

SEISMIC RETROFITTING MANUAL FOR HIGHWAY STRUCTURES: PART 2-RETAINING STRUCTURES, SLOPES, TUNNELS, CULVERTS AND ROADWAYS

By

Maurice Power (Lead Author),
Kenneth Fishman, Faiz Makdisi, Samuel Musser,
Rowland Richards and T. Leslie Youd

December 1, 2006 ■ MCEER-06-SP11





MCEER is a national center of excellence dedicated to establishing disaster-resilient communities through the application of multidisciplinary, multi-hazard research. Headquartered at the University at Buffalo, State University of New York, the Center was originally established by the National Science Foundation (NSF) in 1986, as the National Center for Earthquake Engineering Research (NCEER).

Comprising a consortium of researchers from numerous disciplines and institutions throughout the United States, the Center's mission has expanded from its original focus on earthquake engineering to address a variety of other hazards, both natural and man-made, and their impact on critical infrastructure and facilities. The Center's goal is to reduce losses through research and the application of advanced technologies that improve engineering, pre-event planning and post-event recovery strategies. Toward this end, the Center coordinates a nationwide program of multidisciplinary team research, education and outreach activities.

Funded principally by NSF, the State of New York and the Federal Highway Administration (FHWA), the Center derives additional support from the Department of Homeland Security (DHS)/Federal Emergency Management Agency (FEMA), other state governments, academic institutions, foreign governments and private industry.

**Seismic Retrofitting Manual for Highway Structures:
Part 2 - Retaining Structures, Slopes, Tunnels,
Culverts and Roadways**

by

Maurice S. Power¹ (Lead Author), Kenneth Fishman,²
Faiz Makdisi,³ Samuel Musser,⁴ Rowland Richards⁵
and T. Leslie Youd⁶

Publication Date: December 1, 2006

Technical Report MCEER-06-SP11

Task Number 106-G-3.2

FHWA Contract Number DTFH61-92-C-00106
Contract Officer's Technical Representatives: James Cooper, P.E. HRDI-03,
Wen-huei (Phillip) Yen, P.E., Ph.D., HRDI-07,
John O'Fallon, P.E. HRDI-07,
Federal Highway Administration

- 1 Vice President, Geomatrix Consultants, Inc.
- 2 Principal, McMahan & Mann Consulting Engineers; formerly University at Buffalo, State University of New York
- 3 Principal Engineer, Geomatrix Consultants, Inc.
- 4 Utah Department of Transportation
- 5 Professor, University at Buffalo, State University of New York
- 6 Professor, Brigham Young University

MCEER

University at Buffalo, The State University of New York
Red Jacket Quadrangle, Buffalo, NY 14261

Phone: (716) 645-3391; Fax (716) 645-3399

E-mail: mceer@buffalo.edu; WWW Site: <http://mceer.buffalo.edu>

PREFACE

This manual is a major revision of the Federal Highway Administration publication *Seismic Retrofitting Guidelines for Highway Bridges* which was published in 1983 as Report FHWA/RD-83-007. This original publication was updated in 1994 and an interim revision published as Report FHWA-RD-94-052, *Seismic Retrofitting Manual for Highway Bridges* in May 1995. This current edition expands the coverage of the previous publications by including procedures for seismically-deficient retaining structures, slopes, tunnels, culverts, and roadways, in addition to bridges. It is published in two parts as follows:

Part I: Bridges

Part II: Retaining Structures, Slopes, Tunnels, Culverts, and Roadways

Whereas Part I maintains the basic format of the retrofitting process described in the 1983 Report, major changes have been made in this revision to include advances in earthquake engineering, field experience, and the performance of bridges in recent earthquakes in California and elsewhere.

Part 2 focuses on seismic vulnerability screening, evaluation and retrofitting of the following highway system components: retaining structures, slopes, tunnels, culverts, and roadways. It is the first known effort to capture, in a formal and consistent manner, the important aspects of seismic performance and retrofitting intended to improve performance of highway system structural components other than bridges.

It should be noted that this manual was developed while the Department of Transportation was transitioning to “metric” units. As a consequence, example problems are presented in SI units. However, since most States have switched back to U.S. customary units, the units will also be changed in a future edition.

ACKNOWLEDGMENT

The following people contributed to Part 2 of this manual (in alphabetical order):

Ian Buckle, University of Nevada, Reno; formerly Multidisciplinary Center for Earthquake Engineering Research, University at Buffalo
Brian S.J. Chiou, California Department of Transportation; formerly Geomatrix Consultants, Inc.
Kenneth Fishman, McMahon & Mann Consulting Engineers, P.C.; formerly University at Buffalo
Ian Friedland, FHWA, formerly Applied Technology Council and Multidisciplinary Center for Earthquake Engineering Research, University at Buffalo
Jon Kaneshiro, Parsons Engineering Science; formerly Geomatrix Consultants, Inc.
Faiz Makdisi, Geomatrix Consultants, Inc.
Geoffrey Martin, University of Southern California
Samuel Musser, Utah Department of Transportation
Karthik Narayanan, formerly Geomatrix Consultants, Inc.
Maurice Power, Volume coordinator, Geomatrix Consultants, Inc.
Rowland Richards, University at Buffalo
Dario Rosidi, CH2M Hill; formerly Geomatrix Consultants, Inc.
Zhi-Liang Wang, Geomatrix Consultants, Inc.
T. Leslie Youd, Brigham Young University

The first draft of this document was reviewed by members of the Highway Seismic Research Council for FHWA contract DTFH61-92-C-00106. The second draft was reviewed by the FHWA Office of Infrastructure Research and Development, Turner-Fairbanks Highway Research Center.

The FHWA COTR for this project was Mr. John O'Fallon, assisted by Dr. Phillip Yen.

Editorial assistance was provided by Jane Stoye and Hector Velasco, Multidisciplinary Center for Earthquake Engineering Research, University at Buffalo.

TABLE OF CONTENTS

CHAPTER 1: INTRODUCTION.....	1
1.1 Scope.....	1
1.1.1 Screening.....	2
1.1.2 Detailed Evaluation.....	2
1.1.3 Retrofit Design Strategies.....	2
1.2 Design Earthquakes, Ground Motions, and Performance Criteria for Seismic Screening, Evaluation and Retrofit Design.....	3
1.3 Report Outline.....	4
CHAPTER 2: WALLS AND RETAINING STRUCTURES	5
2.1 Introduction.....	5
2.2 Classification of Wall Types.....	5
2.2.1 Rigid Gravity and Semi-Gravity Walls.....	6
2.2.1.1 Gravity Walls.....	6
2.2.1.2 Semi-Gravity Walls.....	6
2.2.2 Prefabricated Modular Gravity Walls.....	7
2.2.3 Anchored Walls.....	8
2.2.4 Mechanically Stabilized Earth (MSE) Walls.....	9
2.2.5 Other Wall Types.....	10
2.3 Screening.....	10
2.3.1 General Screening Criteria.....	11
2.3.1.1 Level 1.....	11
2.3.1.2 Level 2.....	14
2.3.1.3 Summary.....	14
2.3.2 Anchored Walls.....	16
2.3.3 MSE Walls.....	16
2.4 Evaluation of Retaining Walls.....	17
2.4.1 Information Required for Detailed Evaluation.....	17
2.4.1.1 Wall Details.....	17
2.4.1.1(a) Gravity Walls.....	18
2.4.1.1(b) Concrete Cantilever Retaining Walls (Inverted T-Type).....	19
2.4.1.1(c) Tied-Back Walls.....	20
2.4.1.1(d) MSE Walls.....	20
2.4.1.2 Soil Properties.....	20
2.4.1.3 Ground Motions.....	22
2.4.2 Gravity and Semi-Gravity Walls.....	22
2.4.2.1 External Forces Acting on Gravity or Semi-Gravity Retaining Walls Considering Seismic Loading.....	22
2.4.2.1(a) Seismic Lateral Pressure (Thrust) on Walls.....	23
2.4.2.1(b) Passive Restraint.....	26
2.4.2.1(c) Seismic Bearing Capacity.....	27

TABLE OF CONTENTS (continued)

2.4.2.2	External Stability of Gravity or Semi-Gravity Retaining Walls Considering Seismic Loading: Critical Acceleration k_h for Loss of Equilibrium	30
2.4.2.2(a)	Overturning Stability (Tilting) – Moment Equilibrium.....	30
2.4.2.2(b)	Bearing Capacity Failure - Vertical Equilibrium	32
2.4.2.3	Structural Integrity of Gravity or Semi-Gravity Retaining Walls Considering Seismic Loading.....	33
2.4.2.3(a)	Analysis of Wall Stem	33
2.4.2.3(b)	Analysis of Footing.....	34
2.4.2.4	Loss of Service of Essential Facilities	35
2.4.2.4(a)	Secondary Screening Procedure for Assessing Vulnerability to Seismically Induced Permanent Deformation	36
2.4.2.4(b)	Determination of Threshold Acceleration	37
2.4.2.4(c)	Estimation of Seismically Induced Deformation.....	40
2.4.3	Concrete Cantilever Walls (Inverted T Walls).....	43
2.4.4	Anchored Walls.....	44
2.4.4.1	Secondary Screening Procedure for Anchored Walls.....	44
2.4.4.2	Evaluation Procedure for Anchored Walls	47
2.4.4.2(a)	Passive Toe Failure-Rotation About the Top.....	49
2.4.4.2(b)	Anchor Failure - Rotation of Base	49
2.4.5	MSE Walls	50
2.4.5.1	Evaluation Procedure for MSE Walls for Collapse.....	54
2.4.5.1(a)	Tension in Reinforcements	54
2.4.5.1(b)	Connection Details.....	56
2.4.5.1(c)	Seismic Analysis of Segmental Reinforced Walls and Toppling of the Wall Face	57
2.4.5.2	Proximity of Structures to MSE Walls	58
2.4.5.2(a)	External Sliding Stability.....	59
2.4.5.2(b)	Pullout.....	59
2.4.5.2(c)	Internal Sliding Stability (for SRWs and MCUs).....	60
2.4.5.2(d)	Bulging Shear Failure	60
2.5	Design of Seismic Retrofit for Earth Retaining Structures.....	62
2.5.1	Gravity and Semi-Gravity Walls.....	62
2.5.2	Concrete Cantilever Walls - Structural Failure of the Wall	65
2.5.3	Anchored Walls.....	66
2.5.4	MSE Walls	67
2.6	Screening, Seismic Evaluation and Design of Seismic Retrofit for a Retaining Wall	67

TABLE OF CONTENTS (continued)

CHAPTER 3: SLOPES, EMBANKMENTS, AND ROCKFALLS	97
3.1 Introduction	97
3.2 Classification	97
3.3 Screening Procedures.....	106
3.3.1 Preliminary Screening Procedures	106
3.3.2 Supplemental Screening Criteria for Rockfalls.....	107
3.3.3 Supplemental Criteria for Category III Liquefaction-Induced Landslides.....	113
3.4 Evaluation Procedures	113
3.4.1 Evaluation of Category I Landslides	113
3.4.2 Evaluation of Category II Landslides.....	113
3.4.2.1 Pseudo-Static Slope Stability Analysis Procedure.....	114
3.4.2.1(a) Necessary Data for Analysis	114
3.4.2.1(b) Analysis Procedure	115
3.4.2.1(c) Special Considerations for Rock Slopes.....	117
3.4.2.2 Deformation Analysis Procedures	118
3.4.2.2(a) Yield Acceleration, k_y	119
3.4.2.2(b) Peak Acceleration Induced Within the Sliding Mass, k_{max}	119
3.4.2.2(c) Estimating Deformation, D	119
3.4.3 Evaluation of Category III Landslides	124
3.5 Retrofitting Procedures	124
3.5.1 Rock Slopes.....	125
3.5.2 Soil Slopes.....	131
3.6 Example Problems	136
CHAPTER 4: TUNNELS.....	145
4.1 Introduction.....	145
4.2 Tunnel Classification	145
4.2.1 Bored Tunnels	145
4.2.1.1 Bored Tunnels in Soft Ground	146
4.2.1.2 Bored Tunnels in Rock	146
4.2.2 Cut-and-Cover Tunnels	146
4.2.3 Submerged Tubes	146
4.3 Screening Guidelines	147
4.3.1 Objective of Screening Stage	147
4.3.2 Factors Influencing Tunnel Seismic Performance	148
4.3.2.1 Seismic Hazard	148
4.3.2.2 Geological Conditions	149
4.3.2.3 Tunnel Design, Construction and Condition	149
4.3.3 Screening Guidelines.....	149
4.3.3.1 Screening Guidelines Applicable to All Types of Tunnels.....	149

TABLE OF CONTENTS (continued)

4.3.3.2	Additional Screening Guidelines for Bored Tunnels.....	150
4.3.3.3	Additional Screening Guidelines for Cut-and-Cover Tunnels.....	153
4.3.3.4	Additional Screening Guidelines for Submerged Tubes	153
4.4	Evaluation Procedures	153
4.4.1	Evaluation for Ground Shaking.....	153
4.4.1.1	General.....	153
4.4.1.2	Broad Guidelines for Analyses for Ground Shaking.....	155
4.4.1.3	Evaluation of Axial and Curvature Deformations Along the Longitudinal Tunnel Axis	156
4.4.1.3(a)	Simplified Analyses/Closed Form Solutions.....	157
4.4.1.3(b)	Numerical Analysis.....	166
4.4.1.4	Evaluation of Deformations of Tunnel Cross Section	166
4.4.1.4(a)	Simplified Analyses/Closed-Form Solutions	166
4.4.1.4(b)	Numerical Analysis.....	179
4.4.2	Evaluation for Fault Rupture.....	180
4.4.2.1	General.....	180
4.4.2.2	Assessing the Amount of Fault Displacement.....	181
4.4.2.3	Analyzing Tunnels for Fault Displacement	181
4.4.3	Evaluation for Landsliding or Liquefaction	182
4.5	Retrofit Strategies	186
4.5.1	Ground Shaking-Induced Failure	186
4.5.1.1	Bored Tunnels.....	186
4.5.1.1(a)	Tunnels in Rock.....	186
4.5.1.1(b)	Tunnels in Soil/Soft Ground	188
4.5.1.2	Cut-and-Cover Tunnels.....	191
4.5.1.3	Submerged Tubes.....	191
4.5.1.4	Junctions and Transitions.....	193
4.5.2	Fault Displacement-Induced Failure	196
4.5.3	Landsliding- and Liquefaction-Induced Failure.....	203
4.6	Examples of Tunnel Screening, Evaluation and Retrofit Strategies.....	203
CHAPTER 5: CULVERTS.....		243
5.1	Introduction.....	243
5.2	Classification of Culverts and Background Information	244
5.2.1	Flexible Culverts – Background and Design Philosophies.....	245
5.2.2	Rigid Culverts – Background and Design Philosophies	250
5.2.3	Culvert Joints	252
5.2.3.1	Bell and Spigot Joints	252
5.2.3.2	Tongue and Groove, Keyed and Butt Joints	253
5.2.3.3	Closure Bands and Couplings.....	255
5.2.3.4	Continuous Joints.....	256
5.3	Screening for Potential Seismic Damage.....	257

TABLE OF CONTENTS (continued)

5.3.1	Theoretical Concepts Related to Seismically Induced Culvert Damage	257
5.3.1.1	Permanent Ground Failure	258
5.3.1.2	Transient Ground Motion	259
5.3.2	Empirical Observations of Seismically Induced Culvert Damage	259
5.3.2.1	Embankment Penetration	262
5.3.2.2	Lateral and Embankment Spreading	263
5.3.2.3	Slumping of Fill and Landslides	264
5.3.2.4	Surface Faulting	265
5.3.2.5	Ground Shaking	266
5.3.3	Summary of Culvert Screening Criteria	267
5.3.4	Commentary on Screening Procedure	270
5.4	Evaluation Techniques	273
5.4.1	Permanent Ground Failure	273
5.4.1.1	Embankment and Penetration	275
5.4.1.2	Lateral and Embankment Spreading	275
5.4.1.3	Slumping of Fills and Landslides	275
5.4.1.4	Surface Faulting	276
5.4.2	Transient Ground Motion	276
5.4.2.1	Longitudinal Response of Culverts Due to Transient Ground Motion	277
5.4.2.2	Transverse Response of Culvert Due to Transient Ground Motion	278
5.4.2.3	Examples of Culvert Evaluation Under Transient Ground Motion	278
5.5	Retrofitting Strategies	280
5.5.1	Ground Remediation	280
5.5.2	Remove and Replace	281
5.5.3	Culvert Liners	281
5.5.3.1	Cast-in-Place Liners	283
5.5.3.2	Field Erected Metallic Liners	284
5.5.3.3	Sliplining	284
5.5.4	Joint Retrofit	287
CHAPTER 6: ROADWAYS		289
6.1	Introduction	289
6.2	Classification	289
6.3	Screening and Evaluation Guidelines	290
6.3.1	Stable Embankments and Foundations	290
6.3.1.1	Hazard	290
6.3.1.2	Screen	290
6.3.2	Compaction of Embankment and Foundation Materials	290
6.3.2.1	Hazard	290

TABLE OF CONTENTS (continued)

6.3.2.2	Screen.....	292
6.3.2.3	Evaluation	292
6.3.3	Liquefiable or Soft Embankment and Foundation Materials	295
6.3.3.1	Hazard.....	295
6.3.3.2	Screens for Liquefaction Hazard	300
6.3.3.3	Evaluation	301
6.3.4	Potentially Unstable Embankments, Foundations or Slopes.....	302
6.3.4.1	Hazard.....	302
6.3.4.2	Preliminary Screening and Detailed Evaluation of Slope Instability	306
6.3.5	Active Faults.....	306
6.3.5.1	Screens for Fault Rupture Hazard.....	308
6.3.5.2	Evaluation Procedures	308
6.4	Retrofit Strategies	309
6.4.1	Passive Strategies	309
6.4.2	Active Strategies.....	309
6.4.2.1	Structural Approach Slabs (SAS)	309
6.4.2.2	Use of Easily Repairable Pavement Sections	310
6.4.2.3	Replacement of Inferior Pavement Structures	310
6.4.2.4	Strengthen Foundations Beneath Roadway Grades.....	310
6.4.2.5	Clear and Strengthen Side or Cut Slopes.....	310
APPENDIX A: CHARACTERISTICS OF SURFACE WAVES.....		311
A.1	Introduction	311
A.2	Examples of Prominent Rayleigh Waves During Earthquakes	311
A.3	Summary	313
REFERENCES.....		315

LIST OF FIGURES

2-1	Mass concrete gravity wall	6
2-2	Inverted T-type cantilever wall	7
2-3	Crib wall.....	7
2-4	Anchored wall.....	8
2-5	Generic cross section of MSE structure.....	9
2-6	Seismically induced distress of retaining walls	12
2-7	Structure loaded within zone of active failure wedge.....	13
2-8	Flowchart summarizing the general procedure for screening, evaluation and retrofit of retaining walls.....	15
2-9	Backfill geometry considering construction of the retaining wall.....	18
2-10	Approximate dimensions for various components of a retaining wall	19
2-11	Forces acting on coherent gravity structure	23
2-12	Effect of horizontal and vertical seismic coefficients on active and passive pressure coefficients.....	27
2-13	Ratio of seismic to static bearing capacity factors.....	29
2-14	Assumed distribution of dynamic earth pressure.....	34
2-15	Relationship between static factor of safety and threshold acceleration, k_h^s , for sliding.....	36
2-16	Incremental failure by base sliding.....	41
2-17	Incremental bearing capacity failure by Coulomb sliding wedge mechanism	42
2-18	Chart for seismic screening of anchored walls	44
2-19	Definition of the effective anchor index: $EAI=d/H$	45
2-20	Ratio of active and passive earth pressure coefficients as a decreasing function of k_e	46
2-21	Forces on an anchored wall.....	47
2-22	Seismic effects on anchored walls	48
2-23	Modes of failure for MSE walls.....	52
2-24	Forces acting on MSE wall for external stability analysis.....	52
2-25	Assumed failure surface within the reinforced wall fill.....	53
2-26	Influence of seismic coefficients, k_h and k_v and normalized depth below crest of wall, z/H , on dynamic force amplification factor, r_F	55
2-27	Tensile load in a reinforcement layer due to seismic lateral earth pressure and wall inertia	56
2-28	Overturning moment at an interface within the wall facing of an SRW due to seismic lateral earth pressure and wall inertia	58
2-29	Shear force at an interface within the wall facing of an SRW due to seismic lateral earth pressure and wall inertia	61
2-30	Retrofit strategies for gravity and semi-gravity walls.....	63
2-31	Retrofitting by increasing the width of the base	64
2-32	Seismic effects and retrofit for tied-back walls	66

LIST OF FIGURES (continued)

3-1	Flowchart for screening, evaluating, and retrofitting embankments and slopes adjacent to highway structures.....	98
3-2	Rock fall mechanism and resulting hazard.....	101
3-3	Rock falls along the Pacific Coast highway caused by the 1973 Point Mugu earthquake.....	101
3-4	Examples of toppling failures.....	102
3-5	Aerial view of coalescing disrupted soil slides caused by the 1976 Guatemala earthquake. Slides stripped away vegetation and sheets of sandy residual soil, generally less than 0.6 m thick, exposing white pumice bedrock. Slopes in the foreground are approximately 30 m high.....	103
3-6	Examples of landslides with discrete basal shear surfaces.....	103
3-7	Aerial view of the Native Hospital slide, a large soil block slide in Anchorage, Alaska, caused by the 1964 earthquake.....	104
3-8	Rock slump failure mechanism.....	104
3-9	Soil slump failure mechanism.....	104
3-10	Lateral spread failure mechanism.....	105
3-11	Relationship between corrected “clean sand” blowcount ($(N_1)_{60-cs}$) and underdrained residual strength (S_r) from case studies.....	115
3-12	Horizontal and vertical seismic coefficients for pseudo-static analysis of rock slopes.....	118
3-13	Integration of acceleration time history to determine velocities and displacements.....	120
3-14	Variations of normalized permanent displacement with yield acceleration – summary of all data.....	121
3-15	Variations of average normalized displacement with yield acceleration.....	121
3-16	Upper bound envelope curves of permanent displacements for all natural and synthetic records analyzed.....	122
3-17	Variation of normalized permanent deformation with yield acceleration.....	123
3-18	Categories of rock slope stabilization measures.....	125
3-19	Rock slope reinforcement methods.....	126
3-20	Rock-removal methods for slope stabilization.....	127
3-21	General design criteria for shaped ditches.....	128
3-22	Side view of rock fall restraint net system with fully embedded posts and anchor support.....	129
3-23	Example of rock shed.....	129
3-24	Rock slope mitigation methods used by selected states.....	130
3-25	Rock buttress used to increase forces resisting slope failure.....	134
3-26	Classification scheme for earth retention systems.....	135
3-27	Examples of externally and internally stabilized earth retention systems.....	135
3-28	Types of vertical and horizontal drains used to lower the groundwater in natural slopes.....	136

LIST OF FIGURES (continued)

4-1	Cross sections of submerged tubes	147
4-2	Summary of empirical observations of seismic ground shaking induced damage to bored tunnels	150
4-3	Tunnel response to seismic waves	154
4-4	Approaches for analyzing a tunnel for longitudinal axial and curvature deformations	157
4-5	Example of maximum relative displacements associated with seismic wave propagation. The effects of wave passage and incoherency are shown separately and combined. The dashed lines correspond to constant strains of 10^{-3} and 10^{-4}	158
4-6	Seismic waves causing longitudinal axial and bending strains	158
4-7	Induced forces and moments caused by seismic waves propagating along the longitudinal tunnel axis	160
4-8	Approaches for seismic analysis of tunnel cross section	167
4-9	Pseudo-static stability analysis for weak zone adjacent to tunnel	168
4-10	Forces and moments in tunnel lining due to ovaling	169
4-11	Area and moment of inertia for ovaling analysis of circular tunnel	169
4-12	Definition of terms for Wang (1993) procedure for analysis of racking of a rectangular tunnel	173
4-13	Racking coefficients for rectangular tunnels	176
4-14	Simplified frame analysis models for analysis of racking of a rectangular tunnel	177
4-15	Lateral earth pressures acting on the walls of a cut-and-cover rectangular tunnel	178
4-16	Discrete element model of tunnel	180
4-17	Relationship between maximum surface fault displacement (MD) and earthquake moment magnitude, M_w , for strike-slip faulting	181
4-18	Analytical model of tunnel structure at fault crossing	183
4-19	Schematic illustration of soil-structure model of tunnel at fault crossing	184
4-20	Analytical model of soil restraint for tunnel at fault crossing	185
4-21	Rock bolt stabilization of rock wedge	187
4-22	Rock bolt reinforcement in soft or fractured rock	187
4-23	Precast concrete segmental liner	189
4-24	Example of flexible circumferential joint detail in tunnel lining with seismic isolation washer	190
4-25	Example of a flexible circumferential joint detail in tunnel lining	190
4-26	Corner reinforcing details for seismic design of box-type tunnel	192
4-27	Typical stone column placement around Webster tube	194
4-28	Typical jet grout column around Posey tube	194
4-29	Redesigned joint preventing tension and allowing compression and shear forces between segments of Posey tube	195
4-30	Seismic joint for transbay tube	196
4-31	Seismic joint for North Point tunnel	197
4-32	Enlarged tunnel at fault crossing, plan view, strike-slip faulting	198

LIST OF FIGURES (continued)

4-33	Design of LA Metro tunnel across Hollywood fault zone.....	199
4-34	Enlarged tunnel section with final liner and frangible backpacking to accommodate fault displacement.....	200
4-35	Segment reinforcing and circumferential joint detail, precast concrete segmental liner used in Rose Canyon fault zone for South Bay Tunnel Ocean Outfall Project, San Diego.....	201
4-36	Flexible joint proposed for segmented tunnel lining in fault zone	202
4-37	Flexible joint detail for Coyote Dam outlet tunnel.....	203
5-1	Available types and sizes of flexible culverts.....	246
5-2	Available types and sizes of rigid culverts	247
5-3	Corrugated metal culvert wall profiles	248
5-4	Spiral rib metal culvert wall profiles	248
5-5	Selected examples of thermoplastic culvert wall profiles.....	249
5-6	Selected examples of bell and spigot culvert joints.....	253
5-7	Tongue and groove, keyed and butt joints in reinforced concrete culverts	254
5-8	Selected types of closure bands for corrugated metal culverts.....	255
5-9	Typical coupling for plain end thermoplastic culverts	256
5-10	Penetration of embankment and culvert into liquefied foundation strata.....	262
5-11	Embankment slump (similar effect on culverts as landslide).....	265
5-12	Flowchart of screening procedure for culverts under (a) permanent ground deformation and (b) transient ground deformation.....	268
5-13	Cast-in-place culvert liner.....	283
5-14	Two-flange steel culvert liner plate (top) and four-flange steel culvert liner plate (bottom)	285
5-15	Push and pull techniques for installing HDPE sliplining.....	286
5-16	Internal corrugated sleeve for joining CMP.....	287
6-1	Differential settlement induced by seismic compaction at the easterly approach to bridge 53-1991R in I-5 to I-210 interchange during 1971 San Fernando earthquake.....	291
6-2	Differential settlement across pavement joints near cut-fill boundary on I-5 north of I-405 separation. The settlement is due to seismic compaction of fill during the 1971 San Fernando earthquake.....	292
6-3	Wavy pavement due to differential settlement enhanced by liquefaction during the 1993 Hokkaido-Nansei-Oki, Japan earthquake. The site is on Highway 5 south of Oshamanbe	296
6-4	Failure mechanism beneath embankments that split, settle, and spread due to liquefaction of foundation soils.....	297
6-5	Segment of Highway 36 near Caribbean coast in Costa Rica that split longitudinally, settled and spread laterally during 1991 earthquake by mechanism illustrated in figure 6-4	297

LIST OF FIGURES (continued)

6-6	Disrupted fill and pavement at approach to collapsed Highway 36 bridge over Rio Estrella, Costa Rica. The disruption was due to liquefaction of foundation soils during 1991 earthquake.....	297
6-7	Rigid pavement on I-5 south of I-5/I-210 interchange that sheared and buckled at two localities during the 1971 San Fernando earthquake due to 2 m of lateral spread displacement.....	298
6-8	Extensional fissures in flexible pavement caused by lateral spread of floodplain deposits toward Rio Viscaya during the 1991 Costa Rica earthquake.....	299
6-9	Fractured and overlapped flexible pavement on Highway 229 near northern edge of Assabu River valley. The disruption was due to liquefaction and ground oscillation during 1993 Hokkaido-Nansei-Okii, Japan earthquake; note extensional separation between curb blocks at same locality.....	300
6-10	Liquefaction-induced flow failure of roadway embankment into Lake Merced during 1957 Daly City, California earthquake.....	301
6-11	Slump failure in Highway 5 embankment north of Oshamanbe, Japan during the 1993 Hokkaido-Nansei-Okii earthquake. Failure was due to weakening of soft foundation soils.....	302
6-12	Rigid and flexible pavements disrupted by slump failure of Blucher Avenue near Lower Van Norman reservoir during the 1971 San Fernando earthquake.....	303
6-13	Slump of Highway S22 fill east of Salton Sea during the 1968 Borrego Mountain, California earthquake.....	304
6-14	Sinuous scarp in Summit Road caused by apparent movement of a deep-seated landslide during the 1989 Loma Prieta, California earthquake.....	305
6-15	Disruption to 4th Street, Anchorage, Alaska, caused by deep slump during 1964 Alaska earthquake; headscarp is about 2.8 m high.....	305
6-16	Steep slopes along western shore of Okashiri Island from which numerous rock falls descended onto roadway pavement during the 1993 Hokkaido-Nansei-Okii, Japan earthquake. The debris pitted pavement and blocked highway.....	306
6-17	Rigid and flexible pavements buckled and overlapped by thrust faulting on I-405 south of separation from I-5 during 1971 San Fernando earthquake.....	307

LIST OF TABLES

2-1	Results from application of seismic evaluation procedure for anchored walls (described in Example 2-1)	50
3-1	Characteristics of earthquake-induced landslides	99
3-2	Geologic environments likely to produce earthquake-induced landslides in the Los Angeles region	108
3-3	Description and ratings for the parameters RQD, J_n and J_r	111
3-4	Description and ratings for the parameter J_a	112
3-5	Description and ratings for AF	112
3-6	Comparison of deformation analysis methods.....	124
3-7	Allowable bond stresses in cement-grout anchors.....	126
3-8	Summary of approaches to potential stability problems.....	132
4-1	Assessment of need for seismic evaluations of bored tunnels as related to tunnel lining/support system, geologic conditions, and level of ground shaking	152
4-2	Strains and curvature induced by seismic wave propagating along a tunnel.....	159
4-3	Ratios of ground motion at tunnel depth to motion at ground surface	162
4-4	Ratios of peak ground velocity to peak ground acceleration in rock and soil	163
5-1	Summary of highway culvert performance.....	261
6-1	Expected maximum volumetric strains in dry to moist soils due to seismic shaking	293
6-2	Relative density of sands estimated from standard (SPT) and cone (CPT) penetration test data	294

LIST OF ABBREVIATIONS AND SYMBOLS

ABBREVIATIONS

AASHTO	American Association of State Highway and Transportation Officials
ACI	American Concrete Institute
ACP	Asphaltic Concrete
ACPA	American Concrete Pipe Association
AFTES	Association Francaise des Travaux en Souterrain
AISI	American Iron and Steel Institute
ASCE	American Society of Civil Engineers
ASTM	American Society for Testing and Materials
ATC	Applied Technology Council
BART	Bay Area Rapid Transit
BSSC	Building Seismic Safety Council
CMBC	Corrugated Metal Box Culvert
CMLS	Corrugated Metal Long Span
CMP	Corrugated Metal Pipe
CPT	Cone Penetration Test
EAI	Effective Anchor Index
EP	Embankment Penetration
EPI	Embedment Participation Index
FEMA	Federal Emergency Management Agency
FHWA	Federal Highway Administration
FR	Fault Rupture

FRP	Fiber Reinforced Plastic
GEC	Geotechnical Engineering Circular
GS	Ground Shaking
H/B	Height/Base width
HDPE	High Density Polyethylene
LA	Landslide
LO	Lateral Overpressures
LQ	Liquefaction
LS	Lateral Spread
MCE	Maximum Considered Earthquake
MCEER	Multidisciplinary Center for Earthquake Engineering Research
MCU	Modular Concrete Units
MD	Maximum Displacement
M-O	Mononobe-Okabe
MSE	Mechanically Stabilized Earth
NATM	New Austrian Tunneling Method
NCMA	National Concrete Masonry Association
NEHRP	National Earthquake Hazards Reduction Program
NMSZ	New Madrid Seismic Zone
PCC	Portland Cement Concrete
PGA	Peak Ground Acceleration
PGD	Peak Ground Displacement
PGV	Peak Ground Velocity
PTI	Post Tensioning Institute
PVC	Polyvinyl Chloride

PWPP	Profile Wall Plastic Pipe
RC	Relative Compaction
RCBC	Reinforced Concrete Box Culvert
RCLS	Reinforced Concrete Long Span
RCP	Reinforced Concrete Pipe
RQD	Rock Quality Designation
SAS	Structural Approach Slabs
SG	Strong Ground Shaking
SIDD	Standard Installation for Direct Design
SL	Slumping
SPT	Standard Penetration Test
SRSS	Square Root of the Sum of the Squares
SRW	Segmental Retaining Wall
UCP	Unreinforced Concrete Pipe
UMP	Unreinforced Masonry Pipe
USGS	United States Geological Survey

SYMBOLS

CHAPTER 2: WALLS AND RETAINING STRUCTURES

α_{AE} = Inclination of active failure surface.

β = Wall batter; inclination of the back face of the retaining wall.

β_2 = Batter of the front face of the wall; inclinations of the front face of the retaining wall.

γ = Unit weight.

γ' = Submerged unit weight.

γ_D = Surcharge.

γ_t = Total unit weight of the backfill.

Δ = Total horizontal component of movement.

$\Delta\rho_{AE}$, $\Delta\rho_{PE}$ = Dynamic effects to be added or subtracted to the static values.

δ = Wall/wallfill interface friction angle.

δ_f = Interface friction angle between the base of the foundation and the soil.

δ_w = Wall/soil interface friction angle.

μ = Coefficient of friction between the reinforcement and the wallfill.

ρ_{AE} = Angle of the sliding surface of the active portion of the bearing capacity failure.

ϕ = Angle of friction.

ϕ_b = Wall base/foundation soil interface friction angle.

ϕ_f = Friction angle of the foundation soil.

ϕ_w = Internal friction angle of the backfill.

ψ = Wall batter.

A_D = Anchor force.

A_R = Anchor plate resistance.

B = Width of the footing.

b = Width of reinforcement.

c = Cohesion of the foundation soil.

D = Depth of embedment of the wall toe.

d = Residual displacement; Horizontal distance.

D/H = Embedment depth ratios.

e = Eccentricity.

f = Friction factor.

F = Sum of the horizontal forces.

$F_{\gamma d}$ = Depth factor for soil friction term.

$F_{\gamma i}$ = Inclination factor for soil friction term.

F_A = Design force.

F_a = Site coefficients.

F_c^i = Connection capacities of reinforcement layers.

F_{dyn} = Tension in the reinforcement at depth z ; Dynamic tensile force.

fN = Resisting force.

F_{qd} = Depth factor for surcharge term.

F_{qi} = Inclination factor for surcharge term.

F_{sta} = Static tensile force.

F_{static} = Static factor of safety.

g = Acceleration due to gravity.

h = Height of anchor plate.

H = Height.

\bar{h} = Vertical distance from the line of action of P_{AE} to the toe of the wall footing.

i = Backfill inclination.

j = Facing unit.

K_A = Static lateral earth pressure coefficient.

k_e = Function of the horizontal and vertical seismic coefficients.

k_h = Coefficient of horizontal component of acceleration.

k_h^b = Coefficient of horizontal component of acceleration for yield due to seismic reduction of bearing capacity.

k_h^{OT} = Coefficient of horizontal component of acceleration at threshold of overturning.

k_h^s = Coefficient of horizontal component of acceleration at threshold for sliding.

$(k_h)_{ANC}$ = Critical acceleration for anchor failure.

$(k_h)_{RT}$ = Critical threshold acceleration for rotation about top of wall.

k_o = Peak ground acceleration coefficient accounting for local soil conditions.

k_v = Vertical acceleration component.

L = Length of the wall used to compute N .

L_e = Length of the reinforcement beyond the failure zone defined by ρ_{AE} .

L_w = Width of the wall facing.

M_D = Driving moment.

M_R = Resisting moment capacity.

n = Shear transfer coefficient.

N = Number of reinforcement layers; sum of the vertical forces transmitted to the soil.

N_γ = Soil friction bearing capacity factor.

N_{cE} = Seismic bearing capacity factor.

N_q = Surcharge bearing capacity factor.

N_{qE} = Seismic bearing capacity factor.

$N_{\gamma E}$ = Seismic bearing capacity factor.

q = Overburden due to depth of the footing.

P_{AE} = Active lateral earth pressure.

P_{AS} = Driving force.

p_{IE} = Seismic limit to the bearing pressure.

P_{PE} = Passive resistance from solid placed over the toe of the wall.

R = Rotation mode; Bearing pressure from foundation soil.

r_f = Magnification factor.

S_{dyn} = Interface shear stress.

S_s = Mapped short-period acceleration response parameter.

S_v = Reinforcement spacing.

T = Translation mode.

V = Velocity.

V_u = Shear strength of the interface between modular blocks.

w = Vertical settlement.

W_w = Weight of the retaining wall; Weight of the facing column.

x = Width of contact along the base of the footing. (eq. 2-17).

X_c = Horizontal distance from the centroid of the wall to the toe of the wall footing.

Y_c = Vertical distance from the centroid of the wall to the toe of the wall footing.

Y_c^i = Corresponding moment arms of F_c^i .

z = Depth to the ground water surface below the base of the footing.

CHAPTER 3: SLOPES, EMBANKMENTS, AND ROCKFALLS

A = Peak ground acceleration.

AF = Aperture factor.

a_{max} = Peak ground acceleration.

D = Displacement; deformation.

h = Height of embankment.

J_a = Joint alteration number.

J_n = Joint set number.

J_r = Joint roughness number.

J_v = Total number of joints per cubic meter.

k_a = Peak induced acceleration.

k_{max} = Peak acceleration induced within a sliding mass.

k_y = Yield acceleration.

$(N_1)_{60-CS}$ = Clean sand blowcount.

N_{eq} = Number of cycles.

Q = Rock quality.

Q_{RF} = Seismic rock fall susceptibility index.

S_r = Residual undrained shear strength in psf.

T = Predominant period of the time history.

T_o = Natural period.

V = Velocity.

V_{max} = Low-strain maximum shear wave velocity.

V_s = Strain-dependent shear wave velocity of the soil.

CHAPTER 4: TUNNELS

γ = Shear strain.

γ_{smax} = Maximum free-field shear strain.

γ_t = Total unit weight of geologic medium.

Δ_{ff} = Free-field soil shear deformation over tunnel height.

Δp_E = Lateral earth pressure on tunnel wall.

Δ_r = Racking distortion of the tunnel over tunnel height.

ϵ = Axial strain.

ϵ^{ab} = Maximum axial strain due to combined axial and bending deformations.

σ = Compressive or tensile stress.

σ_{ab} = Maximum axial stress due to combined axial and bending deformations.

σ_v = Vertical total stress.

τ = Shear stress.

ν_l = Poisson's ratio of the liner.

ν_m = Poisson's ratio of geologic medium.

θ = Angle from horizontal of line from center to perimeter of tunnel in plane of tunnel cross section.

ϕ = Angle of direction of seismic wave propagation in horizontal plane with respect to tunnel longitudinal axis.

$1/\rho$ = Curvature.

A_{11} = Cross sectional area of lining (see eqs. 4-6 and 4-7).

A_{12} = Area of unit length of lining (see eq. 4-29 and fig. 4-11).

a_{max} = Peak horizontal ground acceleration at ground surface.

a_p = Peak particle acceleration caused by P-waves.

a_R = Peak particle acceleration caused by R-waves.

a_S = Peak particle acceleration caused by S-waves.

a_v = Peak vertical ground acceleration at ground surface.

C = Compressibility ratio.

C_m = Shear wave velocity of geologic medium.

C'_m = Effective shear wave velocity of geologic medium.

C_p = Apparent propagation velocity of P-waves.

C_R = Propagation velocity of R-waves.

C_S = Apparent propagation velocity of S-waves.

C_V = Seismic earth pressure coefficient.

D = Diameter of tunnel.

D_i = Inside diameter of tunnel lining.

D_o = Outside diameter of tunnel lining ($D_o = D$).

E_1 = Young's modulus of tunnel lining.

f = Maximum frictional force per unit length of tunnel.

F = Flexibility ratio, circular tunnel.

F_r = Flexibility ratio, rectangular tunnel.

g = Acceleration of gravity.

G_m = Shear modulus of geologic medium.

G'_m = Effective shear modulus of geologic medium.

H = Height of tunnel.

h = Depth to center of tunnel.

I_{11} = Moment of inertia of lining cross section (see eq. 4-7).

I_{12} = Moment of inertia of unit length of lining (see eq. 4-17, eq. 4-29 and fig. 4-11).

K_a = Longitudinal soil spring constant per unit length of tunnel.

K_h = Transverse soil spring constant per unit length of tunnel.

K_o = Coefficient of lateral earth pressure at rest.

k_h = Horizontal earthquake coefficient.

L = Wavelength.

M = Moment.

P-wave = Compressional wave.

Q = Tunnel axial force.

$(Q_{\max})_f$ = Maximum frictional force.

R = Reduction factor.

R_r = Tunnel racking coefficient.

R-wave = Rayleigh wave.

S = Tunnel racking stiffness.

S-wave = Shear wave.

t = Lining thickness.

T = Thrust force.

$T_{P,S,R}$ = Period of seismic P-wave, S-wave and R-wave, respectively.

V = Shear force.

V_P = Peak particle velocity caused by P-waves.

V_R = Peak particle velocity caused by R-waves.

V_S = Peak particle velocity caused by S-waves.

w = Tunnel width.

Y = Distance from the neutral axis of the cross section to the extreme fiber of the tunnel lining (see eqs. 4-1, 4-2 and 4-3).

Z = Depth of soil above tunnel.

APPENDIX A: CHARACTERISTICS OF SURFACE WAVES

$C_R(T)$ = Site-specific dispersion curve.

CHAPTER 1: INTRODUCTION

The performance of highway bridges is often considered to be the main determinant in the seismic performance of a highway system. This is due, in large part, to the fact that there are often many more bridges in a region than other types of highway structures or components. Damage to bridges is typically more visible than that to these other types of structures. However, these other components and structures of the highway system may also be important in assuring satisfactory seismic performance of the system.

For example, retaining walls or slopes in highway embankments or excavations provide ground stability at the edges of a highway corridor and protect adjacent property. Tunnels, although much less prevalent than bridges, may comprise important components of the transportation system since, in many cases, a tunnel may provide the only link between two sections of a highway system; i.e., there may be little or no redundancy in the highway or transit system corridor. Consequently, adequate seismic performance of tunnels may be critical. Culverts through or beneath highway embankments are depended on to control surface water flows, and a seismically induced failure could lead to flooding or erosion of a highway or the surrounding area. Finally, failure of a highway roadway due to seismically induced failure of an embankment or its foundation may prevent traffic flow until time-consuming repairs can be made.

In 1983, the Federal Highway Administration (FHWA) published a landmark manual that provided recommendations for screening, evaluating, and retrofitting highway bridges subjected to earthquakes (FHWA, 1983). That manual was updated and reissued in 1995 (FHWA, 1995). Similar guidance, however, has never been developed for these other structures that comprise a typical highway system.

The current edition expands the coverage of the previous publications and is published in two parts. Part 1 covers the screening, evaluation, and retrofitting of highway bridges. It extends the guidance provided in the earlier 1983 and 1995 FHWA manuals, based on recent experiences in California, Japan, and other countries, and the results of comprehensive research programs sponsored by the FHWA, the California Department of Transportation, and other agencies. Part 2 covers these other important highway system structures, namely retaining structures, slopes, tunnels, culverts, and roadways.

1.1. SCOPE

This manual provides guidance on the seismic evaluation and retrofit design of retaining structures, slopes, tunnels, culverts, and roadways. This includes guidance on (a) screening for potential seismic vulnerabilities; (b) conducting a detailed evaluation; and (c) describing strategies for retrofit design. In addition, discussion is provided for classifying each structure by type, construction, or expected performance. This is needed since different types of a given structure (e.g., different types of retaining walls) may have different failure modes and will therefore require

somewhat different approaches to seismic vulnerability screening, detailed evaluation, and retrofitting.

1.1.1. SCREENING

In general, prior to embarking on a detailed seismic evaluation of a highway system structure, an initial screening is carried out to determine whether there is a potential for reduced performance due to a complete or partial seismically induced failure of the structure. The screening methodologies recommended herein are intended to be easy to apply, yet somewhat conservative. If a structure passes the screening criteria, this indicates that there is a low risk of failure and more detailed evaluation or retrofitting is not likely required. If the structure doesn't pass the initial screening step, the owning agency or its designated engineer must decide if a more detailed evaluation, and potential retrofitting, is warranted.

There are a number of considerations that must be included regarding the decision to conduct detailed evaluations and, for those structures deemed vulnerable to seismic demands, retrofitting. Among these are the cost of further evaluation and retrofitting, and the importance of the structure. This is discussed further in section 1.2.

1.1.2. DETAILED EVALUATION

A detailed seismic evaluation is carried out to determine whether or not the structure may fail seismically and, if so, whether a seismic retrofit should be considered. If retrofit is required, these evaluations would continue as a part of retrofit design. Detailed evaluation procedures are presented for each structure type, focusing on the modes of failure most likely to pose the greatest risk. Emphasis, where possible, is on the presentation of step-by-step simplified evaluation procedures that are readily applied yet are reliable and generally accepted in practice. Reference is made to more detailed analytical approaches that should be considered either for more detailed confirmatory analysis or when simplified procedures are not available.

1.1.3. RETROFIT DESIGN STRATEGIES

Guidance is presented regarding alternative approaches and strategies that may be considered in the seismic strengthening of a structure that is determined to be seismically vulnerable from the screening or evaluation process. In some cases, contingency measures are described that may be considered where retrofit design may be judged to be impractical or economically unwarranted. The approaches and strategies presented herein are those that have been utilized in similar retrofit design situations.

1.2. DESIGN EARTHQUAKES, GROUND MOTIONS, AND PERFORMANCE CRITERIA FOR SEISMIC SCREENING, EVALUATION, AND RETROFIT DESIGN

In general, the design earthquakes and ground motions to be used in screening, evaluation, and retrofit design of highway structures covered herein are the same as those described in Part 1. Furthermore, as described in Part 1, a two-level evaluation and design approach may be considered and is encouraged to assure a higher level of performance for more frequently occurring ground motions.

In evaluating the highway system structures described in this report, it is important to recognize that the failure or large deformations of some components may not necessarily comprise a life safety risk. For example, a retaining wall or a slope may translate up to or more than a meter, yet may not pose a life safety risk to users of the highway system. However, consideration must not be restricted to only the impact on the highway system from structure damage, but also to potential collateral damage and life safety for other structures that may be affected by the failure of the highway structure; e.g., a facility or structure located directly above or below a retaining wall or slope.

Furthermore, decisions on whether to seismically retrofit a highway system structure may depend on its importance and criticality, and cost-benefit considerations. For example, a decision may be made to seismically retrofit a tunnel if it provides non-redundant access to an area and if the damage to the tunnel could disrupt post-earthquake traffic flow, even though such damage may not be life threatening. Considerations of facility importance, cost-effectiveness, or prioritization for retrofit are not explicitly considered herein, but their importance must be recognized in developing an overall evaluation and retrofitting program, and in making decisions for individual facilities.

The primary goal of any seismic evaluation and retrofitting program should be to minimize the risk of unacceptable damage and the potential for loss of life; however, such decisions must be tempered by cost considerations and the performance of such structures in prior earthquakes. Transportation structures must be classified as to their importance with respect to traffic flow and the impacts on society due to damage or closure of the structure or associated highway. It is recommended that two classifications of importance be considered for the transportation structures addressed in this report: standard and essential (refer to Part 1, chapter 1).

Decisions regarding the level of detailed evaluation and retrofitting of the highway structures covered in this report should include consideration of its importance and the cost of retrofitting. The owning agency may determine that earthquake damage is acceptable, if it can be easily repaired or functionality can be restored relatively quickly (e.g., gravel or asphalt can be quickly and temporarily applied to damaged roadways). Standard structures may not warrant retrofitting to provide the same level of performance as newly designed structures; however, life safety concerns should be addressed. Essential structures, however, may typically warrant significant investments in evaluation and retrofitting, in order to ensure both life safety and some level of post-earthquake functionality. This is a decision that the owning agency must make.

1.3. REPORT OUTLINE

This report addresses the seismic vulnerability evaluation and retrofitting of the major highway system structures other than bridges. Each chapter contains a section on classification, preliminary screening, detailed evaluation, and retrofitting. Chapter 2 covers retaining structures (other than those directly attached to a bridge), chapter 3 covers slopes and rock fall related to highway cuts and fills, chapter 4 addresses transportation tunnels, chapter 5 covers flexible and rigid culverts, and culvert joints, and chapter 6 addresses rigid and flexible roadways.

CHAPTER 2: WALLS AND RETAINING STRUCTURES

2.1. INTRODUCTION

This chapter on walls and retaining structures describes procedures for classifying earth retaining structures that function as components of a highway system, screening them relative to their seismic vulnerability, and evaluating their performance during earthquake loading using simplified methods. It also describes retrofitting strategies and methods to repair or mitigate the effects of earthquake shaking. This chapter does not cover retaining structures that are an integral part of a bridge, i.e., abutments and wing walls.

Consistent with the performance criteria described in Part 1, the seismic vulnerability of retaining structures is assessed with respect to life safety issues. Life safety issues include collapse of the retaining structure. The possibility of unacceptable damage to nearby essential structures may also give cause for assessing the level of service of the retaining structure.

As demonstrated in the 1995 Kobe earthquake, the most common collapse mechanisms for retaining structures subjected to earthquake loading include excessive tilting leading to an overturning instability, or structural failure, cracking of concrete gravity or cantilever retaining walls (Koseki et al., 1996). This chapter describes a force based approach whereby factors of safety are evaluated relative to external stability, and internal stability is evaluated by comparing the applied loads to the structural resistance. The force based approach for evaluating external stability is employed as a tool to identify cases where excessive deformations leading to collapse are possible. In these cases, more detailed deformation analyses are recommended.

Retaining walls may also slide outward as well as rotate due to seismic loads. The soil behind them slumps possibly causing secondary damage to structures they support, or protect, such as highway fills and buildings above or below the wall. If seismically induced deformation of retaining structures is excessive, nearby essential structures or facilities may suffer unacceptable loss of service including interruption of utilities, structural damage, or loss of access and regress. Therefore, for those cases where the serviceability of nearby essential facilities is deemed important, this chapter will also address level of service issues related to estimating and controlling seismically induced permanent deformations due to sliding, overturning and loss of bearing capacity.

2.2. CLASSIFICATION OF WALL TYPES

Salient details of the wall descriptions appropriate to screening and evaluation for seismic retrofit are presented herein. A complete description of retaining wall classifications and proper terminology are presented in *Geotechnical Engineering Circular No. 2: Earth Retaining Systems* (Sabatini, 1997).

In general, walls are classified as rigid gravity and semi-gravity walls, prefabricated modular gravity walls, anchored walls, mechanically stabilized earth walls, non-gravity cantilevered walls, and in-situ reinforced walls.

2.2.1. RIGID GRAVITY AND SEMI-GRAVITY WALLS

Retaining walls that rely on their mass to resist lateral earth pressures transferred from the backfill are referred to as gravity and semi-gravity walls. The walls are considered rigid and are usually not fully constrained against rotation or displacement at the base. It is generally assumed that deformations are sufficient to mobilize active conditions within the backfill and passive pressure at the toe if buried.

2.2.1.1. Gravity Walls

Gravity retaining walls may be mass concrete (figure 2-1), or masonry. Prior to 1960, these walls were the most popular construction practice. Mass concrete walls are generally proportioned such that a minimum amount of reinforcing steel is required. The mass of the wall limits tensile stress in the concrete. Minimum reinforcing steel may be required to control cracking due to the tendency for concrete to undergo volume changes from shrinkage and temperature variation.

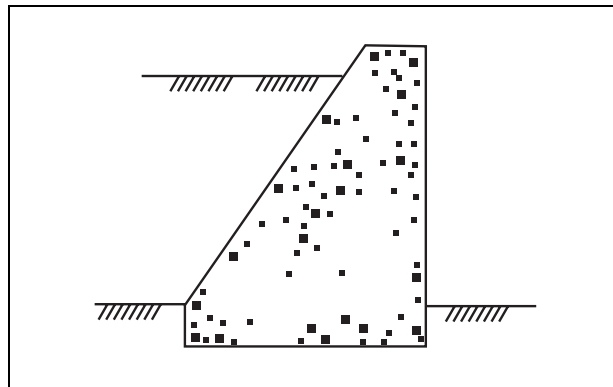


Figure 2-1. Mass concrete gravity wall.

2.2.1.2. Semi-Gravity Walls

Semi-gravity walls including cast in-place concrete cantilever/counterfort retaining walls (figure 2-2) are similar to gravity-type walls, but are designed such that a portion of the backfill is used to contribute to stability. When the stability is evaluated, the wall and the backfill placed over the heel of the footing are considered to act as a unit. Less concrete is used to construct a cantilever wall than for a mass gravity wall. However, large flexural stresses are generated near the base of the wall stem, and heel of the footing. Therefore, these members require significant amounts of reinforcing steel. Counterforts may be added to buttress the wall stem to reduce the moments and reinforcing requirements.

Gravity and semi-gravity retaining walls may be supported on shallow or deep foundations. In general, retaining walls supported by piles or drilled shafts are not vulnerable to collapse except from structural failure of pile-head connections, or liquefaction of the foundation soil. Therefore, the majority of the guidelines for evaluating these wall types is with respect to shallow foundations, i.e., spread footings.

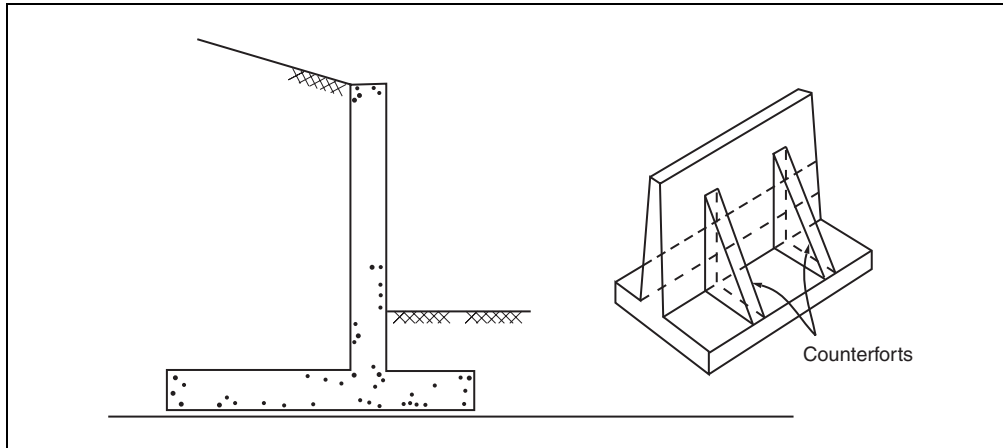


Figure 2-2. Inverted T-type cantilever wall.

2.2.2. PREFABRICATED MODULAR GRAVITY WALLS

Prefabricated modular gravity walls incorporate soil into the mass of the wall system as in crib walls or gabion walls (figure 2-3). These wall types also rely on mass for stability. Materials such as ballast or boulders are contained with cribbing or wrapped within a wire mesh. Cribbed or gabion units are connected to form a coherent mass to resist inertia forces, and applied lateral earth pressures. Internal stability must also be analyzed with respect to sliding, bulging between units, or the structural integrity of the cribbing.

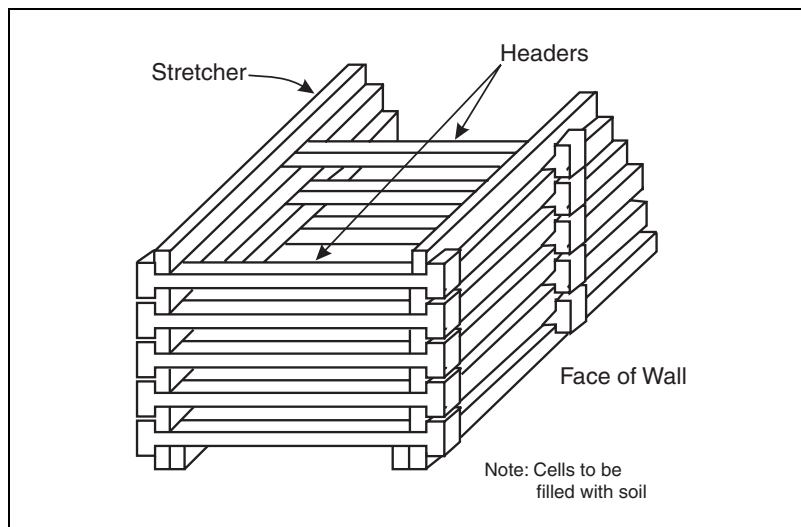


Figure 2-3. Crib wall.

2.2.3. ANCHORED WALLS

Anchored walls are constructed with vertical elements that are embedded into the soil with tie-backs to restrain the top. Facing elements are used to support retained soil. Vertical wall elements may consist of discrete vertical elements (e.g., piles, caissons, drilled shafts) spanned by structural facing (e.g., wood or reinforced concrete lagging, precast or cast in place concrete panels, wire or fiber reinforced concrete, or metal elements such as sheet piles). The discrete vertical elements typically extend deeper into the ground than the facing to provide vertical and lateral support. Alternatively, the vertical wall elements are continuous (e.g., sheet-piles) and, therefore, also form the structural facing. Tie-backs can be anchored to flat “deadmen” or battered piles; or grouted anchors may be used. A typical anchored wall is depicted in figure 2-4.

The most common application of anchored walls is for waterfront structures, but they are also used sometimes in dry or drained conditions. Of particular interest are tied-back walls used to retain highway fills on sloping ground, or for approach embankments. The backfill used to construct tied-back walls in dry conditions is select and often densified.

When used as waterfront structures, tied-back walls are usually constructed by driving sheet-piles and dredging to the desired depth. Often the dredged material is used as additional backfill. Thus, unlike tied-back walls constructed in dry soil, the soil at the toe and anchor of a waterfront tied-back wall necessary to provide passive resistance is often loose, fine grained, and below the water table.

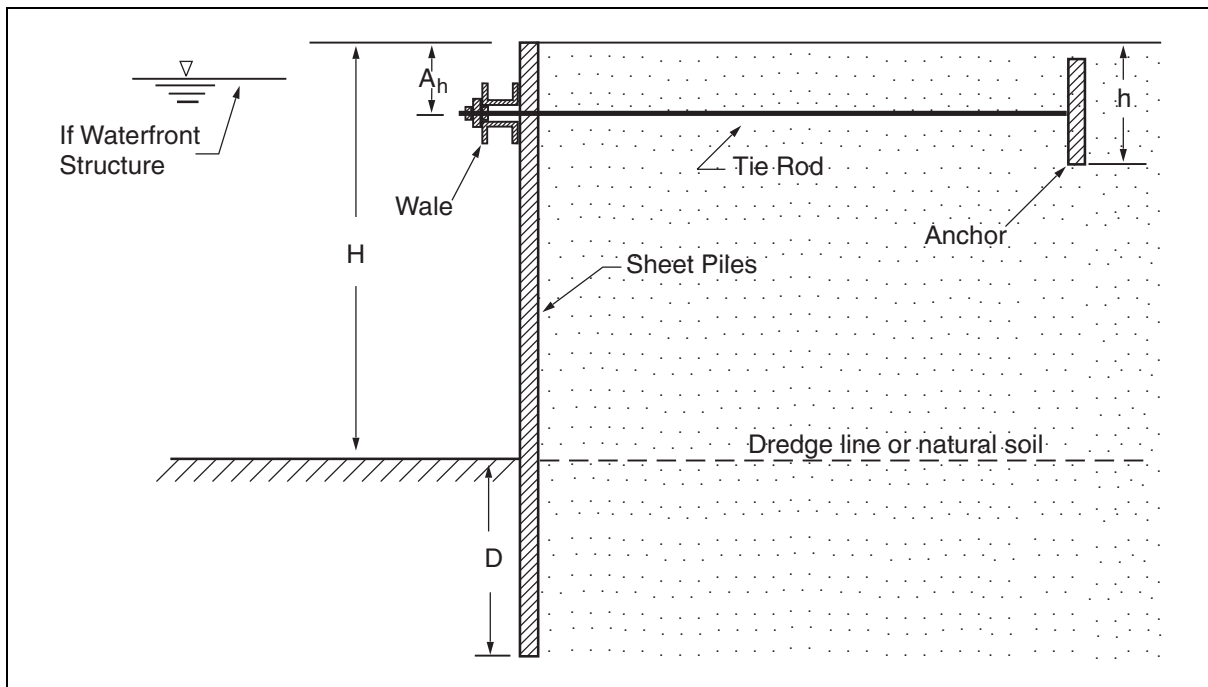
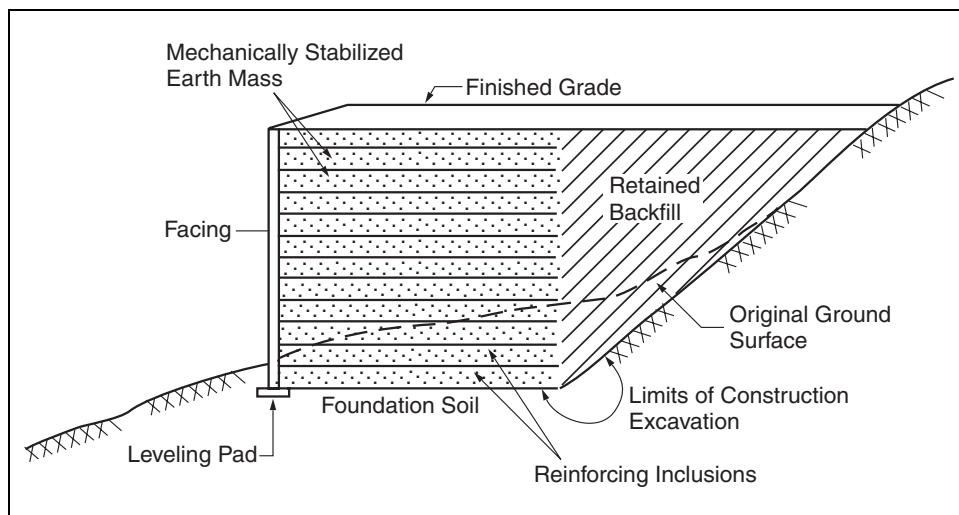


Figure 2-4. Anchored wall.

2.2.4. MECHANICALLY STABILIZED EARTH (MSE) WALLS

MSE walls (i.e., reinforced soil, figure 2-5) incorporate some type of reinforcing element in the soil to help resist lateral earth pressures. The analysis of MSE walls, described in section 2.4.5, treats the reinforced fill, referred to as wall fill, as a gravity retaining wall that supports the unreinforced backfill placed behind it. The external stability analysis of an MSE wall is similar to that of any other gravity-type retaining wall. In addition, an analysis of the internal stability to evaluate structural integrity of the reinforcements must be performed.

Reinforcements may be in the form of strips, sheets, bar mats, or grids. They may be made from metallic materials such as mild steel, galvanized steel, or aluminum. Nonmetallic reinforcements are generally polymeric materials consisting of polypropylene, polyethylene, or polyester polymers. Geotextiles and geogrids are popular types of polymeric reinforcement.



Elias and Christopher, 1997

Figure 2-5. Generic cross section of MSE structure.

Depending on the level of strain required to mobilize the working stress levels in the reinforcement, reinforcements are extensible, or relatively inextensible. The deformation of relatively inextensible reinforcement at failure is much less than the deformability of the soil. Relatively inextensible reinforcement may not reach levels of strain required to develop active earth pressures for the entire height of the wall. For extensible reinforcement, the deformation at failure is comparable to, or even greater than, the deformation of the soil. Typically, metallic strip, or bar mat, type of reinforcement is relatively inextensible and geotextiles are extensible.

Certain details of the screening and evaluation procedure described in sections 2.3.3 and 2.4.5 are related to the type of wall facing incorporated into the MSE wall system. As described by Holtz et al. (1995), a variety of facings may be used with MSE walls including modular concrete units (MCU), wrap around facings, segmental concrete panels, full-height concrete panels, metallic facings, timber facings, or gabion facings. With the exception of MCUs, the wall facing is mainly for protection from erosion and exposure to the environment. MCUs are considered to have mass that contributes to the stability of the MSE wall system.

2.2.5. OTHER WALL TYPES

In addition to the retaining wall types described in the sections above, others are available, including non-gravity cantilever walls with an embedded toe such as sheet-pile walls, etc., soil nail walls, reticulated micropile walls, slurry walls, concrete diaphragm walls, and deep mixed soil walls. These walls are not considered to be a significant portion of the existing inventory, and are not discussed explicitly in the following sections.

Due to their flexibility, analysis of the dynamic response of the backfill behind non-gravity cantilever retaining walls is complicated. Some information on design and analysis of soil nail walls is described by Byrne et al. (1996b). Reticulated micropile walls are described by Bruce and Juran (1997).

Many retaining walls in the larger urban areas support soundwalls that range in height from 3.5 to 5 meters. In some areas, such as the northeast U.S., designers consider a substantial lateral wind load, but in very seismically active areas, such as California, seismic load may control the design. For seismic evaluation of retaining walls that support soundwalls, the forces and moments transferred to the top of the retaining wall should be considered. These details are not included within the analyses and equations presented in this manual.

2.3. SCREENING

Screening of retaining walls is intended to identify those walls susceptible to damage in earthquakes, and therefore candidates for detailed evaluation. The procedure is conservative in the sense that some walls are included in the category for detailed evaluation that will eventually be assessed as not at high risk to seismic loading and no retrofit measures will be required. The screening procedure requires a minimum amount of information including location, site conditions, wall height, base width (if applicable), type of retaining wall, and proximity of essential facilities. This information can be obtained from existing records, soil and geologic maps, and should always entail a site visit.

The screening guidelines presented in this section are for retaining walls in which neither the backfill nor foundation soils will undergo liquefaction. The user must screen the site for the liquefaction hazard as described in chapter 3, Part 1 of this manual.

This section assumes that the user has estimated the anticipated peak ground acceleration (PGA) at the site of the retaining wall. The user is referred to chapter 2, Part 1 of this manual for guidance. Additional guidance on assessing seismic ground motions at retaining walls sites is contained in section 2.4.1.3 in this chapter.

The user must also investigate the possibility of the retaining wall being engulfed in a global failure mechanism. This mode of failure is in the category of slope stability as described in chapter 3, Part 1 of this manual.

2.3.1. GENERAL SCREENING CRITERIA

The general screening criteria are described with respect to gravity and concrete cantilever retaining structures. Special considerations that must be taken into account relative to tied-back and MSE retaining walls are described in sections 2.3.2 and 2.3.3.

Retaining structures are screened with respect to two sets of information described below. The first set (level 1) screens the retaining walls with respect to the potential for seismically induced problems related to life safety issues and possibly with respect to level of service. The second set (level 2) involves visual observation of the wall, condition assessment, and an evaluation of the level of safety of the wall with respect to static loading. Walls that are determined to not require seismic evaluation on the basis of a level 1 screening must still pass the scrutiny of a level 2 screening before a final determination is made. Level 2 screening need not be applied to walls that are selected for detailed seismic evaluation based on the results of level I screening since a site visit is part of the detailed seismic evaluation.

2.3.1.1. Level 1

Relevant modes of failure as they relate to life safety issues are depicted in figure 2-6 (a) and (b). Modes of failure include:

- Overturning of the retaining wall or excessive tilting due to loss of bearing capacity.
- Structural failure of the wall.

Level of service and excessive damage to nearby essential facilities is described in figure 2-6 (c).

Overturning of retaining walls is a concern particularly for tall, slender retaining walls. Increments of seismically induced tilting, or rotation, of the wall accumulate during cycles of strong ground shaking. Long-period and long duration earthquakes are of particular concern due to potentially high ground velocity, or large number of cycles of strong ground shaking, respectively. Screening of the inventory should be performed to identify tall, slender walls and the corresponding seismic hazard. Wall slenderness ratios (height/base width, H/B) greater than 2.0 and/or walls where the horizontal distance from the toe to the center of gravity is less than half the width of the base are a serious concern in areas where the seismic hazard at the site is a peak horizontal ground acceleration in excess of 0.3 g. Slenderness ratios less than two may be a problem for special circumstances, e.g., walls with a high backslope angle.

Seismically induced structural failure of retaining walls is due to overstressing of structural components of the retaining wall system. Accelerations associated with earthquake ground motions, and present within the backfill, have a twofold effect on the lateral earth pressure applied to the backface of a retaining wall. The first is an increase in the lateral thrust, and the second is that the line of action of the lateral thrust is raised with respect to the base of the wall. For high levels of peak ground acceleration, this can lead to significant increases in bending moments within the wall stem, and at the toe and heel of the wall footing. Since for a properly designed reinforced concrete structure a load factor of 1.7 was typically applied to static earth loads (AASHTO, 1996; ACI, 1999), reinforced concrete retaining walls should not suffer a

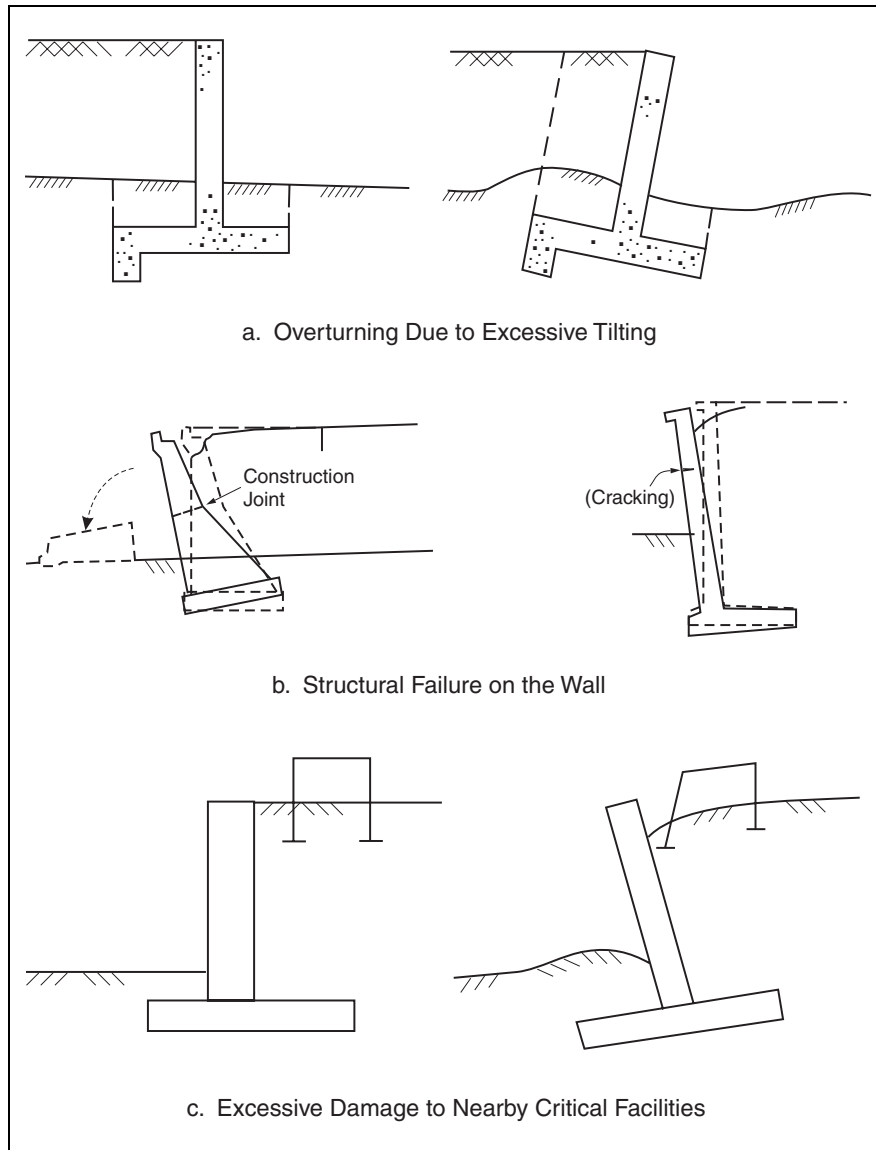


Figure 2-6. Seismically induced distress of retaining walls.

structural failure unless high levels of acceleration are considered or the wall has some form of structural deficiency.

The structural failure shown in figure 2-6(b) is taken from the report prepared by Koseki et al. (1996), and the construction joint is with respect to a particular wall constructed in Japan. Many of the walls that suffered severe structural distress from the Kobe earthquake, as reported by Koseki et al. (1996), were over 60 years old, and unreinforced. Walls designed by today's standards may not fail in this manner, but walls not properly designed or detailed are vulnerable to collapse and need to be evaluated.

Structural deficiencies include inadequate section, poor construction joints, and lack of reinforcement or internal support (buttresses, counterforts). Detailed seismic evaluation is

recommended for sites with a seismic hazard associated with peak horizontal ground accelerations in excess of 0.3 g, or walls with structural deficiencies.

Retaining walls founded on pile foundations (or drilled shafts) may also be vulnerable to structural failure at the pile-head connections. During a seismic event, pile loads will be redistributed and additional shear forces will be transferred to the pile foundation. Pile-head connections should be evaluated for the case of seismic loading applied to the retaining wall system.

Seismically induced damage to nearby structures is due to loss of level of service from deformation of the wall backfill that may result from tilting or sliding of the retaining wall. The potential for damage depends on the proximity of nearby structures or facilities such as pavements, and especially railroad tracks. If structures and facilities on top of the backfill are located within the zone of failure behind the wall, as shown in figure 2-7, small deformations of the retaining wall may be significant. Structures located within 1.5 H of the wall backface may be vulnerable to wall displacement.

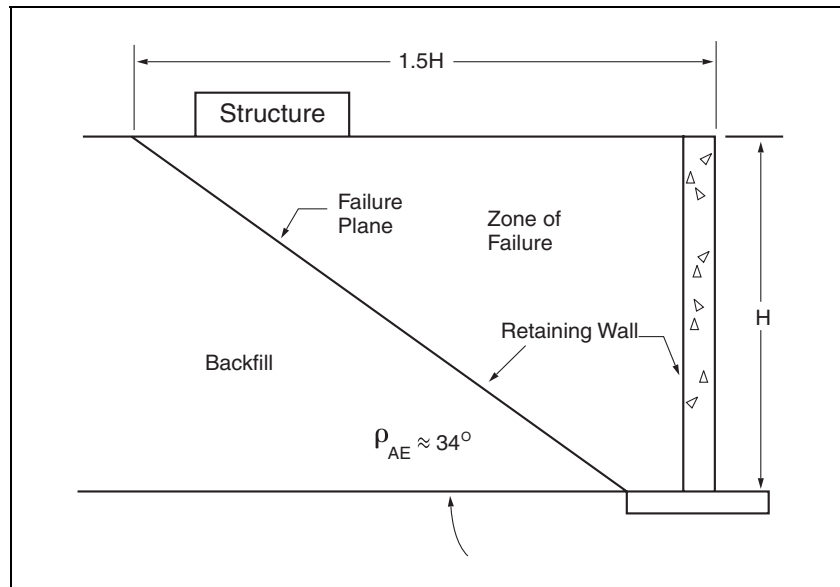


Figure 2-7. Structure loaded within zone of active failure wedge.

Detailed evaluation of retaining walls should be considered whenever essential facilities are located within 1.5 times the height of the wall with respect to the backface, and seismic hazard at the site is associated with a horizontal component of peak ground acceleration in excess of 0.1 g. However, detailed evaluation is not necessary if all the following conditions are satisfied:

- Retaining wall displacements of 75 mm can be tolerated. Seismic hazard at the site is associated with a horizontal component of peak ground acceleration less than 0.3 g.
- Permanent surcharge loads are not applied within 0.5 H of the backface.
- Backfill slope is less than 10° .

- Loose, saturated soils are not present, i.e., saturated cohesionless soils with SPT-N values less than 10.

2.3.1.2. Level 2

Static safety factors should be checked as described in *GEC No. 2: Earth Retaining Systems* (Sabatini, 1997). Soil parameters required for geotechnical engineering considerations may be available from original design calculations or estimated based on knowledge of existing site conditions. Static factors of safety for sliding and overturning should be at least 1.5 and 2.0, respectively. Appropriate factors of safety for bearing capacity and global stability vary depending on subsurface conditions, performance requirements and other conditions (AASHTO, 2002; Vesic, 1973). Compared to the original construction, a change in the wall geometry or soil conditions due to distress and/or lack of appropriate maintenance may result in a safety factor different from that intended in the original design. Distress may include cracking and/or corrosion of the wall or footing, differential settlements or tilting of the wall, or flooding of the backfill or foundation material. Walls not meeting minimum requirements for static loading are certainly candidates for detailed seismic evaluation and should be screened accordingly.

The level 2 screening requires a site visit whereby visual observations are employed to determine the current condition of existing retaining walls. Excessive tilting, or settlement of the wall, are important signs of distress originating in the foundation soil which should be documented. Signs of structural distress that must be documented include spalling concrete at the face of the wall and/or discoloration of the concrete due to corrosion of reinforcing steel; poor construction joints, and excessive cracking of concrete. Retaining walls that exhibit visible signs of excessive distress should be included in the category for detailed evaluation.

2.3.1.3. Summary

In general, for walls that meet the minimum requirements for static factor of safety, detailed evaluation is not required if the following conditions are met:

- No visible signs of distress.
- Backfill or foundation soils are not liquefiable.
- Wall slenderness ratios (height/base width, H/B) are less than 2.0.
- Surcharge loads are low and the backfill slope is not steep.
- Essential facilities are not located in proximity to the wall.
- Seismic hazard at the site is associated with a horizontal component of peak ground acceleration less than 0.3 g.

A flowchart that summarizes application of the general screening guidelines, evaluation procedures and design of retrofit is presented in figure 2-8.

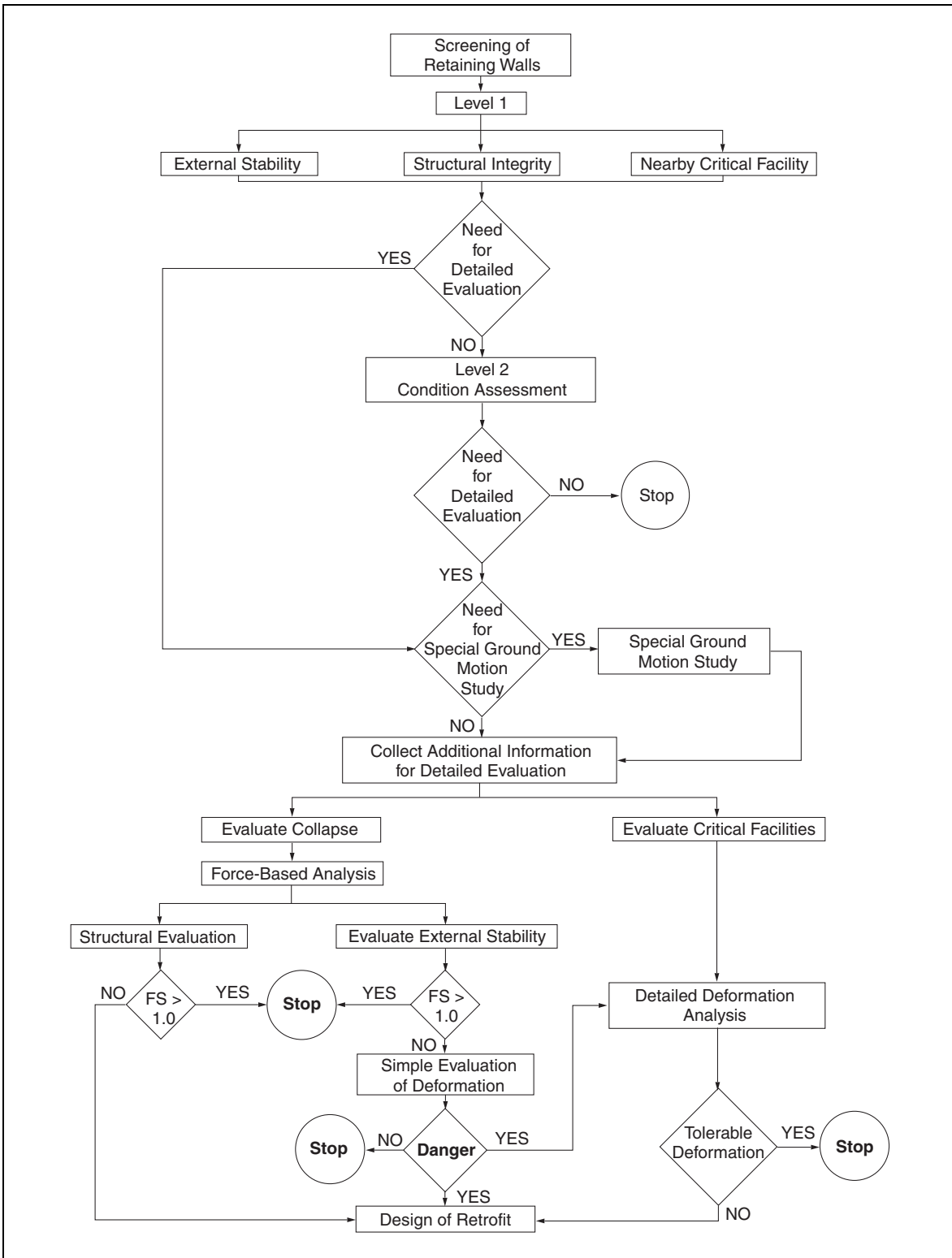


Figure 2-8. Flowchart summarizing the general procedure for screening, evaluation and retrofit of retaining walls.

2.3.2. ANCHORED WALLS

When used as waterfront structures along rivers or for harbor facilities, anchored walls are at great risk due to the liquefaction hazard. The potential for liquefaction is aggravated by the use of dredged material for backfill as described in section 2.2.3. Many such walls have failed dramatically in earthquakes. Waterfront structures must be considered highly suspect and evaluated carefully for retrofit, or replacement, if even a moderate earthquake is anticipated.

In their review of 110 tied-back, waterfront walls in Japan, Gazetas et al. (1990) indicate that, where liquefaction issues are not a concern, it is usually the anchor that is the weak component in current designs. The example presented in section 2.4.4 shows that tied-back walls designed with a static factor of safety of 2 could fail by anchor pullout, causing rotation around the bottom at a coefficient of horizontal acceleration applied within the backfill of approximately 0.2. Thus, tied-back walls not properly designed for seismic effects are at risk even in moderate earthquakes.

A secondary screening procedure is described in section 2.4.4 for rapid evaluation of anchored walls with respect to pullout failure. More detailed evaluation is then performed for walls that are categorized as potentially vulnerable to this failure mechanism.

2.3.3. MSE WALLS

To date, no significant earthquake-induced damage to MSE walls have been reported in the literature. According to Tatsuoka et al. (1995) MSE walls performed very well in the 1995 Kobe earthquake; although at one location some permanent seismically induced displacement was observed. However, conventional gravity walls located in the vicinity of the referenced MSE wall suffered catastrophic damage. Kavazanjian et al. (1997) report that MSE walls also performed well in the 1989 Loma Prieta earthquake.

For MSE walls, the main concern is the effect of earthquake-induced ground accelerations to increase lateral earth pressure and involve a larger volume of soil in the active failure region. The increased lateral earth pressures transfer a dynamic increment of tensile force to the reinforcement. The largest relative increases in reinforcement force occur in the uppermost layers in a reinforced soil wall (Bathurst and Cai, 1995). Also, the critical failure surface becomes flatter, affecting the pullout resistance that can be mobilized along the reinforcement.

Most MSE walls that are found to be deficient from a seismic analysis do not have adequate reinforcement length near the top of the wall. Considering the pullout resistance, as described in section 2.4.5, the length of reinforcement required to resist earthquake-induced tensile forces is typically 10 percent greater than the length required for static loading conditions.

In summary, for MSE walls, there is a need to assess the adequacy of reinforcement near the top of the wall, particularly for walls with facings that include modular concrete units, segmental concrete panels, or gabion facings.

2.4. EVALUATION OF RETAINING WALLS

2.4.1. INFORMATION REQUIRED FOR DETAILED EVALUATION

Detailed seismic evaluation requires considerably more information about the retaining wall than that required for preliminary screening. Additional time and expense is required to collect as-built details of the wall and site features, and to obtain parameters for the backfill and foundation soils.

It may be necessary to conduct a site investigation, and retrieve soil and/or rock samples for laboratory testing. It is also important for the user to document the condition of the retaining walls being evaluated. Man-made construction materials may have decayed or corroded over time, and the wall dimensions and/or material properties used in the initial design may no longer prevail. Nondestructive evaluation to assess the condition of the retaining wall and/or sampling and laboratory testing of materials may be required.

2.4.1.1. Wall Details

Necessary information includes the wall and foundation dimensions, the geometry of the backfill (i.e., slope of the backfill surface), drainage conditions, and depth of burial at the toe of the wall. Most of the necessary information, described in the subsections below, may be obtained from existing construction drawings. If construction drawings are not available, it will be necessary to collect information via a site visit. An invasive, or a nondestructive, evaluation will be necessary if portions of the wall are buried and inaccessible.

The foundation type must be identified as deep or shallow. For a description of methods that may aid in identifying unknown foundation types and conditions, the user is referred to the work of Olsen (1996). For shallow foundations, the bearing grade, thickness, and width of the foundation must be determined. For deep foundations, the length of the foundation elements must be established, as well as their number, distribution, diameter, and reinforcement details; and pile cap, and pile to cap connection details.

A typical backfill geometry considering construction of the retaining wall is shown in figure 2-9. It is likely that during construction of the wall, the contractor minimized placement of backfill to the extent allowed by the owner, or as constrained by site conditions. Often, during construction, in-situ soils are cut back at a steep angle. The use of heavy compaction equipment in close proximity to the wall backface is usually avoided such that backfill soils may not be very well-compacted there. Considering these aspects of wall construction, it is quite possible that backfill and in-situ soils have distinct characteristics. During seismic loading, both are contributing to the response of the retaining wall system and their appropriate strength should be identified for use in the seismic evaluation.

The geometry of the backfill should be assessed during the site investigation. It may possibly be defined by as-built drawings and pre-construction soil investigation. If not, the backfill should be probed with shallow borings or test pits to identify the extent of the backfill placed during construction. The number and depth of borings or test pits are a function of the wall and backfill

geometry, and the depth and character of the backfill and underlying soils. For test borings, Standard Penetration Testing (ASTM D1586, 1984a) should be done at two ft intervals with continuous sampling. Soils retrieved with the split spoon sampler or from test pits should be visually identified at the site by a geotechnical engineer, soil scientist or geologist using the standard practice described in ASTM D2488 (1984b). If fine grained soils are encountered, “undisturbed” samples should be retrieved for testing as described in section 2.4.1.2. The data obtained from the test borings should be analyzed by a geotechnical engineer to identify the interface between backfill and in-situ soils, run appropriate laboratory tests if necessary, and assign appropriate properties to each for use in subsequent analyses.

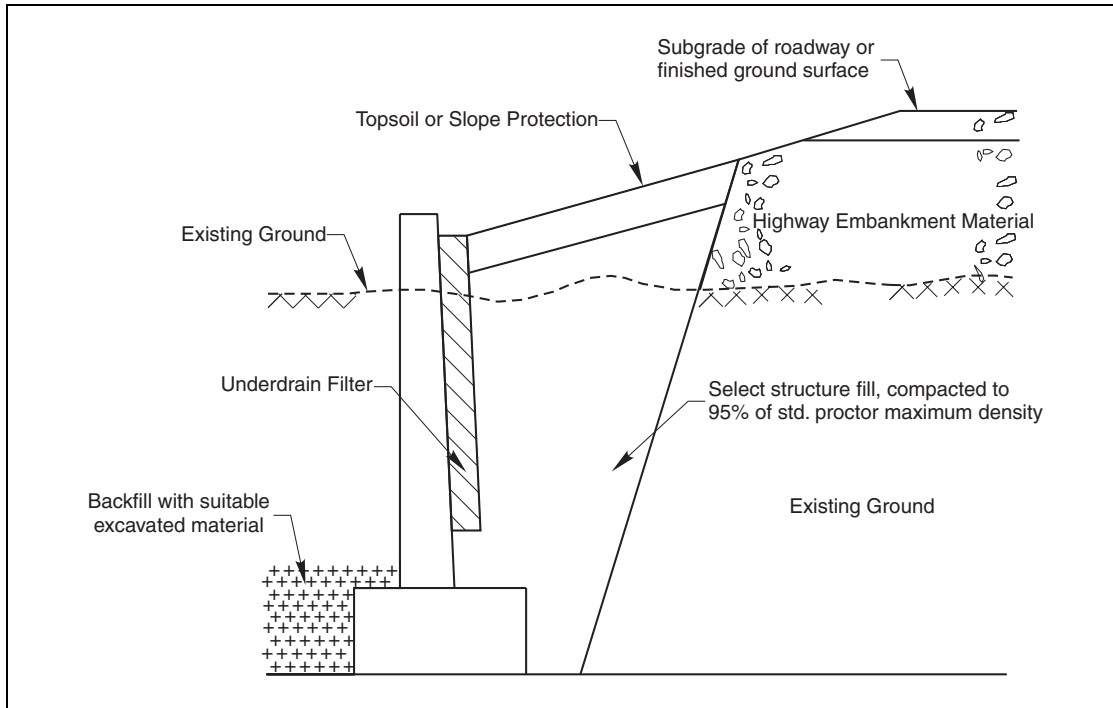


Figure 2-9. Backfill geometry considering construction of the retaining wall.

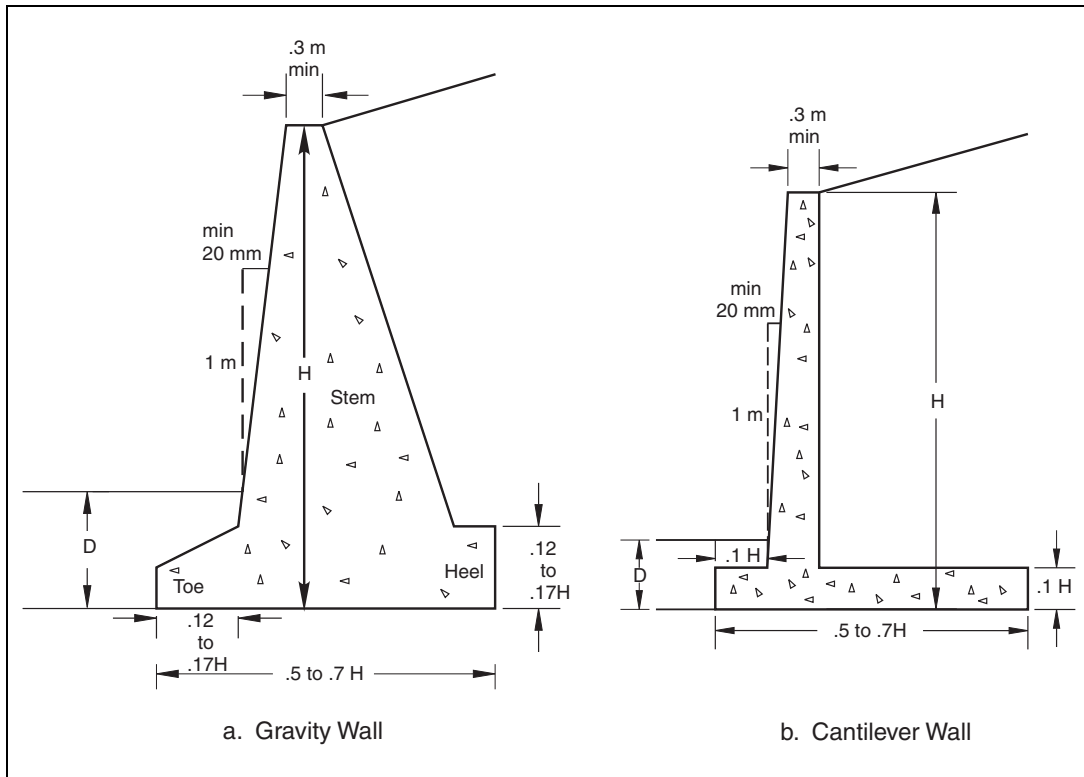
2.4.1.1(a). Gravity Walls

Necessary wall parameters include the wall height, weight, batter, details of the foundation, and backfill drainage conditions. If the wall is vulnerable to tilting (overturning stability), dimensions of the wall must be known to compute the center of gravity for use in the procedure described in section 2.4.2.2(a). Dimensions of the retaining wall should be well established for a detailed analysis. Bowles (1977) provides guidance on the common proportions of gravity retaining walls in terms of the wall height as shown in figure 2-10. Dimensions shown in figure 2-10 are used as a starting point for the design of retaining walls. They may be used as a rough guideline for estimating dimensions. The actual dimensions of constructed walls may deviate significantly from figure 2-10.

It is very important for the analysis of overturning stability to identify the toe of the retaining wall. During the site investigation, the toe of the wall footing should be located by visual observation, if necessary, by excavating a shallow trench. Caution should be exercised when

planning this investigation so as not to remove any toe support required for static stability of the wall. Alternatively, shallow probe holes can be advanced with augers to identify the location of the toe.

Soil samples should be retrieved near the toe of the wall to identify near-surface foundation soils. If these soils are fine grained, and test results are not available, undisturbed samples of the foundation soil should be retrieved and tested as described in section 2.4.1.2.



Bowles, 1977

Figure 2-10. Approximate dimensions for various components of a retaining wall.

2.4.1.1(b). Concrete Cantilever Retaining Walls (Inverted T-Type)

The same information described in the section above is also required for concrete cantilever retaining walls. In addition, the length of the heel of the retaining wall should be established such that soil placed over the heel can be included in the analysis. Details of steel reinforcement used in concrete cantilever walls should also be determined.

If available, construction documents should be utilized, but for older walls this information may not be available. The rough guidelines in figure 2-10 should only be used as a last resort, and used in preliminary calculations. If a more detailed evaluation for retrofit is undertaken, the wall dimensions should be explored as part of a site investigation.

Many retaining wall footings are placed against undisturbed material where the footing concrete is placed without the use of forms. This most likely results in an overpour, i.e., a portion of the footing will be unreinforced. It may be possible to locate the edge of the footing with a probe or soundings as part of the site investigation, but the fact that the concrete may be unreinforced, and is likely cracked, needs to be recognized. If the toe and heel of the footing is exposed, the reinforcing steel may be located with a pacometer. Otherwise, if the edge of the footing appears to be cast directly against the foundation soil, a nominal distance of 0.3 meters should be discounted from the heel and toe of the footing to account for the possibility of an overpour.

2.4.1.1(c). Tied-Back Walls

The user should identify the type of wall system according to the descriptions referenced in section 2.2.3. Dimensions and yield strengths of the structural elements comprising the wall system should be quantified. The depth of embedment of the vertical elements should also be known.

Detailed knowledge of the tie-back system is particularly important to the seismic analysis of the retaining wall system. Knowledge of the type and length of the wall anchor and the anchor head assembly is required. If grouted anchors are employed, the length of the bonded and unbonded portions should be known as well as the level of prestress. In instances where corrosion, or loss of anchorage, is an issue, the user should make an assessment of the in-service state of the tie-back.

2.4.1.1(d). MSE Walls

The user should describe the type of wall system and facing units according to the descriptions given in section 2.2.4. Type, spacing and length of reinforcement should be determined. Dimensions of the wall facing units should also be established as well as details of the connection between the reinforcements and wall facing.

2.4.1.2. Soil Properties

Soil parameters should be obtained for the backfill and foundation soil from the results of a site investigation. The stratigraphy of the foundation soils should be identified as well as the type of soil used for backfill. Knowledge of soil unit weight, and shear strength parameters, including cohesion and angle of friction is needed. For the foundation soil, these values can often be inferred from the results of in-situ testing performed during the preconstruction site investigation. In the United States the *Standard Penetration Test* is the most popular in-situ test. More recent investigations may include results from cone penetration or pressure meter testing.

In-situ test results may not be available for backfill if the site investigation was done prior to construction of the wall. Properties of backfill and in-situ soils may be investigated by sampling and performing appropriate laboratory tests. In lieu of this, a value of 34° is a conservative estimate of the internal angle of friction for a clean, well-graded, free-draining backfill. Fine grained soils are sheared under undrained conditions during seismic loading. Therefore, for fine grained soils, the undrained strength should be used in the evaluation. Appropriate laboratory strength tests should be performed on undisturbed samples retrieved from the site, or appropriate

in-situ testing should be performed to determine the undrained strength. Alternatively, the method described by Ladd (1991) can be used to estimate the undrained strength during shear. Peak and residual strengths should be determined. Details of sampling, testing and proper evaluation of soil properties are described in *Geotechnical Engineering Circular No. 5* (Sabatini, 2002).

Interface friction between the wall face and backfill is estimated based on data available in the literature (AASHTO, 2002). For concrete wall facings and free draining granular backfill, an interface friction coefficient between one-half and two thirds the value of the tangent of the internal friction angle of the backfill is often employed. The base friction angle at the interface between the wall foundation and the foundation soil is often higher than the interface wall friction angle. If concrete is placed directly against a cohesionless foundation soil, the interface friction angle may equal the internal angle of friction for the foundation soil.

Current practice for cohesionless soils is to assume that the internal and interface friction angles are not rate dependent. Friction angles determined for static loading are used in the seismic evaluation procedure. The peak shear strength of the soil is used in the evaluation for seismic resistance and corresponding threshold accelerations. However, when a deformation analysis is performed, the residual strength of the soil should be considered if the soil has undergone large permanent deformation.

The user should also establish the position of the groundwater table(s). The shear resistance of saturated cohesionless soils may degrade during seismic loading. If pore water pressures increase during cycles of shear loading, the effective stress and corresponding shear strength of the soil will decrease. Unless the retaining wall is a waterfront structure (quay wall), the backfill is generally free draining and not saturated. However, for waterfront structures and saturated foundation, soil degradation of shear strength during cyclic loading may be an important issue. Once the properties of the backfill and foundation soil have been evaluated, it is necessary to assess the liquefaction potential at the site of the retaining wall and assess the potential for degradation of shear strength due to cyclic loading of saturated cohesionless soils.

The procedure referred to in chapter 3, Part 1 of this manual may be used to determine if a site is a candidate for detailed evaluation of liquefaction potential. Retaining walls located on sites susceptible to liquefaction will deform due to a severe loss of shear strength within the foundation soil. Procedures for estimating the degradation of shear strength of cohesionless soils as a function of peak ground acceleration are generalized in Edinger (1989). Also, Ebeling and Morrison (1992) describe a method for considering the degradation of shear strength for saturated cohesionless soils.

The static undrained strength of cohesive soils should be reduced by 15 percent per recommendations of Makdisi and Seed (1979) to account for effects from cyclic loading.

Retaining walls located on sites not susceptible to liquefaction may undergo seismically induced permanent deformation due to increased lateral thrust behind the retaining wall and from the inertia force acting on the wall itself. In what follows, procedures to evaluate seismic vulnerability from these effects are discussed for walls classified as gravity walls, concrete cantilever walls (inverted T-walls), tied-back walls, and mechanically stabilized earth walls.

2.4.1.3. Ground Motions

In general, it is acceptable to assume that free-field peak ground accelerations estimated for the site, as described in Part 1 of this manual, are uniformly applicable to the wall and retained soil. However, in some cases, local site soil response effects and/or two-dimensional response effects may be significant and not adequately captured by the site free-field peak ground acceleration. Examples of cases where local response effects may be more significant include: fills of substantial extent constructed behind the wall where the dynamic stiffness of the fill is significantly different from that of the underlying geologic materials for which free-field ground motions were estimated (for example, embankment fills constructed over bedrock); walls with high slopes behind the walls; and tall walls. Conducting a site-specific analysis to evaluate local response effects and accelerations to be used in retaining wall seismic evaluations is always an option to using free-field accelerations defined for the site.

Various methods may be considered for assessing local response effects, including: simplified embankment or slope response analysis methods (refer to chapter 3); one-dimensional analysis of wall backfills above underlying materials to bedrock; and two-dimensional analysis of wall-soil foundation systems (for example, see Kavazanjian et al., 1997). A geotechnical earthquake engineering specialist should evaluate whether special analyses are needed and carry out such analyses.

2.4.2. GRAVITY AND SEMI-GRAVITY WALLS

Seismic evaluation of gravity walls must consider the dynamic increment of lateral earth pressure, the inertial response of the wall, and the effect of seismic loading on the shear strength of the foundation soils and backfill. Evaluation of forces are described in section 2.4.2.1, and their effect on external stability of gravity retaining walls are described in section 2.4.2.2. Section 2.4.2.3 considers the structural integrity of gravity retaining walls for seismic loading conditions. In section 2.4.2.4, a displacement-based analysis is described for evaluation of the potential for damage and loss of serviceability to essential facilities located in close proximity to the wall.

Gravity and semi-gravity retaining walls founded on pile (or drilled shaft) foundations may be vulnerable to collapse if the piles are founded in liquefiable soils. The external stability of retaining walls founded on deep foundations within liquefied foundation soils can be evaluated using procedures described in *Recommended LRFD Guidelines for the Seismic Design of Highway Bridges* (ATC/MCEER, 2003).

2.4.2.1. External Forces Acting on Gravity or Semi-Gravity Retaining Walls Considering Seismic Loading

Figure 2-11 shows the forces acting on a gravity retaining wall during seismic loading. Forces acting on the wall are from inertial response, lateral earth pressure from the backfill (P_{AE}), passive resistance from soil placed over the toe of the wall (P_{PE}), and bearing pressure from the foundation soil (R). Lateral earth pressure includes the static component and the dynamic

increment. It is also important to consider the inertial loading applied to the foundation soil, and its effect on bearing capacity.

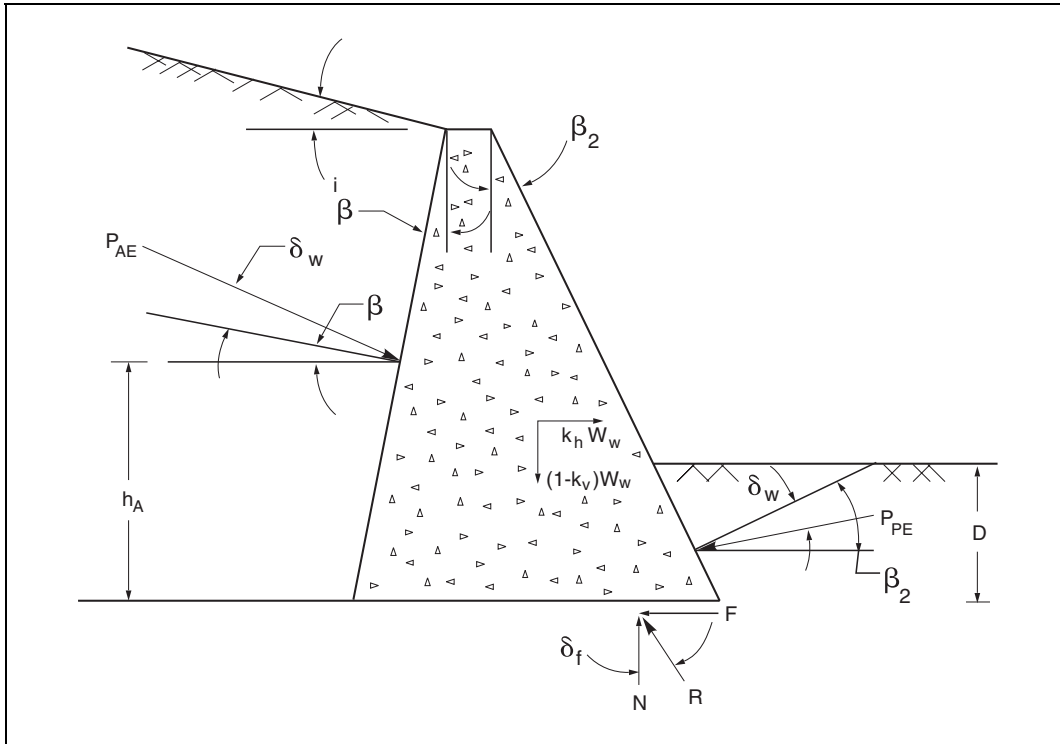


Figure 2-11. Forces acting on coherent gravity structure.

In general, these forces relate to the stability of the retaining wall with respect to sliding, overturning, and loss of bearing capacity. However, from the standpoint of the life safety performance criteria, mechanisms for collapse of gravity or semi-gravity retaining walls include overturning, loss of bearing capacity and/or structural failure of the wall. Unless an essential facility is located within close proximity to the retaining wall, the sliding mode of failure is not catastrophic and, in fact, is the preferred mode of wall movement.

Methods to compute lateral earth pressures and seismic bearing capacity are described in the subsections below. Procedures to evaluate the seismic stability of gravity or semi-gravity retaining walls with respect to overturning and loss of bearing capacity, respectively, are described in section 2.4.2.2.

2.4.2.1(a). Seismic Lateral Pressure (Thrust) on Walls

If the wall is allowed to deform enough to mobilize active earth pressure, lateral earth pressures that develop behind rigid retaining walls during earthquake loading may be evaluated using a rigid plastic model to describe soil behavior. This approach was followed by Okabe (1926), and Mononobe and Matsuo (1929), who performed a modified Coulomb analysis where the inertial load on the failed wedge was included in the analysis. The Mononobe-Okabe (M-O) equation for the active earth pressure coefficient for seismic loading may be expressed as:

$$K_{AE} = \frac{\cos^2(\phi_w - \theta - \beta)}{\cos \theta \cos^2 \beta \cos(\delta_w + \beta + \theta) \left[1 + \sqrt{\frac{\sin(\phi_w + \delta_w) \sin(\phi_w - \theta - i)}{\cos(\delta_w + \beta + \theta) \cos(i - \beta)}} \right]^2} \quad (2-1)$$

where:

$$\theta = \tan^{-1} \left(\frac{k_h}{1 - k_v} \right) \quad (2-2)$$

and:

k_h and k_v are coefficients of horizontal and vertical accelerations,
 ϕ_w is the internal friction angle of the backfill,
 β is the wall batter,
 δ_w is the wall/soil interface friction angle,
 i is the backfill inclination.

The coefficient of horizontal acceleration applied to the backfill, k_h , is taken as the peak ground acceleration divided by the acceleration due to gravity, A_{max}/g , unless: (1) A_{max} is greater than the threshold and (2) the threshold acceleration for sliding is less than the threshold accelerations for overturning or tilting from seismically induced loss of bearing capacity. If conditions (1) and (2) apply, k_h is the threshold acceleration for sliding, k_h^s .

The active thrust, P_{AE} , maybe calculated as:

$$P_{AE} = \frac{1}{2} \gamma_t H^2 (1 - k_v) K_{AE} \quad (2-3)$$

where:

P_{AE} is the active thrust and includes the static component plus the dynamic increment,
 γ_t is the total unit weight of the backfill,
 H is the wall height.

It is important to note that this solution is limited in that:

- A constant value for the angle of wall friction, δ_w , must be assumed.
- There is no moment equilibrium equation so that the line of action of the thrust P_{AE} is not involved.
- Wall deformation must be sufficient to mobilize the active condition within the backfill.
- Cohesion is not included in the analysis.

- Irregular geometry of the backfill surface is not considered.
- The effects of a submerged backfill are not included.
- Equation (2-2) has no real solution of $\theta + i > \phi$. Physically, this implies that an equilibrium condition will not exist.

The orientation of the failure surface associated with equation 2-1 becomes flatter as the level of acceleration increases, and when $\theta + i = \phi$, the predicted failure surface is horizontal. In practice, cohesionless soil is unlikely to be present for a great distance behind a retaining wall and encompass the entire failure wedge under seismic conditions. In some cases, free draining cohesionless soil may only be placed in the static active wedge (i.e., at a 60 degree angle) with the remainder of the soil being cohesive embankment fill ($c - \phi$ soil) or even rock. In these instances, earthquake-induced active pressure should be determined using trial wedges as shown in figure 6-25 in Part 1 of this manual.

In instances where the backfill includes fined grained soils such as clay, silty-clay, or clayey silt, and the shear strength includes a component from cohesion, graphical solutions such as the trial wedge method (see Part 1 of this manual; Bowles, 1977; ASCE, 1994) may be employed to compute the active lateral earth pressure. The trial wedge method for determination of lateral earth pressure may also incorporate irregular geometry of the backfill surface. In the trial wedge method (figure 6-25, Part 1), it is assumed that the failure surface for the active condition is planar. This assumption is consistent with that of Mononobe-Okabe. The retaining wall geometry is drawn to scale and various trial failure wedges are evaluated. Each trial failure wedge has a failure surface with its origin at the base of the retaining wall, but the inclination of the failure surface with respect to the horizontal is varied for each trial. Force polygons are constructed which include:

- The weight of the trial wedge.
- Inertial forces acting on the trial wedge due to vertical and horizontal components of ground acceleration.
- Resultant of the normal force and frictional component of shear resistance along the assumed failure surface.
- Resultant of the pore water pressure acting along the assumed failure surface.
- Resultant of the cohesive component of shear resistance along the failure surface.
- Resultant of the active thrust acting at the wall face.

A number of trial wedges are evaluated from which the maximum active thrust and critical angle of the failure surface are determined. The backfill may be considered to consist of more than one material, however, only one wall interface friction angle and one backfill soil friction angle may be included in the analysis. For backfill with multiple soil layers, total lateral load should be

calculated using an appropriate limiting equilibrium method of analysis as described by ASCE (1994).

This report assumes that backfills are not submerged. For the case of backfills that are either not free draining, or are located along a waterfront, the effects of a submerged backfill on the computation of lateral earth pressure must be included in the analysis. The reader is referred to Ebeling and Morrison (1992) for guidance on including the effects of a submerged backfill on computation of lateral earth pressure.

2.4.2.1(b). Passive Restraint

In many instances, the base of a retaining wall is embedded to some depth within the foundation soil. Effects of foundation embedment include the development of passive restraint against sliding, and a contribution to bearing capacity from the surcharge.

Some deformation is required for the passive restraint to be fully mobilized. As deformations continue, passive restraint is mobilized, and seismic resistance is increased. When full passive restraint is mobilized, a steady state seismic resistance prevails at a given level of acceleration.

For the passive seismic limit state:

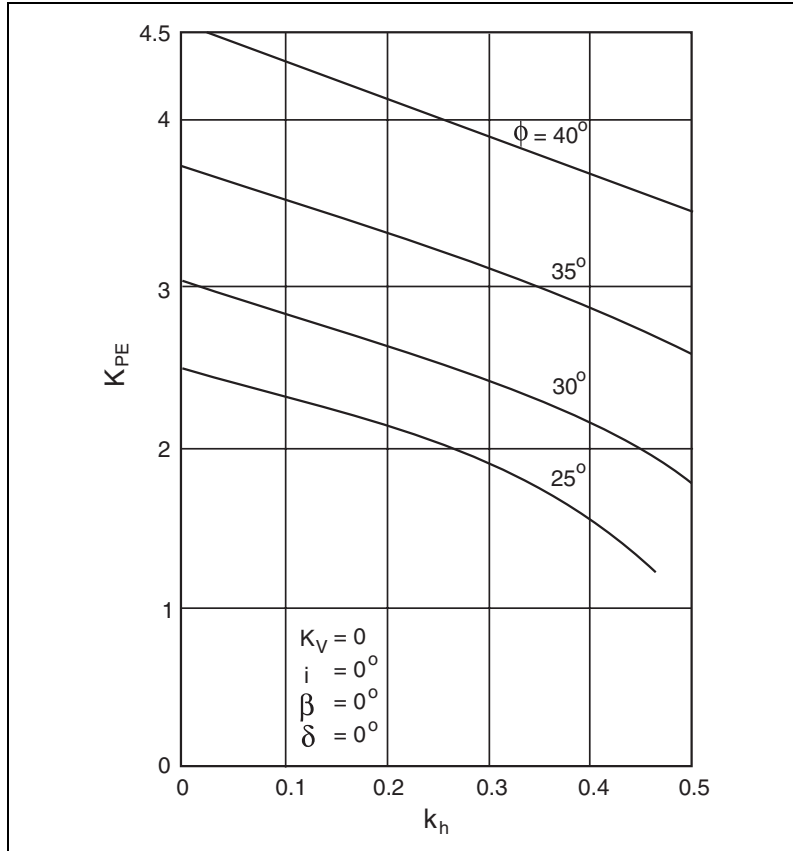
$$P_{PE} = \frac{1}{2} \gamma_t H^2 (1 - k_v) K_{PE} \quad (2-4)$$

where K_{PE} is expressed as:

$$K_{PE} = \frac{\cos^2(\phi_w - \theta + \beta)}{\cos \theta \cos^2 \beta \cos(\delta_w - \beta + \theta) \left[1 - \sqrt{\frac{\sin(\phi_w + \delta_w) \sin(\phi_w - \theta + i)}{\cos(\delta_w - \beta + \theta) \cos(i - \beta)}} \right]^2} \quad (2-5)$$

The value of K_{PE} computed with equation 2-5 increases significantly with increasing wall/soil friction angle, δ_w . The value of δ_w should be chosen carefully to avoid calculating an unconservatively high value of K_{PE} . Morrison and Ebeling (1995) show that eq. (2-5) is unconservative for problems involving low to moderate acceleration fields with interface friction greater than or equal to one-half the angle of internal friction.

Equation 2-5 is plotted in figure 2-12, which portrays how the passive thrust decreases with an increase in level of acceleration. Therefore, at high acceleration levels ($k_h > 0.4 g$), the benefits of embedment at the toe of the retaining wall are diminished compared to that at low levels of acceleration.



Davies et al., 1986

Figure 2-12. Effect of horizontal and vertical seismic coefficients on active and passive pressure coefficients.

2.4.2.1(c). Seismic Bearing Capacity

Richards et al. (1990), Richards and Shi (1991 and 1994) and Shi (1993) studied seismically induced reduction of bearing capacity. Seismic bearing capacity factors are developed considering shear tractions transferred to the soil surface as well as the effect of inertial loading on the soil in the failed region below the footing. For simplicity, a “Coulomb-type” of failure mechanism is considered within the foundation consisting of an active wedge directly beneath the retaining wall and a passive wedge that provides lateral restraint.

For retaining walls, shear transfer between the footing and foundation soil is conveniently described by a shear transfer coefficient, n , where:

$$n = \frac{F}{N \tan \phi_f} \quad (2-6)$$

and:

F is the sum of the horizontal forces,
 N is the sum of the vertical forces transmitted to the soil,
 ϕ_f is friction angle of the foundation soil.

The analytic solution gives a bearing capacity formula in terms of seismic bearing capacity factors N_{qE} , N_{cE} , and $N_{\gamma E}$, similar to its counterpart for the static case, as:

$$p_{IE} = cN_{cE} + qN_{qE} + \frac{1}{2}\gamma B'N_{\gamma E} \quad (2-7)$$

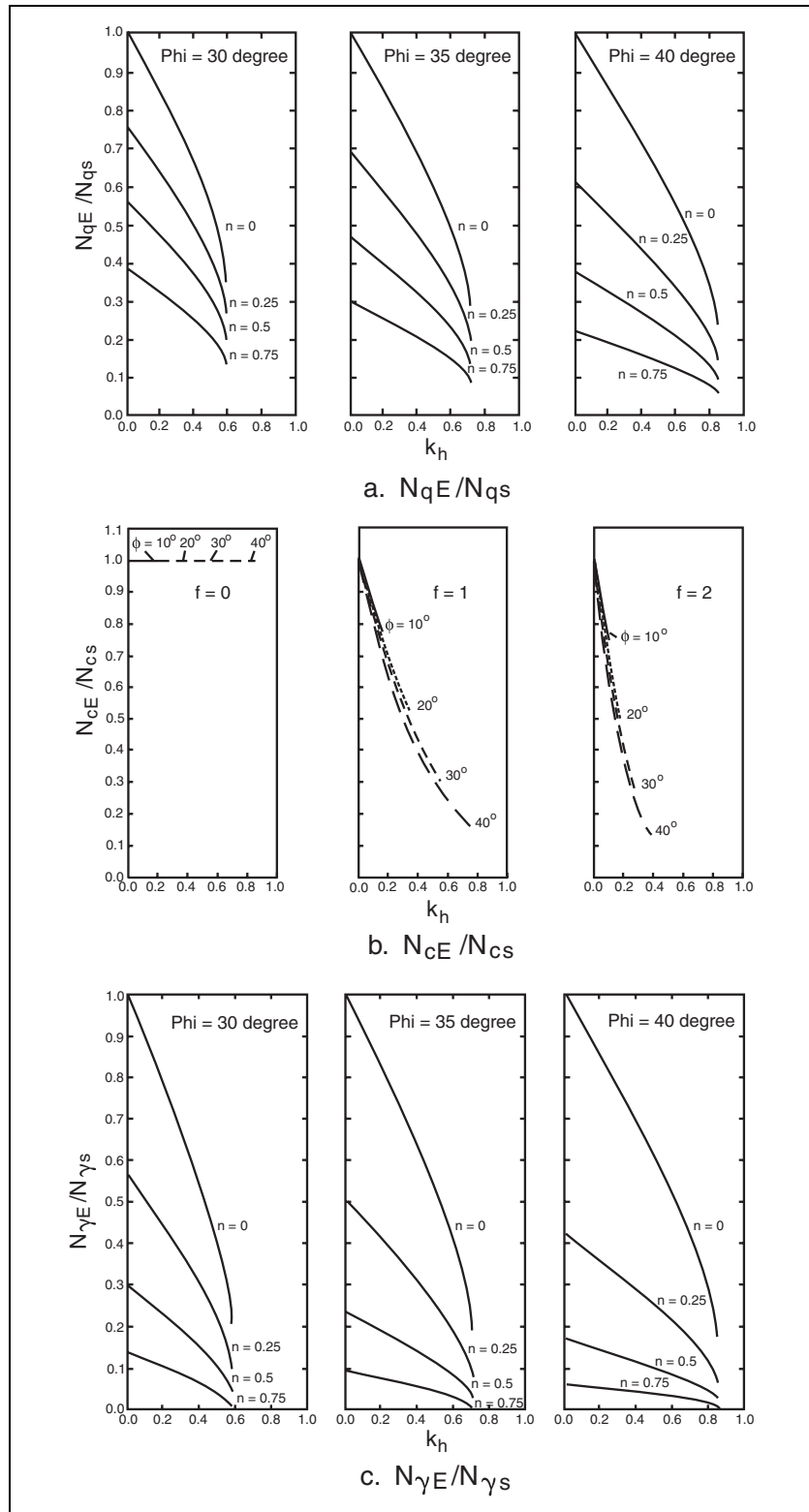
where,

q is the overburden due to depth of the footing, D, i.e., $q = \gamma D$,
 c is the cohesion of the foundation soil,
 γ is the unit weight of the foundation soil,
 B' is equal to $B - 2e$, where B is the width of the footing and e is eccentricity computed as described in section 2.4.2.2(b),
 p_{IE} is the seismic limit to the bearing pressure.

Figure 2-13 presents the ratio of seismic to static bearing capacity factors (N_{qE}/N_{qs} , N_{cE}/N_{cs} , $N_{\gamma E}/N_{\gamma s}$). These ratios depend on the friction angle of the foundation soil, ϕ_f , seismic acceleration coefficient, k_h , and shear transfer coefficient, n. The ratio for N_{cE}/N_{cs} is presented in terms of the friction factor $f = F/Nk_h = n \tan(\phi_f)/k_h$, instead of n. Using the bearing capacity ratios presented in figure 2-13, and static bearing capacity factors for vertical, concentric loading with no depth correction from Vesic (1973), the seismic bearing capacity factors for use in equation 2-7 can be determined.

Equation 2-7 does not include the effect of a submerged, or partially submerged, foundation on the computed bearing capacity. For fine-grained soils and relatively dense, well-graded, coarse-grained soils, equation 2-7 may be modified to incorporate the effect of a submerged foundation. Due to the low permeability of the soil, the pore water and soil skeleton are considered to move in unison during the ground motion. If the foundation soil is submerged above the base of the footing, use the effective stress to compute q in the second term of equation 2-7, and the submerged unit weight in the third term. If the foundation soil is submerged below the base of the footing, use an equivalent unit weight in the third term of equation 2-7 as $\gamma_e = \gamma'(1 - z/B) + \gamma(z/B)$, where γ' is submerged unit weight, z is the depth to the groundwater surface below the base of the footing, and B is the width of the footing. If z is greater than or equal to B, then $\gamma_e = \gamma$.

For foundations with loose, saturated, coarse-grained soils, there is currently no reliable, simplified method for computing seismic bearing capacity. However, since these soils are likely to be susceptible to liquefaction, remediation will be considered as a result of the screening exercise described in section 2.3.



Shi, 1993

Figure 2-13. Ratio of seismic to static bearing capacity factors.

2.4.2.2. External Stability of Gravity or Semi-Gravity Retaining Walls Considering Seismic Loading: Critical Acceleration k_h for Loss of Equilibrium

In this manual, the component of vertical acceleration, k_v , is not included in the calculations for evaluating the external stability of retaining walls. Depending on the correlation with the horizontal component, vertical accelerations may have either a favorable or an unfavorable impact on the stability of the retaining wall system. However, considering the time history of acceleration associated with an earthquake, it is assumed that the net effect of including vertical accelerations in the analyses is not significant. As described in section 2.1, the goal of this retrofit manual is to evaluate vulnerability relative to collapse, or, in some cases, to loss of serviceability due to excessive deformations. For these criteria, the performance depends on the net effect of the time history, and not on a single pulse of acceleration. Therefore, it is considered reasonable to ignore the vertical component of acceleration in calculations for external stability. For the design of new structures, or facilities where yielding of the structure is not allowed, it may be appropriate to include k_v in the calculations as described by Ebeling and Morrison (1992).

2.4.2.2(a). Overturning Stability (Tilting) – Moment Equilibrium

The overturning stability of the retaining wall is evaluated by comparing moments tending to drive the system towards overturning to those tending to resist overturning. A factor of safety is defined as the ratio of the resisting to the driving moments.

Evaluation of overturning stability needs to consider the line of action of the lateral earth pressure. The line of action is determined assuming the dynamic increment of lateral earth pressure acts at 0.6 H from the base of the wall stem and the static component acts at 0.33 H (Seed and Whitman, 1970). The static component of lateral earth pressure is the lateral earth pressure coefficient determined with k_h and k_v equal to zero. The dynamic increment may be determined by subtracting the static component from the total dynamic thrust.

The factor of safety relative to overturning stability is computed as follows:

Driving Moment:

$$M_D = k_h W Y_c + P_{AE} \cos(\delta_w + \beta) \bar{h} + P_{PE} \sin(\delta_w - \beta_2)(D/3)(\sin \beta_2) \quad (2-8)$$

Resisting Moment:

$$M_R = W X_c + P_{AE} \sin(\delta_w + \beta)(B - \bar{h} \sin \beta) + P_{PE} \cos(\delta_w - \beta_2)D/3 \quad (2-9)$$

where:

M_D is the driving moment,

k_h is the coefficient of the horizontal component of peak ground acceleration,

W_w is the weight of the retaining wall,

Y_c is the vertical distance from the centroid of the wall to the toe of the wall footing,

\bar{h} is the vertical distance from the line of action of P_{AE} to the toe of the wall footing.
 X_c is the horizontal distance from the centroid of the wall to the toe of the wall footing,
 B is the width of the wall footing,
 D is the depth of embedment of the wall toe,
 β_2 is the batter of the front face of the wall as shown in figure 2-11.

If the threshold acceleration for sliding is less than the peak ground acceleration, then k_h is limited to the sliding threshold, i.e., $k_h \leq k_h^{slide}$. This applies to the wall inertia term as well as calculation of lateral earth pressure in terms of equations 2-2 (or the graphical procedure for lateral earth pressure) and 2-8, respectively.

Safety Factor Against Overturning Instability:

$$F_s^{O.T.} = \frac{M_R}{M_D} \quad (2-10)$$

The wall is considered stable with respect to overturning if the computed factor of safety is equal to or greater than one. If this is the case, further analysis with respect to the overturning mode of failure is not required. For retaining walls founded on soils, bearing capacity failure, as described in section 2.4.2.2(b), will occur before the overturning mode of failure becomes critical. However, for retaining walls founded on rock, the overturning mode of failure may be relevant.

If the computed safety factor is less than one, more detailed evaluation is required. Further evaluation addresses the seismic resistance, or threshold acceleration, and yielding of the wall system. Computation of threshold acceleration and seismically induced deformation of the retaining wall are discussed in the following paragraphs.

Since earthquake loads are transient, rotation of the retaining wall will only occur when the ground acceleration exceeds some threshold value of acceleration, at which the safety factor is one. The threshold acceleration may be determined by iteration with different values of k_h in equations 2-8 through 2-10. For the purpose of the iteration process, the user is reminded that the values of P_{AE} and P_{PE} depend on k_h .

The wall rotates in increments each time the threshold acceleration is exceeded. Collapse due to overturning is caused by repeated pulses of ground acceleration in excess of the threshold. Due to rotation, the geometry of the wall system is affected. The wall center of gravity is moved closer to the point of rotation. Thus, as the wall rotates, the ability of the wall to sustain a resisting moment is diminished. This phenomenon is referred to as the P- Δ effect. As a simple check on stability, the threshold acceleration is compared to the anticipated peak ground acceleration at the site. If the peak ground acceleration exceeds the threshold acceleration by more than 0.25 g, the wall is not considered safe, and design of retrofit is required as described in section 2.5. Alternatively, in lieu of going directly to retrofit design, the wall deformation may be computed by integrating the equation of motion as described by Zeng and Steedman (2000). This requires selection of an appropriate earthquake record for the analysis. If the more detailed analysis confirms that deformation is excessive and may lead to collapse, design of seismic retrofit is recommended.

For masonry walls, toppling of the wall face must also be considered as described in section 2.4.5.1.

2.4.2.2(b). Bearing Capacity Failure –Vertical Equilibrium

The stability of the retaining wall with respect to seismically induced reduction of bearing capacity is evaluated by comparing the vertical force resultant at the base of the retaining wall to the seismic bearing capacity of the foundation soils computed with equation 2-7. Equation 2-7 requires that the eccentricity of the load with respect to the midpoint of the footing be computed as:

$$e = \frac{B}{2} - \frac{M_R - M_D}{N} \quad (2-11)$$

A factor of safety relative to a bearing capacity failure is defined as the ratio of the seismic bearing capacity to the vertical force resultant. The factor of safety relative to seismically induced loss of bearing capacity is computed as follows:

Vertical Force Resultant:

$$N = P_{AE} \sin(\delta_w + \beta) + W_w - P_{PE} \sin(\delta_w - \beta_2) \quad (2-12)$$

Resultant of Shear Traction Transferred to Foundation Soil:

$$F = P_{AE} \cos(\delta_w + \beta) + k_h W_w - P_{PE} \cos(\delta_w - \beta_2) \leq N \tan \delta_f \quad (2-13)$$

where δ_f is the interface friction angle between the base of the foundation and the foundation soil.

The shear transfer coefficient, n , is computed with equations 2-6, 2-12, and 2-13. Using the shear transfer coefficient, and the friction angle of the foundation soil, ϕ_f , find the seismic bearing capacity factors N_{cE} , N_{qE} , and $N_{\gamma E}$ as described in section 2.4.2.1(c). Compute the seismic bearing capacity, p_{IE} , using equation 2-7 and the safety factor against seismically induced bearing capacity failure as:

$$F_S^{B.C.} = \frac{p_{IE} B'}{N} \quad (2-14)$$

The wall is considered stable with respect to seismically induced loss of bearing capacity if the computed factor of safety for the peak acceleration is equal to or greater than one. If this is the case, further analysis with respect to the seismically induced loss of bearing capacity is not required. If the computed safety factor is less than one, further evaluation is required. Further evaluation is similar to that described in section 2.4.2.2(a). However, in this case, the procedure involves iteration of equations 2-11 through 2-14 to find the threshold acceleration relative to bearing capacity. As a simple check on stability, the threshold acceleration is compared to the anticipated peak ground acceleration that is representative of the earthquake hazard at the site.

For the case of seismically induced loss of bearing capacity, if anticipated peak ground acceleration exceeds the threshold acceleration by more than 0.2 g, the wall is not considered safe, and design of retrofit is required as described in section 2.5. Alternatively, in lieu of going directly to retrofit design, the wall deformation may be computed by integrating the coupled equations of motion as described by Siddharthan et al. (1992). If the more detailed analysis confirms that deformations lead to collapse, design of seismic retrofit is recommended.

2.4.2.3. Structural Integrity of Gravity or Semi-Gravity Retaining Walls Considering Seismic Loading

For evaluating the structural integrity of retaining walls, the vertical component of acceleration, k_v , should be included in the calculations. At an instant of time, vertical accelerations may have a negative impact on structural integrity. Structural failure of retaining wall components is considered to be instantaneous, and does not require the accumulation of deformation as does the consideration of external stability, where k_v is not included in the calculations (see section 2.4.2.2.) Estimation of k_v for use in the analysis is described in Part 1 of this manual.

The structural evaluation compares stresses, shear forces and bending moments computed at critical locations within the wall stem, and at the toe of the wall footing, to the ultimate capacity of the appropriate section. If the ultimate capacities are exceeded, design of seismic retrofit is required as described in section 2.5. Sections 2.4.2.3(a) and (b) describe salient features of the analysis for the wall stem and footing, respectively. It will be assumed that the gravity retaining wall is plain concrete. Application of the procedure for reinforced concrete sections is described in section 2.4.3.

2.4.2.3(a). Analysis of Wall Stem

Analysis of the wall stem requires calculation of shear and bending moments at the critical cross section along the height of the stem. The critical cross section depends upon a combination of the magnitude of shear and bending moment, and the cross sectional area. For a uniform cross section, the critical section is at the base of the stem where the moment and shear force are maximum. For non-uniform cross section, several sections may need to be evaluated in order to locate the critical cross section.

Computation of shear and bending moments need to consider the distribution of seismic lateral earth pressure along the wall stem. The distribution of lateral earth pressure is determined by assuming that the dynamic increment of lateral earth pressure acts at 0.6 H from the base of the wall stem and the static component acts at 0.33 H. This results in the pressure distribution shown in figure 2-14. Lateral earth pressure coefficients, including the dynamic increment, may be determined with equation 2-1. The static component of lateral earth pressure is the lateral earth pressure coefficient determined with k_h and k_v equal to zero. If graphical methods are used to determine active lateral earth pressure, compute the earth pressure coefficient using the thrust determined by the trial wedge method and equation 2-3. The seismically induced inertia force applied to the wall stem must also be included in the calculation of the maximum bending moment and shear force.

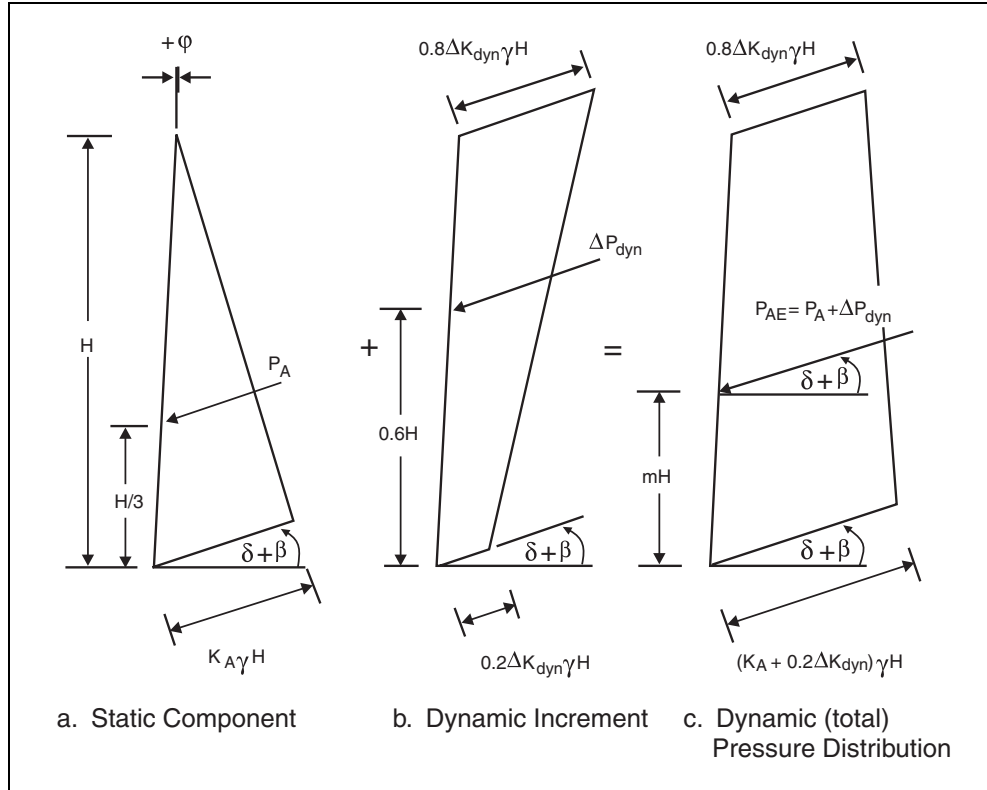


Figure 2-14. Assumed distribution of dynamic earth pressure.

Shear and normal stress at the cross section is computed considering the computed shear force, bending moment, the weight of the stem, and the vertical component of active earth pressure. Allowable stresses for tension, compression, and shear are determined according to ACI (2002). Load factors are taken as unity for seismic evaluation of existing retaining walls.

2.4.2.3(b). Analysis of Footing

The analysis of the structural integrity of the wall footing requires that the contact pressure at the base of the footing be determined. It will be assumed that the contact pressure at the base of the footing varies in a linear fashion, and may be computed with equations 2-15 through 2-17.

The distribution of contact pressure depends on the eccentricity of the resultant of the applied force system. If $e \leq B/6$, the variation of contact pressure follows the shape of a trapezoid with maximum contact pressure at the toe of the footing, and minimum contact pressure at the heel computed as:

$$q_{\max} = \left(1 + \frac{6e}{B}\right) \frac{N}{BL} \quad (2-15)$$

$$q_{\min} = \left(1 - \frac{6e}{B}\right) \frac{N}{BL}$$

If $e > B/6$, there is not full contact at the base of the footing and the variation of contact pressure follows the shape of a triangle with the maximum contact pressure at the toe of the footing computed as:

$$q_{\max} = \frac{4N}{3L(B - 2e)} \quad (2-16)$$

and,

$$x = 1.5(B - 2e) \quad (2-17)$$

where:

L is the length of the wall used to compute N,
x is the width of contact along the base of the footing.

2.4.2.4. Loss of Service of Essential Facilities

Essential facilities may include lifelines, important highways, bridge approach fills, or important structures. Seismically induced deformation of a nearby retaining wall may be responsible for loss of service to essential facilities. Allowable deformation of the wall depends on the deformation that the essential facility may tolerate, and the attenuation relationship for the wall displacement field.

When the tolerable deformation is exceeded, there may be significant loss of service to the facility. Several factors are examined to establish the deformation that a facility may tolerate. These include type of access to the facility, utilities, and the capacity to resist differential settlement. Input is required from a number of disciplines including geotechnical, structural, and emergency management. The tolerable displacement for essential facilities is established on a case-by-case basis. Assessment of the tolerable loss of service to essential facilities is beyond the scope of this chapter. However, to complete the analysis, a determination of tolerable displacement should be made.

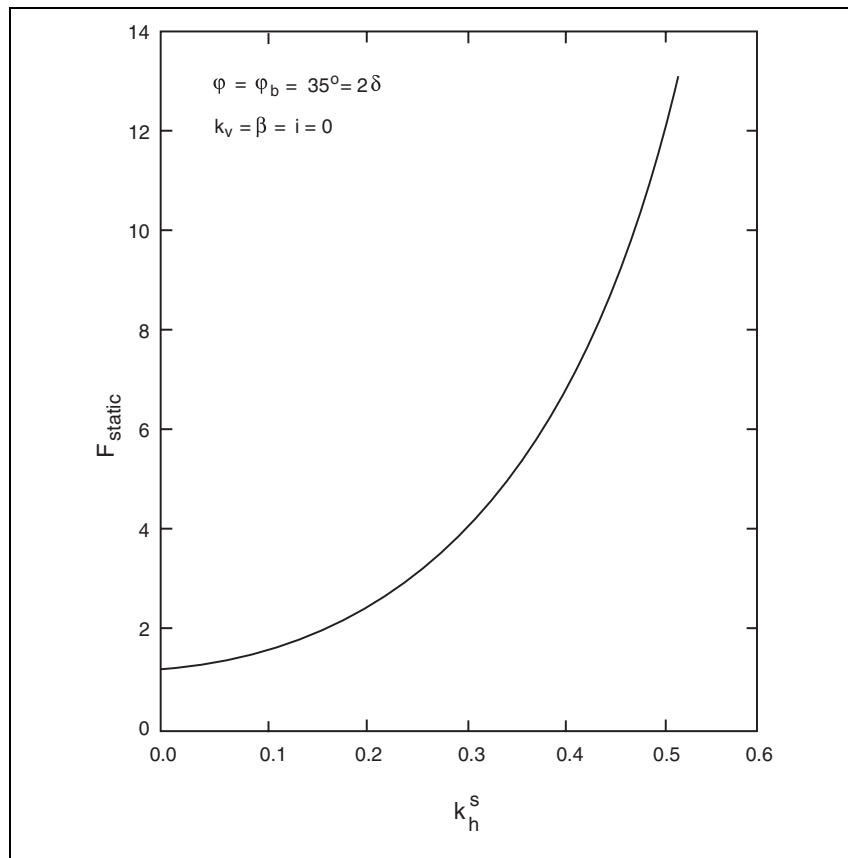
The displacement field is attenuated with respect to distance, therefore distance between the facility and the retaining wall is an important parameter. For backfills with coarse grained soils, assume that (1) the horizontal displacement and the vertical settlement immediately behind the wall are equal, and (2) surface displacements are linearly attenuated within a distance of two times the height of the retaining wall (Clough and O'Rourke, 1990).

This section presents information that may be used to evaluate the potential for the retaining structure to undergo permanent seismically induced deformation and to estimate the magnitude of deformations that may occur. The estimated deformation of the retaining wall is compared to the allowable deformation in order to decide if seismic retrofit is required.

2.4.2.4(a). Secondary Screening Procedure for Assessing Vulnerability to Seismically Induced Permanent Deformation

As discussed in section 2.4.2.2, the threshold coefficient of acceleration is the ground acceleration beyond which the wall will begin to slide or rotate. For gravity or semi-gravity retaining walls that fail in a sliding mode of failure, Richards and Elms (1979) describe a method for computing threshold acceleration. Figure 2-15 presents results obtained by Richards and Elms (1979) showing the relationship between threshold acceleration and static factor of safety for vertical retaining walls with level, cohesionless backfill. For the data presented in figure 2-15, it is assumed that the backfill has an angle of friction, ϕ , equal to 35° , wall/backfill interface friction angle $\delta = \phi / 2$, and wall base/foundation soil interface friction angle, ϕ_b , equal to 35° .

Figure 2-15 is a useful tool for secondary screening of retaining walls that may fail in the sliding mode, and identifying those that are not susceptible to seismic damage. The screening method assumes that the wall will slide before it rotates. The possibility of seismically induced tilting or loss of bearing capacity should be checked, as described in sections 2.4.2.2(a) and (b), to verify that the procedure is appropriate. The following steps describe the screening method for gravity or semi-gravity retaining walls that fail in a sliding mode of failure.



Richards and Elms, 1979

Figure 2-15. Relationship between static factor of safety and threshold acceleration, k_h^s , for sliding.

Screening Method for Gravity or Semi-Gravity Retaining Walls that Fail in a Sliding Model

1. Determine the static factor of safety with respect to a sliding failure of the retaining wall.
2. Using the static factor of safety, and figure 2-15, obtain the threshold acceleration coefficient for sliding, k_h^s .
3. Compare the threshold acceleration coefficient to the estimated peak ground acceleration coefficient at the site of the retaining wall.
4. If the threshold acceleration coefficient is greater than the anticipated peak ground acceleration coefficient, the wall may be eliminated from the list of potential candidates for detailed evaluation (provided other applicable criteria are satisfied).

If some permanent displacement of the retaining wall is acceptable, higher levels of ground acceleration may be tolerated without the need for detailed seismic evaluation and retrofit. Elms and Martin (1979) estimate that, for sliding walls in which k_h^s is greater than the coefficient of peak ground acceleration (k_h) divided by two, the seismically induced permanent translation will be less than $254(k_h)$ (in millimeters) in most cases. This suggests that in areas where the peak ground acceleration coefficient is less than 0.3, detailed evaluation is not necessary for walls if:

- They have a static factor of safety with respect to sliding greater than 2.0.
- They will not fail by tilting or seismic loss of bearing capacity.
- An outward displacement of 75 mm can be tolerated.

If the secondary screening procedure indicates that detailed evaluation is required, the user must follow the procedure for evaluating deformations described in sections 2.4.2.4(b) and (c). The procedure involves the determination of the seismic resistance, or threshold acceleration, as described in section 2.4.2.4(b) followed by estimation of seismically induced deformation described in section 2.4.2.4(c). The procedure considers a variety of possible modes of failure including translation (T mode), rotation with respect to the base of the wall footing (RB mode) and mixed rotation/sliding (R/T mode). The “critical” threshold acceleration for evaluation of seismically induced deformation of the retaining wall is considered the lowest threshold acceleration determined for sliding (k_h^s), seismic reduction of bearing capacity (k_h^b), or overturning (k_h^{OT}). Evaluation of the critical threshold acceleration provides an indication of the prevailing mode of failure.

For masonry walls, internal stability must also be analyzed with respect to sliding or bulging between units. See section 2.4.5.2 for details.

2.4.2.4(b). Determination of Threshold Acceleration

The evaluation of seismically induced deformation of gravity or semi-gravity retaining walls involves the determination of a threshold acceleration beyond which permanent deformation of the gravity or semi-gravity wall will occur. Three values need to be computed from equilibrium;

k_h^s , k_h^{OT} , and k_h^b . A thorough seismic analysis must investigate the possibility of both a sliding mode of failure as well as a bearing capacity failure introducing rotation. The possibility of overturning instability that involves rotation with respect to the toe of the wall footing is discussed in section 2.4.2.2(a). Since seismic bearing capacity factors are dependent on ground acceleration, determination of the threshold acceleration requires an iterative procedure. It is initially assumed that there is no cohesion, no depth of embedment, and $k_v = 0$. These simplifying assumptions are not necessary for the procedure and can be included without much difficulty as described at the end of this section. The procedure for determination of threshold acceleration described below is based on the work of Richards et al. (1996) and Fishman and Richards (1997a, 1997b).

Although the backfill is usually granular, if necessary, the foundation soil may be assumed to have some cohesive strength. There may also be some depth to the foundation. Either or both may be included by using figures 2-13 (a) and (b) for N_{qE}/N_{qs} and N_{cE}/N_{qs} , and equation 2-7 in steps 6 and 7 of the procedure for determination of threshold accelerations.

The threshold acceleration is compared to the peak ground acceleration applied by the design earthquake to the wall system. If k_h^s , k_h^b , and k_h^{OT} are greater than k_h , the local, external stability of the wall is safe from the standpoint of seismic design, and further evaluation is not required if other applicable criteria are satisfied. If k_h^s , k_h^b , or k_h^{OT} are less than k_h , deformation analysis as described in section 2.4.2.4(c) must be performed. If the estimated seismically induced deformations are greater than the acceptable level of deformation, design of seismic retrofit is required as described in section 2.5.

The possibility of a mixed mode failure is evaluated in step 9(b). In this case, the value of k_h^s is less than the peak ground acceleration, and less than the threshold acceleration for bearing capacity, k_h^b . Because shear transfer is limited at the base of the wall, ground acceleration in excess of k_h^s cannot be transferred to the retaining wall. Thus, during sliding deformation, the wall inertia force and lateral earth pressure from the backfill cannot exceed the peak values at which sliding is initiated. However, the inertial force within the foundation soil beneath the retaining wall, as described in section 2.4.2.1(c) will continue to increase in response to the ground motion. Therefore, the possibility for a loss of bearing capacity subsequent to sliding exists. The seismically induced loss of bearing capacity subsequent to a sliding failure mode is referred to as “mixed mode.”

Passive Restraint: In many instances, the base of a retaining wall is embedded to some depth within the foundation soil. Effects of foundation embedment include the development of passive restraint against sliding, and a contribution to bearing capacity from the surcharge. Both of these effects may be incorporated into the analytic method described in this section. Passive resistance may prevent sliding from occurring, resulting in a more damaging failure mode (e.g., overturning).

Procedure for Determination of Threshold Accelerations for Walls that May Fail by Sliding or Loss of Bearing Capacity

1. Assume a trial value for k_h and determine P_{AE} as described in section 2.4.2.1(a).

2. Compute the vertical force resultant, N , as:

$$N = P_{AE} \sin(\delta_w + \beta) + W_w \quad (2-18)$$

3. Compute the result of the shear traction to be transferred to the foundation soil as:

$$F = P_{AE} \cos(\delta_w + \beta) + k_h W_w \quad (2-19)$$

4. Compute the shear transfer coefficient, n , using equation (2-6).

5. Sliding will occur if $F = N \tan \delta_f$ and therefore:

$$F_s^{slide} = \frac{N \tan \delta_f}{F} \quad (2-20)$$

6. where δ_f is the interface friction angle between the abutment footing and the foundation soil.

7. Given the friction angle of the foundation soil, ϕ_f , and the shear transfer co-efficient, n , from step 4, find the seismic bearing capacity factors from figure 2-13.

8. Compute the seismic bearing capacity p_{IE} using equation (2-7).

9. Bearing capacity failure will occur when $N = p_{IE} B'$ and therefore:

$$F_s^{B.C.} = \frac{p_{IE} B'}{N} \quad (2-21)$$

10. Iterate on k_h to determine the threshold values given when $F.S. = 1$. That is:

- a. If $F_s^{B.C.}$ determined in step 8 is nearly equal to one, and F_s^{slide} from step 5 is greater than one, stop the iteration procedure since the assumed value for k_h is the threshold value for bearing capacity failure, k_h^b , which occurs first.
- b. If F_s^{slide} determined in step 5 is nearly equal to one and $F_s^{B.C.}$ is greater than one, stop the iteration procedure since the assumed value for k_h is the threshold value for sliding failure, k_h^s . In this case, when sliding occurs first, there is still the potential for a bearing capacity failure at a higher acceleration introducing a mixed mode. To estimate $k_h^b > k_h^s$ set, N and F at their constant values for sliding, compute N_{IE} from equation (2-7) with $p_{IE} = N/B'$ and determine k_h^b from figure 2-13.
- c. If neither of these conditions are met, select a higher trial value for k_h and return to step 1.

Some deformation is required for the passive restraint to be fully mobilized. Small lateral displacements may occur at sliding threshold accelerations that do not reflect the development of any passive restraint (Fishman and Richards, 1996). As deformations continue, passive restraint is mobilized, and seismic resistance is increased. When full passive restraint is mobilized, a steady-state seismic resistance prevails at a given level of acceleration. Furthermore, the surcharge above the base of the embedded foundation provides a significant increase in the seismic bearing capacity.

To include passive restraint in the procedure for determination of threshold acceleration revise equations 2-18 and 2-20 as follows:

$$N = P_{AE} \sin(\delta_w + \beta) + W_w - P_{PE} \sin(\delta_w - \beta_2) \quad (2-18 \text{ revised})$$

$$FS_{\text{slide}} = \frac{N \tan \delta_f + P_{PE} \cos(\delta_w - \beta_2)}{F} \quad (2-20 \text{ revised})$$

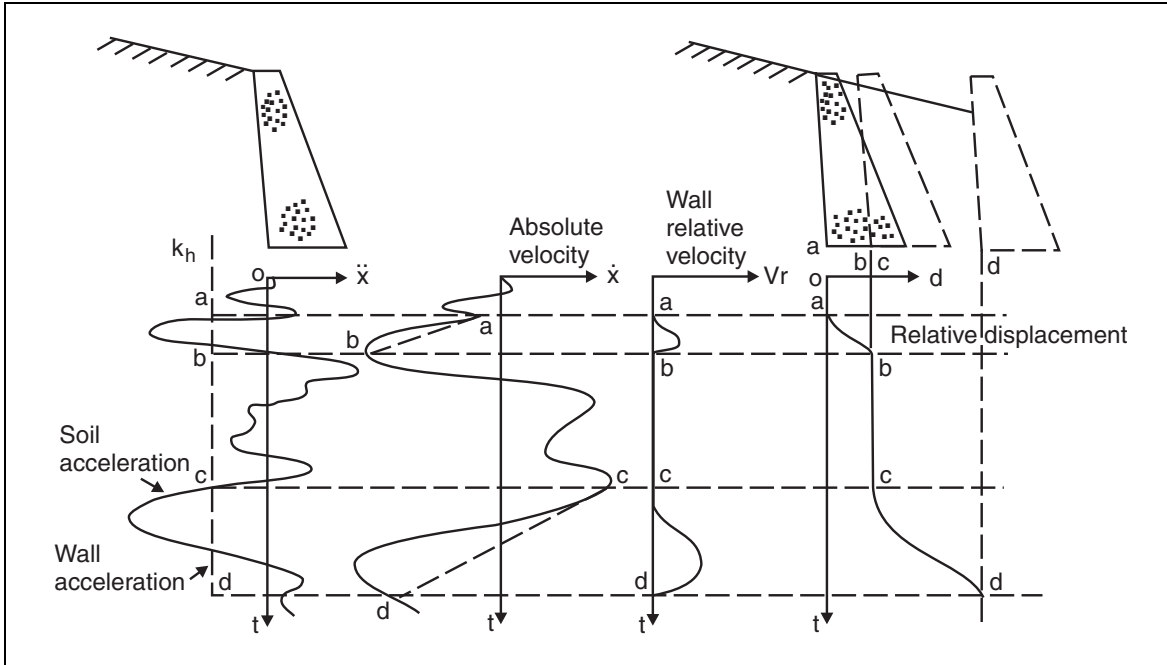
where β and β_2 are the inclinations of the backface and front face of the retaining wall as shown in figure 2-11.

2.4.2.4(c). Estimation of Seismically Induced Deformation

The critical threshold acceleration for evaluation of seismically induced deformation of the retaining wall is considered the lowest threshold acceleration determined for sliding (k_h^s), seismic reduction of bearing capacity (k_h^b), or overturning (k_h^{OT}). If the critical threshold acceleration is k_h^s , the wall will fail in a translation (T) mode of failure. If k_h^b , or k_h^{OT} are critical, the rotation with respect to the base (RB) mode needs to be investigated. If k_h^s is critical, an RB mode of failure is also possible since seismic reduction of bearing capacity occurs during sliding as described in step 9(b) of the procedure for evaluation of critical threshold acceleration.

For gravity or semi-gravity walls that fail in a T mode, a simple, semi-empirical, displacement based seismic analysis may be used. More computational effort is required to evaluate walls that fail in the RB or RB/T mixed modes. The RB and mixed modes will be discussed at the end of this section. For seismic evaluation of existing walls that that fail in a T mode, the following procedure, based on the work of Richards and Elms (1979), is described.

It should be noted that equation 2-22 renders a conservative estimate of displacement. Alternatively, the relative displacement between the retaining wall and foundation soil may be determined by double integration of the difference between an appropriate acceleration time history for the site and corresponding wall acceleration. The corresponding wall acceleration considers the sliding threshold acceleration. Figure 2-16 demonstrates the increments of displacement accumulated by the sliding wall when the ground acceleration exceeds k_h^s .



Richards and Elms, 1979

Figure 2-16. Incremental failure by base sliding.

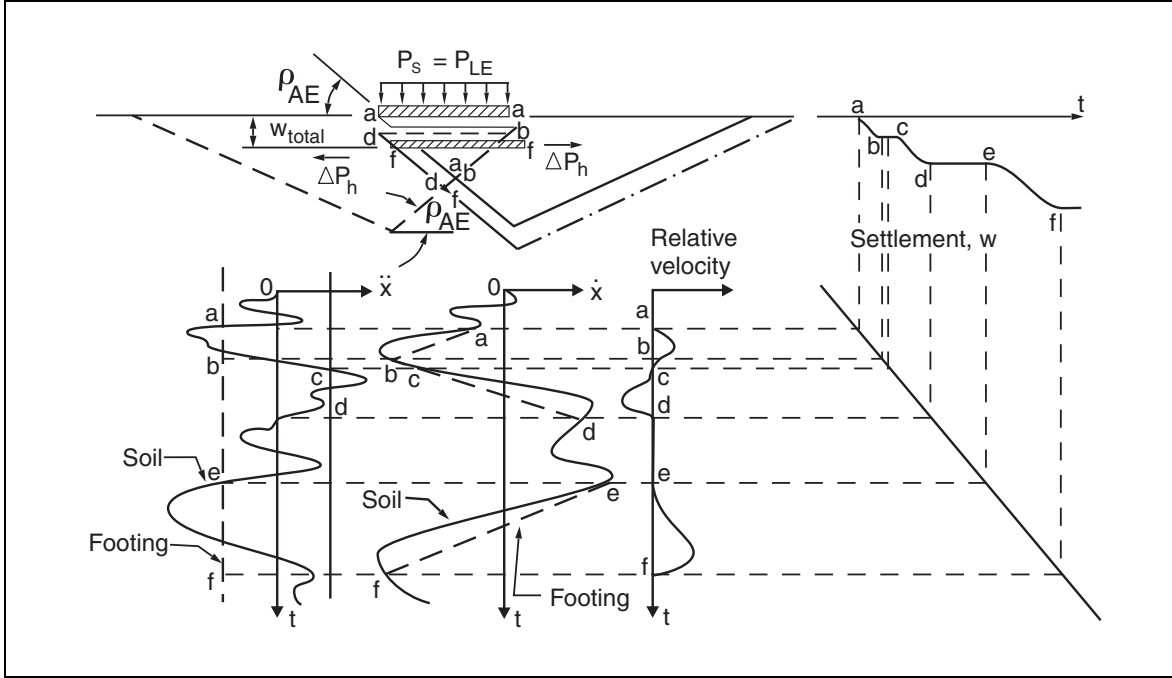
Procedure for Evaluating Walls with a Sliding Mode of Failure (T Mode)

1. Determine the weight of the existing wall.
2. Estimate the peak horizontal ground acceleration coefficient, k_h , and peak horizontal velocity, V , considering the earthquake hazard at the site. The velocity V , corresponding to k_h and distance from the source of the earthquake, may be estimated as described in chapter 4.
3. Using the threshold acceleration, k_h^s , determined from section 2.4.2.4(b), estimate the residual displacement, d , as:

$$d = 0.087 \frac{V^2}{k_h g} \left(\frac{k_h}{k_h^s} \right)^4 \quad (2-22)$$

where g is the acceleration due to gravity. When using equation 2-22, V and g must be in consistent units.

4. Compare the displacement computed in step 3 with the displacement that may be tolerated.



Richards et al., 1993

Figure 2-17. Incremental bearing capacity failure by Coulomb sliding wedge mechanism.

The sliding block approach can be applied to the Coulomb Mechanism described in section 2.4.2.1(c) to estimate movement of footings when the ground acceleration exceeds $k_h^b(g)$ as shown in figure 2-17. This calculation assumes that the line of action of N crosses the wall footing within the middle third and therefore the wall will slide and settle whenever k_h^b is exceeded. The total horizontal component of movement will be the same as that for sliding but computed using k_h^b as the threshold acceleration as:

$$\Delta = u = 0.087 \frac{V^2}{k_h g} \left\{ \frac{k_h}{k_h^b} \right\}^4 \quad (2-23)$$

The vertical settlement will then be:

$$w = 2\Delta \tan \rho_{AE} \quad (2-24)$$

where ρ_{AE} is the angle of the sliding surface of the active portion of the bearing capacity failure region given by,

$$\rho_{AE} = \phi_w - \theta + \tan^{-1} \left[\frac{\sqrt{\tan(\phi_w - \theta - i) \left(\tan(\phi_w - \theta - i) + \cot(\phi_w - \theta - \beta) \right) \left(1 + \tan(\delta_w + \beta + \theta) \cot(\phi_w - \theta - \beta) \right) - \tan(\phi_w - \theta - i)}}{1 + \tan(\delta_w + \beta + \theta) \left[\tan(\phi_w - \theta - i) + \cot(\phi - \theta - \beta) \right]} \right] \quad (2-25)$$

Equations 2-23 and 2-24 do not consider the RB or RB/T mixed modes of failure that may accompany the loss of bearing capacity.

Deformation analyses that consider the RB or mixed RB/T modes of failure are not routine and require the use of specialized software involving numerical integration. A procedure that involves numerical integration of coupled equations of motion is described by Siddharthan et al. (1992). This procedure investigates the possibility of both sliding and rotation modes occurring simultaneously (RB or RB/T modes). Also, a procedure is described by Rafnsson and Prakash (1994) and Prakash et al. (1995a,1995b) for computing both sliding and rocking displacements of rigid retaining walls. For walls that may fail by overturning with respect to the toe (special case of RB mode) the user is also referred to the method described by Zeng and Steedman (2000).

A simple method for assessing the potential for large displacements for walls that fail by tilting or seismic reduction of bearing capacity is described in section 2.4.2.2. If the simple approach indicates that the retaining wall is vulnerable to excessive deformation by tilting or rotation then either a more detailed analysis can be performed to confirm the result, or the design of seismic retrofit is recommended as described in section 2.5.

2.4.3. CONCRETE CANTILEVER WALLS (INVERTED T WALLS)

The analysis for seismic vulnerability of inverted T-shaped cantilever walls follows a similar procedure as that for gravity walls. External stability is evaluated as described in sections 2.4.2.2 (a) and (b). Proximity of nearby structures and the potential for seismically induced deformation is investigated as described in section 2.4.2.4. However, in the case of a cantilever wall, soil placed over the heel of the footing is considered to contribute to the mass of the wall.

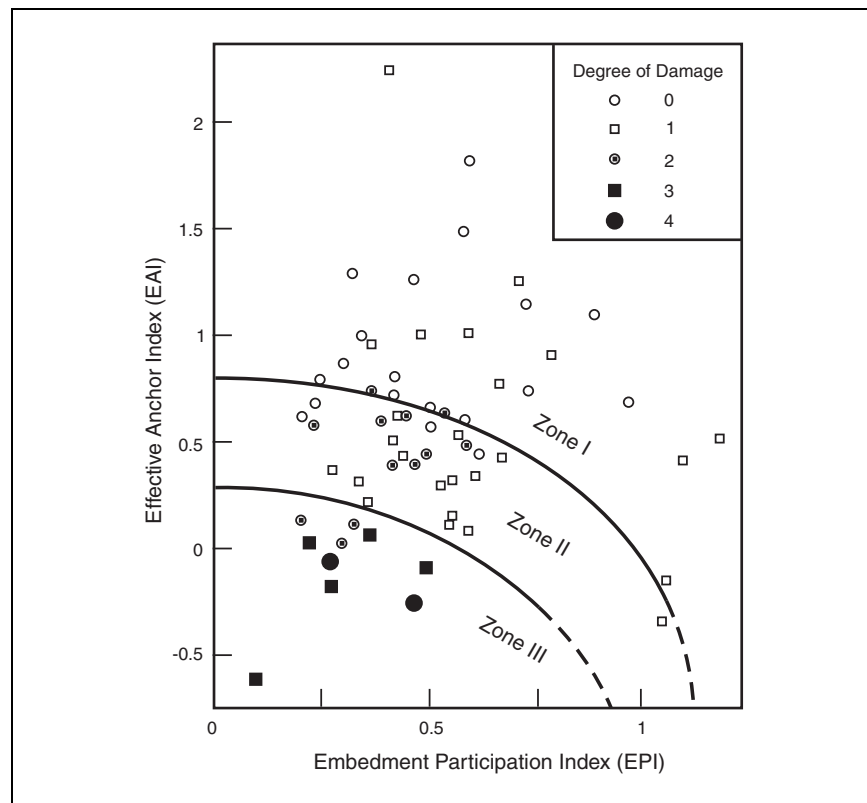
Structural details of the wall stem and footing must also be considered similar to gravity walls as described in section 2.4.2.3. These elements are treated as cantilever sections, subjected to earth pressures from either the backfill or the soil bearing pressures. The wall stem is treated as a cantilever fixed at the top of the footing. The toe of the footing is treated as a cantilever fixed at the front face of the wall stem and acted on by the soil contact pressure. The heel of the footing is treated as a cantilever fixed at the back face of the wall stem loaded by its own weight, the contact soil pressure, the vertical component of active earth pressure (i.e., from friction between backfill placed over the heel and the backfill behind the heel), and that of the backfill placed on top of it. The vertical acceleration component may increase the vertical force applied to the heel.

Due to the cantilever action of the wall elements, reinforced concrete is used to resist the flexural stresses. Ultimate strength design, as described in ACI (2002), is used to check the capacity of the sections. For earthquake loading, and seismic evaluation of existing retaining walls for retrofit, load factors and reduction factors are taken as unity.

2.4.4. ANCHORED WALLS

2.4.4.1. Secondary Screening Procedure for Anchored Walls

Figure 2-18 shows an empirical chart, developed by Gazetas et al. (1990), useful for screening tied-back walls relative to the need for seismic evaluation and possible retrofit. In figure 2-18, anchored sheet-pile walls are screened into one of three distinct zones or categories. Past experience indicates that anchored bulkheads falling into Zone I suffered little or no earthquake-induced damage, those within Zone II have suffered moderate degrees of damage, and those in Zone III have suffered severe, unacceptable, damage. The chart is based on the observed performance of waterfront structures. Before using the chart, the engineer must ensure that liquefaction failure of cohesionless soils in the backfill or foundation is unlikely. Application to bulkheads with backfill and foundation soils that are not submerged should be done with caution. For walls with dry backfill, use of figure 2-18 may be unconservative for high levels of peak ground acceleration, and very tall walls.

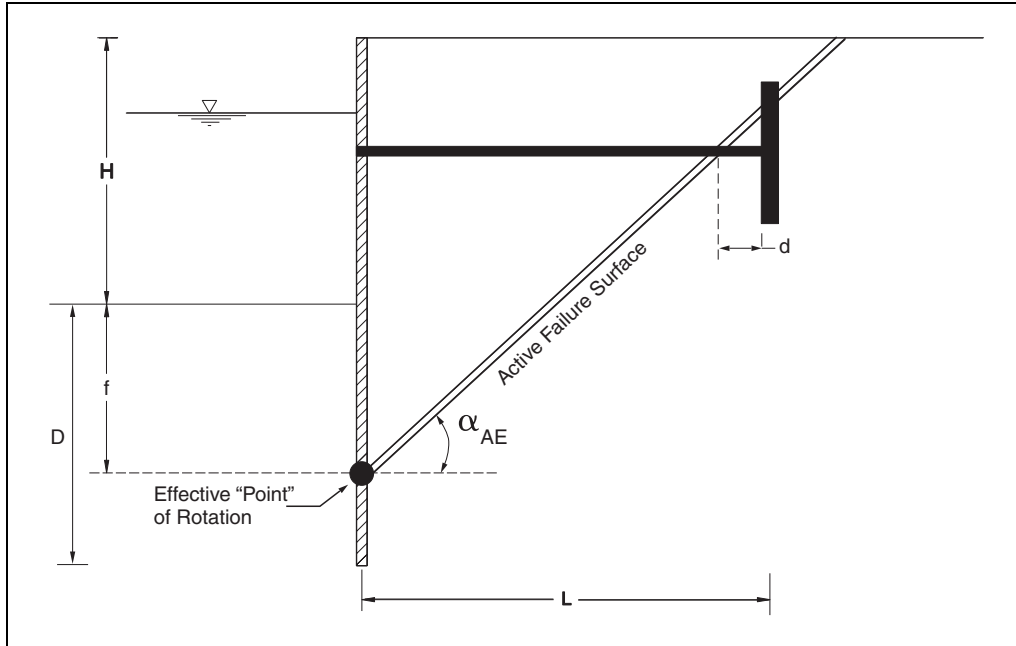


Gazetas et al., 1990

Figure 2-18. Chart for seismic screening of anchored walls.

To use figure 2-18, two indices for the retaining wall must be computed including the Effective Anchor Index (EAI) and the Embedment Participation Index (EPI). The EAI is described with the aid of figure 2-19 in terms of the horizontal distance, d , from the active failure surface to the tie-rod connecting point:

$$EAI = d/H \quad (2-26)$$



Gazetas et al., 1990

Figure 2-19. Definition of the effective anchor index: $EAI = d/H$.

The active failure surface is assumed to originate at the effective “point” of rotation, defined at point f below the dredge line:

$$f \approx \left[0.5(1 + k'_e) - 0.02(\phi - 20^\circ) \right] H \leq D \quad (2-27)$$

where, k_e is a function of the horizontal and vertical seismic coefficients, $k_e = k_h / (1 - k_v)$. Gazetas et al. (1990) recommend that k_h be taken as two thirds of the peak horizontal ground acceleration coefficient. For cohesionless soils under the water table, k_e is increased to $k'_e = 1.5k_e$. Having established k'_e , the angle α_{AE} can be approximated as:

$$\alpha_{AE} \approx 45^\circ + \frac{\phi}{2} - 135(k'_e)^{1.75} \quad (2-28)$$

α_{AE} will become small as k'_e approaches $\tan \phi$.

For uniform backfill and foundation, the EPI can be approximated as:

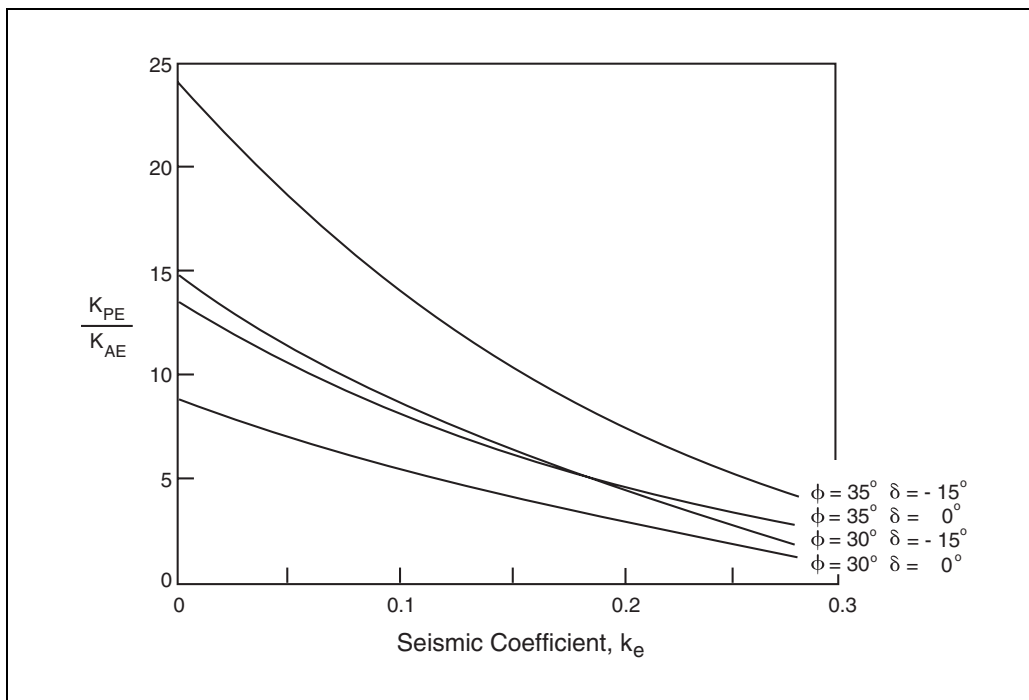
$$EPI \approx \frac{K_{PE}}{K_{AE}} r^2 (1 + r) \quad (2-29)$$

where, $r = f / (f + H)$ and the ratio K_{PE} / K_{AE} can be determined with the aid of figure 2-20.

Figure 2-18 can be used as a screening tool with the following procedure.

Screening Method for Tied-Back Walls

1. Determine the height, H , of the tied-back wall, the depth of embedment, D , and the location of the anchor block.
2. Given the peak ground acceleration at the site, compute $k_e = k_h / (1 - k_v)$ and increase by a factor of 1.5 for cohesionless soils beneath the water table.
3. Using equation 2-27, estimate the location of the effective point of rotation, f , and use equation 2-28 to estimate the inclination of the active failure surface, α_{AE} , behind the wall.
4. Sketch the wall as shown in figure 2-19, find "d" based on "f" and α_{AE} , and compute EAI as described by equation 2-26.
5. Using figure 2-20, determine the ratio of K_{PE}/K_{AE} and compute EPI as described by equation 2-29.
6. Using figure 2-18, and the values of EAI and EPI, determine if the wall is in Category I, II, or III.
7. If the wall is in Category I, further evaluation is not required. If the wall is in Category II, further evaluation is required if movement or noticeable damage of the wall cannot be tolerated. If the wall is in Category III, detailed evaluation and retrofit of the wall is required.



Gazetas et al., 1990

Figure 2-20. Ratio of active and passive earth pressure coefficients as a decreasing function of k_e .

2.4.4.2. Evaluation Procedure for Anchored Walls

The analysis presented in this section is for backfill and foundation soils that are not submerged. While waterfront anchored bulkheads may be the most common form of a anchored wall encountered, they are not often found retaining a highway structure. Many times anchored walls are used to support highway fills, where free water is not involved. See section 2.4.2.1 (a) for guidance on lateral earth pressure computations involving submerged soils.

The vertical acceleration component, k_v , is not included in the calculations for the reasons described in section 2.4.2.2. If the wall is located in proximity to an essential facility, and the wall is not allowed to yield, k_v should be included in the calculations of lateral earth pressure.

Figure 2-21 depicts the forces on a tied-back wall subjected to seismic loading. For a tied-back wall, seismic effects shown in figure 2-22 combine in various ways to reduce the static factor of safety to 1.0, and initiate deformation of the wall. Three effects are involved, and three fundamental modes of failure are possible as follows:

1. Initially, prior to the accumulation of seismically induced deformation, the anchor makes the top part of the wall more rigid and the dynamic increment of lateral earth pressure may exceed that for the active state. This may cause excessive bending moments in the sheet piling, or possibly break the tie rod. However, reports of this mode of failure are infrequent in earthquake reconnaissance reports and the failure mode is not discussed further.
2. The passive resistance at the toe of the wall decreases with increasing acceleration as described by figure 2-12. If the anchor does not fail, this may lead to rotation of the wall about the top as the base lurches outward.

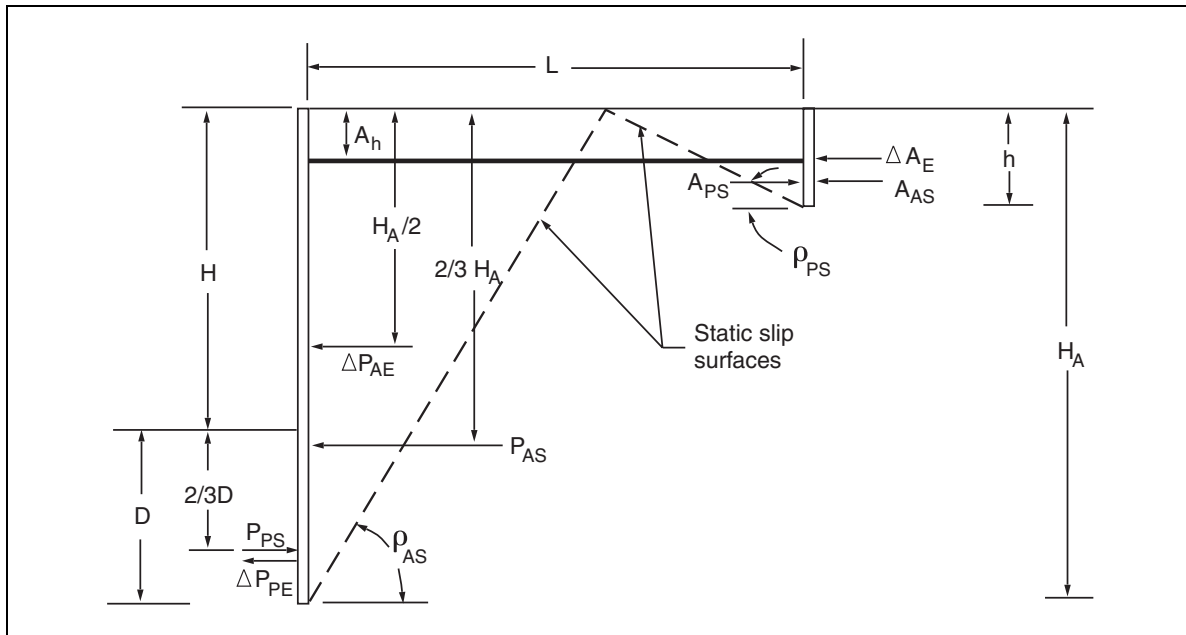


Figure 2-21. Forces on an anchored wall.

3. Finally, and perhaps most important, with increasing levels of ground acceleration, the active wedge behind the wall and passive wedge in front of the anchor grow in size by $\Delta\rho_{AE}$ and $\Delta\rho_{PE}$, respectively. At the point in which there is destructive interference between the active and passive wedges, as shown in figure 2-22, anchor resistance becomes compromised. Destructive interference plus the seismically induced increase in the tie rod force, ΔA_E , can cause premature failure of the anchor and subsequent rotation with respect to the bottom of the wall. Thus, the anchor lurches outward at each excursion of acceleration above the threshold level, triggering outward movement of the top of the wall accompanied by tension cracks and settlement of the ground behind the anchor.

The relationship between ground acceleration and ρ_{AE} and ρ_{PE} is described by equations 2-25 and 2-30. For convenience, equation 2-25 is repeated here.

$$\rho_{AE} = \phi_w - \theta + \tan^{-1} \left[\frac{\sqrt{\tan(\phi_w - \theta - i) (\tan(\phi_w - \theta - i) + \cot(\phi_w - \theta - \beta)) (1 + \tan(\delta_w + \beta + \theta) \cot(\phi_w - \theta - \beta)) - \tan(\phi_w - \theta - i)}}{1 + \tan(\delta_w + \beta + \theta) [\tan(\phi_w - \theta - i) + \cot(\phi_w - \theta - \beta)]} \right]$$

(2-25 repeated)

$$\rho_{PE} = -\phi_w - \theta + \tan^{-1} \left[\frac{\sqrt{\tan(\phi_w - \theta + i) (\tan(\phi_w - \theta + i) + \cot(\phi_w - \theta + \beta)) [1 + \tan(\delta_w + \beta + \theta) \cot(\phi_w - \theta + \beta)] + \tan(\phi_w - \theta + i)}}{1 + \tan(\delta_w - \beta + \theta) (\tan(\phi_w - \theta + i) + \cot(\phi_w - \theta + \beta))} \right]$$

(2-30)

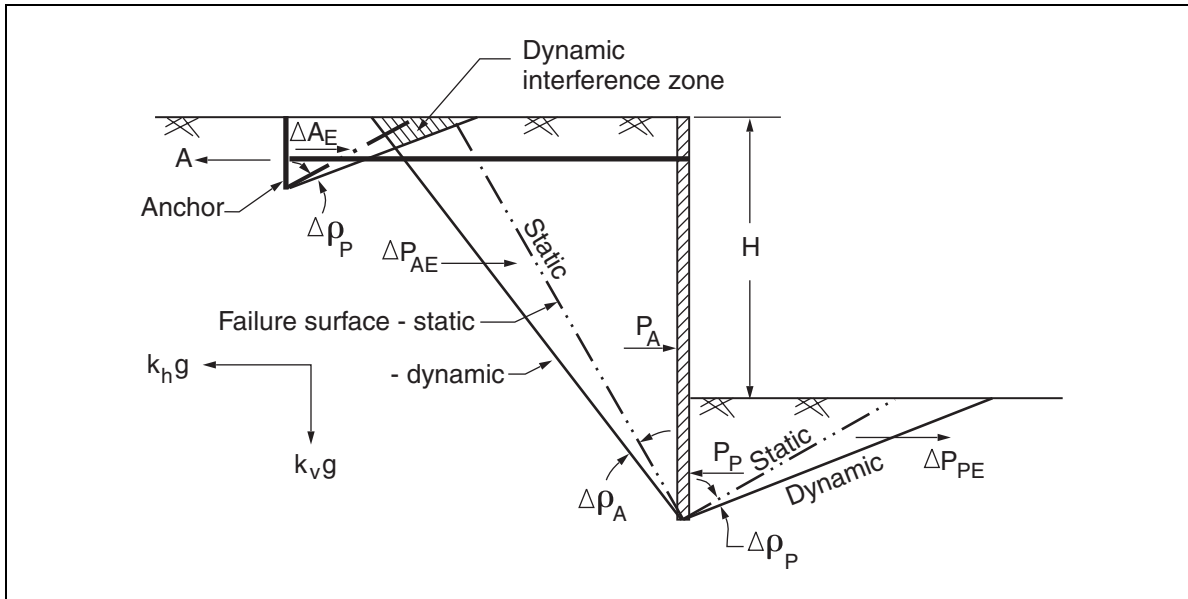


Figure 2-22. Seismic effects on anchored walls.

2.4.4.2(a). Passive Toe Failure - Rotation About the Top

The stress resultants acting on the wall are shown in figure 2-21. In this figure, ΔP_{AE} , and ΔP_{PE} are the dynamic effects to be added or subtracted to the static values and hence:

$$\Delta P_{AE} = P_{AE} - P_{AS} \quad (2-31)$$

$$\Delta P_{PE} = P_{PE} - P_{PS} \quad (2-32)$$

where P_{AE} , P_{PE} , can be determined as described in sections 2.4.2.1(a) and (b). Static values of lateral pressure may be obtained by using $k_h = k_v = 0$. For steel piles, the interface wall friction, $\delta_w = 0$ is a reasonable value (Neelakantan et al., 1992). Assuming that the wall/soil interface friction angle, δ_w , is zero is conservative since active earth pressures are relatively higher, and passive earth pressures are relatively lower compare to values computed with $\delta_w \neq 0$.

The dynamic increments of lateral earth pressure are assumed to act as shown in figure 2-21. From moments taken about the anchor point, the driving moment is:

$$M_D = P_{AS} \left(\frac{2}{3} H_A - A_h \right) + \Delta P_{AE} \left(\frac{H}{2} - A_h \right) \quad (2-33)$$

and the resisting moment capacity is given by:

$$M_R = \left(P_{PS} - \Delta P_{PE} \right) \left(H_A - \frac{D}{3} - A_h \right) \quad (2-34)$$

Thus, the factor of safety against failure by rotation about the top is M_R/M_D , and the critical threshold acceleration, $(k_h)_{RT}$, can be calculated from the condition that $FS = 1.0$ when $M_D = M_R$.

2.4.4.2(b). Anchor Failure - Rotation of Base

The anchor force is computed by summing the forces in the horizontal direction. Thus, the anchor force including static plus seismically induced internal forces is:

$$A_D = \frac{1}{2} \gamma ((H+D)^2 K_{AE} - D^2 K_{PE}) \quad (2-35)$$

In the absence of destructive interference between the active and passive failure wedges in front of the anchor, the resistance that can be provided by an anchor plate is:

$$A_R = \frac{1}{2} \gamma h^2 (K_{PE} - K_{AE}) \quad (2-36)$$

Thus, the factor of safety against anchor failure inducing rotation about the bottom of the wall is A_R/A_D , and the critical acceleration, $(k_h)_{ANC}$, is calculated from the condition that $FS = 1.0$ when $A_D = A_R$.

For any given design, the destructive interference, further reducing the anchor resistance, can be evaluated from equations 2-25 and 2-30 which describe the active and passive slip surface angles for different acceleration levels. It is recommended that the possibility of interference be evaluated from a sketch of the wall system, drawn to scale, that includes the active and passive slip surfaces.

Example 2-1 demonstrates the application of the procedure for seismic evaluation of anchored walls. Table 2-1 is a summary of results from example 2-1.

Table 2-1. Results from application of seismic evaluation procedure for anchored walls (described in Example 2-1).

Recommendation for Static Design	D/H	$A_D = A_R$ Static (kN/m)	$(k_h)_{RT}$ From Eq. 2-33 & 2-34	$(k_h)_{ANC}$ From Eq. 2-35 & 2-36	$A_D = A_R$ Retrofit (kN/m)
(1)	(2)	(3)	(4)	(5)	(6)
1	0.48	59	0.34	0.23	170
2	0.35	48	0.15	0.07	87
3	0.58	59	0.43	0.30	221

2.4.5. MSE WALLS

The seismic evaluation of MSE walls described in this chapter applies to walls less than 12 meters high. Generally, seismic evaluation of MSE retaining walls involves consideration of both external and internal resistance to seismic loading. Potential modes of failure including sliding, bearing capacity, rupture failure, and pullout are depicted in figure 2-23. In addition, slope or general failure should be evaluated as described in chapter 3.

In response to external loading, the reinforced wall fill is treated as a coherent mass (figure 2-24). As such, the external stability analysis for MSE walls follows a procedure similar to that detailed for gravity retaining walls described in section 2.4.2. This includes consideration of sliding, overturning, bearing capacity and global failure modes. Loads on the reinforced wall fill include lateral earth pressure from the unreinforced backfill, inertial loading due to seismic excitation, and from any applied surcharge.

The assumption that the reinforced wall fill behaves as a coherent mass presumes that it is internally stable. Internal stability requires that the reinforcement does not fail by rupture, pullout or at the connection to the wall face. An important issue is the location of the failure surface within the reinforced wall fill as it affects the length required to resist pullout, figure 2-25.

Example 2-1. Application of the Procedure for Seismic Evaluation
of Anchored Walls

A six meter high retaining wall with tie-backs connected one meter below ground level will be evaluated. The soil properties for design are $\phi_w = 35^\circ$, $\delta_w = 0$, and unit weight of backfill and foundation soil, $\gamma = 20 \text{ kN/m}^3$. Seismic evaluations are performed with reference to three different static designs including recommendations of the *BS Code of Practice* (1951) and the *Canadian Foundation Engineering Manual* (1978), the *U.S.S. Steel Sheet Piling Design Manual* (1975), and *The Naval Facilities Design Manual NAVFAC DM-7* (1982). The three recommendations for static design are described below:

1. *BS Code of Practice* (1951) and the *Canadian Foundation Engineering Manual* (1978) recommend that a safety factor of 2.0 be applied to the coefficient of passive earth pressure.
2. The *U.S.S. Steel Sheet Piling Design Manual* (1975) recommends that the theoretical limiting depth of embedment be obtained without incorporating any safety factor. This theoretical depth of embedment is increased by at least 20 percent to arrive at the design depth of embedment similar to AASHTO (2002).
3. *The Naval Facilities Design Manual NAVFAC DM-7* (1982) recommends that a safety factor of 2.0 be applied to the coefficient of passive earth pressure. The theoretical depth of embedment computed with the safety factor is then increased by 20 percent to arrive at the design depth of embedment.

The embedment depth ratios, D/H , and anchor forces, A_D , computed for the static case using each of the recommendations is presented in columns (2) and (3) of table 2-1. The acceleration $(k_h)_{RT}$ to initiate rotation about the anchor position is found by equations 2-33 and 2-34. The acceleration for anchor failure, $(k_h)_{ANC}$, is found by equations 2-35 and 2-36. The height of anchor plate, h , used in equation 2-36 is that which satisfies the static design.

In all cases examined, the acceleration required for anchor failure, $(k_h)_{ANC}$, is less than that required for failure by rotation about the anchor position, $(k_h)_{RT}$. Consequently, the anchor will fail first which is consistent with observations described in section 2.3.2. For any of these static designs, the seismic efficiency of the system can be increased by increasing the anchor resistance, A_R , described by equation 2-36. For example, for the given D/H ratios, the retrofit design of the anchor may be determined from equation 2-35 by putting $k_h = (k_h)_{RT}$. The design anchor forces A_D (retrofit) = A_R (retrofit) thus obtained are presented in column six of table 2-1. These forces are much greater than those found by conventional static methods. Thus, for the same D/H ratio, we can enhance the seismic stability of an anchored retaining wall by retrofitting the anchor(s) to carry the balanced anchor forces. The retrofit anchors must be at a distance L , as shown in figure 2-21 but with P_{AE} and P_{PE} instead of P_{AS} and P_{PS} , to avoid any destructive interference at the retrofit design value of $(k_h)_{RT}$.

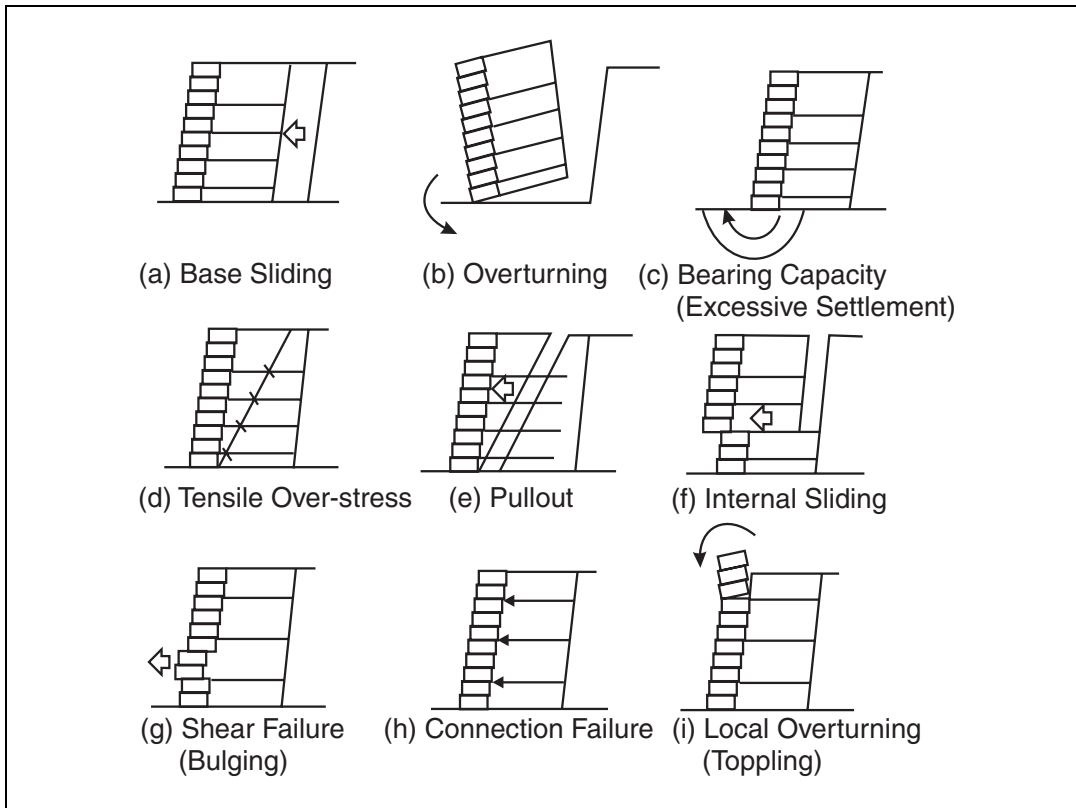


Figure 2-23. Modes of failure for MSE walls.

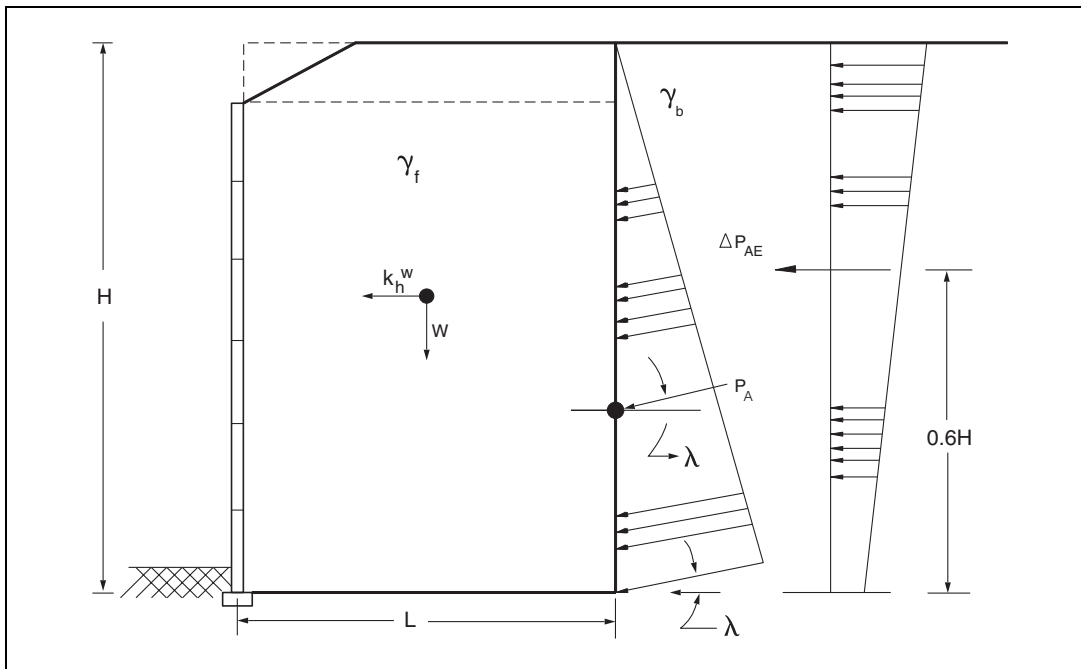


Figure 2-24. Forces acting on MSE wall for external stability analysis.

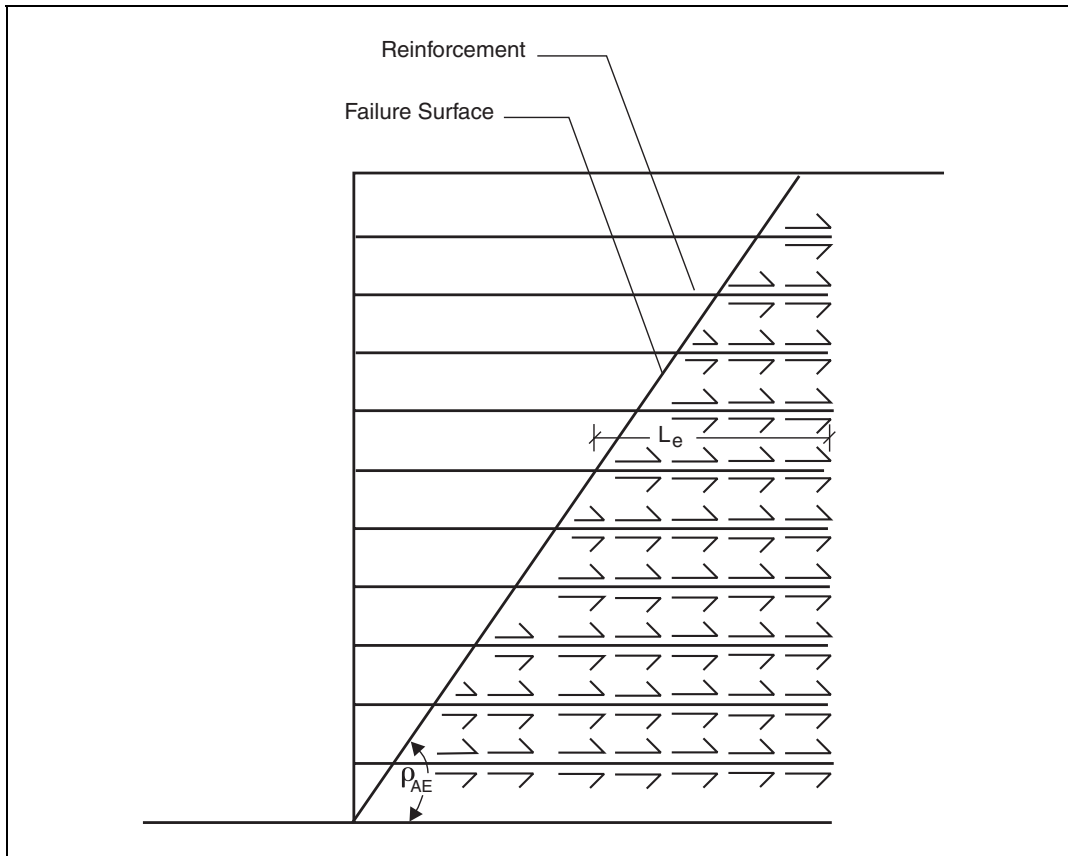


Figure 2-25. Assumed failure surface within the reinforced wall fill.

The seismic internal stability analysis examines the increased reinforcement tension, an increase in the percent of total lateral force carried by reinforcement elements in the upper portions of the wall, and the required increased length of the reinforcement layers.

Seismic lateral earth pressures are computed using equations 2-1, 2-2 and 2-3 from the Mononobe-Okabe analysis described in section 2.4.2.1(a). The peak friction angle is used to represent the shear strength of the soils. Included in the analysis are horizontal accelerations, the inclination of the back face, and the friction at the interface between the wall facing and reinforced fill (an estimate of $\delta_w=2/3\phi_w$ can be used) and between reinforced fill and backfill (an estimate of $\delta=\phi$ can be used).

The maximum acceleration developed in the wall is estimated based on an empirical equation proposed by Segrestin and Bastick (1988).

$$k_h = (1.45 - k_o)k_o \geq k_o \quad (2-37)$$

where:

k_o is the peak ground acceleration coefficient accounting for local soil conditions,
 k_h is the maximum wall acceleration coefficient at the wall centroid.

This equation is intended to consider the dynamic response of the wall. According to Segrestin and Bastick, low ground accelerations are significantly amplified within the wall. The maximum wall acceleration is applied to both the reinforced soil and the wall facing. However, the value of k_h applied to the wall system, including the wall facing, reinforced soil, and retained soil should not exceed the threshold acceleration for sliding. For MSE walls, threshold accelerations for sliding, k_h^s , are generally less than 0.4g.

Procedures that consider potential for collapse of the wall, and loss of serviceability of nearby structures, are described in sections 2.4.5.1 and 2.4.5.2, respectively. The procedures described herein are based on the equations described by Bathurst and Cai (1995).

2.4.5.1. Evaluation Procedure for MSE Walls for Collapse

Collapse of MSE walls from overturning or seismically induced reduction of bearing capacity, as described in sections 2.4.2.2(a) and (b), is not likely. Therefore, these modes of failure need not be investigated for detailed evaluation of the need for seismic retrofit. Potential modes of collapse include tension failure of the reinforcements, failure of connection of the reinforcement to the wall face, and possibly toppling of the wall facing. These modes of collapse are discussed in the following subsections.

2.4.5.1(a). Tension in Reinforcements

The influence of seismic loading on the magnitude of tensile reinforcement loads can be explored by computing a magnification factor, r_f , that is the ratio of dynamic tensile force F_{dyn} , to static tensile force F_{sta} , for a reinforcement layer at depth z below the wall crest. Results of this calculation for reinforcement layers at five different depths below the wall crest reported by Bathurst and Cai (1995) are presented in figure 2-26. The data illustrates that the largest relative increases in reinforcement force occur in the shallowest layers.

In lieu of figure 2-26, reinforcement tension is computed, as shown in figure 2-27, using the contributory area approach and an assumed distribution of the Mononobe-Okabe lateral earth pressure similar to figure 2-14, such that the dynamic increment of lateral thrust acts at 0.6 H from the base and the static component acts at 0.33 H. The inertia force on the wall facing must also be considered in the analysis. Based on this approach, the equation for computing the tensions in the reinforcements considering earthquake loading is:

$$F_{dyn} = \left[0.8\Delta K_{dyn} \cos(\delta - \psi) + (K_A - 0.6\Delta K_{dyn}) \cos(\delta - \psi) \frac{z}{H} + k_h \frac{L_w}{H} \right] \gamma H S_v \quad (2-38)$$

where:

F_{dyn} is the tension in the reinforcement at depth z ,

ΔK_{dyn} is $K_{AE} - K_A$,

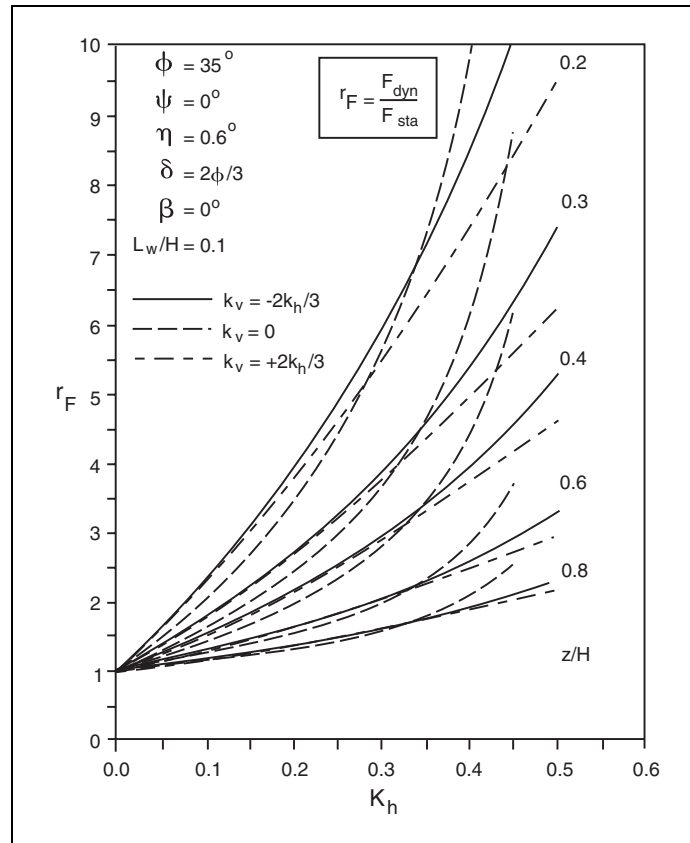
K_A is the static lateral earth pressure coefficient, i.e., with $k_h = 0$,

δ is the wall/wall fill interface friction angle,

ψ is the wall batter ($-\psi = \beta$, see figure 2-11),

L_w is the width of the wall facing,
 γ is the unit weight of the wall fill,
 H is the height of the wall fill,
 S_v is the reinforcement spacing at depth z .

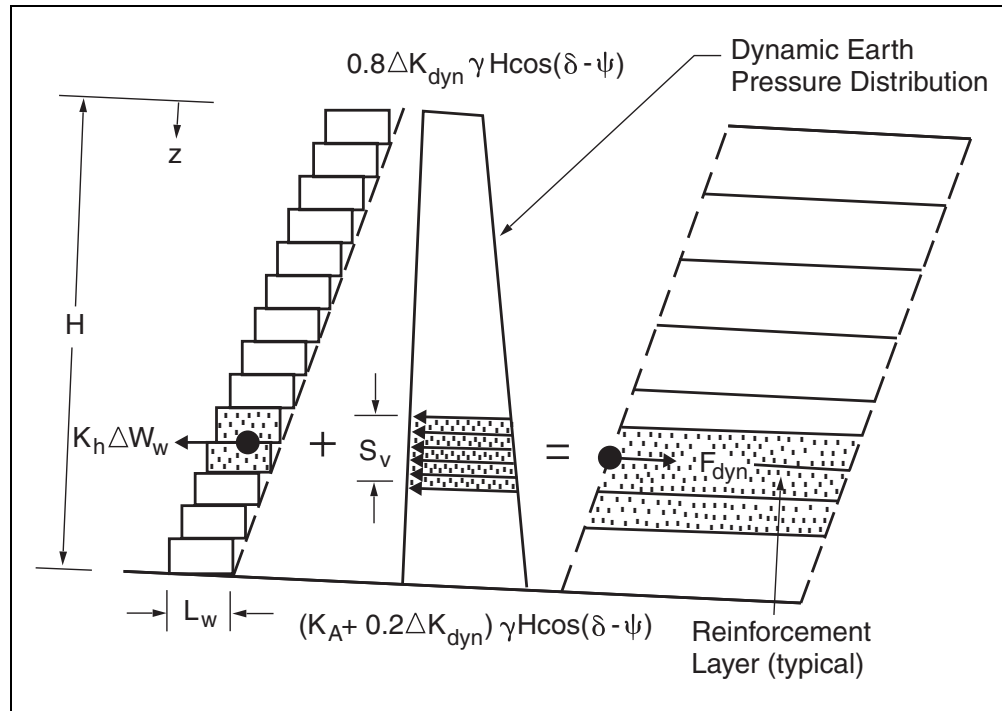
If F_{dyn} is greater than the allowable tension in the reinforcement for seismic loading conditions, design of seismic retrofit is required as described in section 2.5.



Bathurst and Cai, 1995

Figure 2-26. Influence of seismic coefficients, k_h and k_v , and normalized depth below crest of wall, z/H , on dynamic force amplification factor, r_F .

Seismic Design with Polymeric Reinforcement: The stress strain response of HDPE exhibits visco-elastic behavior and is load rate dependent. The tensile strength corresponding to dynamic loads with velocities in the range of seismic loading is greater than the allowable tensile strength for long-term gravity loads. The user should consult the manufacturer’s literature for information on the rate dependent tensile strength of polymeric reinforcement, or conduct tension tests using appropriate rates of loading. Currently, no test standard exists for evaluating the rate dependent tensile strength of polymeric reinforcement.



Bathurst and Cai, 1995

Figure 2-27. Tensile load in a reinforcement layer due to seismic lateral earth pressure and wall inertia.

Considering the increased tensile strength, and the safety factor used for static design, it will often be found that the number of reinforcement layers required for seismic design does not exceed the number required for the long-term gravity loading. However, since the line of action of the dynamic increment of lateral earth pressure is higher than that for long-term gravity loading, the distribution used for the static design may not place enough reinforcement near the top of the wall (Bonaparte et al., 1986).

2.4.5.1(b). Connection Details

The influence of increased dynamic forces on connection load is identical to the analysis described in section 2.4.5.1 (a) for reinforcement overstressing. As described by AASHTO (2002), the tension at the wall face is considered to be between 80 percent and 100 percent of the maximum tension computed in the reinforcement. Compared to static loading, a larger tension in the reinforcements is allowed since it is not necessary to apply a reduction factor for creep effects. The safety factor at the connection is evaluated as the ratio of the connection strength to the tension at the wall face.

If stacked concrete block units are used as facia, the connection strength may be modeled with a Coulomb-type failure law with a maximum cut-off load. For seismic loading, the frictional component of the shear strength is reduced to 80 percent of the value used to compute the static

shear strength (Elias and Christopher, 1997). Peak connection capacities may be sensitive to rates of loading, but further research is required to define this relationship.

If the safety factor at the connection is less than one, design of seismic retrofit is required as described in section 2.5.

2.4.5.1(c). Seismic Analysis of Segmental Reinforced Walls and Toppling of the Wall Face

Bathurst and Cai (1995) propose a method of seismic analysis applicable to segmental retaining walls (SRWs). Segmental retaining walls utilize stacked concrete block units as the fascia system together with extensible sheets of polymeric materials (geosynthetics) that internally reinforce the retained soils and anchor the fascia. Often the wall is battered 3° to 15° from the vertical into the retained soils.

The proposed analysis is a pseudo-static analysis by which factors of safety are computed for various failure modes. Internal and external stability analyses must consider the same failure modes as for other types of MSE retaining walls. Modes of failure, unique to SRWs, that address issues of internal sliding and facing stability (figure 2-23) include:

- Internal sliding along a layer of reinforcement whereby the potential failure surface daylights at the wall face after passing through the interface between the modular blocks.
- Bulging of the modular blocks at the wall face.
- Toppling of the wall face.

For the purpose of evaluating the need for seismic retrofit due to collapse, in addition to the modes of failure discussed in sections 2.4.5.1 (a) and (b), only failure by toppling at the wall face needs to be considered.

Toppling of the wall face: Resistance to overturning is due to the self weight of the column of stacked concrete blocks, and resistance due to the connection capacity of the reinforcement layers above the toe of the target facing unit, as shown in figure 2-28. The factor of safety with respect to toppling is calculated as:

$$FS_{OT} = \frac{M_R (1 \pm k_v) + \sum_{i=1}^N F_c^i Y_c^i}{\left[\frac{1}{6} K_A \cos(\delta - \psi) \frac{Z}{H} + (0.4 - 0.1 \frac{Z}{H}) \Delta K_{dyn} \cos(\delta - \psi) + \frac{1}{2} k_h \frac{L_w}{H} \right] \gamma H Z^2} \quad (2-39)$$

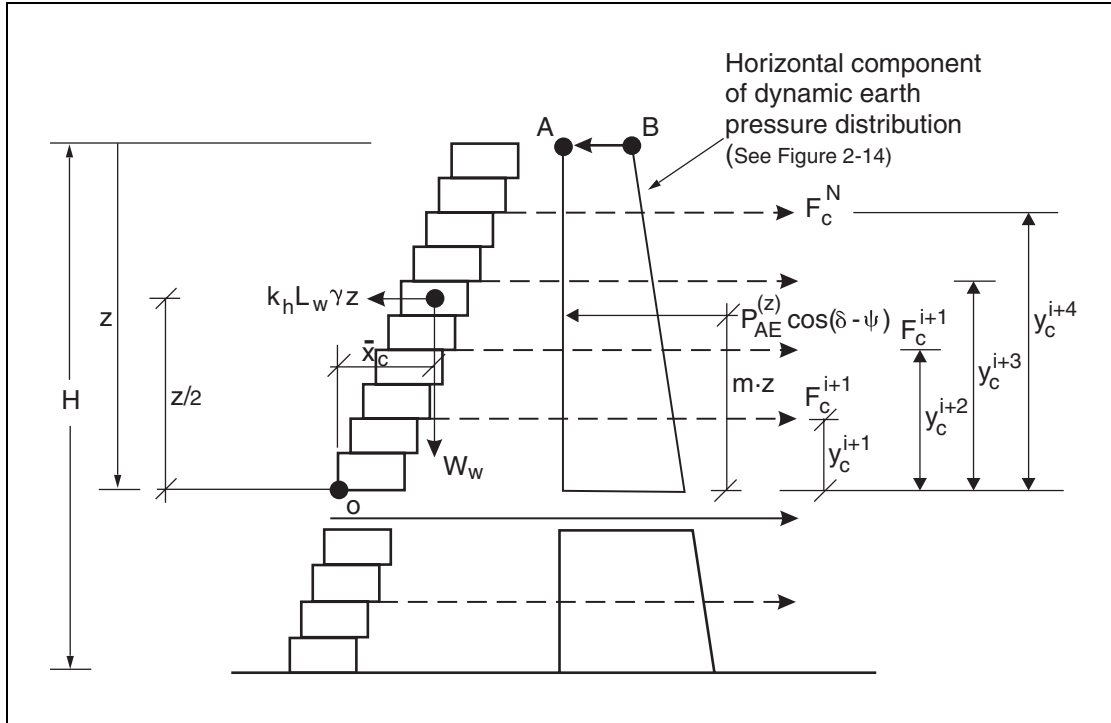
where:

M_R is the resistance to overturning due to facing column self-weight above the toe of the target facing unit,

N is the number of reinforcement layers,

F_c^i is the connection capacities of reinforcement layers,
 Y_c^i are the corresponding moment arms of F_c^i .

If the computed factor of safety with respect to toppling is less than one, seismic retrofit is required as described in section 2.5.



Bathurst and Cai, 1995

Figure 2-28. Overturning moment at an interface within the wall facing of an SRW due to seismic lateral earth pressure and wall inertia.

2.4.5.2. Proximity of Structures to MSE Walls

Nearby essential facilities may be affected by deformations of MSE walls. The potential for these deformations may be evaluated using procedures similar to those for gravity or semi-gravity walls as described in section 2.4.2.4. Potential failure mechanisms that can lead to excessive deformation of MSE walls include external sliding failure, pullout failure of reinforcements; and, for SRWs, internal sliding instability, and bulging of the wall facing. Evaluations of these modes of failure, within the context of loss of serviceability of nearby structures, are described in sections 2.4.5.2(a) through 2.4.5.2(d), respectively.

2.4.5.2(a). External Sliding Stability

MSE walls can be screened relative to the need for detailed evaluation of a sliding failure using the procedure described in section 2.4.2.4(a). The structure is viewed as a gravity retaining wall having the dimensions of the reinforced wall fill. Compared to conventional gravity retaining walls, the static factor of safety relative to a sliding mode of failure for MSE walls is relatively high. This is because the length of reinforcements for MSE walls is often governed by “pullout” requirements rather than sliding stability. For many MSE walls, the static factor of safety for external stability considering the sliding mode is 4 or higher. Figure 2-15 indicates that the threshold acceleration coefficient for this condition is greater than 0.3.

If the screening procedure indicates that deformations are a potential problem, a more detailed evaluation is required. The deformation analysis considers a sliding mode of failure at the base of the reinforced wall fill. The method considers effects from horizontally applied acceleration, including increased lateral thrust applied by the unreinforced backfill, and an inertia force acting within the reinforced wall fill as shown in figure 2-24.

The external sliding analysis is the same as that described in section 2.4.2.4. The analysis is performed for a coherent gravity structure having the dimensions of the reinforced wall fill as shown by figure 2-24. The procedure only considers a sliding mode of failure, therefore steps (6), (7) and (8) of the procedure described in section 2.4.2.4(b) are not necessary and iterations are performed until the threshold acceleration for sliding, k_h^s , is obtained.

2.4.5.2(b). Pullout

The effect of applied horizontal and vertical acceleration on the inclination of the potential failure surface within the reinforced soil, described by equation 2-25 is considered when computing the required anchorage length of the reinforcement. Pullout may lead to unacceptable deformation and damage to nearby essential facilities.

The resistance to pullout from the portion of the reinforcement beyond the potential failure surface is computed as:

$$T_R = 2 L_e \mu \gamma z (1-k_v) b \quad (2-40)$$

where L_e is the length of the reinforcement beyond the failure zone defined by ρ_{AE} , b is the width of reinforcement, and μ is the coefficient of friction between the reinforcement and the wall fill. For sheet reinforcement, use $b = 1$ and T_R as force per unit length. The value of μ should be 80 percent of that determined from static load tests. Studies by Bathurst and Cai (1995) indicate that the required reinforcement anchorage for seismic loading is sensitive to the vertical component of acceleration, k_v . The pullout resistance is compared to the reinforcement tension computed with equation 2-38. If the pullout resistance is less than the computed reinforcement tension, design of seismic retrofit as described in section 2.5 is required.

2.4.5.2(c). Internal Sliding Stability (for SRWs and MCUs)

The analysis for internal sliding stability, figure 2-23, is similar to that for the external stability analysis described in section 2.4.5.2(a). The dimensions of the coherent gravity mass considered in the internal sliding stability analysis are described by the width of the reinforced wall fill and the height of the wall fill above the layer of reinforcement where the potential for sliding is being investigated. Contributions to sliding resistance are from the interlock shear strength between the modular blocks at the facing, and the interface shear resistance along the length of the reinforcement. The shear resistance between modular blocks may also be described with a Coulomb-type failure law. The shear strength between modular blocks is determined as described by NCMA Test Method SRWU-2 (NCMA, 1996). The shear resistance along the reinforcement is often less than for the shear resistance of a failure plane through soil. It is recommended that the user assess the shear strength of the reinforcement/soil interface by laboratory direct shear tests as described by ASTM D5321.

Using the procedure described in section 2.4.2.4(b), equation 2-20 is modified to account for the shear resistance of the modular blocks at the wall face as:

$$F.S._{slide} = \frac{N \tan \delta_f + V_u}{F} \quad (2-41)$$

where

V_u is the shear strength of the interface between modular blocks.

The shear resistance at the wall facing is related to the above weight of the facing column, W_w . At large inclination angles, the magnitude of W_w may be less than the weights of the individual facing units above the interface elevation, due to the effect of the facing column units leaning into the reinforced soil mass. Studies conducted by Bathurst and Cai (1995) indicate the potential for interface shear failure under seismic loading increases with proximity of the shear interface to the crest of the wall. However, the effect of vertical acceleration on calculated dynamic factors of safety diminishes with height of interface.

The procedure only considers a sliding mode of failure, therefore steps (6), (7) and (8) of the procedure described in section 2.4.2.4(b) are not necessary and iterations are performed until the threshold acceleration for sliding, k_h^s , is obtained. The procedure is applied to each reinforcement interface along the height of the wall. The minimum k_h^s thus determined governs the analysis. If the minimum k_h^s is greater than k_h , this mode of failure is not a concern. If the minimum k_h^s is less than k_h , a deformation analysis as described in section 2.4.2.4(c) is performed. The deformations are compared to acceptable levels of deformation to determine if seismic retrofit is required.

2.4.5.2(d). Bulging Shear Failure

Bulging is caused by a shear failure at the interface between modular blocks at the wall face. The wall facing is treated as a shear beam, as shown in figure 2-29, in which the integrated lateral earth pressure (similar to that shown in figure 2-24) must equal the sum of the forces in the

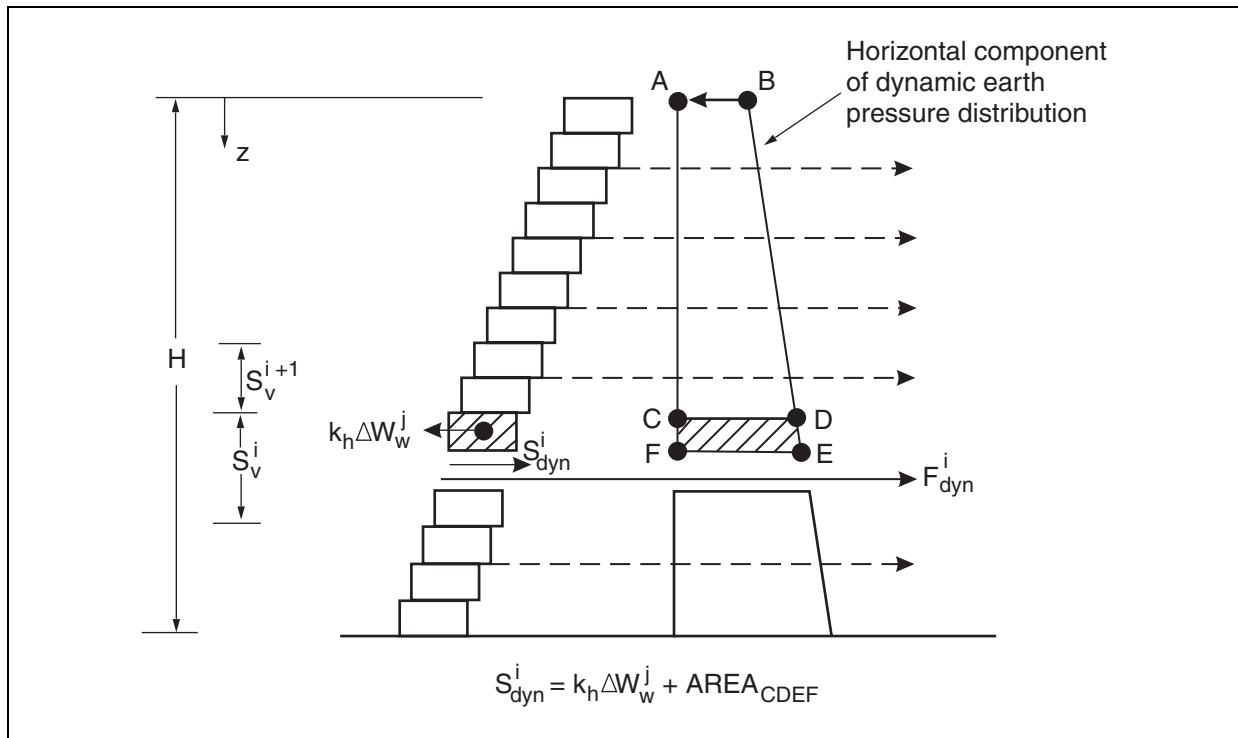
reinforcement layers. The effect of wall inertia is included in the analysis. The total force carried by reinforcement layers located above the facing unit “j” is calculated as the area ABCD of the lateral earth pressure distribution, plus the facing column inertial force over the same height. The out-of-balance force to be carried through shear at the bottom of the facing unit “j” is simply the sum of the incremental column inertia force $k_h \Delta W_w^j$ plus the force due to CDEF in the figure. The locally maximum interface shear forces will occur at reinforcement elevations:

$$S_{\text{dyn}} = [0.8\Delta K_{\text{dyn}} \cos(\delta - \psi) + (K_A - 0.6\Delta K_{\text{dyn}}) \cos(\delta - \psi) \left(\frac{z}{H} - \frac{S_v}{4H}\right) + k_h \frac{L_w}{H}] \frac{\gamma H S_v}{2} \quad (2-42)$$

where

S_{dyn} is the interface shear stress at depth z .

The interface shear strength is compared to the shear strength of the interface between modular blocks, V_u , at each level of reinforcement. If S_{dyn} is greater than V_u , design of seismic retrofit is required as described in section 2.5.



Bathurst and Cai, 1995

Figure 2-29. Shear force at an interface within the wall facing of an SRW due to seismic lateral earth pressure and wall inertia.

2.5. DESIGN OF SEISMIC RETROFIT FOR EARTH RETAINING STRUCTURES

An understanding of the basic concepts presented in section 2.4 will allow the engineer to evaluate various options to strengthen walls and reduce their seismic vulnerability. In fact, results from the evaluation procedures described in section 2.4 suggest the appropriate retrofitting strategies, since not only is the threshold acceleration evaluated, but also the critical failure mode.

In general, retrofitting can involve one or more of the following:

- Tie-backs (with grouted, helical, or expanding anchors).
- Increase in the footing width.
- Reinforcing the concrete wall stems.
- Added passive restraint by burying the toe.
- Minipiles.
- Soil reinforcement near the top.
- Soil modification.

This listing is in the approximate order of their general effectiveness. Tie-backs, for example, are useful in almost every situation for all types of walls, while soil modification by adding admixtures or grouting is more expensive and time consuming.

Retrofit for liquefaction vulnerability is not discussed in this part of the manual. Where walls (particularly tied-back bulkheads used as waterfront structures) are susceptible to liquefaction, special remedial measures may be required as presented in chapter 11, Part 1 of this manual.

2.5.1. GRAVITY AND SEMI-GRAVITY WALLS

From the evaluation procedure described in section 2.4.2, the critical or threshold acceleration corresponding to each mode of failure is determined and an estimate made of the seismic deformation. The mode of deformation with the lowest threshold acceleration occurs first, although for severe earthquakes, mixed types of deformation may occur as less critical failure modes are initiated at higher acceleration levels. Figure 2-30 shows the three modes of failure and appropriate retrofitting measures for each.

As can be seen, tie-backs are a universal retrofitting measure but they must be installed properly. They must be long enough to extend beyond the slip surface described by equation 2-25 with enough anchorage length to develop the design force, F_A . The spacing and size of the tie-backs is computed such that F_A will improve horizontal and moment equilibrium to counter P_{AE} and $k_h W$ to the point where the resulting increase in threshold acceleration eliminates or reduces the seismic displacement to an acceptable level. Equilibrium calculations using the concepts

discussed in section 2.4.2 and 2.4.4 may be applied to establish the required value of F_A and design of the deadman anchorage. Note that the inertia of the gravity wall must be included in the equilibrium equations, and shear resistance at the base of the wall may be included in the force moment equilibrium equations. Tie-backs have the added advantage of increasing the normal force on the slip surface so that not only are the seismic driving forces resisted, but the shear strength resisting slip is increased.

If grouted anchors are employed, the user is referred to Sabatini et al. (1998) for details of the anchor design. The effect of the anchor load on the wall must also be addressed in the design. Effects on the wall from the anchor load include bearing stress, punching shear, bending moment and the associated shear stress.

Increasing the footing width is also an excellent retrofitting strategy for walls where sliding, or rotation about the base, is the failure mode. Various ways of adding to the width are possible and only one of many viable designs is shown in figure 2-31(a). In this approach, heavy wire mesh is used for tensile reinforcement because of its relatively short development length, reducing the amount the original toe must be undercut. Care must be exercised when considering this option such that its implementation does not compromise the original design.

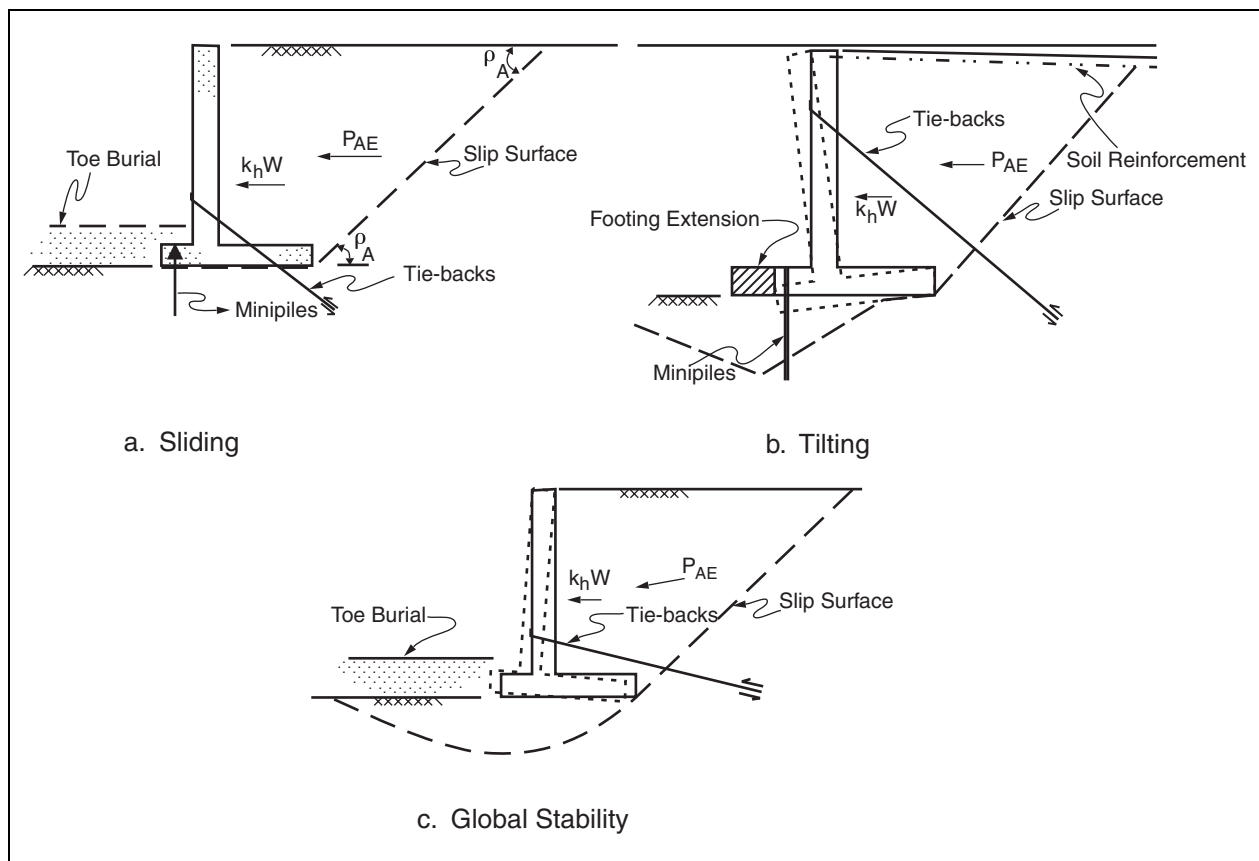


Figure 2-30. Retrofit strategies for gravity and semi-gravity walls.

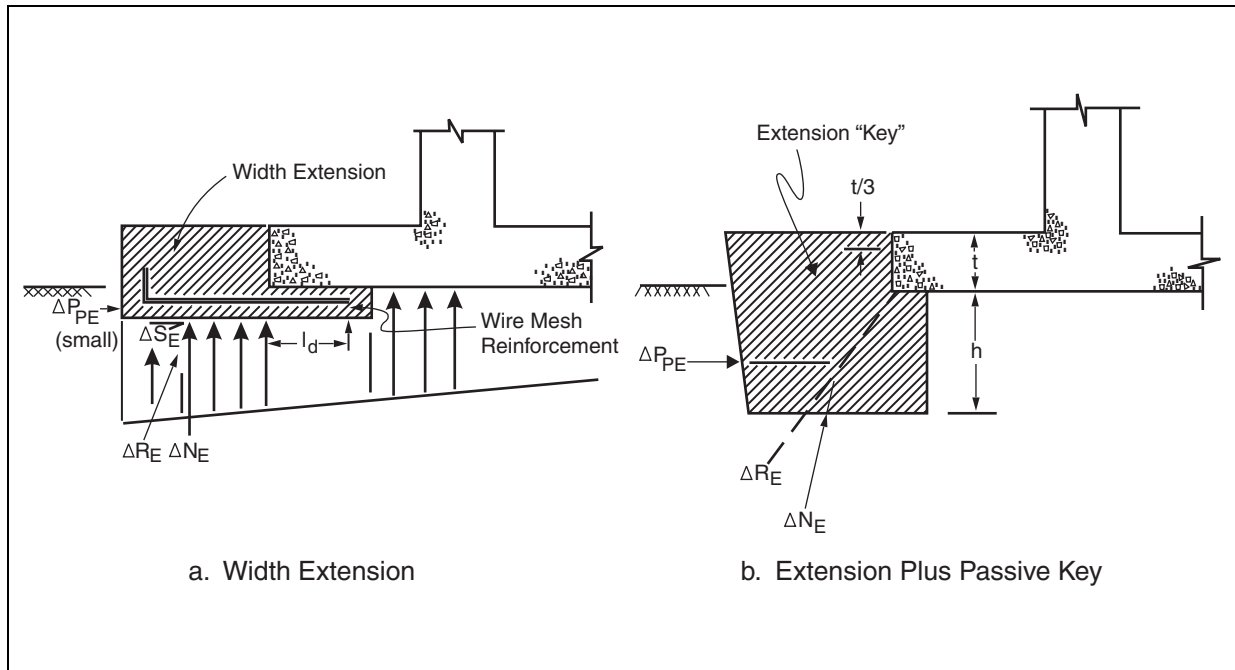


Figure 2-31. Retrofitting by increasing the width of the base.

The increased footing width has an effect on sliding resistance due to the increase in wall weight; overturning stability due to increased wall weight and distance between the toe and centroid of the wall; and seismic bearing capacity due to increase in footing width. The increase in threshold acceleration and corresponding reduction in seismically induced displacement can be evaluated as described in section 2.4.2. Also, the structural integrity of the footing must be evaluated, particularly with respect to the bending moments, which may be higher than those considered in the original design.

Adding passive resistance at the toe by burial is a possible retrofitting strategy for walls where sliding is critical but is not nearly as effective in preventing tilting. The passive resistance can be computed directly from equations 2-4 and 2-5. The increase in seismic bearing capacity due to the surcharge loading is given by use of figure 2-13 and equation 2-7.

Retrofit by adding width to the toe can be combined with added passive resistance by deepening the design of figure 2-31(a), as shown in figure 2-31(b). This, as in all retrofitting strategies, is constrained by the physical conditions of the site, access and material availability. There are added advantages to this design. First, the additional passive restraint at the face of the key is less likely to be disturbed. Secondly, it is possible to design its depth, h , such that the resultant force on the additional block of concrete acts below the upper third of the toe thickness, t . This will reduce the amount of steel reinforcement required. The structural integrity of the footing must also be checked and the effect of concentrated vertical load near the toe with respect to bending moment considered in the design.

Minipiles, as shown in figure 2-30, are certainly a viable retrofitting approach, particularly to prevent tilting of concrete cantilever-type walls. More than one row of piles is desirable, but there may not be enough space at the toe of an existing footing to allow installation of two rows of piles. The retrofit design should include a check for overturning with respect to a pivot point at the pile-heads, and the pile-heads should be designed for moment transfer, i.e., they should be design as fixed head piles. Piles will increase the rigidity of the foundation near the front of the footing, so the design calculations should include analysis of the potential for differential settlement, but the use of short piles will minimize this effect. Also, if pressure grouted mini-piles are used, there will be some improvement in the foundation soil beneath the footing.

The foundation should be analyzed as a spread footing. The pile elements are intended to extend the apparent depth of the footing and provide a deeper-seated failure surface associated with the bearing capacity of the footing. The required pile lengths would be relatively short; less than 3 m.

The piles need to be designed to carry moment, lateral load and transfer the seismic increment of bearing pressure near the toe of the footing. They must be drilled deep enough at the toe to extend below the bearing capacity zone. They will also provide some added resistance to sliding through dowel action. To be most effective, the piles should be battered outward, but generally, there will not be enough clearance at the toe without extending the footing. Minipiles are relatively more expensive but, quick, simple and less disruptive than extending the footing. The reader is referred to Bruce and Juran (1997) for details on the design of minipiles. Similar to tie-backs or grouted anchors, the effect of load transfer on the structural integrity of the footing must be addressed in the design.

The other retrofitting approaches of soil reinforcement and soil modification will generally be less effective and more costly than the four strategies already outlined. Thus, they will not be discussed further. Only in very special cases must the engineer turn to them where there is no room for extending, deepening, or burying the toe, tie-backs for some reason are not feasible, and minipiles cannot be used.

Finally, it should be noted that except for minipiles, these retrofitting strategies are applicable to all types of gravity walls. The figures were drawn for a cantilever wall only for convenience.

2.5.2. CONCRETE CANTILEVER WALLS - STRUCTURAL FAILURE OF THE WALL

For all wall types, structural failure due to increased lateral earth pressures is possible in severe earthquakes with peak horizontal ground acceleration greater than 0.4 g. For design of structural retrofit, the dynamic increment of lateral earth pressure should be assumed to act at 0.6 H from the base of the wall. Thus, for example, in a cantilever wall, if the lateral thrust is doubled due to seismic forces, then the moment at the base of the stem will more than double.

There are a number of methods for adding moment resistance to cantilever wall stems. Use of cover plates is a simple and viable option. Other options include adding buttress elements or tie-backs. The important thing is that the engineer recognizes this potential failure mode for severe

earthquakes. Structural collapse, unlike the accumulation of increments of deformation due to periodic slip, can be catastrophic.

2.5.3. ANCHORED WALLS

The evaluation procedure described in section 2.4.4 dictates the appropriate retrofitting strategies for tied-back walls. As demonstrated by example 2-1, considering walls designed using current standards for static design, the failure mode in an earthquake would be by anchor failure and rotation about the bottom. For current static designs, rotation around the anchor is less likely since the corresponding threshold acceleration is relatively high.

Thus, the best retrofitting approach is to increase the strength of the anchor and increase its embedment length to avoid destructive interference. Thus from figure 2-32, the retrofit anchor should be at:

$$l_E = (H + D) \cot \rho_{AE} + h \cot \rho_{PE} \quad (2-43)$$

and designed to take a seismic anchor force given by equation 2-35. This will increase the threshold acceleration to above 0.35 g for tied-back walls with a D/H ratio greater than 0.5. Even for very severe earthquakes, walls retrofitted to threshold accelerations greater than 0.35 g will not move more than 0.1 meters, unless the anchor fails structurally.

If instability at the toe of the wall is a problem, the retrofit strategy might include installing an additional row of tie-backs.

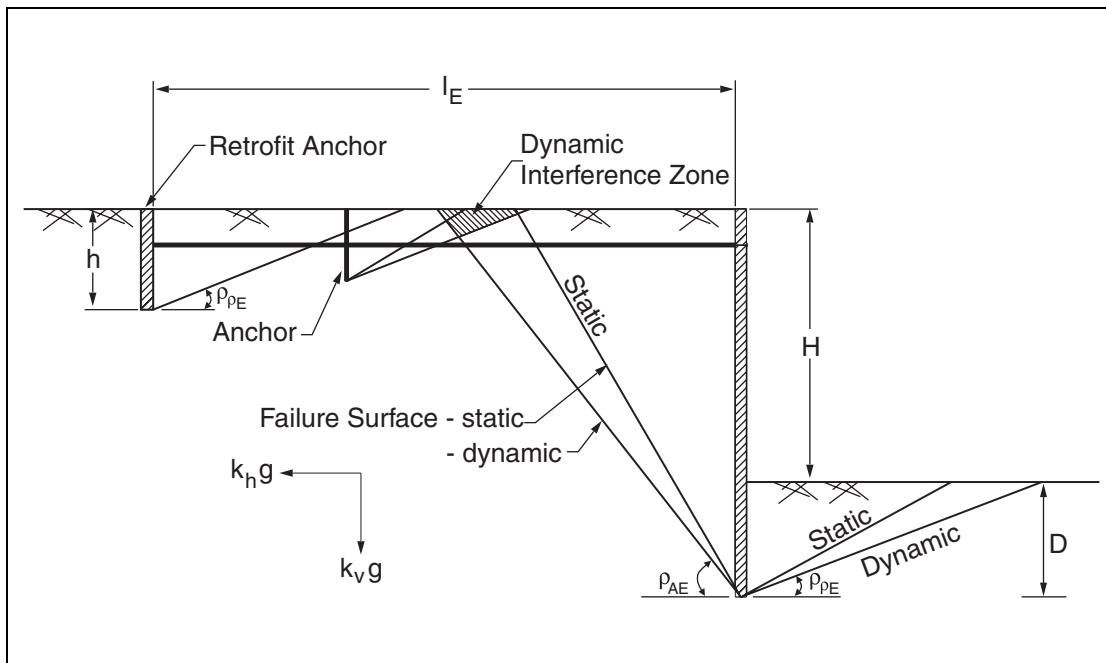


Figure 2-32. Seismic effects and retrofit for tied-back walls.

2.5.4. MSE WALLS

To date, mechanically stabilized earth walls, in all varieties and configurations, have an excellent history of performance in earthquakes. However, the evaluation procedure described in section 2.4.5 will indicate that some, relatively taller, MSE walls in severe earthquake hazard zones may need careful evaluation for possible retrofitting.

If reinforcements near the top of the wall are overstressed, it may be feasible to add additional reinforcements near the top of the wall. If access to the backfill is a problem, soil nails drilled through the existing wall face may be used. Added soil nails may be considered to carry only the dynamic increment in forces because the deformations required to transfer static loads to the nails will not necessarily occur. Bearing plates may be used to distribute the nail loads at the wall face. The user is referred to Byrne et al. (1996b) for details of soil nails.

If the increase in lateral thrust and the potential for a sliding failure is a problem, the front of the wall may be buttressed, or the backfill may be modified to reduce the driving forces. Modification to retained soil may include ground modification such as grouting, partial replacement with lightweight fill, or decreasing the slope angle of the backfill surface.

As discussed in section 2.4.5, the standard static design of MSE walls often leads to insufficient development length for the reinforcement in the upper part of the wall when considering seismic loading. Retrofit options include tying on to the existing reinforcements at the top of the wall to add development length. The splice should be designed to transfer a load equal to the ultimate tensile strength of the reinforcement.

According to Bathurst and Cai (1995), designers of SRWs typically maximize the unreinforced height of wall at the crest while maintaining the required static factor of safety. This strategy results in unacceptably low margins of safety against toppling at the top of the structure under seismic loading conditions. Reinforcement layers with adequate connection capacity must be introduced close to the wall crest to minimize the potential for this failure mechanism.

2.6. SCREENING, SEISMIC EVALUATION AND DESIGN OF SEISMIC RETROFIT FOR A RETAINING WALL

The description and background information for the retaining wall described in this example problem was adapted from Example 3 presented in FHWA Geotechnical Engineering Circular No. 3, *Design Guidance: Geotechnical Earthquake Engineering for Highways, Volume II - Design Examples* (Kavazanjian et al., 1997). This example problem is presented for illustrative purposes only. The data does not apply to any particular location, but are used to illustrate an application of the equations and concepts described in this manual.

EXAMPLE PROBLEM 2 - SCREENING, SEISMIC EVALUATION AND DESIGN OF SEISMIC RETROFIT FOR A RETAINING WALL

An existing retaining wall is part of an underpass along a highway near Memphis, Tennessee. The wall varies in height from 0.5 m to 7 m along the underpass alignment. To complete the screening, evaluation and design of seismic retrofit for the wall, the following tasks need to be performed:

- It has been decided to evaluate the wall for ground motions for the maximum considered earthquake (MCE) which has a seven percent probability of being exceeded in 75 years at this site. Refer to Part 1 of this manual for a discussion of ground motions to be used for retrofit design.
- Apply screening criteria and assess the need for seismic evaluation.
- Check the design of the wall for static loading conditions.
- Perform a seismic evaluation of the wall.
- Design and seismic evaluation of retrofit strategy.

Source Materials Required

The source materials required to solve this problem include:

- *Seismic Retrofitting Manual for Highway Structures*, Parts 1 and 2 (i.e., this manual).
- Subsurface profile information.
- As-built details of the retaining wall.
- *Standard Specifications for Highway Bridges* (AASHTO, 2002).
- *USGS Probabilistic Earthquake Acceleration and Spectral Acceleration Maps for the United States* (1996).
- *NEHRP Guidelines for the Seismic Rehabilitation of Buildings*, FEMA 273 (BSSC, 1997).
- *Building Code Requirements for Structural Concrete* (ACI 318-02) (see ACI, 1995a).
- *Recommendation for Prestressed Rock and Soil Anchors*, PTI (1996).
- FHWA Geotechnical Engineering Circular No. 3, *Design Guidance: Geotechnical Earthquake Engineering for Highways* (Kavazanjian et al., 1997).

Geologic and Seismic Setting

The site is situated in the gulf coastal plain section of the coastal plain physiographic province. The region is referred to as the Mississippi embayment. The topography of the area is characterized as gentle to steep, with occasional discontinuities created by the flat lying alluvial plains of the streams in the area. These topographic features have formed as a result of the glacial erosion of the uppermost tertiary and quaternary formations and by subsequent deposition of a thick covering of loess deposits during the late stages of the pleistocene glaciation.

Approximately 915 to 1200 m of quaternary, tertiary, and cretaceous age sediments were deposited within the Mississippi embayment in the Memphis area. The surface and subsurface geologic units of this area consist predominantly of unconsolidated silt, sand, clay, gravel and lignite deposits.

The retaining wall is located within the New Madrid Seismic Zone (NMSZ), the source of three major earthquakes and several thousand aftershocks between 1811 and 1814. The NMSZ strikes in the northeasterly direction, and extends about 175 km from near Memphis, Tennessee in the south to Cairo, Illinois in the north.

Geotechnical Information

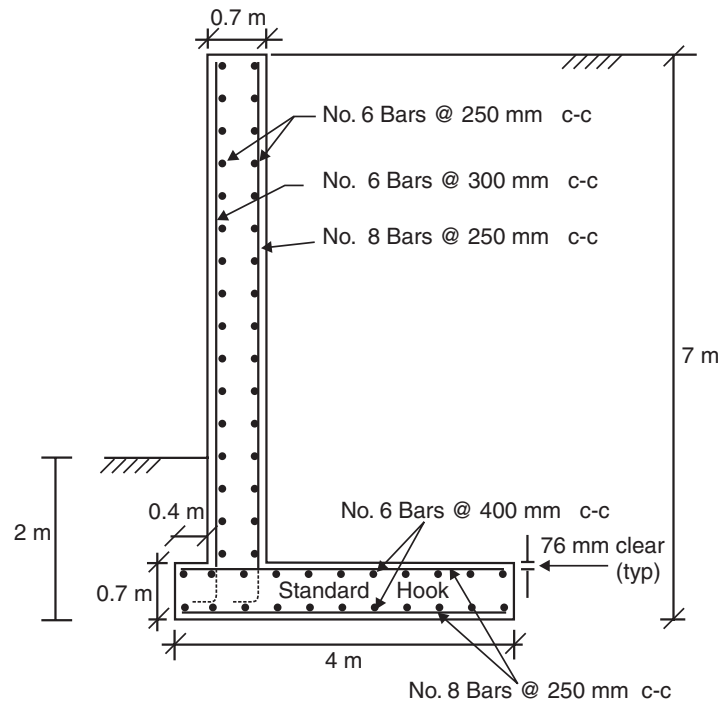
The site is underlain by the Memphis sand formation, which consists mainly of coarse sand with lenses or beds of clay and silt at various horizons.

Subsurface information at the site was obtained through a series of cone penetration tests (CPTs) and borings drilled using rotary wash borings with drilling mud to depths of 60 meters. Standard penetration tests (SPTs) were performed at intervals of 1.5 m in the borings. SPT split-spoon samples recovered from the borings were visually classified, and index property tests were performed on several samples. The normalized and standardized SPT N (blow count) distribution with depth is provided in the following subsections.

Groundwater was not encountered in the test borings. Therefore, the potential for liquefaction is not a factor in the seismic vulnerability of the retaining wall.

Wall Information

The wall is described as a reinforced concrete cantilever wall. The figure below shows the geometry, dimensions, and structural details of the wall.



Step 1: Evaluate Ground Motions at the Site

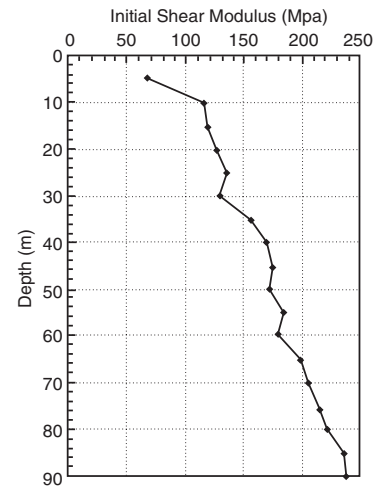
- Site location: 35.15° latitude, 89.6° longitude.
- Maximum considered earthquake has a seven percent probability of exceedance in 75 years.
- Based on USGS (2002) - see website: <http://eqhazmaps.usgs.gov>.
- PGA = 0.31g (this is the PGA in a bedrock outcrop at the site - need to consider site effects).
- Therefore, according to the screening guide, detailed evaluation is required since the PGA > 0.3g.

Step 2: Collect Information Needed for Seismic Evaluation

1. Site conditions:

- Very deep soil deposit which consists mainly of coarse sand with lenses or beds of clay and silt at various horizons.
- Based on CPT data, the variation of initial shear modulus up to a depth of 90 meters is shown in the figure.
- From this figure, the average initial shear modulus is 175 MPa.
- Unit weight is 18 kN/m³ and mass density is $\rho = 1.83 \text{ Mg/m}^3$.
- Average shear wave velocity:

$$V_s = \sqrt{\frac{G}{\rho}} = \sqrt{\frac{175 \times 10^3 \text{ kN/m}^2}{1.83 \text{ Mg/m}^3}} = 309 \text{ m/s}.$$



- Based on FEMA 273 (1997), site class is Class D (stiff soil with $180 \text{ m/s} < V_s < 365 \text{ m/s}$ or with $15 < \bar{N} \leq 50$ or $50 \text{ kPa} \leq S_u < 95 \text{ kPa}$).
- To determine k_h for the seismic evaluation of the retaining wall, multiply the peak bedrock acceleration by the appropriate site coefficient:

F_a = site coefficients,

S_s = mapped short-period acceleration response parameter,

$S_s = 0.60$ from USGS (1996) for 35.15° latitude and 89.6 longitude (see <http://eqhazmaps.usgs.gov>),

$F_a = 1.3$ from FEMA 273 (1997), w/ $S_s \approx 1.0$.

- Therefore, $k_h = F_a \times \text{PGA} = 1.3 \times 0.31 \approx 0.4$.

2. Soil properties:

- Foundation soil

See SPT data shown in the figure.

Average \bar{N} for top 10 m is 12.

for $N = 12$: $\phi \approx 32^\circ$; $D_r \approx 40$ percent; and $\gamma = 18 \text{ kN/m}^3$.

Correlation between N and Φ for sands as described by Peck et al., 1974.

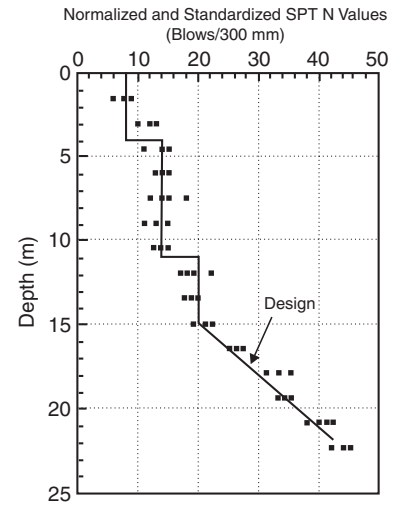
- Wall backfill

$\Phi = 35^\circ$,

$\gamma = 18 \text{ kN/m}^3$,

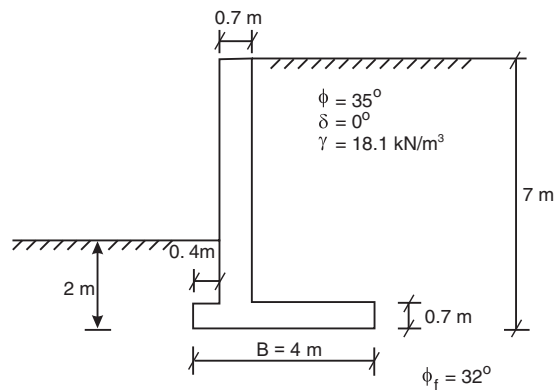
δ_w – wall friction = 0° (conservative assumption),

δ_b – friction at base = 30° (from AASHTO 5-5-2B).



Step 3: Check Design of Wall for Static Loading Conditions

	Weight of Wall	Arm	Moment w.r.t. Toe
Stem	$0.7 \times 6.3 \times 23.5 \text{ kN/m}^3$ $= 104 \text{ kN/m}$	$0.7/2 + 0.4 = .75 \text{ (m)}$	$104 \times .75 = 78 \text{ kN} \times \text{m/m}$
Footing	$0.7 \times 4 \times 23.5 = 65.8 \text{ kN/m}$	$4/2 = 2 \text{ (m)}$	$65.8 \times 2 = 132 \text{ kN} \times \text{m/m}$
Soil	$6.3 \times 2.9 \times 18.1$ $\text{kN/m}^3 = 331 \text{ kN/m}$	$2.9/2 + 1.1 = 2.6 \text{ m}$	$331 \times 2.6 = 861 \text{ kN} \times \text{m/m}$
	501 kN/m		1071 kN x m/m



Evaluate Limit State for Static Loading

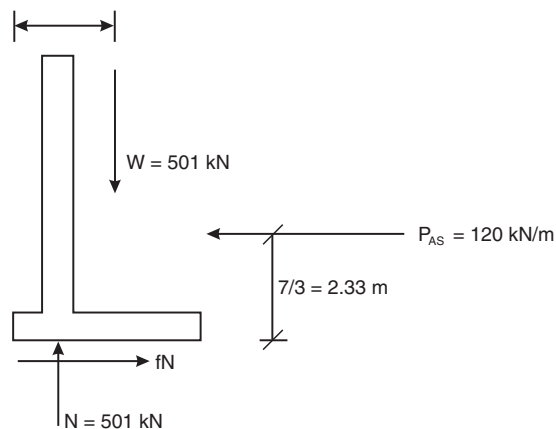
- $P_{AS} = \frac{1}{2} K_{AS} \gamma_S H^2.$

$$K_{AS} = \tan^2 \left(45^\circ - \frac{35^\circ}{2} \right) = 0.271.$$

$$H = 7\text{m}.$$

- Therefore, $P_{AS} = \frac{1}{2} (0.271) (18.1) 7^2 = 120 \text{ kN/m}.$

$$1071/501 = 2.13 \text{ m}$$



1. Check sliding resistance:

- For mass concrete on coarse sand, use $f = \tan 30^\circ = 0.58$ (see AASHTO table 5-5-2-B).

- $$F_{\text{slide}} = \frac{\text{Resisting Force}}{\text{Driving Force}}$$

Resisting Force = $fN = 0.58 (501 \text{ kN}) = 291 \text{ kN}$.
Driving Force = $P_{AS} = 120 \text{ kN}$.

- Therefore, $F_{\text{slide}} = \frac{291}{120} = 2.4 > 1.5$ OK.

2. Check for overturning:

- $M_{\text{Driving}} = P_{AS} (h) = 120 \text{ kN/m} \times 2.33\text{m} = 280 \text{ kN} \times \text{m/m}$.

- $M_{\text{Resistance}} = W \bar{x} = 501 \text{ kN} \times 2.13\text{m} = 1067 \text{ kN} \times \text{m/m}$.

- $F_{\text{Overturn}} = \frac{1067}{280} = 3.8 > 2.0$ OK.

3. Check eccentricity of result:

- $$e = \frac{B}{2} - \frac{M_{\text{Resistance}} - M_{\text{Driving}}}{F_v}$$

$F_v = W$.
 $B = 4\text{m}$.

- Therefore, $e = \frac{4}{2} - \frac{1067 - 280}{501} = 0.429\text{m}$; $\frac{B}{6} = \frac{4}{6} = .67' > e$ OK.

4. Check bearing capacity:

- Generalized bearing capacity equations are from Meyerhoff (1953) with $C = 0$, and shape factors = 1.

- For depth inclination factors, see Meyerhoff (1953) or ASCE (1994).

- $$q_{\text{ult}} = F_{qi} F_{qd} (\gamma D) N_q + \frac{1}{2} F_{\gamma i} F_{\gamma d} \gamma B' N_\gamma$$

F_{qi} = inclination factor for surcharge term;

$$F_{qi} = \left(1 - \frac{\alpha}{90}\right)^2 \quad \alpha = \tan^{-1} \left(\frac{120}{501}\right) = 13.5^\circ$$

- Therefore, $F_{qi} = \left(1 - \frac{13.5}{90}\right)^2 = \underline{\underline{0.72}}$.

$$F_{qd} = \text{depth factor for surcharge term} = 1 + 0.1 \sqrt{K_p} \frac{D}{B}; 1 + 0.1 \tan \left(45 + \frac{32}{2} \right) \frac{2}{4} = 1.09.$$

$$\gamma D = \text{surcharge} = 2 \times 18.1 = \underline{36.2} \text{ kN/m}^2.$$

$$D = 2 \text{ m.}$$

$$\gamma = 18.1 \text{ kN/m}^3.$$

$$N_q = \text{surcharge bearing capacity factor for } \phi = 32^\circ; N_q = \underline{23.18} \text{ (see AASHTO table 4-4-7-1A).}$$

$$F_{\gamma i} = \text{inclination factor for soil friction term.}$$

$$F_{\gamma i} = \left(1 - \frac{\alpha}{\phi} \right)^2 = \left(1 - \frac{13.5}{32} \right)^2 = \underline{0.33}.$$

$$F_{\gamma d} = \text{depth factor for soil friction term} = F_{qd} = 1.09.$$

$$B' = B - 2e = 4 \text{ m} - 2(0.429 \text{ m}) = \underline{3.14 \text{ m.}}$$

$$N_\gamma = \text{soil friction bearing capacity factor for } \phi = 32^\circ; N_\gamma = 30.22. \text{ (see AASHTO table 4-4-7-1A).}$$

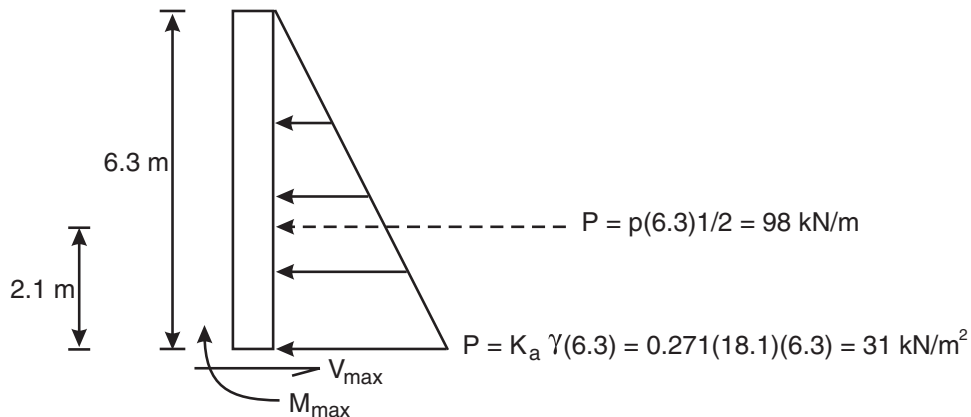
- Therefore, $q_{ult} = (0.72)(1.09)(36.2) 23.18 + \frac{1}{2} (0.33)(1.09)(18.1)(3.14)(30.2)$
 $= 659 + 309 = 968 \text{ kN/m}^2.$

$$q = \frac{N}{B'} = \frac{W}{B'} = \frac{501 \text{ kN/m}}{3.14 \text{ m}} = 159 \text{ kN/m}^2.$$

$$F_{\text{Bearing}} = \frac{q_{ult}}{q} = \frac{968}{159} = 6 > 3 \quad \underline{\text{OK.}}$$

Compute Reinforcing Steel Requirements

1. Find shear and bending moment at base of wall stem:



- $M_{\max} = P h = 98 (2.1) = 206 \text{ kN x m/m} .$
- $M_u = 1.7 M_{\max} = 350 \text{ kN x m/m}$ (from ACI 9-2-4).

- $M_u = \phi A_s f_y \left(d - \frac{0.59 A_s f_y}{f'_c b} \right)$ (from ACI 10-2).

$\Phi = 0.9$ (from ACI 9.3),

$f_y = 414 \text{ MN/m}^2,$

$f'_c = 28 \text{ MN/m}^2,$

$b = 1\text{m},$

$d = 0.7\text{m} - .076\text{m} - .0127 = 0.61$ (from ACI 7-7-1).

2. #8 bars at 250 mm c-c:

- $A_s = 510 \text{ mm}^2 / \#8\text{bar} \times \frac{1000 \text{ mm/m}}{250 \text{ mm/bar}} = 2040 \text{ mm}^2 / \text{m} = .00204 \text{ m}^2 / \text{m} .$

- $M_u = 0.9 (.00204) 414 \left(0.61 - \frac{0.59 (.00204)(414)}{28(1)} \right) = 0.45 \text{ MN/m}$

$= 450 \text{ kN x m/m} > 1.7 M_{\max}$ OK.

- Steel ratio $\rho = \frac{A_s}{bd} = \frac{.00204}{(1)(.61)} = 0.0033 .$

- $\rho_{\min} = \frac{200}{f_y} = \frac{200}{60,000} = .0033$ OK (see ACI 10-5).

- $\rho_{\max} = 0.85 \frac{f'_c}{f_y} \beta \left(\frac{600}{600 + f_y} \right) = 0.0217$ OK (see ACI 10-3-3).

- Requirement for shrinkage and temperature:

$\rho_{\text{set}} = .0018$ OK (see ACI 2-12).

3. Horizontal steel:

- #6 bars @ 250 mm c-c each face.

- $A_s = 2 \text{ faces} \times 284 \text{ mm}^2 / \#6\text{bar} \times \frac{1000}{250} = 2272 \text{ mm}^2 / \text{m} = .002272 \text{ mm}^2 / \text{m} .$

- For walls, $\rho_{\min} = .0025$ (see ACI 14-3-3, based on gross area of concrete).

- $\rho = \frac{.002272}{0.7 \times 1\text{m}} = .0032 > \rho_{\min}$ OK.

Check Shear Capacity

- $V_u = 1.7 (98 \text{ kN/m}) = 167 \text{ kN/m}$.
- $\phi v_c = \phi (0.17) \sqrt{f'_c} bd$ (see ACI 11-3).
- $= 0.85$ (see ACI 9-3-2-3).
- $\phi v_c = 0.85 (.17) \sqrt{28} 0.7(1) = 0.535 \text{ MN/m} = 535 \text{ kN/m}$.
- $\phi v_c > 1.7V$ OK.

Heel Design

- $q = q_1 + q_2 - q_3$.
- $q_1 = \gamma (H - t) = 18.1 \text{ kN/m}^3 \times (7\text{m} - 0.7\text{m}) = 114.0 \text{ kN/m}^2$ (from soil above the heel).
- $q_2 = \gamma_c \times t = 23.5 \text{ kN/m}^3 \times 0.7\text{m} = 16.45 \text{ kN/m}^2$ (from mass of concrete slab).

1. Determine bearing pressures at heel and toe of wall foundation:

- $q_{\text{toe heel}} = \frac{W}{B} \left(1 \pm \frac{6e}{B} \right) = \frac{501 \text{ kN}}{4\text{m}} \left(1 \pm \frac{6(0.429\text{m})}{4\text{m}} \right) = 205.8 \text{ kN/m}^2 = q_{\text{toe}}$
 $= 44.7 \text{ kN/m}^2 = q_{\text{heel}}$

$$\begin{aligned} e &= 0.429 \text{ m,} \\ B &= 4\text{m,} \\ W &= 59 \text{ kN.} \end{aligned}$$

- $q_3 = 44.7 \text{ kN/m}^2 + 40.275 \text{ kN}/(\text{m}^2 \times \text{m}) \times \frac{2.9\text{m}}{2} = 103.09 \text{ kN/m}^2$.
- $V = q \times 2.9 \text{ m} = (114.0 \text{ kN/m}^2 + 16.45 \text{ kN/m}^2 - 103.09 \text{ kN/m}^2) \times 2.9 \text{ m} = 79.3 \text{ kN/m}$.
- $M = (114.0 \text{ kN/m}^2 + 16.45 \text{ kN/m}^2 - 44.7 \text{ kN/m}^2) \times \frac{2.9\text{m}^2}{2} - 40.275 \text{ kN/m}^2 \times \text{m}$.
- $\times \frac{2.9\text{m}^3}{6} = 360.6 \text{ kN} \times \text{m/m} - 163.7 \text{ kN} \times \text{m/m} = 196.9 \text{ kN} \times \text{m/m}$.
- $V_u = 1.7V = 1.7(79.3 \text{ kN/m}) = 134.81 \text{ kN/m}$.
- $M_u = 1.7M = 1.7 (196.9 \text{ kN} \times \text{m/m}) = 335 \text{ kN/m}$.

2. Check for shear:

- $V_c = 0.17 \sqrt{f'_c} bd = 0.17 \sqrt{28 \text{ MN/m}^2} \times 1\text{m} \times 0.7\text{m} = 0.629 \text{ MN/m}.$
- Assume: $b = 1 \text{ m}; d = 0.7 \text{ m}.$
- $\phi V_c = 0.85 \times 629 \text{ kN/m} = 535 \text{ kN/m} > 135.$
- Therefore, section is adequate.

3. Check flexural reinforcement:

- No. 8 bars at 250 mm c-c.
- $A_s = .00204 \text{ m}^2/\text{m}.$
- $\alpha = 0.7\text{m} - .076\text{m} - \frac{.025}{2} = 0.61\text{m}.$
- $M_u = \phi A_s f_y \left(d \times \frac{0.59 A_s f_y}{f'_c b} \right) = 450 \text{ kN/m} > 335 \text{ OK}.$
- $\rho = .0033$ (satisfies ACI 10-5, 10-3-3 and 7-12).

Toe Design

- $q = -q_2 + q_3.$
- $q_2 = \gamma_c t = 23.5 \text{ kN/m}^3 \times (0.7 \text{ m}) = 16.45 \text{ kN/m}^2$ (from mass of concrete slab).
- $q_3 = \text{soil reaction} = 205.8 \text{ kN/m}^2 - 40.275 \text{ kN/m}^2 \times \text{m} \times \frac{0.4\text{m}}{2} = 197.7 \text{ kN/m}^2.$
- $V = q \times 0.4\text{m} = (-16.45 \text{ kN/m}^2 + 197.7 \text{ kN/m}^2) 0.4\text{m} = 72.518 \text{ kN/m}.$
- $V_u = 1.7 (72.518 \text{ kN/m}) = 123.3 \text{ kN/m}.$
- $M = (-16.45 \text{ kN/m}^2 + 205.8 \text{ kN/m}^2) \frac{0.4\text{m}^2}{2} - 40.275 \text{ kN/m}^2 \times \text{m} \frac{(0.4\text{m})^3}{6} = 14.72 \text{ kN} \times \text{m/m}.$
- $M_u = 1.7 (14.72 \text{ kN} \times \text{m/m}) = 25.0 \text{ kN} \times \text{m/m}.$
- Shear is less than that for heel, therefore section is adequate.
- Moment is less than that for heel, therefore $\rho = \rho_{\min}.$
- Use #8 bars spaced at 250 mm c-c.

Step 4: Summary of Static Design Check

1. External stability requirements:

- $F_{\text{slide}} = 2.4 > 1.5$ OK.
- $F_{\text{overturn}} = 3.8 > 2.0$ OK.
- $e = 0.429\text{m} < B/6$ OK.
- $F_{\text{bearing}} = 6 > 3$ OK.

2. Stem:

- $M_{\text{max}} = 206 \text{ kN x m/m}$ $V_{\text{max}} = 98 \text{ kN/m}$
- $M_u = 450 \text{ kN x m/m}$ $\phi V_c = 535 \text{ kN/m}$
- $M_u > 1.7 M_{\text{max}}$ OK $\phi V_c > 1.7 V_{\text{max}}$ OK

3. Heel:

- $M_{\text{max}} = 197 \text{ kN x m/m}$ $V_{\text{max}} = 79.3 \text{ kN/m}$
- $M_u = 450 \text{ kN x m/m}$ $\phi V_c = 535 \text{ kN/m}$
- $M_u > 1.7 M_{\text{max}}$ OK $\phi V_c > 1.7 V_{\text{max}}$ OK

4. Toe:

- $M_{\text{max}} = 14.7 \text{ kN x m/m}$ $V_{\text{max}} = 72.5 \text{ kN/m}$
- $M_u = 450 \text{ kN x m/m}$ $\phi V_c = 535 \text{ kN/m}$
- $M_u > 1.7 M_{\text{max}}$ OK $\phi V_c > 1.7 V_{\text{max}}$ OK

5. Conclusion:

Static design meets existing standards. Since the peak ground motion with a three percent chance of being exceeded in 75 years at this site is greater than 0.3 g, perform a seismic evaluation and determine the need for seismic retrofit.

Step 5: Seismic Evaluation of Wall

1. Sliding threshold:

- Try $k_h^s = 0.34$ (with passive restraint).
- K_{AE} ($\phi = 35^\circ$, $\delta = 0$, $\beta = i = k_v = 0$) = 0.516 @ $k_h = 0.34$ (see eq. 2-1).
- $K_{PE} = 2.97$ (see eqs. 2-1 and 2-5).
- Solve for Equil. $\Sigma F = 0$.
- $\Sigma F = 1/2 K_{AE} \gamma H^2 - 1/2 K_{PE} \gamma D^2 + Wk_h - Wf = 0$.
- Therefore, $\Sigma F = \frac{1}{2} (0.516)(18.1) 7^2 - \frac{1}{2} (2.97) 18.1 (2)^2 + 501 (0.34) - 501 (0.58) = 229 - 108 + 170 - 291 = 0$.
- $k_h^{slide} = 0.34g$ OK.

2. Check sliding threshold with no passive restraint:

- Try $k_h^s = 0.22$.
- $K_{AE} = 0.41$.
- $\Sigma F = \frac{1}{2} (0.41) (18.1) 7^2 + 501 (.22) - 501 (0.58) = 182 + 110 - 291 \approx 0$.
- $k_h^{slide} = 0.22g$ without passive resistance OK.

3. Check overturn - rotation mode:

- Try $k_h^{OT} = 0.35$.
- $h = H/3$ for rotation w.r.t. toe.
- $K_{AE} = 0.53$.
- $K_{PE} = 3.0$.
- $\Sigma M = 0 = \frac{1}{2} K_{AE} \gamma H^2 \frac{H}{3} + Wk_h \bar{Y} - \frac{1}{2} K_{PE} \gamma D^2 \frac{D}{3} - W \bar{X}$ (see eqs. 2-8, 2-9, 2-10).
- $\bar{Y} = \frac{104 \left(\frac{6.3}{2} + 0.7 \right) + 65.8 \left(\frac{.7}{2} \right) + 331 \left(\frac{6.3}{2} + 0.7 \right)}{501} = 3.39$.

- Therefore, $\Sigma M = \frac{1}{2} (0.53) (18.1) \frac{7^3}{3} + 501 (0.35) (3.39) - \frac{1}{2} (3.0) 18.1 \frac{(2)^3}{3} - 501 (2.14) = 548.4 + 594.4 - 72.4 - 1072.14 = -1.74 \approx 0$.

- Therefore, $k_h^{OT} \approx 0.35$.

4. Compute bearing capacity threshold:

- Assume $k_h^{tilt} = 0.2g$.

- $K_{AE} = 0.396$.

- $\Delta K = K_{AE} - K_{AS} = 0.396 - 0.271 = 0.125$.

- $K_{PE} = 3.29$.

4(a). Compute shear stress transferred to base of foundation:

- $$F = \frac{1}{2} K_{AE} \gamma H^2 + Wk_h - \frac{1}{2} K_{PE} \gamma D^2$$

$$= \frac{1}{2} (.396) 18.1 (7)^2 + 501 (0.2) - \frac{1}{2} (3.29) (18.1) (2)^2$$

$$= 175.6 + 100.2 - 119.46 = 156.71$$

- $n = \frac{F}{Nf} = \frac{156.71}{501 (\tan 32^\circ)} = 0.501$ (see eq. 2-6).

- $\frac{N_{qE}}{N_{qS}} = 0.43$ (see figure 2-13).

- Therefore, $N_{qE} = 23.18 \times 0.43 = 9.97$; $N_{qS} = 23.18$.

- $\frac{N_{\gamma E}}{N_{\gamma S}} = 0.21$ (see figure 2-13).

- Therefore, $N_{\gamma E} = 30.2 \times 0.21 = 6.35$; $N_{\gamma S} = 30.2$.

4(b). Compute eccentricity:

- Find h assuming P_{AS} acts at $H/3$ and P_{dyn} acts at $0.6H$.

- $$h = \frac{K_{AS} \frac{H}{3} + \Delta K (0.6) H}{K_{AE}} = \frac{0.271 \left(\frac{7}{3}\right) + .125 (.6) 7}{.396} = 2.923$$

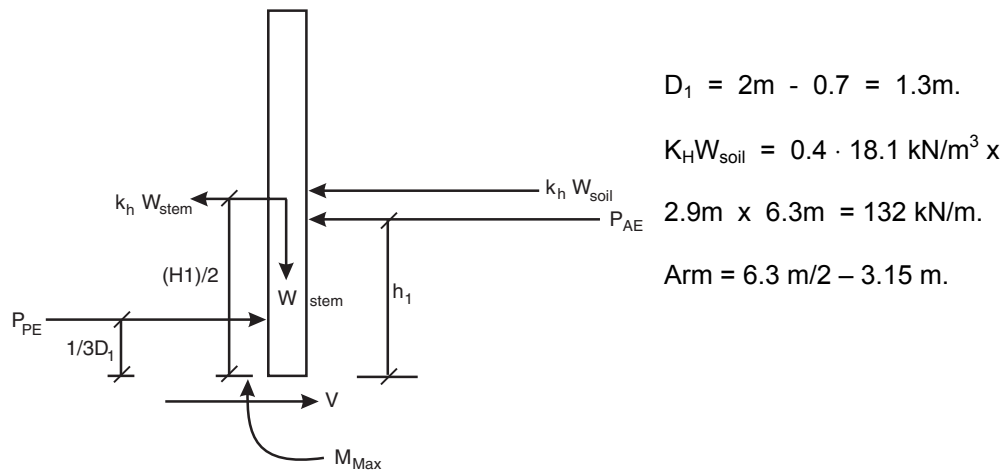
- $M_o = \frac{1}{2} K_{AE} \gamma H^2 h + k_h W\bar{y} = \frac{1}{2} (.396) (18.1) (7)^2 (2.92) + 0.2 (501) 3.39$
 $= 513.3 + 339.7 = 853.0.$
- $M_R = \frac{1}{2} K_{PE} \gamma D^2 \frac{D}{3} + W\bar{x} = \frac{1}{2} (3.29) (18.1) 2^2 \left(\frac{2}{3}\right) + 501 (2.14) = 79.40$
 $+ 1071 = 1150.4$ (see eq. 2-11).
- $e = \frac{B}{2} - \frac{(M_R - M_o)}{N} = \frac{4}{2} - \left(\frac{1150.4 - 853}{501}\right) = 2 - 0.59 = 1.41.$
- $B' = B - 2e = 4 - 2(1.41) = 1.19\text{m}.$
- $q_{ult} = \gamma DN_{qE} + \frac{1}{2}\gamma B'N_{\gamma E} = 18.1(2)9.97 + \frac{1}{2}(18.1)1.19(6.35) = 360.9 + 68.39 = 429.3 \text{ kN/m}^2.$
- $q = \frac{N}{B'} = \frac{501}{1.19} = 421 \approx 429 \text{ kN/m}^2.$
- Therefore, $k_h^{\text{tilt}} = 0.2.$

Summary of Threshold Accelerations		
Sliding	k_h^{slide}	0.34
Overturning	k_h^{rotate}	0.35
Bearing Capacity	k_h^{tilt}	0.2
Therefore, $k_h^{\text{tilt}} < k_h^{\text{rotate}} < k_h^{\text{slide}}$		

- $k_h^{\text{tilt}} = 0.2$ is the critical threshold acceleration. This is considered marginally acceptable since $k_h^{\text{tilt}} + 0.25 = 0.45 \approx k_h$ (see section 2.4.2.2 (b)).

Evaluate Structural Integrity

- Check moment at base of stem using $A = 0.4g$.
- $K_{AE} = 0.581$ $K_{PE} = 2.82$.
- $\Delta K = K_{AE} - K_{AS} = 0.581 - 0.271 = 0.31$.
- Find h_1 assuming P_{AS} acts at $H_1/3$ and P_{dyn} acts at $0.6H_1$.
- $H_1 = \text{height of stem} = 7\text{m} - 0.7\text{m} = 6.3$.
- $h = \frac{K_{AS} H_1/3 + \Delta K(0.6) H_1}{K_{AE}} = \frac{0.271(6.3/3) + 0.31(0.6) 6.3}{0.581} = 3.0\text{ m.}$



- $P_{AE} = \frac{1}{2} \gamma H_1^2 K_{AE} = \frac{1}{2} (18.1) (6.3)^2 (0.581) = 209 \text{ kN/m.}$
 - $W_{\text{stem}} = \gamma_c (d)(H_1) = 23.5 \times 0.7 \times 6.3 = 104 \text{ kN/m.}$
 - $P_{PE} = \frac{1}{2} \gamma D_1^2 K_{PE} = \frac{1}{2} (18.1) (1.3)^2 (2.8) = 43 \text{ kN/m.}$
 - $M_{\text{max}} = W_{\text{stem}} \times k_h \left(\frac{6.3}{2} \right) + P_{AE} (3.0) - P_{PE} (.43) + W_{\text{soil}} \times K_h \times \left(\frac{6.3}{2} \right) = 1155.$
 - $M_u = \phi A_S f_y \left(d - \frac{0.59 A_S f_y}{f'_c (b)} \right).$
 - Use a load factor of 1.0 for collapse prevention objective. Therefore, check $M_{\text{max}} \leq M_u$.
- $\phi = 1.0$ for earthquake loading and collapse prevention objective,
 $f_y = 414 \text{ MN/m}^2,$
 $f'_c = 28 \text{ MN/m}^2,$
 $d = 0.7\text{m} - .076 - .013 = 0.611 \text{ m,}$

$$b = 1 \text{ m},$$

$$A_s = 20.4 \text{ cm}^2/\text{m} - .00206 \text{ m}^2/\text{m}.$$

- $M_u = (1.0) (.00206) (414) \left(.611 - \frac{.59 (.00206) 414}{28 (1\text{m})} \right) = 0.853 (.588) = 0.501 \text{ MN} \times \text{m}/\text{m} = 500 \text{ kN} - \text{m}/\text{m}.$
- $M_{\max} > M_u$ Not Good.

1. Structural integrity of heel:

- Use eccentricity and bearing pressure at the bearing capacity threshold acceleration, k_h^{tilt} .
- $q = q_1 + q_2 - q_3.$
- $q_1 = 114.0 \text{ kN/m}^2$ (from soil above heel).
- $q_2 = \gamma_c \times t = 23.5 \text{ kN/m}^3 \times 0.7\text{m} = 16.45 \text{ kN/m}^2$ (from mass of concrete slab).
- $q_1 + q_2 = 130.45 \text{ kN/m}^2.$
- Determine bearing pressures at heel and toe of wall foundation.

$$q_{\frac{\text{toe}}{\text{heel}}} = \frac{W}{B} \left(1 \pm \frac{6e}{B} \right).$$

$$e = 1.4,$$

$$B = 4 \text{ m},$$

$$W = 501 \text{ kN},$$

$$6e = 8.4.$$

- $6e > B$, therefore, use eq. 2-16.

$$q_{\max} = \frac{4N}{3L(B - 2e)}.$$

$$N = 501 \text{ kN},$$

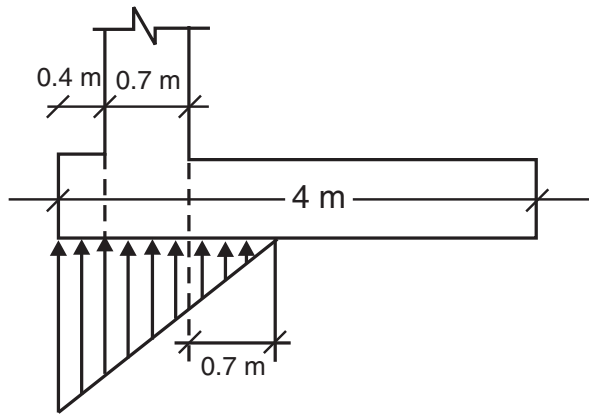
$$L = 1 \text{ m},$$

$$B = 4 \text{ m},$$

$$e = 1.4 \text{ m}.$$

$$= \frac{4(501 \text{ KN})}{3(1\text{m})(4\text{m} - 2(1.4\text{m}))} = 557 \text{ kN/m}^2 \text{ (at toe)}.$$

- $x = 1.5 (B - 2e) = 1.5 (4\text{m} - 2 (1.4\text{m})) = 1.8\text{m}$ (from toe towards heel; see eq. 2-17).



Distribution under heel is then:

$$557 \text{ kN/m}^2 \times \frac{1}{1.8\text{m}} = \frac{309.4 \text{ kN}}{\text{m}^2 \times \text{m}}$$

Pressure at edge of heel is then:

$$309.4 \text{ kN/m}^2 \times \text{m} \times 0.7\text{m} = 216.6 \text{ kN/m}^2.$$

Shear due to bearing pressure at heel is then:

$$216.6 \text{ kN/m}^2 \times \frac{0.7\text{m}}{2} = 75.8 \text{ kN/m}.$$

- $V = 130.45 \text{ kN/m}^2 \times 2.9\text{m} - 75.8 \text{ kN/m} = 302.5 \text{ kN/m}.$
- $M = 130.45 \text{ kN/m}^2 \times \frac{(2.9\text{m})^2}{2} - 75.8 \text{ kN/m} \times \frac{0.7\text{m}}{3} = 530.9 \text{ kN} \times \text{m/m}.$

Check for Shear

- $V_c = 0.17\sqrt{28 \text{ MN/m}^2} \times 1\text{m} \times 0.7\text{m} = 0.629 \text{ MN/m} = 629 \text{ kN/m} > 302.5 \text{ kN/m}.$
- Therefore, the section is OK for shear.

Check Flexural Reinforcement

- $A_s = 0.00206 \text{ m}^2.$
- $d = 0.7\text{m} - 0.076 - 0.013\text{m} = 0.611\text{m}.$
- $M_u = A_s f_y \left(d - \frac{0.59 A_s f_y}{f_c b} \right) = 0.00206\text{m}^2 \times 414 \text{ MN/m}^2$

$$\left(0.611\text{m} - \frac{0.59(0.00206\text{m}^2) \times 414 \text{ MN/m}^2}{28 \text{ MN/m}^2 \times 1\text{m}} \right)$$

 $= 505.7 \text{ kN} \times \text{m/m} < M = 530.9 \text{ kN} \times \text{m/m}.$

- Therefore, the steel is not adequate.

2. Structural integrity of toe:

- $q = -q_2 + q_3.$
- $q_2 = \gamma_c \times t = 23.5 \text{ kN/m}^2 (0.7\text{m}) = 16.45 \text{ kN/m}^2.$

- Soil bearing reaction: $q_{\max} = 557 \text{ kN/m}^2$
 $q_{\min} = 557 \text{ kN/m}^2 - 0.4\text{m} \times 216.6 \text{ kN/m}^2\text{m} = 470.4 \text{ kN/m}^2$.
- $q = -16.45 \text{ kN/m}^2 + 470.4 \text{ kN/m}^2 + 216.6 \text{ kN/m}^2\text{m} \times \frac{X}{2}$.
- $V = 453.91 \text{ kN/m}^2 \times x + 216.6 \text{ kN/m}^2\text{m} \times \frac{x^2}{2}$ ($x = 0.4 \text{ m}$)
 $= 181.56 \text{ kN/m} + 17.33 \text{ kN/m} = 198.9 \text{ kN/m}$.
- $M = 453.91 \text{ kN/m}^2 \times \frac{x^2}{2} + 216.6 \text{ kN/m}^2\text{m} \times \frac{x^2}{2} \times \frac{2}{3}x$
 $= 36.3 \text{ kN} \times \text{m/m} + 4.62 \text{ kN} \times \text{m/m} = 40.92 \text{ kN} \times \text{m/m}$.

The shear resistance from the concrete section is the same as for the heel:

- $629 \text{ kN/m} > 199 \text{ kN/m}$.
- Therefore, the section is adequate.

The moment resistance from the toe is the same as for the heel (same steel):

- $505.7 \text{ kN} \times \text{m/m} > 40.9 \text{ kN} \times \text{m/m}$.

Therefore, the steel is adequate.

Step 6: Summary of Seismic Evaluation

1. Using $k_h = 0.4$, all computed safety factors for external stability are less than one. Therefore, the wall will yield during the MCE.
2. The critical threshold acceleration is 0.2 g and the associated mode of failure is loss of bearing capacity and tilting of the wall. Large rotation (tilting) of the wall may result from the MCE, but the wall is not likely to collapse from overturning.
3. The moment capacity of the wall stem and heel is not adequate to resist the loads from the MCE.

Therefore, seismic retrofit is required. The retrofit strategy needs to address the structural integrity of the wall stem and heel.

Step 7: Design Seismic Evaluation of Retrofit Strategy

Two retrofit strategies are:

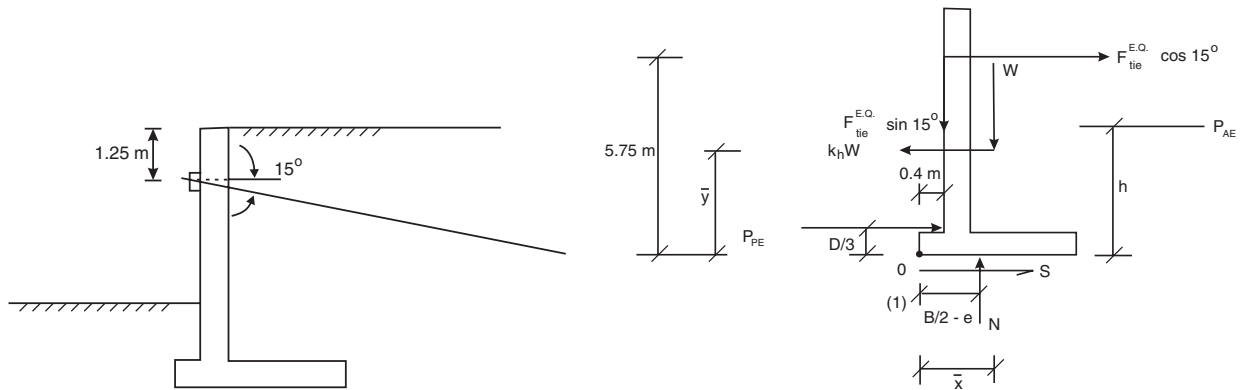
- Increase moment resistance of stem and/or heel; or,
- Decrease moment in stem and/or heel.

It will be difficult to increase the moment resistance at the heel of the wall, since it is buried and access is difficult. Decreasing the maximum moment in the stem and heel is a more readily obtainable objective. Placing a tie-back through the wall stem will serve to reduce moments in both the stem and heel.

The following calculations describe design of the tie-back retrofit strategy. The MCE is considered with a corresponding peak ground acceleration at the site of 0.4 g. First, the tie rod force required for equilibrium is computed and then external stability checks (including sliding and bearing capacity) are pursued.

Moments in the wall stem and heel are checked and, finally, design calculations in support of anchor system details are presented. Anchor system details include the anchor spacing, required total length of the anchor, the length of the bonded zone of the anchor, and transfer of the anchor loads to the wall face.

1. Add tie-back – will reduce moment in stem and heel of wall:



Note: Use e computed for static loading. Consider $F_{tie}^{E.Q.}$ to balance overturning moment from dynamic increment.

- Sum moments about pt. 0 and solve for F_{tie} .
- Sum forces in the horizontal direction and solve for F .
- Check to see if $F \approx N \tan \delta$:

$$\begin{aligned}
 W &= 501 \text{ kN}, \\
 N &= W = 501 \text{ kN}, \\
 \bar{x} &= 2.13\text{m}, \\
 \bar{y} &= 3.39\text{m}, \\
 \frac{B}{2} - e &= \frac{4}{2} - 0.429 = 1.57\text{m}, \\
 k_h &= 0.4g, \\
 K_{AE} &= 0.581, \\
 \Delta K &= 0.31, \\
 K_{AS} &= 0.271, \\
 K_{PE} &= 2.82.
 \end{aligned}$$

- $$h = \frac{K_{AS} \frac{H}{3} + \Delta K(0.6)H}{K_{AE}} = \frac{0.271 \left(\frac{7}{3} \right) + .31 \times (0.6)^7}{0.581} = 3.33\text{m} .$$

2. Sum moments w.r.t. 0 and solve for $F_{tie}^{E.Q.}$:

Force	Arm	Moment
1. $F_{tie}^{E.Q.} \cos 15^\circ$	5.75m	+ $F_{tie}^{E.Q.} (5.75)(.966)$
2. $W = 501 \text{ kN/m}$	$\bar{x} = 2.13 \text{ m}$	+ 1067 kN – m/m
3. $P_{PE} = \frac{1}{2} \gamma D^2 K_{PE} = 102 \text{ kN/m}$	$\frac{D}{3} = \frac{2}{3}(2) = 1.33 \text{ m}$	+ 136 kN x m/m
4. $P_{AE} = \frac{1}{2} \gamma H^2 K_{AE} = 258 \text{ kN/m}$	$h = 3.33 \text{ m}$	- 859 kN x m/m
5. $k_h W = 0.4 (501) = 200 \text{ kN/m}$	$\bar{y} = 3.39 \text{ m}$	- 679 kN x m/m
6. $N = 501 \text{ kN/m}$	$\frac{B}{2} - e = 1.57 \text{ m}$	- 787 kN x m/m
7. $F_{tie}^{E.Q.} \sin 15^\circ$	0.4m	+ $F_{tie}^{E.Q.} (.4)(.26)$

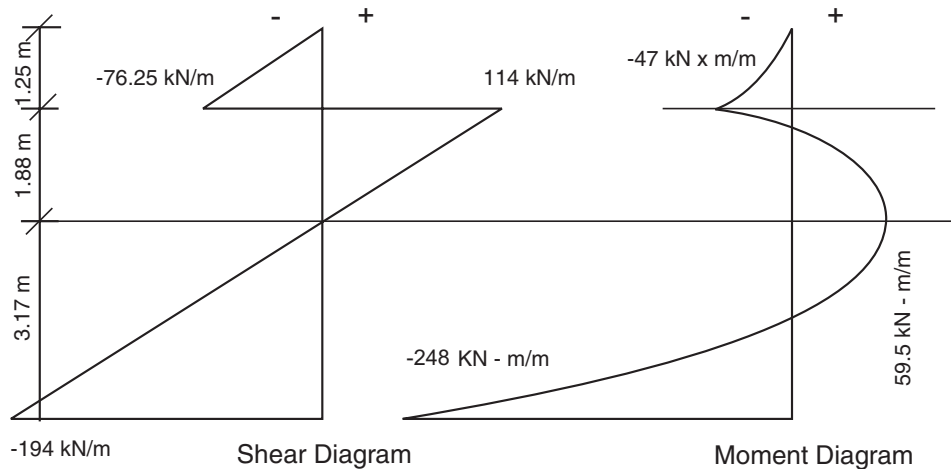
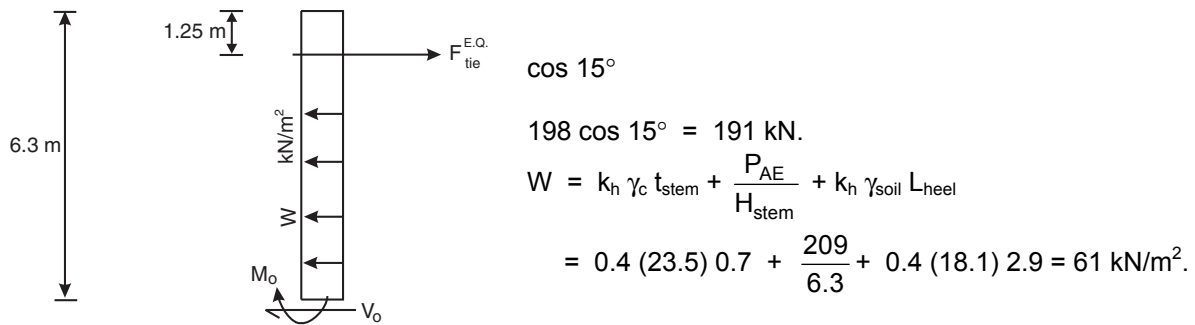
- $\Sigma M_o = 0 = 5.66 F_{tie}^{E.Q.} - 1122.$
- Therefore, $F_{tie}^{E.Q.} = \frac{1122}{5.66} = 198 \text{ kN/m}.$
- Solve for F.
- $\Sigma F_H = 0 = -P_{AE} - k_h W + P_{PE} + S + F_{tie}^{E.Q.} \cos 15^\circ.$
- Therefore, $F = -191 + 258 + 200 - 102 = 165 \text{ kN/m}.$
- Check $F_{max} = N(f) = 501 \times 0.58 = 291 \text{ kN/m}.$
- $F_{max} > F$ is OK.

3. Check bearing capacity with $F_{tie}^{E.Q.}$:

- $k_h = 0.4.$
- $F = 165 \text{ kN/m}.$
- $e = 0.429\text{m}.$
- $B' = 4 - 2(0.429) = 3.14\text{m}.$
- $N = 501 \text{ kN} + 195 \sin 15^\circ = 551 \text{ kN}.$
- Therefore, $n = \frac{F}{N \tan \phi} = \frac{165}{551 \tan 32} = 0.479.$

- $\frac{N_{qe}}{N_{qs}} = 0.33$; $N_{qe} = 23.18 \times 0.33 = 7.65$.
- $\frac{N_{\gamma E}}{N_{\gamma S}} = 0.15$; $N_{\gamma E} = 30.22 \times 0.15 = 4.53$.
- $q_{ult} = \gamma D N_{qE} + \frac{1}{2} (\gamma) B' N_{\gamma E} = 18.1 (2) 7.65 + \frac{1}{2} (18.1) (3.14) 4.53 = 405 \text{ MN/m}^2$.
- $q = \frac{N}{B'} = \frac{551}{3.14} = 175 \text{ kN/m}^2$.
- Therefore, $F_S^{B.C.} = \frac{405}{175} = 2.3$.

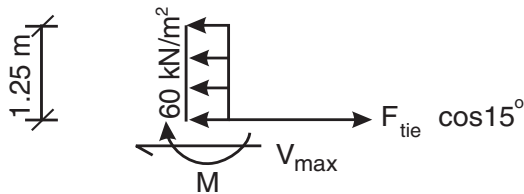
4. Check moment in wall stem with $F_{tie}^{E.Q.}$:



- $M_{min} = -248 \text{ kN x m/m}$ places back row of reinforcing steel in tension.
- $M_u = 500 \text{ kN x m/m}$.

- $M_u > 248$ OK.
- $M_{max} = 65 \text{ kN/m}$ (65 kN/m is placing tension on outside face of wall).
- On outside face, #6 bars are spaced 300 mm c-c.
- Cross sectional area of #6 bar = 284 mm².
- $A_s = 284 \frac{\text{mm}^2}{300\text{mm}} = 0.9466 \text{ mm}^2/\text{mm} = .00095 \text{ m}^2/\text{m}$.
- $M_u = \phi A_s f_y \left(d - \frac{0.59 A_s f_y}{f'_c (b)} \right)$ $d = .7 - .076 - .0095 = 0.623 \text{ m}$
 $= 1.0 (.00095) (414) \left(0.611 - \frac{.59 (.00095) 414}{28 (1\text{m})} \right) = 0.393 (0.603)$
 $= 0.237 \text{ MN} \times \text{m/m} = 237 \text{ kN} \times \text{m/m}$.
- $M_u > 65 \text{ kN/m}$ OK.

5. Check V_{max} (at 2 = 1.25 m):



$$V_{max} = F_{tie}^{E.Q.} \cos 15^\circ - 1.25 (60) = 191 - 75 = 116 \text{ kN/m.}$$

$$V_c = 0.17 \sqrt{f'_c} b d = 0.17 \sqrt{28} (1)(.7) = 629 \text{ kN/m.}$$

$$V_c > V_{max} \text{ OK .}$$

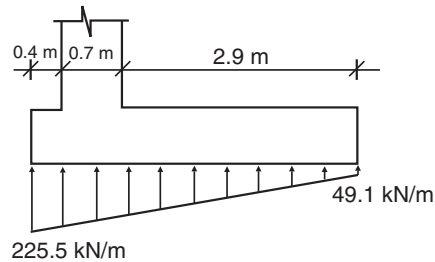
6. Check structural integrity of heel after retrofit:

- $q = q_1 + q_2 - q_3$.
 - $q_1 = 114.0 \text{ kN/m}^2$ (from soil above heel).
 - $q_2 = \gamma_c \times t = 23.5 \text{ kN/m}^3 \times 0.7 \text{ m} = 16.45 \text{ kN/m}^2$ (from mass of concrete slab).
 - $q_1 + q_2 = 130.45 \text{ kN/m}^2$.
 - Determine bearing pressures at heel and toe of wall foundation.
 - $q_{\frac{toe}{heel}} = \frac{F_v}{B} \left(1 \pm \frac{6e}{B} \right) = \frac{551 \text{ kN}}{4\text{m}} \left(1 \pm \frac{6 (0.429\text{m})}{4\text{m}} \right) = 225.46 \text{ kN/m}$ (at toe), 49.1 kN/m (at heel).
- $e = 0.429 \text{ m}$,
 $B = 4 \text{ m}$,
 $W = 501 \text{ kN}$,

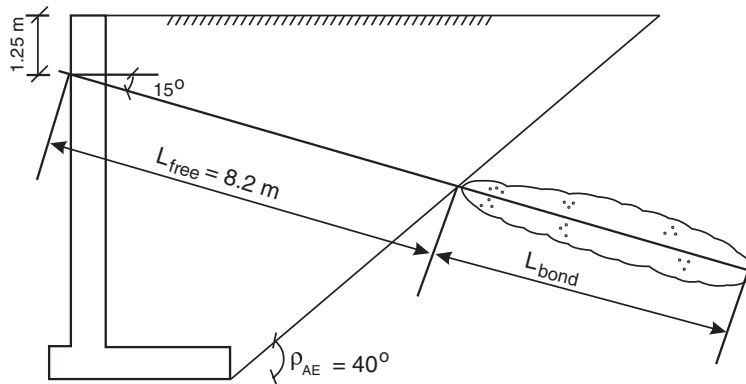
$$F_v = W + F_{tie}^{eq} \sin 15^\circ = 551 \text{ kN},$$

$$6e = 2.574 \text{ m}.$$

- $6e < B$ (equation 2-15) OK.
- Pressure distribution will then be as follows:



- This pressure distribution is practically the same as in the static case. Therefore, the steel in the heel and toe will be adequate for the retrofitted dynamic loading case.
- Geometry of grouted anchor.



$$\phi = 35^\circ,$$

$$k_h = 0.4,$$

$$K_{AE} = 0.581,$$

$$\rho_{AE} = 40^\circ,$$

$$i = \beta = k_v = \delta = 0.$$

- Find L_{bond} and required anchor size.
- Space anchors at 5m c-c.
- $F_{anchor} = 195 \text{ kN/m} \times 5 \text{ m} = 975 \text{ kN}$.
- According to PTI (1995) guidelines, $f_{all} = 0.6 F_u$. (AASHTO, 2002, Section 7, Division 1A, increases by 1.5 for earthquake loading).
- Therefore, $F_u = \frac{975}{0.6 \times 1.5} = 1083 \text{ kN}$.

- Use Dywidag grade 160 36mm diameter prestressing steel bars, $F_u = 1125 \text{ kN}$.

- Find $L_b = \frac{F_{\text{anchor}}}{\pi d \tau_w}$.

d = diameter of the drill hole - use 100 mm,

τ_w = working bond stress along the interface between soil and grout.

- PTI (1996): for pressure grouted anchor in medium coarse sand - medium density average ultimate soil/grout bond stress is $\approx 0.66 \text{ Mpa}$.

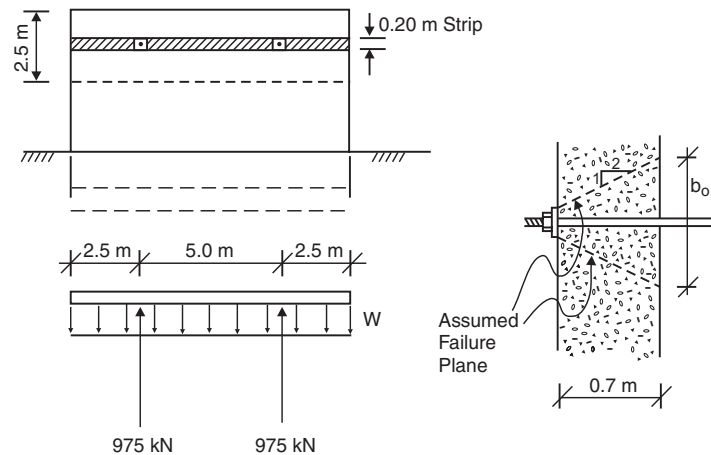
- Use a factor of safety = 2.0 (for proof testing).

- $\tau_w = \frac{0.66}{2} = 0.33 \text{ Mpa}$.

- $L_b = \frac{975 \text{ kN} \times 1000}{\pi(100\text{mm}) \cdot 33\text{MPa}} = 9.4\text{m}$.

- $L_{\text{total}} = L_{\text{free}} + L_b = 8.2 + 9.4 = 17.6\text{m}$.

7. Check wall structural integrity (in long dimension):



- Assume the line load, w , acts uniformly across this strip of the wall

$$w = \frac{975^{\text{kN}} + 975^{\text{kN}}}{2.5\text{m} + 5.0\text{m} + 2.5\text{m}} = 195 \text{ kN/m}.$$

- Maximum shear will occur at tie locations.

- $V = 195 \text{ kN/m} \times 2.5\text{m} = 488 \text{ kN}$.

- $M_{\text{max}} = 195 \text{ kN} \times \frac{2.5^2\text{m}}{2} = 609 \text{ kN} \times \text{m}$.

8. Check one-way shear:

- $v_c = 0.17\sqrt{f'_c} \times b \times d$ (see ACI 11-3).

$$\begin{aligned} f'_c &= 28 \text{ MN/m}^2, \\ b &= 2.5 \text{ m}, \\ d &= 0.7 \text{ m}. \end{aligned}$$

- Therefore $v_c = 0.17\sqrt{28} (2.5)(.7) = 1.57 \text{ MN} = 1570 \text{ kN} > 488 \text{ kN}$ OK.

9. Check two-way shear:

- $v_c = 0.34\sqrt{f'_c} b_o d$ (see ACI 11-37).

- Plate dimensions are 130 mm x 240 mm x 45 mm.

- $b_o = (.13\text{m} + 0.7\text{m})^2 + (.24 + .7\text{m})^2 = 3.54 \text{ m}$ (see ACI 11-12-13).

- $d = 0.7\text{m}$.

- $v_c = 0.34\sqrt{28} 3.54 \times .7 = 4.46 \text{ MN} = 4460 \text{ kN} > 975 \text{ kN}$.

10. Check bearing stress on plate:

- Plate hole $\approx 38 \text{ mm}$ diameter.

- $A_{\text{plate}} = .13\text{m} \times .24\text{m} - \pi \frac{(.038)^2}{4} = .03\text{m}^2 = .85 f'_c A_1 (2) = .85 (28 \text{ MPa}) .03 \text{ m}^2 (2) = 1.428 \text{ MN} >$

0.975 MN (see ACI 10-17, Design Bearing Strength).

11. Compute moment capacity of 2.5m strip of wall:

- $M_u = A_s f_y \left(d - \frac{0.59 A_s f_y}{f'_c b} \right)$.

- #6 bars @ 250mm; area of #6 = 284 mm².

- $A_s = 284 \text{ mm}^2 \times \frac{2500\text{mm}}{250\text{mm}} = 2840\text{mm}^2 = .00284\text{m}^2$.

- $f_y = 414 \text{ MN/m}^2$; $b = 2.5\text{m}$.

- $f'_c = 28 \text{ MN/m}^2$, $d = 0.7\text{m} - .076\text{m} - .025 = 0.6\text{m}$.

- $M_u = .00284 (414) \left[.6 - \frac{0.59(.00284) 414}{28(2.5)} \right] = 0.693 \text{ MN} \times \text{m} = 693 \text{ kN} \times \text{m} > 609 \text{ kN/m}$ OK.

CHAPTER 3: SLOPES, EMBANKMENTS, AND ROCKFALLS

3.1. INTRODUCTION

Earthquake-induced landslides and instability of slopes and embankments have caused extensive damage to highway systems in past earthquakes. This damage has resulted in deaths and significant monetary losses. Earthquake-induced landslides can block or undermine roads, impact and bury vehicles, and seriously inhibit post-earthquake relief efforts. For example, the January 17, 1994 Northridge, California earthquake triggered more than 11,000 landslides (Harp and Jibson, 1995), many of which affected the local highway systems. Rockfalls inundated roadways and landslides, slumps, and blockslides cut off access to many mountain areas for several days following the earthquake.

This section describes procedures for classifying, screening, and evaluating the performance of embankments and slopes that support or are adjacent to highway structures during earthquake loading (figure 3-1). It also describes retrofitting strategies and methods to repair or mitigate the effects of earthquake shaking.

The effects of earthquakes on highway systems include the following phenomena:

- Liquefaction and lateral spreading of subgrade soils beneath a natural slope or a highway embankment that may lead to slope failure.
- Permanent deformations of man-made embankments/natural slopes supporting or adjacent to highway structures that may lead to cracking or failure of roadway pavements.
- Reactivation of old, existing landslides due to earthquake shaking.
- Earthquake-induced rockfalls on nearby slopes that may block or disrupt roadway traffic.

3.2. CLASSIFICATION

For the purposes of screening and evaluating the potential for hazards to highway structures from seismically induced slope instability, landslides, and rockfalls, it is useful to classify and characterize these features based on observed performance and experience during past earthquakes. Keefer (1984) and Keefer and Wilson (1989) have examined earthquake-induced landsliding and slope failures from more than 40 case histories and classified them into 14 types on the basis of topography, material type, and velocity of movement. They further subdivided these landslide types into three categories, as shown in table 3-1.

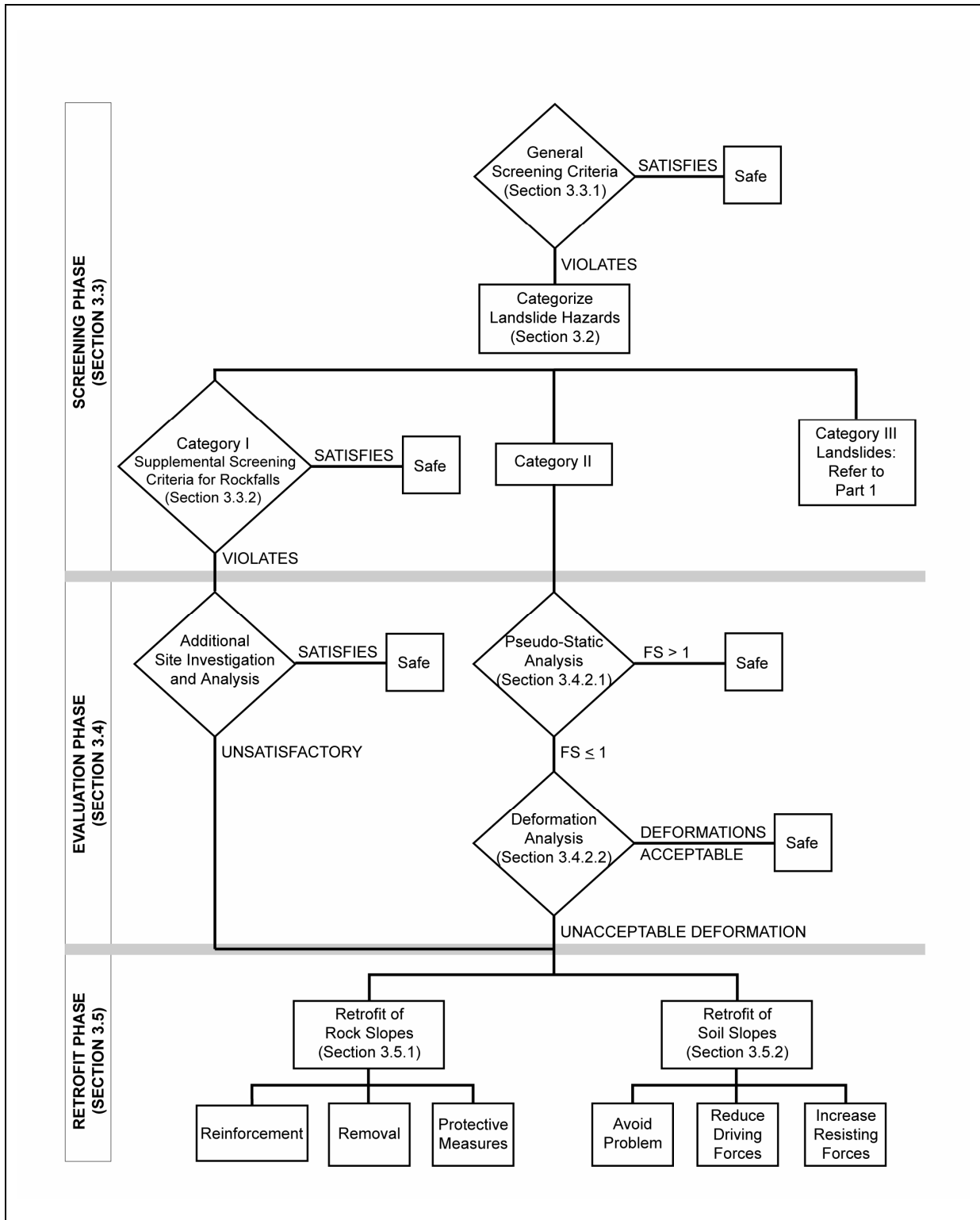


Figure 3-1. Flowchart for screening, evaluating, and retrofitting embankments and slopes adjacent to highway structures.

Table 3-1. Characteristics of earthquake-induced landslides.

Type of Movement	Internal Disruption ¹	Water Content ²	Velocity ³	Depth ⁴
Category I (failure mechanism)	Falls, disrupted slides, and avalanches: highly to very highly disrupted internally, fast-moving, generally shallow, dislodged from steep slopes			
Rock Falls (bounding, rolling, free falling)	High or very high	D-W	Extremely rapid	Shallow
Rock Slides (translational sliding on basal shear surface)	High	D-W	Rapid to extremely rapid	Shallow
Rock Avalanche (complex, involving sliding and/or flow as stream of rock fragments)	Very high	D-W	Extremely rapid	Deep
Soil Falls (bouncing, rolling, free falling)	High	D-W	Extremely rapid	Shallow
Soil Slides (translational sliding on basal shear surface or zone of weakened, sensitive clay)	High	D-W	Moderate to rapid	Shallow
Soil Avalanches (translational sliding; subsidiary flow)	Very high	D-W	Very rapid to extremely rapid	Shallow
Category II (failure mechanism)	Slumps, block slides, and slow earth flows: relatively coherent slides, slower moving than Category I landslides, generally deep-seated, dislodged from moderate to steep slopes			
Rock slumps (sliding on basal shear surface: component of headward rotation)	Slight to moderate	M-W	Slow to rapid	Deep
Rock Block Slides (translational sliding on basal shear surface)	Slight to moderate	M-W	Slow to rapid	Deep
Soil Slumps (sliding on basal shear surface; component of headward rotation)	Slight or moderate	D-W	Slow to rapid	Deep
Soil Block Slides (translational sliding on basal shear surface)	Slight or moderate	D-W	Slow to very rapid	Deep
Slow Earth Flows (translational sliding on basal shear surface; minor internal flow)	Slight	W-VW	Very slow to moderate with very rapid surges	Variable

(Continued)

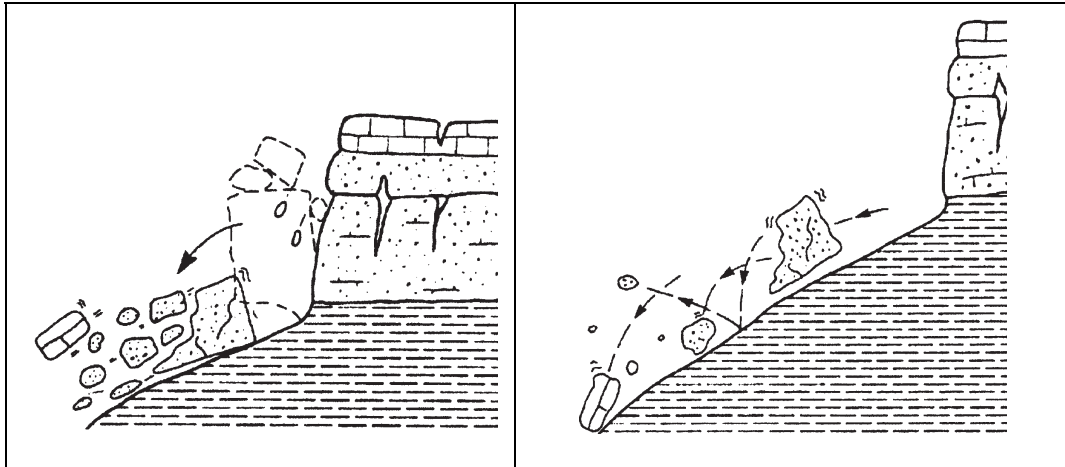
Table 3-1. Characteristics of earthquake-induced landslides (continued).

Type of Movement	Internal Disruption ¹	Water Content ²	Velocity ³	Depth ⁴
Category III (failure mechanism)	Lateral spread and flows: landslides involving significant component of fluid flow, fast-moving, dislodged from gentle to moderately steep slopes			
Soil Lateral Spreads (translational on basal zone of liquefied gravel, sand, silt, or weakened sensitive clay)	Generally moderate occasionally slight or high	W	Very rapid	Variable
Rapid Soil Flows (flow)	Very high	D-W	Very rapid to extremely rapid	Shallow
Subaqueous Landslide (translational on basal zone of liquefied gravel, sand, silt, or weakened, sensitive, clay)	Generally high or very high; occasionally moderate	W-VW	Rapid to extremely rapid	Shallow
Notes: 1. Internal Disruption: <i>Slight</i> , landslide consisting of one or a few coherent blocks; <i>moderate</i> , landslide consisting of several coherent blocks; <i>high</i> , landslide consisting of numerous small blocks and individual soil grains and rock fragments; <i>very high</i> , landslide almost completely disaggregate into individual soil grains or small rock fragments. 2. Water Content: D= <i>Dry</i> , no visible moisture; M= <i>moist</i> , some water but no free water and may behave as a plastic solid but not a liquid; W= <i>wet</i> , contains enough water to act in part as a liquid, has water flowing from it, or supports significant bodies of standing water; VW= <i>very wet</i> , contains enough water to flow as a liquid under low gradients (terms from Varnes, 1978). 3. Velocity: <i>Extremely slow</i> , less than 0.6 m/yr; <i>very slow</i> , between 0.6 and 1.5 m/yr; <i>slow</i> , between 1.5 m/yr and 1.5 m/mo; <i>moderate</i> , between 1.5 m/mo and 1.5 m/d; <i>rapid</i> , between 1.5 m/d and 0.4 m/min; <i>very rapid</i> , between 0.3 m/min and 3 m/s; <i>extremely rapid</i> , more than 3 m/s (terms from Varnes, 1978). 4. Depth: <i>Shallow</i> , generally less than 3 m; <i>deep</i> , generally more than 3 m.				

after Keefer, 1984, and Keefer and Wilson, 1989

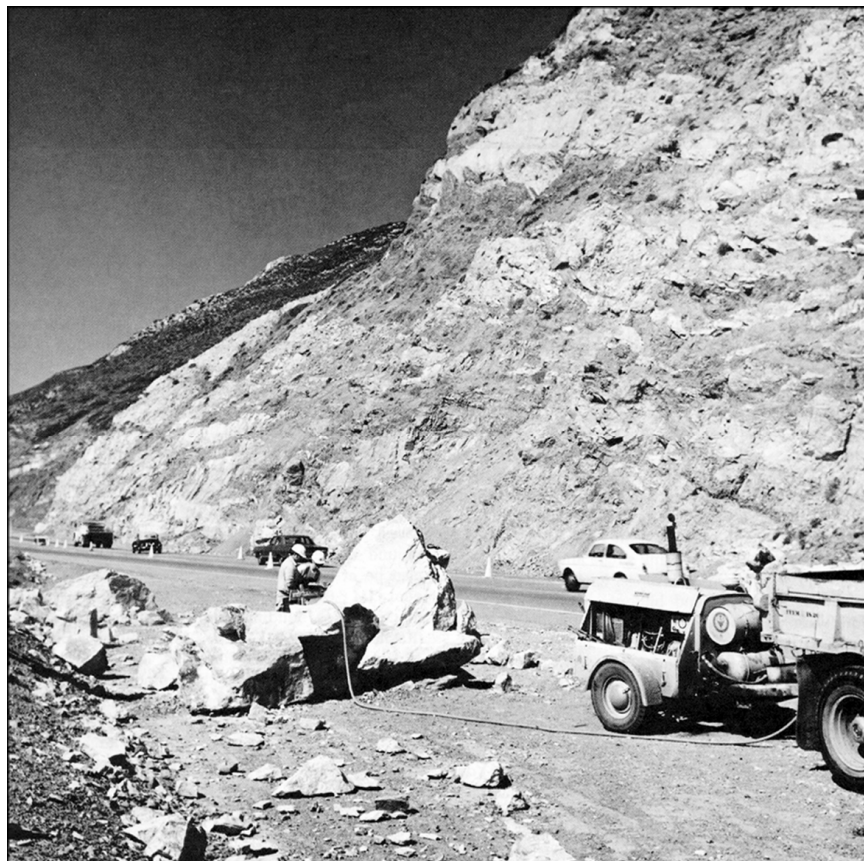
Category I Landslides include rock and soil falls, toppling failures, slides, and avalanches and are generally the most widespread. These are characterized by highly disrupted masses and generally shallow failure surfaces and are fast moving and dislodged from steep slopes.

Rockfalls and rock slides (figure 3-2) are either boulders or disrupted masses of rock that descend down the slope by bounding, rolling, or free fall. Rock properties associated with these failures are: strength of cementation, degree of weathering, and fracture spacing. An example of rockfalls along the Pacific Coast Highway, California, caused by the 1973 Point Mugu earthquake is shown in figure 3-3. Rock avalanches are associated with features such as: closely spaced fractures, moderate or intense weathering, planes of weakness, weak cementation, and evidence of previous failures. Rock falls are the most abundant landslides and the third leading cause of landslide-related deaths in historical earthquakes.



Hansen and Franks, 1991

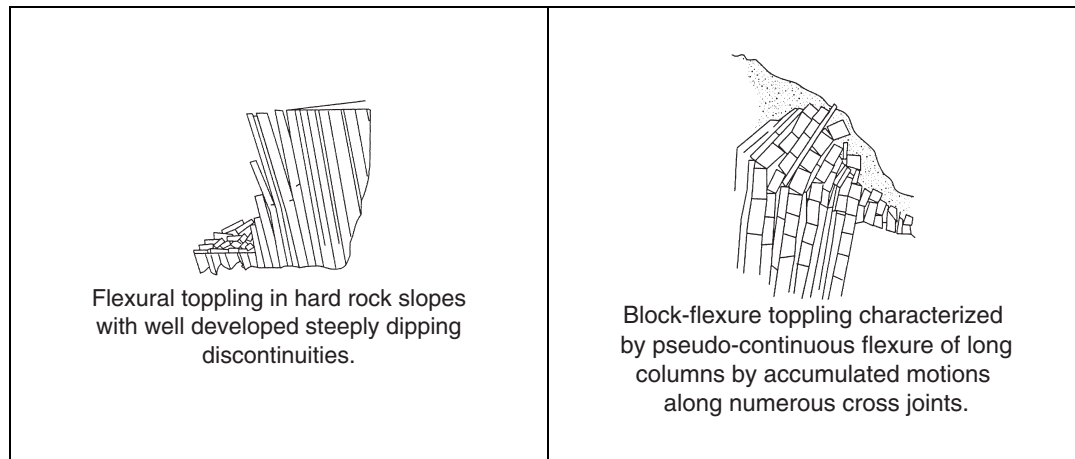
Figure 3-2. Rock fall mechanism and resulting hazard.



Wilson and Keefer, 1985

Figure 3-3. Rock falls along the Pacific Coast highway caused by the 1973 Point Mugu earthquake.

Toppling failures occur when the center of gravity of a rock mass extends beyond its base and causes it to topple over (figure 3-4). Toppling most commonly occurs in columnar rock masses in which the fractures dip steeply into the face of the slope. Columnar basalts and rocks with well-developed bedding or foliation planes are typically susceptible to this mode of failure.



Hoek and Bray, 1981

Figure 3-4. Examples of toppling failures.

Soil slides and soil avalanches are highly disrupted masses that occur in silty or sandy natural soils and poorly compacted fills of low plasticity, or in lightly cemented, weathered, and highly fractured soft rock on generally steep slopes. Examples of this type of landslide are shown in figure 3-5. Hundreds of similar landslides in loose silty and sandy soils were triggered by the 1971 San Fernando earthquake.

Category II Landslides include rock and soil slumps, block slides, and slow earth flows. These are coherent sliding masses that move on bounding basal shear surfaces (figure 3-6). They are slow moving and located on generally deep-seated failure surfaces, occurring mainly on relatively steep slopes. An example of a large block slide in Anchorage, Alaska that occurred during the 1964 earthquake is shown in figure 3-7.

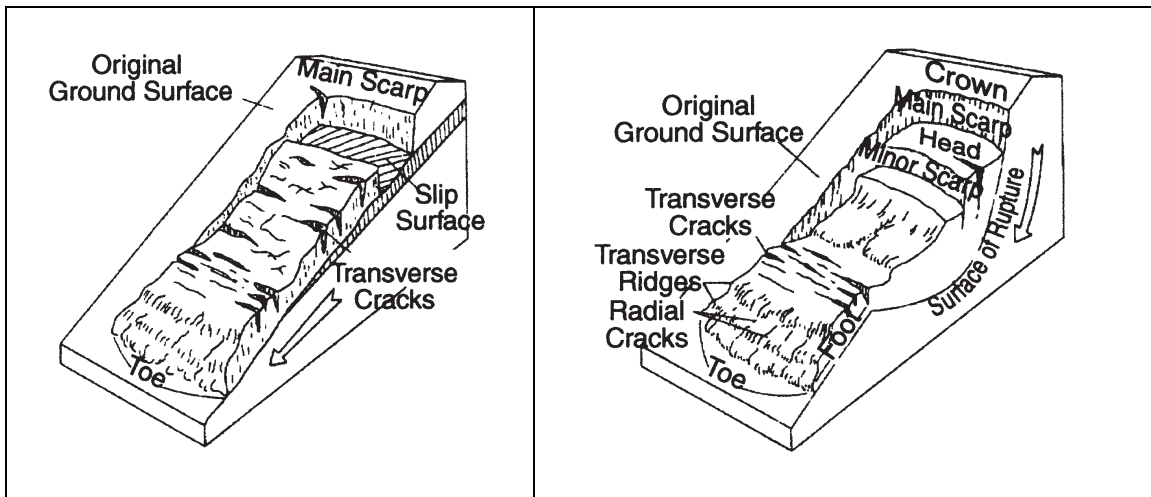
Soil block slides consist of one or a few coherent blocks that slide in a translational manner, exhibiting little or no rotation. Most have grabens at their heads and pressure ridges at their toes. Similar landslides, in somewhat different geologic environments, have been triggered by several southern California earthquakes, including the 1940 Imperial Valley, the 1952 Kern County, the 1966 Parkfield, and the 1971 San Fernando.

Rock slumps and rock slides (see figure 3-8) are most often associated with weakly cemented sedimentary rocks or involve indurated rocks that are intensely weathered, closely fractured, weak, and interbedded with soft material. Many move on a weak bedding plane.



Wilson and Keefer, 1985; photograph taken from Harp et al., 1981

Figure 3-5. Aerial view of coalescing disrupted soil slides caused by the 1976 Guatemala earthquake. Slides stripped away vegetation and sheets of sandy residual soil, generally less than 0.6 m thick, exposing white pumice bedrock. Slopes in the foreground are approximately 30 m high.



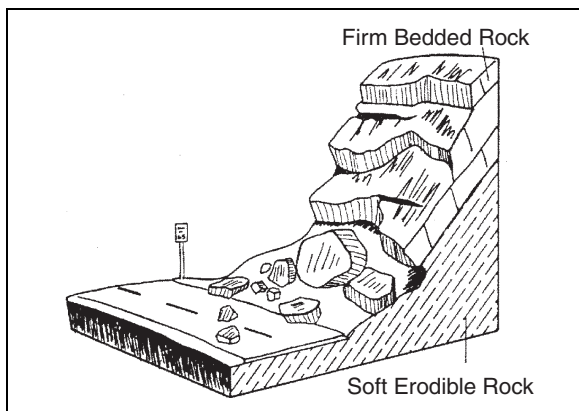
Hansen and Franks, 1991

Figure 3-6. Examples of landslides with discrete basal shear surfaces.



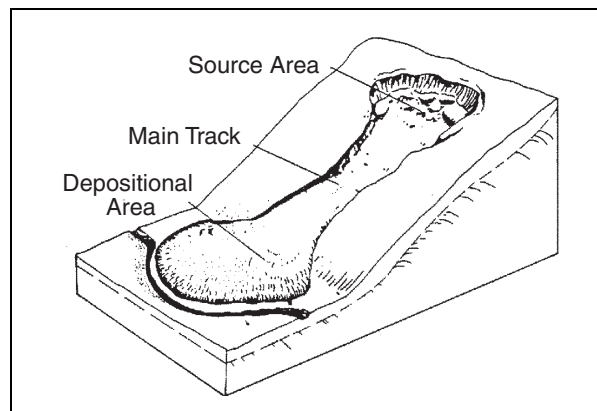
Wilson and Keefer, 1985; courtesy of the U.S. Army

Figure 3-7. Aerial view of the Native Hospital slide, a large soil block slide in Anchorage, Alaska, caused by the 1964 earthquake.



Hansen and Franks, 1991

Figure 3-8. Rock slump failure mechanism.



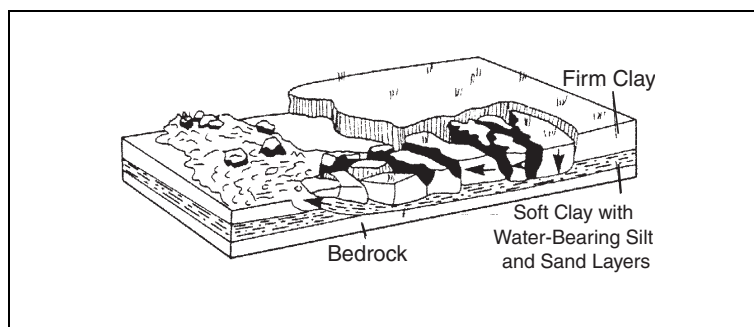
Hansen and Franks, 1991

Figure 3-9. Soil slump failure mechanism.

Soil slumps, soil block slides, and slow soil flows (figure 3-9) are deep-seated rotational failures that occur in natural deposits in alluvial or coastal flood plains. They occur along locally steep free faces such as stream and canal banks. They also occur in gentle to moderately steep hillslopes with shallow or perched water tables.

The most common material involved in earthquake-induced soil slumps is man-made fill (Keefer and Wilson, 1989). Most fills that fail are loose and poorly compacted or are placed on soft foundations such as river channel or marsh deposits. The density and quality of compaction and the foundation conditions are probably more important than the composition of the fill in determining its susceptibility to failure.

Category III Landslides include soil lateral spreads (figure 3-10) and rapid soil flows. These landslides include a significant component of fluid flow, are fast moving, and usually occur on gentle to moderately steep slopes. They are typically initiated as a result of soil liquefaction caused by earthquake-induced buildup of pore pressure in saturated cohesionless deposits, loss of strength in sensitive clays, and poorly constructed man-made fills. These types of failures are addressed in detail in Part 1 of this manual.



Hansen and Franks, 1991

Figure 3-10. Lateral spread failure mechanism.

According to the results of the study by Wilson and Keefer (1985), materials that are most susceptible to earthquake-induced landslides and the predominant types of landslides in each material are as follows:

- Weakly cemented, weathered, or intensely fractured rocks: these are susceptible to rockfalls, slides, avalanches, slumps, and block slides.
- More indurated rocks where predominant discontinuities dip out of slopes: these materials are susceptible to rockfalls and slides, block slides, avalanches, and possibly slumps.
- Loose unsaturated sands: these are susceptible to disrupted soil slides and soil avalanches.
- Loose, partly to completely saturated sand, silt, or loess: these are susceptible to soil slumps, block slides, lateral spreads, subaqueous landslides, and rapid soil flows.
- Saturated soils containing sand and gravel layers alternating with sensitive clay: these are susceptible to disrupted soil slides, soil avalanches, and rapid soil flows.

- Granular soils that are slightly cemented or contain a clay binder: these are susceptible to soil falls.
- Uncompacted or poorly compacted man-made fills containing little or no clay: these are susceptible to soil slumps, block slides, lateral spreads, and rapid soil flows.

3.3. SCREENING PROCEDURES

The potential for landsliding or downslope movement in slopes and embankments is dependent on slope geometry (i.e., slope height and steepness); subsurface soil, rock, and groundwater conditions; past embankment or slope performance; and level and duration of earthquake ground shaking. The procedures for screening involve reviewing geologic and topographic maps, reviewing available data on the subsurface conditions, and performing a reconnaissance of the site and adjacent areas. A review of available aerial photographs is desirable. In some areas, governmental agencies have prepared slope stability maps showing existing landslides and/or areas of relative slope instability; these should be reviewed if available. If appropriate, geologists and engineers in government agencies knowledgeable in the performance of natural slopes in the area should be contacted.

The following general guidelines may be used as screens to delineate highway segments susceptible to seismically induced ground instability. More detailed guidance for delineating areas susceptible to slope instability is given in the Transportation Research Board (TRB) Special Report 247, *Landslides Investigation and Mitigation*, edited by Turner and Schuster (1996).

3.3.1. PRELIMINARY SCREENING PROCEDURES

It can be assumed that a significant hazard due to earthquake-induced landsliding does not exist at a particular site if all of the following criteria are satisfied:

- The site is not located on, above, or below a slope that displays cracking or other signs of actual or incipient slope movement. There is not an obvious hazard to the site from falling rocks or shallow soil flows on slopes located above the site.
- The site is not located within a preexisting active or ancient landslide, and there are no landslides on slopes of similar geometry and geology in the site vicinity.
- The site is not located on or adjacent to a slope with geometric, geologic, and groundwater conditions known to be susceptible to landslides. This criterion should be evaluated based on both local experience and worldwide observations of conditions known to be especially susceptible to earthquake-induced landslides. Based on a United States Geological Survey (USGS) review of case histories of earthquake-induced landslides in the Los Angeles region, Wilson and Keefer (1985) compiled a profile of the general types of geologic environments and characteristics most likely to produce landslides during future earthquakes. These

characteristics are shown in table 3-2 and may generally be applied to other regions with similar seismic and geologic environments.

- The site is not located in a zone that has been mapped as having a moderate or high landslide potential (seismic or static). This criterion utilizes regional maps of observed or postulated landslides that are triggered under static and/or seismic conditions. Seismic slope stability maps based on stability analyses and past seismic performance are available for several areas of the country including: San Francisco Bay Area, California (Wieczorek et al., 1985 and Manson et al., 1990); Los Angeles area, California (Jibson and others, 1998; Harp and Jibson, 1995; and Wilson and Keefer, 1985); urban corridor of Utah (Keaton et al., 1987a and Keaton et al., 1987b); and others. Currently, the California Geological Survey (formerly the California Division of Mines and Geology) is developing seismic slope stability maps that can be accessed by computer on the Internet at www.consrv.ca.gov. Other static and seismic landslide hazard maps may also be used for screening purposes.
- The site is not located on embankments constructed of poorly compacted soils that exhibit signs of settlement and cracking, or on embankments underlain by poor foundation soils.
- The site is not located on potentially liquefiable soils or sensitive clays that could lose significant strength during earthquake shaking.
- The site does not show surface manifestations of the presence of subsurface water (springs and seeps), or potential pathways or sources of concentrated water infiltration on or upslope of the site.
- Judgments from experts familiar with local conditions conclude that an earthquake-induced landsliding hazard is unlikely to exist at the site.

If preliminary screening procedures listed above indicate a potential for landsliding or slope instability at a particular site, then, depending on the importance of the slope and the consequences of failure, an evaluation of its seismic stability should be performed using procedures that are described in section 3.4.

3.3.2. SUPPLEMENTAL SCREENING CRITERIA FOR ROCKFALLS

In addition to the screening criteria provided above, alternate procedures may be used to screen sites for susceptibility to rockfalls. Harp and Noble (1993) developed a rock classification system to evaluate the susceptibility of rockfalls to seismic loading. They modified an engineering classification originally used in tunnel design, known as the rock mass quality designation (Q), for use in rating the susceptibility of rock slopes to seismically induced failure. Based on analysis of Q-value and rockfall concentrations during the 1980 earthquake sequence near Mammoth Lakes, California, they defined a “well-constrained” upperbound relationship that shows that the number of rockfalls for a site decreases rapidly with increasing Q. Using a probability density function, they modeled the decay of number of rockfalls per site versus Q.

Table 3-2. Geologic environments likely to produce earthquake-induced landslides in the Los Angeles region.

Landslide Type	Type of Material	Minimum Slope Inclination in Degrees	Remarks
Rock Falls	Rocks weakly cemented, intensely fractured, or weathered; contain conspicuous planes of weakness dipping out of slope or contain boulders in a weak matrix.	40	Particularly common near ridge crests and on spurs, ledges, artificially cut slopes, and slopes undercut by active erosion.
Rock Slides	(See description above).	35	Occasionally reactivate preexisting rock slide deposits. Particularly common in hillside flutes and channels, on artificially cut slopes, and on slopes undercut by active erosion.
Rock Avalanches	Rocks intensely fractured and exhibiting one of the following properties: significant weathering, planes of weakness dipping out of slope, weak cementation, or evidence of previous landsliding.	25	Restricted to slopes of >150 m relief that are undercut by active erosion.
Rock Slumps	Intensely fractured rocks, preexisting rock slump deposits, shale, and other rocks containing layers of weakly cemented or intensely weathered material.	15	
Rock Block Slides	Rocks having conspicuous bedding planes or similar planes of weakness dipping out of slopes.	15	
Soil Falls	Granular soils that are slightly cemented or contain clay binder.	40	Particularly common on stream banks, terrace faces, coastal bluffs, and artificially cut slopes.
Disrupted Soil Slides	Loose, unsaturated sands.	15	
Soil Avalanches	(See description above).	25	Occasionally reactivate preexisting soil avalanche deposits.
Soil Slumps	Loose, partly to completely saturated sand or silt; uncompacted or poorly compacted man-made fill composed of sand, silt, or clay; preexisting soil slump deposits.	10	Particular common embankments built on soft, saturated foundation materials, in hillside cut-and-fill areas, and on river and coastal flood plains.

(Continued)

Table 3-2. Geologic environments likely to produce earthquake-induced landslides in the Los Angeles region (continued).

Landslide Type	Type of Material	Minimum Slope Inclination in Degrees	Remarks
Soil Block Slides	Loose, partly or completely saturated sand or silt; uncompacted or slightly compacted man-made fill composed of sand or silt; bluffs containing horizontal or subhorizontal layers of loose, saturated sand or silt.	5	Particularly common in areas of preexisting landslides along river and coastal flood plains, and on embankments built on soft, saturated foundation materials.
Slow Earth Flows	Stiff, partly or completely saturated clay and preexisting earth-flow deposits.	10	
Soil Lateral Spreads	Loose, partly or completely saturated silt or sand; uncompacted or slightly compacted man-made fill composed of sand.	0.3	Particularly common on river and coastal flood plains, embankments built on soft, saturated foundation materials, delta margins, sand dunes, sand spits, alluvial fans, lakeshores, and beaches.
Rapid Soil Flows	Saturated, uncompacted or slightly compacted man-made fill composed of sand or sandy silt (including hydraulic-fill earth dams and tailings dams); loose, saturated granular soils.	2.3	
Subaqueous Landslides	Loose, saturated granular soils.	0.5	Particularly common on delta margins.

Notes:

Soil lateral spreads can generally occur on gently sloping ground underlain by liquefied soil. They require earthquake inertia forces to induce liquefaction and temporary instability that result in successive down slope movement during earthquake shaking. Rapid soil flows and flow slides, on the other hand, generally occur in liquefied materials located on steeper slopes or in dams and embankments. Flow movements occur when the gravitational forces acting on a ground slope exceed the strength of the liquefied material within the slope.

Wilson and Keefer, 1985

They developed a seismic rockfall susceptibility index, Q_{RF} , that is calculated with the following equation:

$$Q_{RF} = \left[\frac{115 - 3.3J_v}{J_n} \right] \left[\frac{J_r}{J_a} \right] \left[\frac{1}{AF} \right] \quad (3-1)$$

where:

Q_{RF} is the seismic rockfall susceptibility index,
 J_v is the total number of joints per cubic meter,
 J_n is the joint set number,
 J_r is the joint roughness number,
 J_a is the joint alteration number, and
AF is the aperture factor.

For site-specific screening of rockfall susceptibility using the rockfall susceptibility index, the parameters listed above should be estimated based on field observations by a geologist knowledgeable in rock mechanics. Values for the parameters J_n , J_r , J_a , and AF should be chosen from tables 3-3 through 3-5 based on observed field conditions. The total number of joints per cubic meter, J_v , is measured in the field by adding the number of joints for each joint set. If each of the three orthogonal directions is exposed, J_v is the sum of the joints per meter in each direction. According to Harp and Noble (1993), the aperture factor, which quantifies the openness of rock fractures, is the most significant indicator of earthquake-induced rockfall susceptibility. While this characteristic is not particularly significant for static stability, earthquake vibratory loadings induce relative movement between rock fragments that lead to rocks breaking loose and falling.

Using the model and empirical data from the Mammoth Lakes earthquake sequence, they established four categories of rockfall susceptibility based on percentages of observed rockfalls within areas of different ranges of Q_{RF} . The categories are as follows:

Category A:	$Q_{RF} \leq 1.41$	highly susceptible.
Category B:	$= 1.41 - 2.83$	susceptible.
Category C:	$= 2.83 - 3.87$	moderately stable.
Category D:	≥ 3.87	mostly stable.

Generally, rockfall susceptibility can be screened out for sites classified as Category C and D. However, the above relationship was established for magnitude 6.0 earthquakes, which had peak ground accelerations (in the zone of strong shaking) of about 0.3 g to 0.5 g, and did not account for the effects of the distance from the seismic source on rockfall concentrations. For other earthquakes, however, distance from the seismic source and earthquake magnitude would affect the concentration of rockfalls and have to be accounted for in the analysis. These categories are used only in a preliminary screening analysis. Since measurement and assessment of factors required to calculate Q_{RF} values can be done rapidly, many sites can be evaluated quickly. Q_{RF} values are then used in a preliminary analysis to decide whether a site located near or below rock slopes is unsafe, needs further study, or is relatively safe from seismically induced rockfall hazards.

In addition to the rockfall susceptibility index, the rockfall hazard rating system developed by the Federal Highway Administration (Pierson and Van Vickle, 1993) may be used for rockfall screening. This system was designed to help highway agencies prioritize their rockfall hazard mitigation projects based on factors such as slope and highway geometry, risk to motorists, geologic conditions, past occurrence of rockfalls, and effectiveness of present rockfall mitigation measures. Sites with potential rockfall hazards are prioritized based on a point system. Local

Table 3-3. Description and ratings for the parameters RQD, J_n and J_r .

Rock Quality, $Q = (RQD/J_n) \times (J_r/J_a) \times (J_w/SRF)$	
1. Rock Quality Designation (RQD) ¹	Notes:
A. Very Poor 0-25	(i) Where RQD is reported or measured as ≤ 10 (including 0) a nominal value of 10 is used to evaluate Q in equation 1.
B. Poor 25-50	(ii) RQD intervals of 5, i.e., 100, 95, 90, etc. are sufficiently accurate.
C. Fair 50-75	
D. Good 75-90	
E. Excellent 90-100	
2. Joint Set Number (J_n)	Note:
A. Massive, no or few 0.5-1.0	(i) For intersections ($3.0 \times J_n$).
B. One joint set 2	
C. One joint set plus random 3	
D. Two joint sets 4	
E. Two joint sets plus random 6	
F. Three joint sets 9	
G. Three joint sets plus random 12	
H. Four or more joint sets, random, heavily jointed, "sugar cube," etc. 15	
I. Crushed rock, earthlike 20	
3. Joint Roughness Number (J_r)	Notes:
(a) Rock wall contact and	(i) Add 1.0 if the mean spacing of the relevant joint set is greater than 3 m.
(b) Rock wall contact before 10cm shear	(ii) $J_r = 0.5$ can be used for planar slickensided joints having lineations, provided the lineations are favorably orientated.
A. Discontinuous joints 4	
B. Rough or irregular, undulating 3	
C. Smooth, undulating 2	
D. Slickensided, undulating 1.5	
E. Rough or irregular, planar 1.5	
F. Smooth, planar 1.0	
G. Slickensided, planar 0.5	
(c) No rock wall contact when sheared	
H. Zone containing clay minerals thick enough to prevent rock wall contact 1.0 (nominal)	
I. Sandy, gravelly or crushed zone thick enough to prevent rock wall contact 1.0 (nominal)	
Note:	
¹ RQD is a core recovery ratio in which the lengths of all sound rock core pieces greater than 4 inches are summed and divided by the length of the core run.	

Barton et al., 1974

Table 3-4. Description and ratings for the parameter J_a .

1. Joint Alteration Number (a) Rock wall contact	(J_a)	Φ_r (approx.)	
A. Tightly healed, hard, non-softening, impermeable filling, i.e., quartz or epidote	0.75	(-)	Note: (i) Values of (Φ_r) are intended as an approximate guide to the mineralogical properties of the alteration products if present.
B. Unaltered joint walls, surface only	1.0	(25°-35°)	
C. Slightly altered joint walls, non-softening mineral coatings, sandy particles, clay-free disintegrated rock	2.0	(25°-30°)	
D. Silty- or sandy-clay coatings, small clay fraction (non-softening)	3.0	(20°-25°)	
E. Softening or low-friction clay mineral coatings, i.e., kaolinite, mica. Also chlorite, talc, gypsum and graphite, etc., and small quantities of swelling clays. (Discontinuous coatings, 1-2 mm or less in thickness)	4.0	(8°-16°)	

Barton et al., 1974

Table 3-5. Description and ratings for AF.

1. Aperture	AF	
A. All joints tight	1.0	Notes: (i) If perched or loose rocks are common, increase by one. (ii) If pervasive joints dip out of slope, increase by one.
B. Most joints tight, a few open as much as 2 cm	2.5	
C. Most joints tight, a few loose, open as much as 5 cm	5.0	
D. Significantly (20 percent) open, as much as 10 cm	7.5	
E. Greatly (60 percent) open, as much as 20 cm	10.0	
F. Gaping open, many joints open > 20 cm	15.0	

Harp and Noble, 1993; modified from Barton et al., 1974

seismicity and its effects on the occurrence and magnitude of rockfalls were not considered in this system. Nevertheless, the rockfall hazard rating system may be a useful tool for preliminary screening of rockfall hazards.

3.3.3. SUPPLEMENTAL CRITERIA FOR CATEGORY III LIQUEFACTION-INDUCED LANDSLIDES

Category III Landslides are primarily caused by soil liquefaction (or loss of strength in sensitive clays) induced by earthquake shaking. Section 3.2, Part 1 of this manual contains screening criteria for liquefiable sediments and procedures to evaluate potential for lateral spread and rapid soil flows.

3.4. EVALUATION PROCEDURES

When a potential for landsliding or slope instability is identified during the preliminary screening stage, detailed engineering analyses will be required to evaluate the potential for failure, instability, or downslope movement during a postulated seismic event. In situations where the hazard is judged to be so obvious and severe, the user can proceed directly from screening to retrofit design (eliminating further hazard evaluation, except as needed to design the retrofit).

3.4.1. EVALUATION OF CATEGORY I LANDSLIDES

Well-accepted evaluation procedures for Category I Landslides are not available. If the screening phase indicates a potential for Category I Landslides, additional site-specific seismic stability analyses should be conducted and engineering judgment exercised by individuals with expertise in rock mechanics and rock slope stability.

3.4.2. EVALUATION OF CATEGORY II LANDSLIDES

If the screening phase indicates a potential for Category II Landslides, slope stability analyses should be performed to evaluate the specific hazard. The general method for evaluating seismic stability of slopes and embankments involves both the pseudo-static and deformation analysis procedures. The evaluation is performed in the following sequence:

- Step 1: Perform a pseudo-static slope stability analysis. If the resulting factor of safety is greater than 1.0, no further evaluation or retrofit are necessary. If the factor of safety is less than 1, indicating potential deformations, continue to step 2, or step 2 may be bypassed and retrofitting may conservatively be recommended at this point.
- Step 2: Perform a deformation analysis. If the predicted deformations are acceptable, no further evaluation or retrofit is required. If the predicted deformations are unacceptable, retrofitting strategies should be considered.

3.4.2.1. Pseudo-Static Slope Stability Analysis Procedure

Pseudo-static slope stability analyses conservatively evaluate the potential for occurrence of a slope failure due to earthquake loading. If the results of the pseudo-static analysis indicate a factor of safety less than 1, then the potential for slope movement exists and a deformation analysis may be appropriate to quantify the down slope displacements.

3.4.2.1(a). Necessary Data for Analysis

Prior to performing engineering analyses to assess landslide potential, the data gathered in the screening stage should be supplemented if necessary. More detailed geologic reconnaissance and mapping may be needed. If preexisting landslides were identified at the site in the screening stage, subsurface investigations may be required to assess the slide geometry. Available geotechnical data should be reviewed to assess the engineering properties of the subsurface materials in the slope(s). If sufficient data are lacking, field and laboratory testing may be required. For slopes located in stiff, nonsensitive clays, dry sands, and dense saturated sands that do not liquefy or lose their strength during earthquake shaking, the stability of the slopes can be evaluated using pseudo-static analysis and/or deformation analysis procedures. Slopes on potentially liquefiable soil and sensitive clays can be evaluated using procedures described in Part 1 of this manual.

Several methods are available for determining the appropriate soil strength parameters to be used in pseudo-static and deformation analyses. In-situ and laboratory test methods should be used that measure strengths applicable to short-term loading and, in the case of soils below the water table, undrained conditions. In-situ strength parameters are commonly estimated from unconfined compression, unconsolidated undrained triaxial and consolidated undrained triaxial tests on “undisturbed” samples. Duncan et al. (1990) developed a procedure for evaluating undrained strength under conditions of rapid drawdown, which are similar to conditions during earthquake loading. This procedure incorporates the effects of anisotropic consolidation on the undrained strength, thus avoiding problems associated with estimating pore pressures induced by earthquake shaking. The U.S. Army Corps of Engineers (1970) recommends using a composite shear strength envelop that is constrained by the drained strength envelop at low confining pressures, and the undrained strength envelop at higher confining pressures. This approach provides a conservative strength interpretation compared to Duncan’s (1990) method.

Some engineering methodologies recommend increasing the undrained static shear strength of soils to account for the transient nature of seismic loading. However, soil strength does not always increase during earthquake shaking. When subjected to long durations of strong shaking, some soils decrease in strength due to the effects of pore water pressure buildup. Therefore, unless a reduction can be justified, static undrained strength should be used in pseudo-static analyses. Makdisi and Seed (1978) recommended that the static undrained strength of soft to medium stiff clays be reduced by 20 percent to account for strength loss during strong earthquake shaking.

Residual undrained shear strengths should be used to represent liquefiable sediments. A residual strength condition exists after large strains have occurred and additional shearing will not further decrease the strength or volume of the soil. Seed and Harder (1990) developed a correlation for

residual strength with equivalent clean sand SPT blowcounts , $(N_1)_{60-cs}$ (figure 3-11). The lower bound of the correlation shown in figure 3-11 is thought to be a conservative estimate of residual strength. A curve passing through the lower third of the range shown in figure 3-11 is considered a reasonable estimate to use in stability analyses. This lower-third residual strength is estimated based on the average corrected standard penetration blow counts for a particular stratum.

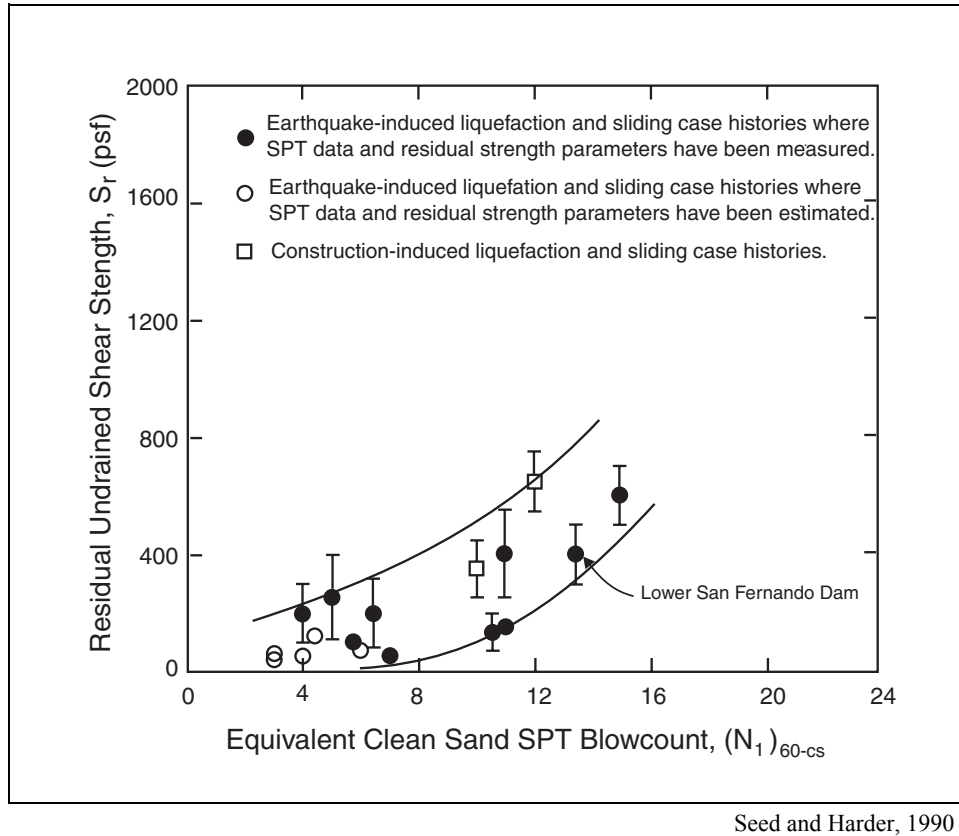


Figure 3-11. Relationship between corrected “clean sand” blowcount $(N_1)_{60-cs}$ and underdrained residual strength (S_r) from case studies.

3.4.2.1(b). Analysis Procedure

In pseudo-static slope stability analyses, inertial forces generated by the earthquake are represented by an equivalent static horizontal force (seismic coefficient) acting on the potential sliding mass. In this analysis, the seismic coefficient should generally be equal to the peak ground acceleration in the vicinity of the slope.

Recommendations for selecting an appropriate pseudo-static seismic coefficient were provided by Seed (1979) and Hynes and Franklin (1984). Both approaches were developed for embankment dams and were based on a level of acceptable deformation that would not compromise the integrity of the embankment. Using a limit of about 1 m (3.3 feet) as a criterion

for acceptable performance, Seed (1979) recommended using seismic coefficients of 0.1 and 0.15 (together with a factor of safety of 1.15) for earthquakes of magnitude 6.5 and 8.25, respectively. This recommendation was made for embankments composed of materials that do not lose more than 15 percent of their strength due to earthquake shaking and that are subjected to peak crest accelerations of less than 0.75 g.

Hynes and Franklin (1984) suggested using a pseudo-static seismic coefficient of one-half the peak acceleration at bedrock underlying the embankment. This recommendation was also based on limiting the permanent deformations to 1 m (3.3 feet), after accounting for amplification effects at the crest of the embankment. It is clear that the level of acceptable or tolerable deformations governs the selection of a seismic coefficient for use in pseudo-static stability analyses. While deformations of 1 m (3.3 feet) may be acceptable for evaluating the performance of earth and rockfill dams and embankments, structures or pavements supported on embankments or on natural or man-made slopes may not tolerate such levels of permanent deformations. Accordingly, the results of earthquake-induced deformations published by Makdisi and Seed (1978) were used to estimate values of the seismic coefficient (used together with a factor of safety of one) for various assumed levels of permanent displacements. Using the ratio of k_y/k_{max} (where k_y is the seismic coefficient resulting in a factor of safety of one, and k_{max} is the peak acceleration induced within a potential sliding mass), and the upper-bound deformations estimated by Makdisi and Seed (1978), values of the seismic coefficient were estimated and found to be a function of the specified permanent deformation and earthquake magnitude. For permanent deformations that usually are tolerated by structures (on the order of 2.5 to 5 cm (one to two inches)), the corresponding seismic coefficient is about 70 to 80 percent of the peak acceleration.

It is therefore recommended that, at the preliminary evaluation phase, a seismic coefficient equal to the peak acceleration induced within the potential sliding mass be conservatively used in the stability analysis. Using this approach, a computed factor of safety greater than one will ensure that estimated earthquake-induced slope deformations are limited to acceptable levels.

The peak or maximum acceleration, k_{max} , induced within a potential sliding mass (average of the peak accelerations over the mass) must be estimated. Often this value is assumed equal to the free-field ground surface acceleration, a_{max} . This neglects possible amplification of accelerations on a slope due to topographic effects, but also neglects decreases in acceleration due to reduction of ground motion with depth and spatial averaging over the sliding mass. A specific evaluation of k_{max} considering amplifying and reducing effects can always be made using dynamic response analysis or simplified methods. Simplified procedures for estimating the response of embankment dams were developed by Makdisi and Seed (1978, 1979). Their procedure provided estimates of the maximum crest acceleration and a distribution of the maximum average acceleration, k_{max} , with depth of sliding surface within the embankment. Ashford and Sitar (1994) performed two-dimensional dynamic response analyses of steep, weakly cemented sand slopes, using a generalized hyper-element method (Deng, 1991). The results of their analyses showed that the peak acceleration computed at the crest of the slope is amplified relative to the free-field ground motions beyond the crest of the slope. The amplification due to topographic effects was dependent on the slope geometry and the frequency content of the input motion. For the sites they analyzed, the computed peak accelerations at the crest of the slope

were, on average, about 50 percent higher than those estimated in the free-field beyond the crest of the slope. They also analyzed steep slopes comprised of soils or weathered rock overlying hard rock formations, and found that amplification of accelerations at the ground surface (beyond the crest of the slopes) due to site response effects were much greater than those due to topographic effects. Thus, Ashford and Sitar (1994) recommended an approach that incorporates site amplification effects by performing one-dimensional site response, and then accounting for topographic effects at the crest of the slope by increasing the peak value of the free-field response by 50 percent. The results of the two-dimensional response analyses showed that the estimated amplification using the Makdisi and Seed Simplified (one-dimensional) procedure for embankments is much higher than that computed for the steep slopes. Ashford and Sitar (1994) also developed curves of normalized k_{\max}/a_{\max} values for various depths of the sliding mass (similar to those of Makdisi and Seed, 1978). Their curves are of the same general shape, but cover a broader range than the profiles developed by Makdisi and Seed (1978). Their k_{\max}/a_{\max} relationship varied with the frequency content of the input motion and the slope angle. The steepest slopes provided the upper bound of the variation k_{\max}/a_{\max} with depth.

The approach to estimating the peak acceleration within a potential sliding mass is as follows: (a) For small slopes having generally uniform subsurface conditions, the free-field peak ground acceleration can be used as an average pseudo-static seismic coefficient. (b) For steep slopes of weathered rock or soil overlying hard rock formations, the approach of Ashford and Sitar (1994) could be used. (c) For sites with complex geometries and material properties, or for essential or critical facilities and structures, a site-specific two-dimensional dynamic response analysis is recommended to estimate k_{\max} . The induced acceleration is estimated in the transverse “down slope” direction of the embankment or slope. For embankment slopes, in addition to the simplified procedure of Makdisi and Seed (described above), an amplification curve developed by Harder (1991) based on recorded motions during several earthquakes (on the crests of embankment dams) can also be used in estimating k_{\max} .

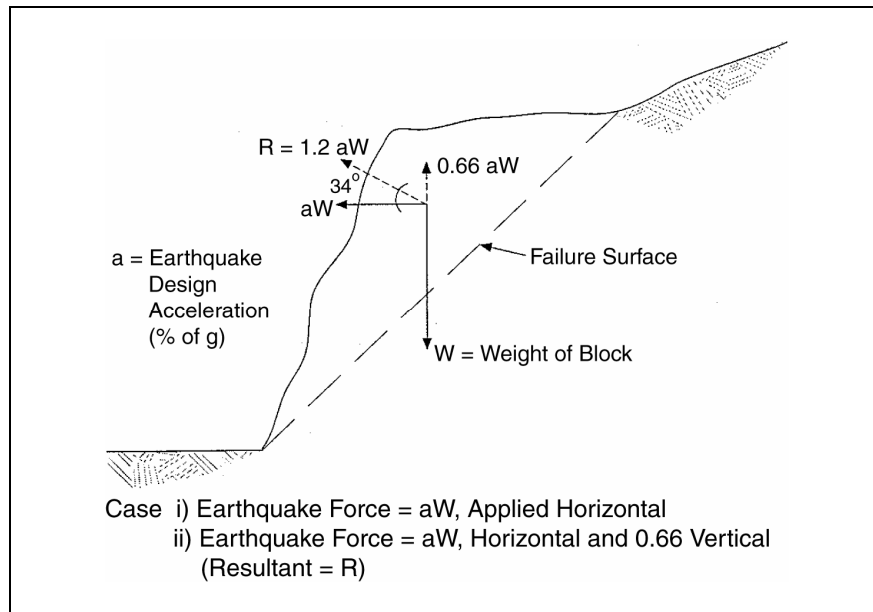
The factor of safety for a given seismic coefficient can be estimated using limit equilibrium slope stability methods. Methods of slope stability analyses for soil slopes are described in detail by Duncan (1996) in the Transportation Research Board, Special Publication 247, *Landslide Investigation and Mitigation*. Several computer programs capable of performing pseudo-static slope stability analyses are available commercially such as UTEXAS3 (Wright, 1991), SLOPE/W (GEO-SLOPE International Ltd., 1998), PCSTABLE (Siegel, 1975), or XSTABL (Sharma, 1997). Use of such computational aids is recommended considering the number of iterations required to locate the critical failure surface.

A computed factor of safety greater than one indicates that the slope is stable and further evaluations are not required. A computed factor of safety of less than one does not imply failure but indicates that the slope will yield and deformations can be expected. In this case, an estimate of the expected slope deformations should be made using the procedures described in section 3.4.2.2.

3.4.2.1(c). Special Considerations for Rock Slopes

The static and seismic stability of rock slopes is often primarily dependent on the orientation and characteristics of the rock bedding, jointing, and fractures rather than on the properties of the

intact rock. Characterization of the engineering properties of the rock mass may require detailed engineering geologic field assessments and laboratory testing. Norrish and Wyllie (1996) present methods for static analyses of rock slopes including kinematic analyses to account for adverse bedding, joints and potential wedge failure. The methods for seismic analysis are not as well developed, but generally consist of applying the pseudo-static seismic coefficient to the rock mass model. Norrish and Wyllie (1996) should be consulted for a description of models and methods of rock slope stability analysis. Figure 3-12 illustrates an analysis model for a simple case.



Norrish and Wyllie, 1996

Figure 3-12. Horizontal and vertical seismic coefficients for pseudo-static analysis of rock slopes.

Due to the variety of failure mechanisms of rock slopes, this document does not review the analytical methods used to analyze the stability of rock slopes. Analytical methods for rock slope stability under seismic loading are presented in Norrish and Wyllie (1996).

3.4.2.2. Deformation Analysis Procedures

Simplified procedures for estimating deformations of slopes during earthquake shaking are based on the concept of yield acceleration originally proposed by Newmark (1965). Newmark's method has been modified and augmented by several investigators (Goodman and Seed, 1966; Ambraseys, 1973; Sarma, 1975; Franklin and Chang, 1977; Makdisi and Seed, 1978; Hynes-Griffin and Franklin, 1984; Wilson and Keefer, 1985; Lin and Whitman, 1986; Ambraseys and Menu, 1988; and Yegian et al., 1991). The procedure assumes that movement occurs on a well defined slip surface and that the material behaves elastically at acceleration levels below the yield acceleration but develops perfectly plastic behavior above yield. The procedure involves the following steps:

- Step 1: Determine the yield acceleration, k_y , using limit equilibrium pseudo-static slope stability methods as described in the preceding section. The yield acceleration corresponds to the seismic coefficient that would result in a factor of safety of one.
- Step 2: Determine the peak horizontal acceleration experienced by the potential sliding mass, k_{max} , as described in the preceding section.
- Step 3: Calculate the ratio of k_y to k_{max} and estimate the potential deformation using one or more of several methods discussed below.

Deformation analysis procedures contained herein can lead to inaccurate results for brittle rocks and soils, which are characterized by a substantial reduction in strength upon yielding. Using deformation analysis procedures that assume perfectly plastic behavior above yield with strengths equal to the yield strength will underestimate deformations in these materials. Brittle soils include weakly cemented sands common in the western U.S. and loess deposits common in the midwestern U.S. Procedures for the evaluation of brittle soils can be found in Ashford and Sitar, 1994, and Sitar and Clough, 1983.

3.4.2.2(a). Yield Acceleration, k_y

A yield acceleration, k_y , i.e., the acceleration at which a potential sliding surface would develop a factor of safety of unity, is determined using limit equilibrium pseudo-static slope stability methods as described above. Values of the yield acceleration are dependent primarily on the slope geometry, the undrained shear strength of the slope material, and the location of the potential sliding surface.

3.4.2.2(b). Peak Acceleration Induced Within the Sliding Mass, k_{max}

Guidance for estimating peak or maximum acceleration, k_{max} , induced within a potential sliding mass (average of the peak accelerations over the mass) is provided in section 3.4.2.1(b).

3.4.2.2(c). Estimating Deformation, D

Several methods for estimating deformation using the Newmark method have been developed. Each of these is based on the following methodology. For a specified potential sliding mass, the induced acceleration, k_{max} , is compared with the yield acceleration, k_y . When the induced acceleration exceeds the yield acceleration, downslope movements will occur along the direction of the assumed failure plane. The movement will stop when the induced acceleration drops below the yield acceleration and when the induced velocity drops to zero. The magnitude of the potential displacements can be calculated by the simple double-integration procedure of an accelerogram as illustrated in figure 3-13 (note that k_y is shown in the figure to vary with the level of acceleration, however, unless the material suffers rapid loss of strength during shaking, k_y is generally assumed to be constant).

The most commonly used simplified method for estimating deformation was developed by Makdisi and Seed (1978) for estimating displacements in embankments. Charts relating the displacements as a function of the ratio of the yield acceleration to the maximum induced acceleration (k_y/k_{max}) are shown in figures 3-14 and 3-15. The displacements shown in figures

3-14 and 3-15 are normalized with respect to the amplitude of the peak induced acceleration, k_{\max} (expressed as a decimal fraction of gravity), the acceleration of gravity, and the predominant natural period of the soil embankment or slope, T_o . The procedure was developed based on T_o values ranging from 0.5 seconds to 1.5 seconds. T_o can be estimated for embankments with the following equation:

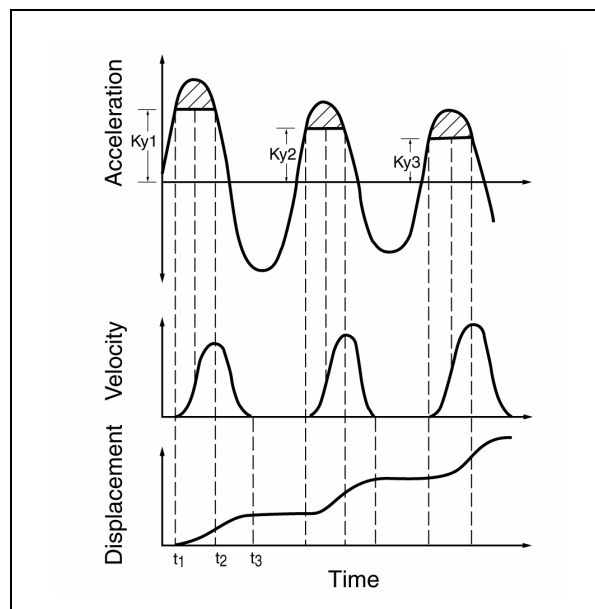
$$T_o = 2.6 \frac{h}{V_s} \quad (3-2)$$

where:

h = height of embankment

V_s = strain-dependent shear wave velocity of the soil

Makdisi and Seed (1979) developed a simplified procedure to estimate strain compatible T_o for embankment slopes. Strain compatible shear wave velocities in soils decrease with increasing levels of ground shaking. In the absence of a dynamic response analysis, recommended values of strain compatible shear wave velocities are as follows: for ground shaking on the order of about 0.1 g, the value of V_s can be assumed equal to $0.8 V_{\max}$ (where V_{\max} is the low-strain maximum shear wave velocity); for strong ground shaking levels of the order of 0.7 g, the value of V_s can be assumed equal to $0.45 V_{\max}$. For small slopes of uniform stiff soil, the predominant period of the earthquake acceleration time history can be used in the analysis. The predominant period of an earthquake acceleration time history is a function of earthquake magnitude, source to site distance, and site conditions. Relationships for estimating the frequency content (natural period) of ground motions were developed by Rathje et al. (1998). Typical values of these periods range between 0.4 and 0.7 seconds.



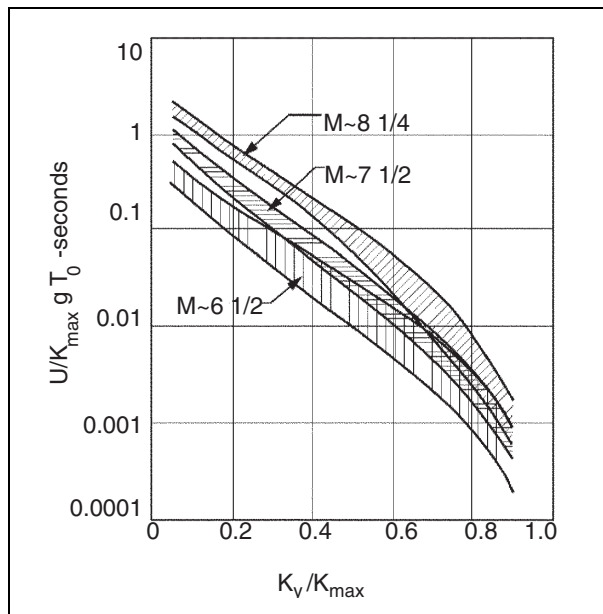
Goodman and Seed, 1966

Figure 3-13. Integration of acceleration time history to determine velocities and displacements.

The displacement relationships shown in figures 3-14 and 3-15 are presented for a range of earthquake magnitudes. The earthquake magnitude can be selected based on either the mean magnitude (de-aggregated) from seismic hazard analyses, or the maximum credible earthquake magnitude obtained from deterministic estimates (see Part I).

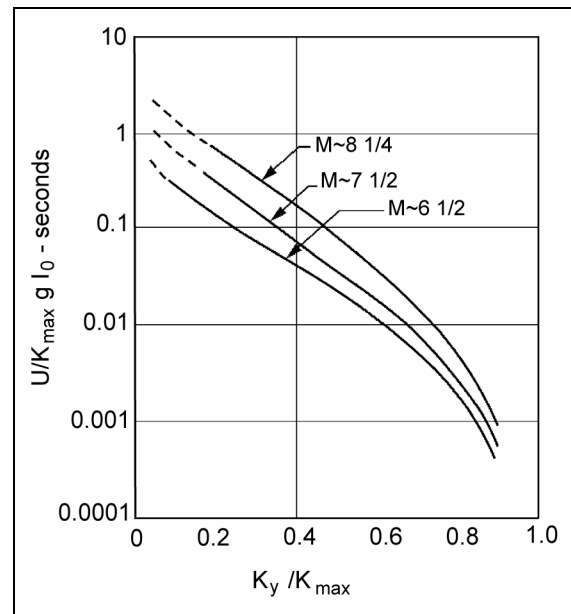
The Newmark sliding block analysis concept was also employed by Franklin and Chang (1977), who computed permanent displacements based on a large number of recorded acceleration time-histories from previous earthquakes and a number of synthetic records. Their results are shown in figure 3-16 in terms of upper bound envelope curves for standardized maximum displacements versus the ratio of the yield acceleration to the maximum earthquake acceleration. The time-histories used by Franklin and Chang (1977) all were scaled to a peak ground acceleration of 0.5g and peak ground velocity of 0.76 m/s (30 inches per second). The displacement, D (in inches), for particular values of peak ground acceleration, A , and velocity, V , may be obtained by multiplying the standardized maximum displacement by the quantity $V^2/1800A$, where V is in units of inches per second and A is a decimal fraction of gravity ($V^2/0.01285A$; where V is in m/s; and D is in meters).

Yegian et al. (1991) performed similar analyses using 86 ground motion records. Their computed normalized displacements are shown in figure 3-17. The computed displacements were normalized with respect to the peak induced acceleration, k_a , the number of equivalent cycles, N_{eq} , and the square of the predominant period of the time history, T .



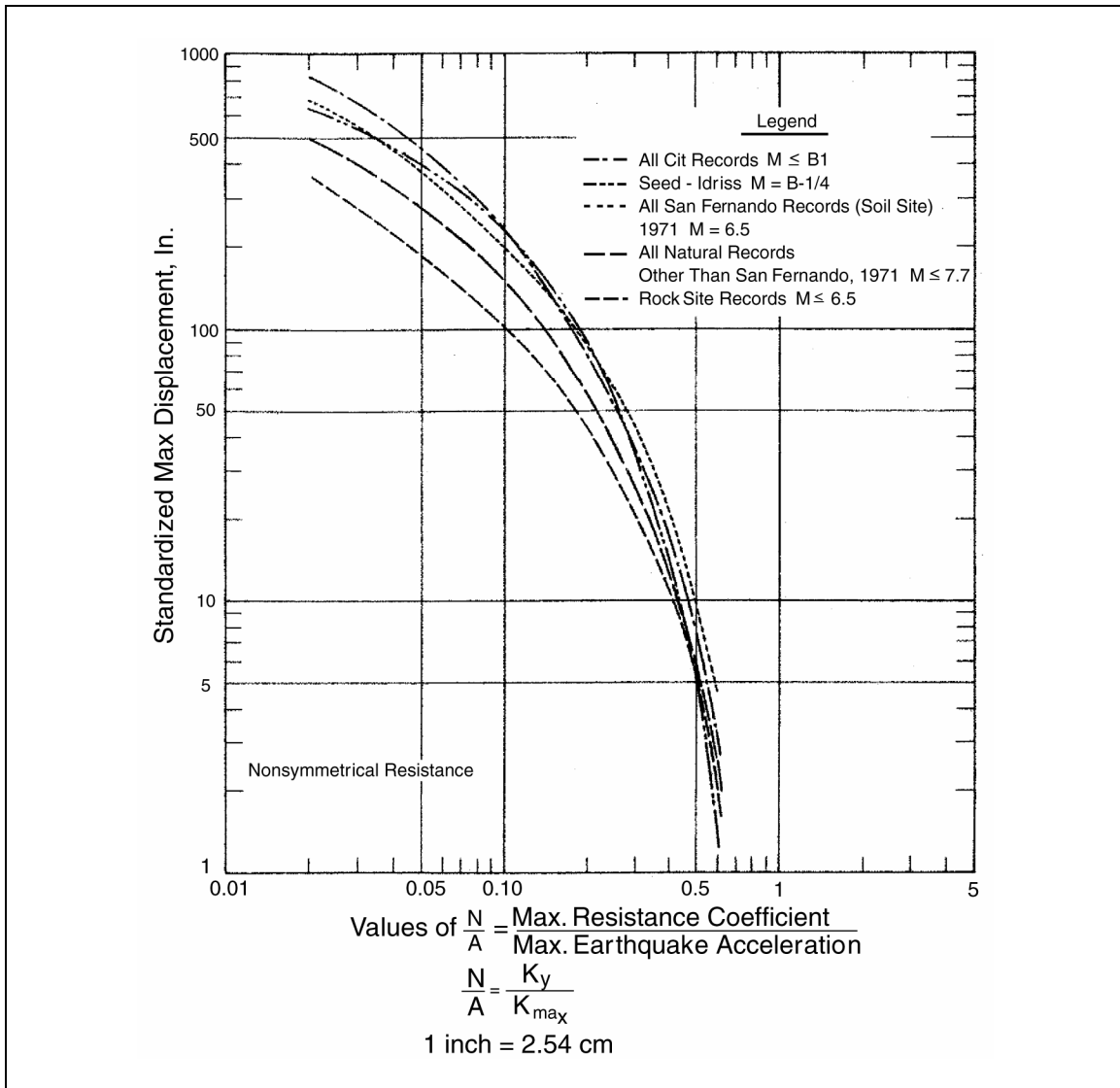
Makdisi and Seed, 1978

Figure 3-14. Variations of normalized permanent displacement with yield acceleration – summary of all data.



Makdisi and Seed, 1978

Figure 3-15. Variations of average normalized displacement with yield acceleration.

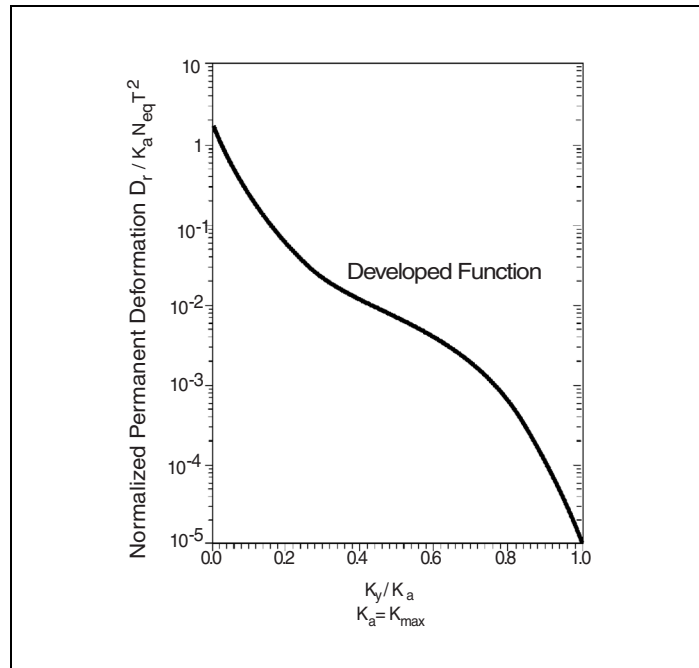


Franklin and Chang, 1977

Figure 3-16. Upper bound envelope curves of permanent displacements for all natural and synthetic records analyzed

The number of equivalent cycles is a function of earthquake magnitude and can be estimated as follows (Seed and Idriss, 1982).

Earthquake Magnitude	Number of Significant Cycles, N_{eq}
5.25	2-3
6	5
6.75	10
7.5	15
8.5	26



Yegian et al., 1991

Figure 3-17. Variation of normalized permanent deformation with yield acceleration.

A simple comparison of the methods described above was made using a postulated magnitude 7.5 earthquake with k_{max} equal to 0.5 g and 0.7 g, and a yield acceleration, k_y of 0.3 is presented in table 3-6. The Franklin and Chang (1977) method, whose curves represent an upper bound relationship, produced the largest deformations for both values of k_{max} . The Makdisi and Seed (1978) and Yegian et al. (1991) methods provided similar deformations for both acceleration levels. Generally, these deformation analysis methods provided similar results. Further illustration of these deformation analysis methods are provided in Example Problem 3.2 (see section 3.6).

In addition to the simplified procedures described above, screening and evaluation procedures were developed by a committee (organized through the ASCE, Los Angeles Section) to implement guidelines of the Division of Mines and Geology (DMG) Special Publication 117-*Guidelines for Analyzing and Mitigating Landslide Hazard in California* (Blake et al., 2002). The document provides guidelines on field and laboratory procedures, preliminary screening procedures, and simplified analyses procedures for evaluating slope stability and earthquake-induced deformations.

For slopes with complex geometries and material properties (that could not be approximated by simplified analysis procedures as described above), and for slopes and embankments supporting essential structures, detailed dynamic analyses and Newmark-type deformation analyses are required. These analyses include the use of equivalent linear (strain-dependant) finite element procedures such as the program QUAD4M (Hudson et al., 1994). This widely used dynamic analysis program provides estimates of earthquake-induced stresses and accelerations within the

Table 3-6. Comparison of deformation analysis methods.

Method	Deformation (cm)		Assumptions
	Case 1: $k_{max}=0.5g$	Case 2: $k_{max} = 0.7g$	
Makdisi & Seed (1978)	3	14	$T_o = 0.36$ sec (Seed et al., 1968)
Yegian et al. (1991)	3.5	13	$T_o = 0.36$ sec (Seed et al., 1968)
Franklin & Chang (1977)	5 (rock) 7 (soil)	19 (rock) 43 (soil)	Velocities estimated using Sadigh and Egan (1998) $K_{max} = 0.5 g$: $v = 50$ cm/s (rock); 60 cm/s (soil) $K_{max} = 0.7g$: $v = 60$ cm/s (rock); 90 cm/s (soil)

entire embankment or slope. The analysis also provides time histories of the average induced seismic coefficient for specified potential sliding masses within the slope. The time histories are compared with the yield acceleration for the corresponding sliding mass and are double-integrated to estimate the earthquake-induced permanent deformations.

Two-dimensional nonlinear finite element and finite difference programs also have recently been used to estimate the dynamic response, liquefaction potential, and permanent deformations of slopes and embankments. The program FLAC (Itasca, 1998), is a finite difference (large strain) computer program that can model nonlinear, coupled effective stress behavior during seismic loading. Such rigorous numerical modeling procedures, however, require considerable experience and judgment to properly calibrate model parameters; and their results are usually compared with commonly used (empirically based) simplified analyses.

3.4.3. EVALUATION OF CATEGORY III LANDSLIDES

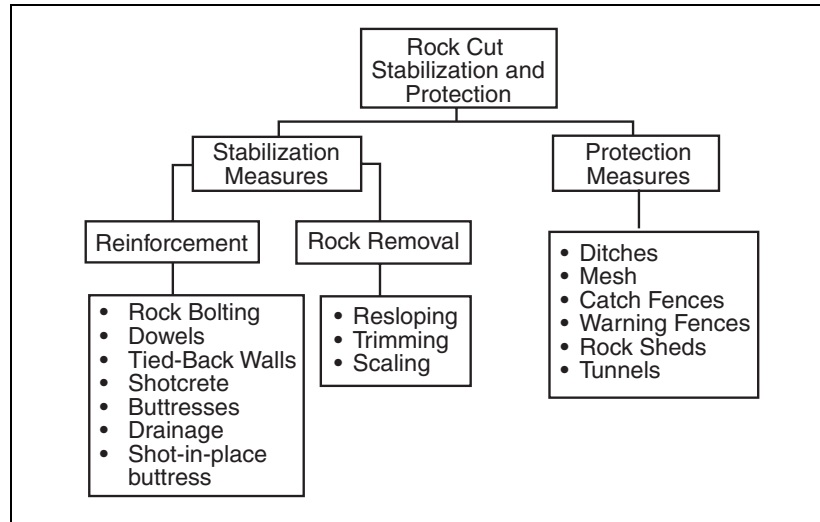
Category III Landslides include soil lateral spreads and rapid soil flows. Procedures to evaluate these conditions are included in Part I of this manual.

3.5. RETROFITTING PROCEDURES

Detailed procedures for stabilizing soil and rock slopes are presented in the Transportation Research Board Special Report 247, *Landslides Investigation and Mitigation* (Turner and Schuster, 1996, editors). Both Category I and II landslides include rock and soil stability issues. Retrofit procedures for landslides are best categorized by whether the slope needing stabilization is composed of rock or soil. Procedures for stabilizing rock slopes are presented by Wyllie and Norrish (1996) and Branwer (1994); stabilization procedures for soil slopes are presented by Holtz and Schuster (1996).

3.5.1. ROCK SLOPES

Methods of stabilization of rock slopes are described in detail by Wyllie and Norrish (1996) and Branwer (1994). Wyllie and Norrish (1996) describe three categories for stabilization and protection of rock slopes: (1) reinforcement; (2) rock removal; and (3) protection. Retrofitting measures in these three categories are listed in figure 3-18. Selecting the appropriate stabilization system is dependent on several issues that are usually site-specific. These issues include service life, importance of highway structure, environmental concerns, construction time, economics and others.



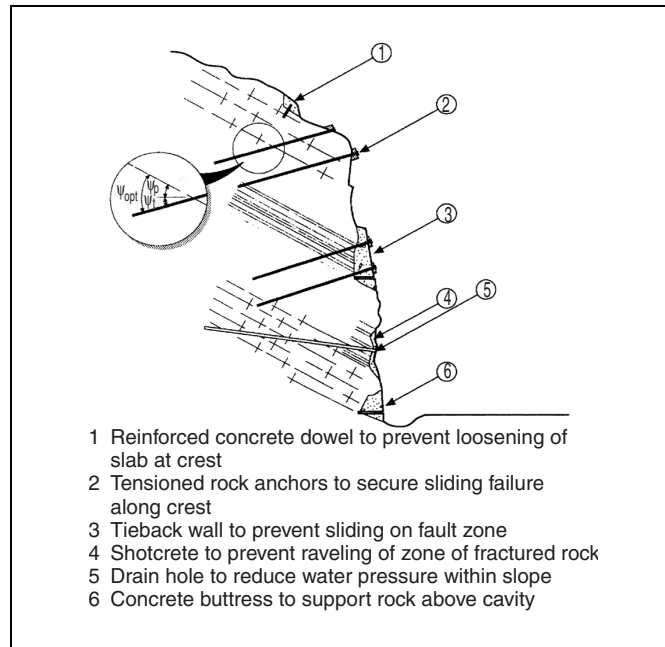
Wyllie and Norrish, 1996

Figure 3-18. Categories of rock slope stabilization measures.

1. Rock Reinforcement

A number of techniques are used for rock slope reinforcement. These techniques are shown schematically in figure 3-19. A feature common to these methods is that they minimize the relaxation and loosening of the rock mass that may take place as a result of excavation and/or seismic loading. These methods include: reinforced concrete dowels; tensioned rock anchors; tie-back walls to prevent sliding on potential fault zones; shotcrete to prevent raveling of fractured rock; drain holes for reduction of pore pressures; and concrete buttresses to fill rock cavities. Potential rock toppling failures also may be stabilized through rock reinforcement. With this approach, multiple rock columns are bolted together in order to move the center of gravity of the combined rock mass to within its base.

Cement grout anchors are commonly used for rock reinforcement because they provide a long service life at a reasonable cost. The grout usually contains non-shrink cement and/or admixtures for high strength, maximum viscosity, and reduced shrinkage. The strength of the rock often governs the strength of the anchor. Approximate values of allowable bond stress between grout and various rock types are listed in table 3-7. These approximate ranges can be used to estimate anchor strengths in the absence of laboratory or field test data.



Wyllie and Norrish, 1996

Figure 3-19. Rock slope reinforcement methods.

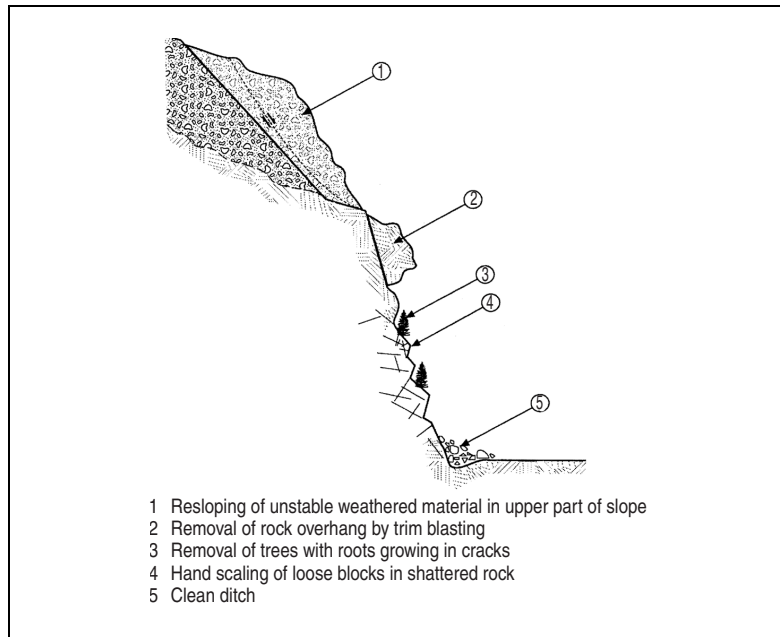
Table 3-7. Allowable bond stresses in cement-grout anchors.

Rock Strength and Type	Allowable Bond Stress (MPa)	Compressive Strength Range (MPa)
Strong	1.05 – 1.40	>100
Medium	0.7 - 1.05	Approx. 50-100
Weak	0.35 - 0.7	Approx. 20-50
Granite, basalt	0.55 - 1.0	
Dolomitic limestone	0.45 - 0.7	
Soft limestone	0.35 - 0.5	
Slates, strong shales	0.3 - 0.45	
Weak shales	0.05 - 0.3	
Sandstone	0.3 - 0.6	
Concrete	0.45 - 0.90	

Wyllie, 1991

2. Rock Removal

Rock removal is an effective method for stabilization of potentially unstable rock slopes because it eliminates the hazard, without the requirement of future maintenance. Rock removal includes resloping zones of unstable rock, trimming overhangs, and scaling of loose individual blocks of shattered rock. Examples of these methods are illustrated in figure 3-20.



Wyllie and Norrish, 1996

Figure 3-20. Rock-removal methods for slope stabilization.

3. Protective Measures Against Rockfalls

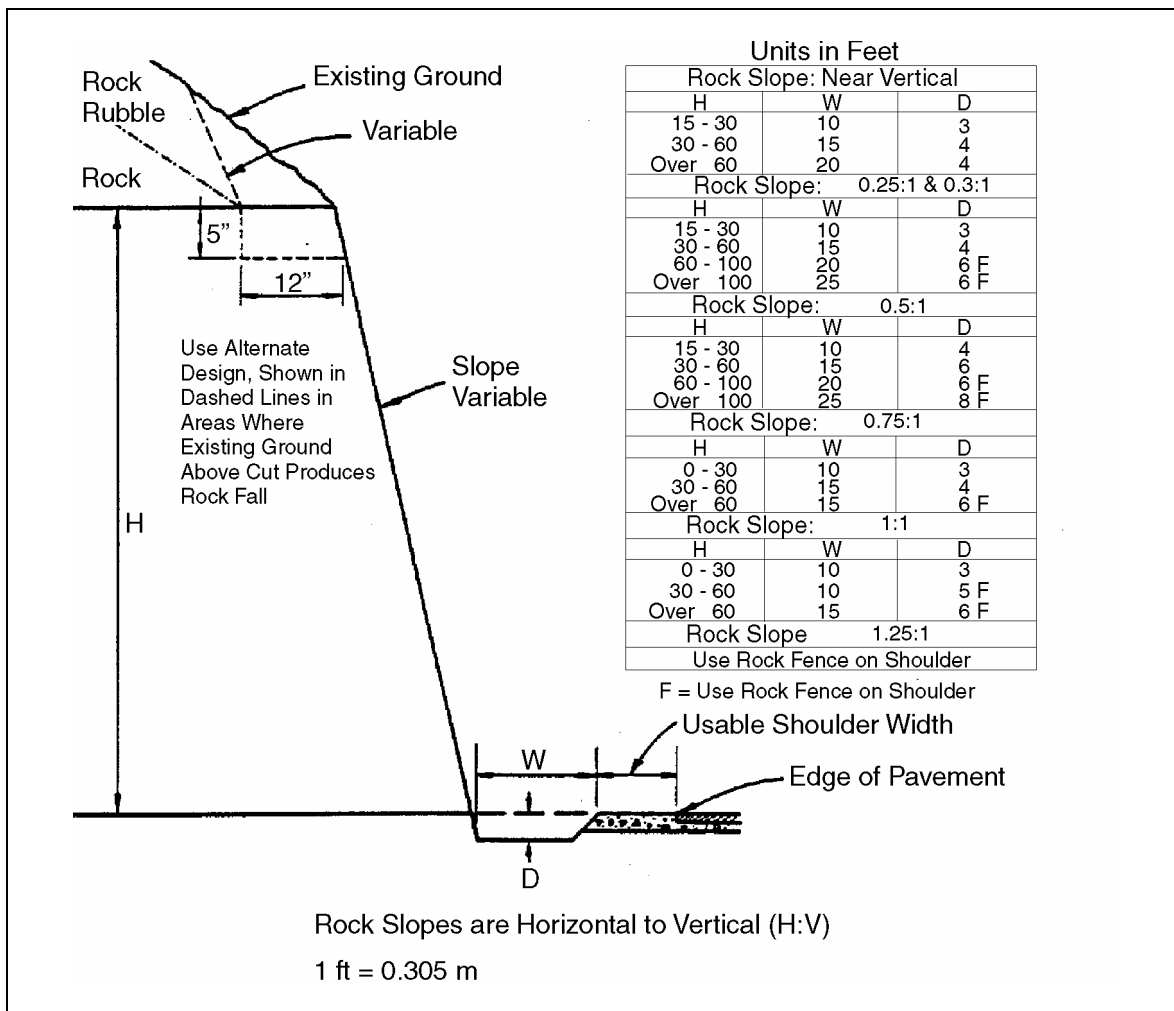
Another effective method of protection against the hazards of rockfalls is to let the falls occur and control the distance and direction of travel. These methods include catchment ditches and barriers, wire mesh fences, mesh lining on the face of the slope, and rock sheds. All these methods rely on the energy-absorbing characteristics of the barrier, which either stop the rockfall over some distance or deflect it away from the facility being protected.

Richie (1963) developed charts for estimating the required width and depth of rock catch ditches in relation to the height and face angle of the nearby slope (figure 3-21). Most catch ditches require a barrier between the ditch and the highway to stop falling or shattered rocks from reaching the roadway. Loose granular material may also be used in the ditch to absorb energy from falling rocks.

A variety of barriers can be constructed to either enhance the performance of excavated ditches or form catchment zones at the toes of slopes. The required type of barrier and its dimensions depend on the energy of the falling blocks, the slope dimensions, and the availability of construction materials.

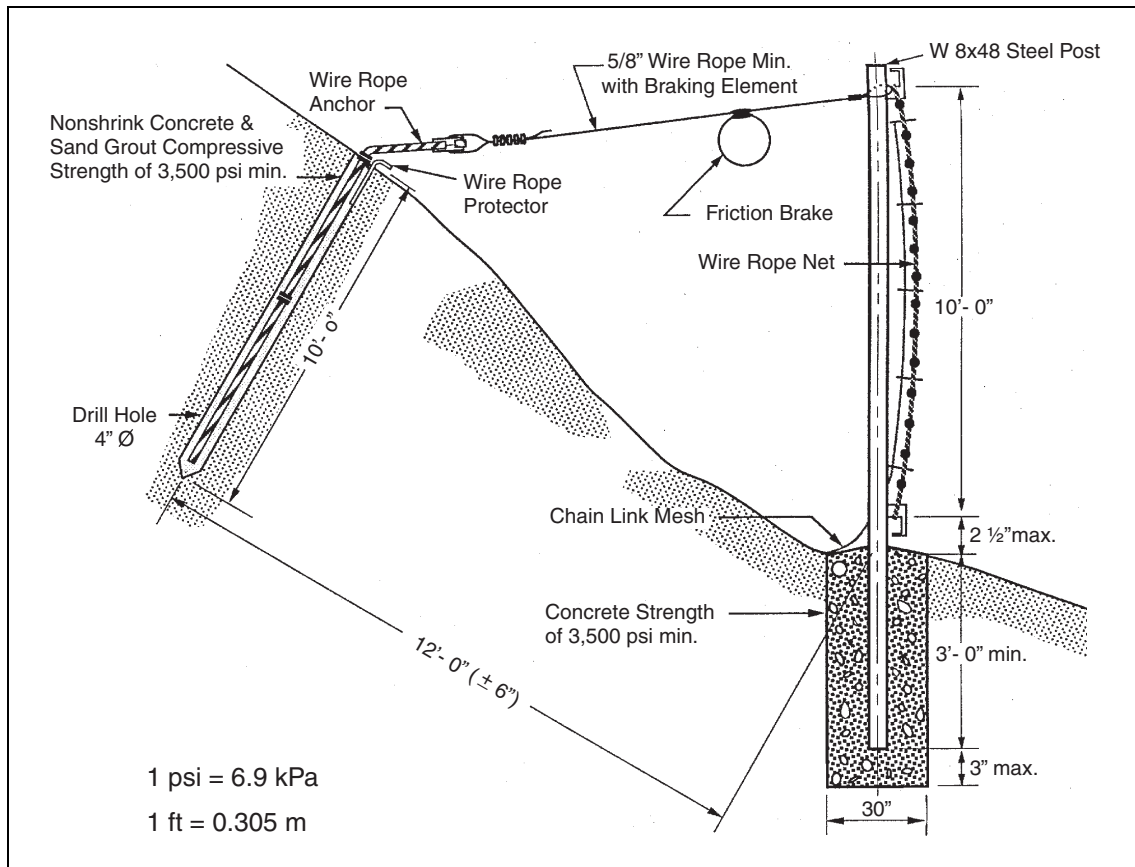
Details of various types of barriers are provided by Wyllie and Norrish (1996). Examples of these barriers include gabions and concrete blocks, and geofabric-reinforced soil barriers. Flexible rock catch fences and attenuators also are commonly used and include woven wire-rope nets, flex-post rockfall fences, and draped wire mesh. Figure 3-22 details the main components of a rockfall retaining net system used by the California Department of Transportation (Smith and Duffy, 1990).

In areas of extreme rockfall hazards where stabilization work may be very costly, construction of rock sheds may be used to protect the highway. The sheds are built with roofs that are inclined at a shallow angle to direct the falling rocks over the pavement or railway rather than to withstand a direct impact (figure 3-23, McCauley et al., 1985). Design of such structures must also be based on the energy required to redirect the falling rocks and boulders. The California Department of Transportation (Caltrans) report on rockfall mitigation (McCauley et al., 1985) evaluated various mitigation techniques that can be used. The Caltrans report also provides a summary of the mitigation methods used by 14 selected states that responded to their survey. The results of the survey are summarized in figure 3-24. From this survey, mesh fences, catch ditches, rock bolts and dowels, controlled blasting, and flattening and scaling slopes were the most widely applied rock slope mitigation methods.



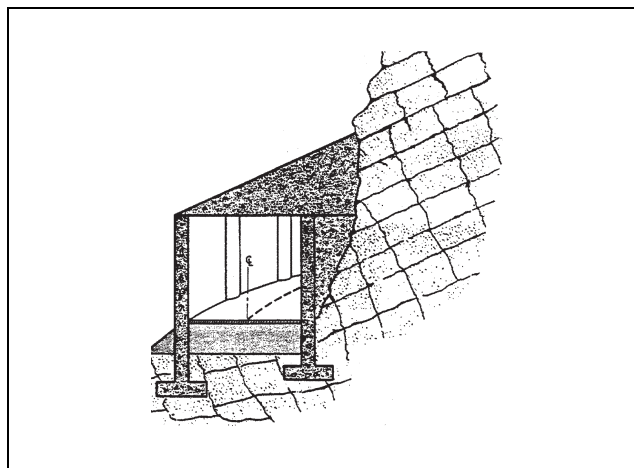
Richie, 1963

Figure 3-21. General design criteria for shaped ditches.



Smith and Duffy, 1990

Figure 3-22. Side view of rock fall restraint net system with fully embedded posts and anchor support.



McCauley et al., 1985

Figure 3-23. Example of rock shed.

States	AK	AZ	CO	HI	ID	MT	NV	NH	NM	OR	UT	VT	WA	WY
Flatten Slope		X				X	X	X	X	X				
Scale or Trim	X	X	X		X	X	X	X			X			
Skewed, Multiple Angle Slopes									X					
Slope Designed to Geology	X											X		
Controlled Blasting	X			X	X				X			X	X	X
Sub-Surface Drainage	X													
Rockbolt or Dowels	X		X				X	X	X	X		X		X
Shotcrete or Gunitite			X						X	X			X	X
Anchored Wire Mesh			X					X	X	X			X	X
Cable Lashing							X							
Retaining Wall		X										X		
Slope at Max. Steepness	X										X			
Highway Relocation		X				X								
Bench		X	X				X			X	X			
Standard Guard Rail							X	X					X	
Metal Barrier						X				X				
PCC Jersey Barrier					X	X	X		X	X				
Gabion	X								X				X	
Earth Berm										X				
Intercepting Slope Ditch								X						
Shaped Ditch at Grade	X		X		X		X	X	X	X	X		X	X
"Telephone Pole" Retainer									X					
Draped Wire Mesh	X		X	X	X		X		X	X	X		X	
Aggregate in Ditch Line								X						
Metal Bin Wall			X											
Wire Mesh Fence		X		X	X		X		X	X	X		X	

Note:

Chart prepared from the responses sent to Caltrans from other states, other methods may also be used by listed states. Combinations of mitigation measures are also used.

McCauley et al., 1985

Figure 3-24. Rock slope mitigation methods used by selected states.

3.5.2. SOIL SLOPES

Approaches to the design of remedial measures for landslides, potential slope failures, and design of stable slopes can be categorized as follows (Holtz and Schuster, 1996):

- Avoid the problem and relocate the facility to a stable site.
- Reduce the driving forces that tend to cause movement and sliding.
- Increase the forces resisting movement.

A summary of these three approaches is given in table 3-8.

- **Avoidance of Problem**

Geologic and geotechnical reconnaissance studies should reveal adverse conditions affecting stability of slopes, such as poor surface drainage, seepage on existing natural slopes, hillside creep, existing landslides, and soft foundations. Facilities could be relocated to avoid these potential problem areas, particularly existing landslides. If relocation or realignment of a proposed facility is not practical, partial or complete removal of the unstable material could be considered. If relocation and/or removal of unstable material is too costly, an alternative design is to span the unstable area with a bridge supported on piles or drilled shafts founded well below the unstable material and capable of withstanding lateral loads from it.

- **Reduction of Driving Forces**

A simple approach to increasing slope stability is to reduce the mass of soil involved in potential sliding. Methods that have been successfully used to improve slope stability include flattening slopes, benching slopes, excavation of material at the top of a landslide, surface and subsurface drainage, and the use of lightweight fills.

Drainage of surface water and groundwater is a widely used method for slope stabilization. Proper drainage will both reduce the weight of the sliding mass and increase the strength of the material in the slope.

Proper surface drainage should be implemented to prevent water from flowing across the face of the slope and from seeping into the slope. Diversion ditches and interceptor drains are used when large volumes of runoff are anticipated. Methods to control subsurface water are discussed in “Increase in Resisting Forces,” below.

Finally, lightweight backfill materials have been used in embankment construction to reduce driving forces tending to cause instability.

Table 3-8. Summary of approaches to potential stability problems.

Category	Procedure	Best Application	Limitations	Remarks
Avoid problem	Relocate facility	As an alternative anywhere	Has none if studied during planning phase; has large cost if location is selected and design is complete; also has large cost if reconstruction is required	Detailed studies of proposed relocation should ensure improved conditions
	Completely or partially remove unstable materials	Where small volumes of excavation are involved and where poor soils are encountered at shallow depths	May be costly to control excavation; may not be best alternative for large landslides; may not be feasible because of right-of-way requirements	Analytical studies must be performed; depth of excavation must be sufficient to ensure firm support
	Install bridge	At sidehill locations with shallow soil movements	May be costly and not provide adequate support capacity for lateral forces to restrain landslide mass	Analysis must be performed for anticipated loading as well as structural capability
Reduce driving forces	Change line or grade	During preliminary design phase of project	Will affect sections of roadway adjacent to landslide area	--
	Drain surface	In any design scheme; must also be part of any remedial design	Will only correct surface infiltration or seepage due to surface infiltration	Slope vegetation should be considered in all cases
	Drain subsurface	On any slope where lowering of groundwater table will increase slope stability	Cannot be used effectively where slide mass is impervious	Stability analysis should include consideration of seepage forces
	Reduce weight	At any existing or potential slide	Requires lightweight materials that may be costly or unavailable; excavation waste may create problems; requires right-of-way	Stability analysis must be performed to ensure proper placement of lightweight materials
Increase resisting forces; Apply external force	Use buttress and counter-weight fills; toe berms	At an existing landslide; in combination with other methods	May not be effective on deep-seated landslides; must be founded on a firm foundation; requires right-of-way	Consider reinforced steep slopes for limited right-of-way

(Continued)

Table 3-8. Summary of approaches to potential stability problems (continued).

Category	Procedure	Best Application	Limitations	Remarks
Increase resisting forces; Apply external force (continued)	Use structural systems	To prevent movement before excavation; where right-of-way is limited	Will not stand large deformations; must penetrate well below sliding surface	Stability and soil-structure analyses are required
	Install anchors	Where right-of-way is limited	Requires ability of foundation soils to resist shear forces by anchor tension	Study must be made of in-situ soil shear strength; economics of method depends on anchor capacity, depth, and frequency
Increase internal strength	Drain subsurface	At any landslide where water table is above shear surface	Requires experienced personnel to install and ensure effective operation	--
	Use reinforced backfill	On embankments and steep fill slopes; land-slide reconstruction	Requires long-term durability of reinforcement	Must consider stresses imposed on reinforcement during construction
	Install in-situ reinforcement	As temporary structures in stiff soils	Requires long-term durability of nails, anchors, and micropiles	Design methods not well established; requires thorough soils investigation and properties testing
	Use biotechnical stabilization	On soil slopes of modest heights	Climate; may require irrigation in dry seasons; longevity of selected plants	Design is by trial and error plus local experience
	Treat chemically	Where sliding surface is well defined and soil reacts positively to treatment	May be reversible; long-term effectiveness has not been evaluated; environmental stability unknown	Laboratory study of soil-chemical treatment must precede field installations; must consider environmental effects
	Use electro-osmosis	To relieve excess pore pressure and increase shear strength at a desirable construction rate	Requires constant direct current power supply and maintenance	Used when nothing else works; emergency stabilization of landslides
	Treat thermally	To reduce sensitivity of clay soils to action of water	Requires expensive and carefully designed system to artificially dry or freeze subsoils	Methods are experimental and costly

Holtz and Schuster, 1996; modified from Gedney and Weber, 1978

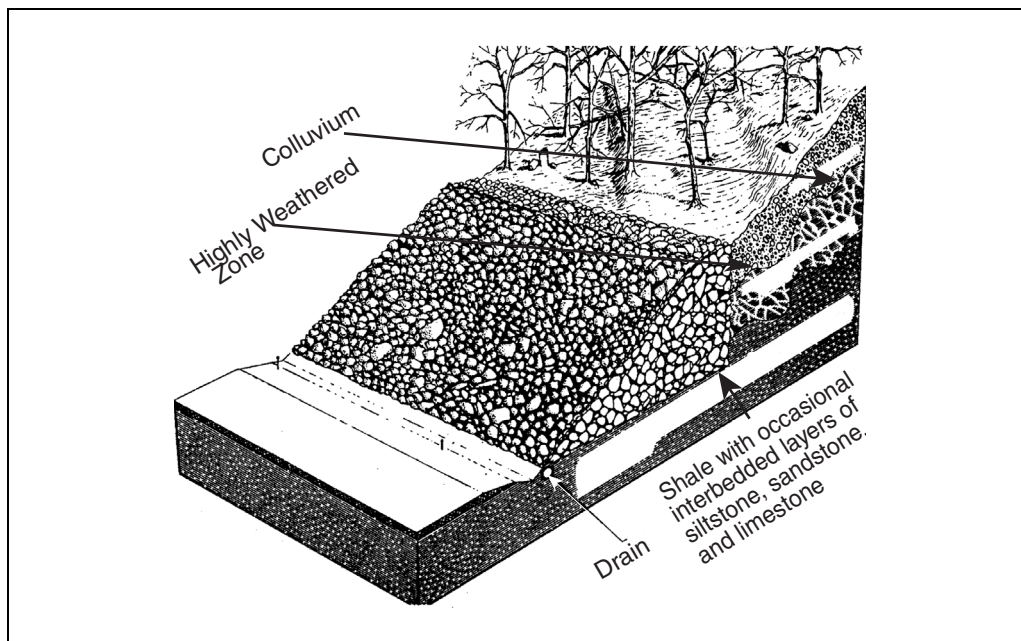
- **Increase in Resisting Forces**

Increasing the resisting forces on a potential or existing landslide can be achieved by applying an external load or a resisting force at the toe of the landslide, or increasing the internal strength of the soils in the failure zone so that the slope would remain stable.

Procedures that have been used to increase the resisting force at the toe of a potential sliding mass include: buttress fills and structural retention systems. Buttresses are often constructed of quarry rock, boulders, cobbles, and coarse gravel fill. An example of a rock buttress is shown in figure 3-25. Notice in this figure that a toe drain was installed to further facilitate drainage.

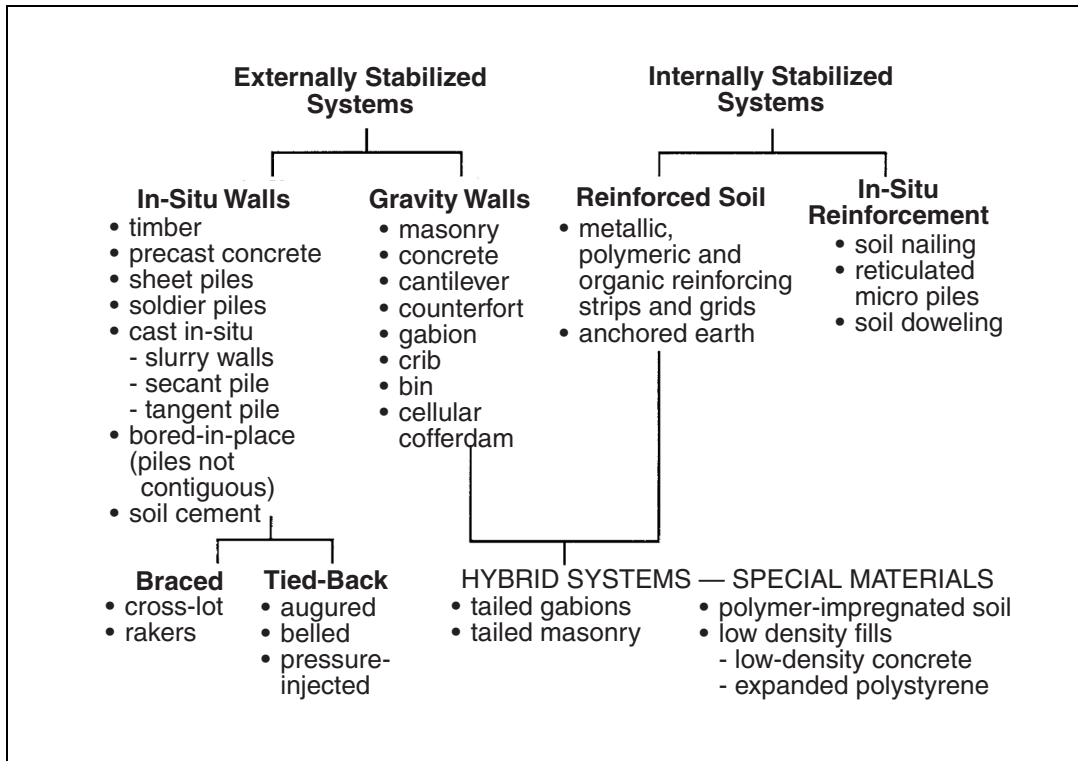
In situations where buttress fills are not feasible because of geometry, cost, or space limitations, conventional retaining structures, piles, and reinforced earth slopes and walls may be used as an alternative. These methods are summarized in figure 3-26. The methods are divided into two groups, depending on whether they provide external or internal support. Examples of both systems are shown in figure 3-27.

Techniques that are used to increase the internal strength of potentially unstable soil include: subsurface drainage, soil reinforcing systems, vegetative and biotechnical stabilization, and other less common methods such as chemical, electrical (electro-osmosis), and thermal stabilization. Details of these procedures are presented by Holtz and Schuster (1996).



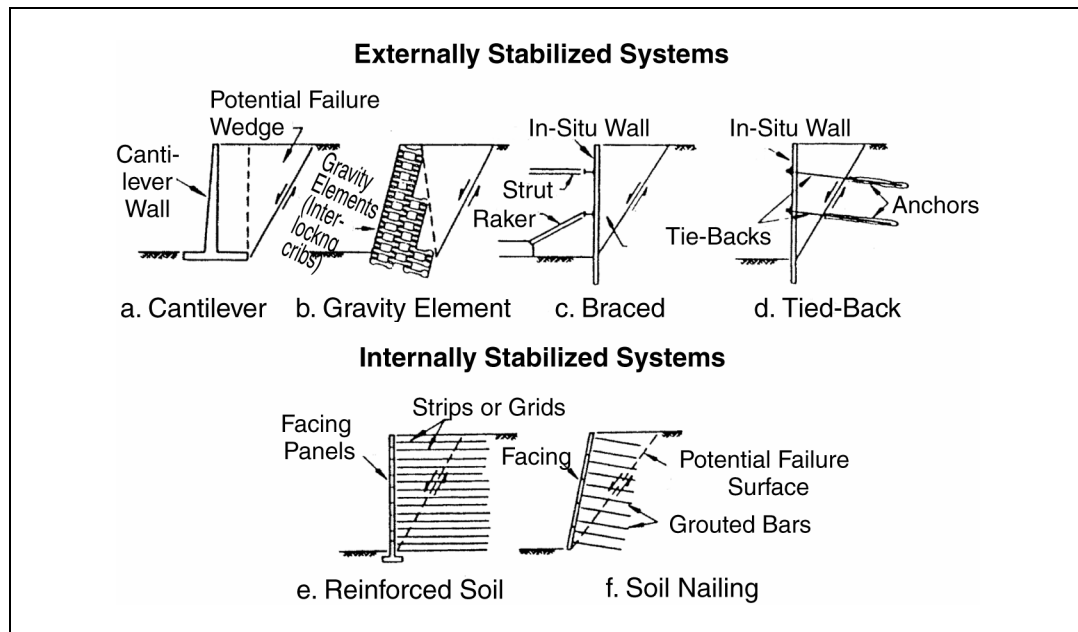
Gedney and Weber, 1978

Figure 3-25. Rock buttress used to increase forces resisting slope failure.



Holtz and Schuster, 1996; modified from O'Rourke and Jones, 1990

Figure 3-26. Classification scheme for earth retention systems.



Holtz and Schuster, 1996; modified from O'Rourke and Jones, 1990

Figure 3-27. Examples of externally and internally stabilized earth retention systems.

Subsurface drainage is used to lower the groundwater table and usually consists of the following procedures: (a) drainage blankets and trenches; (b) drainage wells, galleries, and tunnels; and (c) horizontal and vertical drains. Types of vertical and horizontal drainage methods used in natural slopes are shown in figure 3-28.

Geosynthetic products such as geotextiles and geocomposites have been used for drainage and slope stabilization in several of the situations described above. Geotextiles have often been used as replacements of graded granular filters. Geocomposites have been installed in areas where access is difficult, behind retaining structures, and in other places where interception of seepage is desired.

Other less common methods of improving drainage and controlling groundwater include: electro-osmosis, vacuum dewatering, siphon drains, and blasting of rock slopes.

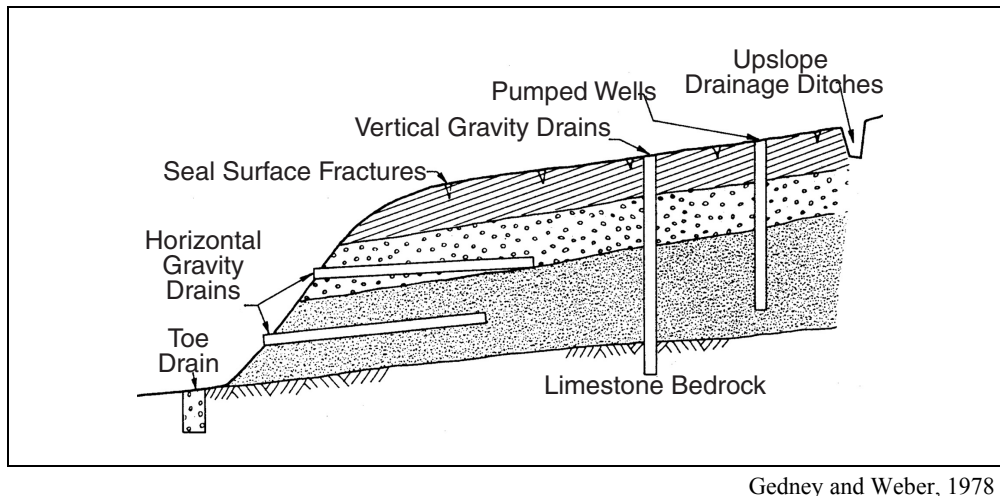


Figure 3-28. Types of vertical and horizontal drains used to lower the groundwater in natural slopes.

3.6. EXAMPLE PROBLEMS

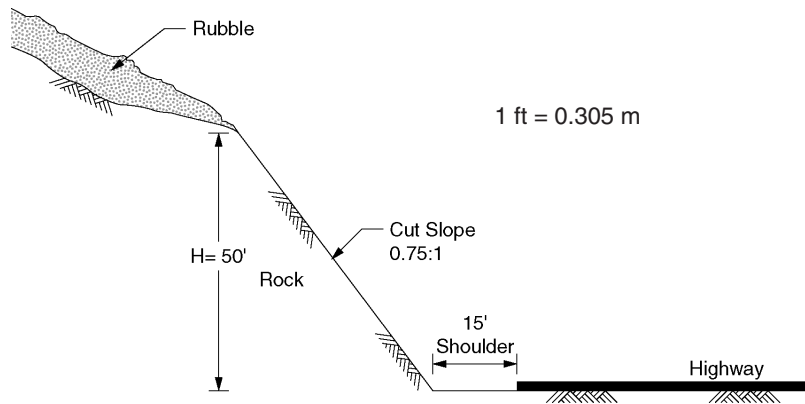
The following are three example cases that illustrate the screening and evaluation procedures described earlier in this chapter. Additional case examples may be found in *Geotechnical Engineering Circular #3, Design Guidance: Geotechnical Earthquake Engineering for Highways, Volume II – Design Examples* (Kavazanjian et al., 1997).

EXAMPLE PROBLEM 3.1 – ROCKFALL HAZARD SCREENING, EVALUATION, AND RETROFIT

This example presents the steps involved in screening and evaluating a site for potential earthquake-induced rockfalls. The example problem is illustrated in accompanying sketches.

a. Review of Available Information

- (1) Site conditions. A highway is located at the base of an approximately 15.2 m (50 ft) high slope cut into rock. The edge of the pavement and usable shoulder is 4.6 m (15 ft) back from the toe of the slope. The ratio of the slope width to the slope height is approximately 0.75:1 (H:V). Inspection of the face of the cut-slope indicates that the slope is stable. The natural slope surface located above the crest of the cut-slope is covered with rock rubble of varying sizes. The highway pavement is founded on competent rock.



- (2) Site history and seismic setting. Minor rockfalls have been known to periodically occur along this section of highway under static conditions. This site has been shaken in the past by several small earthquakes. Rockfalls have occurred following each of these events. Local seismicity indicates that the site is located in an area capable of experiencing moderate to large earthquakes (magnitude 6.5). Seismic landslide hazard maps have not been developed for this area.

b. Earthquake-Induced Landslide Screening

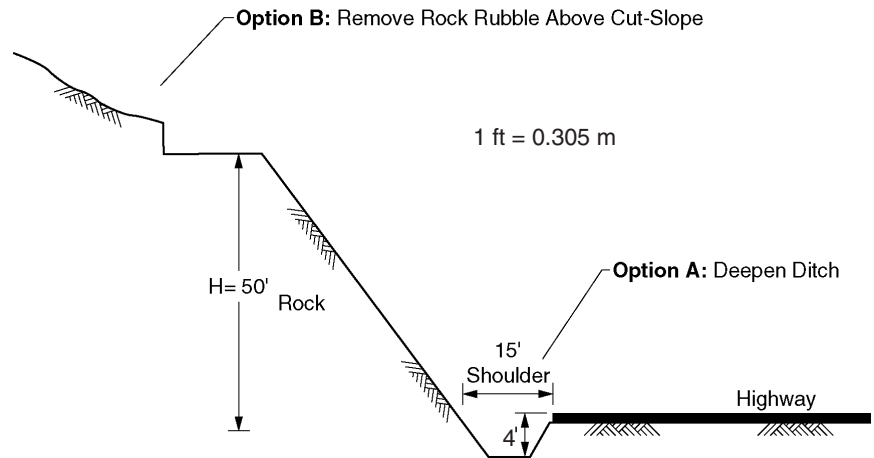
- (1) To conclude that a landsliding hazard does not exist, each of the landslide screening criteria presented in section 3.3.1 must be satisfied. The site is not located in an area designated to have a high susceptibility to earthquake-induced landslides based on available maps. A field visit to the site identified rock rubble above the crest of the cut-slope that may indicate susceptibility to rockfalls. Review of historic site information indicates that rockfalls have been a problem in the past. The occurrence of rockfalls during past earthquakes and under static conditions indicate future susceptibility to earthquake-induced rockfalls. Thus, criterion "a" is not satisfied, indicating that further evaluation is required.

c. Evaluation Procedures

Because rockfall have occurred during historical seismic events, a clear hazard requiring remediation is indicated. Therefore, further hazard evaluations were not needed, and studies were made to identify an appropriate remediation method.

d. Hazard Mitigation

Given the site conditions, two retrofit approaches were considered (see sketch): (1) prevent rockfalls from reaching the highway by constructing a catchment ditch and (2) eliminate the hazard by rock removal.



- (1) Catchment ditch.
The Richie (1963) method for estimating catchment ditch

dimensions was used for this site (figure 3-22). For a slope height of 15.2 m (50 ft) and an inclination of 0.75 horizontal to 1 vertical, the Richie (1963) chart indicates that a ditch would need to be 4.6 m (15 ft) wide and 1.2 m (4 ft) deep to control the travel of falling rocks. This chart also indicates that given the slope geometry, a barrier fence between the ditch and the highway would not be necessary. Based on the chart, we chose to deepen the ditch to 1.2 m (4 ft) below the highway surface. Fortunately, this section of highway was already constructed with a 4.6 m (15 ft) wide unused shoulder. Had less shoulder width been available, then the catchment ditch dimensions would have to be modified or an alternate remediation method considered.

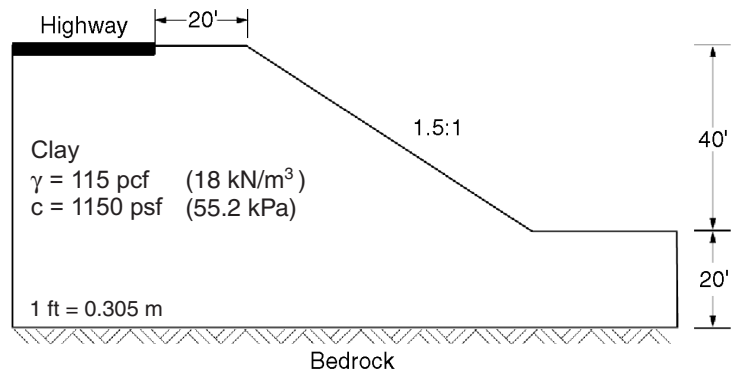
- (2) Rock removal. Figure 3-22 illustrates an alternate rockfall mitigation approach in which the loose rock rubble located above the cut-slope is removed. Physical removal of the rubble is a very effective remediation approach because it essentially eliminates the hazard. However, this approach may be very expensive if the quantity of loose rock is large, access to the slope is difficult, or the site conditions are hazardous.

EXAMPLE PROBLEM 3.2 – LANDSLIDE HAZARD SCREENING AND EVALUATION

This example presents the steps involved in screening and evaluating a site for potential earthquake-induced landsliding hazards. The example problem is illustrated in the accompanying sketch.

a. Review of Available Information

- (1) Soil conditions. A highway pavement is located 6.1 m (20 ft) back from the crest of a 12 m (40 ft) high slope (see sketch). The inclination of the slope is approximately 1.5:1 (H:V). Soil conditions at the site consist of clay with a uniform undrained shear strength (cohesion) of approximately 55.2 kPa (1150 psf) and a unit weight of 18.0 kN/m^3 (115 pcf). Bedrock is located approximately 18 m (60 ft) below the highway surface, and groundwater is not present at the site.



- (2) Historic earthquake effects and postulated earthquake parameters. This site has been shaken by several moderate earthquakes. However, no known historic information indicates that earthquake-induced landsliding occurred. Inspection of the site shows that the slope is stable under static conditions. Seismic landslide hazard maps have not been developed for this area. Site-specific analyses determined the MCE to have a moment magnitude of approximately 6.5 to produce a peak horizontal acceleration at the site of 0.40 g. The predominant period of the induced acceleration time history, T_o , was estimated to be 0.3 seconds.

b. Earthquake-Induced Landslide Screening

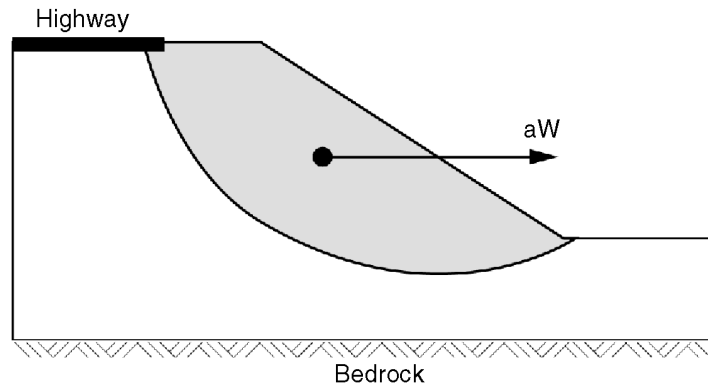
- (1) To conclude that a landsliding hazard does not exist, each of the landslide screening criteria presented in section 3.3.1 must be satisfied. The stability of the slope during past earthquakes and present site conditions indicate no significant susceptibility to landsliding. The site is not located in an area designated to have a high susceptibility to earthquake-induced landsliding based on available maps. A field visit to the site identified several cracks at the crest of the slope that may indicate actual slope movement. Thus, criterion "a" is not satisfied, indicating further evaluation is required.

c. Evaluation Procedures

The general method for evaluating the seismic stability of slopes involves both pseudo-static and deformation analysis procedures, as illustrated below.

- (1) Pseudo-static slope stability analysis

Pseudo-static slope stability analyses conservatively evaluate the potential for slope failure due to earthquake loading. If the results of the pseudo-static analysis indicate potential deformation of the slope (factor of safety < 1), a deformation analysis is performed to estimate the displacement. A static limit-equilibrium slope stability analysis performed for the site (not shown here, but following standard practice) determined that the critical failure surface would intersect the highway pavement (see sketch). This failure surface was then used for the pseudo-static slope stability analysis. The seismic coefficient was assumed to be equal to the peak horizontal



acceleration of 0.40 g. The results of the pseudo-static analysis indicate a marginal susceptibility to earthquake-induced landsliding with a factor of safety of 0.92. A deformation analysis was then performed to estimate the displacement.

(2) Deformation analysis

The deformation analysis procedure is based on Newmark's (1965) concept of yield acceleration. For a specified potential sliding mass, the acceleration induced by the earthquake is compared with the yield acceleration. When the induced acceleration exceeds the yield acceleration, downslope movements will occur along the direction of the assumed failure plane. The movement will stop after the induced acceleration drops below the yield acceleration.

- a. Yield acceleration, k_y . The yield acceleration is the acceleration at which the potential sliding surface would develop a factor of safety of unity. For this site, k_y was determined to be 0.30 g by iteratively adjusting the seismic coefficient in the pseudo-static analysis until the factor of safety reached a value of unity.
- b. Peak or maximum acceleration, k_{max} . This parameter represents the peak or maximum acceleration induced within the sliding mass. k_{max} was assumed to be equal to the peak horizontal acceleration of 0.40 g.
- c. Acceleration ratio. The acceleration ratio is calculated by dividing the yield acceleration, k_y , by the maximum acceleration, k_{max} . For this example, the acceleration ratio is equal to 0.75.
- d. Deformation. Several simplified methods based on the concept of yield acceleration originally proposed by Newmark (1965) are utilized to estimate deformation (see table below).
 1. Makdisi and Seed (1978). The Makdisi and Seed (1978) method normalizes displacement by k_{max} , T_o , and gravity (figure 3.15). Based on the ratio of k_y to k_{max} of 0.75 and a moment magnitude of 6.5, the normalized displacement is equal to approximately 0.003 seconds (note that the units of seconds will be replaced by inches when the normalizing values are factored out). An estimated deformation of 0.4 cm (0.14 inches) was calculated by multiplying the normalized displacement by the values of k_{max} , T_o , and gravity.
 2. Franklin and Chang (1977). The range of the Franklin and Chang (1977) simplified method has a lower bound of 2.5 cm (one inch) of deformation (figure 3.16). The critical acceleration ratio of 0.75 is outside this range. However, judging from the trend of the curves, a deformation of less than 2.5 cm (one inch) can be assessed.

3. Yegian et al. (1991). The Yegian et al. (1991) simplified method for estimating permanent deformation normalizes displacement by k_{max} , T_0^2 , number of cycles, and gravity (figure 3-17). A magnitude 6.5 earthquake contains approximately eight cycles (from Seed and Idriss, 1982). Based on the ratio of k_y to k_{max} of 0.75, the normalized permanent deformation was estimated to be 0.001. An estimated deformation of 0.3 cm (0.1 inch) was determined by multiplying the normalized displacement value of 0.001 by the values of k_{max} , T_0^2 , number of cycles, and gravity.

Method	Estimated Deformation in cm (inches)
Makdisi and Seed (1978)	0.35 (0.14)
Franklin and Chang (1977)	< 2.5 (< 1)
Yegian et al. (1991)	< 0.25 (0.1)

d. Hazard Mitigation

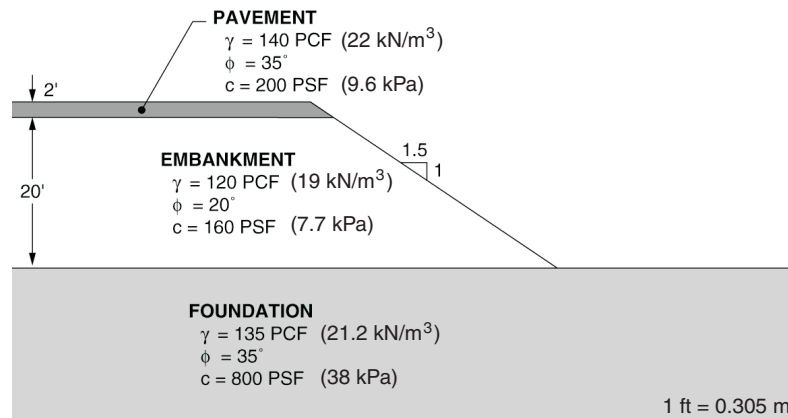
The amount of acceptable deformation is dependent on the tolerance of the pavement and acceptable damage. For this example problem, each deformation analysis method predicted less than 2.5 cm (one inch) of displacement. This magnitude of displacement was determined to be acceptable. Thus, stabilization methods were not needed at this site.

EXAMPLE PROBLEM 3.3 – LANDSLIDE HAZARD SCREENING, EVALUATION, AND RETROFIT OF EMBANKMENTS

This example presents the steps involved in screening, evaluating, and retrofitting a site for potential earthquake-induced landsliding hazards. The example problem is illustrated in accompanying sketches.

a. Review of Available Information

- (1) Soil conditions. A 6.1 m (20 foot) high highway embankment is constructed of poorly compacted fill material (see sketch). The inclination of the embankment slope is approximately 1.5:1 (H:V). The native foundation materials are dense and stable. Groundwater is not present at the site. The embankment does show some signs of settlement and cracking.
- (2) Historic earthquake effects and earthquake parameters. Since the highway was constructed, this site has not been shaken by any moderate to large earthquakes. Inspection of the site shows that the slope is stable under static conditions. Site-specific analyses determined the MCE to have a moment magnitude of approximately 7.5 and a peak horizontal acceleration of 0.50 g. The predominant period of the induced acceleration time history, T_o , was estimated to be 0.3 seconds.



b. Earthquake-Induced Landslide Screening

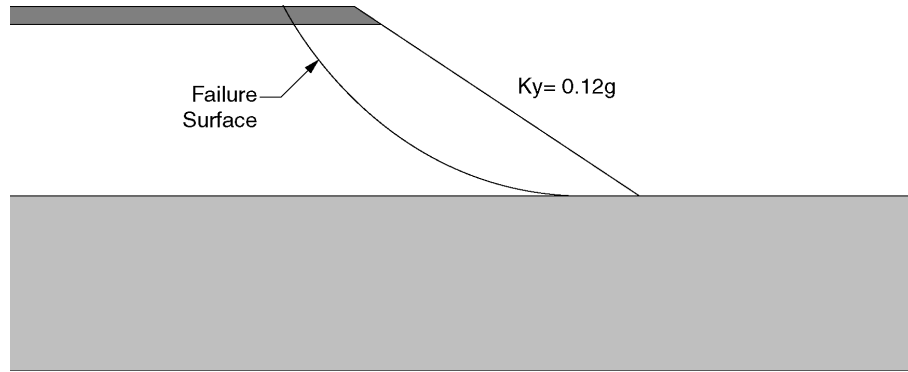
- (1) To conclude that a landsliding hazard does not exist, each of the landslide screening criteria presented in section 3.3.1 must be satisfied. Because this is a man-made embankment, general screening criterion “e” is particularly applicable. The settlement and cracking observed in the embankment indicate that the embankment is constructed of poorly compacted fill or is underlain by poor foundation materials. Thus, criterion “e” is not satisfied, indicating that further evaluation is required.

c. Evaluation Procedures

The general method for evaluating the seismic stability of slopes involves both pseudo-static and deformation analysis procedures, as illustrated below.

- (1) Pseudo-static slope stability analysis

Pseudo-static slope stability analyses conservatively evaluate the potential for slope failure due to earthquake loading. If the results of the pseudo-static analysis indicate a factor of safety < 1 , a deformation analysis is performed to estimate the displacement. A static limit-equilibrium slope stability analysis performed for the site determined that the critical failure surface would intersect the highway pavement (see sketch). This failure surface was then used for the pseudo-static slope stability analysis. The seismic coefficient was assumed to be equal to the peak horizontal acceleration of 0.50 g. The results of the pseudo-static analysis indicate a



significant susceptibility to earthquake-induced landsliding with a factor of safety of 0.58. A deformation analysis was then performed to estimate the displacement.

(2) Deformation analysis

The deformation analysis procedure is based on Newmark's (1965) concept of yield acceleration. For a specified potential sliding mass, the acceleration induced by the earthquake is compared with the yield acceleration. When the induced acceleration exceeds the yield acceleration, downslope movements will occur along the direction of the assumed failure plane. The movement will stop after the induced acceleration drops below the yield acceleration.

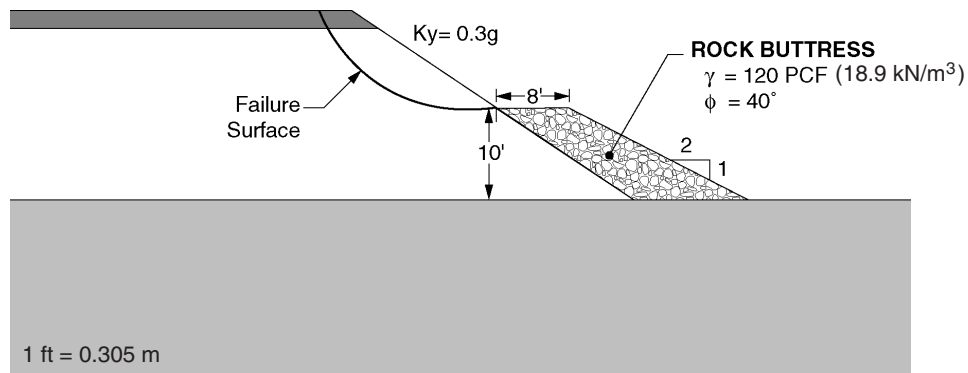
- (a) Yield acceleration, k_y . The yield acceleration is the acceleration at which the potential sliding surface would develop a factor of safety of unity. For this site, k_y was determined to be 0.12 g by iteratively adjusting the seismic coefficient in the pseudo-static analysis until the factor of safety reached a value of unity.
- (b) Peak or maximum acceleration, k_{max} . This parameter represents the peak or maximum acceleration induced within the sliding mass. k_{max} was assumed to be equal to the peak horizontal acceleration of 0.50 g.
- (c) Acceleration ratio. The acceleration ratio is calculated by dividing the yield acceleration, k_y , by the maximum acceleration, k_{max} . For this example, the acceleration ratio is equal to 0.24.
- (d) Deformation. Several simplified methods based on the concept of yield acceleration originally proposed by Newmark (1965) are utilized to estimate deformation (see table below).
 1. Makdisi and Seed (1978). The Makdisi and Seed (1978) method normalizes displacement by k_{max} , T_o , and gravity (figure 3-15). Based on the ratio of k_y to k_{max} of 0.24 and a moment magnitude of 7.5, the normalized displacement is equal to approximately 0.21 seconds (note that the units of seconds will be replaced by inches when the normalizing values are factored out). An estimated deformation of 31 cm (12 inches) was calculated by multiplying the normalized displacement by the values of k_{max} , T_o , and gravity.
 2. Franklin and Chang (1977). The range of the Franklin and Chang (1977) simplified method provides upper bound estimates of permanent ground deformation (figure 3-16). For the critical acceleration ratio of 0.24 and using the curve based on all natural earthquake records, an estimated upper bound deformation of 81 cm (32 in) was calculated.

3. Yegian et al. (1991). The Yegian et al. (1991) simplified method for estimating permanent deformation normalizes displacement by k_{max} , T_0^2 , number of cycles, and gravity (figure 3-17). A magnitude 7.5 earthquake contains approximately fifteen cycles (from Seed and Idriss, 1982). Based on the ratio of k_y to k_{max} of 0.24, the normalized permanent deformation was estimated to be 0.04. An estimated deformation of 26.5 cm (10 in) was determined by multiplying the normalized displacement value of 0.04 by the values of k_{max} , T_0^2 , number of cycles, and gravity.

Method	Estimated Deformation in cm (inches)
Makdisi and Seed (1978)	30 (12)
Franklin and Chang (1977)	80 (32)
Yegian et al. (1991)	35 (10)

d. Hazard Mitigation

The amount of acceptable deformation is dependent on the tolerance of the pavement and acceptable damage. For this example problem, the deformation analysis methods predicted deformations between 26.5 and 81 cm (10 and 32 in). This magnitude of displacement was determined to be unacceptable. Thus, retrofitting was necessary at this site.



Several retrofitting approaches were considered. Based on availability of materials, economics, and other factors, the construction of a rock buttress appeared to be the most feasible. Pseudo-static slope stability analyses of the embankment as described above were repeated with rock buttresses of varying dimensions. The rock buttress served to increase the resisting forces along the slide plane and to force the critical failure surface to exit the embankment above the top of the rock buttress (see sketch). By forcing the critical failure surface to exit above the rock buttress, the mass of sliding material decreases substantially, resulting in reduced permanent ground deformation. The final dimensions of the rock buttress were 3 m (10 ft) in height and 2.4 m (8 ft) wide at the top with a 2:1 (H:V) slope of the outer surface. For the improved embankment, the estimated earthquake-induced displacement is less than 8 cm (3 in).

CHAPTER 4: TUNNELS

4.1. INTRODUCTION

This chapter describes procedures for the seismic screening and evaluation of tunnels and discusses strategies for seismic retrofit design of tunnels. In general, tunnels have performed well during earthquakes in comparison to the performance of aboveground structures. This can be attributed to the fact that a fully embedded tunnel tends to move with the ground and, in general, does not experience the strong inertial response of aboveground structures. The fact that the amplitude of seismic ground motion tends to reduce with depth below the ground surface also reduces tunnel damage.

Nevertheless, moderate to major damage has been experienced by many tunnels during earthquakes, as summarized by Dowding and Rozen (1978), Owen and Scholl (1981), Sharma and Judd (1991), and Power et al. (1998), among others. The greatest incidence of severe damage has been associated with large ground displacements due to ground failure, i.e., fault rupture through a tunnel, landsliding (especially at tunnel portals), and soil liquefaction. Ground shaking in the absence of ground failure has produced a lower incidence and degree of damage in general, but has resulted in moderate to major damage to many tunnels. Near-surface rectangular cut-and-cover tunnels in soil have been especially vulnerable to transient seismic lateral ground displacements, which tend to cause racking of a tunnel over its height and increased lateral pressures on the tunnel walls.

Some tunnels constitute a non-redundant transportation corridor that may be essential in the post-earthquake environment, e.g., highway and transit tunnels. Application of the guidelines for screening, detailed evaluation, and, where necessary, retrofit design of tunnels presented in this chapter can aid in identifying and mitigating life safety hazards in ordinary tunnels or loss of functionality in an essential or critical tunnel.

4.2. TUNNEL CLASSIFICATION

Tunnels can be grouped into three broad categories: (1) bored tunnels; (2) cut-and-cover tunnels; and (3) submerged tubes. These categories of tunnels exhibit distinctly different design features and construction methods.

4.2.1. BORED TUNNELS

Bored (or mined) tunnels are constructed by excavating the opening and constructing the support system below ground. These tunnels may be constructed in a variety of geologic environments ranging from hard rock to soft soils. Construction procedures involve the use of tunneling machines, drilling and blasting, and other techniques. The initial, primary, or temporary

lining/support system is usually constructed as the tunnel is excavated. The cross sectional shape of the tunnel is usually circular or semi-circular (e.g., horseshoe-shaped; straight-sided with semicircular dome). The New Austrian Tunneling Method (NATM) (Rabcewicz, 1964) of tunnel construction utilizes construction and initial support methods that limit the amount of ground deformation and dilation and enhance the ability of the ground to arch and support itself by forming a ground arch reinforced with structural elements. Based upon convergence-confinement theory (AFTES, 1978), the NATM has been successfully used in many ground conditions. In weak or fractured rock, it essentially consists of installing supports in a timely manner before (presupport) or soon after excavation, such as the installation of rock dowels and shotcrete support immediately following a short (2 to 4 feet) advance of the excavation face.

4.2.1.1. Bored Tunnels in Soft Ground

Soft ground tunnels are constructed by either two-pass or one-pass lining methods. In the two-pass method, the initial support system may consist of steel ribs and lagging, liner plate, or precast segmented lining. The final support system consists of a cast-in-place concrete liner. In the one-pass system, the liners are typically bolted and gasketed, precast segmented liners.

4.2.1.2. Bored Tunnels in Rock

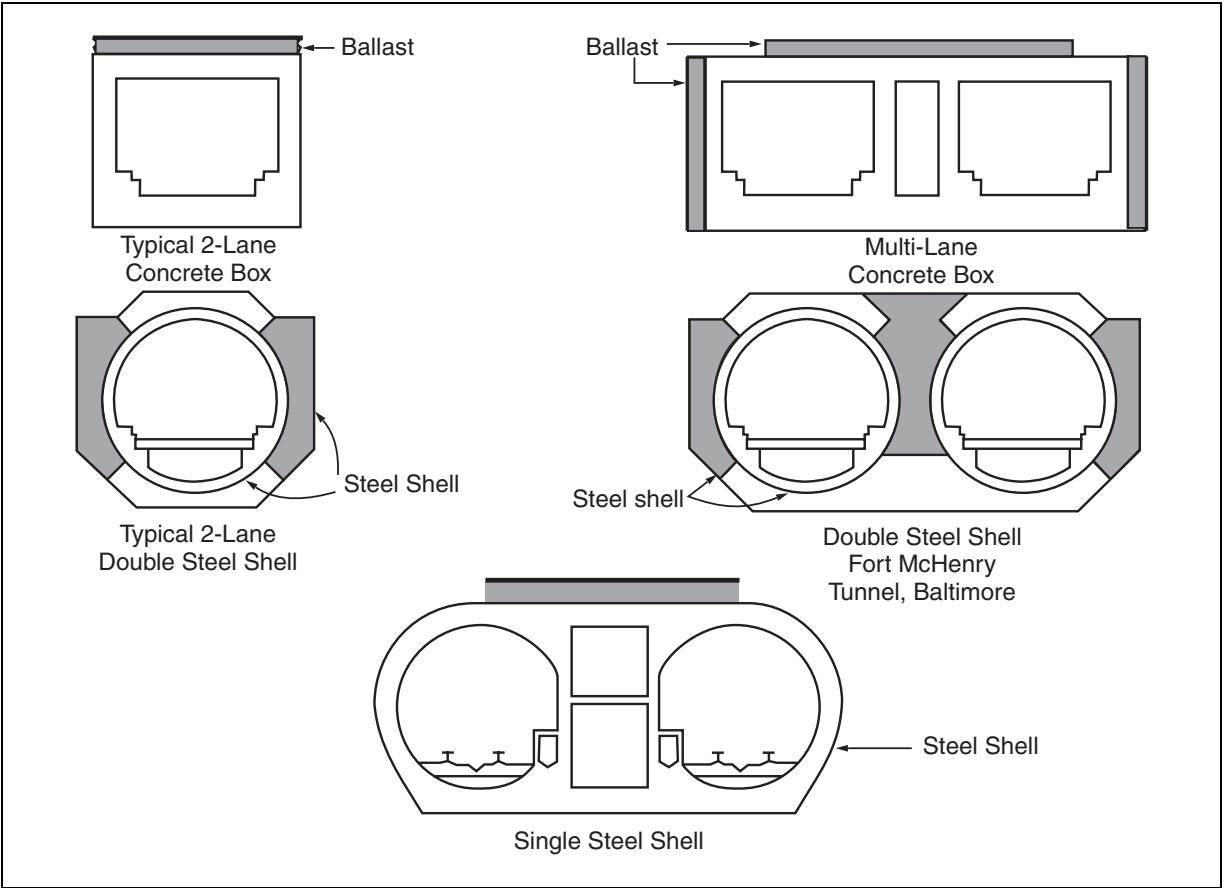
Tunnels in rock have methods of support that vary from none (in massive hard rock) to a temporary rib and lagging liner followed by a cast-in-place concrete final liner. Rock dowels or rock bolts are often installed as the excavation progresses to aid in allowing the rock to support itself and to stabilize loose blocks of rock in the vicinity of the opening.

4.2.2. CUT-AND-COVER TUNNELS

Cut-and-cover tunnels are constructed by excavating the opening from the ground surface, constructing the tunnel structure within the excavated opening, and backfilling above the top of the structure, as well as adjacent to the sides of the structure if it has not been constructed immediately against the excavation face. This method of construction is often used for relatively shallow tunnels (< 50 feet). The tunnel structure is typically rectangular in shape and of cast-in-place reinforced concrete construction.

4.2.3. SUBMERGED TUBES

Submerged tubes are constructed of prefabricated steel or concrete sections placed in shallowly excavated trenches on river and sea bottoms. These segments are floated into position and then sunk and connected. The trench is then backfilled and the tube covered. To overcome buoyancy, submerged tubes typically have enlarged cross sections for increased mass. Tube cross sections may be circular or rectangular (figure 4-1).



Gursoy, 1985

Figure 4-1. Cross sections of submerged tubes.

4.3. SCREENING GUIDELINES

4.3.1. OBJECTIVE OF SCREENING STAGE

The objective of the screening stage is to identify tunnels that have a substantial risk of poor performance during the design earthquake(s). The potential outcomes of the screening process are: (1) the tunnel is expected to meet the performance objective during the design earthquake(s) (see chapter 1), and no further evaluations of the tunnel are required; (2) the tunnel may not meet the performance objective, and further evaluations are needed to assess performance; and (3) the tunnel clearly does not meet the performance objectives, and retrofit measures are required. For tunnels identified through the screening process as falling into categories (2) or (3), the decision as to whether to conduct further evaluations and retrofit design, and the priority for such actions, depends on the importance of the tunnel as established by the responsible agency (see chapter 1).

4.3.2. FACTORS INFLUENCING TUNNEL SEISMIC PERFORMANCE

Various factors may influence tunnel seismic performance. These factors are described briefly below. Guidelines for considering these factors in screening-level evaluations are presented in section 4.3.3.

4.3.2.1. Seismic Hazard

Components of seismic hazard that may influence tunnel performance include:

- **Intensity of Ground Shaking.** The potential effects of vibratory ground shaking range from minor cracking of a concrete liner to collapse of the liner (if present) and major caving of geologic materials into the tunnel. For purposes of evaluating tunnel performance, the intensity of ground shaking is typically quantified by peak ground acceleration (PGA), peak ground velocity (PGV), peak ground displacement (PGD), and strong motion duration. For screening-level evaluations, PGA at the ground surface is usually used as an index of the shaking intensity, since acceleration is the parameter usually recorded and most readily estimated. For more detailed evaluations, ground motions at the depth of the tunnel and frequency content (response spectra) may also be estimated. In addition, for tunnels located close to active faults (within approximately 15 km), the unique characteristics of near-fault ground motion may become important, especially the possible presence of strong long-period pulses of ground motion that can lead to high ground acceleration, velocity, and displacement that may be especially damaging.
- **Fault Rupture.** If an active fault crosses the tunnel alignment, there is a hazard of direct, shearing displacement through the tunnel in the event of a moderate to large magnitude earthquake. Such displacements may range from a few inches to greater than ten feet and, in many cases, may be concentrated in a narrow zone along the fault. Fault rupture can and has had very damaging effects on tunnels. A related hazard is tectonic uplift and subsidence, if such movements cause enough differential deformation of the tunnel to be damaging.
- **Landsliding.** Landsliding through a tunnel, whether statically or seismically induced, can result in large, concentrated shearing displacements and either full or partial collapse of tunnel cross sections. Landslide potential is greatest when a preexisting landslide mass intersects the tunnel. A statically stable landslide mass may be activated by earthquake shaking. The hazard of landsliding is usually greatest in shallower parts of a tunnel alignment and at tunnel portals.
- **Soil Liquefaction.** For tunnels located in soils below the groundwater table, there could be a potential for liquefaction if loose to medium-dense cohesionless soils (sands, silts, gravels) are adjacent to the tunnel. Potential effects of liquefaction of soils adjacent to a tunnel include: (a) increased lateral pressures on the lining or walls of the tunnel, which could lead to failure of the lining or walls depending on their design; (b) flotation or sinking of a tunnel embedded in liquefied soil, depending on the relative weight of the tunnel and the soils replaced by the tunnel; and (c) lateral displacements of a tunnel if there is a free face toward which liquefied soil can move and/or if the tunnel is constructed below sloping ground.

4.3.2.2. Geologic Conditions

Potentially hazardous geologic conditions include fault rupture or tectonic uplift and subsidence, landslides, and liquefiable soils as discussed above. In addition, other unfavorable geologic conditions could lead to unsatisfactory seismic tunnel performance unless recognized and adequately accounted for in the tunnel design and construction. Unfavorable geologic conditions include: soft soils; rocks with weak planes intersecting a tunnel, such as shear zones or well developed weak bedding planes and well developed joint sets that are open or filled with weathered and decomposed rock; failures encountered during tunnel construction that may have further weakened the geologic formations adjacent to a tunnel (e.g., cave-ins or running ground leaving incompletely filled voids or loosened rock behind a lining; squeezing ground with relatively low static factor of safety against lining collapse); and adjacent geologic units having major contrast in stiffness that can lead to stress concentrations or differential displacement.

4.3.2.3. Tunnel Design, Construction, and Condition

Elements of tunnel design, construction, and condition that may influence tunnel seismic behavior include: (1) whether seismic loadings and behavior were explicitly considered in tunnel design; (2) the nature of the tunnel lining and support system (e.g., type of lining, degree of contact between lining/support systems and geologic material, use of rock bolts and dowels); (3) junctions of tunnels with other structures; (4) history of static tunnel performance in terms of failures and cracking or distortion of lining/support system; and (5) current condition of lining/support system, such as degree of cracking of concrete and deterioration of concrete or steel materials over time.

In evaluating an existing tunnel in the screening stage or in a more detailed evaluation, or in designing retrofit measures, it is important to obtain as complete information as possible on the tunnel design, construction, and condition and the geologic conditions along the tunnel alignment. To obtain this information, the design and evaluation team should review the design drawings and design studies, as-built drawings, construction records as contained in the construction engineer daily reports and any special reports, maintenance and inspection records, and geologic and geotechnical reports and maps. Special inspections and investigations may be needed to adequately depict the existing conditions and determine reasons for any distress to the tunnel.

4.3.3. SCREENING GUIDELINES

4.3.3.1. Screening Guidelines Applicable to All Types of Tunnels

There are certain conditions that would clearly indicate a potentially significant seismic risk to a bored tunnel, cut-and-cover tunnel, or submerged tube and thus require more detailed evaluations. These conditions include:

- An active fault intersecting the tunnel.
- A landslide intersecting the tunnel, whether or not the landslide is active.

- Liquefiable soils adjacent to the tunnel.
- History of static distress to the tunnel (e.g., local collapses, large deformations, cracking or spalling of the liner due to earth movements), unless retrofit measures were taken to stabilize the tunnel.

4.3.3.2. Additional Screening Guidelines for Bored Tunnels

If the above conditions do not exist, then the risk to a bored tunnel is a function of the tunnel design and construction, the characteristics of the geologic media, and the level of ground shaking. In this section, additional screening guidelines are presented considering these factors and empirical observations of tunnel performance during earthquakes.

Figure 4-2 presents a summary of empirical observations of the effects of seismic ground shaking on the performance of bored tunnels. The figure is from the study by Power et al. (1998), which updates earlier presentations of tunnel performance data by Dowding and Rozen (1978), Owen and Scholl (1981), and Sharma and Judd (1991). The data are for damage due only to shaking. Damage that was definitely or probably attributed to fault rupture, landsliding, and liquefaction is not included. The data are for bored tunnels only; data for cut-and-cover tunnels and submerged tubes are not included in figure 4-2.

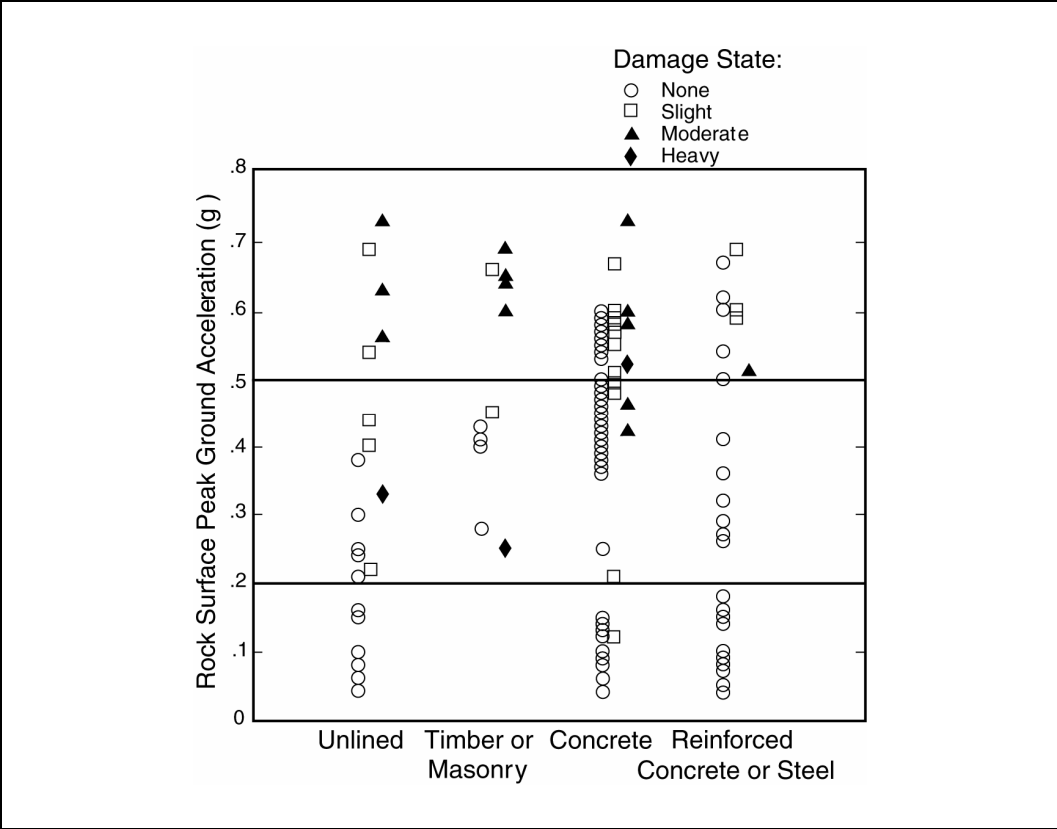


Figure 4-2. Summary of empirical observations of seismic ground shaking induced damage to bored tunnels.

Figure 4-2 incorporates observations for 192 tunnels from ten moderate to large magnitude earthquakes (moment magnitude M_w 6.6 to 8.4) in California, Japan, and Alaska. Note that many of the points in the figure represent multiple observations (i.e., the same damage state, lining types, and estimated acceleration for different tunnels). Ninety-four of the observations are from the moment magnitude M_w 6.9 1995 Kobe, Japan, earthquake. This earthquake produced by far the most observations for moderate to high levels of shaking (estimated peak ground accelerations [PGAs] at ground surface above the tunnels in the range of about 0.4 g to 0.6 g for the Kobe data). Peak ground accelerations in figure 4-2 are estimated for actual or hypothetical outcropping rock conditions at ground surface above the tunnel. Other observations are from moderate to large (M_w 6.7 to 8.4) earthquakes in California and Japan. The complete database is presented in Power et al. (1998). Figure 4-2 shows the level of damage induced in tunnels with different types of linings subjected to the indicated levels of ground shaking. Damage was categorized into four states: none for no observable damage; slight for minor cracking and spalling; moderate for major cracking and spalling, falling of pieces of lining and rocks; and heavy for major cave-ins, blockage, and collapse. The figure indicates the following trends:

- For PGAs equal to or less than 0.2 g, ground shaking caused very little damage in tunnels.
- For PGAs in the range of about 0.2 g to 0.5 g, there are some instances of damage ranging from slight to heavy. Note that the three instances of heavy damage are all from the 1923 Kanto, Japan, earthquake. For the 1923 Kanto earthquake observations with PGA equal to 0.25 g shown on figure 4-2, the investigations for this tunnel indicated the damage may have been due to landsliding. For the other two Kanto earthquake observations, collapses occurred in the shallow portions of the tunnels.
- For PGAs exceeding about 0.5 g, there are a number of instances of slight to moderate damage (and one instance of heavy damage noted above for the Kanto earthquake).
- Tunnels with stronger linings appear to have performed better, especially those tunnels with reinforced concrete and/or steel linings.

The trends in figure 4-2 can be used as one guide in assessing the need for further evaluations of the effects of ground shaking on bored tunnels.

Guidelines for assessing the need for further evaluations of bored tunnels for the failure mode of ground shaking induced damage are presented in table 4-1. The following are examples of poor and good lining/support systems for use with table 4-1.

Poor lining/support system:

- Timber or unreinforced masonry lining.
- Unreinforced concrete in soil or very poor rock.

Table 4-1. Assessment of need for seismic evaluations of bored tunnels as related to tunnel lining/support system, geologic conditions, and level of ground shaking.

Lining/Support System	Geologic Conditions		
	Soil or Extremely Poor Rock	Sheared and Jointed Rock	Sound Rock
Unlined	A	B	C
Poor lining/support system	A	B	C
Good lining/support system	C	C	D

A Evaluation desirable for any ground shaking level.
 B Evaluation desirable for moderate shaking levels, $PGA \geq 0.2$ g.
 C Evaluation desirable for high ground shaking levels $PGA \geq 0.5$ g.
 D No evaluation needed for any ground shaking level.

- Lining/support system in poor condition (e.g., deteriorated or otherwise weak concrete; moderately to severely cracked concrete; moderately to severely corroded metal linings/support systems).
- Linings in poor contact with geologic materials (frequent voids between lining and geologic materials).

Good lining/support system:

- Linings specifically designed for seismic loading consistent with the seismic environment of the tunnel, geologic conditions, and good seismic design practice.
- Reinforced concrete or steel liners in good contact with geologic materials.
- Unreinforced concrete liners in good contact with fair to good rock; rock dowels or rock bolts providing arch support.

Consistent with the criteria in section 1.2 of this manual, the guidelines in table 4-1 are for a performance objective of life safety and collapse prevention for non-critical tunnels during an upper-level rare earthquake. More conservative guidelines may be appropriate for critical or essential tunnels that have functionality performance objectives.

Table 4-1 does not explicitly cover tunnel connections with other structures. If a connection has been well designed to transmit forces or to accommodate displacements, it may be screened on the basis of the third line in table 4-1. However, if the strength or displacement capacity of a connection is questionable, the connection should be screened on the basis of the second line in the table.

4.3.3.3. Additional Screening Guidelines for Cut-and-Cover Tunnels

The seismic performance of shallow cut-and-cover box-like tunnels has been relatively poor in comparison to the performance of bored tunnels. This was especially evident during the 1995 Kobe, Japan, earthquake (O'Rourke and Shiba, 1997; Power et al., 1998). The relatively poor performance of cut-and-cover tunnels may reflect: (1) relatively softer near-surface geologic materials surrounding these types of structures as compared to the harder materials that often surround bored tunnels at greater depths; (2) higher levels of acceleration at and near the ground surface than at depth (due to tendencies for vibratory ground motions to reduce with depth below the ground surface); and (3) vulnerability of these box-like structures to seismically induced racking deformations of the box cross section (figure 4-3d), unless specifically designed for these forces. Cut-and-cover tunnels in soil (the more common geologic condition for these types of tunnels) tend to be more vulnerable than those excavated into rock because of the larger soil shear deformations causing the tunnel racking. Tunnels in soft soil may be especially vulnerable. The most important determinant in assessing whether more detailed seismic evaluations of cut-and-cover tunnels are required is whether the original design considered loadings and deformations consistent with the seismic environment and geologic conditions, and especially, whether racking behavior was taken into account in the seismic analysis, design, and detailing of the structure.

4.3.3.4. Additional Screening Guidelines for Submerged Tubes

Submerged tubes are particularly susceptible to permanent ground movements during seismic shaking. Tubes are typically located at shallow depths and in soft or loose soils. Liquefaction of loose cohesionless soils may cause settlement, uplift (flotation), or lateral spreading. Earthquake shaking may also cause permanent displacement of soft clay soils on sloping ground. Joints connecting tube segments must accommodate the relative displacement of adjacent segments while maintaining a watertight seal. Generally, submerged tubes can be screened out from more detailed evaluations if the original design appropriately considered and analyzed the potential for ground failure modes and if joints have been carefully designed to achieve water tightness.

4.4. EVALUATION PROCEDURES

Described in this section are procedures for the detailed evaluation of tunnels for seismic loading. Procedures for evaluating tunnels for vibratory ground shaking are presented in section 4.4.1. Procedures for the evaluation of tunnels for the hazards of fault rupture displacement, landsliding, and liquefaction are presented in sections 4.4.2 and 4.4.3.

4.4.1. EVALUATION FOR GROUND SHAKING

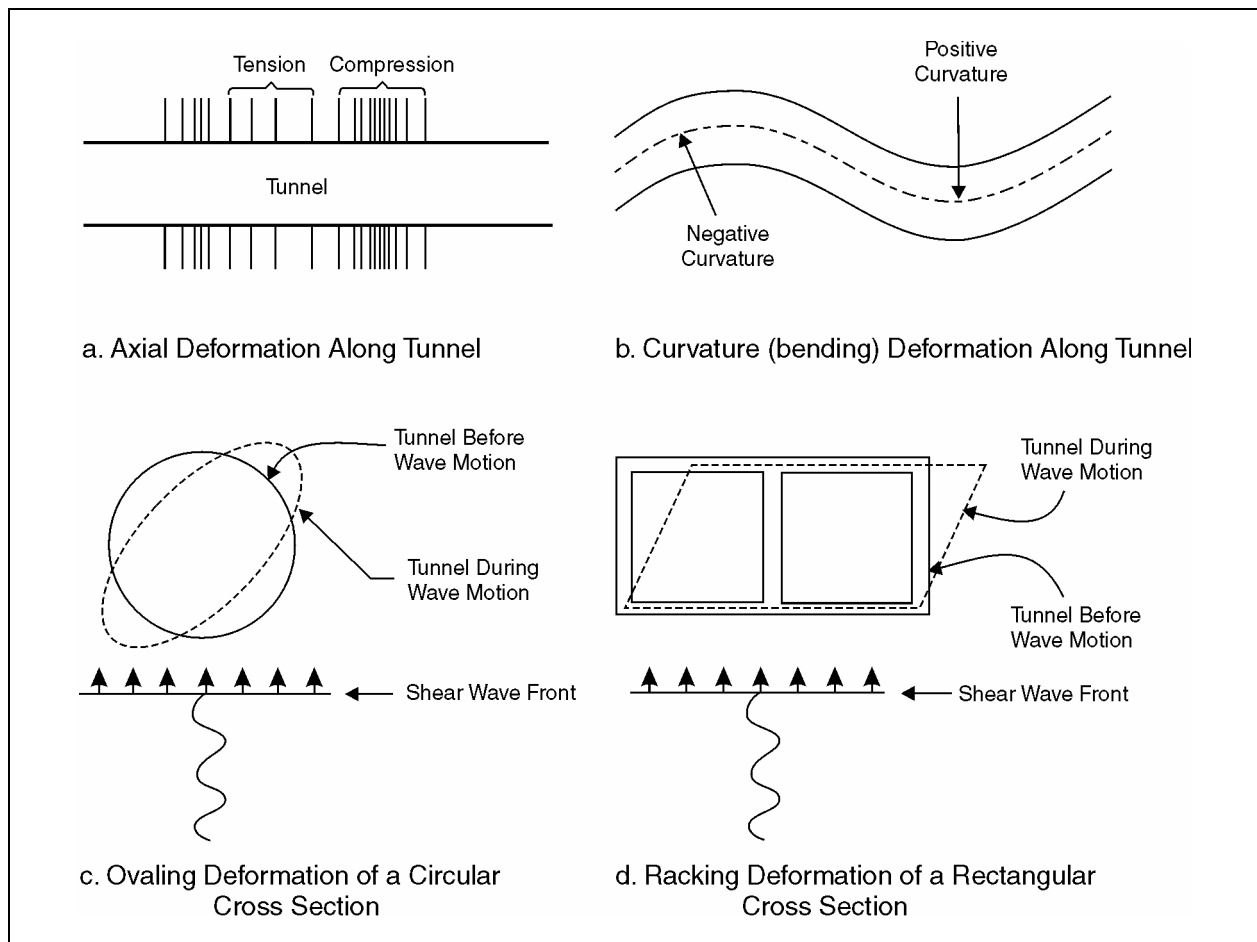
4.4.1.1. General

When a tunnel is subjected to seismic waves, two principal types of deformation occur. The first type consists of deformations occurring along the longitudinal axis of the tunnel, which include

both axial and curvature deformations. The second is deformations perpendicular to the tunnel longitudinal axis in the plane of the tunnel cross section. Figure 4-3 shows these principal types of deformation.

Axial and curvature deformations are induced by components of seismic waves that propagate along the tunnel longitudinal axis (Newmark, 1967; Keusel, 1969; Yeh, 1974; St. John and Zahrah, 1987). Axial deformations are generated by the components of seismic waves that produce particle motions parallel to the longitudinal axis of the tunnel and cause alternating compression and tension (figure 4-3a). Components of seismic waves producing particle motions in directions perpendicular to the longitudinal axis cause curvature (figure 4-3b).

Seismic waves propagating perpendicular to the tunnel longitudinal axis in the plane of the tunnel cross section distort the cross sectional shape of the structure, resulting in “ovaling” deformations of a circular (or semicircular) tunnel cross section (figure 4-3c) and “racking” deformations of a rectangular cross section (figure 4-3d).



Wang, 1993; Owen and Scholl, 1981

Figure 4-3. Tunnel response to seismic waves.

Both axial and curvature deformations along the tunnel longitudinal axis and ovaling and racking deformations of the tunnel cross section can produce significant damage to tunnels. Gross instabilities of the tunnel, involving shaking-induced caving of geologic materials into the tunnel, would generally be associated with inertial forces acting in the plane of the tunnel cross section. Therefore, assessment of the potential for inertial force-induced caving into tunnels is addressed as part of the evaluation procedures for tunnel cross sectional deformation.

The procedures described in subsequent sections provide methods for evaluating shaking-induced strains and stresses in a tunnel. They must be combined with the preexisting static strains and stresses in assessing the effects of earthquake shaking on tunnel performance. The assessment of static loads is described in tunnel design manuals and other publications, e.g., U.S. Army Corps of Engineers (1997). The strains and stresses induced in a tunnel must be assessed relative to the adopted performance criterion or criteria. For a life safety/collapse prevention performance criterion during an upper-level or “maximum” earthquake, strains beyond the elastic range may be acceptable; their effects should be evaluated by structural engineers who are knowledgeable in inelastic structural behavior.

4.4.1.2. Broad Guidelines for Analyses for Ground Shaking

This section provides broad guidelines for the application and relative importance of different types of analyses for ground shaking. These are grouped below into (1) analyses for axial and curvature deformations along the tunnel longitudinal axis, and (2) analyses of tunnel cross sectional response. Then in sections 4.4.1.3 and 4.4.1.4, the analysis methods and their applications are described in detail.

- Evaluation of axial and curvature deformations along tunnel longitudinal axis (section 4.4.1.3 below).
 - Simplified Analyses (section 4.4.1.3(a)). Free-field analyses described in section 4.4.1.3(a) below should be conducted. An important component of the evaluation is a seismological assessment of the type of seismic wave field (body S-waves or surface R-waves) that could be present and govern tunnel response. Generally, S-waves would not result in excessive strains and stresses in a tunnel, but R-waves in basin environments could be more damaging if associated with strong ground motions.

Although simplified soil-tunnel interaction formulations are also presented in section 4.4.1.3(a), these are generally not recommended to be applied because reductions in response due to interaction may not be justified because of uncertainties associated with simplified interaction formulations as well as ground motion phenomena neglected in simplified approaches (i.e., ground motion incoherence described in section 4.4.1.3).

- Numerical Analyses (section 4.4.1.3(b)). More sophisticated numerical analysis methods should be considered if simplified approaches are inconclusive. These approaches should especially be considered for situations where a tunnel abuts structures of significantly different response characteristics such as a portal structure, ventilation structure, or transit station.

- Evaluation of deformations of tunnel cross section (section 4.4.1.4 below).
 - Simplified Analyses (section 4.4.1.4(a)). Except for critical junctions of a tunnel to other structures, the deformations of a tunnel cross section are likely to be a more important mode of response than axial and curvature deformations along the longitudinal axis. Generally, simplified analyses methods described in section 4.4.1.4(a) below should be sufficient to check stability of cross sections against local failure of the lining in weak soil or rock zones or to analyze for the response modes of ovaling or racking of the tunnel cross section. For shallow rectangular cut-and-cover tunnels, seismic earth pressure analyses should also be conducted. However, simplified earth pressure analyses involve more uncertainty than simplified racking analyses.
 - Numerical Analyses (section 4.4.1.4(b)). Numerical analysis methods should be considered in cases where simplified analysis methods are less applicable, more uncertain, or inconclusive, such as earth pressures against rectangular structures, or where case history data indicate relatively higher seismic vulnerability for the type of tunnel, such as rectangular cut-and-cover tunnels.

4.4.1.3. Evaluation of Axial and Curvature Deformations along the Longitudinal Tunnel Axis

Two levels of analytical approaches are described below: simplified or closed-form solutions, and numerical analysis methods. Figure 4-4 summarizes methods for analyzing axial and curvature deformations.

It should be noted that simplified approaches typically incorporate the assumption that the seismic wave field along a tunnel is that of plane waves in which the waves have the same amplitudes at different locations along the tunnel and differ only in their arrival time. Numerical analysis methods may incorporate the same assumptions. However, if local soil conditions would lead to differential soil amplification along a tunnel, these effects would typically be incorporated in numerical analyses.

Wave-scattering and complex three-dimensional wave propagation, which can lead to differences in wave amplitudes along a tunnel, have been neglected in practice. These differences, termed ground motion incoherence (refer, for example, to Abrahamson et al., 1987; Abrahamson, 1993) would tend to increase strains and stresses in the longitudinal direction. For example, figure 4-5, from Abrahamson (1993), illustrates that at shorter separation distances, strains associated with incoherence may equal or exceed those due to plane wave propagation (termed wave passage in figure 4-5). However, the effects of incoherence on tunnel response has not yet been systematically studied. Therefore, until guidance on the effects of incoherence is developed, the results of simplified analyses based on plane wave assumptions should be interpreted conservatively. The effects of incoherence and variable geology on tunnel response can be modeled using numerical analyses if warranted.

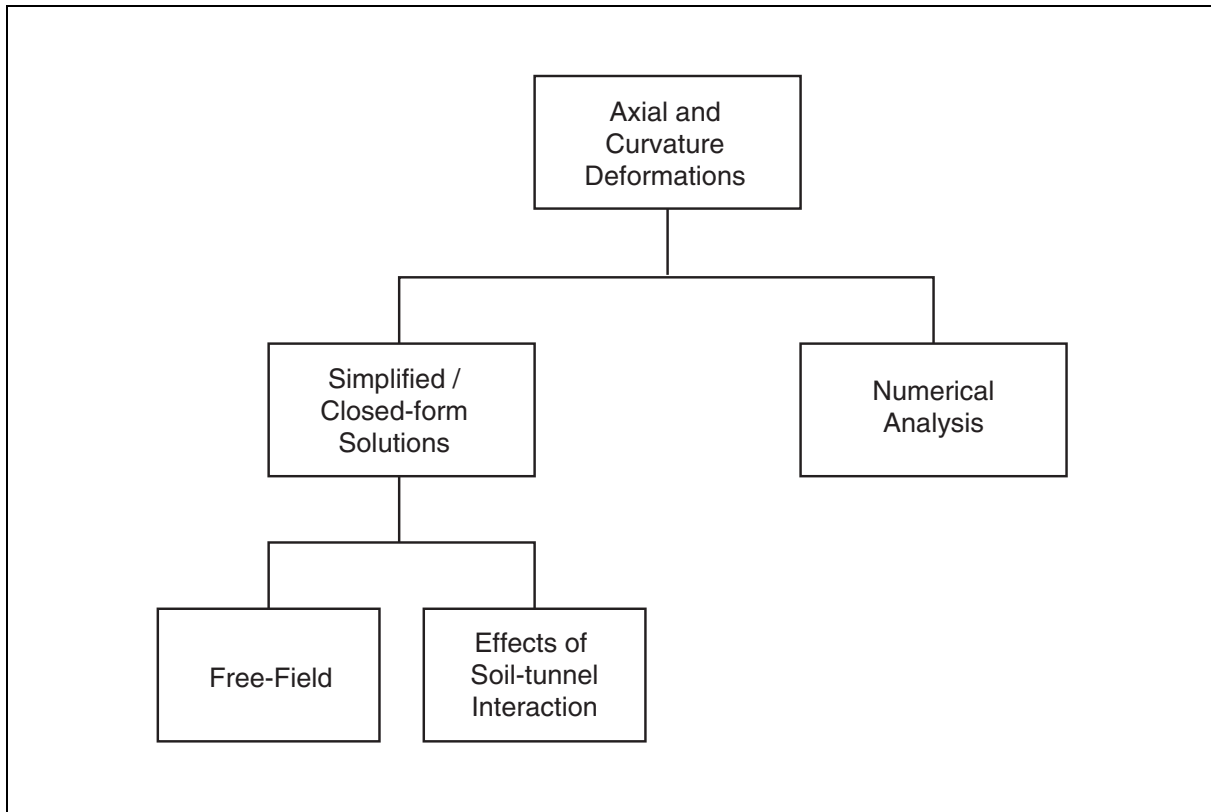
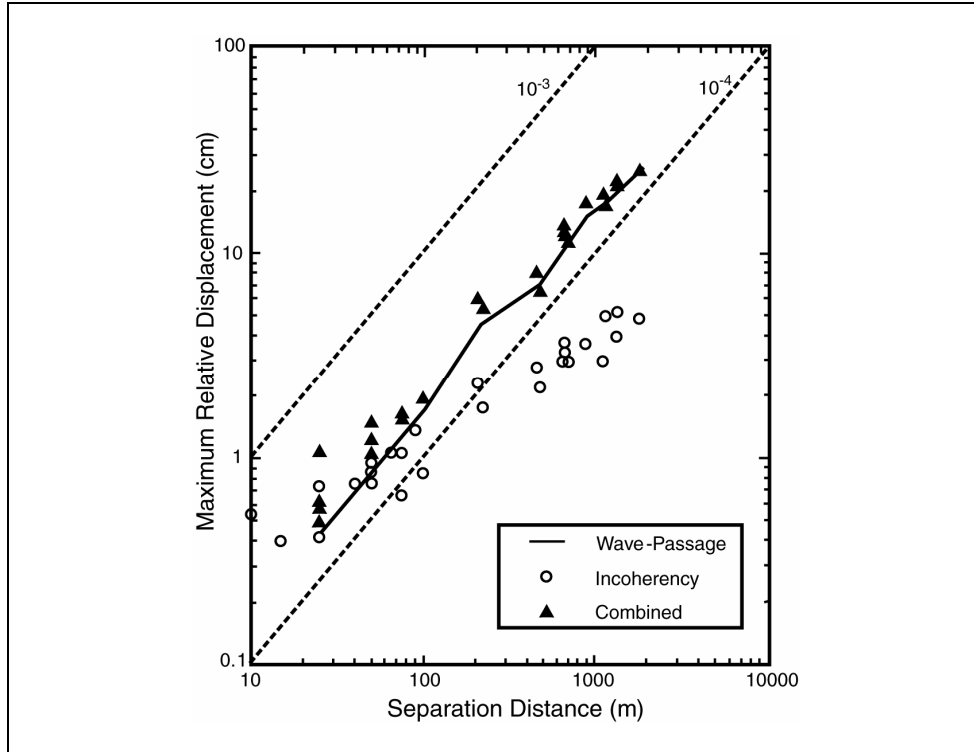


Figure 4-4. Approaches for analyzing a tunnel for longitudinal axial and curvature deformations.

4.4.1.3(a). Simplified Analyses/Closed-Form Solutions

In many cases, tunnels can be considered flexible in response to axial and curvature deformations. In these cases, strains and stresses are estimated using free-field solutions, assuming that the tunnel conforms to the imposed deformations from the surrounding geologic media. Soil-tunnel interaction may reduce response relative to free-field solutions. Simplified analyses for soil-structure interaction are addressed in the section following the presentation of the free-field solutions below.

Free-field Solutions: Table 4-2 summarizes the axial and shear strains and bending curvature generated by seismic waves propagating at an angle ϕ in the horizontal plane with respect to the longitudinal axis of a tunnel (figure 4-6). Equations are given in table 4-2 for strains due to compressional (P) and shear (S) body waves and Rayleigh (R) surface waves, and each strain reaches its maximum value at a different ϕ angle, as shown in the table. Axial strains rather than shear strains are typically of primary significance in tunnel design and performance. In the absence of significant surface waves, S-waves typically cause the largest strains and are the governing wave type. Strains induced by P-waves generally do not govern. Under certain circumstances, R-waves may result in the highest strains and should be considered in design. Figure 4-7 illustrates axial force, shear forces, and moments induced in a tunnel by components of seismic waves propagating in the direction of the tunnel longitudinal axis.



Abrahamson, 1993

Figure 4-5. Example of maximum relative displacements associated with seismic wave propagation. The effects of wave passage and incoherency are shown separately and combined. The dashed lines correspond to constant strains of 10^{-3} and 10^{-4} .

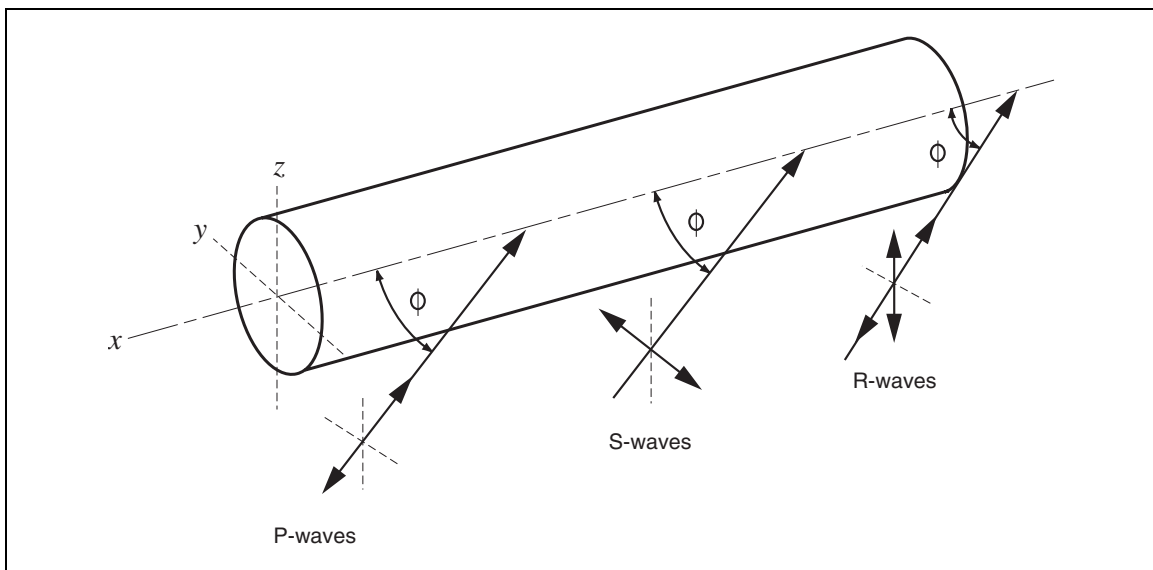


Figure 4-6. Seismic waves causing longitudinal axial and bending strains.

Table 4-2. Strains and curvature induced by seismic wave propagating along a tunnel.

Wave Type		Axial Strain	Shear Strain	Curvature
P-wave		$\epsilon = \frac{V_P}{C_P} \cos^2 \phi$	$\gamma = \frac{V_P}{C_P} \sin \phi \cos \phi$	$\frac{1}{\rho} = \frac{a_P}{C_P^2} \sin \phi \cos^2 \phi$
		$\epsilon_{\max} = \frac{V_P}{C_P}$ for $\phi = 0^\circ$	$\gamma_{\max} = \frac{V_P}{2C_P}$ for $\phi = 45^\circ$	$\frac{1}{\rho_{\max}} = 0.385 \frac{a_P}{C_P^2}$ for $\phi = 35.27^\circ$
S-wave		$\epsilon = \frac{V_S}{C_S} \sin \phi \cos \phi$	$\gamma = \frac{V_S}{C_S} \cos^2 \phi$	$\frac{1}{\rho} = \frac{a_S}{C_S^2} \cos^3 \phi$
		$\epsilon_{\max} = \frac{V_S}{2C_S}$ for $\phi = 45^\circ$	$\gamma_{\max} = \frac{V_S}{C_S}$ for $\phi = 0^\circ$	$\frac{1}{\rho_{\max}} = \frac{a_S}{C_S^2}$ for $\phi = 0^\circ$
R-wave	Compressional Component	$\epsilon = \frac{V_R}{C_R} \cos^2 \phi$	$\gamma = \frac{V_R}{C_R} \sin \phi \cos \phi$	$\frac{1}{\rho} = \frac{a_R}{C_R^2} \sin \phi \cos^2 \phi$
		$\epsilon_{\max} = \frac{V_R}{C_R}$ for $\phi = 0^\circ$	$\gamma_{\max} = \frac{V_R}{2C_R}$ for $\phi = 45^\circ$	$\frac{1}{\rho_{\max}} = 0.385 \frac{a_R}{C_R^2}$ for $\phi = 35.27^\circ$
	Shear Component		$\gamma = \frac{V_R}{2C_R} \cos \phi$	$\frac{1}{\rho} = \frac{a_R}{C_R^2} \cos^2 \phi$
			$\gamma_{\max} = \frac{V_R}{C_R}$ for $\phi = 0^\circ$	$\frac{1}{\rho_{\max}} = \frac{a_R}{C_R^2}$ for $\phi = 0^\circ$
<p>where:</p> <ul style="list-style-type: none"> V_P = soil particle velocity caused by P-waves a_P = soil particle acceleration caused by P-waves C_P = apparent propagation velocity of P-waves V_S = soil particle velocity caused by S-waves a_S = soil particle acceleration caused by S-waves C_S = apparent propagation velocity of S-waves V_R = soil particle velocity caused by R-waves a_R = soil particle acceleration caused by R-waves C_R = propagation velocity of R-waves $1/\rho$ = curvature 				

St. John and Zahrah, 1987; and Yeh, 1974

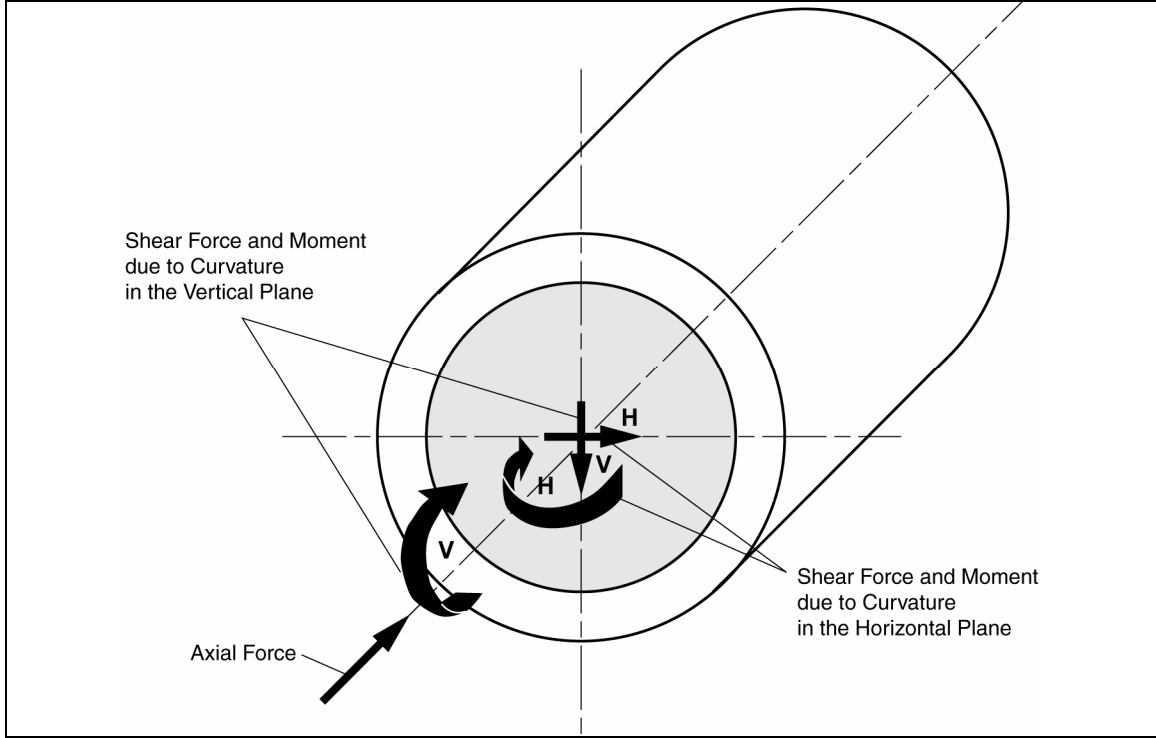


Figure 4-7. Induced forces and moments caused by seismic waves propagating along the longitudinal tunnel axis.

Strains and stresses due to combined axial and curvature deformations can be obtained by treating the tunnel as an elastic beam. Using beam theory, the maximum axial strain, ϵ^{ab} , is given by combining the axial strains generated by longitudinal deformations and curvature deformations in a horizontal plane:

$$\epsilon^{ab} = \left[\frac{V_P}{C_P} \cos^2 \phi + Y \frac{a_P}{C_P^2} \sin \phi \cos^2 \phi \right] \quad \text{for P-waves} \quad (4-1)$$

$$\epsilon^{ab} = \left[\frac{V_S}{C_S} \sin \phi \cos \phi + Y \frac{a_S}{C_S^2} \cos^3 \phi \right] \quad \text{for S-waves} \quad (4-2)$$

$$\epsilon^{ab} = \left[\frac{V_R}{C_R} \cos^2 \phi + Y \frac{a_R}{C_R^2} \sin \phi \cos^2 \phi \right] \quad \text{for R-waves} \quad (4-3)$$

Within the elastic range, the axial stress due to combined axial and curvature deformations is:

$$\sigma^{ab} = E_1 \epsilon^{ab} \quad \text{for P-, S-, and R-waves} \quad (4-4)$$

where:

Y is the distance from the neutral axis of the cross section to the extreme fiber of the tunnel lining,

E_1 is the Young's modulus of tunnel lining,

a_P is the peak particle acceleration associated with P-wave,

a_S is the peak particle acceleration associated with S-wave,

a_R is the peak particle acceleration associated with R-wave,

V_P is the peak particle velocity associated with P-wave,

C_P is the apparent velocity of P-wave propagation,

V_S is the peak particle velocity associated with S-wave,

C_S is the apparent velocity of S-wave propagation,

V_R is the peak particle velocity associated with R-wave, and

C_R is the velocity of R-wave propagation.

The magnitude of axial strain due to curvature deformation is typically small compared to that due to axial deformation. As the radius of the tunnel increases, the contribution to axial strain from curvature deformation increases. The angle of wave propagation, ϕ , that maximizes the combined axial strain depends on the wave characteristics and the geometry of the tunnel, and can be derived by trial and error. If the curvature contribution to axial (longitudinal) strain is insignificant, then the values of ϕ that maximize axial strains are given in table 4-2. If the curvature contribution to axial strain is found to be significant, then it is suggested that the two terms in equations 4-1, 4-2, and 4-3 be combined as the square root of the sum of the squares (SRSS), because peak particle velocity and acceleration will not necessarily be in phase.

In equations (4-1) and (4-2), the P- and S-wave velocities, C_P and C_S , represent apparent horizontal wave propagation velocities at the elevation of the tunnel. Generally, these apparent velocities correspond to seismic wave propagation through the deeper rocks rather than to the velocities of the shallower soils and rocks in which the tunnel may be located. Based on analyses of data from ground motion spatial arrays (O'Rourke et al., 1982; Chang et al., 1986; Abrahamson, 1985, 1992, 1995), the apparent velocity of S-waves in the direction of horizontal wave propagation varies from about 2 to 4 km/sec. A velocity of 2 km/sec is recommended unless larger values can be justified for the specific seismic environment of the tunnel. Apparent P-wave velocities in the direction of wave propagation generally range from about 4 to 8 km/sec. P-wave propagation seldom governs induced strains and stresses in tunnels because the associated peak particle accelerations and velocities are usually much smaller than those associated with S-waves.

When tunnels are present in deep deposits of soil sediments, it is possible that the induced strains and stresses will be governed by surface (Rayleigh) waves. Factors which tend to increase the importance of R-waves relative to S-waves are: (1) R-wave propagation velocities tend to be smaller than S-wave apparent propagation velocities (note that since R-waves propagate horizontally through the shallower geologic media, their wave propagation velocities as measured in spatial arrays are "actual" rather than "apparent" velocities); and (2) maximum axial strain (neglecting contributions from curvature) is equal to V_R/C_R for R-waves and $V_S/2C_S$ from S-waves (table 4-2). Factors which tend to reduce the importance of R-waves relative to S-waves are: (1) the peak particle velocity in a time history is usually associated with S-waves

(velocity, V_S) rather than R-waves (V_R), especially in the near-source region, which is more likely to have potentially damaging strong ground motions; and (2) R-wave amplitudes may decrease faster with depth than S-wave amplitudes, thus reducing the importance of R-waves for deep tunnels.

A seismologic assessment is required to determine whether a tunnel is in a geologic and seismic environment in which surface waves should be considered and to estimate V_R and C_R for strain calculations. In general, surface waves should be considered if the tunnel is located in a sedimentary basin. Examples of sedimentary basins in the United States in which prominent surface waves have been observed include the Los Angeles basin, San Fernando Valley, San Bernardino Valley, and Santa Clara Valley, California. These basins are characterized by soil sediments at least several hundreds of feet deep and valley widths of several kilometers to tens of kilometers. Further discussions of surface waves including current knowledge regarding V_R and C_R are presented in Appendix A. It is noted that with the current state-of-knowledge, selection of parameters for analysis of tunnel longitudinal response due to surface waves involves greater uncertainty than parameter selection for body waves.

Peak particle velocities and accelerations used in the formulations in table 4-2 and equations (4-1) through (4-3) (V_P and a_P for P-waves, V_S and a_S for S-waves, and V_R and a_R for R-waves) represent the velocities and accelerations at the elevation of the tunnel. Because ground motions generally decrease with depth below the ground surface, these parameters generally have lower values than estimated for ground surface motions (e.g., Chang et al., 1986). The ratios of ground motion values at tunnel depths to those at the ground surface may be taken as the ratios summarized in table 4-3 unless lower values are justified based on site-specific assessments.

Ground motion attenuation relationships for estimating ground surface motions that are applicable to the tectonic environment and geologic conditions at the tunnel location should be used to estimate ground surface motions. The ratios summarized in table 4-3 can then be applied to obtain ground motions at the tunnel depth. For tunnels in rock, ground surface motions should be estimated at a hypothetical rock outcrop using rock attenuation relationships and the ratios in table 4-3 applied to the rock outcrop motions.

Table 4-3. Ratios of ground motion at tunnel depth to motion at ground surface.

Tunnel Depth (m)	Ratio of Ground Motion at Tunnel Depth to Motion at Ground Surface
≤ 6	1.0
6 to 15	0.9
15 to 30	0.8
> 30	0.7

A number of attenuation relationships are available for estimating peak ground surface accelerations, but few attenuation relationships are available for estimating peak ground surface velocities. The ratios of peak ground velocity (km/sec) to peak ground acceleration (g) for soil and rock summarized in table 4-4 may be used to estimate peak ground velocities in the absence

of site-specific assessments. The relationships in table 4-4 are for use with peak ground acceleration attenuation relationships for shallow crustal earthquakes in the western United States. These types of earthquakes are the primary sources of seismic hazard in most parts of the western United States. For subduction zone earthquakes, such as those that occur along coastal regions of Washington, Oregon, northwest California and Alaska, and for earthquakes in the central and eastern United States, ground motion prediction relationships developed for those regions should be used.

Due to the vertical component of a Rayleigh (R) wave, axial strain due to curvature in the vertical plane is equal to (see table 4-2):

$$\epsilon^{ab} = Y \frac{a_R}{C_R^2} \cos^2 \phi \quad \text{for R-waves} \quad (4-5)$$

which is out of phase with the axial strains due to the horizontal component of an R-wave given in equation 4-3.

Example calculations of axial strains and stresses in a tunnel using free-field solutions are provided in examples 4-1 and 4-2 for shear (S) waves and Rayleigh (R) waves, respectively.

Table 4-4. Ratios of peak ground velocity to peak ground acceleration in rock and soil.

Moment Magnitude, M_w	Ratio of Peak Ground Velocity (cm/sec) to Peak Ground Acceleration (g)		
	Source-to-Site Distance (km)		
	0 - 20	20 - 50	50 - 100
Rock*			
6.5	67	80	90
7.5	97	110	124
8.5	120	130	145
Stiff Soil*			
6.5	92	98	104
7.5	130	135	140
8.5	150	155	161
Soft Soil*			
6.5	138	147	156
7.5	195	203	210
8.5	225	233	242
* In this table, the sediment types represent the following low-strain shear wave velocity (C_m) ranges: rock \geq 750 m/sec; stiff soil 200 m/sec – 750 m/sec; and soft soil < 200 m/sec. The relationship between peak ground velocity and peak ground acceleration in soft soils is poorly constrained.			

adapted from Sadigh and Egan, 1998

Effects of Soil-Tunnel Interaction: The effects of soil-tunnel interaction on reducing axial strain (ϵ), shear strain (γ), and curvature ($1/\rho$) in a tunnel can be estimated using reduction factors given by St. John and Zahrah (1987) using beam-on-elastic-foundation theory. The free-field values of ϵ , γ , and ($1/\rho$) given in table 4-2 may be multiplied by the following reduction factors, R , to account for soil-tunnel interaction:

$$\text{For axial strain, } R = \frac{1}{1 + \frac{E_l A_{ll}}{K_a} \left(\frac{2\pi}{L}\right)^2 \cos^2 \phi} \quad (4-6)$$

For shear strain and curvature in a horizontal plane,

$$R = \frac{1}{1 + \frac{E_l I_{ll}}{K_h} \left(\frac{2\pi}{L}\right)^4 \cos^4 \phi} \quad (4-7)$$

where:

E_l is the Young's modulus of tunnel lining,

A_{ll} is the cross sectional area of the lining,

K_h is the transverse soil spring constant per unit length of tunnel,

K_a is the longitudinal soil spring constant per unit length of tunnel,

L is the wavelength of the P-, S-, or R-wave, and

I_{ll} is the moment of inertia of the lining cross section.

$$\text{(e.g., for circular liners: } I_{ll} = \frac{\pi(D_o^4 - D_i^4)}{64} \text{)}$$

St. John and Zahrah (1987) indicate that the transverse and longitudinal soil spring constants for use in equations 4-6 and 4-7 are the same and equal to:

$$K_a = K_h = \frac{16\pi G_m (1 - \nu_m) H}{(3 - 4\nu_m) L} \quad (4-8)$$

where:

H is the height of tunnel (diameter, D , for circular tunnels),

G_m is the shear modulus of the medium,

ν_m is the Poisson's ratio for the medium,

D_o is the outside diameter of tunnel lining ($D_o = D$), and

D_i is the inside diameter of tunnel lining.

For shear or bending in a vertical plane, the spring constant K_v is used in the preceding equations, and tunnel height, H , is replaced by width, w . If the geologic medium is of approximately equal stiffness all around the tunnel, K_v can be taken equal to K_h (equation 4-8). If the soil medium above the tunnel is much softer than the geologic medium beneath it, such as for a near-surface cut-and-cover tunnel or a tube, then:

$$K_v = \frac{2 \pi G_m}{(1 - \nu_m)} \frac{w}{L} \quad (4-9)$$

The wavelength, L , of P-waves, S-waves, and R-waves is related to the apparent velocity of P-wave and S-wave propagation, C_P and C_S ; the velocity of R-wave propagation, C_R ; and the wave period, $T_{P,S,R}$, for the respective waves, by:

$$L = (C_P, C_S \text{ or } C_R) T_{P,S,R} \quad (4-10)$$

For purposes of using this expression, $T_{P,S,R}$ can be assumed equal to the period at which the maximum displacement occurs. Typically, displacements occur at relatively long periods, and a value of $T_{P,S,R}$ equal to 2 seconds may be assumed unless L is evaluated from a site-specific study.

Shear modulus, G_m , is related to shear wave velocity, C_m , of the geologic medium adjacent to the tunnel by the equation:

$$G_m = \frac{\gamma_t}{g} C_m^2 \quad (4-11)$$

where:

γ_t is the total unit weight of the geologic medium,
 g is the acceleration of gravity.

For calculation of soil-structure interaction effects, it is recommended that “effective” values of G_m and C_m be used. Use of the effective values accounts in an approximate way for nonlinear soil behavior, i.e., the decrease of soil shear modulus with increasing level of ground shaking and soil shear strain. The effective values are denoted G'_m and C'_m . For rock, the ratio of C'_m / C_m , where C_m is the low-strain or maximum shear wave velocity, can be assumed equal to 1.0. For soil, in the absence of a site-specific study, C'_m / C_m can be assumed equal to 0.45 for a peak ground acceleration (PGA) at the ground surface of 0.7 g and equal to 0.8 for a PGA of 0.1 g. Values of C'_m / C_m may be interpolated for other accelerations.

The axial force in the lining is limited by the maximum frictional forces that can be developed between the lining and the surrounding soils. The maximum frictional force, $(Q_{\max})_f$, can be estimated to be equal to the frictional force per unit length times one-quarter of the wavelength (Sakurai and Takahashi, 1969):

$$(Q_{\max})_f = \frac{fL}{4} \quad (4-12)$$

where:

f is the maximum frictional force per unit length of the tunnel.

Examples 4-1 and 4-2 illustrate the calculation of the soil-structure interaction effect.

In section 4.4.1.3, it was suggested that the results of simplified analyses of axial and curvature deformations be interpreted conservatively, because the effects of ground motion incoherence might add significantly to the response, yet guidance for a systematic evaluation of incoherence effects has not yet been developed. There is also uncertainty regarding soil-structure interaction effects calculated using simplified procedures; for example, different approaches for the evaluation of soil spring constants have been proposed (e.g., St. John and Zahrah (1987); Owen and Scholl (1981); Public Works Research Institute (1976); SFBART (1960)). Therefore, in applying simplified procedures, it is recommended that the effect of soil-structure interaction in reducing axial and curvature deformations be neglected, except for limiting the maximum frictional force using equation 4-12. However, if equations 4-6 and 4-7 should be applied, it is recommended that the reduction factor, R , be limited to a minimum value equal to 0.7.

Junctions: At a junction of a tunnel to a stiffer structure, such as a ventilation structure or a transit station, strains will tend to be larger than along the running tunnel. Assuming the structure is a rigid boundary, the axial strain can be approximated as twice the strain calculated using the formulations presented in the preceding paragraphs.

4.4.1.3(b). Numerical Analysis

Generally, the inertia of a tunnel is small compared to that of the surrounding soil mass. Therefore, it is possible to conduct the analysis of axial and curvature deformations as a quasi-static analysis in which displacement time histories are applied to soil springs connected to a model of the tunnel. Computer codes available for this type of numerical model include ADINA (1996), ABAQUS (Hibbitt, Karlsson & Soreson, Inc., 1998), and SADSAP (Wilson, 1998).

4.4.1.4. Evaluation of Deformations of Tunnel Cross Section

Similar to approaches for the analysis of axial and curvature deformations, both simplified/closed-form solutions and numerical analysis methods may be used for the analysis of the tunnel cross section. Figure 4-8 summarizes the analytical methods, which are described below.

4.4.1.4(a). Simplified Analyses/Closed-Form Solutions

Analysis of Bored Tunnels

Pseudo-static Stability Analysis: A check should be made of the ability of the tunnel support system (lining and/or rock bolts or dowels) to resist inertia forces applied to the roof of the tunnel. The inertia forces can be approximated as a pseudo-static force equal to the estimated peak vertical ground acceleration (expressed as a decimal fraction of g) at the tunnel level times the static loads used for the roof design. The vertical peak ground acceleration may be assumed equal to the horizontal peak ground acceleration estimated as described in section 4.4.1.3(a). This may be somewhat conservative because vertical peak ground accelerations tend to be smaller than horizontal peak ground accelerations. However, for close distances to earthquake sources, ratios of vertical to horizontal peak ground accelerations tend to exceed the commonly used two-thirds ratios (e.g., Silva, 1997).

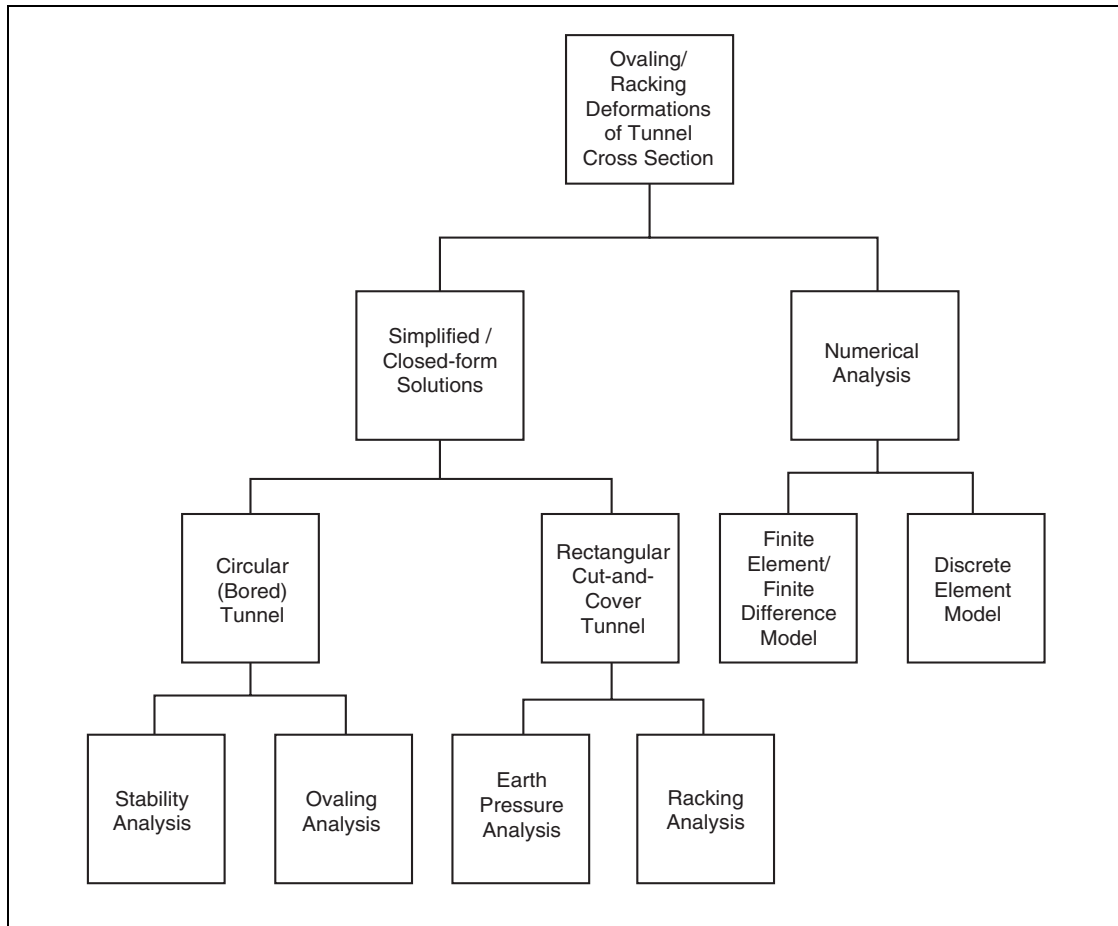


Figure 4-8. Approaches for seismic analysis of tunnel cross section.

A pseudo-static analysis is inherently conservative because the seismic inertia forces act in a destabilizing direction only for short instances of time. Nevertheless, the analysis is useful in indicating a potential stability problem.

If a weak zone, such as a zone of soft, sheared rock, exists adjacent to a tunnel, or a zone of relatively weak bedding or joint planes dips toward the tunnel, a pseudo-static analysis can also be made of the potential for caving of the weak mass into the tunnel. The analysis is illustrated schematically in figure 4-9.

Analysis of Ovaling of Circular Tunnels: The cross section of a tunnel should be analyzed for the ovaling deformations imposed by the geologic media assuming vertically propagating shear waves (figure 4-3c). Simplified analyses using static solutions generally may be used. Dynamic amplification effects on the response of the cross section can generally be neglected because these effects typically do not increase lining stresses by more than 5 percent to 15 percent (SFBART, 1960; Chen et al., 1979; Owen and Scholl, 1981). In general, if the predominant wavelength of the vertically propagating shear waves is greater than eight times the tunnel height, dynamic amplification effects will be insignificant (Merritt et al., 1985).

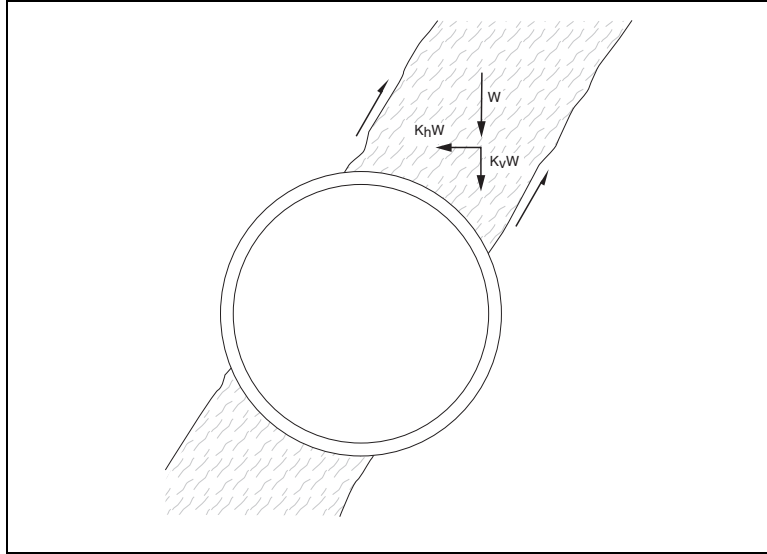


Figure 4-9. Pseudo-static stability analysis for weak zone adjacent to tunnel.

For purposes of assessing whether there is a potential for significant dynamic amplification, the predominate wavelength of the vertically propagating shear wave can be estimated as the product of the predominant period of acceleration ground shaking times the effective or strain-dependent shear wave velocity, C'_m , of the medium in which the tunnel is located. The predominant period of acceleration ground shaking is typically about 0.3 second for stiff soils and rocks and longer than 0.3 second for soft soils. A period of 0.3 second can be assumed in the absence of a site-specific study. The effective or strain-dependent shear wave velocity is discussed in section 4.4.1.3(a) following equation 4-11.

If the predominant wavelength calculated using these guidelines is less than eight times the tunnel height, a dynamic amplification of 15 percent above the forces and moments obtained from the static solutions presented below may be assumed. Alternatively, either the predominant wavelength may be estimated from a one-dimensional site response analysis discussed later in this section, or a dynamic time history soil-structure interaction analysis may be conducted to determine tunnel response, as discussed in section 4.4.1.4(b).

The closed-form elastic static solutions of Wang (1993) and Penzien and Wu (1998) may be used to estimate the dynamic (pseudo-static) thrust force (T), shear force (V), and moment (M) in the tunnel lining (figures 4-10 and 4-11). These solutions account for the interaction of the tunnel lining with the surrounding soil or rock. Wang (1993) adapted earlier solutions for external loading on a tunnel by Peck et al. (1972) (based on previous work by Burns and Richard, 1964; and Hoeg, 1968) to the seismic loading case for the condition of full slip (zero tangential shear stress) between tunnel and geologic medium. Similarly, he adapted the solution of Schwartz and Einstein (1980) (based on Hoeg's work) for the no-slip condition (continuity of displacements at tunnel and geologic medium interface). Penzien and Wu (1998) independently developed solutions for full-slip and no-slip conditions.

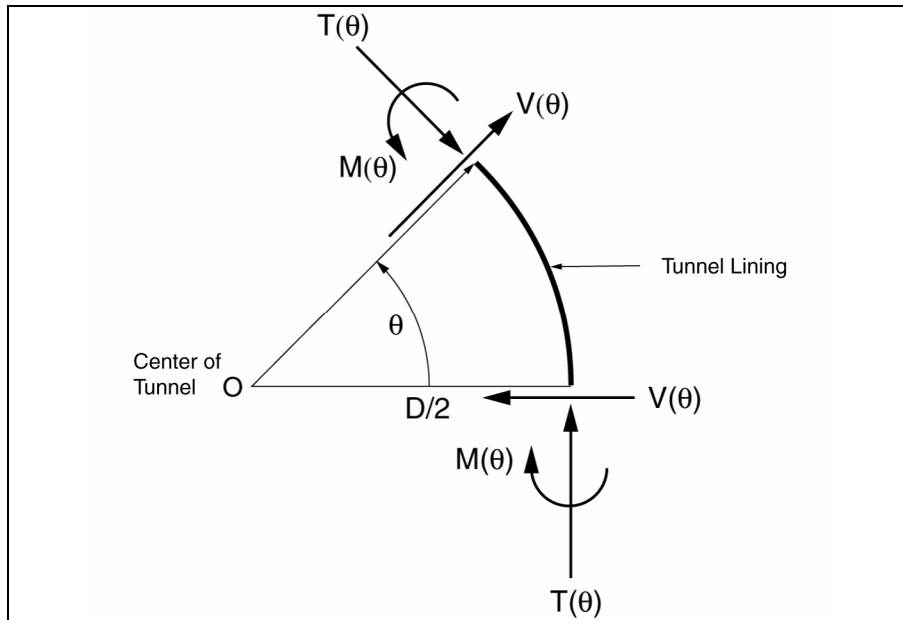


Figure 4-10. Forces and moments in tunnel lining due to ovaling.

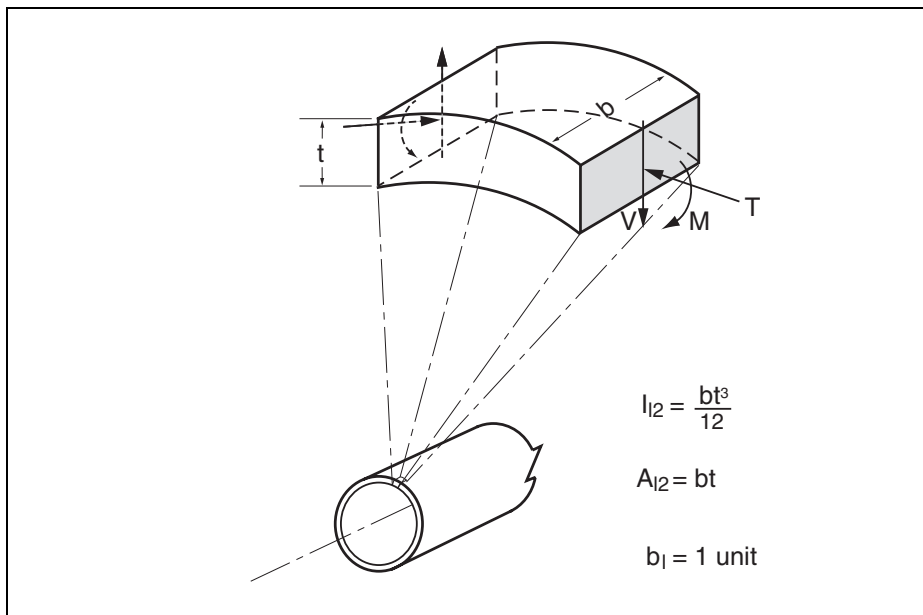


Figure 4-11. Area and moment of inertia for ovaling analysis of circular tunnel.

The solutions of Wang (1993) and Penzien and Wu (1998) for full slip are the same and can be expressed as follows:

$$\text{Thrust force, } T(\theta) = G'_m DK \gamma_{s\max} \sin 2\theta \quad (4-13)$$

$$\text{Shear force, } V(\theta) = 2G'_m DK \gamma_{s\max} \cos 2\theta \quad (4-14)$$

$$\text{Moment, } M(\theta) = \frac{1}{2} G'_m D^2 K \gamma_{s\max} \sin 2\theta \quad (4-15)$$

$$\text{where: } K = \frac{1 - \nu_m}{F + 2.5 - 3\nu_m} \quad (4-16)$$

F, termed the flexibility ratio, is the ratio of the shear stiffness of the geologic medium to that of the tunnel liner:

$$F = \frac{G'_m (1 - \nu_1^2) D^3}{24E_1 I_{12}} \quad (4-17)$$

where:

θ is the angle relative to horizontal axis through center of tunnel (figure 4-10),

D is the diameter of the tunnel,

$\gamma_{s\max}$ is the free-field shear strain at tunnel elevation induced by earthquake ground shaking,

G'_m is the effective shear modulus of the geologic medium (refer to text following equation 4-11 for evaluation of G'_m),

E_1 is the Young's modulus of the liner,

ν_m is the Poisson's ratio of geologic medium,

ν_1 is the Poisson's ratio of the liner, and

I_{12} is the moment of inertia of the lining cross section per unit length of tunnel (fig. 4-11).

The formulations of Penzien and Wu (1998) for the no-slip condition are the following:

$$\text{Thrust force, } T(\theta) = 2G'_m DK' \gamma_{s\max} \sin 2\theta \quad (4-18)$$

$$\text{Shear force, } V(\theta) = 2G'_m DK' \gamma_{s\max} \cos 2\theta \quad (4-19)$$

$$\text{Moment, } M(\theta) = \frac{1}{2} G'_m D^2 K' \gamma_{s\max} \sin 2\theta \quad (4-20)$$

where:

$$K' = \frac{1 - \nu_m}{F + 3 - 4\nu_m} \quad (4-21)$$

Note that equations 4-13 through 4-16 and 4-18 through 4-21 have been rearranged from the equations originally presented by Penzien and Wu (1998).

The formulation of Wang (1993) for thrust for the no-slip condition can be expressed as:

$$T(\theta) = \frac{1}{2} G'_m (1 + a_2) \gamma_{s\max} \sin 2\theta \quad (4-22)$$

Following the same approach used by Wang (1993), the formulation for moment for the no-slip condition is derived as:

$$M(\theta) = \frac{1}{8} G'_m D^2 (1 - a_2 - 2a_3) \gamma_{s\max} \sin 2\theta \quad (4-23)$$

where:

$$a_2 = \left\{ F(1 - 2v_m)(1 - C) - \frac{1}{2} C(1 - 2v_m)^2 + 2 \right\} / a_0 \quad (4-24)$$

$$a_3 = \left\{ F \left[C(1 - 2v_m) + 1 \right] - \frac{1}{2} C(1 - 2v_m) - 2 \right\} / a_0 \quad (4-25)$$

$$a_0 = F \left[(3 - 2v_m) + (1 - 2v_m)C \right] + C \left[\frac{5}{2} - 8v_m + 6v_m^2 \right] + 6 - 8v_m \quad (4-26)$$

Flexibility ratio, F , is given by equation 4-17. Compressibility ratio, C , is :

$$C = \frac{G'_m (1 - v_1^2) D}{E_1 t (1 - 2v_m)} \quad (4-27)$$

where:

t is the lining thickness (figure 4-11).

The earthquake loading for the calculation of ovaling is represented by the maximum free-field shear strain, $\gamma_{s\max}$, over the height of the tunnel produced by vertically propagating shear waves.

The maximum free-field shear strain preferably should be estimated using numerical methods such as a one-dimensional site response analysis (e.g., SHAKE [Schnabel et al., 1972; Idriss and Sun, 1992]). For deep tunnels, $\gamma_{s\max}$ can be approximated as:

$$\gamma_{s\max} = \frac{V_S}{C'_m} \quad (4-28)$$

where:

V_S is the peak particle velocity in the geologic medium at the tunnel depth.

C'_m is the effective shear wave velocity of the geologic medium at the tunnel depth.

These parameters can be estimated as discussed in the paragraphs following equations 4-4 and 4-11.

The maximum thrust force and bending moment both occur at angles of 45 degrees from the horizontal diametric axis of the tunnel (figure 4-10).

The maximum compressive and tensile stresses in the cross section induced by the earthquake can be obtained by combining the stresses from the thrust force and bending moment:

$$\sigma = \frac{T(\theta)}{A_{12}} \pm \frac{M(\theta)(t/2)}{I_{12}} \quad (4-29)$$

where:

t , A_{12} , and I_{12} are, respectively, the thickness, area, and moment of inertia of the lining cross section (figure 4-11).

In general, the equations for a full-slip condition lead to higher moments than the equations for a no-slip condition. Higher thrust forces are generally obtained for a no-slip condition, and thrust forces predicted by the Wang (1993) formulation are generally much higher than those predicted by the Penzien and Wu (1998) formulation, especially for stiffer geologic media. The reasons for the difference in the thrust force from the two formulations for the no-slip condition are not understood at present.

In application, it is recommended that the maximum stress from equation 4-29 be obtained using the full-slip or no-slip formulation that leads to the highest stress (equations 4-13 and 4-15 for a full-slip condition; equations 4-18 and 4-20 or equations 4-22 and 4-23 for a no-slip condition).

Example 4-3 illustrates the calculation of dynamic (pseudo-static) stresses in a circular tunnel due to ovaling. Example 4-5 illustrates the calculation of the combined static and dynamic (pseudo-static) stresses in circular tunnels for two different types of tunnel linings and for soft and stiff geologic media. Penzien and Wu (1998) present an example showing how the critical tension stress in a concrete lining increases and then decreases with increasing lining thickness due to soil-lining interaction.

It should be noted that the equations in this section were derived assuming the structure behaves elastically. When inelastic deformations are predicted to occur in the lining, nonlinear inelastic analyses should be performed when necessary to ensure that the lining will have adequate ductility.

Analysis of Rectangular Tunnels

Similar to the analysis of circular tunnels for ovaling, rectangular tunnel sections should be analyzed for the imposed racking deformations assuming vertically propagating shear waves. In addition, the walls and roof of the tunnel should be analyzed for dynamic earth pressures.

Racking Deformation Analysis: Wang (1993) developed a simplified procedure incorporating soil-structure interaction for the analysis of racking of rectangular tunnels (figure 4-3d). The procedure was developed based on a series of dynamic finite element analyses of a number of cases with varying soil and structural dynamic properties and structure geometries. The cases analyzed covered the following conditions:

- The ratio of the depth to the center of the structure, h , to the structure height, H , ranged from 1.1 to 2.0 (figure 4-12).
- Average shear modulus of the soils surrounding the structure ranged from 11,000 to 72,000 kPa (230 to 1500 ksf), with corresponding shear wave velocities of 75 to 200 m/sec (250 to 650 ft/sec).
- The vertical distance between the bottom of the structure and the top of underlying stiff soils/rock was equal to or greater than the height of the structure.
- Rigid body rotation was excluded.
- Five types of one-barrel and two-barrel rectangular structures were investigated. Structure widths, w , ranged from 4.6 to 27.5 m (15 to 90 feet), and structure heights, H , ranged from 4.6 to 8 m (15 to 26 feet).
- Two artificial earthquake ground motion time histories, representing western and northeastern U.S. earthquakes, were used.

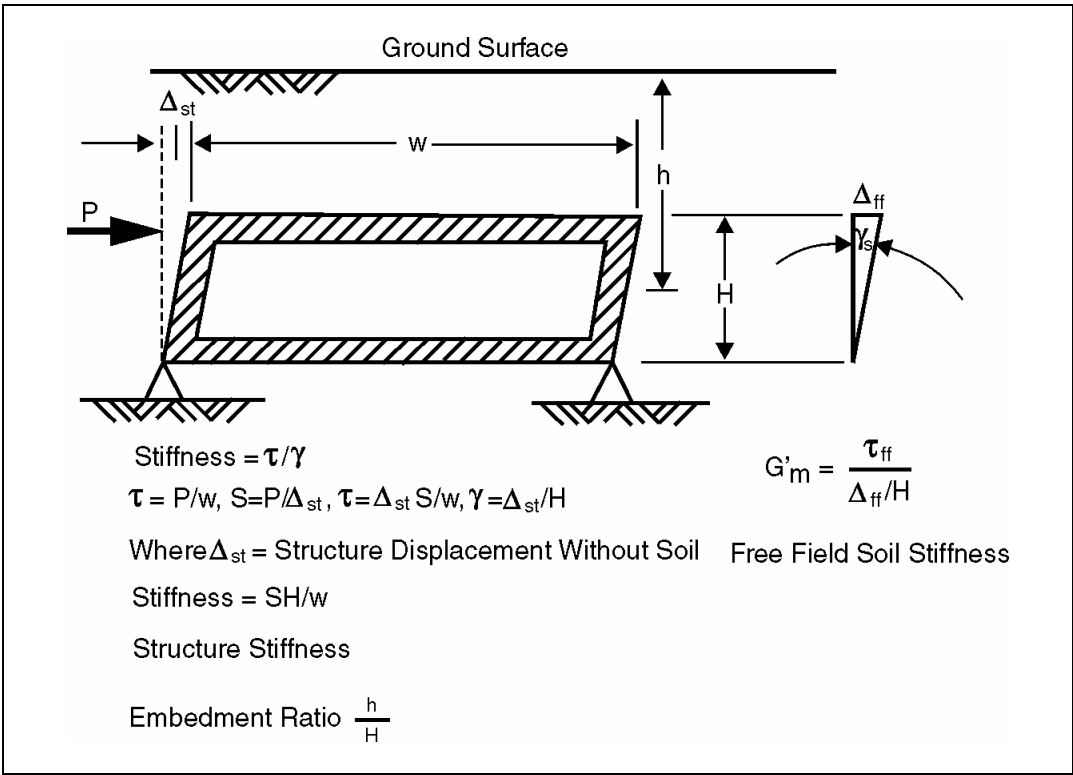


Figure 4-12. Definition of terms for Wang (1993) procedure for analysis of racking of a rectangular tunnel.

The following procedure is followed to assess the structure response and behavior:

Step 1: Estimate the free-field effective soil shear deformation, Δ_{ff} , over the height of the structure, H , due to vertically propagating shear waves (figure 4-12).

The free-field shear deformation, Δ_{ff} , should be estimated using site response analyses (e.g., computer code SHAKE [Schnabel et al., 1972; Idriss and Sun, 1992]). Due to the influence of seismic waves reflecting from the ground surface, shear strain is more reliably estimated for shallow tunnels using site response analyses than using simplified formulations (equation 4-28).

Step 2: Determine the relative flexibility of the soil and the structure.

A flexibility ratio, F_r , is defined as the ratio of the free-field effective soil shear stiffness to that of the structure, and is given by:

$$F_r = \frac{G'_m w}{S H} \quad (4-30)$$

where:

S is the racking stiffness, i.e., the force required to cause a unit racking deflection of the structure,

w is the width of the structure,

H is the height of the structure, and

G'_m is the shear modulus of the medium.

These terms are defined in figure 4-12.

Step 3: Estimate the racking distortion of the structure.

From a series of dynamic finite element analyses, Wang (1993) presented results showing the relationship between the structure racking and the flexibility ratio. The racking coefficient, R_r , is the ratio of the racking distortion of the structure embedded in the soil, Δ_r , to that of the free-field soils, Δ_{ff} , over the height of the structure:

$$R_r = \frac{\Delta_r}{\Delta_{ff}} \quad (4-31)$$

The values of R_r vs. F_r obtained from the dynamic finite element analyses are shown in figures 4-13(a) and 4-13(b). Also shown in these figures are curves from closed-form static solutions for circular tunnels. The solutions shown in the figures are from the full-slip solution presented by Wang (1993) and Penzien (2000) and the no-slip solution presented by Penzien (2000). As can be seen in the figures and previously reported by Wang (1993) and Penzien (2000), the curves from the closed-form solutions provide a good approximation of the finite element analysis results. These curves can therefore be used to provide a good estimate of the racking of a rectangular tunnel as a function of the flexibility ratio defined by equation 4-30. The analytical expressions for the curves in figure 4-13 are the following:

$$\text{For full slip: } R_r = \frac{4(1-\nu_m)F_r}{F_r + 2.5 - 3\nu_m} \quad (4-32)$$

$$\text{For no slip: } R_r = \frac{4(1-\nu_m)F_r}{F_r + 3 - 4\nu_m} \quad (4-33)$$

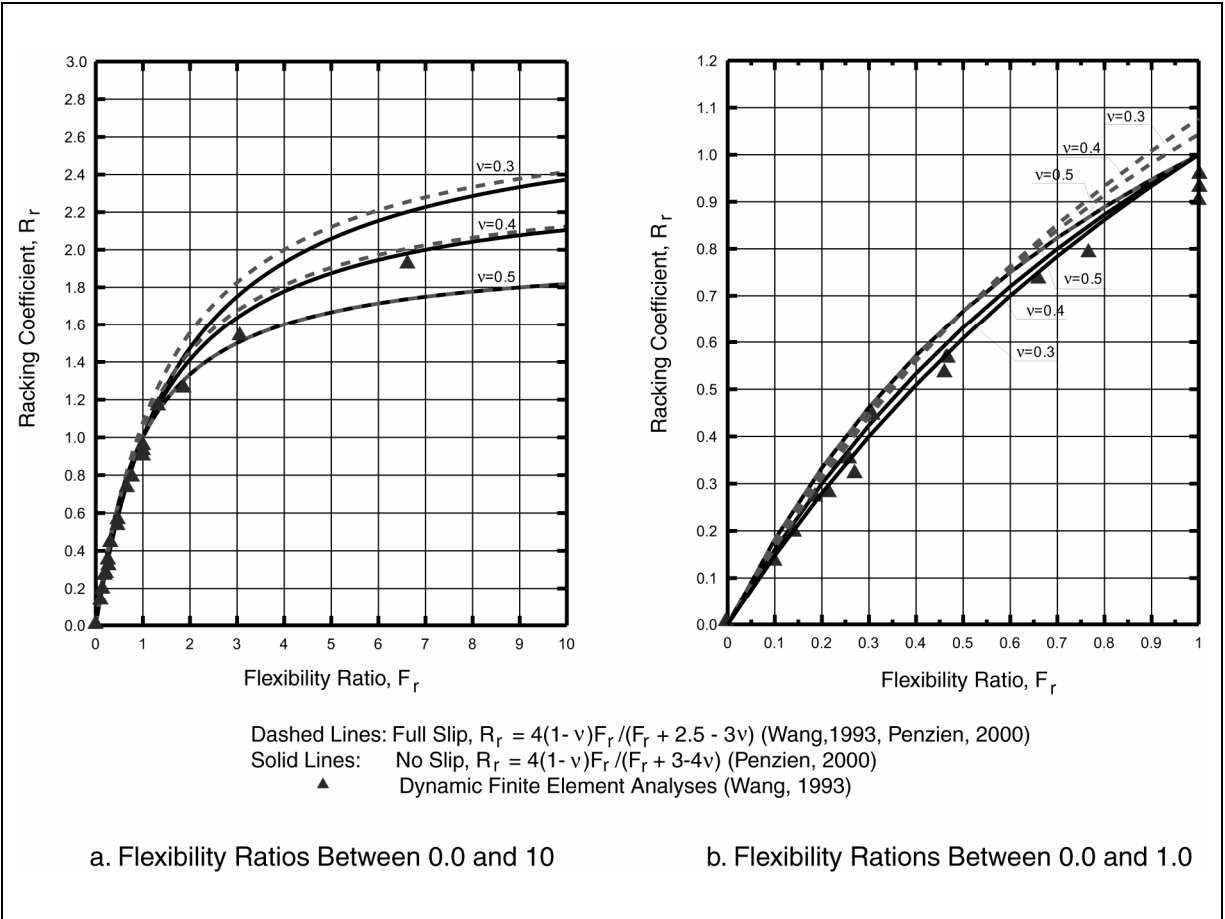
Several observations can be made from figure 4-13. When F_r is equal to zero, the structure is perfectly rigid, no racking distortion is induced, and the structure moves as a rigid body during earthquake loading. When F_r is equal to 1, the racking distortion of the structure is approximately the same as that of the soil (exactly equal to that of the soil for the no slip condition). For a structure that is flexible relative to the surrounding ground, ($F_r > 1$), racking distortion of the structure is greater than that of the free-field. As noted by Penzien (2000), if the structure has no stiffness (i.e., $F_r \rightarrow \infty$), R_r is approximately equal to $4(1-\nu_m)$, which is the case of an unlined cavity. $R_r = 4(1-\nu_m)$ also describes the racking ratio of an unlined circular cavity (Penzien and Wu, 1998).

Step 4: Perform structural analysis to determine forces, moments, and detailing requirements.

Two pseudo-static lateral force models are recommended by Wang (1993) (figure 4-14). The lateral forces should be applied to produce a racking deformation on the structure equal to the calculated value. If the displacements are large enough to cause inelastic deformation of the structure, inelastic pushover analyses (ATC, 1995) should be performed to assess structural behavior. The more critical responses from the two force models should be used for design.

Under the loading from the maximum design earthquake, inelastic deformation in the structure may be allowed depending on the performance criteria and provided that overall stability of the tunnel is maintained. Detailing of the structural members and joints should provide for adequate internal strength, ductility, and energy absorption capability.

Wang (1993) conducted parametric analyses to identify the influences of relative stiffness, structure geometry, ground motion characteristics, embedment depth, and foundation stiffness on the racking coefficient, R_r . Results of these analyses indicate that the relative stiffness between the rectangular structure and the surrounding medium has the most significant influence on R_r . The effects of structure geometry and ground motion characteristics were negligible. Additional analyses were performed to determine the influence of embedment depth. In these analyses, depths of embedment ranged from 0 to 40 feet for a structure with a height of 15 feet. The results indicate that the calculated racking coefficient is relatively independent of embedment depth when $h/H > 1.5$ (figure 4-12). Penzien (2000) further observed that as h/H reduces below 1.5, the racking coefficient decreases rather slowly, and the reduction is only about 20 percent for a reduction of h/H from 1.5 to 0.5.

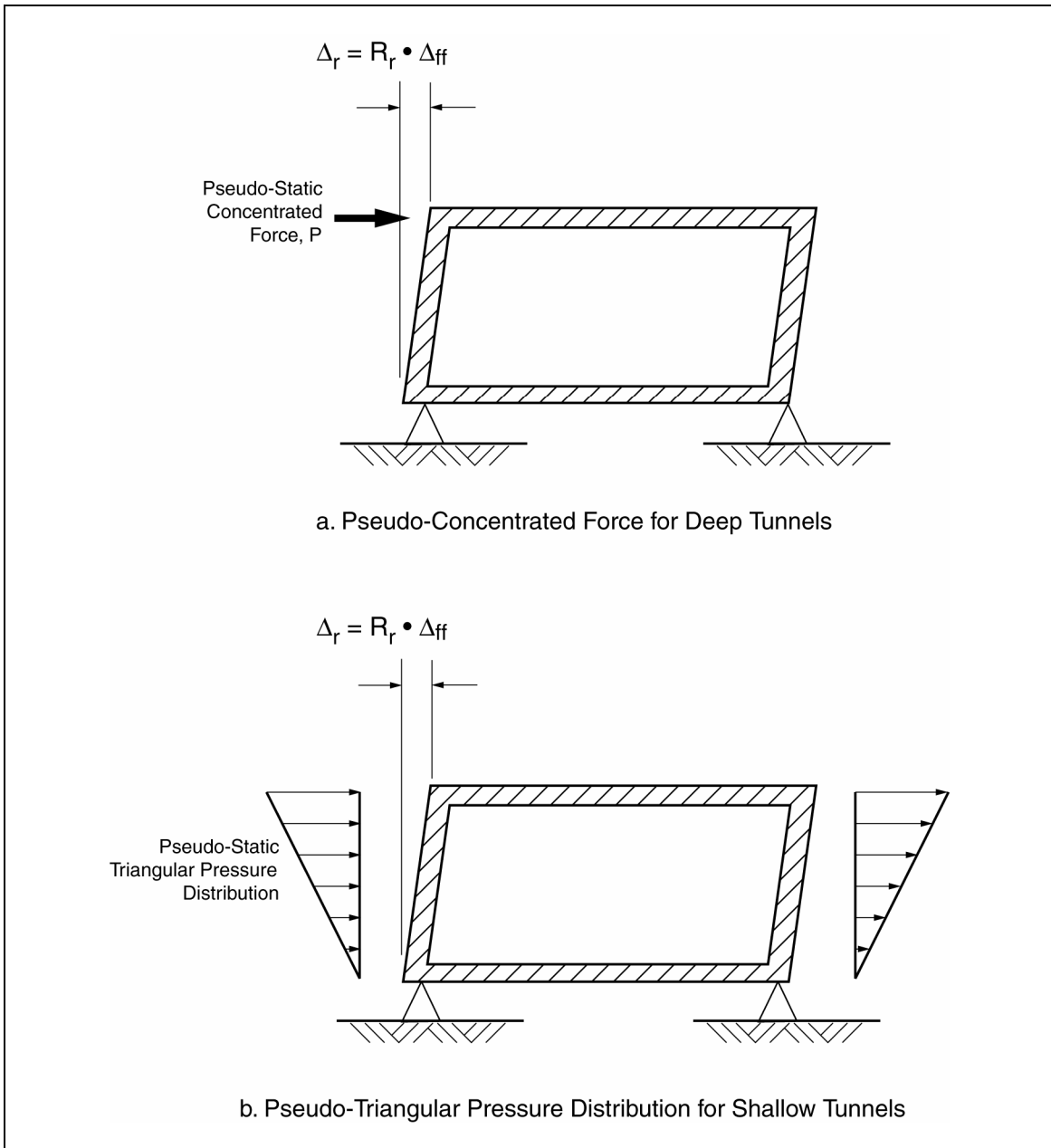


modified from Wang, 1993

Figure 4-13. Racking coefficients for rectangular tunnels.

Example 4.4 illustrates the calculation of racking of a rectangular tunnel.

Earth Pressure Analysis: For a tunnel that is stiff relative to the surrounding soil (i.e., flexibility ratio, $F_r \leq 1.0$, equation 4-30), the walls of the structure should be further checked for their capacity to withstand dynamic earth pressures. Dynamic lateral earth pressures acting on the walls are the increment of inertia-induced earth pressures that are added to or subtracted from the static lateral earth pressures (see figure 4-15). They tend to increase earth pressures on one side of a structure while simultaneously reducing earth pressures on the opposite side. A check should be made that the tunnel racking induced by the dynamic pressures does not unreasonably exceed the shear deformations of the surrounding ground.



Wang, 1993

Figure 4-14. Simplified frame analysis models for analysis of racking of a rectangular tunnel.

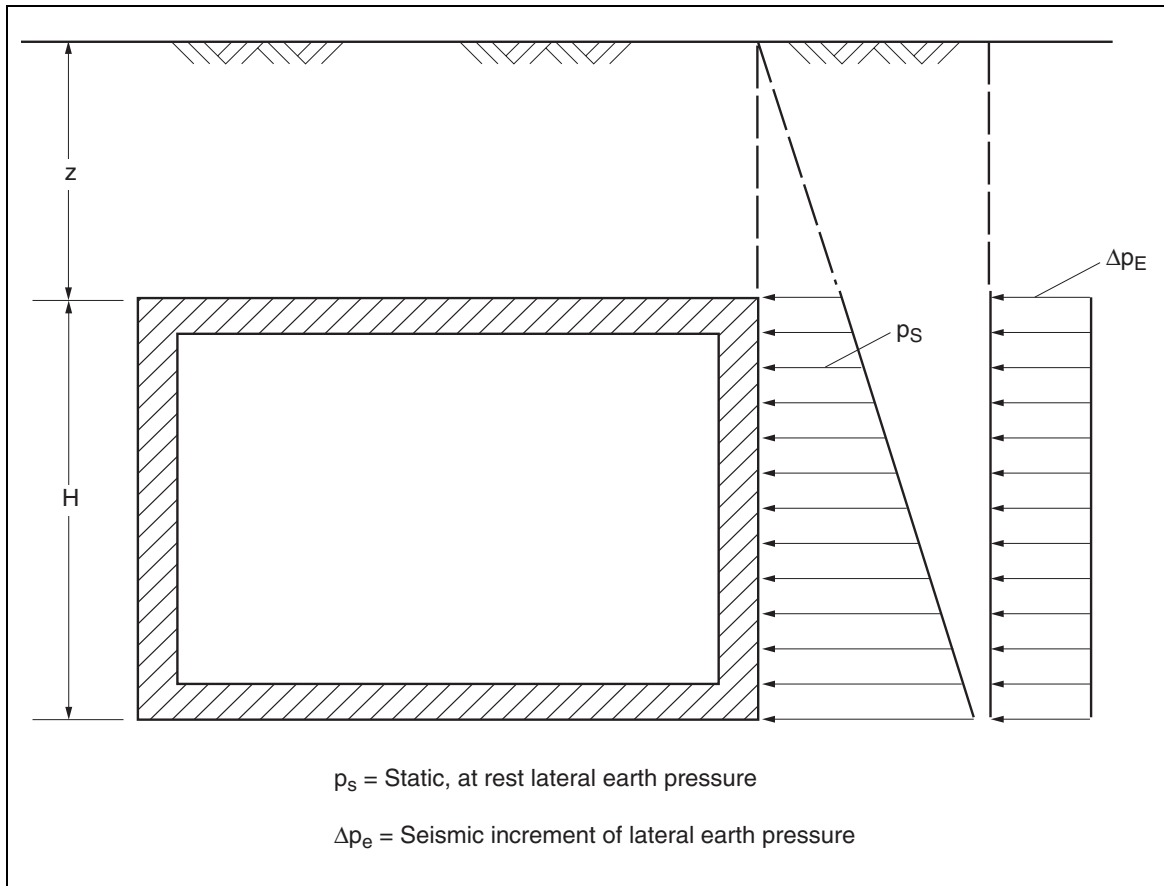


Figure 4-15. Lateral earth pressures acting on the walls of a cut-and-cover rectangular tunnel.

The dynamic lateral earth pressure on a tunnel wall, Δp_E , may be estimated by the following equation for shallowly embedded tunnels where the ratio of the depth of soil above the tunnel, Z , to the height of the tunnel wall, H , is less than 0.5:

$$\Delta p_E = C_V k_h \gamma_t (H + Z) \quad (4-34)$$

where:

C_V is the seismic earth pressure coefficient,
 k_h is the horizontal earthquake coefficient,
 γ_t is the total unit weight of soils,
 H is the height of the wall, and
 Z is the depth of soil above the tunnel.

As shown in figure 4-15, Δp_E is assumed to act on the wall as a uniform pressure. This formulation is based on the dynamic lateral earth pressure procedures developed by Seed and Whitman (1970) and Wood (1973) as summarized in Power et al. (1998). The seismic earth pressure coefficient, C_V , may be assumed equal to 0.4 and 1.0 for tunnels founded on soil and

rock, respectively. k_h should be taken, perhaps somewhat conservatively, as the horizontal ground surface acceleration expressed as a decimal fraction of gravity.

Considerable uncertainty exists regarding the magnitude of these pressures, especially for a fully embedded structure such as a tunnel. Numerical analyses should be considered for estimating dynamic lateral earth pressures, especially for depths of embedment to the top of the tunnel exceeding approximately one-half the tunnel height (i.e., $Z/H > 0.5$). A state-of-the-art review of dynamic earth pressures is presented by Whitman (1991).

Vertical seismic forces may be exerted on the roof of a cut-and-cover tunnel due to vertical accelerations in the soil backfill mass above the tunnel. The seismic forces in a backfill over a shallow tunnel can be obtained by multiplying the estimated vertical peak ground acceleration times the backfill mass.

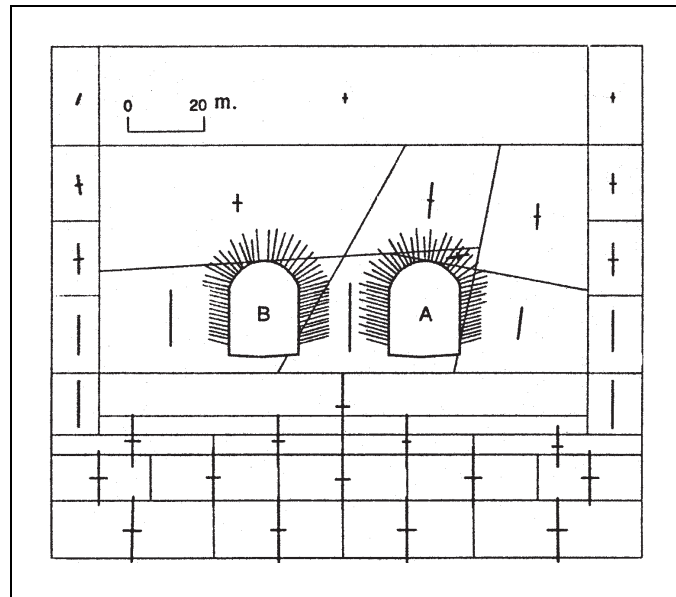
Having estimated the seismic (and static) earth pressures, structural analysis is carried out to check the capacity of the walls and roof to resist these pressures. The static (gravity) and inertial forces in the roof and the inertial forces in the walls should be added to the earth pressures in determining the total static plus seismic loads.

4.4.1.4(b). Numerical Analysis

Two-dimensional finite element and finite difference models may be used to analyze the cross section of a tunnel. Equivalent linear methods may be used to approximate nonlinear behavior of soils. Computer codes for linear or equivalent linear dynamic time history analysis include FLUSH (Lysmer et al., 1975), SASSI (Lysmer et al., 1991), and QUAD4-M (Hudson et al., 1994). The computer program FLAC (Itasca, 1998; Wang and Makdisi, 1999) can incorporate nonlinear behavior in soil materials through the incorporation of nonlinear (or bilinear) constitutive models.

In cases where movement along weak planes in the geologic media (shear zones, bedding planes, joints) may potentially cause local stress concentrations and failures in a tunnel, dynamic time history analyses using discrete element models may be considered. In these models, the soil/rock mass is modeled as an assemblage of discrete blocks. The blocks may be modeled as either rigid or deformable materials, each behaving according to a prescribed stress-strain relationship. The relative movements of the blocks along weak planes are modeled using force-displacement relationships in both normal and shear directions. Figure 4-16 illustrates an example of a discrete element model, where joints and bedding planes are included for analyses. UDEC (Itasca, 1992) and DDA (Shi, 1989) are two computer codes that can be used for this type of numerical analysis.

Because of the complexity of the tunnel-soil interaction problem, consideration should be given to using numerical analysis methods. Use of these methods is especially desirable for analysis of the cross sections of cut-and-cover box tunnels in soil because of the relative seismic vulnerability of these structures (as compared to bored tunnels) based on earthquake observations.



Akky et al., 1994

Figure 4-16. Discrete element model of tunnel.

4.4.2. EVALUATION FOR FAULT RUPTURE

4.4.2.1. General

Assessing the behavior of a tunnel that may be subject to the direct shear displacements along a fault includes, first, characterizing the free-field fault displacement (i.e., displacements in the absence of the tunnel) where the fault zone crosses the tunnel and, second, evaluating the effects of the characterized displacements on the tunnel.

In general, if moderate to large fault displacements occur in narrow zones in relatively hard geologic media, the tunnel may experience severe local damage that can be reduced only by special design to accommodate the displacements or must be anticipated in contingency repair plans. Design and contingency measures are discussed in section 4.5.2. Severe local damage to linings or walls of tunnels could generally be expected for fault movements on the order of a few inches or more occurring on discrete planes in rock. On the other hand, if displacements are small and/or are distributed over a wide zone, it is possible that only minor or moderate damage to tunnels may occur, especially if the tunnel is ductile or articulated. The effect of cracking or joint separation on the water tightness and potential for flooding of a tunnel should be carefully evaluated.

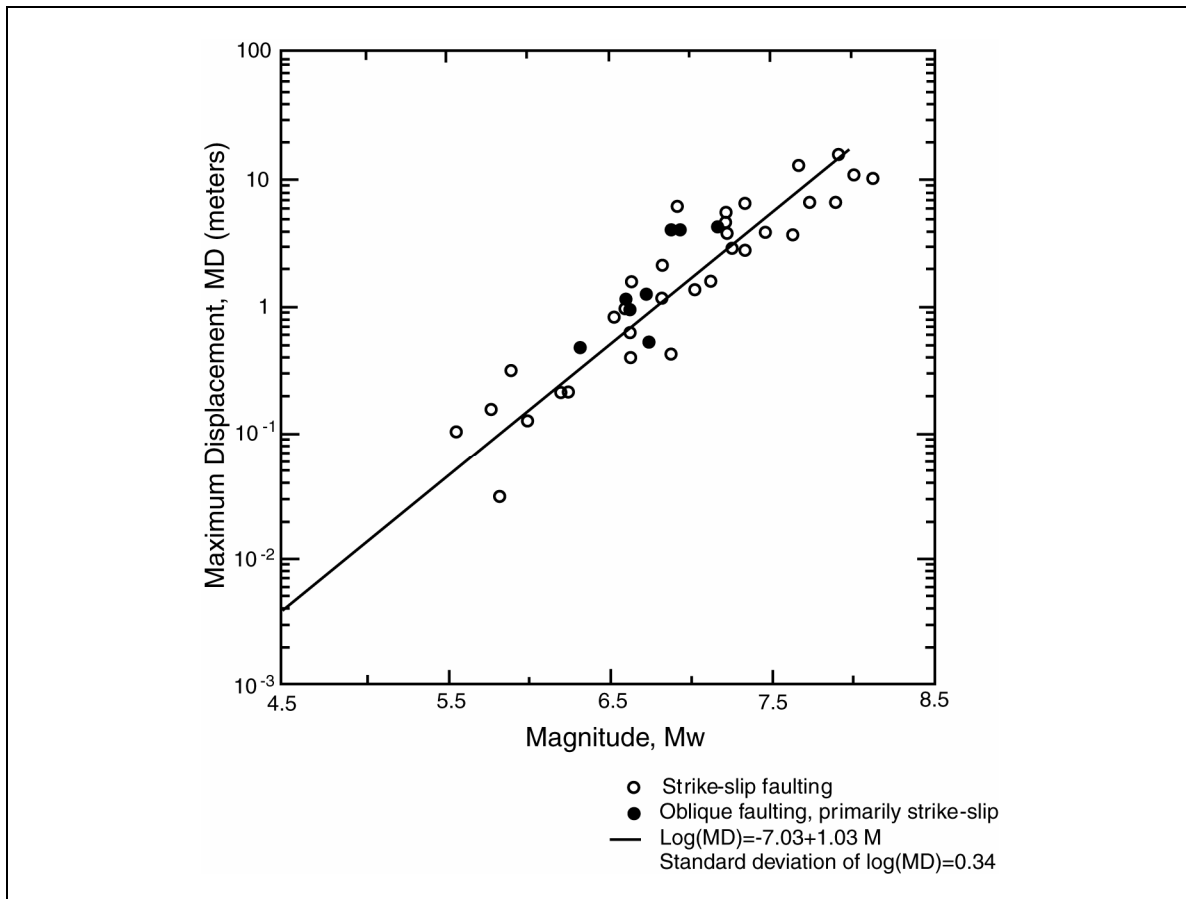
One factor that affects the behavior of a tunnel in a fault rupture zone is the direction of slip relative to the tunnel axis. For steel linings susceptible to buckling, relative slip that would place a tunnel in compression tends to be more damaging than slip that would elongate the tunnel. The development of cracks or gaps in a lining due to either elongation or compression may result in unacceptable water inflow.

4.4.2.2. Assessing the Amount of Fault Displacement

Assessing the amount and distribution of fault displacement is an activity requiring the effort of geologists who are knowledgeable of the character of displacements in fault rupture zones. Empirically based relationships, such as those developed by Wells and Coppersmith (1994), can be utilized to estimate the amount of fault displacement as a function of earthquake magnitude and type of faulting. Figure 4-17 is an example of such a relationship, which shows that the amount of displacement is strongly dependent on earthquake magnitude and can reach maximum values of several feet or even tens of feet for large-magnitude earthquakes.

4.4.2.3. Analyzing Tunnels for Fault Displacement

When subjected to fault differential displacements, a buried structure with shear and bending stiffness tends to resist the deformed configuration of the fault offset, which induces axial and shear forces and bending moments in the structure. The axial deformation is resisted by the frictional forces that develop at the soil-tunnel interface in the axial direction, while shear and curvature deformations are caused by the soil resistance normal to the tunnel lining or walls.



Wells and Coppersmith, 1994

Figure 4-17. Relationship between maximum surface fault displacement (MD) and earthquake moment magnitude, M_w , for strike-slip faulting.

In general, analytical procedures for evaluating tunnels subjected to fault displacements follow those used for buried pipelines. Three analytical methods have been utilized in the evaluation and design of linear buried structures (ASCE Committee on Gas and Liquid Fuel Lifelines, 1984). They are:

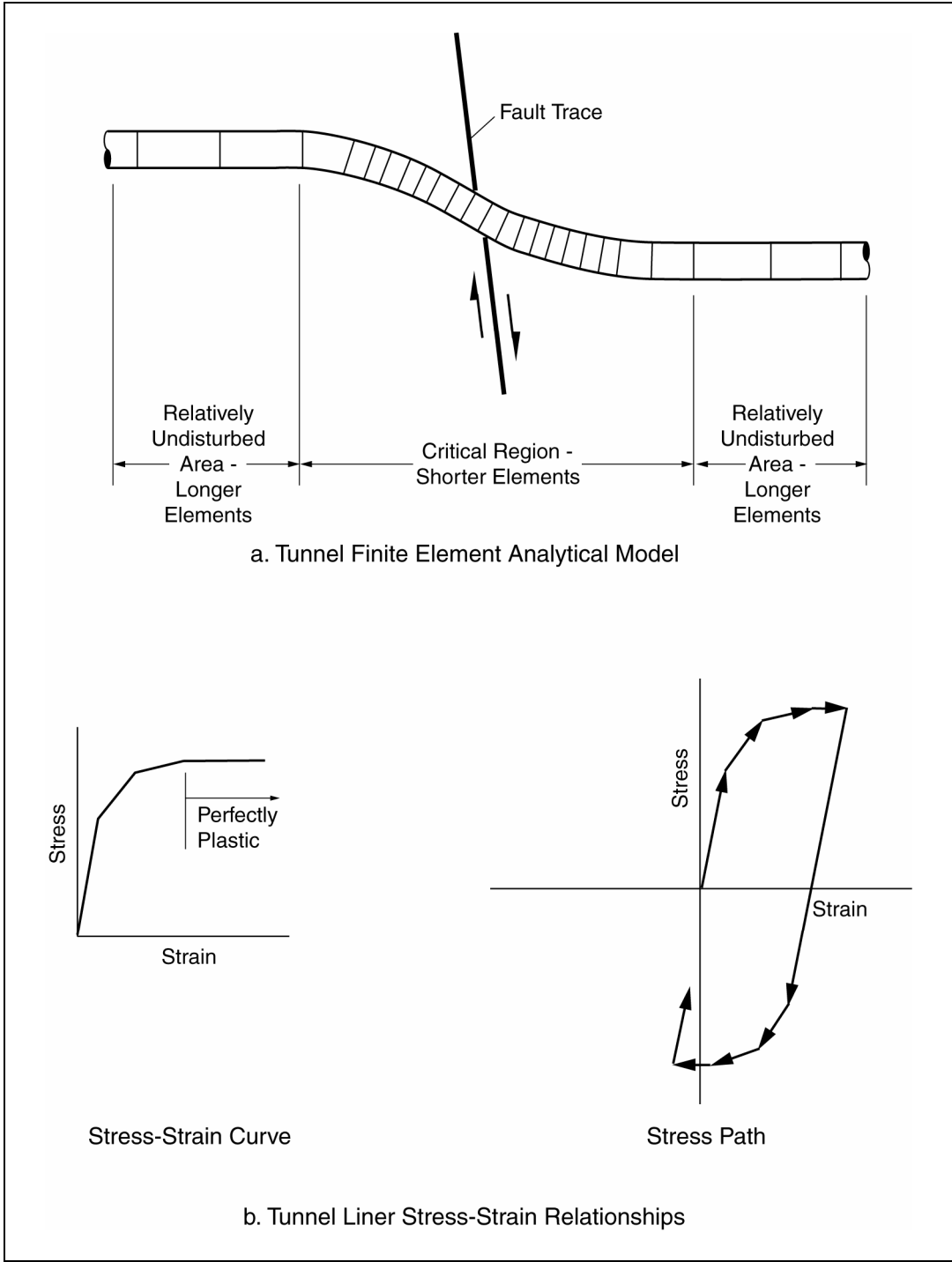
- Newmark-Hall procedure.
- Kennedy et al. procedure.
- Finite element approach.

The Newmark-Hall (1975) and Kennedy et al. (1977) approaches were originally developed for analyzing buried pipelines subjected to discrete fault displacements. Both approaches assume that the structural axial deformation is restrained by the soil-structure frictional forces. In the Newmark-Hall method, it is assumed that the structure “breaks free” from the surrounding soils by climbing out of a shallow trench and remains straight between two anchored points. In the Kennedy et al. approach, the buried structure is modeled like a cable; induced curvatures and resulting bending stresses are calculated ignoring the bending stiffness of the structure.

The Newmark-Hall method is generally not applicable to tunnels because the size of the tunnel and depth of burial would generally preclude the possibility of the tunnel climbing out of the ground and straightening itself out. The Kennedy et al. method may be used, although the bending stiffness is not negligible for many tunnels. This method would generally overestimate the bending curvature by neglecting the bending stiffness. The finite element method is preferred because it can incorporate the most realistic models of the tunnel and surrounding geologic media. The tunnel is modeled using finite elements, which may incorporate nonlinear behavior (figure 4-18). Transverse and axial springs connected to the tunnel model soil normal pressures on the tunnel lining or walls and axial frictional resistance (figure 4-19); these springs may also incorporate nonlinear behavior if applicable (figure 4-20). Many finite element codes may be considered for analyzing the response of tunnels to fault displacement. A few of these are ADINA (1996), ABAQUS (Hibbitt, Karlsson and Sorensen, 1998), PIPLIN (Structural Software Development Co., 1981), ANSR-III (Oughourlian and Powell, 1982), and STARDYNE (Research Engineers, 1995).

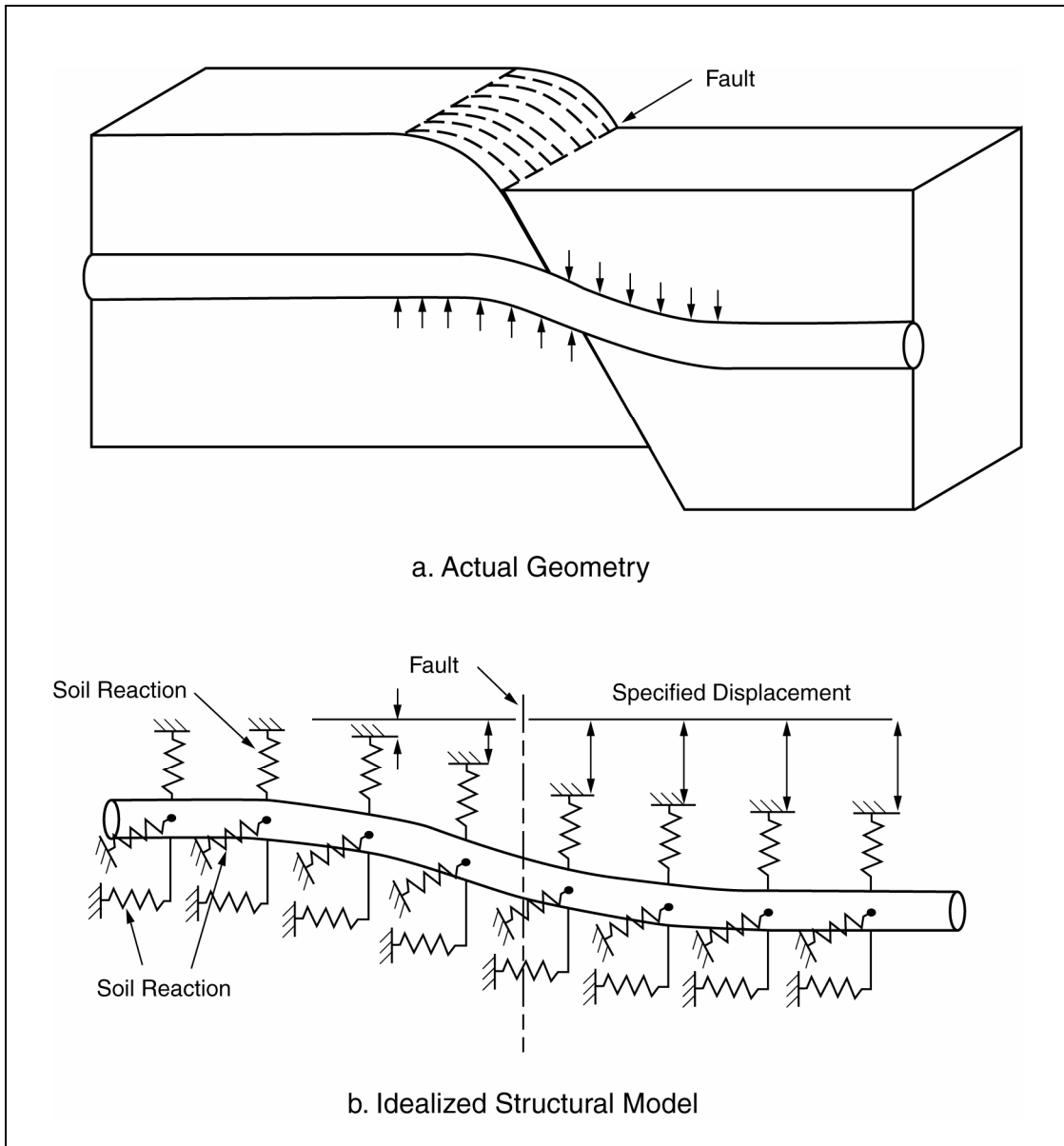
4.4.3. EVALUATION FOR LANDSLIDING OR LIQUEFACTION

If liquefiable soil deposits or unstable soil masses susceptible to landsliding are identified along the tunnel alignment, then more detailed evaluations may be required to assess whether liquefaction or landsliding would be expected to occur during the design earthquake and to assess impacts on the tunnel.



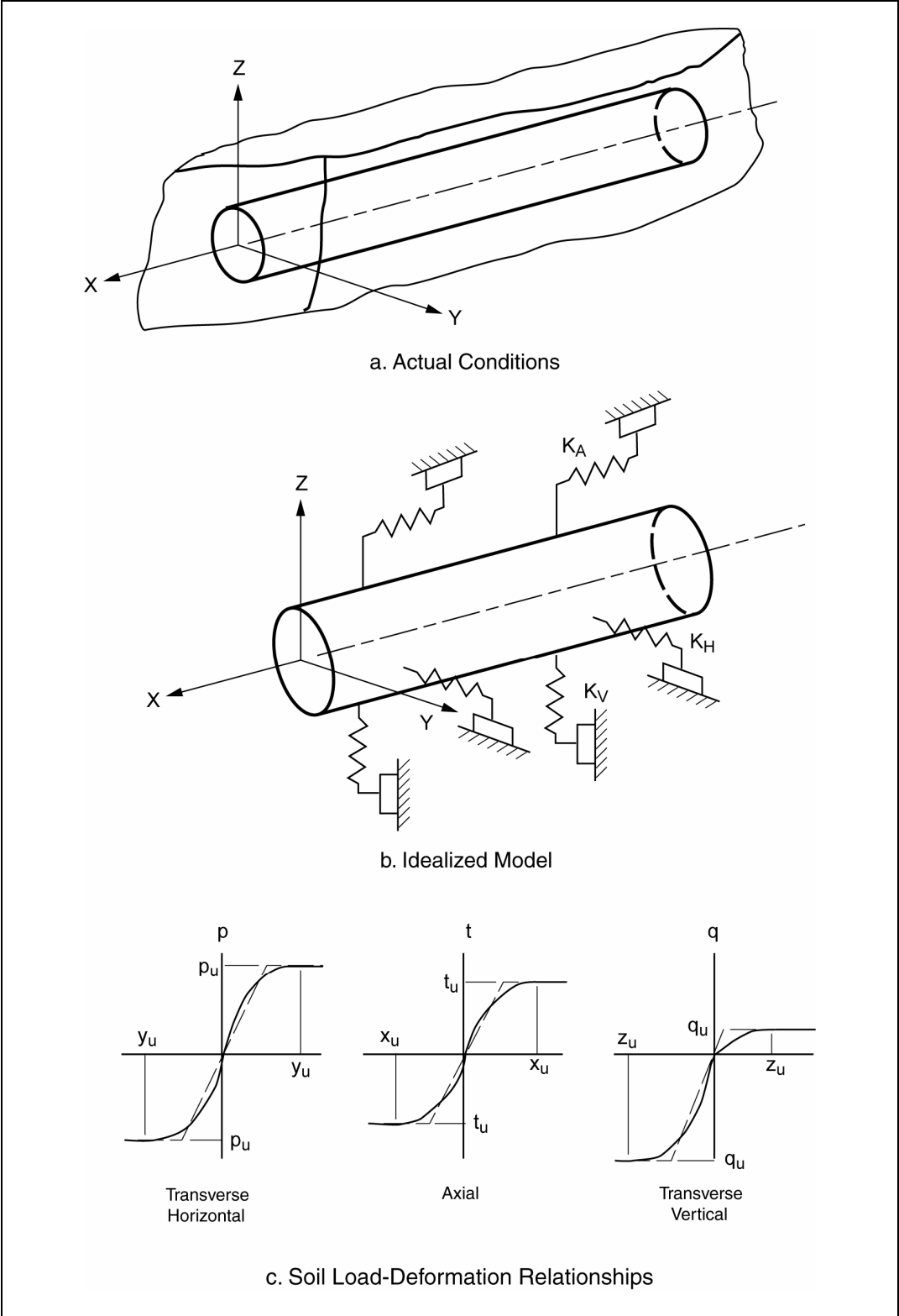
ASCE Committee on Gas and Liquid Fuel Lifelines, 1984

Figure 4-18. Analytical model of tunnel structure at fault crossing.



ASCE Committee on Gas and Liquid Fuel Lifelines, 1984

Figure 4-19. Schematic illustration of soil-structure model of tunnel at fault crossing.



ASCE Committee on Gas and Liquid Fuel Lifelines, 1984

Figure 4-20. Analytical model of soil restraint for tunnel at fault crossing.

If slope movements due to landsliding or lateral spreading movements due to liquefaction intersect a tunnel, the potential effects of these movements on the tunnel are similar to those of fault displacement. As is the case for fault displacements, tunnels generally would not be able to resist landsliding or lateral spreading concentrated displacements larger than a few inches without experiencing locally severe damage.

If liquefaction were predicted to occur adjacent to a tunnel lining or wall, a potential consequence could be yielding of the lining or wall due to the increased lateral earth pressure in the liquefied zone. The pressure exerted by a liquefied soil may be as large as the total overburden pressure. The potential for liquefaction to cause uplift of a tunnel embedded in liquefied soil, or for the tunnel to settle into the soil, should also be checked.

4.5. RETROFIT STRATEGIES

Retrofit strategies are discussed in the following subsections for the potential failure modes of ground shaking-induced failure, fault displacement-induced failure, and landsliding- and liquefaction-induced failure.

4.5.1. GROUND SHAKING-INDUCED FAILURE

4.5.1.1. Bored Tunnels

4.5.1.1(a). Tunnels in Rock

Tunnels in rock have levels of support that range from a temporary rib and lagging liner with a cast-in-place concrete final liner, to rock bolts and rock dowels, to little or no support. To enhance seismic, as well as static, performance of tunnels in rock, retrofit methods should be used that limit the amount of deformation and enhance the ability of the ground to support itself by forming a ground arch reinforced with structural elements (Bischoff and Smart, 1976; Lang 1962, 1972, 1981). Weak zones or rock wedges should be supported by rock bolts, stronger liners, or other methods to prevent them from shaking loose and producing additional loads on and possibly collapsing a liner during seismic loading (figure 4-21). For tunnels in weak rock, it may be desirable to install a continuous or patterned system of rock bolts and dowels and shotcrete support (figure 4-22). Chemical grouting may be considered in areas of highly jointed or fractured rock.

In rock tunnels for railroads, the tunnels are often enlarged to carry higher-profile and higher-capacity cargo cars (see for example Millar et al., 1991). Typically, the crown of the tunnel is mined, and new more “flexible” support consisting of rock bolts and shotcrete is installed. Older railroad tunnels are often supported with large timbers, which have rotted away or burned (from engine smoke). The timbers are removed and the tunnel enlarged and provided with larger clearances by replacing the timbers with rock bolts and shotcrete. Rehabilitation methods similar to those used for enlarging railroad tunnels may also be applied to seismic retrofitting of highway tunnels.

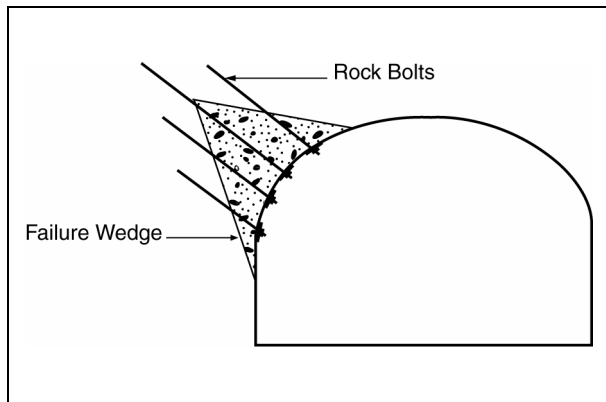


Figure 4-21. Rock bolt stabilization of rock wedge.

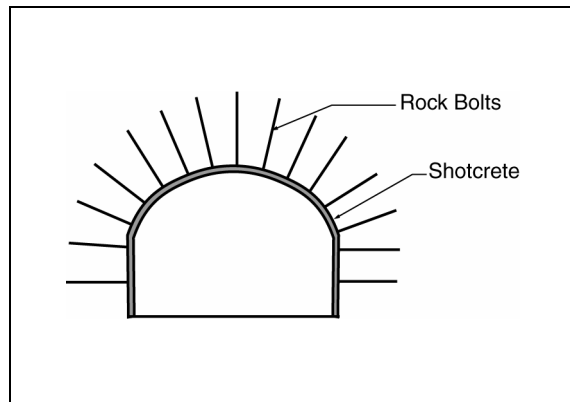


Figure 4-22. Rock bolt reinforcement in soft or fractured rock.

It is critical that a tunnel lining be in good contact with the geologic media (whether rock or soil). The quality and completeness of contact grouting between the liner and the geologic media may be investigated by taking core samples as well as by geophysical techniques (e.g., ground penetrating radar or impact echo techniques). Contact grouting should be employed if significant voids are present behind a liner. Various materials may be used for contact grouting, including conventional grout, cellular or foam concrete, and polyurethane or other chemical grouts. Examples of application of contact grouting are described by Grimm and Parish (1985), Russel (1987, 1993), Navin and Hutchinson (1992), and Grodner et al. (1998). An example of the combined application of rock bolts, shotcrete, and contact grouting to rehabilitate a tunnel is the FHWA/National Park Service Ft. Baker-Ft. Barry tunnel originally constructed in 1918 (California Builders and Exchange, 1994).

If tunnel linings are locally weak due to cracked, deteriorated, or otherwise low-strength concrete or masonry, spot repairs may be employed by removing and replacing weak zones with shotcrete or alternative materials such as resin-impregnated fabric or polymeric membranes. Use of such materials when a limited area needs structural rehabilitation is discussed by Abramson and Boscardin (1999) and Russell (1999). Weak zones of existing liners may be removed by conventional methods such as jack-hammering or techniques such as hydro-demolition (e.g., Soast, 1989). After the concrete or masonry is removed, additional reinforcement may be added and a new shotcrete or concrete liner placed.

Extensively deteriorated, cracked, or otherwise weak concrete or masonry liners may require either the demolition and replacement of the liner or the strengthening of the liner by constructing an inner liner or installing stiffeners and arch beams (Madden, 1999). Typically, strains in tunnel liners in rock will be small, and reinforcing steel in concrete liners may not be required. Nevertheless, the use of reinforcing steel is desirable to provide a more ductile and stronger material if strong seismic shaking is anticipated.

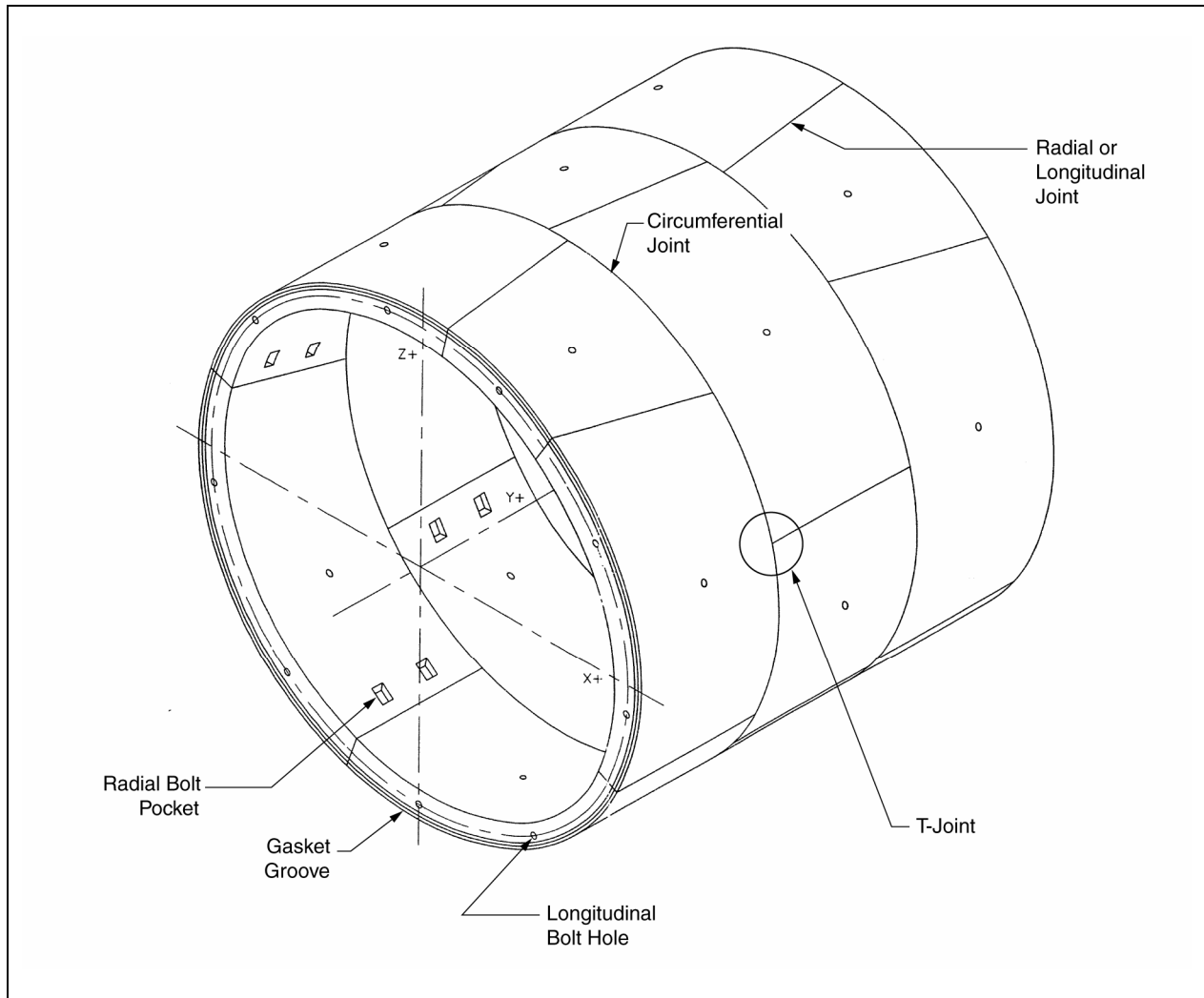
4.5.1.1(b). Tunnels in Soil/Soft Ground

As indicated in section 4.2.1.1, circular tunnels in soil are typically constructed using a two-pass or one-pass lining system. In the two-pass system, the primary, initial, or temporary support typically consists of steel ribs and lagging, liner plate, or precast concrete segmented lining. The final support consists of a cast-in-place liner. While many concrete tunnel liners do not require reinforcing, based on calculations for static-plus-seismic loading, it is desirable to provide reinforcing if strong seismic shaking could occur. During strong shaking, reinforcing provides a lattice to hold cracked concrete together without major spalling or collapse.

Single-pass liners are typically bolted and gasketed steel plate or precast concrete segmented liners. The segments are typically staggered along the length of the tunnel so the segments' radial or longitudinal joints are not continuous, forming "T" joints as shown in figure 4-23. Segments forming a continuous radial joint have the disadvantage that all the gaskets meet at four corners, increasing the potential for groundwater leakage. Staggering the segments is beneficial from a seismic point of view because it provides better interlocking among adjacent segments. Bolting together the segments of the liner is desirable for seismic design to provide continuity of the lining and reduce the potential for local lining failure. At the same time, the steel bolts provide a ductile fastening material. The Japan Tunneling Association indicated that there were no reports of damage to segmented-lining tunnels from the Kobe earthquake (Fukuchi, 1995).

Unbolted segmented liners are frequently used. Advantages and disadvantages of various joint shapes are discussed by McCusker (1989) and Iftimie (1994). The potential seismic advantage of unbolted radial joints is that the moments induced by racking behavior can be further reduced, since little or no moment is transmitted across the joint. On the other hand, such joints are locations of shear weakness and are more susceptible to local failure during racking distortion. A variation of an unbolted radial joint is the use of a guide rod centered on the radial joint surface (AFTES, 1999). The guide rod is made of hard plastic and does not provide for any clamping force or moment or tension connection. It does allow rotation and provides a mechanical shear connector. Clough (1981) observed that the ability of unbolted liners to withstand earthquake loading requires research.

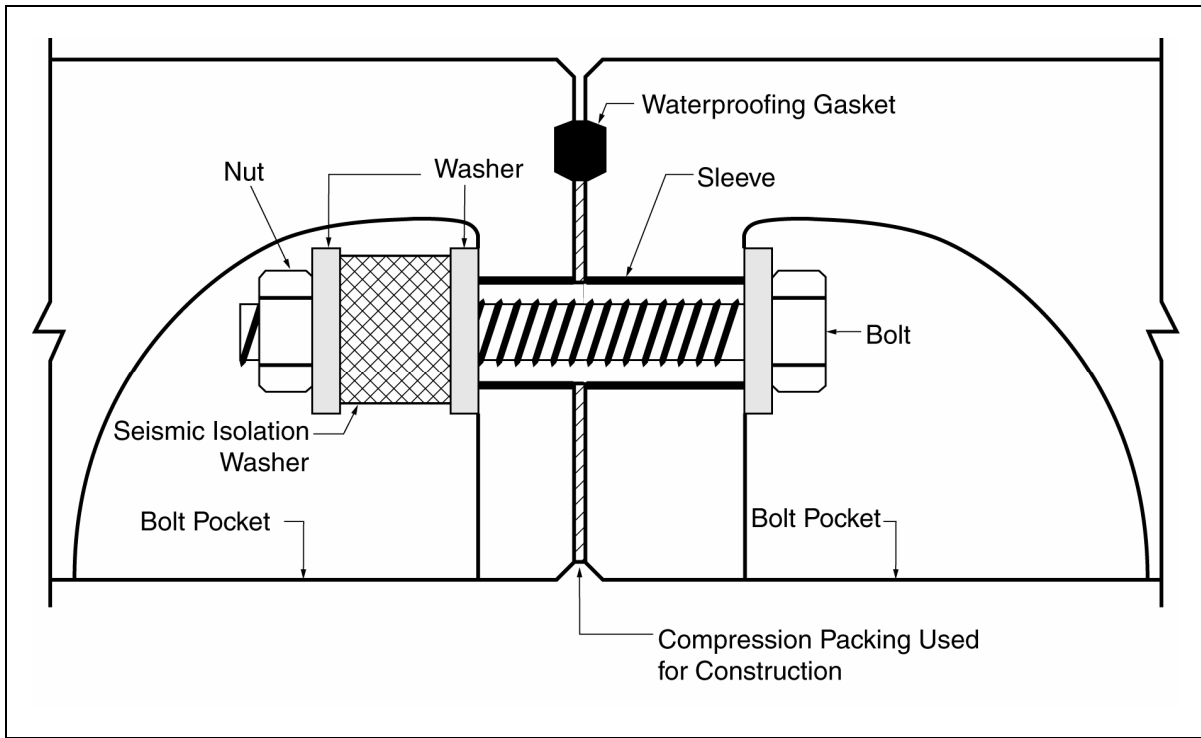
Special connectors across circumferential joints in tunnel liners in soft soil may sometimes be desirable to accommodate large axial strains and curvatures. If such connectors are installed, it is important that they not become weak points where local transverse shear deformation might occur. Examples of joint details are shown in figures 4-24 and 4-25. The "seismic isolation washer" shown in figure 4-24 is a highly compressible element that was proposed for the Trans-Tokyo Bay highway tunnel. The detail in figure 4-25, which was proposed for the Osaka South Port Tunnel, incorporates a rubber gasket to resist the compressive force, a cable to resist tensile force, and an omega-shaped rubber gasket for secondary water tightness. The effect of joints on potential for water inflow and design measures to achieve the required water tightness should always be evaluated.



City of San Diego, CA/Parsons Engineering Science, 1995

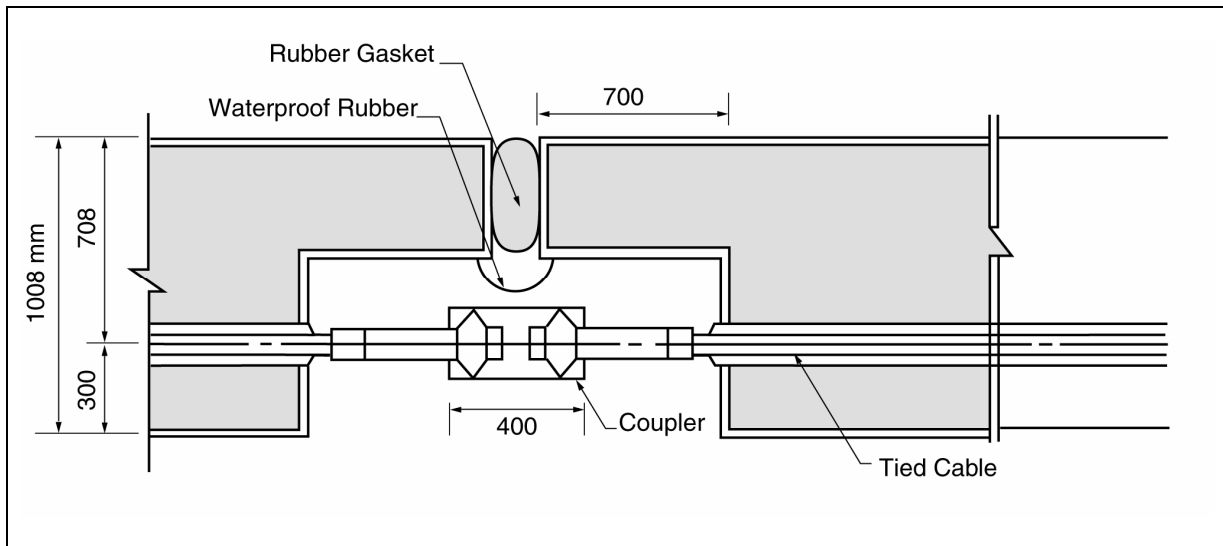
Figure 4-23. Precast concrete segmental liner.

Other joint designs which accommodate larger movements may incorporate practices employed on other projects, not originally intended for seismic shaking. Circumferential joints, for example, may be reinforced with continuous longitudinal bolts through the segments as was used for the West Akli tunnel in Seattle for an ancient landslide crossing (Madden et al., 1994) and the South Bay Ocean Outfall in San Diego for active fault crossings (Kaneshiro et al., 1996a, 1996b) (the design for the latter project is discussed in section 4.5.2 and illustrated in figure 4-35).



modified from Ono et al., 1992

Figure 4-24. Example of flexible circumferential joint detail in tunnel lining with seismic isolation washer.



Kiyomiya, 1995

Figure 4-25. Example of a flexible circumferential joint detail in tunnel lining.

Many retrofit strategies for soil tunnels may be similar to those for rock tunnels and include the following:

- Spot repairs over a limited area by removing weak concrete and installing shotcrete, concrete, or alternative materials. Tunnels with steel liner plates may be strengthened in corroded or otherwise vulnerable areas with welded steel plates.
- Contact grouting.
- Ground improvement by chemical or compaction grouting.
- Demolishing an existing liner and constructing a new liner with temporary ground support provided and/or liner replacement performed in short segments using sequential excavation methods.
- Constructing an inner liner of reinforced concrete or a steel pipe with concrete in the annulus between the pipe and the existing liner.
- Increasing deformation capacity of a liner by construction of special joints, such as the “seismic isolation washer” (figure 4-24) and joint details described in sections 4.5.1.3 and 4.5.1.4.
- Strengthening or increasing ductility of joints of segmented liners by local concrete removal and installation of steel connectors.

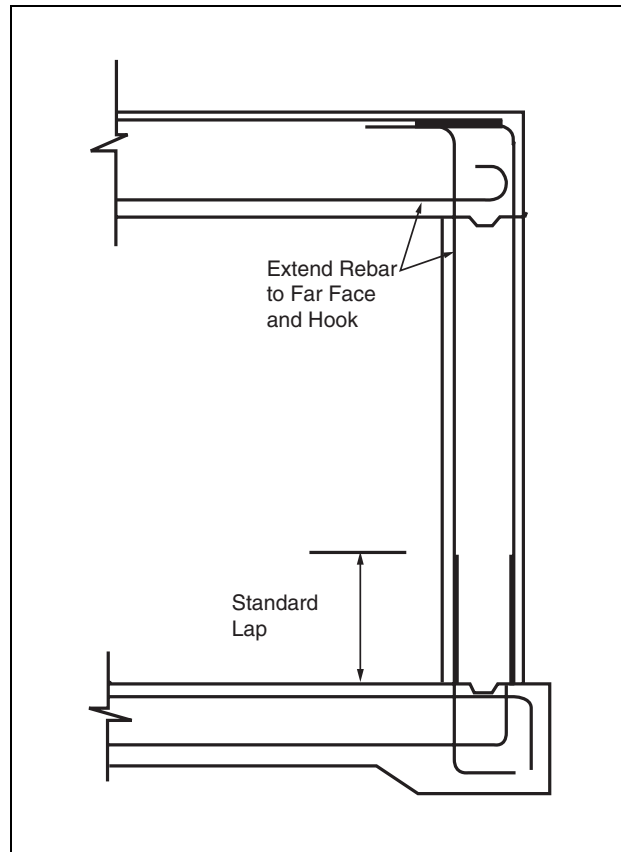
Water inflow may limit retrofit choices for some tunnels in soil.

4.5.1.2. Cut-and-Cover Tunnels

The key to the retrofit of reinforced concrete, box-type cut-and-cover tunnels is to capture the main modes of behavior in the analysis of the tunnel cross section, including uncertainty in the induced stresses due to uncertainties in soil properties and uncertainties in response of the tunnel-soil system. Modes of behavior that must be adequately quantified include racking (figure 4-3d) and bulging of sidewalls and roof due to static-plus-seismic earth pressures. As pointed out by Owen and Scholl (1981), the seismically induced racking behavior of box-type cut-and-cover tunnels results in tension being induced on the inside faces of the corners of the box, whereas earth pressures result in tension at the inside middle part of the walls and roof. To design for the racking behavior, they recommended that longitudinal reinforcing steel in the walls be extended into the adjacent slabs and hooked at the far face, as illustrated in figure 4-26. Not shown in figure 4-26 is the transverse confinement reinforcing which is important for ductile behavior.

4.5.1.3. Submerged Tubes

Submerged tubes present several seismic retrofit challenges. Liquefaction-induced flotation is a potential concern when tubes are placed on and backfilled with loose sandy soil. Settlements could occur due to liquefaction and consolidation of sandy soils below a tunnel. Lateral



Owen and Scholl, 1981

Figure 4-26. Corner reinforcing details for seismic design of box-type tunnel.

movement of a tunnel on gently sloping ground is a potential concern due to earthquake-induced lateral spreading in either liquefied soils or soft clays.

The seismic vulnerability evaluation and retrofit design of the Posey and Webster Street tubes by Caltrans is summarized in the following paragraphs as an illustration of vulnerabilities and retrofit strategies for this type of tunnel (Caltrans/Parsons Brinckerhoff, 1998; Anderson, 1998; Schmidt and Hashash, 1998; Hashash et al., 1998; Boulanger et al., 1998; Schmidt and Hashash, 1999). These tube-type vehicular tunnels pass beneath the Oakland estuary between the communities of Oakland and Alameda, California. During the 1989 Loma Prieta earthquake, accelerations at the tunnel locations were low enough that the tunnels did not experience significant structural damage. However, the earthquake caused some leaking at the connections between the tube segments, which was thought to have been caused by some liquefaction of the soil adjacent to the tubes (Yashinsky, 1998). Also, backfill soils over the tubes at the Alameda portals liquefied during the earthquake. Backfill around the tubes consists of sand for the Webster Street tube and a mixture of soft clay and sand for the Posey tube. For both these tunnels, seismic vulnerability studies conducted by Caltrans concluded that backfill around the tubes would likely liquefy and cause flotation of the tubes during potential earthquakes that could be larger and much closer to the sites than the Loma Prieta earthquake. In addition, dynamic analysis of the tunnels indicated that continuous joints connecting the approximately

200 foot-long tube segments (made continuous during the original construction by connecting the reinforcing bars of adjacent tube sections) would experience large tensile and shear forces that could result in uncontrolled cracking of the tubes, leakage of water, and possible flooding. The analysis also indicated that large compressive forces would be transmitted at the continuous connections of the tubes to the portal buildings at the tube ends, causing damage to the buildings and the tubes.

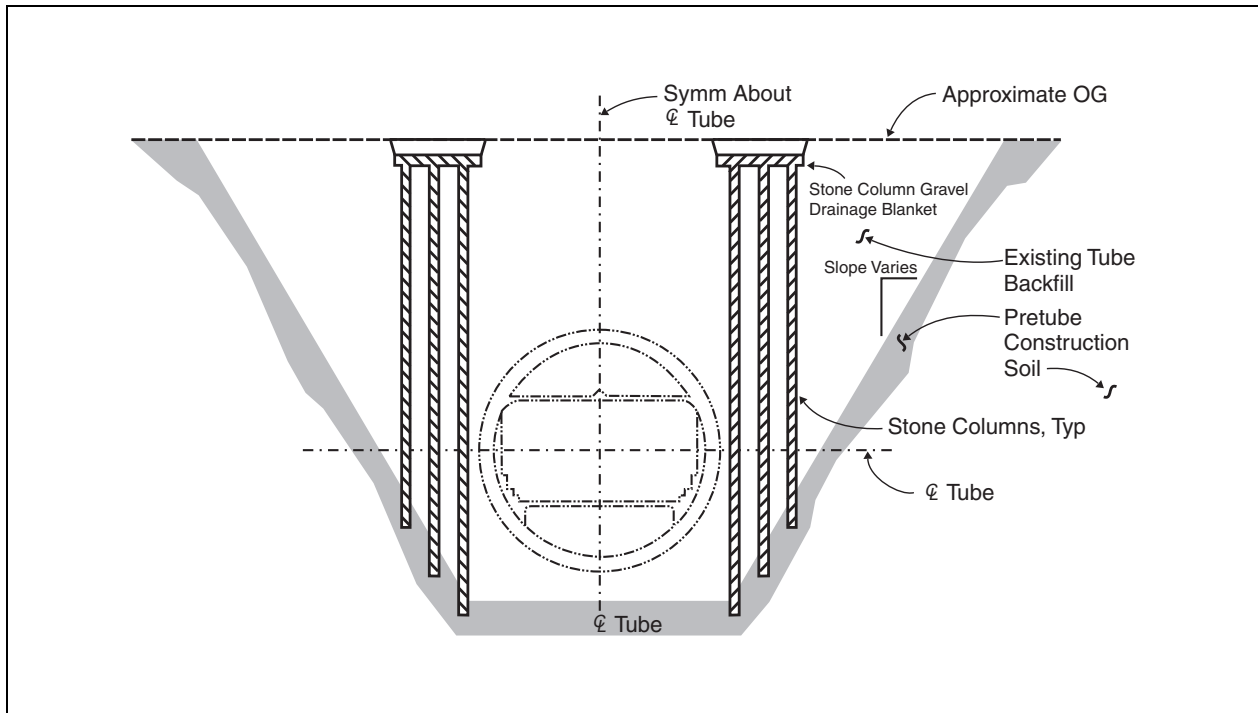
Retrofit design measures adopted by Caltrans for these tunnels included: (1) ground improvement to prevent flotation of the tubes; (2) cutting loose the joints and redesigning them so they would not transmit tensile forces while maintaining compression and shear capacity; and (3) providing gaps at the tube-portal-building joints to minimize the transmittal of interaction forces between the tubes and the buildings.

The concept adopted to prevent tube flotation was to construct isolation walls using ground improvement methods adjacent to the tubes that would prevent liquefied soils outside the walls from moving beneath the tubes. This concept is not intended to prevent liquefaction of soils beneath the tube; rather it is intended to prevent flotation by interrupting the flotation mechanism. The ground improvement methods adopted to create the isolation walls consist of three rows of stone columns constructed in the backfill sands of the Webster Street tube and a continuous jet grout column wall constructed in the mixed clay and sand backfill of the Posey tube. Typical cross sections illustrating the isolation wall designs are shown in figures 4-27 and 4-28. A typical detail of the as-built, redesigned joint between Posey tube segments is shown in figure 4-29.

4.5.1.4. Junctions and Transitions

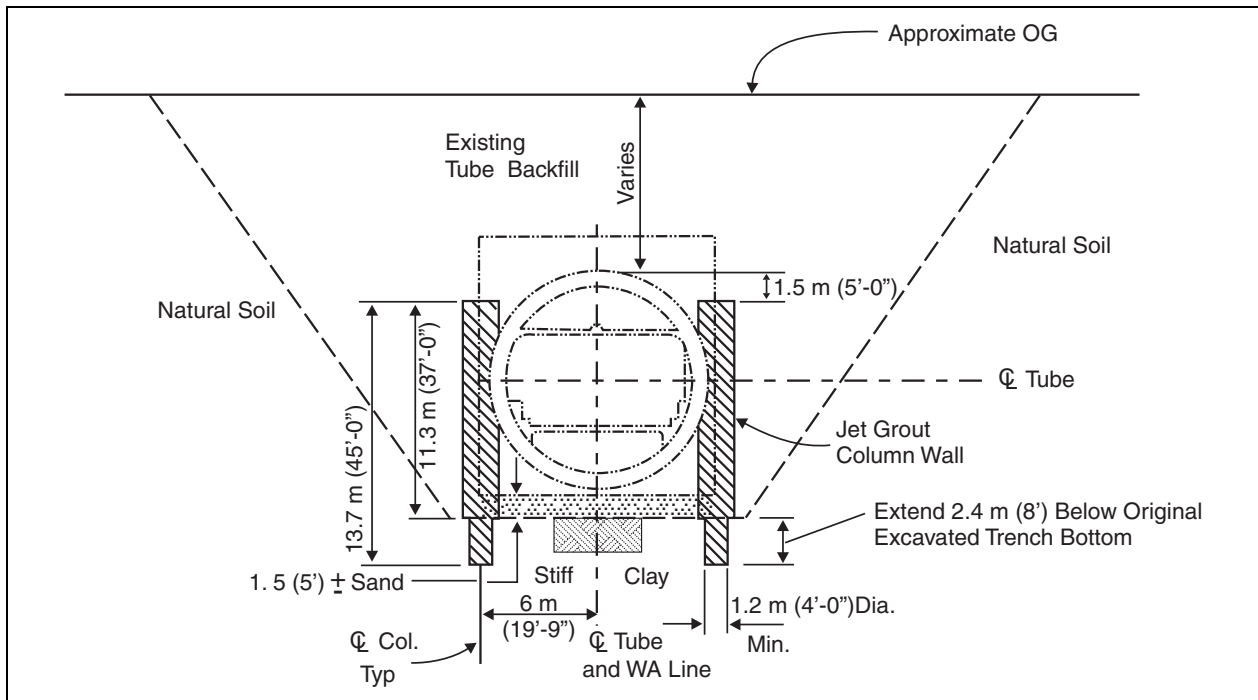
Special detailing may need to be considered at the junction of a tunnel to a relatively stiffer structure such as a ventilation structure or a transit station, because relatively large seismically induced strains and forces may be generated at such junctions (see section 4.4.1.3(a)). This situation, for example, was found for the tubes connecting to portal buildings described in section 4.5.1.3. Special joints may need to be provided to allow movement between the tunnel and the adjoining structure and therefore reduce forces at these junctions. Figure 4-30 illustrates a seismic joint designed to allow three-dimensional movement at the junction of the transbay tube and a ventilation structure of the San Francisco Bay Area Rapid Transit (BART) (Douglas and Warshaw, 1971; Bickel and Tanner, 1982); sixty of these joints were provided around the perimeter of the transbay tube.

Stresses also tend to be concentrated at locations along a tunnel where there is an abrupt change in stiffness of the geologic media, such as where a tunnel passes from rock to soil. Again, stresses and strains can be reduced by providing flexible joints at such transitions. The North Point tunnel in the San Francisco Wastewater System, for example, passes through an abrupt soil-rock interface (Owen and Scholl, 1981). For this interface, a special seismic joint was designed to accommodate 0.3 m of lateral displacement over a length of 15 m. A 2.5 cm thickness of crushable foam in the joint allowed the pipe to conform to the predicted displacements (figure 4-31). Another approach to design at an abrupt soil-rock transition is overexcavation of the rock and backfilling with soil to create a more gradual transition.



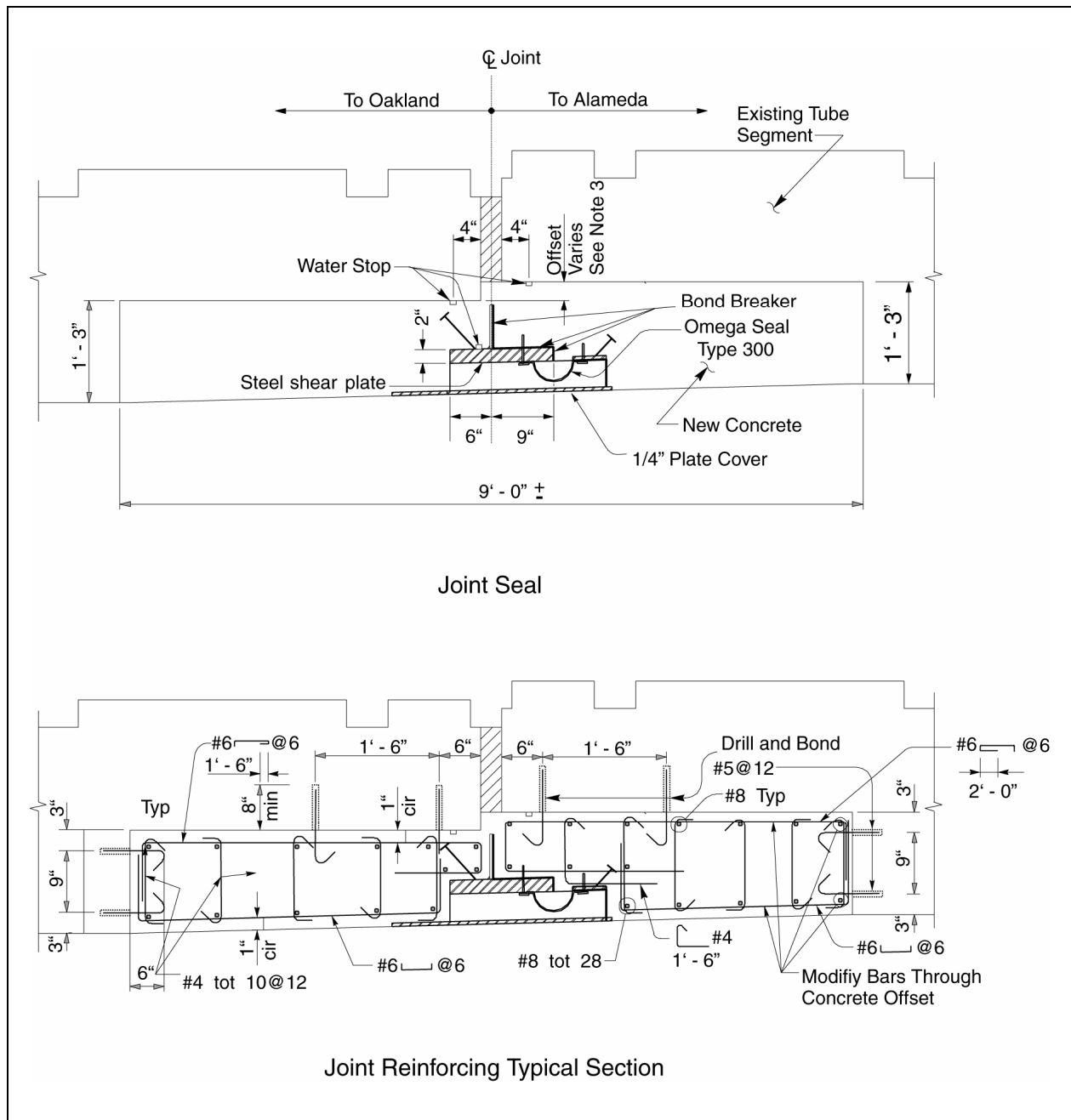
Caltrans/Parsons Brinckerhoff, 1998

Figure 4-27. Typical stone column placement around Webster tube.



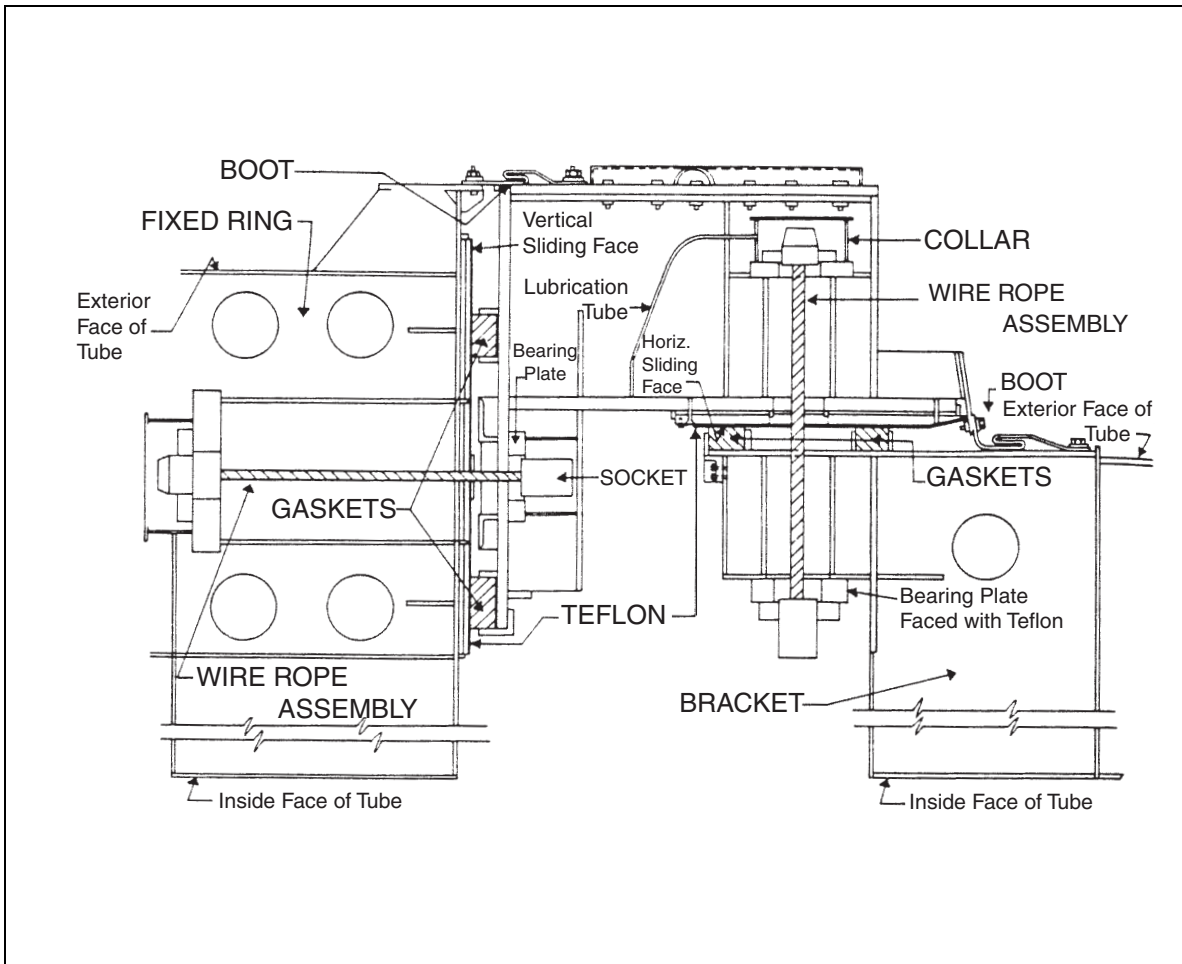
Caltrans/Parsons Brinckerhoff, 1998

Figure 4-28. Typical jet grout column around Posey tube.



Caltrans/Parsons Brinckerhoff, 1998
T. Jackson, personal communication, 2003

Figure 4-29. Redesigned joint preventing tension and allowing compression and shear forces between segments of Posey tube.



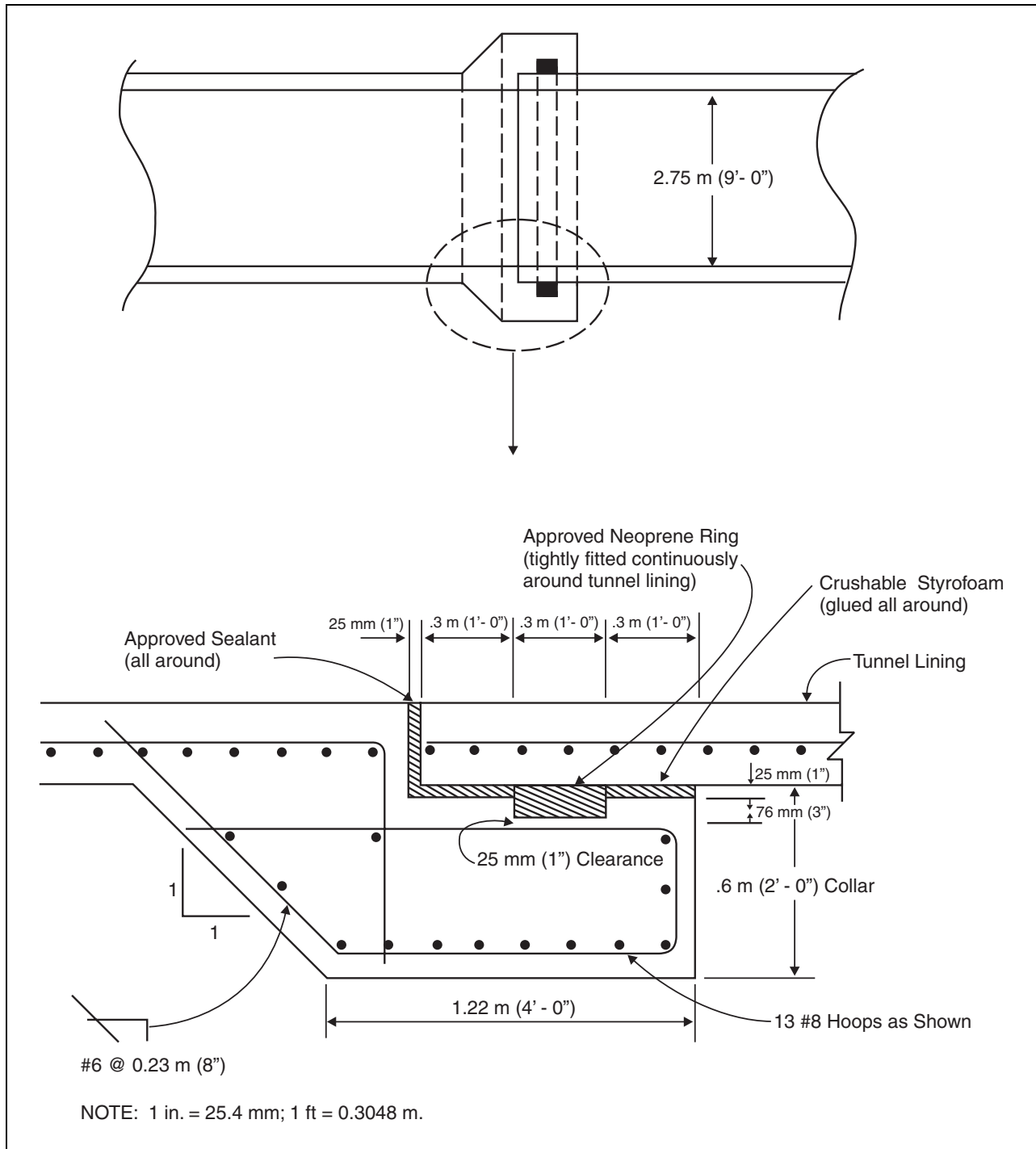
Douglass and Warshaw, 1971; Bickel and Tanner, 1982

Figure 4-30. Seismic joint for transbay tube.

4.5.2. FAULT DISPLACEMENT-INDUCED FAILURE

Retrofit strategies for portions of tunnels crossing active faults and potentially subject to fault displacement depend on the magnitude of the displacement and the width of the zone over which the displacement is distributed, as well as the geologic conditions.

If large displacements are concentrated in a narrow zone, a retrofit strategy is to enlarge the tunnel across and beyond the displacement zone. This has been discussed or suggested in a number of publications, including Rosenbluth (1977), Owen and Scholl (1981), Brown et al. (1981), Desai et al. (1989), Rowe (1992), and Abramson and Crawley (1995), and has been implemented in rapid transit tunnels including San Francisco's BART and Los Angeles' Metro tunnels.



Owen and Scholl, 1981

Figure 4-31. Seismic joint for North Point tunnel.

The concept of an enlarged tunnel to accommodate fault displacement is illustrated in figure 4-32. The tunnel is made wide enough that the fault displacement will not close the tunnel and traffic can be resumed after repairs are made. Repairs include removal of lining and rock debris in the damaged tunnel sections, restoration of lining continuity, and repair of the pavement section in a highway tunnel, or realignment of the rails in a transit tunnel. The length of tunnel over which enlargement is made is a function of both the amount of fault displacement and the permissible curvature of the roadway or trackway. An S-shaped roadway or trackway is required after the earthquake in the enlarged tunnel region. The longer the enlarged tunnel, the smaller the post-earthquake curvature. The design of the enlarged Los Angeles Metro tunnel across the Hollywood fault zone is illustrated in figure 4-33. As shown in the cross section in the figure, the design allows for fault movement upward and to the left. After fault movement, the track in the enlarged tunnel, resting on ballast rock, would be realigned and ballast rock placed at the new line and grade after repair.

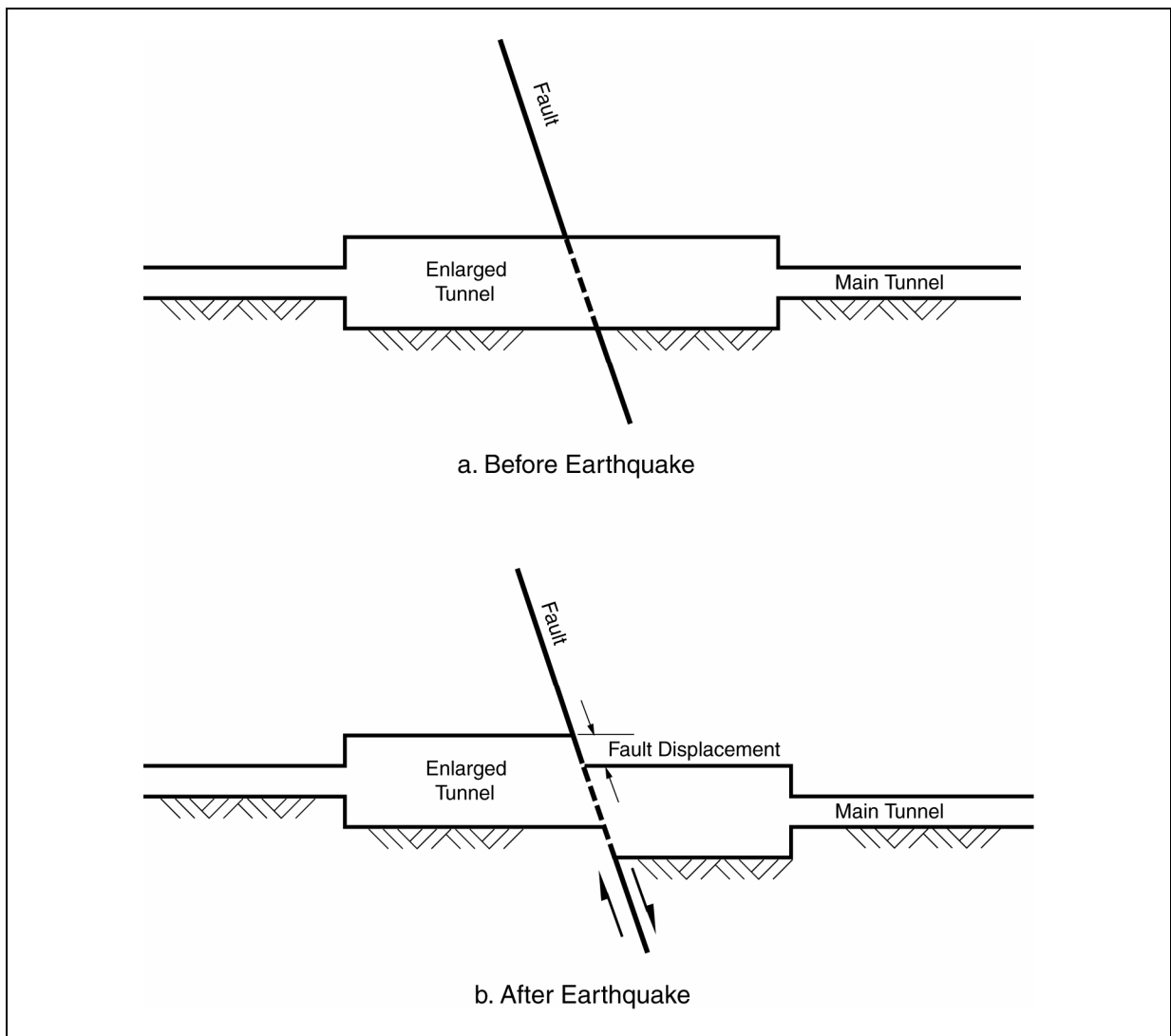
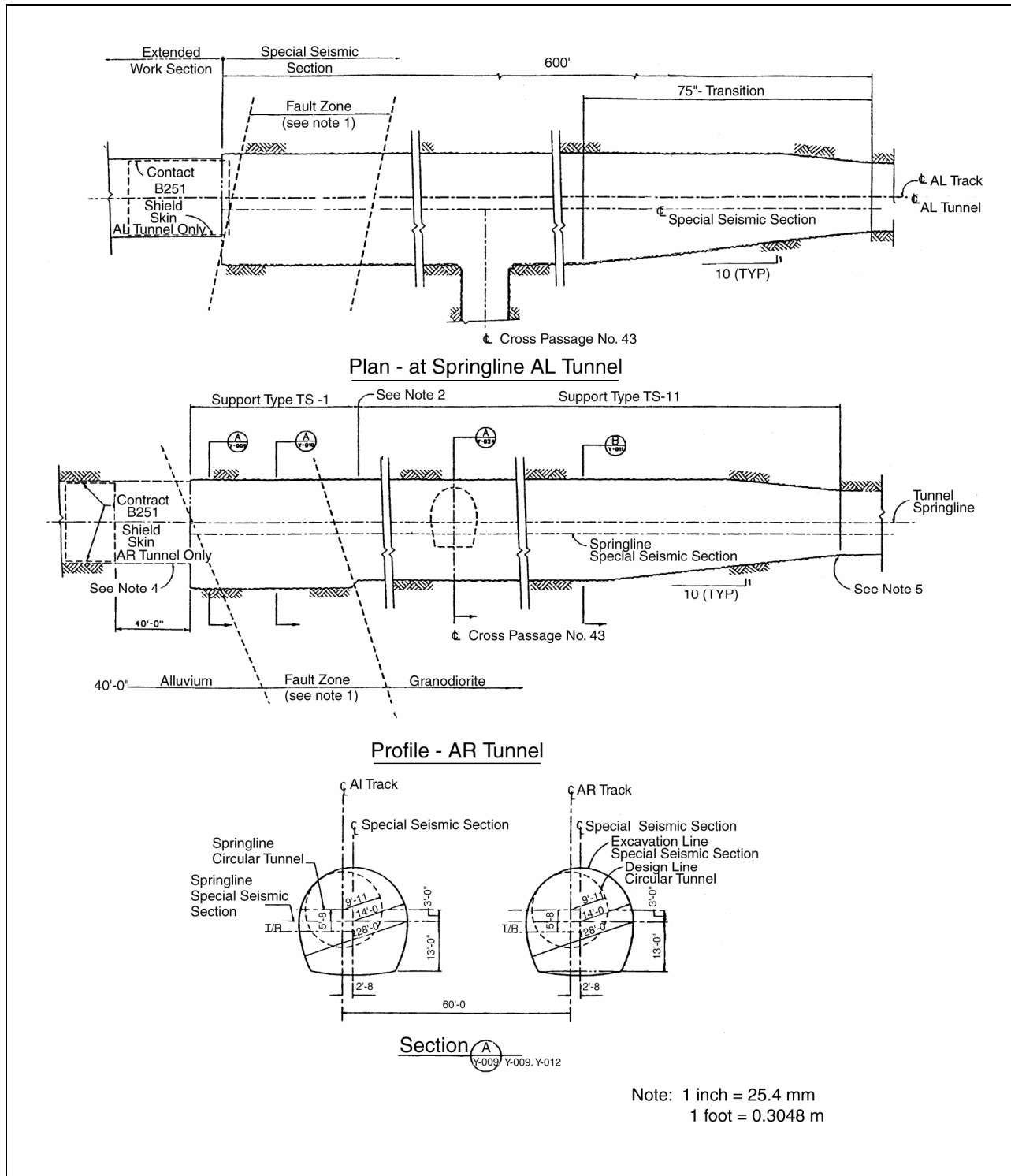


Figure 4-32. Enlarged tunnel at fault crossing, plan view, strike-slip faulting.



LA County MTA/Parsons Brinckerhoff, 1994

Figure 4-33. Design of LA Metro tunnel across Hollywood fault zone.

An enlarged tunnel may also surround an inner tunnel that is backfilled with frangible backpacking such as cellular concrete (figure 4-34). Cellular concrete is readily available at low cost and has a history of use in underground projects (Huff, 1971). It can be made with varying amounts of void space and may be engineered to have unit weights as low as 2.4 to 3.9 kN/m³. It also has a relatively low yield strength to minimize lateral loads on the tunnel liner, but has adequate strength to resist normal soil pressures and other seismic loads such as minor ground shock and soil “loosening” load or other vertical loads above the excavation. It is highly compressible at strains of 60 percent or even more. It also has stable long-term properties with respect to hardening, chemical resistance, and creep behavior.

If fault movements are small and/or distributed over a relatively wide zone, it is possible that a tunnel may be designed to accommodate the fault displacement by providing articulation of the tunnel liner using ductile joints. The effect is to allow the tunnel to distort into an S-shape through the fault zone without rupture and with repairable damage. The closer the joint spacing, the better the performance of the liner. This approach may not be feasible for fault displacements exceeding a few inches.

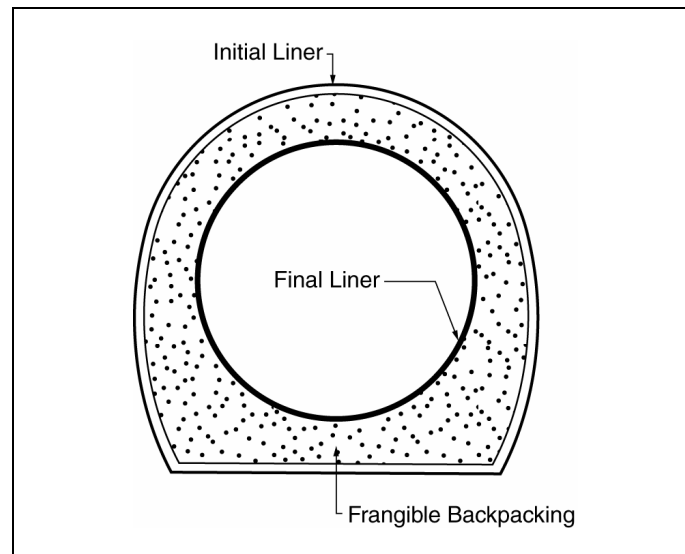
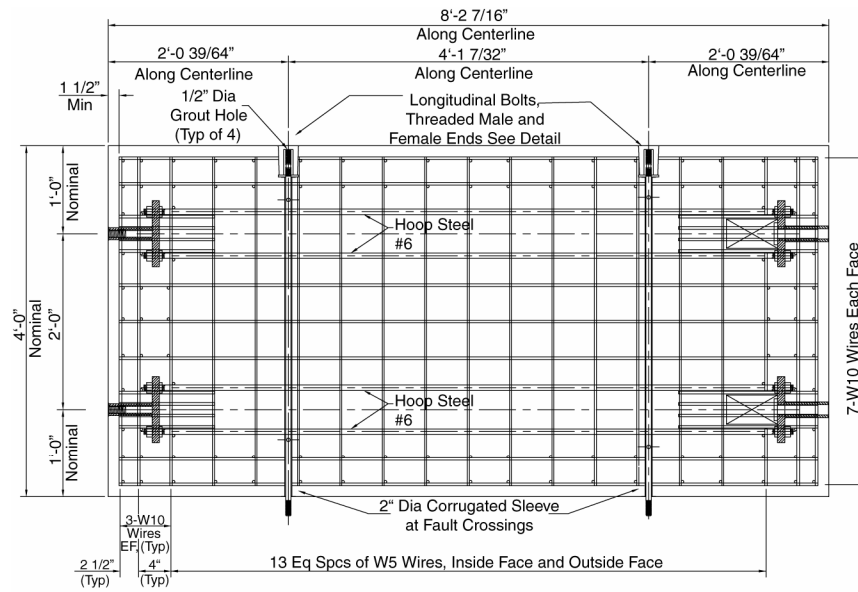


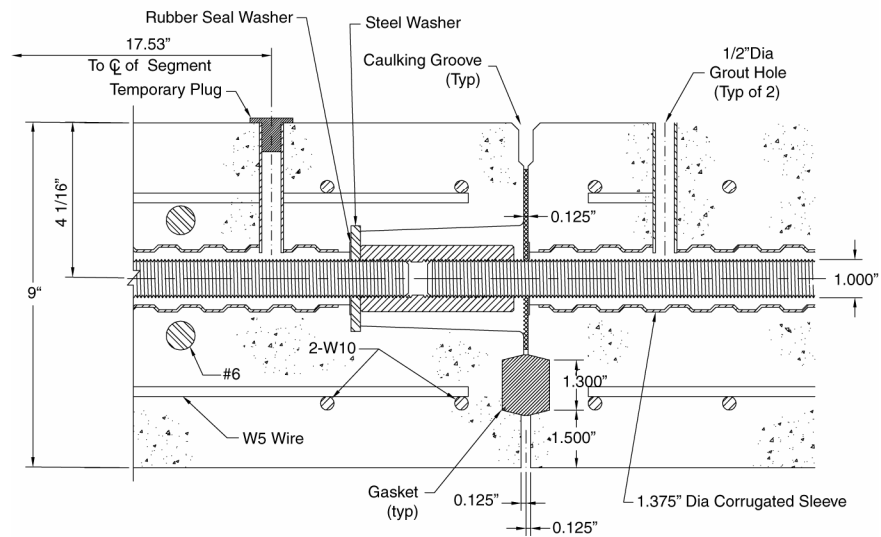
Figure 4-34. Enlarged tunnel section with final liner and frangible backpacking to accommodate fault displacement.

Design of a lining to accommodate fault displacement becomes more feasible in soft soils where the tunnel lining can more effectively redistribute the displacements. The requirements for tunnel water-tightness must be evaluated when considering the use of joints.

An example of a segmented lining designed to accommodate small fault displacements is that of the South Bay Ocean Outfall shown in figure 4-35 (Kaneshiro et al., 1996a, 1996b). Large-diameter longitudinal bolts extending through the precast concrete segments provide a certain amount of ductility for longitudinal extension and articulation in the fault zone. Figure 4-36 illustrates a different approach to joints in segmented tunnels to withstand small fault movements. The joint design and neoprene seals permit extensional, compressional, and rotational movements while maintaining water-tightness.



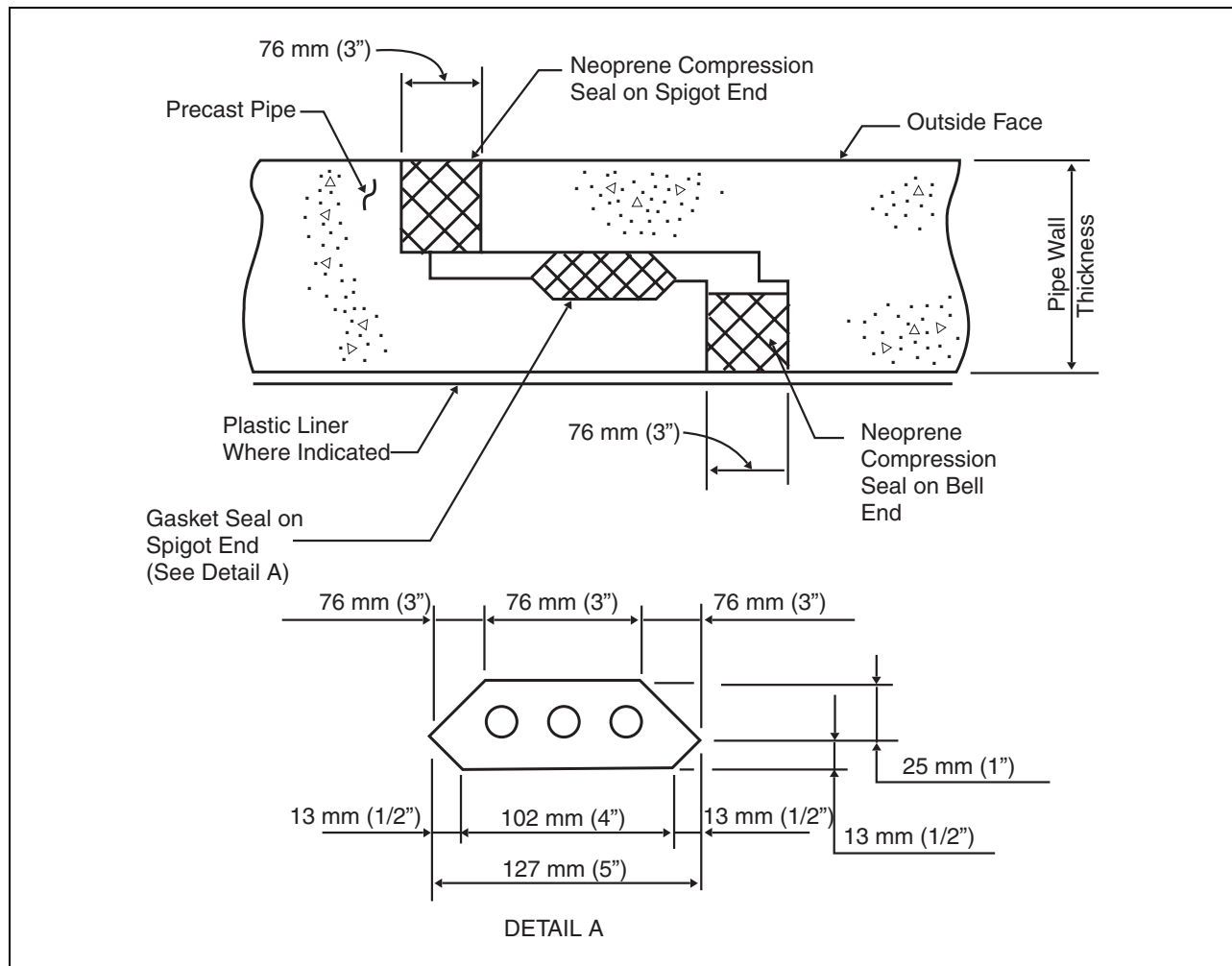
Plan Along Centerline



Fault Crossing
Circumferential Joint Detail

Kaneshiro et al., 1996

Figure 4-35. Segment reinforcing and circumferential joint detail, precast concrete segmental liner used in Rose Canyon fault zone for South Bay Tunnel Ocean Outfall Project, San Diego.

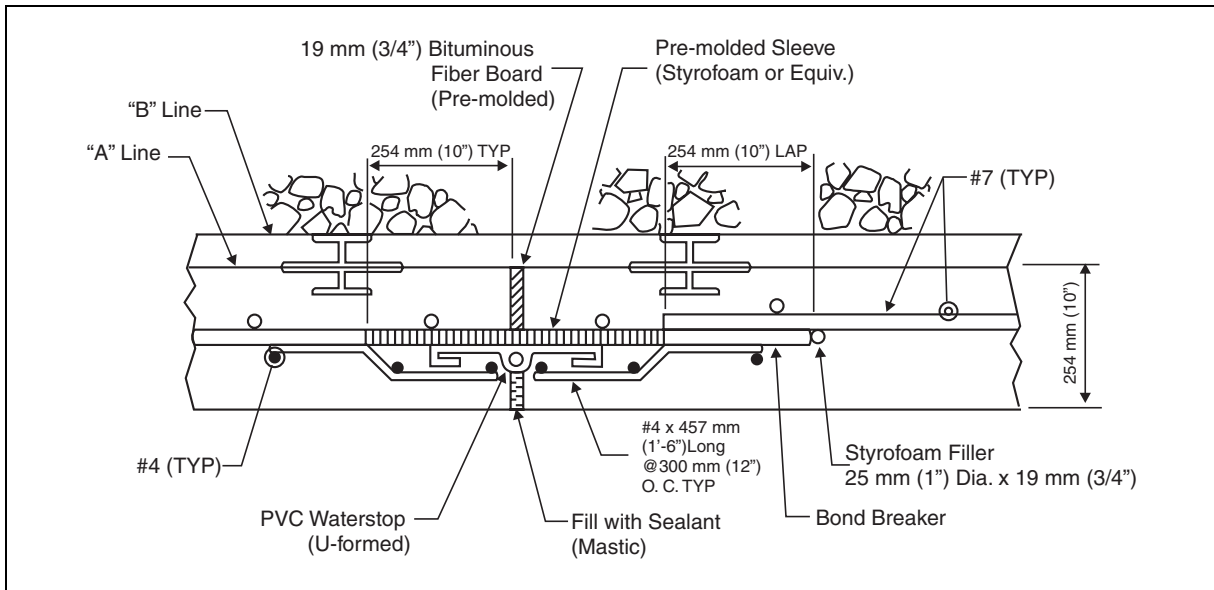


Desai et al., 1989

Figure 4-36. Flexible joint proposed for segmented tunnel lining in fault zone.

An example of a joint designed to accommodate small fault displacements in a cast-in-place reinforced concrete tunnel lining is shown in figure 4-37. Compressive and tensile movement of the joint occurs in the fiberboard joint filler and through placing the No. 7 reinforcing bars in a pre-molded sleeve and bond breaker. The joints were placed on 10 foot centers (3 m) over a distance of about 56 m (185 feet) to resist a total displacement of approximately 300 mm (12 inches) in any direction.

An alternative to retrofitting a tunnel to withstand faulting displacements is to instead make contingency plans to facilitate repair as rapidly as possible after the earthquake. Modifications to portal structures may be made to facilitate safe ingress and emergency repair. Temporary supports and other materials essential to the rapid repair of the tunnel may be stockpiled, and tunneling and other specialty contractors may be put under contract in advance of the earthquake event.



Frame, 1995

Figure 4-37. Flexible joint detail for Coyote Dam outlet tunnel.

4.5.3. LANDSLIDING- AND LIQUEFACTION-INDUCED FAILURE

If landsliding- or liquefaction-induced lateral spreading movements through a tunnel are a significant hazard, the hazard may be mitigated by stabilizing the landslide or stabilizing the ground to prevent liquefaction and/or resulting lateral spreading movements. It is doubtful that a tunnel can be designed to resist or accommodate the movements associated with these phenomena unless the hazard is localized and the amount of rock or soil involved in the phenomena is small. Other hazard mitigation approaches are rerouting the tunnel to avoid the hazard or making contingency plans.

If the predicted effects of liquefaction are to cause local buildup of pore water pressure adjacent to the walls of a tunnel, an alternative retrofit measure is to strengthen the walls to resist the increased lateral earth pressures.

Seismic (as well as static) landsliding has historically been a cause of failure at tunnel portals. The most effective mitigation is generally to stabilize the unstable earth mass. Portal structures also represent locations of change in geometry and stiffness and therefore are locations for concentrated forces at the connection of the tunnel and the portal. Either the connection must be strong enough to resist the large forces that may develop, or a joint must be designed to allow relative movement and reduce the forces.

4.6. EXAMPLES OF TUNNEL SCREENING, EVALUATION, AND RETROFIT STRATEGIES

Examples 4-1 through 4-4 illustrate details of analytical methodologies for seismic evaluation of tunnels. Example 4-5 provides a hypothetical example of the overall process of seismic screening, seismic evaluation, and development of seismic retrofit strategies.

EXAMPLE PROBLEM 4.1 – AXIAL AND CURVATURE DEFORMATION ALONG THE TUNNEL LONGITUDINAL AXIS DUE TO S-WAVES

1. Earthquake parameters:

Earthquake moment magnitude, $M_w = 7.5$
 Earthquake source-to-site distance = 10 km
 Peak ground acceleration at ground surface above the tunnel, $a_{max} = 0.5 g$

2. Tunnel parameters:

Reinforced concrete circular tunnel:

$D = 6 \text{ m}$
 $t = 0.3 \text{ m}$
 $E_l = 24.8 \times 10^6 \text{ kPa}$
 $I_{l1} = 25.4 \text{ m}^4$
 $A_{l1} = 5.65 \text{ m}^2$
 Depth = 100 m

3. Soil parameters:

$\gamma_t = 19.0 \text{ kN/m}^3$
 $C'_m = 800 \text{ m/s}$
 $v_m = 0.3$
 $f = 6,000 \text{ kN/m}$

Assume that the shaking at the tunnel elevation is dominated by shear (S) body waves (i.e., for purposes of this example, an assessment has been made that significant surface waves are unlikely to occur at the tunnel during the design earthquake).

a. Determine the seismic ground shaking parameters at the tunnel depth:

$$a_s = 0.7 a_{max} = 0.7(0.5 g) = 0.35 g \quad (\text{Table 4-3})$$

$$V_s = (97 \text{ cm/s } g) (0.35 g) = 34 \text{ cm/s} = 0.34 \text{ m/s} \quad (\text{Table 4-4})$$

$$C_s = 2 \text{ km/s and } T_s = 2 \text{ seconds (default values)}$$

$$L = C_s \cdot T_s = 2000 \text{ m/s (2 s)} = 4000 \text{ m} \quad (\text{Eq. 4-10})$$

b. Determine the axial strain and stress from combined longitudinal and curvature deformations, assuming negligible soil-tunnel interaction:

$$\varepsilon^{ab} = \left[\frac{V_s}{C_s} \sin \phi \cos \phi + Y \frac{a_s}{C_s^2} \cos^3 \phi \right] \text{ for S-waves} \quad (\text{Eq. 4-2})$$

$$\varepsilon^{ab} = \left[\frac{0.34}{2000} \sin 45^\circ \cos 45^\circ + 3 \frac{0.35(9.81)}{2000^2} \cos^3 45^\circ \right]$$

$$\varepsilon^{ab} = 0.000085 + 9.1(10^{-7}) = 0.000085$$

$$\sigma^{ab} = 0.000085(24.8 \cdot 10^6 \text{ kPa}) = 2100 \text{ kPa} \quad (\text{Eq. 4-4})$$

c. Evaluate the effect of soil-tunnel interaction:

$$G'_m = \frac{\gamma_t}{g} C'_m{}^2 = 1.24(10^6) \text{ kPa} \quad (\text{Eq. 4-11})$$

$$K_a = K_h = \frac{16\pi G'_m (1-v_m) D}{(3-4v_m) L} \quad (\text{Eq. 4-8})$$

$$K_a = K_h = \frac{16\pi 1.24(10^6)(1-0.3)}{(3-4(0.3))} \frac{6}{4000} = 36,300 \text{ kPa}$$

$$R = \left\{ 1 + \frac{E_t A_{It}}{K_a} \left(\frac{2\pi}{L} \right)^2 \cos^2 \phi \right\}^{-1} \quad (\text{Eq. 4-6})$$

$$R = \left\{ 1 + \frac{24.8(10^6)5.65}{36300} \left(\frac{2\pi}{4000} \right)^2 \cos^2 45^\circ \right\}^{-1} = 0.99$$

Based on the above calculation, the effects of soil-tunnel interaction will not significantly reduce the longitudinal strains or stresses in the tunnel lining.

d. Check the axial force, Q , against the maximum force that can be developed by friction of the soil against the tunnel lining:

$$Q = \sigma^{ab} \cdot A_{It} = 2100 \cdot 5.65 = 11,900 \text{ kN}$$

$$(Q_{\max})_f = \frac{fL}{4} = \frac{(6000)(4000)}{4} = 6,000,000 \text{ kN} \quad (\text{Eq. 4-12})$$

$Q < (Q_{\max})_f$; thus, the axial force is not limited by frictional capacity.

EXAMPLE PROBLEM 4.2 - AXIAL AND CURVATURE DEFORMATION ALONG THE TUNNEL LONGITUDINAL AXIS DUE TO R-WAVES

1. Earthquake parameters:

Earthquake moment magnitude, $M_w = 7.5$
 Earthquake source-to-site distance = 20 km

2. Tunnel parameters:

Reinforced concrete circular tunnel

$D = 6$ m
 $t = 0.3$ m
 $E_l = 24.8 \times 10^6$ kPa
 $I_{l1} = 25.4$ m⁴
 $A_{l1} = 5.65$ m²
 Depth to top of tunnel, $Z = 15$ m

3. Soil parameters:

$\gamma_t = 17.0$ kN/m³
 $C'_m = 250$ m/s
 $v_m = 0.45$
 $f = 1500$ kN/m

Assume that the shaking at the tunnel elevation is dominated by Rayleigh (R) surface waves (i.e., for purposes of this example, an assessment has been made that significant surface waves producing the strong ground velocities and displacements are likely to occur at the tunnel during the design earthquake).

a. *Determine the seismic ground shaking parameters at the tunnel depth. From a site-specific assessment, it was determined that:*

$$\begin{aligned} a_R &= 0.20 \text{ g} \\ V_R &= 30 \text{ cm/s} = 0.30 \text{ m/s} \\ C_R &= 500 \text{ m/s and } T_R = 2 \text{ seconds} \\ L &= C_R \cdot T_R = 500 \text{ m/s (2 s)} = 1000 \text{ m} \end{aligned} \quad (\text{Eq. 4-10})$$

b. *Determine the axial strain and stress from combined longitudinal and curvature deformations in the horizontal plane, assuming negligible soil-tunnel interaction:*

$$\epsilon^{ab} = \left[\frac{V_R}{C_R} \cos^2 \phi + Y \frac{a_R}{C_R^2} \sin \phi \cos^2 \phi \right] \text{ for R-waves} \quad (\text{Eq. 4-3})$$

$$\epsilon^{ab} = \left[\frac{0.30}{500} \cos^2 0^\circ + 3 \frac{0.20(9.81)}{500^2} \sin 0^\circ \cos^2 0^\circ \right]$$

$$\epsilon^{ab} = 0.0006 + 0 = 0.0006$$

$$\sigma^{ab} = E_l \epsilon^{ab} = 14,880 \text{ kPa} \quad (\text{Eq. 4-4})$$

- c. Determine the axial strain and stress from curvature deformations in the vertical plane, assuming negligible soil-tunnel interaction:

$$\varepsilon^{ab} = Y \frac{a_R}{C_R^2} \cos^2 \phi \text{ for R-waves} \quad (\text{Eq. 4-5})$$

$$\varepsilon^{ab} = 3 \frac{0.20 (9.81)}{500^2} \cos^2 0^\circ = 0.00002$$

(Negligible compared to axial strain determined in (b) above.)

- d. Evaluate the effect of soil-tunnel interaction:

$$G'_m = \frac{\gamma_t}{g} C_m'^2 = 108,000 \text{ kPa} \quad (\text{Eq. 4-11})$$

$$K_a = K_h = \frac{16\pi G'_m (1-v_m) D}{(3-4v_m) L} \quad (\text{Eq. 4-8})$$

$$K_a = K_h = \frac{16\pi (108000)(1-0.45)}{(3-4(0.45))} \frac{6}{1000} = 15,000 \text{ kPa}$$

$$R = \left\{ 1 + \frac{E_t A_{lt}}{K_a} \left(\frac{2\pi}{L} \right)^2 \cos^2 \phi \right\}^{-1} \quad (\text{Eq. 4-6})$$

$$R = \left\{ 1 + \frac{24.8(10^6)(5.65)}{15,000} \left(\frac{2\pi}{1000} \right)^2 \cos^2 0^\circ \right\}^{-1} = 0.730 \quad (\text{Eq. 4-6})$$

$$\sigma^{ab} = E_t \varepsilon^{ab} R = 10,900 \text{ kPa}$$

- e. Check the axial force, Q , against the maximum force that can be developed by friction of the soil against the tunnel lining:

$$Q = \sigma^{ab} \cdot A_{lt} = 10,900 (5.65) = 61,600 \text{ kN}$$

$$(Q_{\max})_f = \frac{fL}{4} = \frac{(1500)(1000)}{4} = 375,000 \text{ kN} \quad (\text{Eq. 4-12})$$

$Q < (Q_{\max})_f$; thus, the axial force is not limited by frictional capacity.

EXAMPLE PROBLEM 4.3 - OVALING DEFORMATION OF A CIRCULAR TUNNEL

1. Earthquake parameters:

Earthquake moment magnitude, $M_w = 7.5$
 Earthquake source-to-site distance = 10 km
 Peak ground acceleration at ground surface above the tunnel, $a_{\max} = 0.5 \text{ g}$

2. Tunnel parameters:

Reinforced concrete circular tunnel

$D = 6 \text{ m}$

$t = 0.3 \text{ m}$

$E_1 = 24.8 \times 10^6 \text{ kPa}$

$I_{12} = 0.0023 \text{ m}^4/\text{m}$

$A_{12} = 0.3 \text{ m}^2/\text{m}$

$\nu_1 = 0.2$

Depth to top of tunnel, $Z = 15 \text{ m}$

3. Soil parameters:

$\gamma_t = 19.0 \text{ kN/m}^3$

$C'_m = 250 \text{ m/s}$

$\nu_m = 0.3$

a. Determine the seismic ground shaking parameters at the tunnel depth:

$$a_s = 0.85 a_{\max} = 0.85(0.5 \text{ g}) = 0.425 \text{ g} \quad (\text{Table 4-3})$$

$$V_s = (130 \text{ cm/s g}) (0.425 \text{ g}) = 55 \text{ cm/s} = 0.55 \text{ m/s} \quad (\text{Table 4-4})$$

$$\gamma_{s\max} = \frac{V_s}{C'_m} = \frac{0.55}{250} = 0.0022 \quad (\text{Eq. 4-28})$$

b. Determine the normal stress in the liner assuming full slippage condition:

$$G'_m = \frac{\gamma_t}{g} C_m'^2 = 121,000 \text{ kPa} \quad (\text{Eq. 4-11})$$

$$F = \frac{G'_m (1 - \nu_1^2) D^3}{24 E_1 I_{12}} \quad (\text{Eq. 4-17})$$

$$F = \frac{121000 (1 - (0.2)^2) 6^3}{24(24.8(10)^6)0.0023} = 18.3$$

$$K = \frac{1 - \nu_m}{F + 2.5 - 3\nu_m} = \frac{1 - 0.3}{18.3 + 2.5 - 3(0.3)} = 0.0351 \quad (\text{Eq. 4-16})$$

$$T(\theta) = G'_m DK \gamma_{smax} \sin 2\theta \quad (\text{Eq. 4-13})$$

$$T(45^\circ) = (121000)6(0.0351)(0.0022)\sin 2(45^\circ) = 56.1 \text{ kN/m}$$

$$M(\theta) = \frac{1}{2} G'_m D^2 K \gamma_{smax} \sin 2\theta \quad (\text{Eq. 4-15})$$

$$M(45^\circ) = \frac{1}{2} (121000)6^2(0.0351)(0.0022) \sin 2(45^\circ) = 168 \text{ kN} \cdot \text{m/m}$$

$$\sigma = \frac{T}{A_{l2}} \pm \frac{M(t/2)}{I_{l2}} = \frac{56.1}{0.3} \pm \frac{168(0.3/2)}{0.0023} = 11,100 \text{ kPa} \quad (\text{Eq. 4-29})$$

c. Determine the normal stress in the liner assuming no slippage condition using Penzien and Wu (1998):

$$K' = \frac{1 - v_m}{F + 3 - 4v_m} = \frac{1 - 0.3}{18.3 + 3 - 4(.3)} = 0.0348 \quad (\text{Eq. 4-21})$$

$$T(\theta) = 2G'_m DK' \gamma_{smax} \sin 2\theta \quad (\text{Eq. 4-18})$$

$$T(45^\circ) = 2 (121000)6(0.0348)(0.0022)\sin 2(45^\circ) = 111 \text{ kN/m}$$

$$M(\theta) = \frac{1}{2} G'_m D^2 K' \gamma_{smax} \sin 2\theta \quad (\text{Eq. 4-20})$$

$$M(45^\circ) = \frac{1}{2} (121000)6^2(0.0348)(0.0022)\sin 2(45^\circ) = 166 \text{ kN} \cdot \text{m/m}$$

$$\sigma = \frac{T}{A_{l2}} \pm \frac{M(t/2)}{I_{l2}} = \frac{111}{0.3} \pm \frac{166(0.3/2)}{0.0023} = 11,200 \text{ kPa} \quad (\text{Eq. 4-29})$$

d. Determine the normal stress in the liner assuming no slippage condition using Wang (1993):

$$C = \frac{G'_m (1 - v_1^2) D}{E_t t (1 - 2v_m)} = \frac{121000(1 - 0.2^2)6}{24.8(10^6)0.3(1 - 2(0.3))} = 0.234 \quad (\text{Eq. 4-27})$$

$$a_o = F[(3 - 2v_m) + (1 - 2v_m)C] + C \left[\frac{5}{2} - 8v_m + 6v_m^2 \right] + 6 - 8v_m \quad (\text{Eq. 4-26})$$

$$a_o = 18.3[(3 - 2(0.3)) + (1 - 2(0.3))0.234] + 0.234 \left[\frac{5}{2} - 8(0.3) + 6(0.3)^2 \right] + 6 - 8(0.3)$$

$$a_o = 49.5$$

$$a_2 = \left\{ F[(1-2v_m)(1-C)] - \frac{1}{2}C(1-2v_m)^2 + 2 \right\} / a_o \quad (\text{Eq. 4-24})$$

$$a_2 = \left\{ 18.3[(1-2(0.3))(1-0.234)] - \frac{1}{2}(0.234)(1-2(0.3))^2 + 2 \right\} / 49.5 = 0.152$$

$$a_3 = \left\{ F[C(1-2v_m) + 1] - \frac{1}{2}C(1-2v_m) - 2 \right\} / a_o \quad (\text{Eq. 4-25})$$

$$a_3 = \left\{ 18.3[0.234(1-2(0.3)) + 1] - \frac{1}{2}(0.234)(1-2(0.3)) - 2 \right\} / 49.5 = 0.362$$

$$T(\theta) = \frac{1}{2}G'_m D(1 + a_2)\gamma_{smax} \sin 2\theta \quad (\text{Eq. 4-22})$$

$$T(45^\circ) = \frac{1}{2}121000(6)(1 + 0.152)0.0022 \sin 2(45^\circ) = 920 \text{ kN/m}$$

$$M(\theta) = \frac{1}{8}G'_m D^2(1 - a_2 - 2a_3)\gamma_{smax} \sin 2\theta \quad (\text{Eq. 4-23})$$

$$M(45^\circ) = \frac{1}{8}121000(6)^2(1 - 0.152 - 2(0.362))0.0022 \sin 2(45^\circ) = 149 \text{ kN} \cdot \text{m/m}$$

$$\sigma = \frac{T}{A_{l2}} \pm \frac{M(t/2)}{I_{l2}} = \frac{920}{0.3} \pm \frac{149(0.3/2)}{0.0023} = 12,800 \text{ kPa} \quad (\text{Eq. 4-29})$$

e. *Conclusion:*

It is recommended that the maximum stress be obtained using the formulation that produces the highest stress. Of the three methods for estimating stress in the liner due to cross sectional deformation, the Wang (1993) no slippage condition formulations estimate the highest normal stress (12,800 kPa) in the liner.

EXAMPLE PROBLEM 4.4 - RACKING DEFORMATION OF A RECTANGULAR TUNNEL

1. Earthquake parameters:

Earthquake moment magnitude, $M_w = 7.5$

Earthquake source-to-site distance = 10 km

Peak horizontal ground acceleration at ground surface above the tunnel, $a_{max} = 0.5 g$

Peak vertical ground acceleration at ground surface above the tunnel, $a_v = 0.4 g$

2. Tunnel parameters:

Width, $w = 18$ m

Height, $H = 6$ m

Depth to top of tunnel, $Z = 5$ m

Tunnel founded on soil

3. Soil parameters:

$\gamma_t = 17.0$ kN/m³

$C'_m = 80$ m/s

$v_m = 0.4$

Racking Deformation Analysis

a. Determine the free-field soil shear deformation, Δ_{ff} :

$\gamma_{s\ max} = 0.0056$ (estimated using site response analyses)

$\Delta_{ff} = \gamma_{s\ max} H$

$\Delta_{ff} = (0.0056)(6) = 0.034$ m

b. Determine the flexibility ratio, F_r :

$$G'_m = \frac{\gamma_t}{g} C_m'^2 = 11,000 \text{ kPa} \quad (\text{Eq. 4-11})$$

$$F_r = \frac{G'_m w}{SH} \quad (\text{Eq. 4-30})$$

Through structural analysis, the force required to cause a unit racking deflection (1 m) for a unit length (1 m) of the cross section, S , was determined to be 150,000 kPa. Note that for the flexibility ratio, F_r , to be dimensionless, the units of S must be in force per area.

$$F_r = \frac{11000(18)}{150000(6)} = 0.22$$

For $F_r = 0.22$ and $V_m = 0.4$, the full slip relationship produces a racking coefficient, R_r , of 0.34 and the no-slip relationship produces a $R_r = 0.32$ (figure 4-13b). The greater racking coefficient produced by the full-slip relationship is used to determine the racking deformation of the tunnel.

- c. Determine the racking deformation of the structure, Δ_r :

$$\Delta_r = R_r \Delta_{fr} \quad (\text{Eq. 4-31})$$

$$\Delta_r = 0.34(0.034) = 0.012 \text{ m}$$

- d. Determine the stresses in the structure by performing a structural analysis with an applied racking deformation of 0.012 m as shown in figure 4-14. Both the point load and triangularly distributed load pseudo-lateral force models should be applied to identify the maximum forces in each location of the liner.

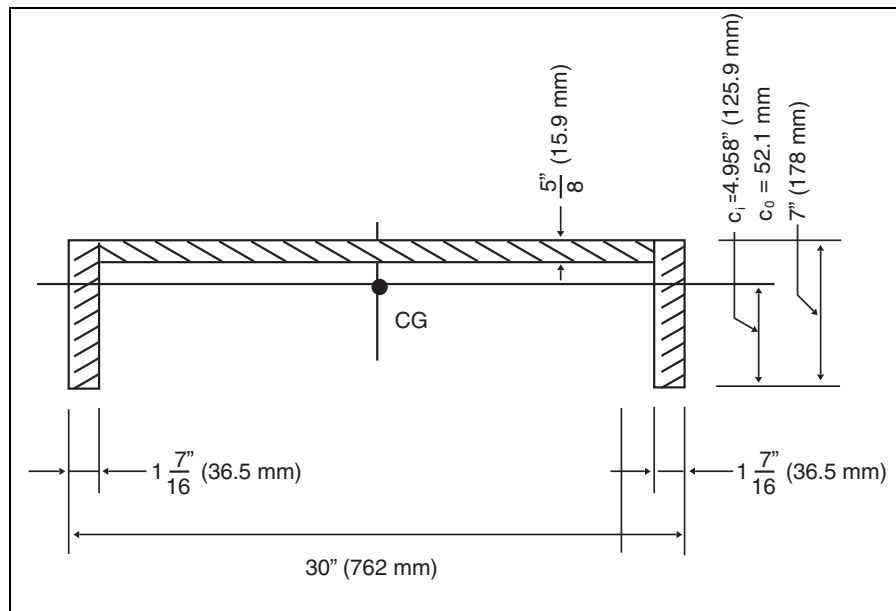
EXAMPLE PROBLEM 4.5 - SEISMIC SCREENING EVALUATION AND RETROFIT STRATEGIES FOR A HYPOTHETICAL TUNNEL

Description of Tunnel

A bored transit tunnel 18 feet (5.49 m) in diameter passes through bedrock and into a soil-filled sedimentary basin. The depth to the top of the tunnel in both rock and soil is 15 m. The bedrock is moderately jointed and locally intensely sheared. The soil at the tunnel grade is a medium stiff clay. The groundwater table is 3 m below the ground surface. The tunnel in rock has a 0.3 m-thick unreinforced concrete liner that is moderately cracked locally. The tunnel in soil has a steel segmented liner having the cross section shown in the figure below (after Penzien and Wu, 1998). Assessment of the concrete lining by inspection, coring, and geophysical sounding indicates that the concrete has moderate strength but has frequent voids behind the lining. The segmented lining appears to be undamaged and is constructed immediately against the excavation face.

Seismic Environment

An active earthquake fault capable of generating a moment magnitude M_w 7.5 earthquake is located a closest distance of 2 km from the tunnel at the basin edge. Based on current national seismic ground motion maps, the level of ground shaking for seismic evaluation and retrofit design (if required) is a peak acceleration of 0.50 g at the ground surface at the basin edge. This acceleration is judged to be applicable to soil or rock.



Penzien and Wu, 1998

Screening

Based on the screening guidelines in section 4.3.3 and table 4-1, the level of ground shaking, soil and geologic conditions, and the condition of the liner, the tunnel cannot be screened out as seismically adequate for ground shaking. The tunnel is not known to be intersected by an active fault, a landslide, or liquefiable soils (section 4.3.3.1). Therefore, further seismic evaluation is required only for ground shaking.

Evaluation and Retrofit

1. Concrete liner parameters:

$$\begin{aligned}D &= 5.49 \text{ m} \\A_{l2} &= 0.3 \text{ m}^2/\text{m} \\I_{l2} &= 2.25 \times 10^{-3} \text{ m}^4/\text{m} \\f'_c &= 20.7 \times 10^3 \text{ kPa} \\t &= 0.3 \text{ m} \\E_l &= 22 \times 10^6 \text{ kPa} \\v_l &= 0.2 \\c_o &= c_i = 0.15 \text{ m (distance to outer and inner fiber of lining from center of gravity of lining)} \\Z &= 15 \text{ m} \\H_w &= 12 \text{ m (distance to groundwater table above tunnel)}\end{aligned}$$

2. Steel liner parameters:

$$\begin{aligned}D &= 5.49 \text{ m} \\A_{l2} &= 0.0314 \text{ m}^2/\text{m} \\I_{l2} &= 9.63 \times 10^{-5} \text{ m}^4/\text{m} \\f_y &= 249 \times 10^3 \text{ kPa} \\E_l &= 20.4 \times 10^{10} \text{ N/m}^2 \\v_l &= 0.3 \\c_o &= 0.0521 \text{ m (figure 4-38)} \\c_i &= 0.1259 \text{ m (figure 4-38)} \\Z &= 15 \text{ m} \\H_w &= 12 \text{ m (distance to groundwater table above tunnel)}\end{aligned}$$

3. Soil parameters:

$$\begin{aligned}\gamma_t &= 17.0 \text{ kN/m}^3 \\C'_m &= 80 \text{ m/s} \\G'_m &= 1.109 \times 10^7 \text{ N/m}^2 \text{ (eq. 4-11)} \\E'_m &= 32.1 \times 10^6 \text{ N/m}^2 [= 2(1 + v_m)G'_m] \\v_m &= 0.45 \\K_o &= 0.5 \text{ (coefficient of static lateral earth pressure at rest)} \\\gamma_{s\text{-max}} &= 0.007\end{aligned}$$

4. Rock parameters:

$$\begin{aligned}\gamma_t &= 19.65 \text{ kN/m}^3 \\C'_m &= 800 \text{ m/s} \\G'_m &= 12.8 \times 10^8 \text{ N/m}^2 \\E'_m &= 33.3 \times 10^8 \text{ N/m}^2 [= 2(1 + v_m)G'_m] \\v_m &= 0.3 \\K_o &= 0.3 \text{ (coefficient of static lateral earth pressure at rest)} \\\gamma_{s\text{-max}} &= 0.0005\end{aligned}$$

Note: The elastic properties of the soil and rock under static and dynamic conditions have been assumed to be equal. It was judged that the softening of the soil and rock resulting from construction of the tunnel would be similar to the softening that would occur during earthquake shaking.

Axial and Curvature Deformations Along the Tunnel Longitudinal Axis (section 4.4.1.3)

Concrete tunnel in rock, response due to S-waves:

Peak ground acceleration, a_s , peak ground velocity V_s , and apparent wave propagation velocity, C_s at tunnel level:

$$a_s = 0.85 (0.50 \text{ g}) = 0.425 \text{ g} \quad (\text{Table 4-3})$$

$$V_s = 0.425 \text{ g} (97 \text{ cm/s}) = 41 \text{ cm/s} \quad (\text{Table 4-4})$$

$$C_s = 2 \text{ km/s (default value)}$$

Axial strain and stress induced by axial component of S-wave:

$$\varepsilon = \frac{V_s}{C_s} \sin \phi \cos \phi \quad (\text{Eq. 4-2})$$

$$\varepsilon = \frac{0.41 \text{ m/s}}{2000 \text{ m/s}} \sin 45^\circ \cos 45^\circ = 0.0001$$

$$\sigma = 0.0001 (22 \cdot 10^6) \text{ kPa} = 2.2 \cdot 10^3 \text{ kPa}$$

Axial strain and stress due to bending induced by transverse component of S-wave:

$$\varepsilon = Y \frac{a_s}{C_s^2} \cos^3 \phi$$

$$\varepsilon = (2.745 \text{ m}) \frac{(0.425 \text{ g})(9.81 \text{ m/s}^2)}{(2000 \text{ m/s})^2} \cos^3 45^\circ = 1.01 \times 10^{-6} \quad (\text{Eq. 4-2})$$

(Note: Negligible for $\phi = 45^\circ$ which maximizes strain due to axial component of S-wave.)

$$\sigma = E_s \varepsilon = (22 \cdot 10^6)(1.01 \cdot 10^{-6}) = 22 \text{ kPa (negligible)}$$

Steel tunnel in soil, response due to S-waves:

a_s , V_s , and C_s at tunnel level:

$$a_s = 0.85 (0.50 \text{ g}) = 0.425 \text{ g} \quad (\text{Table 4-3})$$

$$V_s = 0.425 \text{ g} (195 \text{ cm/s}) = 83 \text{ cm/s} \quad (\text{Table 4-4})$$

$$C_s = 2 \text{ km/s (default value for S-waves)}$$

Axial strain and stress due to axial component of S-wave:

$$\varepsilon = \frac{V_s}{C_s} \sin \phi \cos \phi \quad (\text{Eq. 4-2})$$

$$\varepsilon = \frac{0.83 \text{ m/s}}{2000 \text{ m/s}} \sin 45^\circ \cos 45^\circ = 0.00021$$

$$\sigma = 0.00021(20.4 \cdot 10^7) = 42.8 \cdot 10^3 \text{ kPa}$$

Axial strain and stress due to bending induced by transverse component of S-wave: negligible, as above for rock.

Steel tunnel in soil, response due to R-waves:

From a site-specific seismological assessment, it was determined that significant R-waves would be generated farther into the basin. From this assessment, it was determined that:

$$V_R = 30 \text{ cm/s}$$

$$C_R = 0.5 \text{ km/s}$$

Axial strain and stress due to axial component of R-wave:

$$\varepsilon = \frac{V_R}{C_R} \cos^2 \phi \quad (\text{Eq. 4-3})$$

$$\varepsilon = \frac{0.30 \text{ m/s}}{500 \text{ m/s}} \cos^2 0^\circ = 0.0006$$

$$\sigma = 0.0006(20.4 \cdot 10^7) = 122 \cdot 10^3 \text{ kPa}$$

Axial strain and stress due to bending induced by the vertical component of R-wave: The vertical R-wave component is out of phase with the horizontal component and produces negligible axial strain compared to the horizontal component (see eq. 4-5).

Discussion of Axial and Curvature Response Along the Tunnel Longitudinal Axis:

In this example, the calculated axial stresses are much less than the concrete compressive strength and steel yield strength but are approximately equal to the tensile strength of concrete taken as $0.1 f'_c$. Soil-structure interaction (eq. 4-6), neglected in the calculations, would further reduce tunnel response in soil, but ground motion incoherence could increase response (section 4.4.1.3). Strains in the vicinity of the soil-rock contact could be increased by the geologic discontinuity. If increased by a factor of two, as discussed in section 4.4.1.3(a), stresses in the concrete liner would still be well below compressive strength while being about twice the tensile strength. The effects of the formation of circumferential tension cracks in the concrete liner in the vicinity of the soil-rock contact require structural evaluation.

Seismic Retrofit:

The analysis of tunnel longitudinal response (longitudinal axial strains) indicates that axial stresses are well below the compressive strength of the concrete lining or the yield strength of the steel lining. Axial stresses may substantially exceed concrete tensile strength in the vicinity of the soil-rock contact. A structural evaluation is required to assess effects of tensile cracking. If retrofit is judged to be needed in the local region of the soil-rock contact, an appropriate retrofit measure would consist of removal of the unreinforced concrete lining and placement of a reinforced concrete lining. An alternative, if space permits, would be installation of an inner steel liner with grout in the annulus between steel and existing concrete.

In areas where voids were found behind the concrete lining during inspection, grouting is desirable to assure continuous contact between the lining and the soil and rock. Areas where the lining was found to be moderately cracked during inspection could be considered for additional retrofit. If the cracking were indicative of locally excessive pressures against the lining due to geologically weak zones (e.g., a zone of highly sheared rock), strengthening of the liner by removal and replacement of sections of the liner with a reinforced concrete liner or placement of an interior steel liner could be considered.

STEEL TUNNEL IN SOIL: OVALING DEFORMATION OF TUNNEL CROSS SECTION (SECTION 4.4.1.4)

Analyses of stresses in the steel tunnel in soil are conducted in this section using two formulations. The conditions of full-slip and no-slip at the soil-tunnel interface are considered in both formulations. First, the formulation of Schwartz and Einstein (1980) is used for the calculation of static stresses; these static stresses are combined with the dynamic stresses computed using the method of Wang (1993). Second, the formulation of Penzien and Wu (1998) is used to calculate static and dynamic stresses.

The intermediate calculations in these examples contain more significant figures than what is typically used in hand calculations. This was done to minimize the transmission of errors from the intermediate steps to the solutions. Calculations were conducted in the program Mathcad (Mathsoft, 1998).

Equations for static stresses using the formulations of Schwartz and Einstein (1980) and Penzien and Wu (1998) can be found in the respective publications. Reference numbers for these equations are followed by "†" or "††" and do not appear in this manual. Equations for dynamic stresses are presented in this manual.

The sign convention used for static and dynamic forces and moments is shown on figures 4-10 and 4-11. Compressive stresses are taken to be positive. The sign convention used for the calculation of static forces and moments by the formulation of Penzien and Wu (1998) has been changed to be consistent with figures 4-10 and 4-11. Thrusts and moments vary with position in the tunnel liner (i.e., vary with angle θ). The definition of θ is shown on figure 4-10.

Steel Tunnel in Soil - Static Stresses in Soil at Tunnel Mid-depth:

Vertical total stress

$$\sigma_v = \left(Z + \frac{D}{2}\right)\gamma_t = \left(15 + \frac{5.49}{2}\right)(17 \cdot 10^3) = 301 \text{ kPa}$$

Pore water stress

$$u = \left(H_w + \frac{D}{2}\right)\gamma_w = \left(12 + \frac{5.49}{2}\right)(9.81 \cdot 10^3) = 144 \text{ kPa}$$

Vertical effective stress

$$\sigma'_v = \sigma_v - u = 301 - 144 = 157 \text{ kPa}$$

Steel tunnel in Soil - Static Moment, Thrust, and Stress by Method of Schwartz and Einstein (1980) for the Condition of **No-Slip** between the Tunnel and the Soil:

$$C^* = \frac{E'_m r(1 - \nu_l^2)}{E_l A_{l2}(1 - \nu_m^2)} = \frac{(32.1 \cdot 10^6)(2.745)(1 - 0.3^2)}{(2.04 \cdot 10^{11})(0.0314)(1 - 0.45^2)} = 0.015696 \quad (\text{Eq. A-3}^\dagger)$$

$$F^* = \frac{E'_m r^3 (1 - v_m^2)}{E_{I_2} (1 - v_m^2)} = \frac{(32.1 \cdot 10^6)(2.745^3)(1 - 0.3^2)}{(2.04 \cdot 10^{11})(9.63 \cdot 10^{-5})(1 - 0.45^2)} = 38.56438 \quad (\text{Eq. A-6}^\dagger)$$

$$a_0^* = \frac{C^* F^* (1 - v_m)}{C^* + F^* + C^* F^* (1 - v_m)} \quad (\text{Eq. A-36}^\dagger)$$

$$= \frac{(0.015696)(38.56438)(1 - 0.45)}{(0.015696) + (38.56438) + (0.015696)(38.56438)(1 - 0.45)} = 8.555 \cdot 10^{-3}$$

$$\beta = \frac{(6 + F^*)C^* (1 - v_m) + 2F^* v_m}{3F^* + 3C^* + 3C^* F^* (1 - v_m)} \quad (\text{Eq. A-41b}^\dagger)$$

$$= \frac{(6 + 38.56438)(0.015696)(1 - 0.45) + 2(38.56438)(0.45)}{3(38.56438) + 3(0.015696) + 3(0.015696)(38.56438)(1 - 0.45)} = 0.30147$$

$$b_2^* = \frac{C^* (1 - v_m)}{2[C^* (1 - v_m) + 4v_m - 6\beta - 3\beta C^* (1 - v_m)]} \quad (\text{Eq. A-41c}^\dagger)$$

$$= \frac{(0.015696)(1 - 0.45)}{2[(0.015696)(1 - 0.45) + 4(0.45) - 6(0.30147) - 3(0.30147)(0.015696)(1 - 0.45)]}$$

$$b_2^* = -0.541$$

$$a_2^* = b_2^* \beta = (-0.540)(0.30147) = -0.163 \quad (\text{Eq. A-41d}^\dagger)$$

Static thrust:

$$T_s = \frac{r\sigma'_v}{2} [(1 + K_0)(1 - a_0^*) + (1 - K_0)(1 + 2a_2^*) \cos(2\theta)] \quad (\text{Eq. A-48a}^\dagger)$$

$$T_s = \frac{(2.745\text{m})(157\text{kPa})}{2} [(1 + 0.5)(1 - 8.556 \cdot 10^{-3}) + (1 - 0.5)(1 + 2(-0.163)) \cos(2\theta)]$$

$$= 320 + 72.6 \cos(2\theta) \text{ kN/m}$$

Add component of thrust due to hydrostatic water pressure:

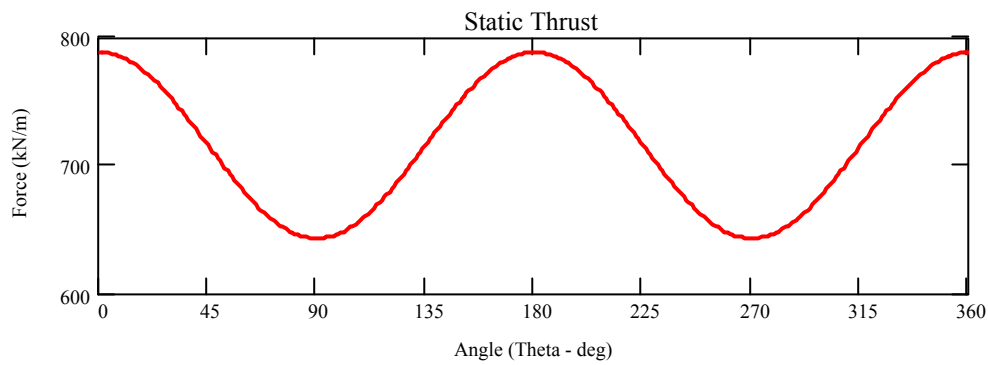
$$T_h = ur = (144\text{kPa})(2.745\text{m}) = 395 \text{ kN/m}$$

$$T_s = (320 + 395) + 72.6 \cos(2\theta) = 715 + 72.6 \cos(2\theta) \text{ kN/m}$$

Maximum and minimum static thrusts:

$$\max(T_s) = 788 \text{ kN/m}$$

$$\min(T_s) = 643 \text{ kN/m}$$



Static moments:

$$M_s = \frac{r^2 \sigma'_v}{4} (1 - K_0) (1 - 2a_2^* + 2b_2^*) \cos(2\theta) \quad (\text{Eq. A-48b}^{\dagger})$$

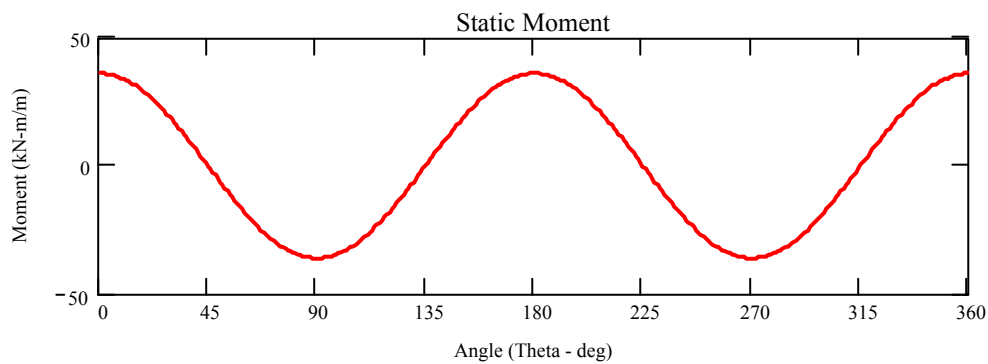
$$M_s = \frac{(2.745^2)(157\text{kPa})}{4} (1 - 0.5) (1 - 2(-0.163) + 2(-0.540)) \cos(2\theta)$$

$$M_s = 36.3 \cos 2\theta$$

Maximum and minimum static moments:

$$\max(M_s) = 36.3 \text{ kN} \cdot \text{m} / \text{m}$$

$$\min(M_s) = -36.3 \text{ kN} \cdot \text{m} / \text{m}$$



Combine stresses from static thrust and moment.

Stress at outer fiber of liner:

$$\sigma_{so} = \frac{T_s}{A_{l2}} - \frac{M_s c_o}{I_{l2}}$$

Stress at inner fiber of liner:

$$\sigma_{si} = \frac{T_s}{A_{l2}} + \frac{M_s c_i}{I_{l2}}$$

Maximum and minimum combined stresses:

$$\max(\sigma_{so}) = 4.00 \cdot 10^4 \text{ kPa}$$

$$\min(\sigma_{so}) = 5.55 \cdot 10^3 \text{ kPa}$$

$$\max(\sigma_{si}) = 7.23 \cdot 10^4 \text{ kPa}$$

$$\min(\sigma_{si}) = -2.67 \cdot 10^4 \text{ kPa}$$

Steel Tunnel in Soil - Dynamic Moment, Thrust, and Stresses by Method of Wang (1993) for the Condition of **No-Slip** between the Tunnel and the Soil:

$$G'_m = \frac{\gamma_t C'_m{}^2}{g} = \frac{(17 \cdot 10^3)(80^2)}{(9.81)} = 1.109 \cdot 10^7 \text{ N/m}^2 \quad (\text{Eq. 4-11})$$

$$F = \frac{G'_m(1-v_i^2)D^3}{24E_t I_{l2}} = \frac{(1.109 \cdot 10^7)(1-0.3^2)(5.49^3)}{24(2.04 \cdot 10^{11})(9.63 \cdot 10^{-5})} = 3.54323 \quad (\text{Eq. 4-17})$$

$$C = \frac{G'_m(1-v_i^2)D}{E_t t(1-2v_m)} = \frac{(1.109 \cdot 10^7)(1-0.3^2)(5.49)}{(2.04 \cdot 10^{11})(0.0314)(1-2(0.45))} = 0.08653 \quad (\text{Eq. 4-27})$$

$$a_0 = F[(3-2v_m) + (1-2v_m)C] + C\left(\frac{5}{2} - 8v_m + 6v_m^2\right) + 6 - 8v_m \quad (\text{Eq. 4-26})$$

$$a_0 = 3.54323[(3-2(0.45)) + (1-2(0.45))(0.08653)] + (0.08653)\left(\frac{5}{2} - 8(0.45) + 6(0.45^2)\right)$$

$$+ 6 - 8(0.45) = 9.881$$

$$a_2 = \left[[F(1-2v_m)(1-C)] - \frac{1}{2}C(1-2v_m)^2 + 2 \right] \frac{1}{a_0} \quad (\text{Eq. 4-24})$$

$$a_2 = \left[[(3.54323)(1-2(0.45))(1-(0.08653))] - \frac{1}{2}(0.08653)(1-2(0.45))^2 + 2 \right] \frac{1}{(9.881)}$$

$$= 0.235$$

$$a_3 = \left[F[C(1-2v_m) + 1] - \frac{1}{2}C(1-2v_m) - 2 \right] \frac{1}{a_0} \quad (\text{Eq. 4-25})$$

$$a_3 = \left[(3.54323)[(0.08653)(1-2(0.45)) + 1] - \frac{1}{2}(0.08653)(1-2(0.45)) - 2 \right] \frac{1}{(9.881)} = 0.159$$

Dynamic thrust:

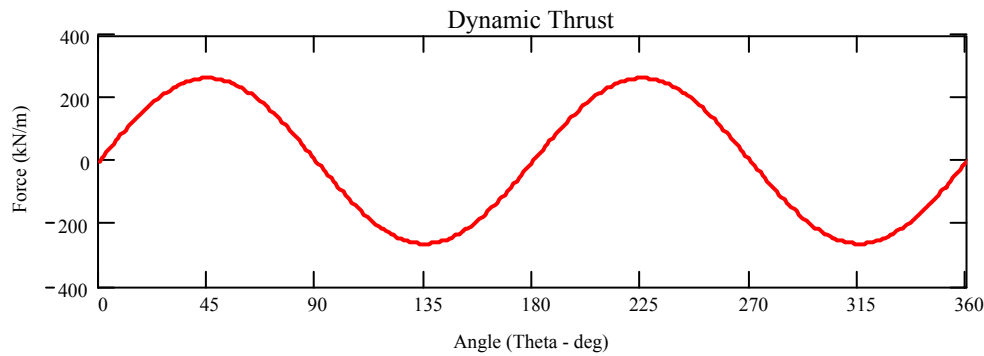
$$T_d = \frac{1}{2} G'_m D (1 + a_2) \gamma_{smax} \sin(2\theta) \quad (\text{Eq. 4-22})$$

$$= \frac{1}{2} (1.109 \cdot 10^7) (5.49) (1 + 0.235) (0.007) \sin(2\theta) = 263 \sin(2\theta) \text{ kN/m}$$

Maximum and minimum dynamic thrusts:

$$\max(T_d) = 263 \text{ kN/m}$$

$$\min(T_d) = -263 \text{ kN/m}$$



Dynamic moment:

$$M_d = \frac{1}{8} G'_m D^2 (1 - a_2 - 2a_3) \gamma_{smax} \sin(2\theta) \quad (\text{Eq. 4-23})$$

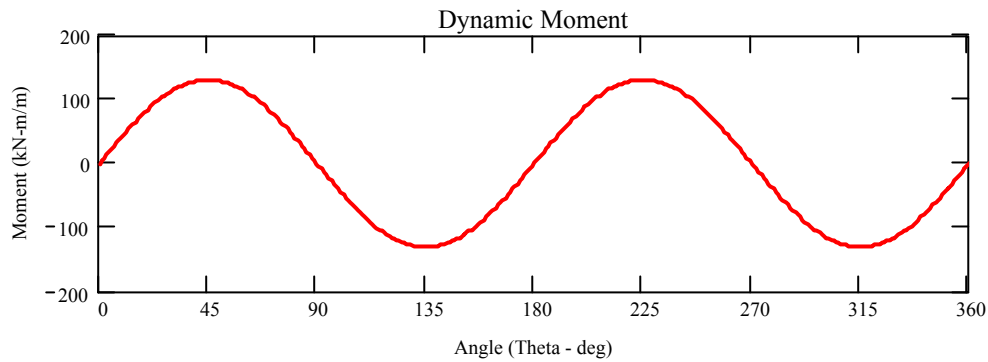
$$M_d = \frac{1}{8} (1.109 \cdot 10^7) (5.49^2) (1 - (0.235) - 2(0.159)) (0.007) \sin(2\theta)$$

$$M_d = 131 \sin(2\theta) \text{ kN} \cdot \text{m/m}$$

Maximum and minimum dynamic moments:

$$\max(M_d) = 131 \text{ kN} \cdot \text{m/m}$$

$$\min(M_d) = -131 \text{ kN} \cdot \text{m/m}$$



Combine stresses from dynamic thrust and moment.

Dynamic stress at outer fiber of liner:

$$\sigma_{do} = \frac{T_d}{A_{l2}} - \frac{M_d c_o}{I_{l2}}$$

Dynamic stress at inner fiber of liner:

$$\sigma_{di} = \frac{T_d}{A_{l2}} + \frac{M_d c_i}{I_{l2}}$$

Maximum and minimum combined dynamic stresses:

$$\max(\sigma_{do}) = 6.240 \cdot 10^4 \text{ kPa}$$

$$\min(\sigma_{do}) = -6.240 \cdot 10^4 \text{ kPa}$$

$$\max(\sigma_{di}) = 1.794 \cdot 10^5 \text{ kPa}$$

$$\min(\sigma_{di}) = -1.794 \cdot 10^5 \text{ kPa}$$

Steel Tunnel in Soil - Combined Static and Dynamic Stresses by Method of Schwartz and Einstein (1980) and Wang (1993) for the Condition of **No-Slip** Between the Tunnel and the Soil:

Stress at outer fiber of liner:

$$\sigma_o = \sigma_{so} + \sigma_{do}$$

Stress at inner fiber of liner:

$$\sigma_i = \sigma_{si} + \sigma_{di}$$

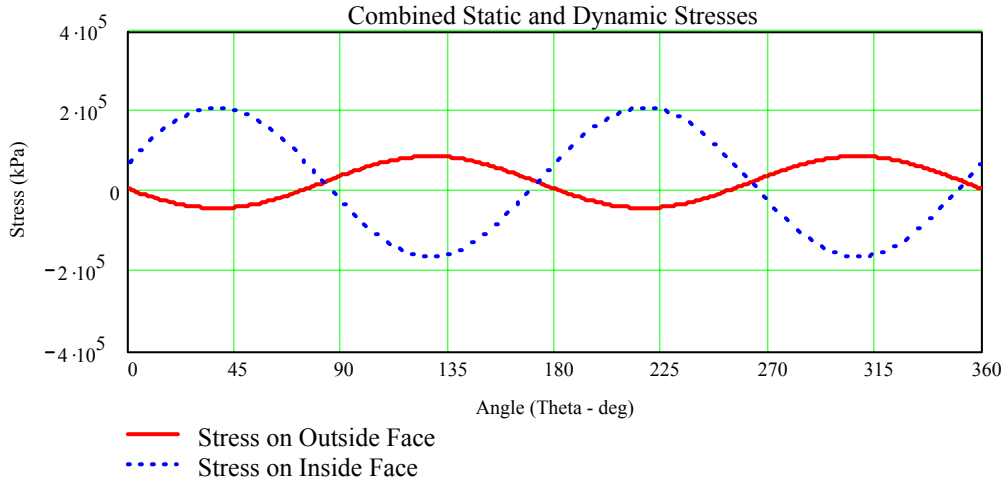
Maximum and minimum combined stresses:

$$\max(\sigma_o) = 8.75 \cdot 10^4 \text{ kPa}$$

$$\min(\sigma_o) = -4.19 \cdot 10^4 \text{ kPa}$$

$$\max(\sigma_i) = 2.09 \cdot 10^5 \text{ kPa}$$

$$\min(\sigma_i) = -1.63 \cdot 10^5 \text{ kPa}$$



Maximum tensile and compressive stresses occur on the inside face of the liner. The maximum tensile and compressive stresses are 64 and 84 percent, respectively, of the yield stress.

Steel Tunnel in Soil - Static Moment, Thrust, and Stresses by Method of Schwartz and Einstein (1980) for the Condition of **Full-Slip** between the Tunnel and the Soil:

$$C^* = \frac{E'_m r (1 - \nu_l^2)}{E_l A_{l2} (1 - \nu_m^2)} = \frac{(32.1 \cdot 10^6)(2.745)(1 - 0.3^2)}{(2.04 \cdot 10^{11})(0.0314)(1 - 0.45^2)} = 0.015696 \quad (\text{Eq. A-3}^\dagger)$$

$$F^* = \frac{E'_m r^3 (1 - \nu_l^2)}{E_l I_{l2} (1 - \nu_m^2)} = \frac{(32.1 \cdot 10^6)(2.745^3)(1 - 0.3^2)}{(2.04 \cdot 10^{11})(9.63 \cdot 10^{-5})(1 - 0.45^2)} = 38.56438 \quad (\text{Eq. A-6}^\dagger)$$

$$a_0^* = \frac{C^* F^* (1 - \nu_m)}{C^* + F^* + C^* F^* (1 - \nu_m)} \quad (\text{Eq. A-32a}^\dagger)$$

$$= \frac{(0.015696)(38.56438)(1 - 0.45)}{(0.015696) + (38.56438) + (0.015696)(38.56438)(1 - 0.45)} = 8.555 \cdot 10^{-3}$$

$$a_2^* = \frac{(6 + F^*)(1 - \nu_m)}{2F^* (1 - \nu_m) + 6(5 - 6\nu_m)} = \frac{(6 + 38.56438)(1 - 0.45)}{2(38.56438)(1 - 0.45) + 6(5 - 6(0.45))} = 0.436 \quad (\text{Eq. A-32b}^\dagger)$$

Static thrust:

$$T_s = \frac{r\sigma'_v}{2} [(1+K_0)(1-a_0) + (1-K_0)(1-2a_2) \cos(2\theta)] \quad (\text{Eq. A-47a}^\dagger)$$

$$T_s = \frac{(2.745\text{m})(157\text{kPa})}{2} [(1+0.5)(1-8.556 \cdot 10^{-3}) + (1-0.5)(1-2(0.436)) \cos(2\theta)]$$

$$= 320 + 13.7 \cos(2\theta) \text{ kN/m}$$

Add component of thrust due to hydrostatic water pressure:

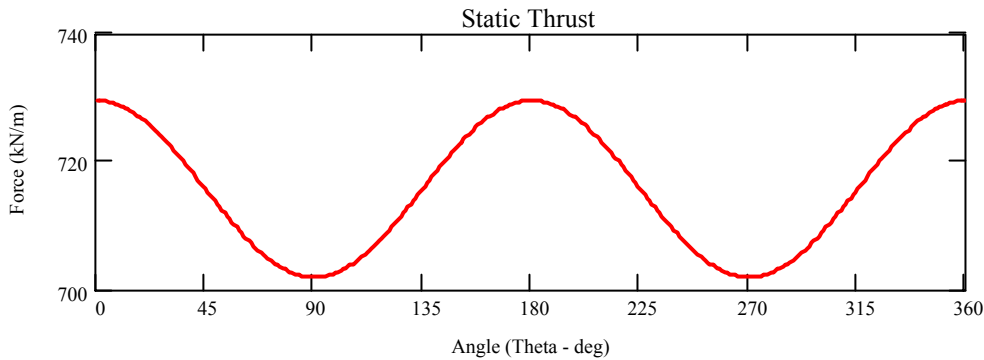
$$T_h = ur = (144\text{kPa})(2.745\text{m}) = 395 \text{ kN/m}$$

$$T_s = (320 + 395) + 13.7 \cos(2\theta) = 715 + 13.7 \cos(2\theta) \text{ kN/m}$$

Maximum and minimum static thrusts:

$$\max(T_s) = 729 \text{ kN/m}$$

$$\min(T_s) = 701 \text{ kN/m}$$



Static moment:

$$M_s = \frac{r^2\sigma'_v}{2} (1-K_0)(1-2a_2) \cos(2\theta) \quad (\text{Eq. A-47b}^\dagger)$$

$$M_s = \frac{(2.745^2)(157\text{kPa})}{2} (1-0.5)(1-2(0.436)) \cos(2\theta)$$

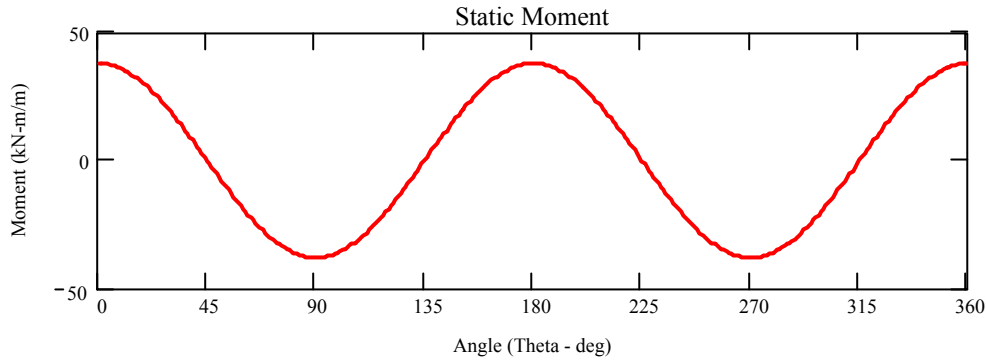
$$M_s = 37.8 \cos 2\theta \text{ kN} \cdot \text{m/m}$$

Maximum and minimum static moments:

$$\max(M_s) = 37.8 \text{ kN} \cdot \text{m} / \text{m}$$

$$\min(M_s) = -37.8 \text{ kN} \cdot \text{m} / \text{m}$$

Combine stresses from static thrust and moment.



Stress at outer fiber of liner:

$$\sigma_{so} = \frac{T_s}{A_{l2}} - \frac{M_s c_o}{I_{l2}}$$

Stress at inner fiber of liner:

$$\sigma_{si} = \frac{T_s}{A_{l2}} + \frac{M_s c_i}{I_{l2}}$$

Maximum and minimum combined stresses:

$$\max(\sigma_{so}) = 4.28 \cdot 10^4 \text{ kPa}$$

$$\min(\sigma_{so}) = 2.74 \cdot 10^3 \text{ kPa}$$

$$\max(\sigma_{si}) = 7.27 \cdot 10^4 \text{ kPa}$$

$$\min(\sigma_{si}) = -2.71 \cdot 10^4 \text{ kPa}$$

Steel Tunnel in Soil - Dynamic Moment, Thrust, and Stresses by Method of Wang (1993) for the Condition of **Full-Slip** between the Tunnel and Soil:

$$G'_m = \frac{\gamma_t C'_m{}^2}{g} = \frac{(17 \cdot 10^3)(80^2)}{(9.81)} = 1.109 \cdot 10^7 \text{ N/m}^2 \quad (\text{Eq. 4-11})$$

$$F = \frac{G'_m (1 - \nu_l^2) D^3}{24 E_{l2}} = \frac{(1.109 \cdot 10^7)(1 - 0.3^2)(5.49^3)}{24(2.04 \cdot 10^{11})(9.63 \cdot 10^{-5})} = 3.54323 \quad (\text{Eq. 4-17})$$

$$K = \frac{1 - v_m}{F + 2.5 - 3v_m} = \frac{1 - 0.45}{3.54323 + 2.5 - 3(0.45)} = 0.11719 \quad (\text{Eq. 4-16})$$

Dynamic thrust:

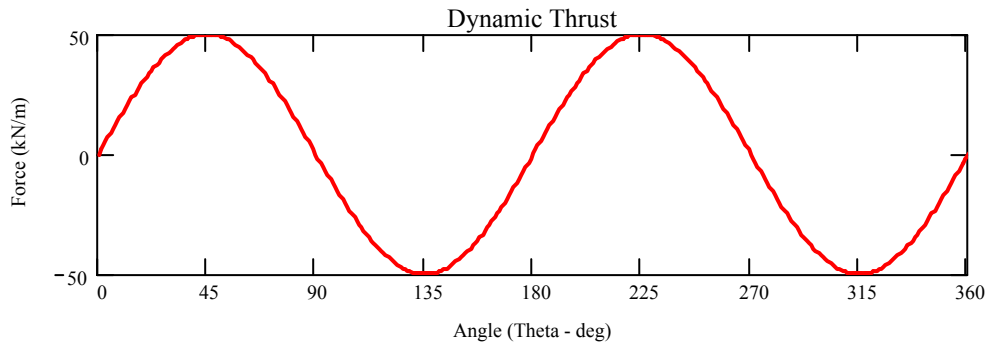
$$T_d = G'_m D K \gamma_{smax} \sin(2\theta) \quad (\text{Eq. 4-13})$$

$$= (1.109 \cdot 10^7)(5.49)(0.11719)(0.007) \sin(2\theta) = 49.9 \sin(2\theta) \text{ kN/m}$$

Maximum and minimum dynamic thrusts:

$$\max(T_d) = 49.9 \text{ kN/m}$$

$$\min(T_d) = -49.9 \text{ kN/m}$$



Dynamic moments:

$$M_d = \frac{1}{2} G'_m D^2 K \gamma_{smax} \sin(2\theta) \quad (\text{Eq. 4-15})$$

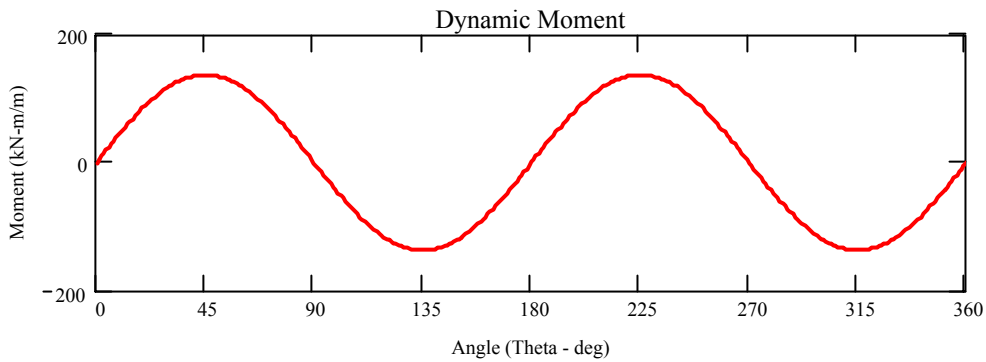
$$M_d = \frac{1}{2} (1.109 \cdot 10^7)(5.49^2)(0.11719)(0.007) \sin(2\theta)$$

$$M_d = 137 \sin(2\theta) \text{ kN} \cdot \text{m/m}$$

Maximum and minimum dynamic moments:

$$\max(M_d) = 137 \text{ kN} \cdot \text{m/m}$$

$$\min(M_d) = -137 \text{ kN} \cdot \text{m/m}$$



Combine stresses from dynamic thrust and moment.

Dynamic stress at outer fiber of liner:

$$\sigma_{do} = \frac{T_d}{A_{I2}} - \frac{M_d c_o}{I_{I2}}$$

Dynamic stress at inner fiber of liner:

$$\sigma_{di} = \frac{T_d}{A_{I2}} + \frac{M_d c_i}{I_{I2}}$$

Maximum and minimum combined dynamic stresses:

$$\max(\sigma_{do}) = 7.26 \cdot 10^4 \text{ kPa}$$

$$\min(\sigma_{do}) = -7.26 \cdot 10^4 \text{ kPa}$$

$$\max(\sigma_{di}) = 1.80 \cdot 10^5 \text{ kPa}$$

$$\min(\sigma_{di}) = -1.80 \cdot 10^5 \text{ kPa}$$

Steel Tunnel in Soil – Combined Static and Dynamic Stresses by Method of Schwartz and Einstein (1980) and Wang (1993) for the Condition of **Full-Slip** between the Tunnel and Soil:

Stress at outer fiber of liner:

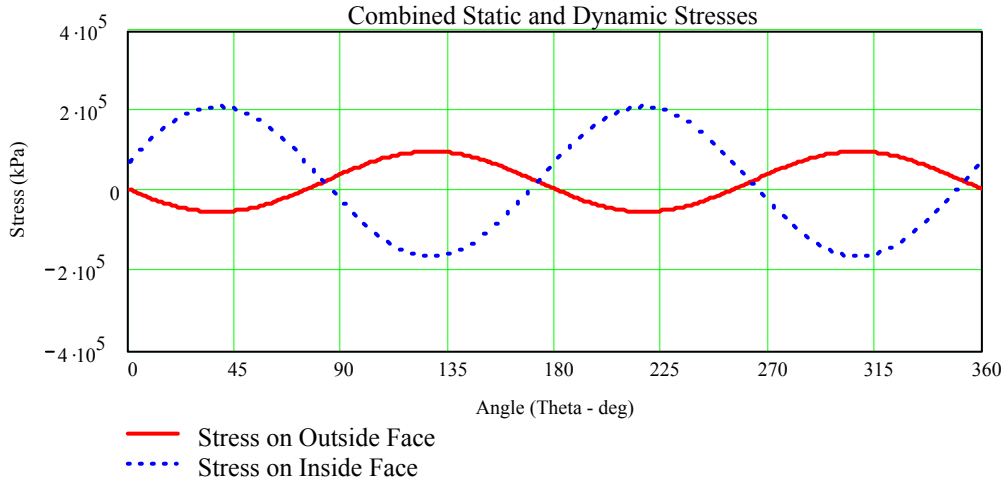
$$\sigma_o = \sigma_{so} + \sigma_{do}$$

Stress at inner fiber of liner:

$$\sigma_i = \sigma_{si} + \sigma_{di}$$

Maximum and minimum combined stresses:

$$\begin{aligned}\max(\sigma_o) &= 9.81 \cdot 10^4 \text{ kPa} \\ \min(\sigma_o) &= -5.25 \cdot 10^4 \text{ kPa} \\ \max(\sigma_i) &= 2.10 \cdot 10^5 \text{ kPa} \\ \min(\sigma_i) &= -1.64 \cdot 10^5 \text{ kPa}\end{aligned}$$



Maximum tensile and compressive stresses are very similar to those previously presented for the no-slip case.

Steel Tunnel in Soil - Static Moment, Thrust, and Stresses by Method of Penzien and Wu (1998) for the Condition of **No-Slip** between the Tunnel and Soil:

$$\alpha_d = \frac{E_i A_{i2} (1 + \nu_m)}{E'_m r (1 - \nu_i^2)} = \frac{(20.4 \cdot 10^{10})(0.0314)(1 + 0.45)}{(32.1 \cdot 10^6)(2.745)(1 - 0.3^2)} = 115.835 \quad (\text{Eq. 47}^{tt})$$

$$\begin{aligned}\Delta_{dl} &= \frac{\sigma'_r(1 + K_o)(1 + \nu_m)}{E'_m(1 + \alpha_d)} + \frac{2ur^2(1 - \nu_i^2)\alpha_d}{E_i A_{i2}(1 + \alpha_d)} = \frac{(157 \cdot 10^3)(2.745)(1 + 0.5)(1 + 0.45)}{32.1 \cdot 10^6 (1 + 115.835)} \\ &+ \frac{2(144 \cdot 10^3)(2.745^2)(1 - 0.3^2)(115.835)}{(20.4 \cdot 10^{10})(0.0314)(1 + 115.835)} = 5.57 \cdot 10^{-4} \text{ m}\end{aligned} \quad (\text{Eq. 49}^{tt})$$

$$P_d = \frac{E_i A_{i2} \Delta_{dl}}{2r (1 - \nu_i^2)} = \frac{(20.4 \cdot 10^{10})(0.0314)(5.57 \cdot 10^{-4})}{2(2.745)(1 - 0.3^2)} = 7.142 \cdot 10^5 \text{ N/m} \quad (\text{Eq. 58}^{tt})$$

$$\begin{aligned}\alpha_s &= \frac{6E_i I_{i2}(1 + \nu_m)(3 - 4\nu_m)}{r^3 E'_m (1 - \nu_i^2)} = \frac{6(20.4 \cdot 10^{10})(9.63 \cdot 10^{-5})(1 + 0.45)(3 - 4(0.45))}{(2.745^3)(32.1 \cdot 10^6)(1 - 0.3^2)} \\ &= 0.339\end{aligned} \quad (\text{Eq. 51}^{tt})$$

$$\Delta_{sl} = \frac{\sigma'_v r(1-K_o)(1+v_m)(3-4v_m)}{E'_m(1+\alpha_s)} = \frac{(157 \cdot 10^3)(2.745)(1-0.5)(1+0.45)(3-4(0.45))}{32.1 \cdot 10^6(1+0.339)}$$

$$= 8.271 \cdot 10^{-3} \text{ m} \quad (\text{Eq. 50}^{\dagger\dagger})$$

$$P_s = \frac{3E_{I_2}\Delta_{sl}}{r^3(1-v_1^2)} \cos 2\theta = \frac{3(20.4 \cdot 10^{10})(9.63 \cdot 10^{-5})(8.271 \cdot 10^{-3})}{(2.745^3)(1-0.3^2)} \cos 2\theta$$

$$= 2.731 \cdot 10^4 \cos 2\theta \text{ N/m} \quad (\text{Eq. 59}^{\dagger\dagger})$$

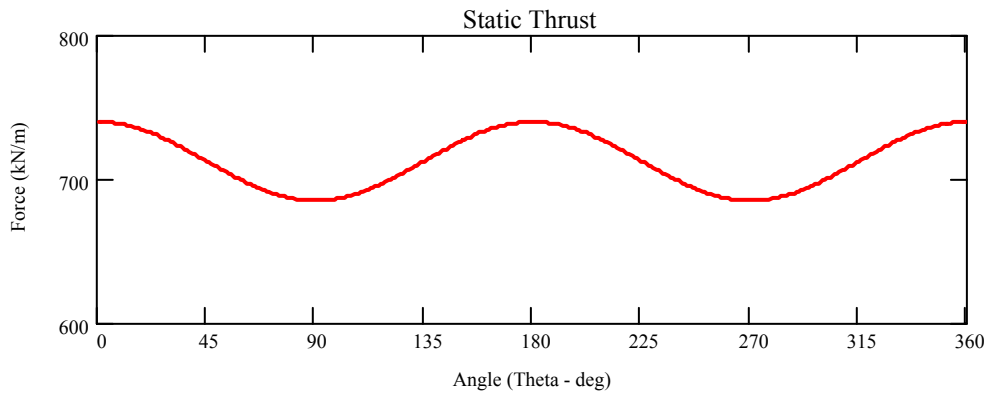
Static thrust:

$$T_s = P_s + P_d = 2.731 \cdot 10^4 \cos 2\theta + 7.142 \cdot 10^5 \text{ N/m}$$

Maximum and minimum static thrusts:

$$\max(T_s) = 741 \text{ kN/m}$$

$$\min(T_s) = 686 \text{ kN/m}$$



Static moment:

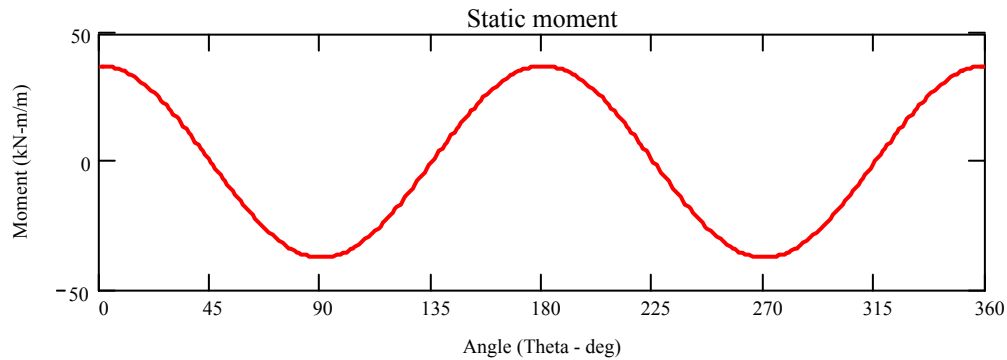
$$M_s = \frac{3E_{I_2}\Delta_{sl}}{2r^2(1-v_1^2)} \cos 2\theta = \frac{3(20.4 \cdot 10^{10})(9.63 \cdot 10^{-5})(8.271 \cdot 10^{-3})}{2(2.745^2)(1-0.3^2)} \cos 2\theta$$

$$= 3.748 \cdot 10^4 \cos 2\theta \text{ N} \cdot \text{m/m} \quad (\text{Eq. 59}^{\dagger\dagger})$$

Maximum and minimum static moment:

$$\max(M_s) = 37.4 \text{ kN} \cdot \text{m/m}$$

$$\min(M_s) = -37.4 \text{ kN} \cdot \text{m/m}$$



Combine stresses from static thrust and moment.

Stress at outer fiber:

$$\sigma_{so} = \frac{T_s}{A_{I2}} - \frac{M_s c_o}{I_{I2}}$$

Stress at inner fiber:

$$\sigma_{si} = \frac{T_s}{A_{I2}} + \frac{M_s c_i}{I_{I2}}$$

Maximum and minimum combined stresses:

$$\max(\sigma_{so}) = 4.215 \cdot 10^4 \text{ kPa}$$

$$\min(\sigma_{so}) = 3.336 \cdot 10^4 \text{ kPa}$$

$$\max(\sigma_{si}) = 7.261 \cdot 10^4 \text{ kPa}$$

$$\min(\sigma_{si}) = -2.713 \cdot 10^4 \text{ kPa}$$

Steel Tunnel in Soil – Dynamic Moment, Thrust, and Stresses by Method of Penzien and Wu (1998) for the Condition of **No-Slip** between the Tunnel and Soil:

$$G'_m = \frac{\gamma_t}{g} C_m^2 = \frac{17 \cdot 10^3}{9.81} 80^2 = 1.109 \cdot 10^7 \text{ N/m}^2 \quad (\text{Eq. 4-11})$$

$$F = \frac{G'_m (1 - \nu_t^2) D^3}{24 E_{I2}} = \frac{1.109 \cdot 10^7 (1 - 0.3^2) (5.49^3)}{24 (20.4 \cdot 10^{10}) (9.63 \cdot 10^{-5})} = 3.54323 \quad (\text{Eq. 4-17})$$

$$K' = \frac{1 - \nu_m}{F + 3 - 4\nu_m} = \frac{1 - 0.45}{3.54323 + 3 - 4(0.45)} = 0.11595 \quad (\text{Eq. 4-21})$$

Dynamic thrust:

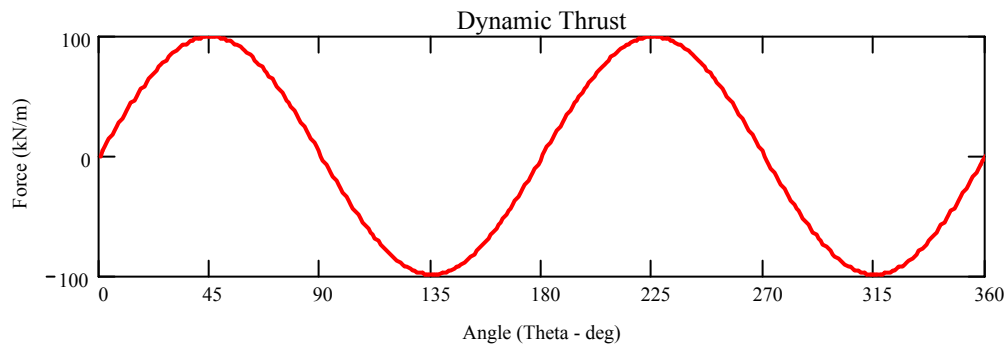
$$T_d = 2G'_m DK' \gamma_{s-\max} \sin 2\theta = 2(1.109 \cdot 10^7)(5.49)(0.11595)(0.007) \sin 2\theta$$

$$= 9.887 \cdot 10^4 \sin 2\theta \text{ N/m} \quad (\text{Eq.4-18})$$

Maximum and minimum dynamic thrusts:

$$\max(T_d) = 98.88 \text{ kN/m}$$

$$\min(T_d) = -98.88 \text{ kN/m}$$



Dynamic moment:

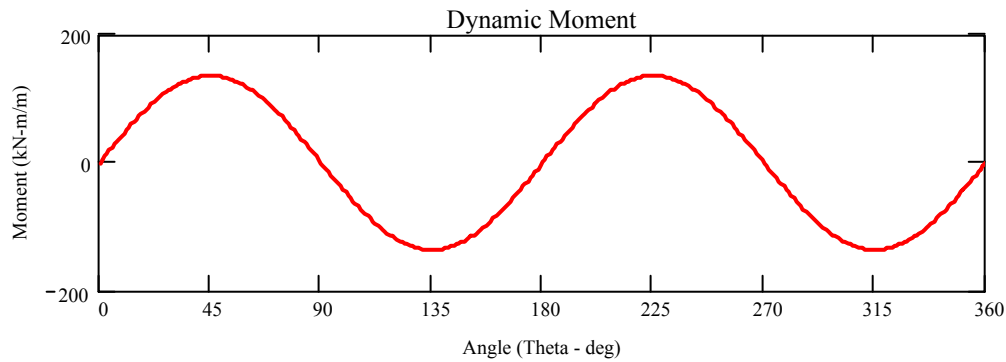
$$M_d = \frac{1}{2} G'_m D^2 K' \gamma_{s-\max} \sin 2\theta = \frac{1}{2} (1.109 \cdot 10^7) (5.49^2) (0.11595) (0.007) \sin 2\theta$$

$$= 1.356 \cdot 10^5 \sin 2\theta \text{ N} \cdot \text{m/m} \quad (\text{Eq. 4-20})$$

Maximum and minimum dynamic moments:

$$\max(M_d) = 136 \text{ kN} \cdot \text{m/m}$$

$$\min(M_d) = -136 \text{ kN} \cdot \text{m/m}$$



Combine stresses from dynamic thrust and moment.

Dynamic stress at outer fiber of liner:

$$\sigma_{do} = \frac{T_d}{A_{l2}} - \frac{M_d c_o}{I_{l2}}$$

Dynamic stress at inner fiber of liner:

$$\sigma_{di} = \frac{T_s}{A_{l2}} + \frac{M_s c_i}{I_{l2}}$$

Maximum and minimum dynamic stresses:

$$\max(\sigma_{do}) = 7.02 \cdot 10^4 \text{ kPa}$$

$$\min(\sigma_{do}) = -7.02 \cdot 10^4 \text{ kPa}$$

$$\max(\sigma_{di}) = 1.80 \cdot 10^5 \text{ kPa}$$

$$\min(\sigma_{di}) = -1.80 \cdot 10^5 \text{ kPa}$$

Steel Tunnel in Soil – Combined Static and Dynamic Stresses by Method of Penzien and Wu (1998) for the condition of **No-Slip** between the Tunnel and Soil

Stress at outer fiber:

$$\sigma_o = \sigma_{so} + \sigma_{do}$$

Stress at inner fiber

$$\sigma_i = \sigma_{si} + \sigma_{di}$$

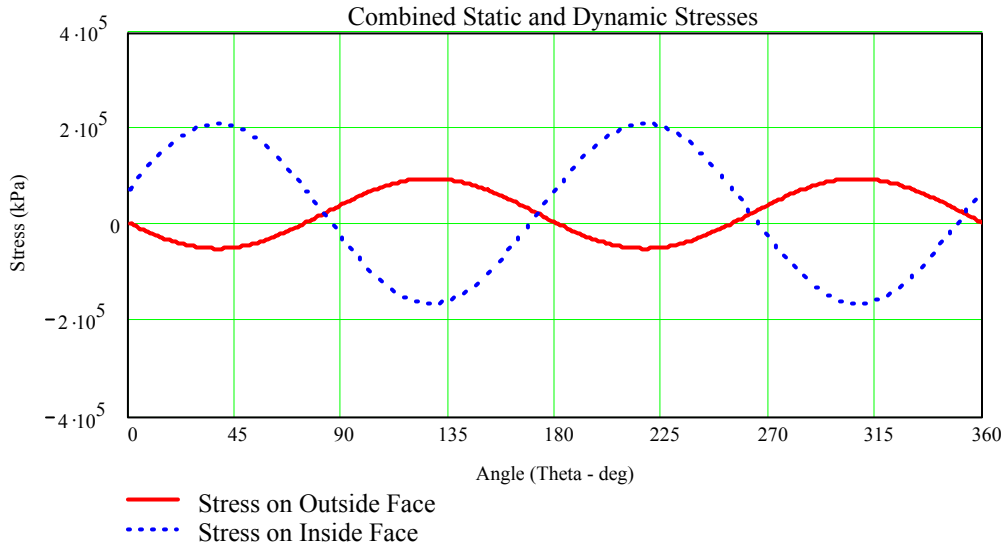
Maximum and minimum combined stresses

$$\max(\sigma_o) = 9.564 \cdot 10^4 \text{ kPa}$$

$$\min(\sigma_o) = -5.016 \cdot 10^4 \text{ kPa}$$

$$\max(\sigma_i) = 2.101 \cdot 10^5 \text{ kPa}$$

$$\min(\sigma_i) = -1.646 \cdot 10^5 \text{ kPa}$$



Maximum tensile and compressive stresses are very similar to those previously presented for the methods of Schwartz and Einstein (1980), and Wang (1993) for no-slip and full-slip cases.

Steel Tunnel in Soil - Static Moment, Thrust, and Stresses by Method of Penzien and Wu (1998) for the Condition of **Full-Slip** between the Tunnel and Soil:

$$\alpha_d = \frac{E_I A_{I2} (1 + \nu_m)}{E'_m r (1 - \nu_l^2)} = \frac{(20.4 \cdot 10^{10})(0.0314)(1 + 0.45)}{(32.1 \cdot 10^6)(2.745)(1 - 0.3^2)} = 115.835 \quad (\text{Eq. 47}^{\dagger\dagger})$$

$$\Delta_{dl} = \frac{\sigma'_v r (1 + K_o)(1 + \nu_m)}{E'_m (1 + \alpha_d)} + \frac{2ur^2(1 - \nu_l^2)}{E_I A_{I2} (1 + \alpha_d)} = \frac{(157 \cdot 10^3)(2.745)(1 + 0.5)(1 + 0.45)}{32.1 \cdot 10^6 (1 + 115.835)} + \frac{2(144 \cdot 10^3)(2.745^2)(1 - 0.3^2)(115.835)}{(20.4 \cdot 10^{10})(0.0314)(1 + 115.835)} = 5.57 \cdot 10^{-4} \text{ m} \quad (\text{Eq. 49}^{\dagger\dagger})$$

$$P_d = \frac{E_I A_{I2} \Delta_{dl}}{2r(1 - \nu_l^2)} = \frac{(20.4 \cdot 10^{10})(0.0314)(5.57 \cdot 10^{-4})}{2(2.745)(1 - 0.3^2)} = 7.142 \cdot 10^5 \text{ N/m} \quad (\text{Eq. 58}^{\dagger\dagger})$$

$$\alpha_s = \frac{3E_{I_2}(1+\nu_m)(5-6\nu_m)}{r^3E'_m(1-\nu_1^2)} = \frac{3(20.4 \cdot 10^{10})(9.63 \cdot 10^{-5})(1+0.45)(5-6(0.45))}{(2.745^3)(32.1 \cdot 10^6)(1-0.3^2)} = 0.325 \quad (\text{Eq. 51}^{\dagger\dagger})$$

$$\Delta_{sl} = \frac{\sigma'_v r(1-K_o)(1+\nu_m)(3-4\nu_m)}{E'_m(1+\alpha_s)} = \frac{(157 \cdot 10^3)(2.745)(1-0.5)(1+0.45)(3-4(0.45))}{32.1 \cdot 10^6(1+0.325)} = 8.814 \cdot 10^{-3} \text{ m} \quad (\text{Eq. 50}^{\dagger\dagger})$$

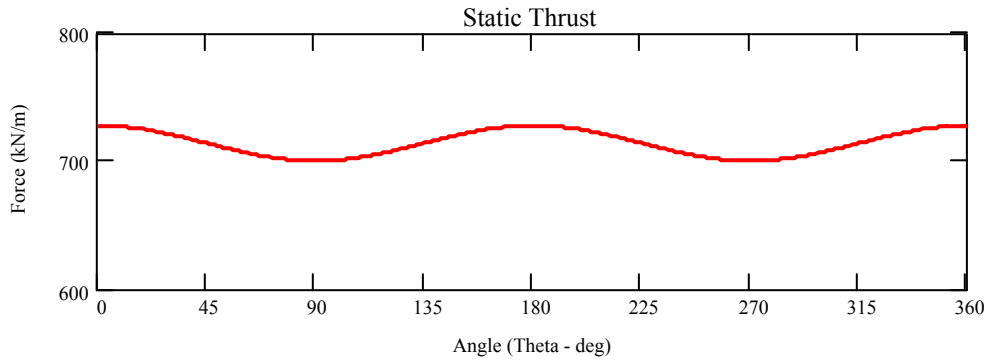
$$P_s = \frac{3E_{I_2}\Delta_{sl}}{2r^3(1-\nu_1^2)} \cos 2\theta = \frac{3(20.4 \cdot 10^{10})(9.63 \cdot 10^{-5})(8.814 \cdot 10^{-3})}{2(2.745^3)(1-0.3^2)} \cos 2\theta = 1.380 \cdot 10^4 \cos 2\theta \text{ N/m} \quad (\text{Eq. 59}^{\dagger\dagger})$$

Static thrust:

$$T_s = P_s + P_d = 1.380 \cdot 10^4 \cos 2\theta + 7.142 \cdot 10^5 \text{ N/m}$$

Maximum and minimum static thrusts:

$$\begin{aligned} \max(T_s) &= 728 \text{ kN/m} \\ \min(T_s) &= 700 \text{ kN/m} \end{aligned}$$



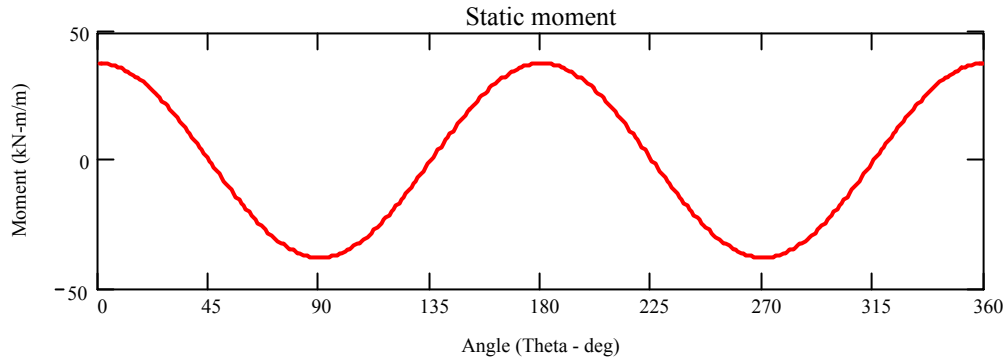
Static moment:

$$M_s = \frac{3E_{I_2}\Delta_{sl}}{2R^2(1-\nu_1^2)} \cos 2\theta = \frac{3(2.04 \cdot 10^{11})(9.63 \cdot 10^{-5})(8.814 \cdot 10^{-3})}{2(2.745^2)(1-0.3^2)} \cos 2\theta = 3.788 \cdot 10^4 \cos 2\theta \text{ N} \cdot \text{m/m} \quad (\text{Eq. 59}^{\dagger\dagger})$$

Maximum and minimum static moment:

$$\max(M_s) = 37.8 \text{ kN} \cdot \text{m}/\text{m}$$

$$\min(M_s) = -37.8 \text{ kN} \cdot \text{m}/\text{m}$$



Combine stresses from static thrusts and moment.

Stress at outer fiber:

$$\sigma_{so} = \frac{T_s}{A_{I_2}} - \frac{M_s c_o}{I_{I_2}}$$

Stress at inner fiber:

$$\sigma_{si} = \frac{T_s}{A_{I_2}} + \frac{M_s c_i}{I_{I_2}}$$

Maximum and minimum combined stresses:

$$\max(\sigma_{so}) = 4.280 \cdot 10^4 \text{ kPa}$$

$$\min(\sigma_{so}) = 2.690 \cdot 10^4 \text{ kPa}$$

$$\max(\sigma_{si}) = 7.271 \cdot 10^4 \text{ kPa}$$

$$\min(\sigma_{si}) = -2.722 \cdot 10^4 \text{ kPa}$$

Steel Tunnel in Soil – Dynamic Moment, Thrust, and Stresses by Method of Penzien and Wu (1998) for the Condition of **Full-Slip** between Tunnel and Soil:

$$G'_m = \frac{\gamma_t}{g} C'_m{}^2 = \frac{17 \cdot 10^3}{9.81} 80^2 = 1.109 \cdot 10^7 \text{ N/m}^2 \quad (\text{Eq. 4-11})$$

$$F = \frac{G'_m (1 - \nu_t^2) D^3}{24 E_{I_2}} = \frac{1.109 \cdot 10^7 (1 - 0.3^2) (5.49^3)}{24 (20.4 \cdot 10^{10}) (9.63 \cdot 10^{-5})} = 3.54323 \quad (\text{Eq. 4-17})$$

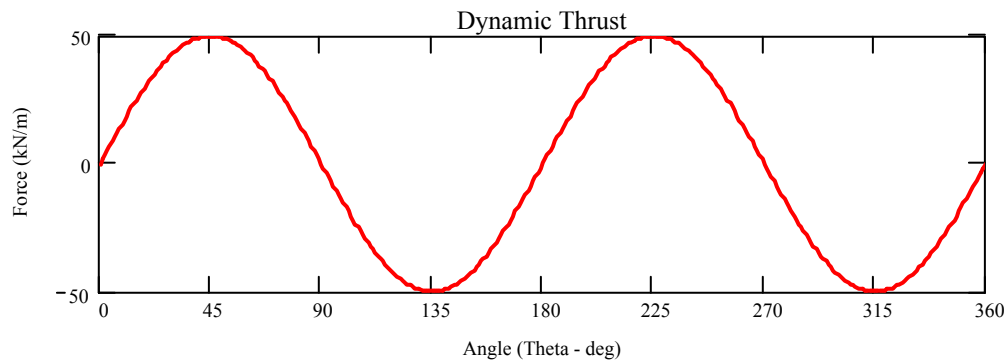
$$K = \frac{1 - v_m}{F + 2.5 - 3v_m} = \frac{1 - 0.45}{3.54323 + 2.5 - 3(0.45)} = 0.11719 \quad (\text{Eq. 4-16})$$

Dynamic thrust:

$$\begin{aligned} T_d &= G'_m D K \gamma_{s-\max} \sin 2\theta = (1.109 \cdot 10^7)(5.49)(0.11719)(0.007) \sin 2\theta \\ &= 4.997 \cdot 10^4 \sin 2\theta \text{ N/m} \end{aligned} \quad (\text{Eq. 4-13})$$

Maximum and minimum dynamic thrusts:

$$\begin{aligned} \max(T_d) &= 49.9 \text{ kN/m} \\ \min(T_d) &= -49.9 \text{ kN/m} \end{aligned}$$

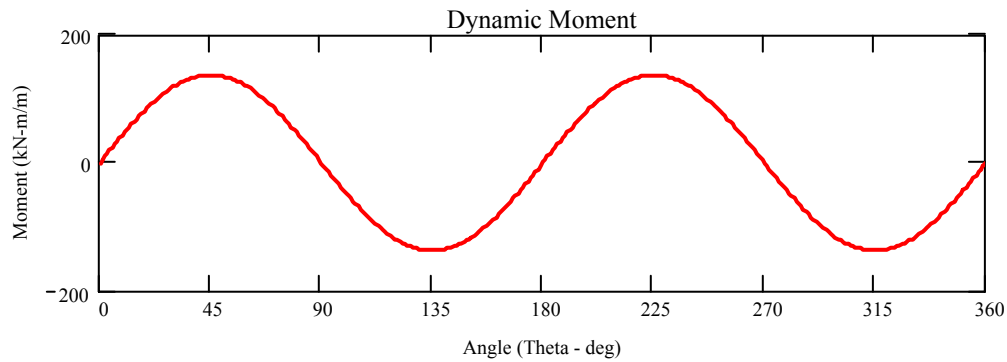


Dynamic moment:

$$\begin{aligned} M_d &= \frac{1}{2} G'_m D^2 K \gamma_{s-\max} \sin 2\theta = \frac{1}{2} (1.109 \cdot 10^7)(5.49^2)(0.11719)(0.007) \sin 2\theta \\ &= 1.372 \cdot 10^5 \sin 2\theta \text{ N} \cdot \text{m/m} \end{aligned} \quad (\text{Eq. 4-15})$$

Maximum and minimum dynamic moments:

$$\begin{aligned} \max(M_d) &= 137.2 \text{ kN} \cdot \text{m/m} \\ \min(M_d) &= -137.2 \text{ kN} \cdot \text{m/m} \end{aligned}$$



Dynamic stress at outer fiber of liner:

$$\sigma_{do} = \frac{T_d}{A_{l2}} - \frac{M_d c_o}{I_{l2}}$$

Dynamic stress at inner fiber of liner:

$$\sigma_{di} = \frac{T_d}{A_{l2}} + \frac{M_d c_i}{I_{l2}}$$

Maximum and minimum dynamic stresses:

$$\max(\sigma_{do}) = 7.261 \cdot 10^4 \text{ kPa}$$

$$\min(\sigma_{do}) = -7.261 \cdot 10^4 \text{ kPa}$$

$$\max(\sigma_{di}) = 1.806 \cdot 10^5 \text{ kPa}$$

$$\min(\sigma_{di}) = -1.806 \cdot 10^5 \text{ kPa}$$

Steel Tunnel in Soil – Combined Static and Dynamic Stresses by Method of Penzien and Wu (1998) for the Condition of **Full-Slip** between the Tunnel and Soil:

Stress at outer fiber:

$$\sigma_o = \sigma_{so} + \sigma_{do}$$

Stress at inner fiber

$$\sigma_i = \sigma_{si} + \sigma_{di}$$

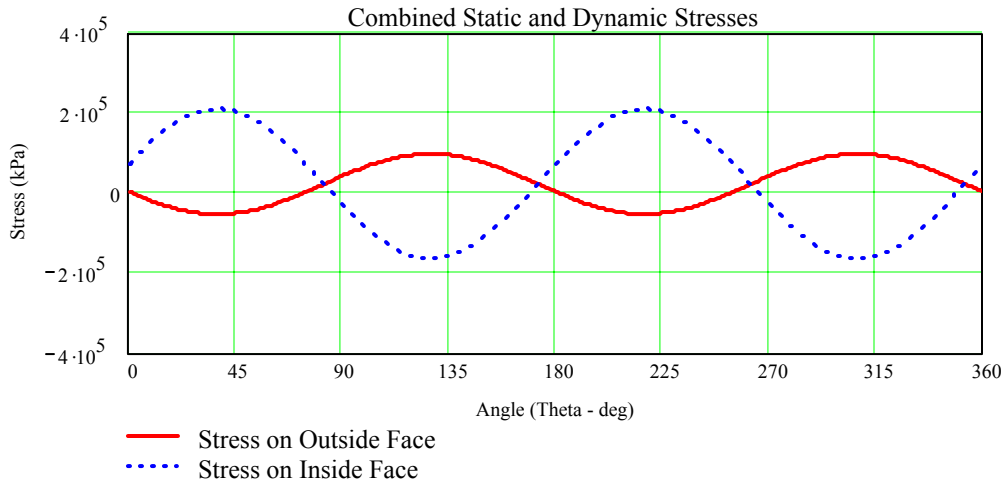
Maximum and minimum combined stresses

$$\max(\sigma_o) = 9.80 \cdot 10^4 \text{ kPa}$$

$$\min(\sigma_o) = -5.25 \cdot 10^4 \text{ kPa}$$

$$\max(\sigma_i) = 2.10 \cdot 10^5 \text{ kPa}$$

$$\min(\sigma_i) = -1.64 \cdot 10^5 \text{ kPa}$$



Steel Tunnel in Soil - Summary of Thrusts and Moments:

			NO SLIP		FULL SLIP	
			SE/W**	PW	SE/W**	PW
STATIC	Thrust (kN/m)	Maximum	788	741	729	728
		Minimum	643	686	701	700
	Moment (kN·m/m)	Maximum	36.3	37.4	37.8	37.8
		Minimum	-36.3	-37.4	-37.8	-37.8
DYNAMIC	Thrust (kN/m)	Maximum	263	98.8	49.9	49.9
		Minimum	-263	98.8	-49.9	-49.9
	Moment (kN·m/m)	Maximum	131	137	136	137
		Minimum	-131	-137	-136	-137

Steel Tunnel in Soil - Summary of Stresses*:

			NO SLIP		FULL SLIP	
			SE/W**	PW	SE/W**	PW
STATIC (MPa)	Inside Face	Maximum	72.3	72.6	72.7	72.7
		Minimum	-26.7	-27.1	-27.1	-27.2
	Outside Face	Maximum	40.0	42.1	42.8	42.8
		Minimum	5.55	33.3	2.74	26.9
DYNAMIC (MPa)	Inside Face	Maximum	179	180	180	180
		Minimum	-179	-180	-180	-180
	Outside Face	Maximum	62.4	70.2	72.6	72.6
		Minimum	-62.4	-70.2	72.6	72.6
COMBINED (MPa)	Inside Face	Maximum	209	210	210	210
		Minimum	-163	-164	-164	-164
	Outside Face	Maximum	87.5	95.6	98.1	98.0
		Minimum	-42.1	-50.1	-52.5	-52.5

* Positive stresses are compressive, negative stresses are tensile.

** Schwartz and Einstein (1980) was used for static, Wang (1993) was used for dynamic.

Discussion of Ovaling Deformation of Steel Tunnel in Soil:

Similar combined static and dynamic stresses were computed for the formulations of Schwartz and Einstein (1980), and Wang (1993), for static and dynamic stresses, respectively, and Penzien and Wu (1998) for static and dynamic stresses. Maximum tensile and compressive stresses were found to occur on the inside fiber (i.e., the inner edge of the flange) of the steel liner. Maximum tensile and compressive stresses are about 64 percent and 84 percent, respectively, of the yield stress. A need for retrofit is not indicated by the analysis.

Concrete Tunnel in Rock - Ovaling Deformation of Tunnel Cross Section

An ovaling analysis similar to that described in the preceding sections for the steel tunnel in soil was carried out for a concrete tunnel in rock. The results are summarized below.

Concrete Tunnel in Rock - Summary of Thrusts and Moments:

			NO SLIP		FULL SLIP	
			SE/W**	PW	SE/W**	PW
STATIC	Thrust (kN/m)	Maximum	679	377	576	376
		Minimum	472	373	574	374
	Moment (kN·m/m)	Maximum	2.47	2.79	2.80	2.80
Minimum		-2.47	-2.79	-2.80	-2.80	
DYNAMIC	Thrust (kN/m)	Maximum	1447	28.4	14.2	14.2
		Minimum	-1447	-28.4	-14.2	-14.2
	Moment (kN·m/m)	Maximum	34.5	39.0	39.0	39.0
Minimum		-34.5	-39.0	-39.0	-39.0	

Concrete Tunnel in Rock - Summary of Stresses*:

			NO SLIP		FULL SLIP	
			SE/W**	PW	SE/W**	PW
STATIC (MPa)	Inside Face	Maximum	2.42	1.44	2.10	1.43
		Minimum	1.40	1.05	-1.72	1.06
	Outside Face	Maximum	2.09	1.43	2.10	1.44
Minimum		1.73	1.07	1.73	1.06	
DYNAMIC (MPa)	Inside Face	Maximum	7.12	2.69	2.65	2.65
		Minimum	-7.12	-2.69	-2.65	-2.65
	Outside Face	Maximum	2.52	2.50	2.55	2.55
Minimum		-2.52	-2.50	-2.55	-2.55	
COMBINED (MPa)	Inside Face	Maximum	9.06	3.95	4.57	3.91
		Minimum	-5.22	-1.45	-0.742	-1.40
	Outside Face	Maximum	4.44	3.76	4.48	3.81
Minimum		0.61	-1.26	-0.646	-1.31	

* Positive stresses are compressive, negative stresses are tensile.

** Schwartz and Einstein (1980) was used for static, Wang (1993) was used for dynamic.

Discussion of Ovaling Deformation of Concrete Tunnel in Rock:

As with the steel tunnel liner in soil, the maximum combined static and dynamic stresses occur on the inside face of the concrete liner. The magnitude of the tensile and compressive stresses varies considerably with the assumption of full-slip or no-slip using the formulations of Schwartz and Einstein (1980), and Wang (1993). The formulation of Penzien and Wu (1998) gave similar stresses for both full-slip and no-slip, and in both cases, peak stresses were lower than the strength of the liner. Maximum tensile and compressive stresses computed using the formulation of Penzien and Wu (1998) were about 70 and 19 percent of the liner strength, respectively. The formulation of Schwartz and Einstein (1980) and Wang (1993) gave peak stresses lower than the strength of the liner for the full-slip case: Peak tensile and compressive stresses were approximately 36 and 22 percent, respectively, of the liner strength. The no-slip formulation of Schwartz and Einstein (1980) and Wang (1993) gave much higher stresses than the other formulations, mainly due to higher computed dynamic thrusts. For this formulation, peak tensile and compressive stresses were about 250 and 44 percent, respectively, of the liner strength. Considering that some slip is likely to occur, it is judged that the ovaling deformations will not be large enough to cause collapse or significant spalling of the concrete tunnel in rock.

Concrete Tunnel in Soil - Ovaling Deformation of Tunnel Cross Section

An additional case of an unreinforced concrete tunnel in soil was considered to obtain the stresses for a concrete liner in relatively soft soil. The concrete tunnel and soil properties are the same as those described at the beginning of Example 4.5. The static and dynamic thrusts, moments, and stresses are summarized below:

Concrete Tunnel in Soil - Summary of Thrusts and Moments:

			NO SLIP		FULL SLIP	
			SE/W*	PW	SE/W*	PW
STATIC	Thrust (kN/m)	Maximum	797	762	740	738
		Minimum	634	665	691	689
	Moment (kN·m/m)	Maximum	64.4	66.2	67.4	67.4
		Minimum	-64.4	-66.2	-67.4	-67.4
DYNAMIC	Thrust (kN/m)	Maximum	295	174	89.0	89.0
		Minimum	-295	-174	-89.0	-89.0
	Moment (kN·m/m)	Maximum	233	239	244	244
		Minimum	-233	-239	-244	-244

Concrete Tunnel in Soil - Summary of Stresses*:

			NO SLIP		FULL SLIP	
			SE/W**	PW	SE/W**	PW
STATIC (Mpa)	Inside Face	Maximum	6.95	6.95	6.96	6.96
		Minimum	-2.18	-2.19	-2.19	-2.20
	Outside Face	Maximum	6.41	6.63	6.80	6.79
		Minimum	-1.63	-1.87	-2.03	-2.03
DYNAMIC (Mpa)	Inside Face	Maximum	16.5	16.5	16.5	16.5
		Minimum	-16.5	-16.5	-16.5	-16.5
	Outside Face	Maximum	14.5	15.4	16.0	16.0
		Minimum	-14.5	-15.4	-16.0	-16.0
COMBINED (Mpa)	Inside Face	Maximum	19.5	19.5	19.6	19.5
		Minimum	-14.7	-14.8	-14.8	-14.8
	Outside Face	Maximum	17.5	18.3	18.9	18.9
		Minimum	-12.7	-13.6	-14.2	-14.2

* Positive stresses are compressive, negative stresses are tensile.

** Schwartz and Einstein (1980) was used for static, Wang (1993) was used for dynamic.

Discussion of Ovaling Deformation of Concrete Tunnel in Soil:

As with the steel tunnel in soil and the concrete tunnel in rock, the maximum stresses for the concrete tunnel in soil occur on the inside face of the liner. Similar to the preceding analyses, stresses in the unreinforced concrete tunnel were calculated using the formulations of Schwartz and Einstein (1980) and Wang (1993), and Penzien and Wu (1998) for full-slip and no-slip. Similar stresses were obtained for all cases. Maximum compressive stresses were about 95 percent of the compressive strength of the tunnel. Tensile stresses were about seven times the tensile strength of the concrete liner. Because the tensile strength of the unreinforced concrete liner is exceeded, the analysis assumption of elastic behavior is not satisfied. However, the results indicate the need for retrofit of the unreinforced concrete tunnel in soil. Retrofit schemes to be considered include demolition of the existing liner and construction of a reinforced concrete or steel liner with temporary support provided during construction, and constructing an inner liner consisting of a steel pipe with concrete filling the annulus between the pipe and the existing liner.

CHAPTER 5: CULVERTS

5.1. INTRODUCTION

Culverts are very common in the nation's transportation corridors. So far, their performance record during major earthquakes has been very positive, on the average, especially when compared to reported damage of other highway components, such as bridges. The primary reason is believed to be the ground level position that culverts occupy in the seismic force field. This position reduces and, in some cases, may eliminate the consideration of dynamic inertial forces, the major seismic design criterion for aboveground structures. However, seismic activity also produces transient ground motion and may produce permanent ground deformations, both of which can affect culvert performance under some circumstances.

In addition, culverts exist in a wide variety of sizes, shapes, and types. Therefore, another reason why culvert failures do not widely occur may be that most culverts have small diameters that may be only marginally affected by earthquakes. Large span culverts that would be expected to experience greater seismic vulnerability are relatively sparse, partly because the demand for their capacity is not as common and because they are relatively new and highly distributed among infrastructure systems. Hence, they do not have the same exposure risk from seismic activity as smaller diameter culverts.

The risk of catastrophic consequences due to the collapse or failure of a culvert generally can be related to both the size and type of culvert. Generally, small diameter culverts do not sustain major damage during an earthquake unless the entire highway system, of which they are a part, also suffers the same level of damage. However, when medium to large size culverts are damaged to the point where they become partially or totally incapacitated and can no longer handle their design hydraulic capacity, impoundment of the inflow and eventual overtopping of the highway surface can result. For the hydraulic flows normally associated with medium to large size culverts, overtopping of the highway can lead to loss of the pavement, scour of the embankment and silt contamination of the downstream ecology. Secondary damage to the road surface can be life threatening due to the resulting hazard faced by the traveling public.

While many factors in addition to the size of the culvert can contribute to its failure during a seismic event, reported case histories seem to indicate that the type of culvert also may be a factor under some circumstances. Permanent ground failure cases, particularly those related to liquefaction, can cause distortion or loss of soil envelope support. Flexible culverts (defined below under the culvert classification section) may distort or collapse due to the loss of support provided by the surrounding soil envelope. This, in turn, can lead to embankment loss and damage to the road surface, thus threatening lives.

One of the goals of this chapter is to increase understanding of the factors that affect culvert performance during seismic events. This will be pursued through a combination of theoretical considerations and documented case histories. Other goals include the delineation of a systematic approach for screening culverts to determine the susceptibility of seismically induced

damage and evaluating the need and extent for employing retrofit measures. Finally, a number of useful retrofit strategies to fortify culverts against this damage are reviewed.

Large culverts over 6 m in span are becoming more commonplace every year. They are employed not only as hydraulic structures but also as grade separation structures. Damage or collapse of a large box culvert has similar consequences to the failure of a bridge. Yet, current AASHTO specifications do not require consideration of seismic design criteria for any type of buried structure, except as follows:

Seismic effects for box culverts and buried structures need not be considered, except where they cross active faults (AASHTO, 2002). AASHTO does not provide guidance on how to design culverts when buried structures cross active faults.

In addition, a systems approach to the development of culvert retrofit strategies is encouraged. Rather than considering culverts as discrete components in a facilities inventory, their role as links in a much bigger chain is important. Seismic retrofit strategies for culverts should be based on the levels of service and priorities of the particular transportation corridor of which they are a part. General considerations affecting the level of evaluation and the need for retrofitting culverts and other elements of the highway system are covered in chapter 1 of this report.

Culverts, like other transportation facilities, require the input of multiple engineering disciplines in the design process. In addition to structural and geotechnical aspects, successful culvert performance requires application of the principles of hydraulics, hydrology, economics, roadway geometric design, as well as traffic capacity and safety considerations. A discussion of the entire process for culvert design is beyond the scope of this chapter.

Many highway culverts utilize end appurtenances of some kind to channel hydraulic flows into and out of the culvert without causing erosion. Special end sections are available for small diameter culverts and typically require no additional design consideration. However, as the size of the culvert increases, these end appurtenances often become endwalls and wingwalls, which are essentially types of retaining walls. The seismic vulnerability and retrofit of retaining walls are addressed in chapter 2 of this report.

5.2. CLASSIFICATION OF CULVERTS AND BACKGROUND INFORMATION

Culverts comprise a diverse group of products with large variations in the availability of material properties, geometric wall sections, sizes and shapes. For instance, diameters as small as 300 mm and spans 15 m and larger are used in highway applications. They can be composed of concrete, steel, aluminum, plastic, and combinations of these.

For the purposes of compiling and maintaining a national bridge inventory, the Federal Highway Administration (FHWA) differentiates culverts from bridges by the width of the span parallel to the roadway. Structures having less than a 6 m span are classified as culverts. However, this distinction is arbitrary from both a functional and a design viewpoint. The American Association of State Highway and Transportation Officials (AASHTO, 2002) publish design specifications for culverts that apply over a continuous range of sizes that extend well beyond the

FHWA limit. General information on culverts can also be found in Highway Drainage Guidelines (AASHTO, 1999; FHWA, 2001) and in *The Culvert Inspection, Material Selection and Rehabilitation Guideline*, Volume 14 (AASHTO, 1999).

In this chapter, highway culverts are defined as structures of any size that are fully surrounded and supported by a highway embankment or an earth fill at or near existing grade level. They may be factory-made in modular components, field constructed, or a combination. They may be based on standard designs covering a range of performance criteria or may be custom designed for a specific application. Their end purpose may be either to convey runoff or traffic (vehicular, pedestrian or wildlife) across a highway corridor. Ballinger and Drake (1995) compiled a list of manufactured culvert types, along with the range of sizes typically available in each type. These are illustrated in figures 5-1 and 5-2.

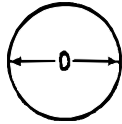
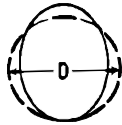
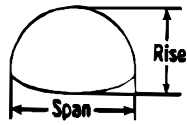
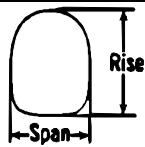
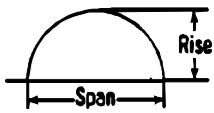
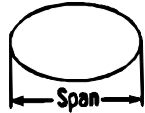
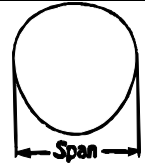
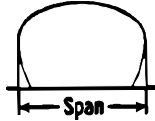

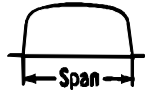
Occasionally, culvert-like materials or assemblies are used for underground tunnels that extend significantly below the surface of the ground and underwater tubes that extend to great lengths beyond the crossing of highway corridors at or near grade level. These structures require additional and specialized design considerations that are beyond the scope of this chapter. Tunnels and underwater tubes are discussed in chapter 4.

Structurally, culverts are complex. They perform as elements in a composite system consisting of the culvert itself and the soil continuum. The soil acts as both a load and resistance element in the composite. When a stable soil mass is properly compacted around the culvert, the load-carrying capacity of the culvert-soil system exceeds the capacity of the culvert alone. The integrity of both elements in the composite is critical to its performance, not only under the action of static loads, but under dynamic excitation of earthquakes. Therefore, any consideration of the capacity of culverts must include recognition of the role played by the soil envelope.

Culverts generally are divided into two major classes: flexible and rigid. Flexible culverts respond to loads differently than rigid culverts. Because their ring stiffness is small relative to the adjacent soil, flexible culverts depend upon a large strain capacity and the interaction with the surrounding soil to hold their shape while supporting the external pressures imposed upon them. On the other hand, the strain capacity of rigid culverts is much lower. Therefore, rigid culverts must develop significant ring stiffness and strength to support external pressures. Hence, they are not as dependent upon soil support as flexible culverts. More specific aspects of both flexible and rigid culverts relative to their seismic resistance are discussed in the following sections.

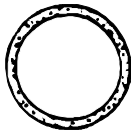
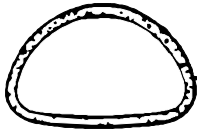
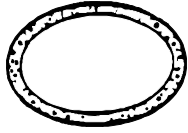



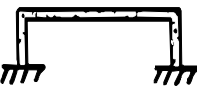

5.2.1. FLEXIBLE CULVERTS - BACKGROUND AND DESIGN PHILOSOPHIES

Flexible culverts typically are composed of either metal or thermoplastic materials. Highly efficient wall sections have evolved that maximize their section properties while conserving material. Corrugated metal pipe (CMP), originally composed of iron, was the first type of flexible culvert to be developed in the early part of this century. Modern CMP culverts are available in both steel and aluminum. A family of corrugated profiles having wall sections that are composed of a series of arcs and tangents are illustrated in figure 5-3. These sections have been shown to be stable structurally but may suffer in hydraulic performance compared to other

Shapes	Range of Sizes	Common Uses
Round 	Diameter 0.15 m to 7.9 m	Culverts, subdrains, sewers, service tunnels (all materials in smaller diameters, structural plate in larger diameters).
Vertical Ellipse (5% Common) 	Diameter 1.2 m to 6.4 m nominal; before elongating	Culverts, sewers, service tunnels, recovery tunnels (CMP and structural plate).
Pipe Arch 	Span x Rise 1.42 m x 0.33 m to 6.27 m x 4.01 m	Where headroom is limited. Has hydraulic advantages at low flows (CMP and structural plate).
Underpass 	Span x Rise 1.73 m x 1.75 m to 6.20 m x 5.41 m	For pedestrians, livestock or vehicles (structural plate).
Arch 	Span x Rise 1.83 m x 0.55 m to 7.62 m x 3.81 m	For low clearance large waterway opening, and aesthetics (structural plate).
Horizontal Ellipse 	Span 2.1 m to 12.2 m	Culverts, grade separations, storm sewers, tunnels (CMP and structural plate).
Pear 	Span 7.6 m to 9.1 m	Grade separations, culverts, storm sewers, tunnels (structural plate).
High Profile Arch 	Span 6.1 m to 13.7 m	Grade separations, culverts, storm sewers, tunnels, ammo ammunition magazines, earth covered storage (structural plate).
Low Profile Arch 	Span 6.1 m to 15.2 m	Low, wide waterway enclosures, culverts storm sewers (structural plate).
Box Culvert 	Span 3.0 m to 7.9 m	Low, wide waterway enclosures, culverts, storm sewers (structural plate).
Specials	Various	For lining old structures or other special purposes. Special fabrication.

adapted from Ballinger and Drake, 1995

Figure 5-1. Available types and sizes of flexible culverts.

Shapes	Range of Sizes	Common Uses
Round 	Diameter 0.3 m to 4.6 m (reinforced); 0.1 m to 0.9 m (non-reinforced)	Culverts, storm drains, sewers.
Pipe Arch 	Span x Rise 0.4 m to 3.4 m equivalent diameter	Culverts, storm drains, sewers. Used where head room is limited.
Horizontal Ellipse 	Span x Rise 0.5 m to 3.7 m equivalent diameter	Culverts, storm drains, sewers. Used where head room is limited.
Vertical Ellipse 	Span x Rise 0.9 m to 3.7 m equivalent diameter	Culverts, storm drains, sewers. Used where lateral clearance is limited.
Rectangular Box Culvert 	Span 0.9 m to 3.7 m	Culverts, storm drains, sewers. For wide openings with limited head room.
Arch 	Span 7.3 m to 12.5 m	Culverts and storm drains. For low, wide waterway enclosures.
Flat Top 3-Sided 	Span 4.3 m to 10.7 m	Culverts and storm drains. For low, wide waterway enclosures.
Arch Top 3-Sided 	Span 4.9 m to 11.0 m	Culverts and storm drains. For low, wide waterway enclosures.

adapted from Ballinger and Drake, 1995

Figure 5-2. Available types and sizes of rigid culverts.

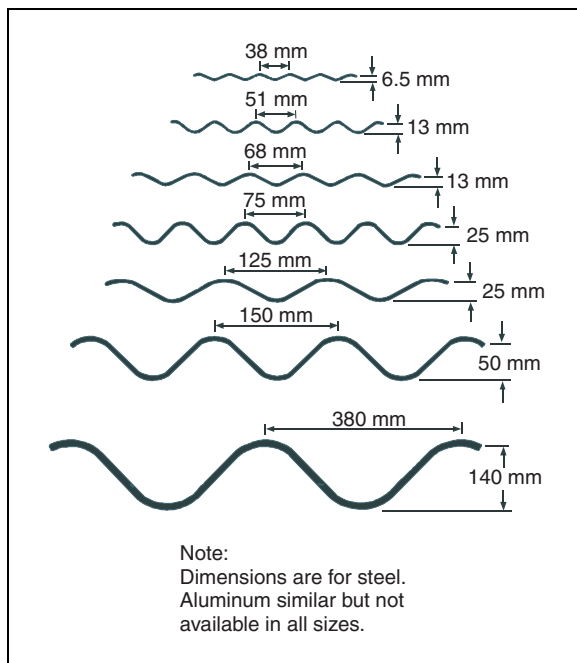
culvert products. They are available in a variety of factory-made and field-assembled shapes ranging in size from 300 mm in diameter to 15 m in span and larger. In smaller diameters, they may be fabricated with either annular or helical corrugations. In larger sizes and special shapes, they are only available in field-erected modular plates having annular corrugations.

Spiral rib is a more recent corrugation innovation. Also available in both steel and aluminum, its wall section consists of alternating lengths of smooth wall and box corrugations as illustrated in

figure 5-4. They are known to be less structurally robust as the arc and tangent corrugation, but are more efficient from both material and hydraulic viewpoints.

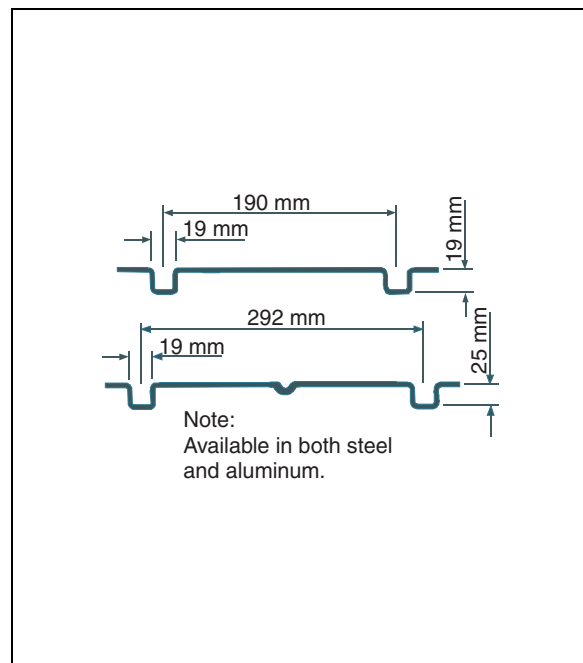
Culverts manufactured from thermoplastic materials employ one of two types: high-density polyethylene (HDPE) or polyvinyl chloride (PVC). Many formulations are available in each type. Also, a broad range of manufacturing processes for thermoplastic culverts facilitates maximization of both their structural and hydraulic efficiencies. As a result, many varieties of cross sections have evolved, some of which are illustrated in figure 5-5. Since their engineering properties are a function of both the formulation of the material and the wall section profile, significant variability exists from one product to the next. In addition, strength and modulus parameters of thermoplastic materials are temperature, time and stress history dependant, thus further complicating their design.

Current AASHTO specifications deal with the complications inherent in thermoplastic culverts through simplistic lower bound assumptions, which are thought to be generally conservative. However, some issues remain to be addressed. These include local buckling control of thin-walled sections, recognition of the reduced load transfer that occurs from the soil envelope to the culvert wall compared to traditional high modulus (metal and concrete) culverts, and material formulations that assure long-term ductility and oxidation resistance. Research investigations on these topics are expected to result in future additional refinements to the material and design specifications of thermoplastic culverts.



AISI, 1993

Figure 5-3. Corrugated metal culvert wall profiles.



AISI, 1993

Figure 5-4. Spiral rib metal culvert wall profiles.

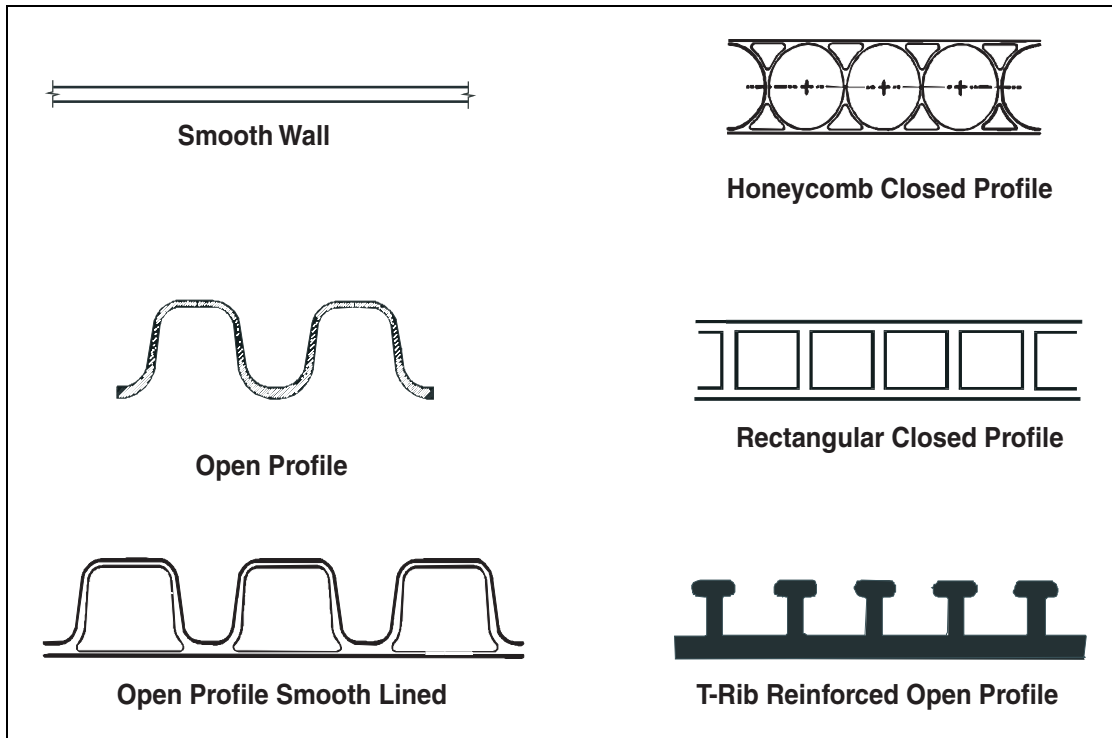


Figure 5-5. Selected examples of thermoplastic culvert wall profiles.

The primary design considerations for small diameter flexible culverts are ring compression and resistance to general buckling (cross sectional collapse). For larger sizes and shapes other than circular, the flexural strength required by nonsymmetrical and concentrated live loads, including seismic loads, must be considered. To accomplish this, some applications may require the use of computerized numerical methods (Katona et al., 1976, 1979, 1981; Duncan, 1979; Leonards et al., 1981; Musser, 1989a). Secondary design considerations include resistance to local buckling of thin-wall sections and fatigue of pavement sections over installations having shallow covers in combination with heavy live loads.

Implicit in the design assumptions for flexible culverts is the existence of adequate soil support. This is achieved by employing stable backfill materials surrounding the circumference of the culvert. Both the size of the envelope of stable material, and its placement method and quality, are factors that affect the successful performance of flexible culverts.

From a seismic performance perspective, flexible culverts are attractive because they are very ductile. Five percent strain or higher is available in the basic material properties of steel, aluminum and thermoplastics. And, even higher equivalent strain capabilities are available in the longitudinal direction of corrugated sections due to accordion action. Statically safe flexible culverts generally have sufficient ductility to withstand seismic forces without permanent deformation or collapse. The weakness of flexible culverts is their dependence upon soil support, which can be reduced or lost during liquefaction of other permanent ground failure mechanisms associated with seismic events. Distortion or collapse of the culvert cross section is

likely if soil support is reduced or lost. Thus, for seismic consideration, distortion or collapse of flexible culverts is generally associated with liquefaction, slope instability or faulting, all which are geotechnical or geologic issues rather than structural issues.

5.2.2. RIGID CULVERTS – BACKGROUND AND DESIGN PHILOSOPHIES

Modern rigid highway culverts consist primarily of reinforced concrete shapes that are either precast or cast-in-place. In the past, some unreinforced culverts were placed either as precast or cast-in-place pipe. The use of unreinforced concrete culverts is now limited for highway applications and they are not recognized in current AASHTO specifications (AASHTO, 2002). Because of their brittleness, unreinforced concrete culverts are not recommended for use in seismic regions. Reinforced concrete pipe (RCP) is almost always furnished precast in diameters ranging from 300 mm to 3,600 mm. Above this range of sizes, RCP is precast on the site or constructed cast-in-place. Rectangular four-sided box culverts can be furnished precast in spans ranging from 900 mm to 3,600 mm. Larger spans and multiple cell four-sided box culverts typically are constructed cast-in-place. Three-sided precast box culverts are a relatively recent innovation and can be furnished in spans up to 15 m.

Whether precast or cast-in-place, the concrete cross sections are relatively smooth on both the inside and outside. Material efficiency is achieved by optimizing the wall thickness, the strength of the concrete and in the case of reinforced concrete, the placement and quantity of the steel reinforcement. In the case of precast circular cross sections, elliptically shaped reinforcement or specially placed reinforcing mats are sometimes employed to increase efficiency.

The rupture strain of typical concrete under uniaxial compression is between 0.1 and 0.25 percent, but can vary over a greater range, depending upon the quantity and characteristics of the aggregate and upon the water/cement ratio of the paste (Hobbs, 1983). Under uniaxial tension, the rupture strain capacity is an order of magnitude less, ranging between 0.005 and 0.01 percent. On the other hand, modern reinforcing steel can develop rupture tensile strains between seven and nine percent. However, the strain capacity of rebar at yield is approximately 0.2 percent.

It is the approximate compatibility of the definable limit state strains between concrete rupture in compression and steel yield in tension that is used in the design of the reinforced concrete composite. The unused strain capacity of the steel beyond yield may further contribute to the inelastic ductility of the composite, provided adequate consideration is given to concrete confinement and to limiting concrete compressive and shear strains. But, since the concrete tension strain capacity is so low, some cracks in the tension surface of reinforced concrete bending members are nearly always anticipated, even at service loads. Exceptions to this are pretensioned and post-tensioned members.

The width of tension surface cracks typically is regulated through both design criteria and quality assurance practices during manufacture and construction. In the case of highway applications, AASHTO specifications currently limit the width of surface cracks in reinforced concrete culverts to about 0.3 mm (AASHTO, 2002).

The primary design method used for precast concrete pipe, either reinforced or unreinforced, is known as the *Indirect Design Method*. This means simply that their design is based on a

laboratory test, known as the three-edge bearing test. The testing protocol calls for concentrated vertical loads applied at the crown and invert of a pipe specimen. The test results include the load at which the specimen either ruptures (in the case of unreinforced pipe) or exceeds allowable crack width requirements (in the case of reinforced pipe). Empirical bedding factors are used to translate three-edge bearing laboratory test values into actual field support conditions at the haunch and invert. The end result is that adequate soil envelope support from these regions of the pipe circumference are assumed in the design. However, this is much less than requiring that the total periphery of the soil envelope support the wall section, which is the case with flexible pipe.

The *Indirect Design Method* was developed by Marston during the first quarter of this century (Marston et al., 1917; Marston, 1930). Since that time, a number of refinements have been made that provide a more direct design procedure that accounts for moments, shears, and thrusts around the periphery of the culvert wall (Paris, 1921; Olander, 1950). The latest methods employ computerized numerical models that evaluate the contribution provided by soil-structure interaction (Hegar, 1982). These have evolved into what is termed the *Direct Design Method*. Also, new installation types, known as SIDD (Standard Installations for Direct Design), have been developed to replace the empirical bedding factors developed by Marston. These installation types better represent the soil support conditions typically obtained using modern construction practices (ASCE, 1993).

While the designs resulting from these refinements can be more efficient, their assumptions may be less tolerant to loss of backfill support, such as seismically induced ground instability, than earlier, less efficient designs. Currently, AASHTO jurisdictions are mixed on their adoption of direct versus indirect methodologies for design of RCP culverts. This is also the case with adoption of the new SIDD factors versus continuing to use the older Marston bedding factors. More work is required to quantify the difference in seismic retrofit requirements for RCP designed under the older versus the newer methodologies.

Four-sided and three-sided box culverts, whether precast or cast-in-place, are designed using the same criteria as other reinforced concrete beams and columns. Rectangular shapes are analyzed assuming an indeterminate elastic frame and active or neutral soil pressures against the side, but do not account for soil-structure interaction. Most computer software currently available to the typical engineer can perform the structural analysis required for design. In addition, specialty software has been developed for this purpose (McGrath et al., 1988).

On the other hand, arched-top three-sided box culverts account for soil-structure interaction by depending upon the passive soil restraint at the side to support the arching action of the top. Therefore, their design and analysis requires the use of computerized numerical models that can account for this interactive support (Katona et al., 1976, 1981; Beach, 1988; Musser, 1989a; McGrath et al., 1996).

The advantage that rigid culverts have over flexible ones during earthquakes is their ability to provide a greater degree of *brute strength* during the loss of soil envelope support that might occur as a result of permanent ground deformations. A disadvantage is their brittle nature (ultimate strain capacity less than 0.1 percent). When the *brute strength* limit is reached, rigid culverts cannot shift overloads to the soil envelope through passive restraint without causing

permanent damage to the structural shell. Also, they do not respond as well to transient ground motions where ductility is important. However, even if irreparable damage results, cases of catastrophic collapse of RCP during seismic events have not been documented in the literature.

5.2.3. CULVERT JOINTS

The primary objective of the seismic design of culvert joints is to maintain joint closure during ground shaking and after the occurrence of permanent ground deformation. Open joints can lead to soil fines migration, which over time can lead to loss of the backfill envelope and the collapse of the culvert and road surface. However, this action takes considerable time to develop and is not classed as an immediate threat to life safety or serviceability of the roadway. A secondary objective of the joint design is to relieve longitudinal stress built up in the continuous part of the culvert wall, provided that the primary objective of joint tightness is not compromised.

During ground shaking, the optimum joint would provide longitudinal ductility in both tension and compression without reaching the end of its design travel length and without the loss of joint tightness. Joints that are assembled tightly in compression but are relatively free to move in tension are subject to joint hammering during the high frequency longitudinal oscillations typically associated with seismic ground shaking. This hammering can result in damage to the joint and a loss of joint tightness. In addition, joints that open as soon as they are extended in tension may allow infiltration of soil fines. This action may prevent them from fully closing during subsequent cycles of shaking, thus leading to further loss of soil tightness.

During permanent ground deformation, the optimum joint would be capable of developing the full strength capacity of the culvert wall section in tension, compression, and shear while still remaining ductile. This is because the deformation demand at ground failure sites can become so great that typical joint designs utilizing the *push-on* type of assembly cannot accommodate such large seismically induced deformations without coming apart. The best design to withstand permanent ground deformations would be jointless culverts that could also maintain longitudinal ductility and cross sectional strength, even after losing the support of the confining soil envelope. No real culvert systems available today can provide all of these characteristics. However, some types approach this optimum performance more closely than others.

As will be seen in the case histories that follow, culvert joints can be the *weak link* in the chain of total culvert performance during earthquakes. Hence, adequate joint design to resist the action of earthquakes is perhaps as strategic to overall culvert performance as the design of the wall section. Therefore, to increase understanding regarding this aspect of culvert performance, several types of commonly available joints are reviewed in the following subsections.

5.2.3.1. Bell and Spigot Joints

Bell and spigot joints are available for a number of thermoplastic and precast reinforced concrete pipe products, as shown in figure 5-6. They are generally furnished with rubber gaskets. Thermoplastic pipe joints typically allow 25-50 mm of longitudinal joint translation as well as 1-3 degrees of joint rotation. Normal RCP bell and spigot designs do not allow for much longitudinal translation or rotation while still maintaining a sealed joint. An RCP joint

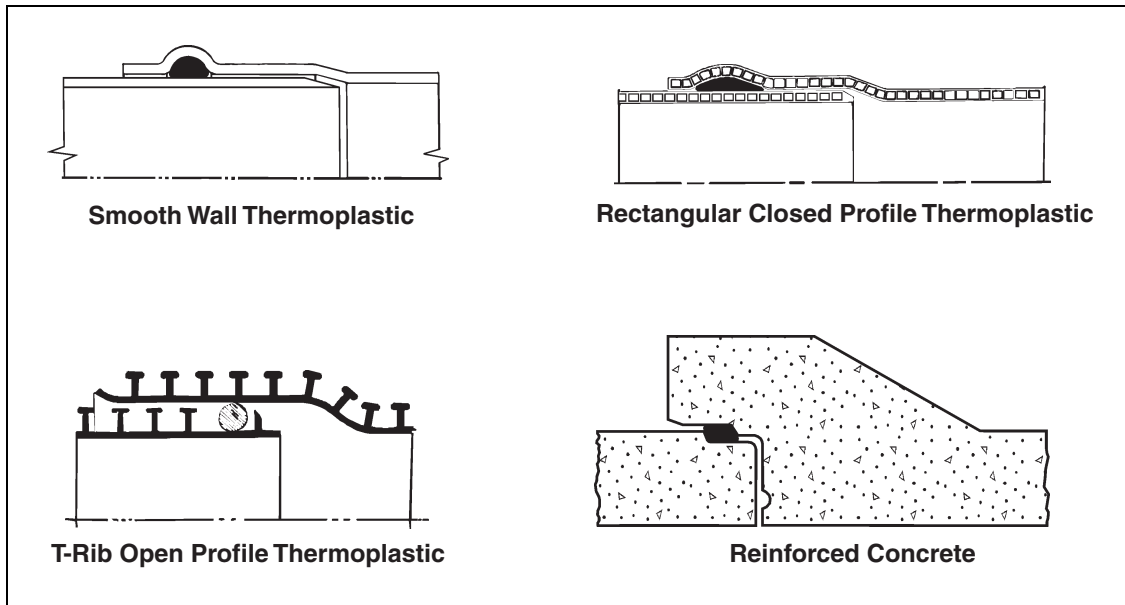


Figure 5-6. Selected examples of bell and spigot culvert joints.

configuration allowing 50-100 mm of joint translation is available by special order in some markets.

While most thermoplastic and RCP bell and spigot designs develop some level of transverse shear strength at the joint, the full shear capacity of the culvert wall generally cannot be developed. This is due to a number of factors. Some RCP designs do not carry the full quantity of shell reinforcement into the joint. Even when the full wall sectional capacity is carried into the joint, the bell portion is acting at a slightly larger diameter, which is accompanied by a proportionate decrease in strength. This is true for both RCP and thermoplastic materials. Also, transverse forces tend to develop stress concentrations at one point around the joint circumference. Deformation mechanics suggests that flexible materials will distribute these stress concentrations more uniformly than rigid materials, hence developing a higher percentage of wall strength at the joint.

The typical installation practice for bell and spigot joints is to push the pipe *home*, or in other words, to assemble the joint with the spigot end fully inserted into the bell. While this provides the greatest pull-out (tension) ductility available from a given design, it leaves no ductility in compression. Ideal installation practice for seismic performance would be 50 percent insertion. However, for most commercially available culvert products, the resulting travel length available in each direction (tension and compression) would be of little use during a seismically induced ground failure event.

5.2.3.2. Tongue and Groove, Keyed and Butt Joints

Tongue and groove, keyed and butt joints are used in many precast concrete culverts and in the expansion joints of nearly all cast-in-place concrete designs. Examples of these joints are shown

in figure 5-7. The tongue and groove and keyed joints are similar because they both provide some level of restraint and strength to resist transverse forces. However, like bell and spigot RCP joints, they provide very little longitudinal or rotational ductility without separating. The spaces between both the tongue and groove and keyed joints typically are filled with cement grout but also may be fitted with an elastomeric pad or other sealant. In either case, the joint can be subjected to longitudinal hammering during dynamic shaking that can lead to cracking and spalling. This damage can result in loss of soil tightness. Also, as the joint opens or is damaged, backfill soil can infiltrate and prevent it from fully closing during subsequent cycles of shaking.

The butt joint is used in some precast reinforced concrete designs. It is not usually grouted closed during construction but is assembled as close as possible. It is often wrapped with a geotextile or waterproofing membrane. However, the effectiveness of these wraps in maintaining joint closure during dynamic shaking is not known. Also, butt joints obviously provide no transverse strength and can be subject to damage from longitudinal hammering.

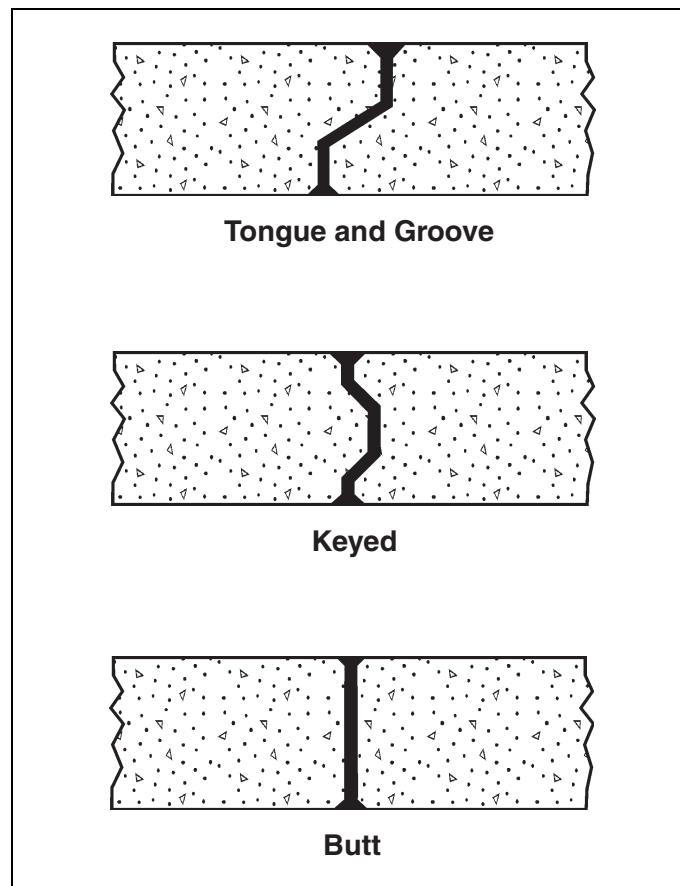


Figure 5-7. Tongue and groove, keyed and butt joints in reinforced concrete culverts.

5.2.3.3. Closure Bands and Couplings

Closure bands are used primarily with corrugated and spiral rib metal pipes. They are manufactured in a wide variety of configurations. Examples of closure bands are illustrated in figure 5-8. Designs for culverts with annular corrugations utilize sections of matching corrugated pipe wall that are joined by angle iron flanges welded to the ends of the sections at two or three points around the circumference, thus forming a complete band. The band is tightened by cinching the flanges together with bolts located external to the pipe. The width of the band typically engages two or three annular corrugations on each culvert end that it joins.

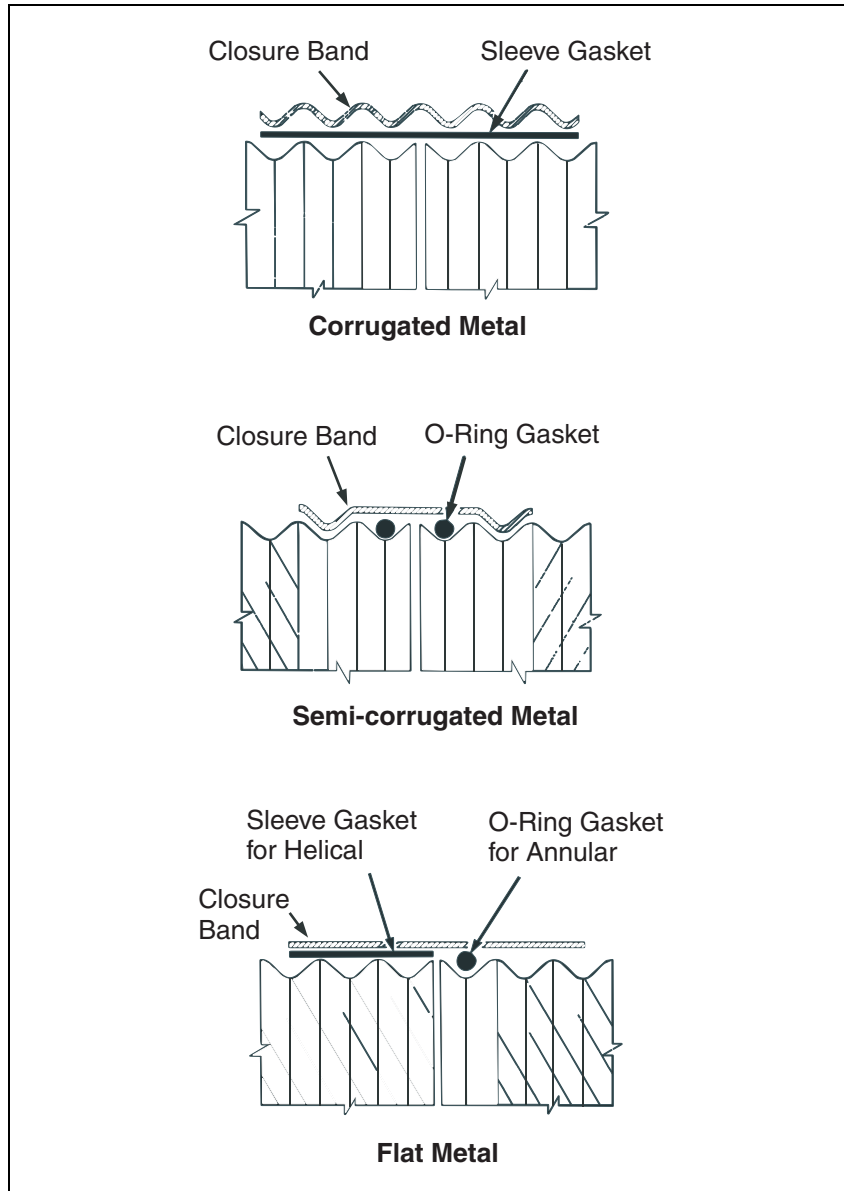


Figure 5-8. Selected types of closure bands for corrugated metal culverts.

This design provides both ductility and strength in all three degrees of freedom, as well as good closure against soil migration. However, pull-apart tests reveal that this type of closure band falls short of developing the full culvert wall strength. The bolted connections at the flanges are the weak link. An elastomeric gasket is sometimes inserted between the band and the pipe wall to improve water tightness but may also decrease the pull-apart strength of the connection.

Another type of closure band employs flat steel sheet fabricated with edge corrugations (semi-corrugated). Its typical use is to join spirally corrugated culverts having ends that are reformed into annular corrugations. It engages the reformed end in only one of its corrugations. Hence, while it is more efficient in materials, it lacks the same pullout capacity of the fully corrugated band that engages at least two corrugations on each end. Otherwise, the semi-corrugated design shares most of the other characteristics of the fully corrugated band.

Flat or dimpled closure bands are provided for culverts with plain end spiral corrugations or spiral ribs. They provide some level of transverse strength but almost no longitudinal or rotational restraint. Since the band does not fit snugly into spirally corrugated culvert walls, the surrounding backfill envelope can be lost when spirally corrugated culverts without reformed ends are employed under some hydraulic conditions and when fine-grained soils are present.

Most profile wall thermoplastic culverts employ shaped couplings to join plain end sections. These couplings are designed to fit the specific profile configuration of the culvert wall. They typically include a shaped rubber gasket to provide tightness against both moisture and soils migration. An example of such a coupling is shown in figure 5-9. Other designs employ a type of closure band. Molded plastic sheets with edges that match the exterior of the profile wall fit around the pipe ends and snap shut. Thermoplastic couplings perform similarly to thermoplastic bell and spigot joints in terms of their longitudinal and rotational ductility. They also provide some transverse strength.

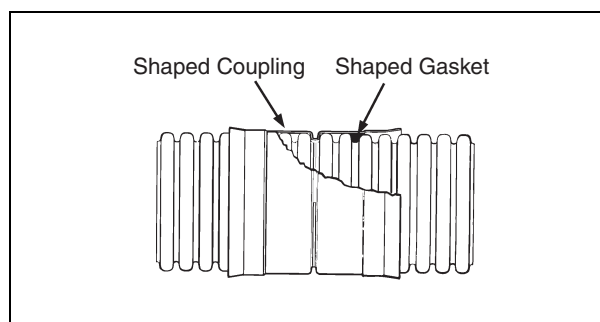


Figure 5-9. Typical coupling for plain end thermoplastic culverts.

5.2.3.4. Continuous Joints

Three types of continuous joints are available for certain applications. Cast-in-place reinforced concrete often utilizes construction joints that are formed similar to tongue and groove or keyed joints, but carry dowels of reinforcing steel across the joints. A second type is corrugated metal structural plates that are field assembled with bolted connections. A third type is thermoplastic pipe with ends that are fused together, either by heat or solvent. The first two are used for relatively large culvert applications.

The third type is used as a liner of relatively small diameter culverts, the outer shell of which consists of one of the other culvert types described herein.

All three types of continuous joints share common characteristics relative to seismic performance. The most important aspect is that they develop a large portion of their wall-sectional strength and ductility in all three degrees of freedom.

5.3. SCREENING FOR POTENTIAL SEISMIC DAMAGE

The objective of the screening process is to identify a subset of culvert sites that may require further evaluation at a more detailed level while dismissing sites that would not be expected to suffer significant damage and remain functional after an earthquake. Techniques for performing detailed evaluations of culverts are provided in section 5.4.

Screening of culvert sites to determine the potential for earthquake-induced damage requires an understanding of the interrelationship between many complex factors, such as the following:

- Magnitude of the earthquake.
- Probable location of its origin.
- Intensity of ground shaking expected to occur at the culvert site.
- Likelihood that the fault displacement might rupture the ground surface or induce other ground failure mechanisms in the vicinity of the culvert.
- Response of the culvert system to any of the factors listed above.

Only the last item is dealt with exclusively in this chapter. The remaining factors are discussed briefly below. However, since they can influence the behavior of other highway system components as well, more detailed descriptions have been provided elsewhere in this manual.

This section presents both the theoretical concepts related to seismically induced culvert damage as well as case histories that document the nature and extent of actual damage. These discussions provide important background that will be needed to support implementation of the decision-tree screening model given at the end of this section.

5.3.1. THEORETICAL CONCEPTS RELATED TO SEISMICALLY INDUCED CULVERT DAMAGE

Similar to other structures, seismic events can damage culverts through two primary causative mechanisms, permanent ground failure and transient ground shaking, the latter of which may also induce significant inertial forces. Permanent ground failures generally cause the largest deformations and greatest damage to culverts. Transient ground shaking can also damage culverts, but typically to a much more limited extent. Seismically induced inertial forces, which

are the primary cause of damage to aboveground structures, seem to have little effect on culverts except for large diameter pipes and non-circular shapes, including box culverts, under heavy loads.

The first step in screening culverts to determine the need for retrofit measures is to assess the potential that the causative mechanisms described above will occur at any given site. Theoretical concepts related to the occurrence and manifestation of these causative factors will be reviewed briefly in the following subsections. In addition, the likely responses to these causative factors will be discussed.

5.3.1.1. Permanent Ground Failure

Permanent ground failure can result from either of two major causes, fault rupture or ground deformation due to ground shaking. Fault rupture by itself can induce ground surface deformations in the vicinity of the rupture zone. The extent of this zone is typically limited to a distance of a few hundred meters from the principal trace of surface fault rupture. The resulting ground surface deformations can range from very slight to severe.

Mild tectonic deformations may appear as undulations, bulges or depressions that extend over large areas but may produce only small differential effects local to a given culvert. Hence, they generally have little effect on culvert performance. On the other hand, severe tectonic deformations can produce compression zones, tension zones, ground surface offsets, either horizontal, vertical, or both, or the possible formation of chasms or ridges. The most severe of these manifestations would be impossible to protect against and, certainly, would impair the performance of culvert structures that happened to exist in their path.

Nonetheless, where the existence of these challenges have been identified, other utilities, such as pressure water or gas pipelines, have devised engineered solutions that have successfully dealt with at least moderate tectonic deformations. These solutions typically have used one of two types of constructions. The first employs continuous ductile pipelines having full strength (often welded) joints. The second utilizes multiple sections of short pipes connected by flexible joints capable of developing significant tension, compression and lateral ductility without suffering pull-apart, damage or other loss of functionality. Similar technologies as these are also available for culverts.

Ground shaking alone can also cause permanent ground failure. Liquefaction, collapse or sliding of unstable soil masses are the causative factors in these cases. Permanent ground failure that impacts culvert performance is often accompanied by the following site manifestations:

- Embankment penetration.
- Lateral and embankment spreading.
- Slumping of fill and landslides.

Identification of potential sites that might experience permanent ground failure requires significant expertise as well as the availability of site-specific geotechnical and seismological characteristics. Once estimates of ground deformations are provided for the design earthquake,

they can be used to devise retrofit strategies. Or, they may lead to a decision favoring some means of ground remediation or stabilization to prevent ground failure, in which case culvert retrofit may not be necessary. Both ground failure prediction and ground remediation methods are discussed in Part 1 of this manual.

5.3.1.2. Transient Ground Motion

Transient ground motion may not result in permanent ground failure but still may induce strains and stresses in culverts that can lead to structural damage. The extent of this damage depends upon the level of shaking as well as the design and condition of the culvert.

Transient ground motion produces both axial and transverse culvert strains or deformations. Components of seismic waves that propagate along the longitudinal axis of a culvert can produce joint hammering, joint pull-apart or transverse cracking. Components of seismic waves that propagate transversely to the longitudinal axis can produce ovaling, racking and other distortions of the culvert cross section. Transverse waves, whether vertical or horizontal, can also affect longitudinal culvert alignment.

These manifestations of culvert distress caused by transient ground motion generally are not catastrophic except for the possible collapse of flexible types of culverts due to loss of soil support. Most culverts are believed to be too short in length and small in cross section to suffer major damage or immediate collapse as a direct result of such distress. However, joint separations and other induced damage can produce catastrophic collapse over time if there is erosion of soil into the culvert leading to loss of soil envelope support. In areas that suffer heavy shaking, post-seismic inspection and repair may be necessary in order to assure the long-term survivability of the culvert system.

Transient ground shaking can also mobilize inertial forces induced in the backfill materials around and over the top of culverts. These inertial forces produce both horizontal and vertical overpressures that can increase the stress in the culvert cross section. Such transient stress risers do not typically lead to collapse, although they may induce local buckling or cracking of the wall. But, since all culverts depend to some degree upon the surrounding soil for their strength, these stress risers, when acting in conjunction with liquefaction or other causes of ground instability, can exacerbate the effect of the inertial forces due to reduction or elimination of support provided by the soil envelope. The extent of resulting damage depends upon the severity of this combination of effects but can produce distortion or collapse of the culvert cross section.

Seismic ground accelerations are typically three-dimensional and are not necessarily in phase orthogonally. Hence, buried structures can experience tilting, racking, shear and unbalanced pressure increases, both horizontally and vertically. The longitudinal and transverse components of buried structure deformation and the types of seismic waves that can produce them are more fully discussed and illustrated in chapter 4.

5.3.2. EMPIRICAL OBSERVATIONS OF SEISMICALLY INDUCED CULVERT DAMAGE

In reviewing the following empirical data on seismically induced culvert damage, it is useful to differentiate between the causative mechanisms of damage and their manifestations. For

instance, permanent ground failure caused by liquefaction can manifest itself in many forms of damage including misalignment, separation of joints, uneven settlement and even collapse of the culvert cross section. However, the likely causative factor, (i.e., liquefaction, collapse, slumping, fault rupture, etc.) can be readily ascertained by other site characteristics, such as the presence of unconsolidated sands or clays, the depth of the water table, the slope of the ground surface, observed tectonic ground deformations in the vicinity, etc. On the other hand, transitory longitudinal ground shaking, with or without inertial effects, can manifest itself in joint hammering, cross sectional deformation, cracking, etc.

Of course, empirical observations will produce a mix of causative factors acting together. The challenge is to deduce the mechanisms that produce the most significant effects in any given observation. Accurate identification of the causes will result in selection of more appropriate evaluation techniques and retrofit strategies.

Perhaps the most complete survey to date of culvert performance during seismic events was performed by Youd and Beckman (1996). Through a combination of personal observations and published reports, they documented culvert performance during six North American earthquakes. They identified not only effects but also probable causes of the damage. Table 5-1 categorizes their findings by culvert type and extent of damage.

Another significant study by Davis and Bardet (1998) reported on the performance of 61 CMP and structural plate culverts that were shaken by the 1994 Northridge earthquake. Included in this study were 29 culverts that were 1 m or smaller in diameter and 32 that ranged from 1.07 m to 4.78 m in diameter or span. All 61 culverts were in the vicinity of the Van Norman Water Treatment Complex in the northern San Fernando Valley. Peak ground accelerations in this vicinity ranged from 0.48 g to 1.08 g horizontal and from 0.32 g to 0.85 g vertical.

With the exception of one culvert that was damaged due to a severely corroded invert, none of the culverts 1 m and smaller in diameter suffered damage during this event. Of these smaller diameter culverts, two were in areas that may have suffered some degree of permanent ground deformations. The nature, causative factors or extent of deformations at these sites were not reported.

The performance of the larger culverts ranged from no damage to complete collapse. While all of these larger culverts appeared to sustain some deformations, four seemed to be influenced by permanent ground deformations to some degree. Four others seemed to be influenced by preexisting conditions such as poor backfill and severe corrosion of the invert. No surface faulting occurred at this site.

The following paragraphs describe in more detail specific observations of culvert damage and the causative mechanisms that produced them. Contributions from both Youd and Beckman (1996) and Davis and Bardet (1998) are included.

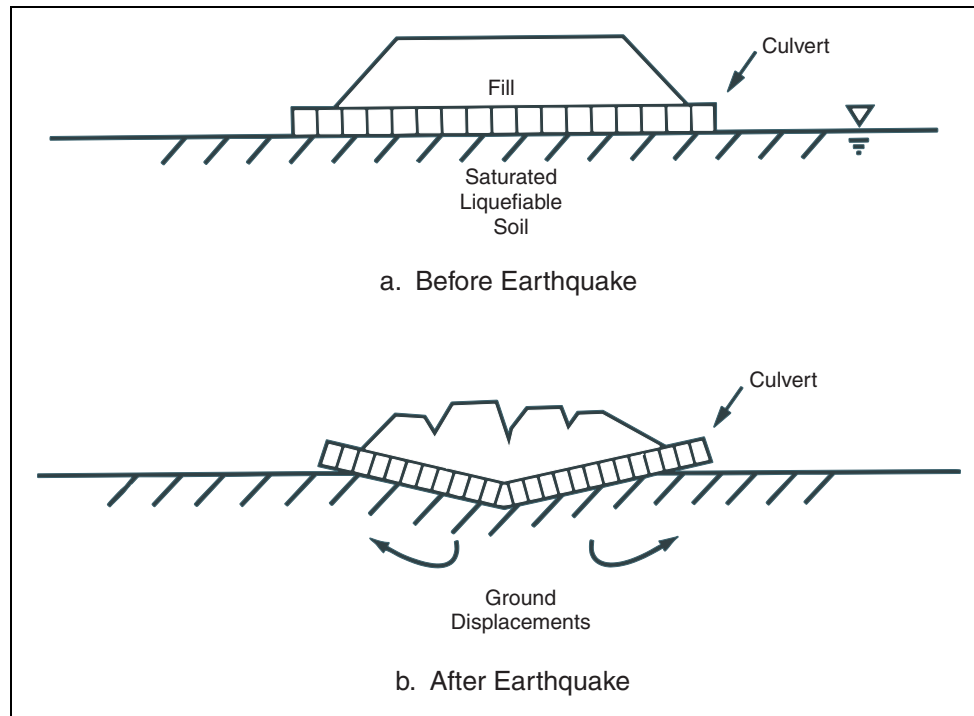
Table 5-1. Summary of highway culvert performance.

Site Manifestation of Seismic Event	Permanent Ground Deformation						Transient Ground Deformation			Totals
	EP	LS	SL	LQ	LA	FR	SG	GS	LO	
CMP Pipe										
Replace	4	1	1						1	7
Repair		1							1	2
No Repair	1						24			25
Thermoplastic Pipe										
Replace										0
Repair										0
No Repair							1			1
Reinforced Concrete Pipe										
Replace						1				1
Repair		1			1		1			3
No Repair										0
Unreinforced Concrete Pipe										
Replace								1		1
Repair										0
No Repair										0
Reinforced Concrete Box										
Replace						1			1	2
Repair	2	4						3		9
No Repair				1			4	14	1	20
<p>Notes: EP = Embankment Penetration LS = Lateral Spread SL = Slumping LQ = Liquefaction LA = Landslide FR = Fault Rupture SG = Strong Ground Shaking GS = Ground Shaking LO = Lateral Overpressures</p>										

compiled from Youd and Beckman, 1996

5.3.2.1. Embankment Penetration

Strong ground shaking occurring during moderate to high magnitude seismic events can trigger the collapse of liquefiable or sensitive foundation soil layers below highway embankments. The resulting subsidence of these layers causes penetration of embankments into the unstable stratas and can damage highway culverts located in the vicinity of these stratas. This can lead to longitudinal and transverse bending of the culvert barrel sections, separation, misalignment and fracturing of the culvert joints and raising of the culvert ends above the flow line. A typical failure diagram is shown in figure 5-10.



Youd and Beckman, 1996

Figure 5-10. Penetration of embankment and culvert into liquefied foundation strata.

While any culvert type would be subject to damage from embankment penetration into unstable foundation soils, Youd and Beckman (1996) reported that it was the most common cause of CMP culvert failure in the six earthquakes that they investigated. These events experienced magnitudes ranging from 6.4 to 9.2. The cause of damage at five CMP culvert sites and two cast-in-place reinforced concrete box culvert sites was attributed to embankment penetration. Four of the five CMP sites required major repair or replacement of the culvert. In two of the CMP cases, the road was rendered impassible by embankment penetration. At only one of the five sites, the battery of culverts maintained limited hydraulic functionality after the earthquake. Only minor repair was required at the two box culvert sites.

Damage to the CMP culverts included vertical misalignment of the flow line, buckling or bending of the pipe underneath the fill, possibly at the joints, and raising of the culvert ends. Documented culvert sizes ranged from 760 to 1,070 mm in diameter. The embankments subsided as much as 0.9 m and spread laterally as much as 6 m. The resulting subsidence in the

center of the embankment raised the culvert ends as much as 1.8 m. At most of the above described sites, the embankments and the surface pavements also suffered major damage.

Damage to the two cast-in-place reinforced concrete box culverts were less severe than those described above. Longitudinal bending of the culverts opened transverse cracks, which were in the weak direction of reinforcement. The widths of the cracks ranged from as much as 13 mm in the floors of the boxes to hairline cracks in the top slabs. The box configurations included a triple-celled 2.6 m wide by 1.8 m high as well as a single-celled 2.4 m high by 2.4 m wide cross sectional configuration. In both of these cases, embankment penetration was slight. Surface damage included cracks in the pavement at the edge of the culverts and at other locations in the liquefied zone not over the culverts. In one case, blocks of asphalt road surface and concrete gutter were buckled and pulled apart. Total vertical misalignments of 6 to 10 mm were reported.

It should be noted that a similar reinforced concrete box culvert as well as four CMP culverts were identified in the vicinity of the damaged box culverts described above. Upon inspection, they were found to have suffered no damage, even in the presence of 0.5 g accelerations. Obviously, ground instability was not a factor at these additional sites.

Davis and Bardet (1998) inspected two CMP culverts that suffered beam-type bending during the Northridge earthquake. Both measured 1.52 m in diameter and were encased in concrete. Both performed well during the earthquake. Although the joints slightly separated due to foundation and embankment deformations, the concrete surrounding these culverts remained intact. Liquefaction was observed in the area. However, the magnitude of permanent ground deformation experienced at the culvert site was not reported. Concrete encasement appears to be a promising retrofit measure to prevent CMP joint pull-apart under embankment penetration.

5.3.2.2. Lateral and Embankment Spreading

Like embankment penetration, lateral spreading of ground surfaces and embankments are also caused by unstable foundation soils that either liquefy or collapse during strong ground shaking. Significant lateral spreading can occur, even over very gently sloping ground. Culvert damage usually associated with lateral spreading includes vertical and horizontal misalignment, pull-apart of the joints and separation of the culverts from end appurtenances such as headwalls, wingwalls and flared end sections. Also, unbalanced horizontal and vertical pressures can overload culvert walls, causing ovaling, racking and overstress.

Youd and Beckman (1996) documented culvert damage due to lateral spreading that extended as much as 1.8 m horizontally and 1.4 m vertically. Two CMP and two RCP culverts suffered major damage, although no road closures occurred. One of the CMP culvert sites was part of a dam. In addition to these four, one reinforced concrete box culvert suffered only minor damage.

For most CMP, the major damage was observed to be joint and end appurtenance separation. However, in the case of a liquefaction zone experiencing ground accelerations exceeding 1.0g, a 2,400 mm diameter CMP culvert collapsed. The cause of the collapse was attributed to excessive unbalanced lateral pressure. The height of cover over the failed section varied from 4.2 to 12 m. The portion of the culvert having less than 3.7 m of cover did not appear to be

damaged. The CMP was an extension of an older RCP of the same diameter. The connection was made at the deepest point. No damage was noted in the adjacent section of RCP.

Considering these facts, another likely contributing factor to this failure was the loss of the soil envelope support due to the reduction of shear strength in the liquefied soil. Flexible culverts, such as CMP and plastic, depend almost entirely upon the shear capacity in soil support to maintain their shape under load.

However, reporting on this same collapse, Davis and Bardet (1998) noted that only a portion of the culvert segments were in the liquefied zone. The remaining segments were in non-liquefiable bedrock and alluvium. Hence, they contend that strong ground shaking alone triggered the collapse along at least a portion of the culvert's length.

Damage in RCP culverts due to lateral spreading generally occurred at the joints. In addition, some RCP culverts suffered joint hammer, or opening and closing of the joints, during ground oscillations. This could have occurred with impact, intensifying the damage. Spalled concrete surfaces at joints and exposed rebar were noted during the inspections.

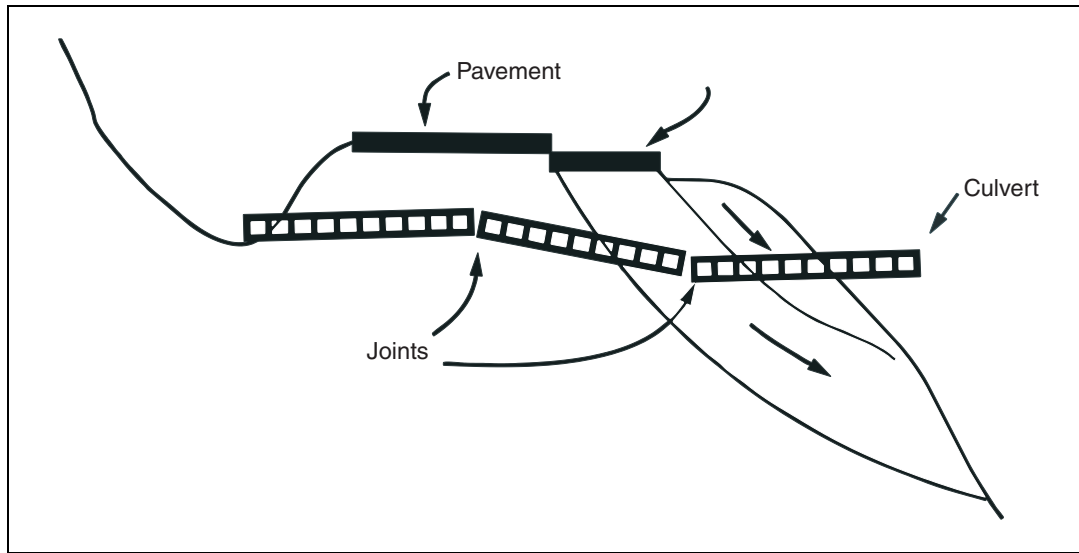
Several cases of lateral spreading were also noted at sites having multiple barrels of cast-in-place reinforced concrete box culverts. Even where the construction joints in these structures were designed for strength transfer from one section to another, tension rupture of the rebar, spalling of the concrete and separation of the construction joints were observed. This may be indicative of a design deficiency that inadequately represents the strength capacity required for the joint to withstand a seismic event.

Notwithstanding this type of misalignment and joint damage, the barrels between the joints of CMP, precast reinforced concrete and cast-in-place reinforced concrete culverts all generally performed well under lateral spread.

5.3.2.3. Slumping of Fill and Landslides

This type of ground failure occurs at steep slopes composed of materials that becomes unstable during strong ground shaking. Slumping of fill or landslides can damage highway culverts installed at these locations. Damage could include longitudinal and transverse bending of culvert barrel sections or separation, misalignment and fracturing of the culvert joints. A typical failure diagram is illustrated in figure 5-11.

Youd and Beckman (1996) reported only one instance of this type of culvert failure. The slump rotated and slid downward about 0.9 m. The 900 mm diameter CMP did not crush or tear, but rather rotated and stretched at the joints. The joints were pulled apart as much as 150 mm. Angular rotations about the joints were as much as 5 degrees. However, this particular culvert was over-wrapped with a 0.3 m to 0.6 m length of curved corrugated metal sheet at each joint. Hence, even though joint separation occurred, the culvert continued to function after the earthquake without being blocked by slumping soil. However, the road was impassible as a result of the slump. Apparently, the original design of the culvert assumed the potential occurrence of slope instability, since over-wrapping has not been a standard installation practice.



Youd and Beckman, 1996

Figure 5-11. Embankment slump (similar effect on culverts as landslide).

5.3.2.4. Surface Faulting

Surface faulting occurs when a fault rupture extends to the ground surface. Tectonic deformation zones can include vertical and lateral surface fractures, compression buckling, and crustal uplift or subsidence. Also, strong ground shaking generally accompanies surface faulting. Culvert failures associated with surface faulting include longitudinal and transverse bending of the culvert barrel sections, separation, misalignment and fracturing of the culvert joints and separation, fracture and collapse of culvert end sections.

In an area where surface faulting, diffuse tectonic deformations and strong ground shaking of 0.4 g occurred, Youd and Beckman (1996) inspected approximately 20 CMP and one plastic culvert. They found virtually no damage to the culverts or to the associated road pavements that could be attributable to the seismic event. However, none of these culvert alignments intersected surface fractures, even though many fractures occurred in the vicinity. Also, the ground upheaval due to faulting did not render the road impassible at the culvert sites. Nonetheless, the culverts had been subjected to strong ground shaking and mild tectonic deformations.

Reinforced concrete pipe was also documented to do well in surface faulting zones experiencing mild tectonic deformations and where no surface fractures intersected the culvert alignment. However, they did find examples of RCP in areas where ground upheaval, fractures and significant offsets had occurred. Here moderate-to-severe damage of the RCP joints were noted. This included joint separations, misalignment, shear failure, spalling and exposure of the reinforcing steel. It was considered likely that some of the joint damage was attributable not only to surface faulting but to ground oscillations produced by longitudinal compression waves that resulted in joint hammering. However, no barrel fractures or spalling beyond the joints were noted. The road was passable after the earthquake. However, two RCP culverts required major repair or replacement of some sections as a result of the faulting.

Reinforced concrete box culverts were also studied in areas of surface faulting. Where diffuse tectonic deformation occurred, cracks developed in the tension zones of wall cross sections. In many cases, these cracks were repairable. However, in areas of severe tectonic deformations and ground fracture, major shear and moment failures in the walls, inverts and roofs were experienced. Characteristically, the walls were deflected inward as much as 0.3 m at mid-height. Again, the road was passable but major repairs and replacement of portions of the culvert were required.

5.3.2.5. Ground Shaking

All of the above empirical observations involved permanent ground failure in one form or another. Ground shaking is transitory and, of course, occurs integrally with and is a part of the other responses detailed above. However, when it is not accompanied by some type of permanent ground failure mechanism, experience has shown that even strong ground shaking does not appear to cause catastrophic damage to smaller diameter highway culverts (1 m or less), whether flexible or rigid. Nevertheless, there are some circumstances under which ground shaking, acting alone or in combination with inertial effects, can impact culvert performance. These include culvert joints with little or no ductility in either tension or compression, large span culverts, culverts under high cover, culverts with non-circular cross sections and unreinforced concrete or masonry culverts.

Youd and Beckman (1996) reported instances where RCP culverts experienced damage in the presence of ground shaking. However, none rendered the roads impassable. The evidence suggested that permanent ground failure mechanisms, such as liquefaction, were absent at these sites. In one case, a 2,210 mm diameter by 63.4 m length of RCP culvert under about 8 m of fill was damaged during the 1971 San Fernando earthquake. Distress was concentrated at the joints and included spalling with exposed rebars that were twisted and/or sheared. Cracks varied from 5 to 10 mm in width. Also, displacements of 38 to 51 mm were noticeable at the joints. The culvert was later repaired using a protective steel liner plate.

Youd and Beckman (1996) also inspected a number of reinforced concrete box culverts in areas that experienced 0.5 g to 1.0 g under 3 m or less of cover. Again, evidence of ground failure mechanisms was absent. No visible damage was detected in any of those inspected. However, a box culvert under 7.6 m of cover and another one under 20 m of cover suffered significant damage, which included lateral racking and cracks in the walls and ceiling. Transient ground deformation likely contributed to the damage under these heavy covers. This damage was repaired after the earthquake.

A 2,100 mm diameter unreinforced concrete pipe was also reported to have sustained damage in the presence of 0.5 g ground shaking, but without the presence of other ground failure mechanisms. Longitudinal cracks were practically continuous, mainly between the 8 and 11 o'clock and 2 and 4 o'clock positions. Cracks up to one inch wide with lateral offsets up to one inch were noted. Also, peripheral cracks at joints were observed. A 183 m length was badly damaged and appeared no longer serviceable. The investigators suggested that unreinforced concrete may be too weak and brittle to provide satisfactory culvert performance in earthquake prone areas.

Davis and Bardet (1998) suggested that either transverse or longitudinal ground shaking, or both, triggered axial and/or lateral deformation, wall buckling and bolt shear of one structural plate and portions of two CMP culverts during the Northridge earthquake. The structural plate was 3.81 m in diameter. The CMP culverts, although at different locations, were both 2.44 m in diameter. As noted earlier, peak ground accelerations exceeding 1.0 g were experienced in the vicinity of these culverts.

5.3.3. SUMMARY OF CULVERT SCREENING CRITERIA

The above described theoretical and empirical observations of culvert performance under various modes of seismic response do not provide a statistically meaningful basis for analysis of all the factors involved in the resistance of culverts to seismic damage. However, they do provide a basis for a number of general and qualitative conclusions, which are summarized in the paragraphs that follow.

First, zones of permanent ground failure were observed to produce the largest deformations and the greatest damage to culverts. Also, no culvert types, shapes or sizes were found to be immune to damage by this cause. However, the empirical observations reviewed above reveal that, under cases of moderate to severe liquefaction, thin-walled flexible culverts were found to be more susceptible to buckling or collapse of the cross section than rigid culverts. On the other hand, in areas exposed to slumping of fills, landslides or fault ruptures, joints that fail to provide continuity and ductility were found to exhibit the greatest liability. Furthermore, the deformations that could develop in zones of permanent ground failure may be so great that the capacity of normally available culvert systems of any type may not have the capacity to accommodate them without special design.

Second, strong ground shaking, when not accompanied by ground failure, generally has not appeared to cause significant damage to small culverts one meter or less in diameter, regardless of type. However, the empirical evidence has shown that the damaging effect of ground shaking on culverts increases with size and length. This effect also varies with culvert shape and type. Circular cross sections are more resistant than noncircular. Ductile materials, such as metal, plastic or reinforced concrete perform better than unreinforced or brittle materials. Moreover, in the presence of strong ground shaking, longitudinal joint ductility in both tension and compression was observed to be important. Numerous cases of damage from joint hammering were noted, primarily in the rigid joint designs.

These limited empirical observations as well as the theoretical considerations given above provide a basis for screening culverts relative to their need for further evaluation and, possibly, retrofit. The suggested logic for doing so is illustrated in figure 5-12.

Only culvert systems commonly employed in highway applications are included. Still, the potential range of shapes, sizes, types, ground conditions and seismic effects make all but the most generalized treatment a daunting task. Undoubtedly, more detailed screening criteria could be developed and might be justified under some circumstances.

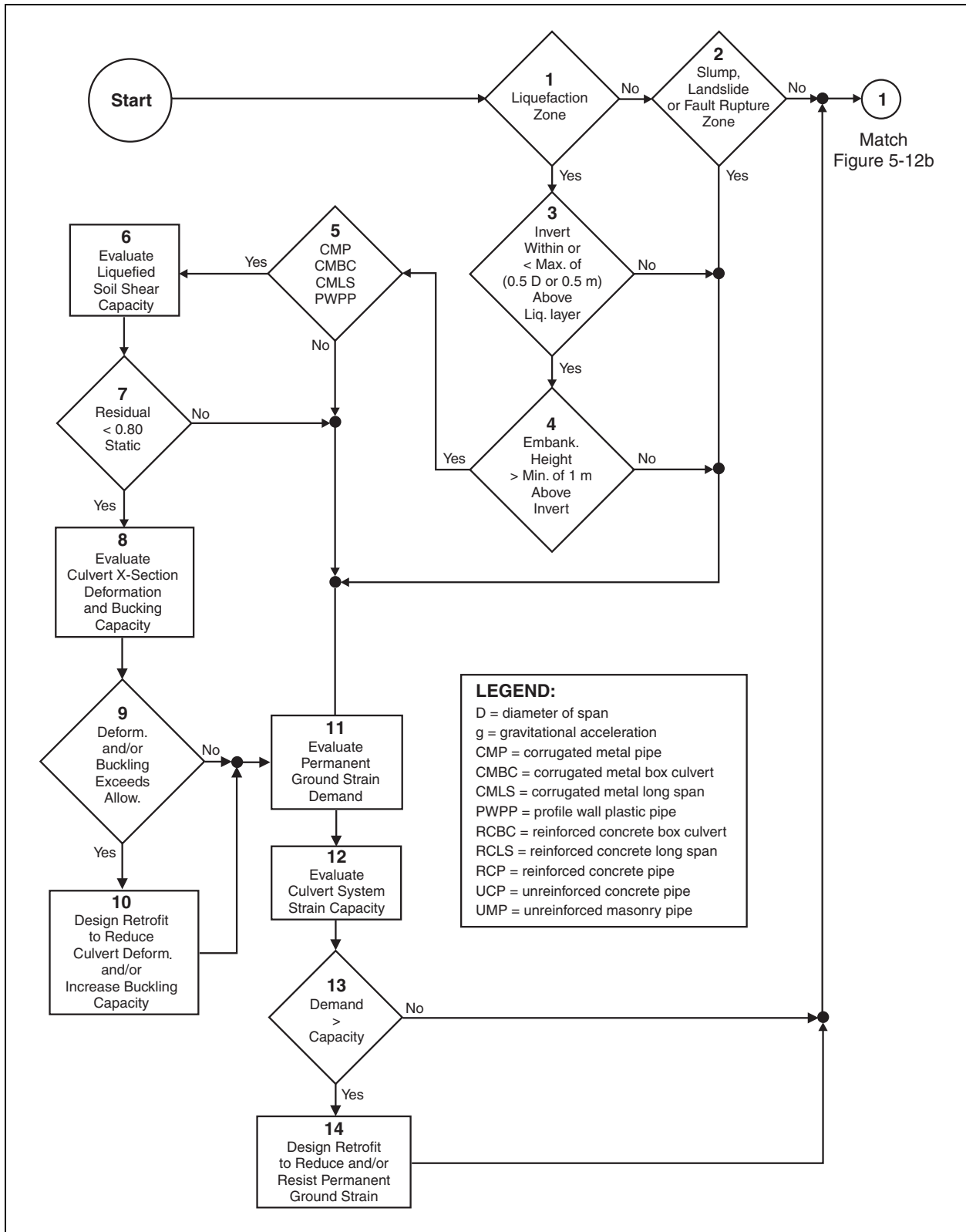


Figure 5-12. Flowchart of screening procedure for culverts under (a) permanent ground deformation and (b) transient ground deformation.

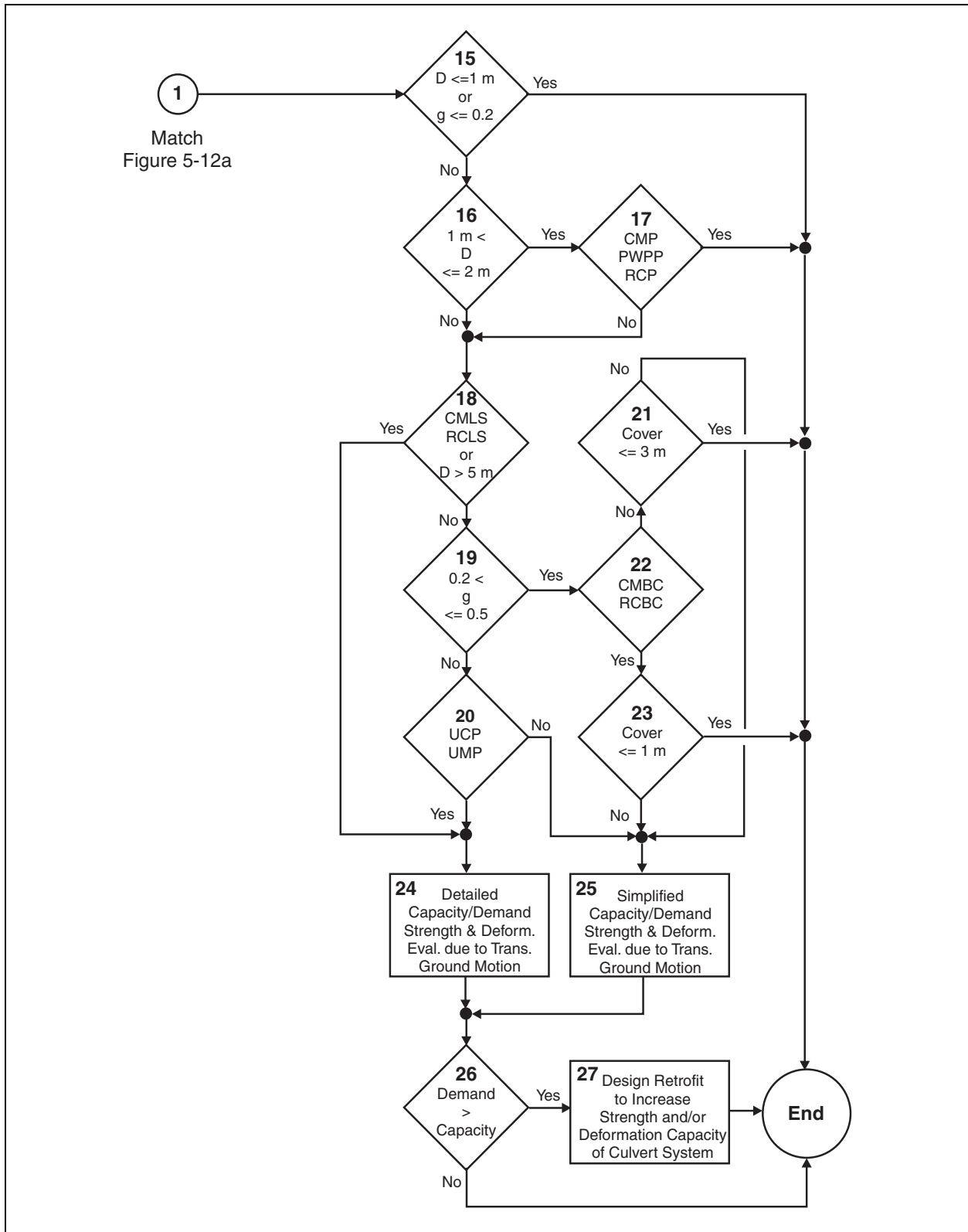


Figure 5-12. Flowchart of screening procedure for culverts under (a) permanent ground deformation and (b) transient ground deformation.

Figure 5-12(a) proposes logic for screening culverts under the action of permanent ground deformation. In order to make a retrofit decision, both the ground strain demand and the culvert system strain capacity must be evaluated in all three principal axes. Cases in which the liquefaction zone or its overburden would experience only minor strains are neglected, or screened-out. However, when flexible culverts exist in major liquefaction zones, an extra step is required. If a significant reduction in shear strength is predicted due to liquefaction, still another evaluation is then required to assess the magnitude of culvert deformations and the potential for buckling of the culvert cross section that could occur as a result of the loss of side support.

Once a retrofit decision is made regarding permanent ground deformations and/or buckling of flexible culverts due to liquefaction, strong ground shaking alone must be considered. Figure 5-12(b) proposes logic for screening culverts under the action of transient ground motion. Here the retrofit decision is based on the strength and deformation capacity of the culvert system compared to the demand generated by ground shaking. This requires a fundamentally different evaluation process than for permanent ground deformations, hence the development of two separate decision matrices. Again, the effects of transient ground motion must be evaluated in all three principal axes.

Because case histories and theoretical considerations suggest that the influence of ground shaking is graduated over some scale, the decision matrix shown in figure 5-12(b) is also graduated. Smaller culverts and low level seismic events are screened out immediately. Culverts of intermediate size that are subjected to moderate loads and midlevel seismic events undergo a simplified evaluation process. Large, non-circularly shaped and unreinforced culverts subjected to mid and high level seismic events undergo a detailed evaluation process. It is anticipated that 95 percent (or higher) of highway culverts will be screened out by this decision matrix, not requiring retrofit. This is in agreement with both current perception of culvert performance during earthquakes as well as the limited case histories of ground shaking alone.

Based on these flowcharts, two shortcuts can be observed for sites not susceptible to permanent ground displacements. First, retrofitting is not recommended for any culverts less than 1 m in diameter or with a design acceleration less than 0.2 g. Secondly, for CMP, plastic pipe, and rigid culverts with diameter less than 2 m, no retrofitting is recommended.

The limits shown for the various branches of the decision matrices of figure 5-12(a) and (b) are thought to be somewhat conservative. However, it should be emphasized that no statistical basis for these limits can be reasonably derived from the small sample of case histories of culvert performance during earthquakes that has been documented to date.

5.3.4. COMMENTARY ON SCREENING PROCEDURE

The purpose of the screening procedure shown in figure 5-12(a) and (b) is to provide a rapid, low-cost approach to identify culverts with significant probability of collapsing or sustaining unacceptable damage during future earthquakes. Because culverts are generally resistant to seismic forces and because highway damage due to culvert damage or collapse can usually be repaired rapidly, highway agencies generally have not been concerned about the seismic hazards associated with culverts. However, to assure post-earthquake operability of critical highway

segments, culverts must remain functional. Critical highways include those where closure, even for a short period of time, could immediately and adversely effect national defense, public safety, or emergency response, or where culvert blockage could lead to unacceptable environmental damage. Screening provides a logical first step for assessment of culvert performance. Although the screening procedure presented here is specifically for critical highway segments, the procedure may be applied to any highway system.

The first step in the screening procedure (see figure 5-12(a)) is to determine whether the culvert lies in a liquefaction, slump, landslide or fault rupture hazard zone (Elements 1 and 2). If the culvert is not in one of these zones, then damage due to permanent ground deformation is unlikely, and the screening proceeds to an evaluation of effects of transient ground motions (figure 5-12(b)). If the culvert lies in one of these hazard zones, then culvert stability and permanent ground strain potential need to be evaluated. If the site is nonliquefiable, but within a slump, landslide or fault hazard zone (Element 2), the screening proceeds directly to an evaluation of permanent ground strain potential (Element 11). Procedures for estimating permanent ground strains are provided in chapters 3 and 4 of this manual.

If the culvert lies in a liquefaction hazard zone, then damage is possible due to loss of side support (Element 3) or penetration of the highway embankment into the liquefied soil (Element 4). To assure that loss of side support will not occur, the culvert should not lie within or immediately above the liquefiable layer. Based on past performance and conservative engineering judgment, significant loss of side support does not occur when the liquefiable layer lies more than twice the culvert diameter or a minimum of 0.5 m beneath the culvert invert (Element 3).

Embankment penetration does not occur unless the embankment has sufficient weight to cause compression or shear failure within the liquefied foundation soil. Based on past performance, embankment heights greater than 1.0 m are required for significant penetration to occur. Thus, if the embankment height is less than 1.0 m (Element 3), penetration is not a significant hazard and the screening procedure proceeds to an evaluation of ground strain potential (Element 11). Procedures for estimating ground strain at liquefaction sites are provided in Part 1 of this manual.

If the ground surrounding or overlying a culvert is susceptible to loss of sidewall support or embankment penetration, the screening continues to Element 5, culvert types. If the culvert is a rigid type, such as reinforced concrete (RCP) or unreinforced concrete (UCP) or masonry (UMP) pipe, the culvert is not vulnerable to loss of sidewall support or collapse due to embankment penetration and the screening proceeds directly to an evaluation of ground strain potential (Element 11).

If the culvert is a flexible type of culvert, corrugated metal pipe (CMP), corrugated metal box culverts (CMBC), corrugated metal long span (CMLS) culverts or profile wall plastic pipe (PWPP), the screening proceeds to Element 6, evaluation of the shear strength of the liquefied soil. If the estimated residual strength of the liquefied soil is greater than 0.8 times the static shear strength, damaging loss of sidewall support is not likely and again the screening proceeds to Element 11, evaluation of permanent ground strain potential. If the soil is susceptible to large strength loss (greater than 20 percent), an evaluation of the deformation and buckling and capacity of the culvert is required (Element 8). If excess deformation or buckling is possible

(Element 9), retrofit is needed to increase the buckling capacity to assure post-earthquake highway operability. Even after retrofit to prevent buckling, the culvert may still be vulnerable to failure due to excess ground strain. Thus, the screening proceeds to Element 11, an evaluation of permanent ground strain potential.

If the calculated ground strains (Element 11) are less than the calculated strain capacity of the culvert (Elements 12 and 13), the culvert is not vulnerable to damage due to permanent ground displacement and the screening proceeds to an evaluation of the effects of transient ground motions (see figure 5-12(b), Element 15). If the calculated ground strains are greater than the capacity of the culvert can withstand, then retrofit is required to improve seismic culvert performance (Element 14). Such retrofit could include ground improvement to decrease ground strain potential or structural modification to improve culvert strain capacity. Procedures for these improvements are discussed in Part 1, and chapters 3 and 4 in this manual.

The flowchart in figure 5-12(b) carries the screening process through an evaluation of culvert performance due to excitation by transient ground motions. If the culvert diameter is less than 1.0 m or the anticipated peak acceleration, a_{max} , is less than 0.2 g (Element 15), the culvert is too small or the motions too weak for damage to occur. The inherent strength of small-diameter culverts makes them very resistant to damage due to transient ground motions, and ground strains generated by motions with a_{max} less than 0.2 g are too weak to damage even the most vulnerable culvert types. Thus, if the answer to the question in Element 15 is yes, the screening is complete and seismic damage is highly unlikely.

If the diameter of the culvert is between 1.0 m and 2.0 m (Element 16) and the culvert is constructed from CMP, PWPP, or RCP (Element 17), the culvert is also immune to seismically generated damage and the analysis is complete. These types of culverts have proven to be resistant to transient seismic forces during past earthquakes.

If the culvert diameter is greater than 5.0 m or the type is CMLS or RCLS, detailed strain capacity and demand analyses are required to assure that the culvert can withstand strains likely to be generated by the transient ground motions (Element 24). Few of these types of culverts have been shaken by large transient ground motions during past earthquakes to test their performance, so specialized analyses are required to assure their safety. If one of these long span culverts should collapse, the damage to the highway could present a safety hazard and be very disruptive to highway operations.

If the culvert is less than 5.0 m diameter, the estimated a_{max} is greater than 0.5 g (Element 19), and the culvert is unreinforced masonry (UMP) or concrete (UCP) pipe (Element 20), the structure is vulnerable to collapse and detailed seismic capacity/demand analyses are required to assure culvert safety (Element 24).

If a_{max} is greater than 0.5 g, the culvert type is other than UCP or UMP, and the cover is less than 3.0 m thick (Elements 20 and 21), the culvert is immune to earthquake damage and the screening is complete. If the cover is greater than 3.0 m, inertial forces applied to the culvert through the cover material may be sufficient to overstress it and detailed capacity/demand analyses are required. Similarly, if the culvert is a box structure (CMBC or a RCBC) and the cover is less than 1.0 m, it is immune to seismically induced damage and the screening is complete. If the

cover over a box structure is greater than 1.0 m thick, however, inertial forces may damage the culvert (Element 23) and analyses are required to assure safety. In this instance, simplified capacity/demand analyses may be applied to evaluate culvert performance (Element 25). These criteria are based on observed culvert performance and conservative engineering judgment.

If the capacity/demand analyses (Elements 24 and 25) indicate that expected transient ground strains will not overstress the culvert, it is classified as safe and the screening and analysis is complete. If unacceptable damage is likely, then retrofit is required to strengthen the culvert.

5.4. EVALUATION TECHNIQUES

The flowcharts shown in figure 5-12(a) and (b) call for evaluations to be performed if certain criteria are met. In the case of permanent ground failure, the primary evaluation step requires estimation of the ground strains that are likely to be produced in directions that are both parallel and perpendicular to the axes of the culvert. These strain demands are compared with the capacity of the culvert system to either accommodate or resist them, which provides the basis for a retrofit decision.

In liquefaction zones, an additional evaluation step is required for flexible culverts. The residual soil shear capacity must be determined. If it is found to be significantly less than the static capacity, the ability of the culvert cross section to resist buckling and large deformations must then be evaluated.

In the case of transient ground motions, both the inertial force fields and transient ground strains that are likely to develop during the earthquake must be estimated for both the longitudinal and transverse axes of the culvert. These demands are then compared with the strength and deformation capacities of the culvert system to determine if seismic retrofit is needed.

The following paragraphs describe some of the evaluation methods available to determine the effects of both permanent ground failure and transient ground motion on culverts. Since some of these methods apply to other highway components as well as to culverts, they may be treated elsewhere in this report, and references to other chapters are cited where appropriate.

5.4.1. PERMANENT GROUND FAILURE

To evaluate permanent ground failure, the basic assumption employed is that culverts will move coincidentally with the ground as seismically generated ground failure occurs. This assumption is conservative in that it neglects any deformation of the ground around the culvert and slippage between the culvert and the backfill. Most culvert types are not sufficiently strong to resist the forces imposed by ground failure; hence ignoring deformation and slippage is reasonable. During ground failure, culverts may be forced to undergo deformations that could be much larger than they are typically designed to accommodate, which can lead to damage.

If the predicted ground displacements and strains are greater than the culvert can withstand without rupture, retrofit measures may be considered. Such displacements, however, would

likely disrupt the roadway surface and joint separation of an underlying culvert may be of secondary importance. As noted in chapter 6, highway agencies in general prefer to rely on post-earthquake repair of roadway damage as a mitigation strategy, rather than pre-earthquake retrofit measures. This preference also applies to culverts because culvert damage rarely leads to immediate catastrophic roadway damage. Thus, as part of any post-earthquake roadway repair, damaged culverts may also be repaired or replaced. Because active strategies are not being proposed or applied by highway agencies, no procedures or example calculations are given here for retrofit of culvert structures.

Once permanent ground strain demands are estimated in both the longitudinal and transverse directions of the culvert axes, they must be compared to the strain capacity of the culvert system. If the demand exceeds the capacity, a retrofit decision must then be made. To avoid damage, retrofit strategies must be developed and deployed that will allow the culvert to accommodate the required deformations or remediate the ground and, thus, eliminate the cause of the potential ground failure. In some cases, a combination of both retrofit strategies may be the most cost effective solution.

In order to design a culvert retrofit measure for potential ground failure, the first step is to estimate the strains that would likely be associated with this failure. Part 1 of this manual describes the analysis for liquefaction and its resulting ground strains. Analyses procedures for liquefaction induced ground failures are described in chapter 4. In this report, chapter 3 describes methods for estimated slope stability and associated ground movements, and chapter 4 describes methods for estimating fault displacements and assessing their effects on tunnels. However, since these methods were not developed and verified specifically for culverts, they may or may not be directly applicable to all the varieties and specific design aspects of culverts. Hence, their applicability must be assessed for the specific case under consideration.

In addition, a number of other investigators have applied various theoretical and empirical evaluation methods to the prediction of the seismic performance of buried pipelines under the action of permanent ground failure. These include O'Rourke, T., et al. (1985, 1986), Wang et al. (1991), Yeh and Wang (1991), Miyajima and Kitaura (1991a, 1991b), Lopez and Berrones (1994), Honegger (1994), Liu and O'Rourke, M. (1997), and Trifunac and Todorovska (1997). However, these methods were developed primarily for pressure pipelines that extend over significant lengths. They have not been directly applied to culvert installations. While it is expected that many of these methodologies may be successfully adapted to culverts, much more theoretical development and experimental verification is needed to confirm the validity of such adaptation.

Even though very little experience has been developed regarding the prediction of culvert performance during seismically induced permanent ground failure, it is expected that consideration of this aspect of performance will be required for important highway facilities that include medium to large culverts. A brief discussion of each major permanent ground failure mechanism and the recommended factors to be considered during evaluation are given below.

5.4.1.1. Embankment Penetration

Analytical or empirical procedures for predicting embankment penetration have not been developed for application in engineering practice. The following paragraphs provide guidance on factors controlling penetration and general procedures that could be applied to predict penetration and associated ground deformation. Embankment penetration is the vertical settlement of an embankment cross section caused by a classic shear failure of the underlying strata. Either single or double shear planes could develop. Some outward and upward motion of material within the failure envelope is likely to occur at the toe of the embankment slope.

The first step in preventing damage to culverts due to embankment penetration is identification of locations where ground instability is likely to occur in the foundation soil below an embankment. The second step requires predicting the magnitude of the deformation. The following factors are known to be important in predicting the occurrence and magnitude of embankment penetration:

- Presence of liquefiable or sensitive soil layers below embankments.
- Presence of a water table.
- Thickness of unstable strata.
- Magnitude of ground shaking.
- Height and geometry of embankment.

5.4.1.2. Lateral and Embankment Spreading

Guidance for the prediction of liquefaction and lateral spread displacement are covered in Part 1, chapter 4. These procedures can be applied to predict the occurrence of liquefaction and amount of possible lateral spread displacement at culvert sites. Liquefaction and lateral spread can occur with or without the presence of an embankment. Conservative estimates of the amount of extension of a culvert due to lateral spread can be made using the procedures in Part 1, chapter 4

5.4.1.3. Slumping of Fills and Landslides

Slumping of fills during ground shaking is a classical slope stability problem with a dynamic component. The slope deformation analysis methods described in chapter 3 can be used to predict both the occurrence of a slope failure due to earthquakes as well as the approximate travel length of the failure wedge. However, predicting the relative movements of a road surface or culvert within the sliding mass may be problematic except for small movements and simple geometric layouts. The following factors are known to be important in predicting the occurrence of slope failure during earthquakes:

- Magnitude of ground shaking.
- Slope of ground surface.

- Geometry of critical failure surface.
- Presence and depth of groundwater.
- Geometry of the roadway cross section within the failure surface.
- Frictional and cohesive strength of the in-situ materials.

5.4.1.4. Surface Faulting

If the surface trace of an active fault crosses a culvert alignment, geotechnical studies are required to assess the potential displacements that may occur in the event of an earthquake on the fault. Earthquake magnitude is an important factor in determining the amount of displacement, and correlations of fault displacement with magnitude have been developed as described in chapter 4. The determination of the possible distribution of displacements within the defined active fault zone (whether concentrated in a very narrow zone or distributed over a broad zone) requires geological assessments.

5.4.2. TRANSIENT GROUND MOTION

To evaluate the transient ground motion effects on culverts, the basic assumption employed for permanent ground failure regarding coincidental movement still applies to culvert deformations. However, transient ground deformations are typically much smaller than those experienced during permanent ground failures. Hence, they are not as likely to lead to culvert failures or to immediate collapse. Nevertheless, as documented previously, joint hammer and pull-apart due to transient ground motion can lead to the migration of fine soil particles, thus to the development of sink holes and, ultimately, to the collapse of road surfaces, which can be both expensive to repair and deadly to the unsuspecting motorist.

On the other hand, the assumption of coincidental movement does not strictly apply to the component of transient ground motion responsible for inertia. This is because the intensity of inertial forces during a dynamic event is related to differences in mass rather than strain. Since culverts represent low mass inclusions, consisting mostly of air, that are surrounded by a high mass (soil) media, the potential for the development of inertial forces exists. Inertial effects can produce both racking and overpressure forces in the transverse axis of the culvert and frictional forces in the longitudinal axis.

However, experience has shown that both transient ground strain and inertial forces are negligible for small culverts. Acting in all three principal axes, these effects become more dominant as earthquake intensities, culvert sizes and cover heights increase and with shapes that deviate from a circular cross section. Hence, the screening flowchart in figure 5-12(b) suggests a graduated consideration of culvert size, height of cover, and shape for transient ground motion.

Due to their small numbers compared to other culvert types, little is known regarding the seismic performance of the largest and most noncircular culvert sizes and shapes. These include all large (long) spans of either concrete or metal as well as other types with diameters or spans greater than 5 m. For these types of culverts, detailed evaluations are recommended for moderate-to-

intense seismic events. The primary detailed evaluation method available for this culvert class consists of dynamic numerical modeling that assumes, as a minimum, linear elasticity. If permanent ground failure is also anticipated, large deflection theory and nonlinear material relationships should be included in the numerical analysis, the results of which should also be compared with empirical methods and case histories.

On the other hand, seismic case histories are more available for culverts with intermediate sizes and shapes. Therefore, generally they can be safely evaluated for transient ground motion using simplified techniques. These simplified methodologies typically are closed-formed, equivalent static relationships that assume linear elasticity. Also, they are generally limited to circular or rectangular shapes. The results may be more conservative than would be obtained from the detailed methods described above. However, depending upon the size and length of the facility, the difference in the retrofit demand predicted by a detailed versus a simplified analysis may be overshadowed by the cost differential for performing these two types of evaluations.

There is a large database of seismic performance histories for small diameter culverts. Generally, this history justifies neglecting the effects of transient ground motion for these facilities. Possible exceptions include unreinforced concrete and unreinforced masonry culverts subjected to intense ground shaking.

In order to design a culvert retrofit measure that can accommodate transient ground motion, the first step is to estimate both the ground strains and the inertial forces associated with the seismic event being considered. The following subsections suggest methodologies that can be employed to evaluate these effects on culverts.

5.4.2.1. Longitudinal Response of Culverts Due to Transient Ground Motion

The following factors are known to be important in estimating the level of axial strain in a culvert associated with seismic waves propagating along the culvert longitudinal axis:

- Types of seismic waves dominating the ground motion in the vicinity of the culvert.
- Magnitude of acceleration and velocity components of these waves.
- Frictional and cohesive strength of the site materials.
- Height of cover.
- Soil profile at the site.
- Culvert wall materials and geometry.
- Joint ductility.

The analytical procedures described in chapter 4 for tunnels may be adequate for estimating the axial strains and stresses in a culvert wall due to seismic waves propagating along the culvert longitudinal axis. The modes of deformation are described in chapter 4 and illustrated in figure 4-3(a) and (b).

Under the action of transient ground motion, rigid culvert types are stiffer longitudinally than the surrounding soil. Also, they are stronger in this direction than the frictional forces that typically develop in an earthquake. Hence, any damage due to this response tends to concentrate at the joints. This damage typically consists of joint hammer and/or pull-apart (Youd and Beckman, 1996).

On the other hand, flexible culvert types typically have corrugated walls of one form or another, which results in a lower stiffness longitudinally than the surrounding soil (Takada et al., 1991). Hence, most of the longitudinal energy of transient ground motion is absorbed by flexible culverts without damage to either the culvert wall or to the joints.

5.4.2.2. Transverse Response of Culvert Due to Transient Ground Motion

Transient ground motions in the transverse direction of the culvert axis tend to produce racking or ovaling of the cross section. These deformation modes are illustrated in figure 4-3(c) and (d) in chapter 4 for circular and rectangular cross sections. In addition, transient ground motions can develop both horizontal and vertical inertial forces that can further exacerbate the distress in the cross section of the culvert. The horizontal component of these inertial forces can produce horizontal shear forces acting on the culvert roof as well as additional lateral earth pressures acting on the sides of the culvert. The vertical component can increase the vertical loads transmitted to the culvert roof from the overlying fill. At the same time, it can further add to the lateral earth pressures as well as produce frictional forces acting vertically on the sides of the culvert.

Arching of the overlying fill generally is assumed to reduce the vertical static load pressures on culverts by some factor that depends upon both the culvert type and the backfill material. While arching action would be expected to persist under light to moderate ground shaking, it is not known whether it could continue to be maintained during heavy ground shaking. In the absence of experimental verification, it is safer to assume that arching action could not continue to be counted upon aboveground shaking that exceeded 0.5 g for non-liquefiable foundation materials.

In chapter 4, closed form solutions and simplified procedures are presented for analyzing the cross sectional response of tunnels subjected to strong ground shaking. The solutions may be used for some culverts subject to the conditions of applicability described in chapter 4. For culverts that are assessed to be relatively seismically vulnerable (e.g., unreinforced concrete culverts, or culverts having marginal stability under static loads) and having an unacceptable consequence of failure, dynamic analyses using two-dimensional finite element or finite difference computer codes may be considered. Computer codes that could be considered for this purpose include FLUSH (Lysmer et al., 1975); SASSI (Lysmer et al., 1991), and FLAC (Itasca, 1995). The program FLAC has the advantage over the linear or equivalent linear programs, such as FLUSH and SASSI, of incorporating nonlinear soil constitutive relationships that are able to model soil yielding under higher excitation levels.

5.4.2.3. Examples of Culvert Evaluation Under Transient Ground Motion

A number of investigators have applied various theoretical and empirical evaluation methods to the prediction of the seismic performance of buried pipelines under transient ground motion.

These include O'Rourke, M. et al. (1978, 1980, 1981, 1984, 1988, 1990), Shah and Chu (1974), O'Rourke, T. et al. (1985), Yun and Kyriakides (1988), Miyajima and Kitaura (1991a and 1991b), and Trifunac and Todorovska (1997). However, like those described above for permanent ground failures, these methods were developed primarily for pressure pipelines that extend over significant lengths. They have not been directly applied to culvert installations. Only a few examples of evaluation methods for transient ground motions applied to culverts or to culvert-like structures were available from published and unpublished sources. Some of these have been summarized below.

Byrne et al. (1996a) investigated a three-hinged semi-circular reinforced concrete arch having a 10.5 m span and a 5.2 m rise under 15 m of cover. They considered a seismic event having a peak horizontal ground acceleration of 0.2 g and a peak vertical ground acceleration of 0.13 g. Using full dynamic methods, they found seismically induced bending moments in the wall as high as 140 percent greater than static while wall compression forces were only 8 percent greater than static. These differences were based on the maximum for separate horizontal and vertical components. These investigators also employed equivalent static methods, which produced even greater differences between static and dynamic effects.

Fenves (1989) and Musser (1989b) analyzed the seismic performance of a 13.0 m span by 5.3 m rise multi-radius corrugated steel earth covered (aboveground) arch used for military munitions storage. For ground accelerations that were about 25 percent greater than used by Byrne et al., and employing full dynamic methods, they found that seismically induced bending moments in the wall were as high as 200 percent greater than static while wall compression forces were about 19 percent greater. Possessing much less soil confinement than a typical highway culvert, this example could provide insight into the upper limit of seismic responses that buried highway structures would be expected to undergo.

Chen and Krauthammer (1987) performed an interesting dynamic parametric analysis of a 4 m square reinforced concrete box culvert under three configurations: on the surface, partially buried, and fully buried. They found that under the same dynamic regime, the accelerations it experienced were reduced by 25 to 30 percent when buried to its mid-height, compared to what it experienced sitting on the ground surface and subjected to the inertial effects of its own weight. When buried to a depth equal to its height, accelerations were reduced by 53 to 59 percent of what they were at the surface. Clearly, burial reduces inertial effects as well as adding to confinement and stiffness, which is why culverts perform better during earthquakes than aboveground structures.

Davis and Bardet (1998) investigated a 2.4 m diameter corrugated metal culvert, part of which collapsed during the 1994 Northridge earthquake. They developed a pseudo-static buckling analysis method that was able to account for the failure. They also performed a limited parametric evaluation of the soil profiles along the culvert alignment, some of which did not collapse, and found that the peak ground acceleration and the reduction in stiffness of the embedding soil due to pore pressure buildup were the primary causative factors. They concluded that liquefaction was a contributing but not a necessary factor for failure. Indeed, while complete liquefaction would have most definitely led to collapse, partial liquefaction or other causes of reduction in the stiffness of the backfill envelope or the buckling capacity of the culvert cross section also could have led to collapse.

5.5. RETROFITTING STRATEGIES

The decisions surrounding seismic retrofit of culverts should be based on an optimization of structural, hydraulic, geotechnical and economic considerations. Many choices are available to achieve the same end. The timing of the culvert retrofit may be coordinated with normal repair or replacement cycles of other highway components, such as pavements. Linking culvert retrofit with other repair or replacement programs may influence the retrofit strategies selected.

The design of the culvert retrofit strategy to resist either permanent ground failure or transient ground motion is based on an assessment of the seismic demand compared to the existing capacity of the culvert. Any shortfalls in capacity must be supplied by the retrofit feature or measure. The evaluation section of this chapter suggests methodologies for assessing seismic demand and dynamic capacity. Many culvert guides and design specifications, including those by AASHTO (1999) propose methodologies for assessing static culvert capacity. Some general guidelines are given below.

5.5.1. GROUND REMEDIATION

As noted earlier, most of the culvert damage associated with an earthquake occurs in conjunction with ground instability. Therefore, a primary culvert retrofit measure consists of identifying and remediating unstable ground that may exist along the culvert alignment. Identifying unstable ground and remediation planning measures are dealt with in chapters 3 and 4 as well as in Part 1 of this manual. Therefore, they will not be treated in detail here. Some measures found to be effective in remediating seismically induced ground instability include:

- Dynamic compaction.
- Vibro-compaction.
- Stone columns.
- Slope stabilization.
- Soil reinforcement.
- Overexcavation/replacement.
- Grouting.

Dynamic compaction or vibro-compaction would induce stresses in a culvert due to both the overpressures and the settlement that occurs. These methods would generally not be applicable unless the culvert was removed while the ground was being stabilized. The removal option is discussed in more detail below.

Some of the techniques listed above may be more effective for remediation of one type of ground instability than another. Also, a combination of these techniques may result in the most cost

effective alternative. The primary design strategy involves estimating the reduction of both vertical or horizontal ground deformations that are to be achieved by remediation.

5.5.2. REMOVE AND REPLACE

Seismic retrofit of a transportation corridor requiring significant ground remediation may also require removal and replacement of the culverts along the corridor during construction of the remediation measure. In these cases, a secondary consideration includes the economic choice of replacing the existing culvert with a new one or salvaging and reinstalling the existing one. Obviously, only certain circumstances would justify salvaging and reinstalling an existing culvert. Some cases where this could be cost effective include relatively new culverts under shallow cover that are made of precast or pre-manufactured sections. Also, large, high value culvert installations that can be easily disassembled and reassembled in the field may fall into this category.

If a salvaging option is selected, care must be exercised during removal of culverts in order to avoid mechanical damage that could be inflicted by earthmoving equipment. Another consideration is the necessity of preventing unbalanced earth or equipment loading that could rupture or collapse the culvert pipe during removal. Some types and sizes of flexible culverts may not be cost effective to salvage during removal, due to the careful excavation that would be required to avoid damage.

In addition to the case of ground remediation, removal and replacement of a culvert makes sense if the cost of retrofitting the culvert exceeds the cost of replacing it with a more seismically resistant design. Still another case is if the culvert to be retrofitted is near the end of its useful life or is undersized. On the other hand, removal and replacement generally is not a practical option for deeply buried or cast-in-place culverts.

5.5.3. CULVERT LINERS

Many liners are available for the repair of culvert and pipeline interiors. This includes some of the new cured-in-place thermosetting plastic liner systems that are formed in-situ to fit snugly against the culvert wall interior. Most liners have been developed to inhibit corrosion and/or infiltration or exfiltration. An excellent review of these repair methodologies is given by Ballinger and Drake (1995) and will not be repeated here. These liners may be applicable to the seismic retrofit of culverts where improved joint ductility or the prevention of fines migration at damaged joints is needed. However, many liners are not specifically designed to improve the ductility or structural capacity of the culvert cross section, which limits their applicability to seismic retrofit.

Liners that provide any significant structural improvement to the cross section may also reduce the hydraulic capacity of the culvert, simply because they reduce the existing cross section. The impact of whether this is important depends upon whether the culvert is designed to function at capacity and whether it operates under inlet or outlet control during the design hydrologic event. It is currently common practice by highway agencies to install small diameter culverts that are oversized from a hydraulic consideration in order to avoid future maintenance costs. In these

cases, reducing the existing hydraulic capacity of the retrofitted culvert by installing a liner may not be an issue.

Many embankment cross culverts operate under inlet control at their design discharge. That is, the culvert inlet acts as an orifice that controls the discharge of the culvert. In this case, the culvert barrel could be lined along most of its length without suffering any hydraulic consequences. The transition at the inlet end could then be reconstructed to a larger cross section in order to make up the capacity lost due to the wall thickness of the liner material. Typically, the inlet occurs at the toe of the embankment slope where cover height is minimal, further facilitating this retrofit approach. However, the inlet slope protection would also have to be modified or reconstructed in order to accommodate the larger opening.

Culvert hydraulic capacity should be checked using the procedures in the *Model Drainage Manual* (AASHTO, 1999; FHWA, 2001). Culverts that operate under outlet control are affected by both the diameter and the frictional characteristics of the entire barrel length. In these cases, smooth-walled liners may be able to provide the hydraulic capacity lost due to their thickness, if they are used to line existing culverts that are internally corrugated. However, when this is not the case and a reduction in hydraulic capacity cannot be tolerated, another option is to install a parallel culvert. This additional culvert could be installed by jacking, augering, micro-tunneling, tunneling, or cut and cover methods. It could either augment or replace the existing one.

As can be seen, many factors are involved and many options are available when using liners as a retrofit alternative. Therefore, the decision to line existing culverts and with what materials, or to add parallel culverts, should be based on an analysis of all the structural, hydraulic and economic risks associated with the requirements of the retrofit design scenario.

Once a decision has been made to use a culvert retrofit strategy based on liners, a number of design and installation issues must also be addressed. For instance, it is important to clean the inside of the existing culvert thoroughly and to remove all deleterious material prior to installation. Except for cast-in-place liners, it is also important to fill the annular space between the liner wall and the existing culvert wall with grout. This is because liner design generally assumes full support around the periphery of the liner conduit. Often, culverts are subjected to hydrostatic pressure from groundwater, which without the support of the grout fill, could damage, severely deform or collapse the liner, if left unsupported. In addition to providing circumferential support, the grout fill prevents soil fines from migrating into the annular space between the liner and the host culvert through damaged or leaking joints, which can lead to the formation of sink holes and pavement settlement. However, successful grouting is generally limited to liners large enough in diameter to allow safe personnel access.

During installation, grouting itself can cause damage to culvert liners if not properly controlled. It is important to use low-volume, bottom feed systems that are pressure controlled. Also, sufficient numbers of grout nipples must be provided, both in the cross sectional and longitudinal direction, to assure equal distribution of the grout as well to provide for air relief. Procedures for grouting lined culverts are treated in greater detail by Ballinger and Drake (1995).

In summary, liners can improve the performance of joints and/or they can improve the performance of the barrel. To design the liner for joint performance, longitudinal ductility is the

critical criterion. In the case of barrel performance, cross sectional strength and ductility are the critical criteria.

In general, liners are perhaps the most versatile as well as the most cost effective retrofit materials currently available for improving the seismic performance of many existing culverts. Therefore, a more detailed discussion of specific liner types is given below.

5.5.3.1. Cast-in-Place Liners

Cast-in-place liners have been used extensively for repair of culverts damaged due to seismic activity, deterioration or other causes. To be effective as a seismic retrofit, the liner must be designed as a structural element with adequate reinforcement to develop both ductility and strength. An advantage of cast-in-place liners is that they can be custom fit to each application. An example of a circular cast-in-place liner is illustrated in figure 5-13.

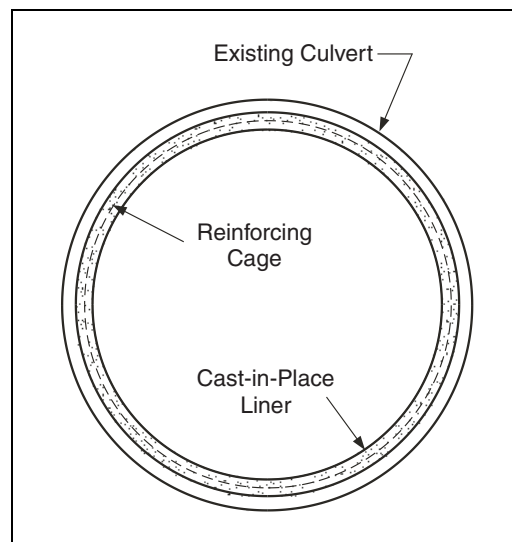


Figure 5-13. Cast-in-place culvert liner.

Shotcrete is the material typically employed for cast-in-place liners. This material can include either wet or dry mortars, or concrete, that is pneumatically projected at high velocity onto the surface to be lined. For tunnel and overhead applications, the dry variety is most commonly employed. Shotcrete can be formulated to have both structural and durable qualities. Its manufacture and application can be strictly specified (ACI, 1995b). In addition, shotcrete can be applied in a thickness that would embed reinforcement and thus, be consistent with the strength and ductility objectives of the seismic retrofit objective. However, the application of shotcrete in these thicknesses requires personnel access to the facility. Therefore, a minimum culvert diameter of about 1,500 mm is required before this method is applicable. Also, strict adherence to specifications and the employment of experienced personnel are the key to a quality installation.

Thorough cleaning and surface preparation are important in order to assure long-term adhesion of the liner to the substrate. Wire mesh or deformed rebar should be attached securely to the existing culvert barrel in order to maintain its position during placement. The design criteria of

the reinforcement should be to maintain tension ductility as well as to enhance concrete confinement during the seismic event.

Generally, the liner would be made continuous over the entire length of the culvert. If control joints are required, they should be carefully detailed so as to not defeat the purpose of the seismic retrofit. This generally means that they should be staggered to be opposite the joints of the host culvert.

This may seem to contradict normal good construction practices that would position control joints where shrinkage cracks are most likely to develop, i.e., at the existing joints of the host culvert. However, depending upon the seismic design scenario, the greatest retrofit reinforcement may be required at the joints of the host culvert. Since control joints must have a reduced structural capacity to work properly, they should be placed where they are least needed for structural capacity. This generally means that they should be staggered opposite the joints of the host culvert. Undoubtedly, shrinkage and temperature cracks will still develop in the liner at the locations of host culvert joints. However, their structural consequence in a seismic event is insignificant compared to the goal of the retrofit strategy to increase the ductility of the host culvert joint.

5.5.3.2. Field Erected Metallic Liners

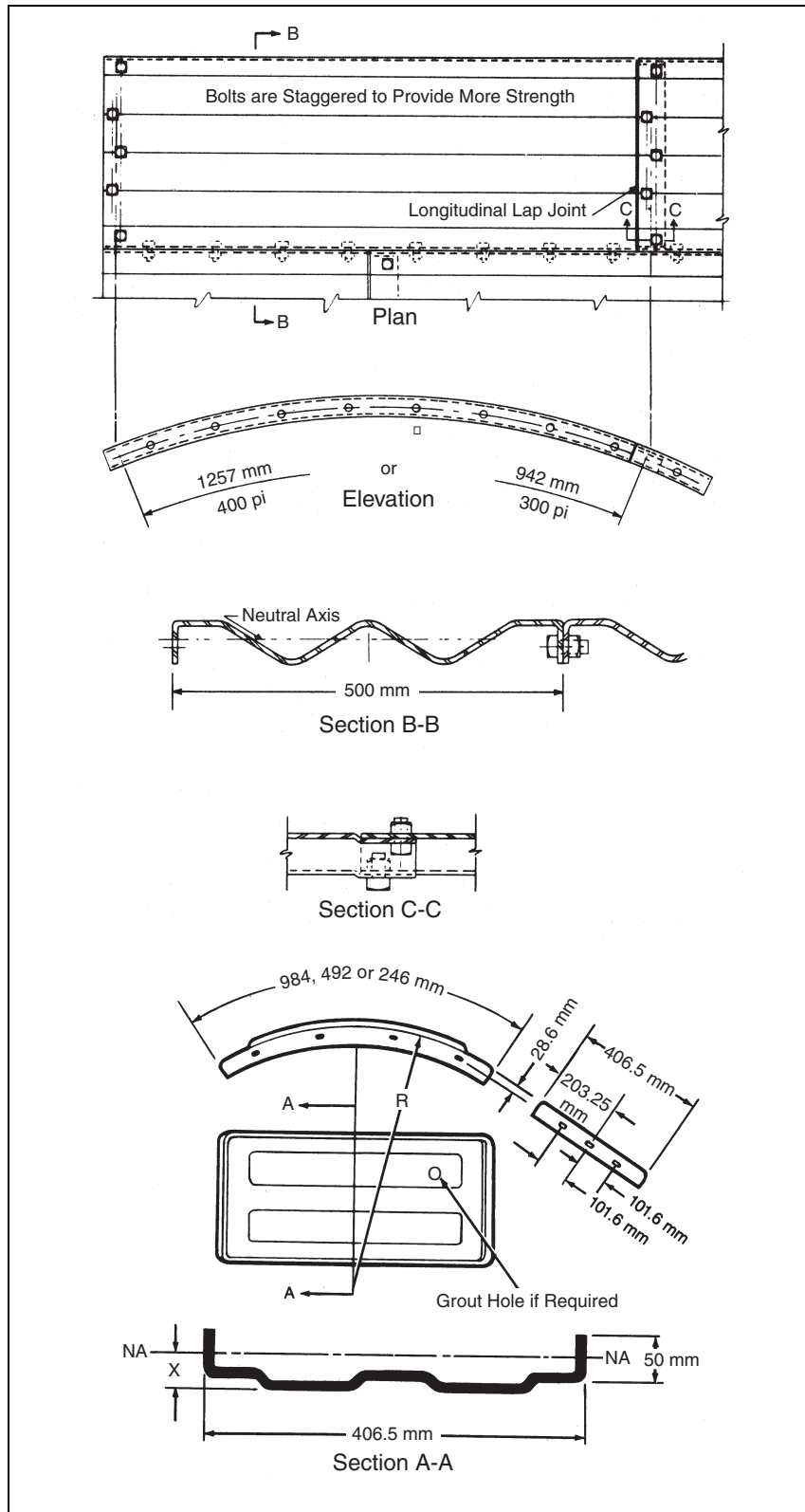
Like cast-in-place liners, field erected metallic liners also have been used extensively for repair of culverts damaged due to a number of causes. The most commonly available metallic liners are fabricated from steel sheets or plates into elements of a circular cross section that can be field bolted together from the inside. Two types are available, two-flange and four-flange as shown in figure 5-14. These lining systems are available in specific wall thicknesses and diameter increments ranging from about 1,500 mm to 7,500 mm. They can be fitted with grout nipples during fabrication to facilitate grouting the annular space between the liner and the existing culvert wall. They can be furnished galvanized to prolong their life in corrosive environments.

The advantages of these liners are that they provide ductility and strength. The strength capacity exceeds that of the liner material itself because the liner provides confinement of the grout fill. This increases the shear capacity of the composite section. A disadvantage is that the hydraulic roughness of the finished interior surface is high.

5.5.3.3. Sliplining

Sliplining is the process of pushing or pulling sections of culvert pipe inside of an existing culvert and grouting the annular space between the old and new cross sections. Many types of materials as well as a wide range of sizes and shapes are available for this purpose including:

- Corrugated metal.
- Spiral rib metal.
- Profile wall thermoplastic.



AISI, 1993

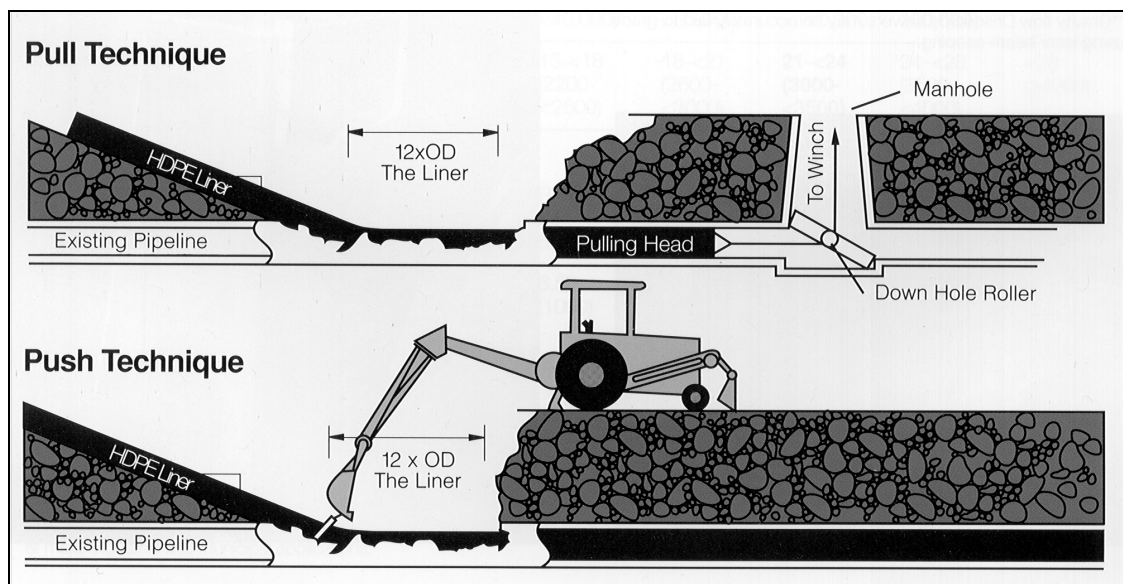
Figure 5-14. Two-flange steel culvert liner plate (top) and four-flange steel culvert liner plate (bottom).

- Smooth wall thermoplastic.
- Fiber reinforced plastic (FRP).
- Precast concrete.

The design of the slipliner material depends upon the retrofit strategy employed. For slipliners that are intended to prevent joint separation and soil fines migration, the primary design criterion is longitudinal ductility. In this case, smooth wall thermoplastics may be the optimum choice.

For slipliners that must help resist cross sectional deformation and buckling, a stiffer wall profile may be more desirable. Slipliners that act as combined structural elements with an existing culvert wall and with the grouted annular space between them can develop significantly increased structural capacity compared to the original culvert wall acting alone. If sufficient roughness can be shown to exist at the interfaces of the inner and outer components of this composite, then at least a portion of full composite action can be developed that will dramatically increase the structural capacity of the total section.

Most potential slipliner materials must be adapted from standard precast or prefabricated products. Their primary application may have been as standalone culvert materials. Hence their joints, clearance dimensions, adaptability to the addition of grout nipples, and their ability to be pushed or pulled into place may not be compatible with the demands of the seismic retrofit objectives. Because the concept of seismically retrofitting culverts is so new, both the designer and the manufacturer may have to exercise significant ingenuity in order to develop systems that are both economically viable and structurally adequate for the intended installation techniques. Typical slipliner installation setups for both the push and pull cases are illustrated in figure 5-15.



Phillips Driscopipe, 1995

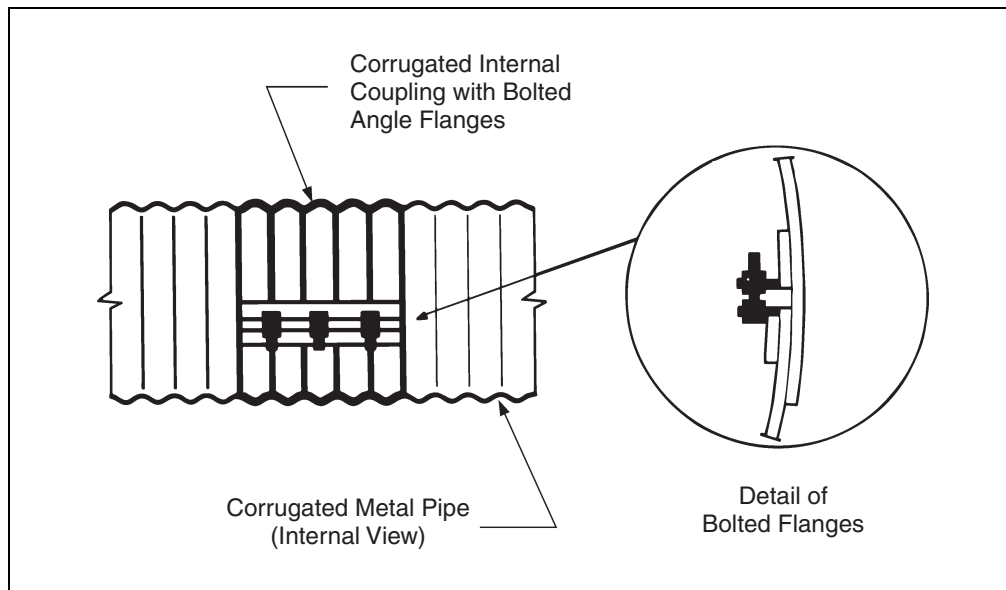
Figure 5-15. Push and pull techniques for installing HDPE sliplining.

5.5.4. JOINT RETROFIT

As stated earlier, one of the primary objectives of a culvert seismic retrofit is to maintain joint closure during ground shaking and after the occurrence of permanent ground deformation. Seismic retrofit schemes for culvert joints should evaluate both the longitudinal and rotational strain demand that are likely to be imposed on the joints by the design earthquake as well as the capacity of the existing joints to accommodate these strains without damage or separation. Details of joint performance can be obtained from manufacturer's literature (ACPA, 1992; AISI, 1993; Uni-Bell, 1991).

As with other structural components, when the strain demand of joints exceeds their capacity, a retrofit is recommended. Many of the lining systems described above are effective for retrofitting culvert joints. They do this by making the joints continuous.

In larger culvert sizes that afford personnel access, another method of retrofitting joints employs specially fabricated internal metal sleeves with angle brackets and bolts. These can be designed to maintain joint closure even if the original culvert joints undergo damage or pull apart. These can be adapted to almost any pipe type or joint configuration. An example of this type of sleeve is illustrated in figure 5-16 for a corrugated metal pipe.



AISI, 1993

Figure 5-16. Internal corrugated sleeve for joining CMP.

CHAPTER 6: ROADWAYS

6.1. INTRODUCTION

Pavement damage has occurred during most large earthquakes. Permanent ground deformation or ground failure, however, has generally been the direct cause of damage. In a few instances, pavement disruption has occurred due to very intense ground motions that locally uplifted or flung pavement sections. These instances, however, have been relatively rare. Consequently, the great majority of pavement damage has been restricted to roadways underlain by poorly compacted embankment materials or foundation materials that are susceptible to seismically induced ground displacement. Common causes of foundation displacement include liquefaction of loose saturated granular layers, slope instability, and surface fault rupture. Hazard evaluation and retrofit procedures for these sources of damage are discussed in the following subsections.

Although retrofit or other mitigative procedures are available to reduce or eliminate most pavement damage, these procedures generally are too expensive to be economically viable for all but the most critical pavement structures. Consequently, most highway agencies have elected to use a passive strategy of rapid repair of pavement damage after an earthquake, rather than an active strategy of retrofitting to prevent damage. Rapid repair is an acceptable mitigative strategy in that pavement damage can usually be repaired rather quickly compared to other types of damage, such as bridge and tunnel damage, and the potential for loss of life or personal injury is small. Thus, pavement damage generally classifies as an acceptable risk and little retrofit activity is occurring among highway agencies. There may be critical highway segments, however, that must be usable immediately after an earthquake where retrofit measures are warranted. The following subsections provide guidance for hazard identification, analysis, and implementation of retrofit measures for those critical highway segments.

6.2. CLASSIFICATION

Pavements are classified into two principal types: flexible pavements constructed of asphaltic concrete (ACP), and rigid pavements constructed of portland cement concrete (PCCP). Each pavement type is supported by a structural section consisting of a base course, embankment where needed, and foundation soil.

For earthquake hazard consideration, further classification is based on potential for permanent deformation of the structural section. In nearly all instances of past earthquake-induced pavement damage, the damage was caused by permanent deformation of the supporting embankment or foundation rather than by failure solely within the paved surface. Many pavements are supported by embankments or foundations that are not susceptible to earthquake-induced permanent deformation. Pavements on such stable substructures are practically immune to earthquake damage. Where foundations or embankments are likely to deform, damage to pavements and disruptions to traffic operations are likely to occur. At particularly vulnerable localities, pavement damage may be so severe that roadways are obstructed and repairs required

before traffic operations can resume. Permanent deformation of embankments and foundations have adversely affected both flexible and rigid pavements. Causes of permanent deformation include:

- Differential settlement due to seismic compaction of embankment or foundation materials.
- Penetration, settlement, flow or spreading of highway embankments due to liquefaction or other weakening of embankment or foundation soils.
- Vertical displacement of pavement sections due to embankment of slope instability.
- Differential displacement due to fault rupture.

6.3. SCREENING AND EVALUATION GUIDELINES

6.3.1. STABLE EMBANKMENTS AND FOUNDATION

6.3.1.1. Hazard

In the absence of deformation or displacement of the foundation or embankment materials, even the most intense seismic shaking has not caused significant damage to flexible or rigid pavements. For example, numerous stable interstate, primary arterial, and secondary roadways were strongly shaken during the 1971 San Fernando, 1989 Loma Prieta, and 1994 Northridge earthquakes without damage to flexible or rigid pavements. Pavement damage occurred only at localities susceptible to some form of permanent embankment or foundation deformation or displacement.

6.3.1.2. Screen

Based on past performance, pavements supported by embankments and foundations not susceptible to ground deformation or failure have performed well. Special analysis or retrofit measures are not required for these pavements. Embankment and foundation failure modes that have caused damage to highway pavements are described in the following sections.

Pavement sections can be considered safe against earthquake damage unless possible deleterious foundation or embankment deformation is indicated by one of the following assessments.

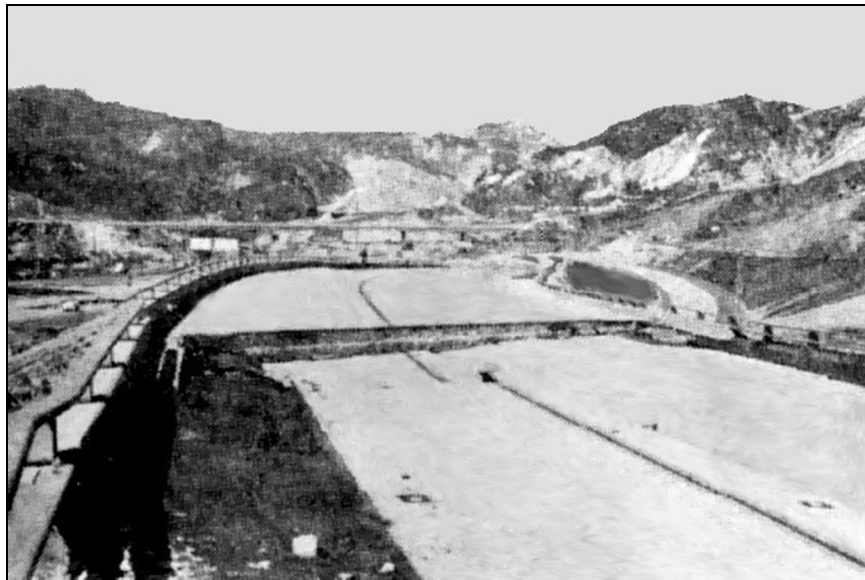
6.3.2. COMPACTION OF EMBANKMENT AND FOUNDATION MATERIALS

6.3.2.1. Hazard

Settlements induced by seismic compaction of embankment and/or foundation soils may be disruptive to both flexible and rigid pavements. The breadth of the zone across that differential settlement occurs is generally as important to pavement damage as the amount of settlement. Where settlements are small, uniform, or distributed across wide zones, little damage occurs to either rigid or flexible pavements. Rigid pavements are generally able to bridge areas of small

differential settlement and flexible pavements are usually sufficiently ductile to absorb small differential movements without damage. Where large differential settlements have occurred across narrow zones, both rigid and flexible pavements have fractured and separated, disrupting traffic operations and requiring repairs.

Seismic compaction of approach fills adjacent to bridge abutments has been a major cause of damaging differential settlements. The stronger and longer the earthquake shaking, the thicker the fill, and the poorer the state of compaction, the greater the amount differential settlement and pavement damage. The photograph reproduced in figure 6-1 shows about 600 mm of differential settlement that offset the paved surface and blocked traffic at the easterly approach to Bridge 53-199R during the 1971 San Fernando earthquake (M6.6). That bridge was part of a connector from northbound I-5 to eastbound I-210 in Sylmar, California. The highway was still under construction at the time of the 1971 San Fernando earthquake. This settlement was caused by seismic compaction and perhaps some spreading of the approach embankment.



Caltrans, reproduced from Prysoc and Egan, 1981

Figure 6-1. Differential settlement induced by seismic compaction at the easterly approach to bridge 53-1991R in I-5 to I-210 interchange during 1971 San Fernando earthquake.

Backfills placed against bridge abutments have been particularly vulnerable to seismic compaction. Difficulties in operating mechanized compaction equipment near walls is one reason for the poor compaction at these localities. The rigidity of the abutment wall also tends to concentrate and accentuate differential settlement.

Contacts between cuts and fills are also locations where differential settlements commonly occur. Materials in the cut section are usually more rigid and less compressible than material in the fill. Also, the cut-fill contact may impede the maneuvering of compaction equipment leaving a poorly compacted section. For example, figure 6-2 shows pavement disruption due to 100 mm

to 200 mm of differential settlement and offset between pavement slabs at a cut-fill contact. This damage occurred on I-5 east of Van Norman Lake and about 500 m north of the junction of I-5 and I-405 during the 1971 San Fernando earthquake.

Pavements supported by poorly compacted embankment materials and/or loose or collapsible foundation soils are also vulnerable to large settlements. Such conditions are more likely to occur beneath sections of older highways than under highways built in accordance with modern codes and construction practices.



Caltrans, reproduced from Prysoc and Egan, 1981

Figure 6-2. Differential settlement across pavement joints near cut-fill boundary on I-5 north of I-405 separation. The settlement is due to seismic compaction of fill during the 1971 San Fernando earthquake.

6.3.2.2. Screen

The primary criteria for identifying pavement sections susceptible to seismic compaction is to identify areas underlain by thick, poorly compacted embankments or loose foundation soils. Localities where these conditions typically occur include older roadways placed on embankments greater than a meter or two thick, newer roadways on fills greater than a few meters thick, or on foundation soils composed of loose natural materials such as collapsible soils or late Holocene deposits of sand, silts, or gravels. Areas most susceptible to differential settlement include bridge abutment-fill contacts and cut-fill contacts.

6.3.2.3. Evaluation

The first step in evaluating potential for settlement is to identify zones where poorly compacted materials could be incorporated into or lie beneath highway embankments. For screening purposes, this evaluation begins with an inventory of embankment thicknesses, ages of

construction, and the compaction criteria applied during construction. The criteria listed in table 6-1 may then be applied with this information to develop rough but generally conservative or high estimates of possible pavement settlement. This procedure is valid for settlements due to seismic compaction of dry to moist embankment fills. Settlement due to seismic compaction of foundation soils can also be estimated by extrapolation from this table. For this extrapolation, the criteria listed in table 6-1 are applied to granular foundation materials, including silts, sands and gravels. The thickness and compaction state of the foundation materials may be estimated from foundation reports, geologic information, etc. Table 6-2 provides criteria for estimating the density state of sands from standard penetration test (SPT) and cone penetration test (CPT) data, where such data is given in foundation reports. These criteria were developed for clean sands, but may be extrapolated to gravely and silty sands for screening purposes. As noted above, the most susceptible foundation materials to seismic compaction are granular sediments deposited during late to early Holocene age. Late Holocene sediments would likely be characterized by relative compactations less than 90 percent; early Holocene to late Pleistocene sediments would likely be characterized by relative compactations between 90 and 95 percent; and middle Pleistocene and older granular sediments would likely be characterized by relative compactations greater than 95 percent. Clay-rich sediments are generally immune to seismic compaction.

Rough, but generally conservative estimates of embankment settlement can be calculated by multiplying the thickness of the embankment and susceptible foundation materials by appropriate volumetric strain values from table 6-1 and then summing the calculated settlements for the fill and foundation. This calculation assumes one-dimensional strain in the vertical direction. Where embankment spreading can occur, the actual vertical displacements may be greater than those predicted. Greater settlements than those estimated from table 6-1 may also occur where foundation soils or embankments are saturated and where increased pore water pressures or liquefaction may lead to enhanced settlement and other deleterious effects. Liquefaction is discussed in a later section.

Table 6-1. Expected maximum volumetric strains in dry to moist soils due to seismic shaking.

Earthquake		Soil Condition - Relative Compaction (RC)		
Magnitude M_w	Acceleration Coefficient A	Loose $RC \leq 90\%$	Moderately Dense $90\% < RC < 95\%$	Dense $RC \geq 95\%$
$M \geq 7$	$A \geq 0.4$	10%	5%	1%
$M \geq 7$	$0.2 < A < 0.4$	5%	2%	0.5%
$M \geq 7$	$A \leq 0.2$	2%	0.5%	0.1%
$5 < M < 7$	$A \geq 0.4$	6%	3%	0.5 %
$5 < M < 7$	$0.2 < A < 0.4$	2%	1%	0.2%
$5 < M < 7$	$A \leq 0.2$	1%	0.2%	0.05%
$M \leq 5$	$A \geq 0.4$	3%	1%	0.2%
$M \leq 5$	$0.2 < A < 0.4$	1%	0.2%	0.05%
$M \leq 5$	$A \leq 0.2$	0.5%	0.1%	0.01%

Table 6-2. Relative density of sands estimated from standard (SPT) and cone (CPT) penetration test data.

SPT N-value	Normalized CPT tip resistance (q_c/P_a)	Relative Density	Approximate Relative Compaction (RC)
0-4	< 20	Very Loose	RC < 90%
4-10	20-40	Loose	RC < 90%
10-30	40-120	Medium	90 % < RC < 95 %
30-50	120-200	Dense	RC > 95 %
Over 50	> 200	Very Dense	RC > 95 %

modified from Terzaghi et al., 1996; Kulhaway and Mayne, 1990

If settlements estimated using the criteria in table 6-1 are small (less than 50 mm), pavement damage from fill and ground settlement is unlikely. For most flexible or rigid pavements, settlements of a few tens of millimeters can be accommodated without obstructing traffic flow. Larger settlements (up to 0.5 m) will likely fracture the pavement and cause uneven surfaces that will greatly slow traffic flow, but without complete obstruction. If such settlements occur at bridge abutments without structural approach slabs or at other discontinuities in foundation, however, the roadway will likely be impassible until emergency repairs are made.

Where subsurface conditions are uniform, settlements are likely to be rather even and non-damaging. Differential settlements are generally caused by local variations or discontinuities in subsurface soil conditions. The width of the zone of differential settlement generally decreases with the sharpness of the discontinuity. Pavement disruption is as much a function of the concentration or width of the zone of differential settlement as the total settlement. Thus, settlements near a bridge abutment or cut-fill contacts are generally more disruptive than similar settlements at localities without sharp lateral discontinuities in foundation materials.

Where preliminary estimates indicate unacceptably large settlements, additional analyses of strain potential and settlement should be conducted. For example, settlement analyses using the Tokimatsu and Seed (1987) procedure might be applied. If the analyses continue to indicate larger than acceptable settlements, mitigation should be considered. Mitigative measures are described in a later section of this chapter.

Table 6-1 was developed for this retrofit manual by evaluating and generalizing past observations of embankment settlement. For example, Prysoc and Egan (1981) documented roadway damage and differential settlements following the 1971 San Fernando earthquake. These investigators reported several instances of 50 mm to 100 mm (2 to 4 in) of differential settlement at bridge abutments in the heavily shaken Sylmar and San Fernando areas. Assuming an average embankment height of 4 m, the average vertical strains at these sites were between 1 percent and 3 percent. That earthquake had a magnitude of 6.5 and peak accelerations in the heavily shaken area exceeded 0.4 g. Assuming that the fills were moderately dense (relative compaction between 90 percent and 95 percent), a conservative value of 3 percent was listed in table 6-1 for these seismic and fill conditions.

Settlements as great as 600 mm (2 ft) were reported by Prysoc and Egan for a few bridge approach fills (figure 6-1). These larger settlements were confined to fills greater than 5 m thick and zones within 3 m of an abutment wall. The total vertical strains at these localities were between 5 percent and 10 percent, indicating that the effected embankments were looser (relative compaction less than 90 percent) than those where smaller strains developed. A vertical strain of 6 percent is listed in the table for these soil conditions.

Little settlement was observed at the fill-abutment contacts for several bridges on the Golden State Freeway (I-5) south of the separation of I-405. These bridges were in the heavily shaken area but pavements were unaffected. Vertical strains in these fills were 1 percent or less. Assuming those fills were well-compacted (relative compaction greater than 95 percent), a conservative strain of 1 percent is listed in the table.

Strain values for other earthquake magnitudes and peak accelerations were extrapolated from the reported San Fernando settlements and verified using the procedure of Tokimatsu and Seed (1987) for calculating vertical strain.

6.3.3. LIQUEFIABLE OR SOFT EMBANKMENT AND FOUNDATION MATERIALS

6.3.3.1. Hazard

Liquefaction of soils has been a major cause of embankment and foundation deformation as well as pavement damage. Both flexible and rigid pavements have been adversely affected. Liquefaction may lead to any of the types of ground deformation or ground failure listed below, depending on geometric and soil conditions at the site. Types and amounts of displacement depends on several factors including height and steepness of embankments, ground slope, and the depth, thicknesses and continuity of liquefiable layers. Similarly, very soft foundation soils under embankments have compressed or sheared during earthquake shaking, causing embankment deformation and pavement damage.

Enhanced Ground Settlement—As noted in the previous section, earthquake shaking is an effective compactor of granular or cohesionless soils, dry, moist or saturated. Where loose soils are saturated and drainage is impeded, excess pore pressures develop during strong ground shaking. Soft saturated cohesive soils may also develop increased pore water pressures in zones of high cyclic stresses. Such pressures lead to progressive softening, greater cyclic shear deformations within the soil, and compaction or shear deformation. As pore pressures reach a certain critical level, effective stresses approach zero and the soil behaves as a liquid rather than a solid. At that point, liquefaction has occurred, which greatly enhances soil deformation and ground settlement, particularly beneath heavy embankments.

Where highways are underlain by low embankments and flat terrain, ground settlement commonly mimics the thickness of underlying liquefiable layers in the foundation soils. Figure 6-3 shows a section of Highway 5 south of Oshamanbe, Japan that settled differentially during the 1993 Hokkaido-Nansei-Okai earthquake (M7.8). In this instance, differential settlement generated waves in the highway that gave the flexible pavement a roller coaster appearance. Differential vertical displacements were as great as 0.6 m between crests and troughs of the induced waves (Youd et al., 1995).

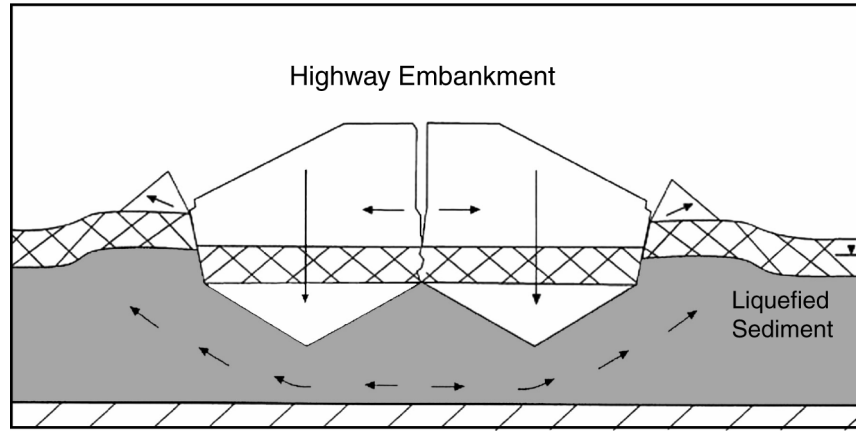


Kiso-Jiban Consultants Co., Inc., Tokyo, reproduced from Youd et al., 1995

Figure 6-3. Wavy pavement due to differential settlement enhanced by liquefaction during the 1993 Hokkaido-Nansei-Oki, Japan earthquake. The site is on Highway 5 south of Oshamanbe.

Penetration and Spreading of Embankment Structures—Liquefaction or increased pore water pressures in soft soils beneath embankments usually leads to penetration of the embankment into the weakened soil, forming a bearing capacity type of failure as illustrated in figure 6-4. During penetration, the embankment usually fractures longitudinally and may spread laterally, generating long open fissures oriented roughly along the centerline of the embankment. In some instances, one or both sides of the embankment may subside and rotate forming a rotational slump. For example, figure 6-5 shows a segment of Highway 36, along the Caribbean coast in eastern Costa Rica, that split longitudinally during the 1991 Limon Province Costa Rica earthquake (M7.5).

The longitudinal fissure is indicative of embankment penetration and spreading. Greater penetration and disruption is illustrated in figure 6-6 that shows the Highway 36 approach to the Rio Estrella Bridge, also in eastern Costa Rica. This approach fill subsided about 2 m and spread laterally due to a combination of soil compaction, embankment penetration and embankment spreading. These actions severely disrupted the embankment and paved surface. In total, about 30 percent of all highway pavements in the lowlands of eastern Costa Rica were disrupted by the effects of liquefaction, primarily embankment penetration and spreading, during the 1991 earthquake (Cole et al., 1991).



modified from Youd et. al, 1995

Figure 6-4. Failure mechanism beneath embankments that split, settle, and spread due to liquefaction of foundation soils.



University of Costa Rica

Figure 6-5. Segment of Highway 36 near Caribbean coast in Costa Rica that split longitudinally, settled and spread laterally during 1991 earthquake by mechanism illustrated in figure 6-4.



University of Costa Rica

Figure 6-6. Disrupted fill and pavement at approach to collapsed Highway 36 bridge over Rio Estrella, Costa Rica. The disruption was due to liquefaction of foundation soils during 1991 earthquake.

Lateral Spread—Lateral spread is a form of ground failure characterized by lateral displacement of surface soil layers over an underlying liquefied layer. The surface of the mobilized ground is commonly disturbed by open fissures, differential settlements, scarps, lateral shear zones, pressure ridges, etc. Structures built over or within lateral spreads, including highways, are commonly disrupted and displaced along with the underlying ground. Lateral spreads generally move down gentle slopes (usually less than 6 percent) or toward a free face, such as an incised river channel. Horizontal displacements typically range up to a few meters, but where shaking is particularly intense or of long duration and ground conditions are extremely vulnerable, larger displacements have occurred. Figure 6-7 shows a section of the Golden State Freeway (I-5) that was translated laterally by as much as 2 m from a large lateral spread (called the Juvenile Hall spread) during the 1971 San Fernando earthquake. Sheared and buckled pavement marked the lateral shear zones at either margin of the failure zone. Between these margins, the lateral spread and highway shifted as much as 2 m westward, causing minor curvature of the roadway.

Where a highway is aligned parallel to the direction of movement, lateral spreads usually induce extensional features, such as open fissures and pulled apart pavement slabs at the head, and compressional features, such as pressure ridges and buckled pavement, at the toe. Figure 6-8 shows a section of Highway 36 in Costa Rica that crossed the head of a lateral spread that shifted toward the Rio Viscaya. The spreading movement generated deep open fissures in the ground and overlying highway embankment and pavement. Extensional movement at the head of the spread was compensated by compression at the toe, that was beneath the Rio Viscaya bridge. The displacement beneath the bridge sheared bearings and connections, causing the superstructure to collapse into the river (Priestly et al., 1991).



R.F. Scott, reproduced from Scott, 1971

Figure 6-7. Rigid pavement on I-5 south of I-5/I-210 interchange that sheared and buckled at two localities during the 1971 San Fernando earthquake due to 2 m of lateral spread displacement.



M.J.N. Priestly, reproduced from Priestly et al., 1991

Figure 6-8. Extensional fissures in flexible pavement caused by lateral spread of floodplain deposits toward Rio Viscaya during the 1991 Costa Rica earthquake.

Ground Oscillation—Ground oscillation generally occurs on nearly level ground underlain by a liquefied layer. In this instance, the liquefied layer decouples the surface layers from underlying nonliquefied ground. The decoupling allows large transient ground movements or waves to develop that may alternatively pull apart surficial soil layers and overlying structures, creating open fissures and fractures, and then jam the separated ground and structural elements back together, creating compressional shear and buckling. Permanent ground displacements at oscillation sites are generally small and chaotic, both in magnitude and in direction. Figure 6-9 shows asphaltic concrete pavement on Highway 229 near the northern edge of the Assabu River valley that was fractured and overlapped due to ground oscillation during the 1993 Hokkaido-Nansei-Oki, Japan earthquake. The photo shows separated curb blocks, indicative of ground extension, near overlapped pavement structures, indicative of compression, at the same locality. Such juxtapositions of compressional and extensional features are common by-products of ground oscillation. Oscillation also typically occurs during the lateral spreading process, with mobilized soil blocks oscillating back and forth as they migrate horizontally down slope or toward a free face.

Flow Failure—Flow failure is the most catastrophic form of ground dislocation associated with liquefaction. Flow failures occur on relatively steep (greater than 6 percent) slopes or embankments that are underlain by loose saturated granular materials. Under these adverse conditions, seismic shaking generates large reductions in soil strength and massive ground displacements. Substantial internal deformation usually occurs within the mobilized soil mass and overlying structures. Pavements on such failures are nearly always displaced and destroyed.



T.L. Youd, reproduced from Youd et al., 1995

Figure 6-9. Fractured and overlapped flexible pavement on Highway 229 near northern edge of Assabu River valley. The disruption was due to liquefaction and ground oscillation during 1993 Hokkaido-Nansei-Oki, Japan earthquake; note extensional separation between curb blocks at same locality.

Figure 6-10 shows a flow failure that occurred in a highway fill along the western edge of Lake Merced in San Francisco during the 1957 Daly City, California earthquake (M5.2). This failure dislodged a section of highway embankment that flowed into the lake, severing the roadway and blocking traffic.

6.3.3.2. Screens for Liquefaction Hazard

Detailed procedures for evaluating liquefaction hazard are given in Part 1 of this manual. These procedures should be used in detailed site investigations for implementation of retrofit measures. In addition, Youd (1998) prepared a screening guide for rapid assessment of liquefaction hazard at highway bridge sites. This guide is also generally valid for assessing liquefaction hazard to pavement structures as well, and may be used for initial hazard assessment. The screening guide presents a systematic application of standard criteria for assessing liquefaction and ground displacement potential. The general principle of screening, and the approach provided by Youd



M.G. Bonilla, reproduced from Youd and Hoose, 1978

Figure 6-10. Liquefaction-induced flow failure of roadway embankment into Lake Merced during 1957 Daly City, California earthquake.

(1998), begins with re-evaluation of available analyses of liquefaction hazard at a site or in the area surrounding a site. The procedure continues with the application of geologic, seismic, hydrologic, and geotechnical criteria. The assessment progresses from the least complex, least time-consuming, and least data intensive to the more complex, time-consuming, and rigorous site-specific analyses. By this procedure, many sites may be evaluated and classified as low hazard with very little time and effort. Only sites with significant hazard need to be evaluated with the more sophisticated and time-consuming procedures.

At each step, a conservative assessment of hazard is made. If there is clear evidence that liquefaction or damaging ground displacements are unlikely, the site is classified as low liquefaction hazard and low priority for further investigation, and the evaluation is complete for that site. If the available information indicates a higher hazard rating, or if the data is inadequate, incomplete or unclear, the site is classified as having a possible liquefaction hazard, and the analysis proceeds to the next step. If the available site information is insufficient to complete a liquefaction hazard analysis, then simplified seismic, geologic, and hydrologic criteria are used to prioritize the site for further investigation.

6.3.3.3. Evaluation

Procedures for evaluating the liquefaction hazard to highway grades and pavements, as well as other works, proceed in two steps: first, liquefaction susceptibility is evaluated using the procedures noted above and in Part 1. Second, potential for ground deformation and displacement is evaluated using procedures outlined in Part 1, chapter 4, and in the screening guide prepared by Youd (1998).

6.3.4. POTENTIALLY UNSTABLE EMBANKMENTS, FOUNDATIONS OR SLOPES

6.3.4.1. Hazard

Slumps, block glides, rock and soil falls, and other types of landslides caused by unstable embankments, foundations or slopes have disrupted or impacted highway pavements during past earthquakes. The following incidents illustrate pavement damage caused by slope instability.

Shallow Slump—Shallow slump of highway embankments located on steep slopes or weak foundations has been a major cause of disruption to highway grades and pavements during past earthquakes. Figure 6-11 shows a section of slumped embankment on Highway 5 between Oshamanbe and Yakumo, Japan (Harp and Youd, 1995). The slump occurred during the 1993 Hokkaido-Nansei-Oki earthquake. In this instance, a major highway embankment slipped down a steep slope, destroying the highway and blocking the roadway to traffic for several weeks until repairs were made. The cause of failure was weakening of marshy foundation soils over where the embankment had been constructed. Liquefaction of sand layers within the marshy deposits also may have occurred.



Oshamanbe Fire Department, reproduced from Harp and Youd, 1995

Figure 6-11. Slump failure in Highway 5 embankment north of Oshamanbe, Japan during the 1993 Hokkaido-Nansei-Oki earthquake. Failure was due to weakening of soft foundation soils.

Slumps with small displacements commonly fracture and offset pavement structures, but usually do not require embankment reconstruction, making repairs much easier to implement. Figure 6-12 shows a highway section with both flexible and rigid highway pavement that was fractured and displaced a few hundred millimeters by slump movement during the 1971 San Fernando earthquake. This locality was on Blucher Avenue immediately east of the lower Van Norman reservoir. In this instance, repairs to the flexible pavement were more easily constructed, both temporarily and permanently, than to the rigid pavement. In general, flexible pavements are more easily repaired than rigid pavements.

Shallow slumps, such as those described above, could have been prevented by ground modification to strengthen foundation soils prior to embankment construction. Remedial measures can also be applied after construction has been completed, but the cost is generally prohibitive except for the most critical structures. Hence, retrofit by strengthening of slopes to prevent pavement damage is rarely applied.

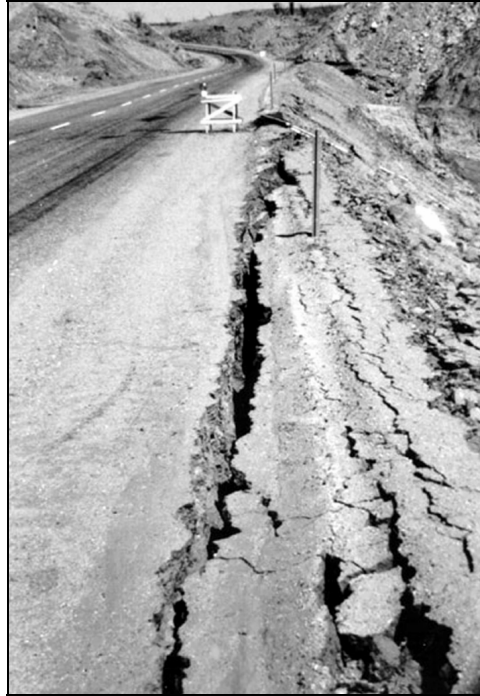
Shoulders of causeways or embankments occasionally slide or slump due to steepness of the slope and poor compaction materials near the embankment face. Figure 6-13 shows a shoulder of a secondary roadway (California State Highway S22) that slid about 0.5 m down a steep embankment during the 1968 Borrego Mountain, California earthquake (M6.4). In this instance, the edge of the steep fill had been poorly compacted, allowing the shoulder to slip. The slumping produced a fissure and scarp between the unstable material in the shoulder and the well-compacted fill beneath the interior of the roadway.



Caltrans, reproduced from Prysoc and Egan, 1981

Figure 6-12. Rigid and flexible pavements disrupted by slump failure of Blucher Avenue near Lower Van Norman reservoir during 1971 San Fernando earthquake.

Deep-Seated Landslides—Deep-seated slumps and block slides involve movement of large masses of soil or rock over failure surfaces that plunge tens of meters into underlying strata. These types of landslides typically generate surface displacement across narrow zones or a series of discrete rupture zones separated by blocks of intact ground. Figure 6-14 shows a single fissure and scarp across Summit Road in the Santa Cruz Mountains induced by movement of a deep-seated slide that slipped a few hundred millimeters during the 1989 Loma Prieta earthquake (M7.1). That displacement separated and vertically offset the flexible roadway pavement.



U.S. Geological Survey, reproduced from
Castle and Youd, 1972

Figure 6-13. Slump of Highway S22 fill east of Salton Sea during the 1968 Borrego Mountain, California earthquake.

Some of the more dramatic damage to urban streets and other structures as a consequence of deep-seated slumps and block glides occurred in Anchorage during the 1964 Alaska earthquake (M9.2). Figure 6-15 shows the massive disruption to 4th Street caused by the 4th Street landslide. The roadway was vertically offset by as much as 2.8 m across the headscarp and broken up within a graben area that formed below the headscarp. Away from the headscarp and graben areas, pavement damage was less severe, consisting of a few fissures within the interior of the slide and several pressure ridges at the margins and near the toe. Some ground dislocation and pavement damage also occurred at distances as far as 130 m inland from the headscarp, a consequence of a few tenths of a meter of sympathetic ground movement toward the landslide (Hansen, 1966).

While shallow slumps may be prevented through ground remediation, deep-seated landslides, such as those shown in figures 6-14 and 6-15, are practically untreatable. These slides cut deeply into the underlying terrain with shear zones that are difficult to detect and strengthen, making remediation a formidable and generally prohibitively expensive task.



E.W. Hart, reproduced from Hart et al., 1990

Figure 6-14. Sinuous scarp in Summit Road caused by apparent movement of a deep-seated landslide during the 1989 Loma Prieta, California earthquake.



U.S. Geological Survey

Figure 6-15. Disruption to 4th Street, Anchorage, Alaska, caused by deep slump during 1964 Alaska earthquake; headscarp is about 2.8 m high.

Debris Slides—Debris shaken loose from cut slopes and steep hillsides commonly accumulate on roadway surfaces. This debris may impede or block traffic and may damage the highway pavement. Rock fall debris has been particularly destructive to asphaltic concrete pavements. Figure 6-16 shows a steep rock slope from where rock fragments, some several meters in diameter, fell or bounced onto the highway pavement, temporarily blocking the roadway and pitting the surface where impacts occurred. The resulting divots were as much as 0.5 m deep. This damage occurred to a roadway around the perimeter of Okashiri Island during the 1993 Hokkaido-Nansei-Oki, Japan earthquake.



T.L. Youd

Figure 6-16. Steep slopes along western shore of Okashiri Island from which numerous rock falls descended onto roadway pavement during 1993 Hokkaido-Nansei-Oki, Japan earthquake. The debris pitted pavement and blocked the highway.

6.3.4.2. Preliminary Screening and Detailed Evaluation of Slope Instability

Procedures for preliminary screening of slope instability hazard and for detailed analysis of stability for implementation of retrofit measures are presented in chapter 2, and are not repeated here.

6.3.5. ACTIVE FAULTS

Surface fault ruptures have disrupted highway pavements during several past earthquakes. For example, pavements were fractured and buckled at several localities due to a combination of thrust and strike-slip faulting during the 1971 San Fernando earthquake. Figure 6-17 shows buckled and overlapped rigid and flexible pavement structures on Highway I-5 immediately north of the junction with I-405. The pavement disruption was caused by thrust faulting near the Lower Van Norman reservoir during the 1971 San Fernando earthquake. The pavement damage was caused by approximately 0.3 m horizontal compression, 0.2 m left-lateral strike-slip, and 0.3 m differential uplift across the fault rupture zone (Yerkes, 1992; Yerkes et al., 1974).

Although both rigid and flexible pavements buckled and fractured, the flexible pavement was more easily repaired, both temporarily and permanently. Flexible pavements on many city streets were disturbed by fault rupture during the 1971 earthquake, but with only minor disruption to traffic operations. Rupture of rigid pavements generally created greater traffic obstructions and repair difficulties.



Caltrans, reproduced from Prysoc and Egan, 1981

Figure 6-17. Rigid and flexible pavements buckled and overlapped by thrust faulting on I-405 south of separation from I-5 during 1971 San Fernando earthquake.

Strike-slip faulting without a major dip-slip component is typically less disruptive to highway pavements than thrust or normal faulting. For example, during the 1979 Imperial Valley earthquake (M6.5), the rigid pavement of Interstate Highway 8 east of the Meloland overcrossing was offset about 0.6 m right laterally across two fault strands about 150 m apart. The faulting caused minor rotation and offset of rigid pavement slabs and curvature of the roadway, but no pavement buckling and little disruption to traffic. Similar magnitudes of right lateral displacement caused little damage to flexible pavements on county routes, such as McCabe and Heber Roads. At a few other roadway crossings, such as at Ralph Road, right-lateral displacement was accompanied by normal faulting with displacements as great as 0.4 m across narrow fault zones. This vertical faulting fractured and offset flexible pavements, but natural ramping up the scarps allowed traffic to cross the faulted section with only minor hindrance to the free flow of traffic on this country road (Sharp et al., 1982).

6.3.5.1. Screens for Fault Rupture Hazard

The following procedures for evaluation of fault rupture hazard are summarized from *California Division of Mines and Geology Special Publication 42* (Hart, 1988) and from *NEHRP Recommended Provisions for Seismic Regulations for New Buildings, Part 2 - Commentary* (BSSC, 1994). The evaluation of fault rupture hazard is based extensively on recency of slip along existing faults. The magnitude, sense, and frequency of surface fault rupture varies for different faults and in many instances along the same fault. Even so, past occurrences of faulting have generally mimicked previous faulting episodes, both in location, magnitude, and sense of displacement.

The following three steps, in order of implementation, are commonly used for rapid screening of fault rupture hazard. Where the first step indicates negligible fault rupture hazard, the second and third steps may be abbreviated or eliminated.

1. Active faults should be identified and delineated from review and analysis of published and unpublished geologic reports applicable to the region in question. Identification studies incorporate evaluation of regional fault patterns as well as local fault features along the highway alignment. From these studies, regional and local fault traces, groundwater barriers, and other fault features are delineated on topographic maps. The character of past faulting episodes should be noted, including widths of rupture zones, amounts and senses of displacements, dates of past activity, etc., as a basis for estimating future faulting hazard.
2. A stereoscopic study of aerial photographs and other remotely sensed images incorporating the highway alignment may provide additional information on the locality and character of a potential fault rupture hazard. Data to be collected from a stereoscopic study include delineation of fault-related topography, vegetation and soil contrasts, and other lineaments of fault origin. Predevelopment air photos are essential to the detection of fault features.
3. A field reconnaissance may be needed to further develop and define fault-related information, such as geologic and soil units, geomorphic features, springs, and deformation of man-made structures, etc. The field study should be detailed near the highway alignment (within a few hundred meters) and much less detailed beyond that proximity.

6.3.5.2. Evaluation Procedures

Evaluation of surface fault rupture hazard to engineered construction includes the following primary considerations: how large and what type of displacement is likely to occur and what is the probability of occurrence. Standardized procedures have not been developed for these calculations; engineering geologists and seismologists, however, routinely make estimates of total fault displacement using empirical criteria. These estimates require specialized procedures that are beyond the scope of this manual. Reviews of existing criteria and procedures, their application, and background information are given by Wells and Coppersmith (1994) and Reiter (1990). The reader is referred to these texts for methodologies for estimating fault rupture displacement and probability of occurrence. Further discussion of fault displacement, as it relates to retrofit of tunnels, is given in section 4.4.2.

6.4. RETROFIT STRATEGIES

Only a few retrofit measures have been applied to prevent earthquake-induced pavement damage. These measures are termed “active” strategies. The policy of nearly all highway departments is not to apply active retrofit measures, except for the construction of structural approach slabs, but to repair pavement damage as rapidly as possible following an earthquake. The wait and repair approach is termed a “passive” strategy. Because no active strategies are proposed or being applied by highway agencies, other than structural approach slabs which are discussed in Part 1, section 6.3.1.1, no guidance and example calculations are given here for the retrofit of pavement structures.

6.4.1. PASSIVE STRATEGIES

The general procedure or policy of most highway departments is to repair pavement damage as quickly as possible after an earthquake, rather than to take active measures to retrofit or mitigate pavement damage prior to the event. Most highway agencies are experienced and prepared to respond to emergencies requiring pavement repair. A few pavement engineers contacted during preparation of this manual felt that timely and efficient pavement repairs could be made following an earthquake without specific advanced preparation or stockpiling of materials. These engineers further indicated that repair of pavement damage will likely be a rather minor concern compared to other emergency needs, such as repair of bridge damage. Because of these more important seismic issues, little action or concern is being given to prevention or specific rapid repair strategies.

6.4.2. ACTIVE STRATEGIES

Active strategies may be necessary at critical sites where pavement damage cannot be tolerated. For example, post-earthquake operability of highways critical to national defense or emergency response may be sufficiently important that retrofit measures are warranted to prevent pavement damage. In addition, some particularly vulnerable localities may require retrofit measures for safety. For example, wire netting is routinely applied on steep rock slopes adjacent to major highways to restrain rockfall debris from entering traffic lanes. This safety procedure is justifiable for both static and earthquake conditions. Foundation strengthening or construction of structural slabs are viable measures at sites where embankment or foundation settlement or deformations are likely to occur across narrow zones that can be defined prior to an earthquake. Retrofit measures might include strengthening the foundation, construction of structural slabs to bridge narrow susceptible zones, or replacement of rigid pavements with flexible pavement for ease of repair.

6.4.2.1. Structural Approach Slabs (SAS)

Because approach fills to bridge abutments are likely to undergo compaction and settlement during seismic shaking, structural approach slabs (SAS) are a viable retrofit measure to reduce the likelihood of pavement damage and traffic obstruction at these localities. Design of settlement slabs is considered in Part 1, section 6.3.1.1 and is not considered further here. However, maintenance of structural approach slabs is an important issue to seismic performance.

One major maintenance problem has been washing of materials from beneath slabs by storm water, creating voids beneath the SAS. If these voids become too large, they could lead to fracture of the slab. Such fracture could be triggered by seismic shaking. As a maintenance measure, the fill supporting SAS should be checked for voids during routine bridge inspections. If voids are detected, the voids should be filled with grout as a retrofit measure and slab drainage improved to prevent recurrence of these deleterious features.

6.4.2.2. Use of Easily Repairable Pavement Sections

At localities of persistent or expected ground movement, such as active landslides, creeping or active faults, etc., easily repaired pavements may be utilized to expedite repairs as pavement deformation and damage occurs. Such localities might include areas susceptible to seismic compaction, liquefaction, slope instability, and fault rupture. A plausible retrofit measure is replacement of rigid pavement with flexible pavement to provide more ductility to absorb deformation and to facilitate post-earthquake pavement repairs. Other retrofit measures might include reduced joint spacing to increase flexibility of rigid pavements in critical areas.

6.4.2.3. Replacement of Inferior Pavement Structures

Pavements supported by poorly compacted embankments or soft foundations are more susceptible to settlement and embankment deformation than pavements on well-compacted fill. Also, embankments with narrow shoulders and steep side slopes are more susceptible to damage than wider, more stable embankments. Thus, an important retrofit measure is to replace older, poor-quality embankments with higher-quality well-compacted materials. Such replacement should be scheduled during regular highway maintenance and improvement projects.

6.4.2.4. Strengthen Foundations Beneath Roadway Grades

Much of the pavement damage during past earthquakes has been due to foundation deformation and instability. Thus, a major retrofit measure is to strengthen potentially unstable foundation soils. Such strengthening might include any or all of the following procedures:

- Compact soft or loose soils to reduce settlement and ground deformation potential.
- Improve foundation drainage to lower water tables and increase foundation strength and liquefaction resistance.
- Add berms or struts to embankments to improve slope stability.

6.4.2.5. Clear and Strengthen Side or Cut Slopes

Pavement damage as well as roadway obstruction has occurred from sliding, toppling, or falling of rock and soil debris from cut or side slopes. Possible retrofit measures include:

- Clearance of loose debris from slopes to prevent slippage or falling onto paved surfaces.
- Placement of wire netting to restrain debris.
- Flattening of grades, rock-bolting, or otherwise strengthening slopes to improve stability and prevent slippage or falling of landslide debris.

APPENDIX A: CHARACTERISTICS OF SURFACE WAVES

A.1. INTRODUCTION

A seismic surface wave is generated by the constructive interference of multiply reflected body waves trapped in a waveguide. Important shallow crustal waveguides include layered sedimentary deposits and sedimentary basins (nonplanar structures). These two types of waveguide typically exhibit a significant velocity contrast between them and the underlying geologic materials.

A surface wave is transmitted along the free surface of the earth (i.e., it propagates horizontally) and its vibration is restricted to near the free surface. Because of their slower velocity, surface waves arrive after the main S-waves. There are two types of surface waves, Love waves and Rayleigh waves. The latter is of main interest for tunnels because of their capacity to induce large axial strain under certain conditions. The particle motion of a Rayleigh wave is elliptical and could be either retrograde or prograde (Mooney and Bolt, 1966). Another unique feature of a surface wave is the velocity dispersion; i.e., its propagation velocity is a function of the wave period. The material properties and the geometry of a waveguide determine the style of particle motion, amplitude (varying with depth), and velocity dispersion of a surface wave. In a multi-layer medium, the surface wave velocity lies between that of the top layer and that of the bottom layer, with long-period surface waves having velocities approaching the latter. This property is useful when making a quick assessment of surface wave velocity in a layered medium. A more complete description and theoretical treatment of surface waves can be found in textbooks such as Bullen and Bolt (1985) and Aki and Richards (1980).

A.2. EXAMPLES OF PROMINENT RAYLEIGH WAVES DURING EARTHQUAKES

Rayleigh waves normally are considered a less important element of the recorded strong ground motions than S-waves because they generally produce weaker shaking than S-waves. However, when a surface wave is adequately excited or amplified, its particle velocity or displacement may be comparable to or even larger than the S-wave amplitude. The following summarizes several situations in which Rayleigh waves have been considered to be a significant element in recorded long-period motions.

Example 1. 1995 Kobe earthquake

Late-arriving, long-duration waves (two- to five-second period) were identified as Rayleigh waves at the soil sites of Takami (in Osaka City, about 40 km from the epicenter) and Osaka Meteorological Observatory (Yokoyama, 1996). The peak ground displacement at the site Takami is carried by the late arriving surface wave. Surface waves were insignificant or not found at the nearby rock sites of Kobe Meteorological Observatory and Chihaya. The velocity at which Rayleigh waves traveled across the Osaka plain was estimated to be 0.6 km/sec. The identified Rayleigh waves produced the peak horizontal displacement at Takami.

Example 2. April 25, 1989 (M_s6.9) Guerrero earthquake – A case of incident surface waves being amplified by a sedimentary basin

A broadband wave packet (1.0- to 12.5-second period) recorded at TACY (in the hill zone of Mexico City, about 300 km from the epicenter of the 1989 Guerrero earthquake) was identified as Rayleigh waves. Rayleigh waves were amplified by the soft soils of Mexico City as they entered the basin and contributed to the lengthening in ground shaking at recording stations D56 and NZ31 inside the lake-bed zone (Gomez-Bernal and Saragoni, 1996). This observation is in line with the hypothesis that the large and long-duration shaking in the lake-bed zone of Mexico City during the M 8.0 1985 Michoacan Earthquake resulted from the interaction of deeply guided surface waves with local one-dimensional resonance (Chavez-Garcia et al., 1995).

Chavez-Garcia et al. (1996) reported a Rayleigh wave velocity greater than 2.5 km/sec for two of the Rayleigh wave packets and a low velocity of 0.1 km/sec for the third packet that appeared only locally.

Example 3. 1971 San Fernando earthquake

Development of Rayleigh waves and their subsequent dispersion were observed along recording stations that lie on similar source-to-site azimuths (Hanks, 1975). Results of the two-dimensional simulation of the Los Angeles basin and San Fernando Valley (Vidale and Helmberger, 1988) suggest that both basins convert direct shear waves into surface waves. O'Rourke et al. (1984) analyzed eight pairs of nearby displacement records and suggested that the maximum observed horizontal strains can be modeled by the propagation of Rayleigh waves.

Example 4. Loma Prieta earthquake and its aftershocks – A case of valley-induced surface waves

The late-arriving ground motion (about three-second period) in the Colton Avenue record (at a distance of 29 km to the fault rupture) of the 1989 Loma Prieta mainshock earthquake was interpreted by Frankel et al. (1991) as caused by surface waves. The identified surface waves caused the peak ground velocity (37 and 36 cm/sec) and peak ground displacement (19 and 17 cm) on both horizontal components of the record. Rayleigh waves were also identified on the array recordings of several Loma Prieta aftershocks inside the Santa Clara Valley (Frankel et al., 1991). The interpretation of these Rayleigh waves as valley-induced waves is supported by a three-dimensional basin response simulation (Frankel and Vidale, 1992). The estimated Rayleigh wave propagation velocity ranges from 1.0 km/sec to 2.0 km/sec.

Pei and Papageorgiou (1996) interpreted the complex waveforms following the S-wave arrival on the mainshock recordings of the Gilroy array, which is also inside the Santa Clara Valley, as valley-induced surface waves. The fundamental mode and the first two higher modes of Rayleigh waves were interpreted: the phase velocity was estimated to be 0.4 km/sec for the fundamental mode and 1.2 km/sec for the first higher mode. The peak ground velocity of the Gilroy array records is carried by the direct S-wave; the particle velocity of the interpreted surface wave is less than 20 cm/sec and less than half of the peak ground velocity.

Example 5. 1992 Landers-Big Bear aftershocks

Analysis of records from a dense array inside the San Bernardino Valley indicated the existence of one- to three- second period surface waves at deep soil sites (Frankel, 1994). A three-dimensional finite difference simulation of the San Bernardino Valley's response to incident S-waves (Frankel, 1994) supported the interpretation that these observed ground motions were caused by basin-induced surface waves. The Rayleigh wave velocity was estimated to be approximately 1.0 km/sec.

Example 6. Observations from the Los Angeles basin

Joyner (2000) used the distance dependence of the time of maximum amplitude to distinguish surface waves and body waves. He studied the pseudovelocity response spectra of strong motion records from the Los Angeles basin and showed that late arriving surface waves with group velocity of about 1km/sec dominate the ground motion for periods of three seconds and longer. He explained the observed surface waves as basin-induced surface waves generated by conversion by body waves at the boundary of the Los Angeles basin. Joyner also speculated that between periods of 0.75 and three seconds, the maximum amplitude is carried by the body waves on some records and by the surface waves on others.

Example 7. Observations from the 1999 M_w 7.6 Chi-Chi Taiwan earthquake

Preliminary examination of the strong motion data provided by the Central Weather Bureau in Taiwan indicates numerous cases of possible surface waves dominating the recorded motions in sedimentary basins and alluvial plains. Surface-wave-like phases in several recordings in Ilan, which is about 80 km northeast of the fault rupture, carry the peak ground velocity (in the range of 25 cm/sec to 30 cm/sec). Other likely examples of dominating surface waves are in the alluvial plain west of the fault rupture at a distance range of 30 to 80 km and with peak ground velocities of 20 cm/sec to 30 cm/sec. The period of the surface-wave-like arrival is five seconds and longer. There is one observation with a particle velocity of 50 cm/sec at a distance of 20 km (station CHY104) from the fault. It should be noted that these observations are preliminary and further studies are needed to verify the wave type and to estimate the propagation velocity.

A.3. SUMMARY

In summary, the above seven examples indicate that surface waves can be an important element of ground motions in sedimentary deposits at periods of about one second and longer. These surface waves are explained as due to either soil amplification of surface waves incident from the epicentral region or the conversion of incident S-waves into surface waves inside a sedimentary basin (basin-induced surface waves). The majority of these examples occurred at a distance of 20 km or more from the earthquake source. In some records, the observed peak ground velocity is carried by the identified surface wave, while in others the particle velocity associated with the identified surface wave is only a fraction of the peak velocity. The two largest peak particle velocities of the identified surface wave described in the above examples are 30 cm/sec (Colton Ave. recording of the Loma Prieta earthquake) and 50 cm/sec (CHY104 station of the Chi-Chi earthquake). However, further work is needed to confirm the wave type of the latter. Most of the observed surface wave velocities, C_R , are in a range of approximately 0.5 to 2.5 km/sec. This

large variation reflects the diversity of the subsurface conditions and the surface wave period in each observation. It should be noted that when the subsurface velocity structure is known, numerical methods could also be used to determine the site-specific dispersion curve $C_R(T)$. The dispersion curve for a multiple-layer medium is relatively simple to calculate (Haskell, 1953; Mooney and Bolt, 1966). However, the calculation of surface wave velocity inside a sedimentary basin usually requires a complicated numerical method (for examples, Lysmer and Drake, 1972; Drake, 1972; Bard and Bouchon, 1980; Papageorgiou and Kim, 1993).

REFERENCES

- Abrahamson, N.A., 1985, *Estimation of Seismic Wave Coherency and Rupture Velocity Using the SMART-1 Strong Motion Array Recordings*, Report EERC/UCB/85-02, Earthquake Engineering Research Center.
- Abrahamson, N.A., 1992, *Spatial Variation of Earthquake Ground Motion for Application to Soil-Structure Interaction*, TR-100463, Electric Power Research Institute.
- Abrahamson, N.A., 1993, "Spatial Variation of Multiple Support Inputs," *Proceedings of the First U.S. Seminar, Seismic Evaluation and Retrofit of Steel Bridges*, University of California at Berkeley, Department of Civil Engineering and California Department of Transportation, Division of Structures, San Francisco, October 18.
- Abrahamson, N.A., 1995, *Review of Apparent Seismic Wave Velocities from Spatial Arrays*, Report to Geomatrix Consultants, San Francisco, California.
- Abrahamson, N.A., Bolt, B.A., Darragh, R.B., Penzien, J., and Tsai, Y.B., 1987, "The SMART 1 Accelerograph Array (1980-1987): A Review," *Earthquake Spectra*, Volume 3, Number 2, pp. 263-287.
- Abramson, L.W. and Crawley, J.E., 1995, "High Speed Rail Tunnels in California," Williamson, G.E., and Gowing, I.M., (eds.), *Proceedings of Rapid Excavation and Tunneling Conference*, San Francisco, California, June 18-21, Chapter 37.
- Abramson, L.W. and Boscardin, M.D., 1999, "Tunnel Rehabilitation," Fernandez, G., and R.A. Bauer, (eds.), *Proceeding of Geo-Engineering for Underground Facilities*, Geotechnical Special Publication No. 90, American Society of Civil Engineers, New York, pp. 925-935.
- ADINA, 1996, *Automatic Dynamic Incremental Nonlinear Analysis Finite Element Code*, Version 6.3.
- Aki, K. and Richards, P.G., 1980, *Quantitative Seismology: Theory and Methods*, Volumes 1 and 2, W.H. Freeman, San Francisco, California.
- Akky, R., Rosidi, D., Madianos, M., and Kaneshiro, J., 1994, "Dynamic Analysis of Large Underground Caverns Using Discreet Element Codes – Verification and Reliability," *Proceedings of the International Congress on Tunneling and Ground Conditions*, Cairo, Egypt, April.
- Ambraseys, N.N., 1973, "Dynamics and Response of Foundation Materials in Epicentral Regions of Strong Earthquakes," *Proceedings of the Fifth World Conference on Earthquake Engineering*, Rome.
- Ambraseys, N.N. and Menu, J.M., 1988, "Earthquake-Induced Ground Displacements," *Earthquake Engineering and Structural Dynamics*, Volume 16, pp. 985.

AASHTO (American Association of State Highway and Transportation Officials), 1996, *Standard Specification for Highway Bridges*, 16th Edition, AASHTO, Washington, DC.

AASHTO (American Association of State Highway and Transportation Officials), 1998, *LRFD Bridge Design Specifications - SI*, Second Edition (with Interim Specifications), AASHTO, Washington, DC.

AASHTO (American Association of State Highway and Transportation Officials), 1999, *Highway Drainage Guidelines*, Third Edition, Vol. I-XII and XIV, Culvert Inspection and Rehabilitation, AASHTO, Washington, DC.

AASHTO (American Association of State Highway and Transportation Officials), 2002, *Standard Specification for Highway Bridges*, Division I, 17th Edition, AASHTO, Washington, DC. (with Interim Specifications).

ACI (American Concrete Institute), 1995a, *ACI-318 Building Code Requirements for Structural Concrete and Commentary*, American Concrete Institute, Detroit, Michigan.

ACI (American Concrete Institute), 1995b, *Specification for Materials, Proportioning, and Application of Shotcrete*, Publication No. ACI 506.2-95, American Concrete Institute, Detroit, Michigan.

ACI (American Concrete Institute) 1999, *Building Code Requirements for Structural Concrete*, ACI 318-99, American Concrete Institute, Farmington Hills, Michigan.

ACI (American Concrete Institute) 2002, *Building Code Requirements for Structural Concrete*, ACI 318-02, American Concrete Institute, Farmington Hills, Michigan.

ACPA (American Concrete Pipe Association), 1992, *Concrete Pipe Design Manual*, American Concrete Pipe Association, Vienna, Virginia.

AISI (American Iron and Steel Institute), 1993, *Handbook of Steel Drainage & Highway Construction Products*, fourth edition, American Iron and Steel Institute, Washington, DC.

ASCE (American Society of Civil Engineers) Committee on Gas and Liquid Fuel Lifelines, 1984, *Guidelines for the Seismic Design of Oil and Gas Pipeline Systems*, Technical Council on Lifeline Earthquake Engineering, American Society of Civil Engineers, New York.

ASCE (American Society of Civil Engineers), 1993, *Standard Practice for Direct Design of Buried Precast Concrete Pipe Using Standard Installations (SIDD) with Appendix A - Manufacturing Specification and Commentary*, American Society of Civil Engineers.

ASCE (American Society of Civil Engineers), 1994, *Retaining and Floodwalls*, Technical engineering and design guides as adapted from the U.S. Army Corps of Engineers, No.4, American Society of Civil Engineers Press, New York.

ASTM (American Society for Testing and Materials), 1984a, *Standard Method for Penetration Test and Split-Barrel Sampling of Soils*, ASTM Standard D1586.

ASTM (American Society for Testing and Materials), 1984b, *Standard Practice for Description and Identification of Soils*, ASTM Standard D2488.

Anderson, R., 1998, California Department of Transportation (personal communication).

Applied Technology Council, 1995, *Structural Response Modification Factors*, including "Appendix A, Evaluation of Building Strength and Ductility," Report ATC-19, 70 pp.

ATC/MCEER Joint Venture, 2003, *Recommended LRFD Guidelines for the Seismic Design of Highway Bridges, Specifications and Commentary*, Applied Technology Council/Multidisciplinary Center for Earthquake Engineering Research Joint Venture, MCEER-ATC-49.

Ashford, S.A. and Sitar, N., 1994, *Seismic Response of Steep Natural Slopes*, Report No. UCB/EERC-94/05, Earthquake Engineering Research Center, University of California at Berkeley, May.

AFTES (Association Francaise des Travaux en Souterrain), 1978, "Tunnel Stability by Convergence-Confirmation Method," *Proceedings of the Paris Conference*, October 26, 1978; reprinted in *Underground Space*, Volume 4, Numbers 4, 5, and 6, 1980.

AFTES (Association Francaise des Travaux en Souterrain), 1999, *AFTES Recommendations, The Design, Sizing, and Construction of Precast Concrete Segments at the Rear of a Tunnel Boring Machine*.

Ballinger, C.A. and Drake, P.G., 1995, *Culvert Repair Practices Manual: Volumes I and II*, Report No. FHWA-RD-94-096, Federal Highway Administration, Washington, DC.

Bard, P.Y. and Bouchon, M., 1980, "The Seismic Response of Sediment-filled Valleys, Part II, The Case of Incident P and SV Waves," *Bulletin of the Seismological Society of America*, Volume 70, pp. 1921-1941.

Barton, N., Lien, R., and Lunde, J., 1974, *Engineering Classification of Rock Masses for the Design of Tunnel Support*, Norwegian Geotechnical Institute, Oslo, Norway, 48 pp.

Bathurst, R.J. and Cai, Z., 1995, "Pseudo-Static Seismic Analysis of Geosynthetic-Reinforced Segmental Retaining Walls," *Geosynthetics International*, Volume 2, Number 5, pp. 787-830.

Beach, T.J., 1988, "Load Test Report and Evaluation of a Precast Concrete Arch Culvert," *Culverts and Tiebacks*, Transportation Research Record No. 1191, pp. 12-21, Transportation Research Board, Washington, DC.

Bickel, J.O. and Tanner, D.N., 1982, "Sunken Tube Tunnels," Bickel, J.O. and Keusel, T.R. (eds.), *Tunnel Engineering Handbook*, Chapter 13, Van Nostrand-Reinhold.

Bischoff, J.A. and Smart, J.D., 1976, "A Method of Computing a Rock Reinforcement System Which is Structurally Equivalent to an Internal Support System," *Proceedings of the Sixteenth U.S. Symposium on Rock Mechanics*.

Blake, T.F., Hollingsworth, R.A., and Stewart, J.P. (editors), 2002, *Recommended Procedures for Implementation of DMG Special Publication 117, Guidelines for Analyzing and Mitigating Landslide Hazard in California*, Committee organized through ASCE Los Angeles Section Geotechnical Group, published by the Southern California Earthquake Center, June.

Bonaparte, R., Schmertman, G.R., and Williams, N.D., 1986, *Seismic Design of Reinforced Slopes with Tensar Geogrids*, Tensar Technical Note, TTN:SR2.

Boulanger, R., Idriss, I.M., Stewart, D.P., Hasash, Y.M.A., and Schmidt, B., 1998, "Drainage Capacity of Stone Columns or Gravel Drains for Mitigating Liquefaction Potential," *Geotechnical Earthquake Engineering and Soil Dynamics Conference*, American Society of Civil Engineers, Seattle, Washington, May 31-June 4.

Bowles, J.E., 1977, *Foundation Analysis and Design*, Second Edition, McGraw Hill Inc.

Branwer, C.O., 1994, *Rockfall Hazard Mitigation Methods Participant Workbook*, Publication No. FHWA SA-93-085, Federal Highway Administration, Washington, DC.

British Standard (BS) Code of Practice No. 2, 1951, *Earth Retaining Structures*, Institute of Structural Engineers, London, UK.

Brown, I., Brekke, T., and Korbin, G., 1981, *Behavior of the Bay Area Rapid Transit Tunnels through the Hayward Fault*, UMTA Report No. CA-06-0120-81-1, U.S. Department of Transportation.

Bruce, D.A. and Juran, I., 1997, *Drilled and Grouted Minipiles: State-of-the-Art Review*, Report No. FHWA-RD-96-017, Federal Highway Administration, Washington, DC, National Technical Information Service, Springfield, Virginia.

BSSC, 1994, *NEHRP Recommended Provisions for Seismic Regulations for New Buildings: Part I Provisions; Part II Commentary*, Report FEMA 222A and 223A, Building Seismic Safety Council, Washington, DC.

BSSC, 1997, *NEHRP Guidelines for the Seismic Rehabilitation of Buildings*, FEMA 273-274, Federal Emergency Management Agency, Washington, DC.

Bullen, K.E. and Bolt, B.A., 1985, *An Introduction to the Theory of Seismology*, fourth edition, Cambridge University Press.

Burns, J.Q. and Richard, R.M., 1964, "Attenuation of Stresses for Buried Cylinders," *Proceedings of the Symposium on Soil-Structure Interaction*, University of Arizona, Tempe.

Byrne, P.M., Anderson, D.L., and Hendra, J., 1996a, "Seismic Analysis of Large Buried Culvert Structures," *Structures, Culverts and Tunnels*, Transportation Research Record No. 1541, pp. 133-139, National Academy Press, Washington, DC.

Byrne, R.J., Cotton, D., Porterfield, J., Wolschlag, C., and Ueblacker, G., 1996b, *Manual for Design and Construction of Soil Nail Walls*, Report No. FHWA-SA-96-069, Federal Highway Administration, Washington, DC, National Technical Information Service, Springfield, Virginia.

California Builders and Exchange, 1994, *Value Engineering and Low-density Cellular Concrete Play Major Roles in Tunnel Project*, Volume 7, May 2.

California Department of Transportation (Caltrans)/Parsons, Brinckerhoff, Quade, and Douglas, 1998, "Posey and Webster Street Tubes, Seismic Retrofit Project," *Second 100% Structural PS&E Submittal, Volume II – Design Plans*.

Canadian Geotechnical Society, 1978, *Canadian Foundation Engineering Manual*, CGS Foundation Committee, Toronto, Canada.

Castle, R.O. and Youd, T.L., 1972, *Engineering Geology, The Borrego Mountain Earthquake of April 9, 1968*, U.S. Geological Survey Professional Paper 787, pp. 158-174.

Chang, C.Y., Power, M.S., Idriss, I.M., Somerville, P.G., Silva, W., and Chen, P.C., 1986, *Engineering Characterization of Ground Motion - Task II: Observational Data on Spatial Variations of Earthquake Ground Motion*, Report prepared for U.S. Nuclear Regulatory Commission, NUREG/CR-3805, Volume 3.

Chavez-Garcia, F.J., Ramos-Martinez, J., and Romero-Jimenez, E., 1995, "Surface-wave Dispersion Analysis in Mexico City," *Bulletin of the Seismological Society of America*, Volume 85, pp. 1116-1126.

Chavez-Garcia, F.J., Ramos-Martinez, J., and Romero-Jimenez, E., 1996, "A Detailed Analysis of Ground Motion in Mexico City during the 4.25.89 Guerrero earthquake," *Eleventh World Conference on Earthquake Engineering*, Paper No. 888.

Chen, P.C., Deng, D.Z.F., and Birkmyer, A.J., 1979, "Considerations of Dynamic Stress Concentrations in the Seismic Analysis of Buried Structures," *Proceedings of the Second U.S. National Conference on Earthquake Engineering*, Stanford, California, August 22-24.

Chen, Y. and Krauthammer, T., 1987, "Soil-Structure Interface Effects on Dynamic Interaction Analysis of Reinforced Concrete Lifelines," *Developments in Geotechnical Engineering, No. 43 - Soil-Structure Interaction*, A.S. Cakmak, (ed.), Elsevier, Amsterdam.

City of San Diego/Parsons Engineering Science, 1995, *Contract Package Number 2, South Bay Ocean Outfall*, Drawing Number 5-1.40.

Clough, G.W., 1981, "Innovations in Tunnel Construction and Support Techniques," *Bulletin of the Association of Engineer Geologists*, Volume XVIII, Number 2, May.

Clough, G.W. and O'Rourke, T.D., 1990, "Construction Induced Movements of Insitu Walls," *Design and Performance of Earth Retaining Structures*, Geotechnical Special Publication Number 25, American Society of Civil Engineers, New York, pp 439-470.

- Cole, E., Leeds, D.J., Santana, G.S., and Singh, J.P., 1991, "Introduction," *Costa Rica Earthquake of April 22, 1991 Reconnaissance Report, Earthquake Spectra*, Volume 7, Supplement B, pp. 1-14.
- Davies, T.G., Richards, R., and Chen, K.H., 1986, "Passive Pressure During Seismic Loading," *Journal of Geotechnical Engineering*, American Society of Civil Engineers, Volume 112, Number 4, pp. 470-483.
- Davis, C.A. and Bardet, J.P., 1998, "Seismic Analysis of Large-Diameter Flexible Underground Pipes," *Journal of Geotechnical and Geoenvironmental Engineering*, American Society of Civil Engineers, Volume 124, Number 10, pp. 1006-1015.
- Deng, N., 1991, *Two-Dimensional Site Response Analyses*, thesis presented to University of California at Berkeley, in partial satisfaction of the requirements for the degree of Doctor of Philosophy.
- Desai, D.B., Merritt, J.L., and Chang, B., 1989, "Shake and Slip to Survive - Tunnel Design," Pond, R.A. and Kenny, P.B. (eds.), *Proceedings of Rapid Excavation and Tunneling Conference*, Los Angeles, California, June 11-14, Chapter 2.
- Douglas, W.S. and Warshaw, R., 1971, "Design of Seismic Joint for San Francisco Bay Tunnel," *Journal of the Structural Division*, American Society of Civil Engineers, Volume 97, Number St4, pp. 1129-1141.
- Dowding, C. and Rozen, A., 1978, "Damage to Rock Tunnels from Earthquake Shaking," *Journal of Geotechnical Engineering*, American Society of Civil Engineers, Volume 104, Number GT 2, February.
- Drake, L.A., 1972, "Love and Rayleigh Waves in Non-horizontally Layered Media," *Bulletin of the Seismological Society of America*, Volume 62, pp. 1241-1258.
- Duncan, J.M., 1979, "Behavior and Design of Long-Span Metal Culverts," *Journal of Geotechnical Engineering*, American Society of Civil Engineers, Volume 105, Number GT3, Proceedings Paper 14429, pp. 399-418.
- Duncan, M.J., 1996, *Slope Stability Analysis: Landslides Investigation and Mitigation*, Special Report 247, Transportation Research Board, pp. 337-388.
- Duncan, M.J., Wright, S.G., and Wong, K.S., 1990, "Slope Stability During Rapid Drawdown," *H. Bolton Seed Memorial Symposium Proceedings*, May 1990, Volume 2, pp. 253-272.
- Ebeling, R.M. and Morrison, E.E., 1992, *The Seismic Design of Waterfront Retaining Structures*, U.S. Army Technical Report No. ITL-92-11, National Technical Information Service, Springfield, VA.
- Edinger, P.H., 1989, "Seismic Response Considerations in Foundation Design," *Foundation Engineering: Current Principles and Practices*, Proceedings of American Society of Civil Engineers Conference, Evanston, Illinois, Northwestern University.

Elias, V. and Christopher, B.R., 1997, *Mechanically Stabilized Earth Walls and Reinforced Slopes*, Report No. FHWA-SA-96-071, Federal Highway Administration, Washington, DC, National Technical Information Service, Springfield, VA.

Elms, D.A. and Martin, G.R., 1979, "Factors Involved in the Seismic Design of Bridge Abutments," *Proceedings, Workshop on Seismic Problems Related to Bridges*, Applied Technology Council.

FHWA (Federal Highway Administration), 1983, *Seismic Retrofitting Guidelines for Highway Bridges*, Report No. FHWA-RD-83-007, Federal Highway Administration, Washington, DC.

FHWA (Federal Highway Administration), 1995, *Seismic Retrofitting Guidelines for Highway Bridges*, Report No. FHWA-RD-94-052, Federal Highway Administration, Washington, DC, May.

FHWA (Federal Highway Administration), 2001, *Hydraulic Design Series No. 6, Hydraulic Design of Highway Culverts*, Report No. FHWA NHI-01-020, Federal Highway Administration, Washington, DC.

Fenves, G.L., 1989, *Seismic Evaluation of the Syro Igloo Structure*, A Report to Syro Steel Company, Western Division, Centerville, Utah (unpublished).

Fishman, K.L. and Richards, R., 1996, "Seismic Analysis and Model Studies of Bridge Abutments," *Analysis and Design of Retaining Walls Against Earthquakes*, Geotechnical Special Publication No. 60, S. Prakash (ed.), American Society of Civil Engineers, New York, pp. 77-99.

Fishman, K.L. and Richards, R., 1997a, *Sliding Analysis and Design of Bridge Abutments Considering Sliding and Rotation*, Technical Report NCEER-97-0009, National Center for Earthquake Engineering Research, University at Buffalo.

Fishman, K.L., Richards, R., and Divito, R., 1997b, *Seismic Analysis for Design or Retrofit of Gravity Bridge Abutments*, Technical Report NCEER-97-0011, National Center for Earthquake Engineering Research, University at Buffalo.

Frame, P.A., 1995, "Evaluation of Fault Offset for the Coyote Dam Outlet Work," *Association of Engineering Geologists News*, Volume 38, Number 2, pp. 26-28.

Frankel, A., 1994, "Dense Array Recordings in the San Bernardino Valley of Landers-Big Bear Aftershocks: Basin Surface Waves, Moho Reflections, and Three-dimensional Simulations," *Bulletin of the Seismological Society of America*, Volume 84, pp. 613-624.

Frankel, A., Hough, S., Friberg, P., and Busby, R., 1991, "Observations of Loma Prieta Aftershocks from a Dense Array in Sunnyvale, California," *Bulletin of the Seismological Society of America*, Volume 81, pp. 1900-1922.

Frankel, A. and Vidale, J., 1992, "A Three-dimensional Simulations of Seismic Waves in the Santa Clara Valley, California, from a Loma Prieta Aftershock," *Bulletin of the Seismological Society of America*, Volume 82, Number 5, pp. 2045-2074.

- Franklin, A.G. and Chang, F.K., 1977, *Earthquake Resistance of Earth and Rockfill Dams: Permanent Displacements of Earth Embankments by Newmark Sliding Block Analysis*, Miscellaneous Paper S-71-17, Report 5, U.S. Army Corps of Engineers, Waterways Experiment Station, Vicksburg, Mississippi.
- Fukuchi, G., 1995, personal communication to J.Y. Kaneshiro, March.
- Gazetas, G., Dakoulas, P., and Dennehy, K., 1990, "Empirical Seismic Design Method for Waterfront Anchored Sheetpile Walls," *Design and Performance of Earth Retaining Structures*, Geotechnical Special Publication No. 25, P.C. Lambe and L.A. Hansen (eds.), American Society of Civil Engineers, New York.
- Gedney, D.S. and Weber, W.G., 1978, "Design and Construction of Soil Slopes," *Special Report 176: Landslides: Analysis and Control*, Chapter 8, Transportation Research Board, National Research Council, Washington, DC, pp. 172-191.
- GEO-SLOPE International Ltd., 1998, *User's Guide SLOPE/W Version 4*, Calgary, Alberta, Canada.
- Gomez-Bernal, A. and Saragoni, R.G., 1996, "Oscillations of the Mexico City Surface Layer Excited by Surface Seismic Waves," *Eleventh World Conference on Earthquake Engineering*, Paper Number 718.
- Goodman, R.E. and Seed, H.B., 1966, "Earthquake-Induced Displacements in Sand Embankments," *Journal of the Soil Mechanics and Foundations Division*, American Society of Civil Engineers, Volume 92, Number SM2, pp. 125-146.
- Grimm, D. and Parish, W.C.P., 1985, "Foam Grout Saves Tunnel," *ASCE Civil Engineering Magazine*, September, pp. 64-65.
- Grodner, M., Mclellan, G., and Brystrum, L., 1998, "Cure for Thinning Concrete," *ASCE Civil Engineering Magazine*, December, pp. 49-51.
- Gursoy, A., 1985, "Immersed Steel Tube Tunnels: an American Experience," *Tunneling and Underground Space Technology*, Volume 10, Number 4, pp. 439-453.
- Hanks, T.C., 1975, "Strong Ground Motion of the San Fernando, California, Earthquake: Ground Displacements," *Bulletin of the Seismological Society of America*, Volume 65, Number 1, pp. 193-225.
- Hansen, A. and Franks, C.A.M., 1991, "Characterization and Mapping of Earthquake Triggered Landslides for Seismic Zonation," *Fourth International Conference on Seismic Zonation*, Earthquake Engineering Research Institute, Stanford University, August.
- Hansen, W.R., 1966, *Effects of the Earthquake of March 27, 1964, at Anchorage, Alaska*, U.S. Geological Survey Professional Paper 542-A, 68 pp.

- Harder, L.F., 1991, "Performance of Earth Dams during Earthquakes," *Proceedings of the Second International Conference on Recent Advances in Geotechnical Earthquake Engineering and Soil Dynamics*, St. Louis, Missouri, March 11-15, Paper No. LP 05.
- Harp, E.L., Wilson, R.C. and Wieczorek, G.F., 1981, *Landslides from the February 4, 1976 Guatemala Earthquake*, U.S. Geological Survey Professional Paper 1204-A, 35 p.
- Harp, E.L. and Noble, M.A., 1993, "An Engineering Rock Classification to Evaluate Seismic Rock-fall Susceptibility and Its Application to the Wasatch Front," *Bulletin of the Association of Engineering Geologists*, Volume XXX, Number 3, pp. 293-319.
- Harp, E.L. and Jibson, R.W., 1995, *Inventory of Landslides Triggered by the 1994 Northridge, California Earthquake*, U.S. Geological Survey Open-file Report 95-213.
- Harp, E.L. and Youd, T.L., 1995, "Landslides," *Earthquake Spectra*, EERI, Volume 11, supplement A, pp. 41-48.
- Hart, E.W., 1988, *Fault Rupture Zones in California*, Special Publication 42, California Division of Mines and Geology.
- Hart, E.W., Bryant, W.A., Wills, C.J., and Treiman, J.A., 1990, "The Search for Fault Rupture and Significance of Ridge Top Fissures, Santa Cruz Mountains, California," *The Loma Prieta (Santa Cruz Mountains), California Earthquake of 17 October 1989*, Special Publication 104, California Division of Mines and Geology, pp. 83-94.
- Hashash, Y.M.A., Tseng, W.S., and Kirimotat, A., 1998, "Seismic Soil-structure Interaction Analysis for Immersed Tube Tunnels Retrofit," *Geotechnical Earthquake Engineering and Soil Dynamics Conference*, American Society of Civil Engineers, Seattle, Washington, May 31-June 4.
- Haskell, N.A., 1953, "The Dispersion of Surface Waves in Multilayered Media," *Bulletin of the Seismological Society of America*, Volume 43, Number 1, pp. 17-34.
- Heger, F.J., 1982, *Structural Design Method for Precast Reinforced Concrete Pipe*, Transportation Research Record No. 878, National Academy Press, Washington, DC.
- Hibbitt, Karlsson, and Soresen, Inc., 1998, *ABAQUS, User's Manual*.
- Hobbs, D.W., 1983, "Failure Criteria for Concrete," *Handbook of Structural Concrete*, F.K. Kong, et al. (eds.), McGraw-Hill, New York.
- Hoeg, K., 1968, "Stresses Against Underground Structural Cylinders," *Journal of the Soil Mechanics and Foundation Division*, American Society of Civil Engineers, Volume 94, Number SM4, April.
- Hoek, E. and Bray, J.W., 1981, *Rock Slope Engineering*, Third Edition, Institution of Mining and Metallurgy, London, 402 pp.

Holtz, R.D. and Schuster, R.L., 1996, *Stabilization of Soil Slopes: Landslide Investigations and Mitigation*, Special Report 247, Transportation Research Board, pp. 474-504.

Holtz, R.D., Christopher, B.R., and Berg, R.R., 1995, "Geosynthetics Design and Construction Guidelines," *Participant Notebook NHI Course No. 13213*, National Technical Information Service, Springfield, VA.

Honegger, D.G., 1994, "Assessing Vulnerability of BC Gas Pipelines to Lateral Spread Hazards," *Proceedings of the Fifth U.S.-Japan Workshop on Earthquake Resistant Design of Lifeline Facilities and Countermeasures Against Soil Liquefaction*, T.D. O'Rourke and M. Hamada (eds.), Technical Report NCEER-94-0026, National Center for Earthquake Engineering Research, University at Buffalo, pp. 515-530.

Hudson, M., Idriss, I.M., and Beikae, M., 1994, *User's Manual for QUAD4M, A Computer Program to Evaluate Seismic Response of Soil Structures Using Finite Element Procedures and Incorporating A Compliant Base*, Center for Geotechnical Modeling, University of California, Davis.

Huff, G.C., 1971, *Low-density Concrete Backfills for Lined Tunnels*, American Concrete Institute, Paper SP 29-12.

Hynes-Griffin, M.E. and Franklin, A.G., 1984, *Rationalizing the Seismic Coefficient Method*, Miscellaneous Paper GL-84-13, U.S. Army Corps of Engineers, Waterways Experiment Station, Vicksburg, Mississippi.

Idriss, I.M. and Sun, J.I., 1992, *SHAKE91, A Computer Program for Conducting Equivalent Linear Seismic Response Analyses of Horizontally Layered Soil Deposits*, Center for Geotechnical Modeling, Department of Civil and Environmental Engineering, University of California at Davis.

Iftimie, T., 1994, "Prefabricated Lining, Conceptual Analysis," and "Comparative Studies for Optimal Solution," Abel Salam, M.E. (ed.), *Proceedings of the International Congress on Tunneling and Ground Conditions*, Cairo, Egypt, April 3-7.

Itasca, 1992, *UDEC - Universal Distinct Element Code, User's Guide*, Itasca Consulting Group, Inc., Minneapolis, Minnesota.

Itasca, 1995, *FLAC, Fast Lagrangian Analysis of Continua, Version 3.3*, Itasca Consulting Group, Inc., Minneapolis, Minnesota.

Itasca, 1998, *FLAC, Fast Lagrangian Analysis of Continua, Version 3.40 User's Guide*, Itasca Consulting Group, Inc., Minneapolis, Minnesota.

Jackson, T.B., 2003, Parsons Brinckerhoff, Personal Communication to M.S. Power, October.

Jibson, R.W., Harp, E.L., and Michael, J.A., 1998, *A Method for Producing Digital Probabilistic Seismic Landslide Hazard Maps: An Example from the Los Angeles, California Area*, U. S. Geological Survey Open File Report 98-113, 17 pp., 2 plates.

Joyner, W.B., 2000, "Strong Motion from Surface Waves in Deep Sedimentary Basins," *Bulletin of the Seismological Society of America*, Volume 90, No. 6B, pp. 95-112.

Kaneshiro, J., Korbin, G., and Hart, J., 1996a, "Fault Crossing Design and Seismic Considerations for the South Bay Ocean Outfall," *Proceedings of the American Society of Civil Engineers Pipelines Crossings Conference*, June 16-19, Burlington, Vermont.

Kaneshiro, J., Navin, S., and Korbin, G., 1996b, "Unique Precast Concrete Segmented Liner for the South Bay Ocean Outfall Project," Ozdemir, L.O. (ed.), *Proceedings of the International Conference on North American Tunneling '96 and 22nd General Assembly of the International Tunneling Association*, April.

Katona, M.G., Smith, J.M., Odello, R.S., and Allgood, J.R., 1976, *CANDE – A Modern Approach for the Structural Design and Analysis of Buried Culverts*, Report No. FHWA-RD-77-5, Federal Highway Administration, Washington, DC.

Katona, M.G., Meinhert, D.F., Orillac, R., and Lee, C.H., 1979, *Structural Evaluation of New Concepts for Long-Span Culverts and Culvert Installations*, Report No. FHWA-RD-79-115, Federal Highway Administration, Washington, DC.

Katona, M.G., Vittes, P.D., Lee, C.G., and Ho, H.T., 1981, *CANDE-1980: Box Culverts and Soil Models*, Report No. FHWA/RD-80/172, Federal Highway Administration, Washington, DC.

Kavazanjian, E., Matasovic, N., Hadj-Hamou, T., and Sabatini, P.J., 1997, *Geotechnical Engineering Circular No. 3 Design Guidance: Geotechnical Earthquake Engineering for Highways, Volume II Design Examples*, Report No. FHWA-SA-97-077, Federal Highway Administration, Washington, DC.

Keaton, J.R., Anderson, L.R., Topham, D.E., and Rathbun, D.J., 1987a, *Earthquake-Induced Landslide Potential in and Development of a Seismic Slope Stability Map of the Urban Corridor of Utah, Weber, Box Elder, and Cache Counties, Utah*, 47 pp.

Keaton, J.R., Topham, D.E., Anderson, L.R., and Rathbun, D.J., 1987b, "Earthquake-Induced Landslide Potential in and Development of a Seismic Slope Stability Map of the Urban Corridor of Davis and Salt Lake Counties, Utah," *Proceedings from the 23rd Symposium on Engineering Geology and Soils Engineering*, Logan, Utah, April 6-8, Volume 23, pp. 57-80.

Keefer, D.K., 1984, "Landslides Caused by Earthquakes," *Geologic Society of America Bulletin*, Volume 95, pp. 406-421.

Keefer, D.K. and Wilson, R.C., 1989, "Predicting Earthquake-Induced Landslides with Emphasis on Arid and Semi-Arid Environments," *Publication of the Inland Geological Society*, Volume 2, pp. 118-149.

Kennedy, R.P., Chow, A.W., and Williamson, R.A., 1977, "Fault Movement Effects on Buried Oil Pipeline," *Journal of the Transportation Engineering Division*, American Society of Civil Engineers, Volume 103, Number TE5.

- Keusel, T.R., 1969, "Earthquake Design Criteria for Subways," *Journal of the Structural Division, Proceedings of the American Society of Civil Engineers*, Volume 95, Number st6, June.
- Kiyomiya, O., 1995, "Earthquake-resistance Design Features of Immersed Tunnels in Japan," *Tunneling and Underground Space Technology*, Volume 10, Number 4, pp. 463-475.
- Koseki, J., Tateyama, M., Tatsuoko, F., and Horri, K., 1996, "Back Analysis of Soil Retaining Walls for Railway Embankments Damaged by the 1995 Hyogoken-Nambu Earthquake," *The 1995 Hyogoken-Nambu Earthquake- An Investigation into the Damage to Civil Structures*, Committee of Earthquake Engineering, Japan Society of Civil Engineers, pp.101-114.
- Kulhawy, F.H. and Mayne, P.W., 1990, *Manual on Estimating Soil Properties for Foundation Design*, Report No. EPRI EL-6800, Electric Power Research Institute, Palo Alto, CA.
- Ladd, C.C., 1991, "Stability Evaluation During Staged Construction," *Journal of Geotechnical Engineering*, American Society of Civil Engineers, New York, Volume 117, Number 4, pp. 540-615.
- Lang, T.A., 1962, "Theory and Practice of Rock Bolting," *Transactions, AIME (Mining)*, Volume 23.
- Lang, T.A., 1972, "Rock Reinforcement," *Bulletin of the Association of Engineering Geologists*, Volume IX, Number 3.
- Lang, T.A., 1981, "Rock Reinforcement Design," *Leeds Hill and Jewett Report for Reverse Curve Tunnel*.
- Leonards, G.A., Wu, T.H., and Juang, C.H., 1981, *Predicting Performance of Buried Conduits*, Report No. FHWA/IN/JHRP-81/3, Indiana State Highway Commission, Indianapolis.
- Lin, J.S. and Whitman, R.V., 1986, "Earthquake-Induced Displacements of Sliding Blocks," *Journal of Geotechnical Engineering Division*, American Society of Civil Engineers, Volume 112, Number 1, pp. 44-59.
- Liu, X. and O'Rourke, M.J., 1997, "Behavior of Continuous Pipeline Subject to Transverse PGD," *Earthquake Engineering and Structural Dynamics*, A.K. Chopra, (ed.), Volume 26, pp. 989-1003, Wiley, New York.
- Lopez, V.T. and Berrones, R.F., 1994, "Pipeline Design Against Sand Liquefaction in Isla Del Carmen, Mexico," *Fifth U.S.-Japan Workshop on Earthquake Resistant Design of Lifeline Facilities and Countermeasures Against Soil Liquefaction, Proceedings*, T.D. O'Rourke and M. Hamada, (eds.), Technical Report No. NCEER-94-0026, National Center for Earthquake Engineering Research, University at Buffalo, pp. 531-545.
- Los Angeles County Metropolitan Transportation Authority/Parsons Brinckerhoff, 1994, *Design Drawings for LA CBD to North Hollywood STA 630+00 to Universal City Tunnel Special Seismic Section Plan, Profile, and Section*, Drawing No. Y-009, Sheet Number 118.

- Lysmer, J. and Drake, L.A., 1972, "A Finite Element Method for Seismology," Chapter 6, *Methods in Computational Physics II: Seismology*, Alder, B., Fernbach, S., and Bolt, B.A. (eds.), Academic Press, New York.
- Lysmer, J., Udaka, T., Tsai, C.F., and Seed, H.B., 1975, *FLUSH, A Computer Program for Approximate 3-D Analysis of Soil-Structure Interaction Problems*, Report No. EERC 75-30, Earthquake Engineering Research Center, November.
- Lysmer, J., Ostadan, F., Tabatabaie, M., Tajirian, F., and Vahdani, S., 1991, *SASSI, A System for Analysis of Soil-Structure Interaction, User's Manual*, Geotechnical Engineering Division, Civil Engineering Department, University of California, Berkeley, and Bechtel Corporation, San Francisco, California.
- Madden, P., 1999, "Strengthening Part of London's Tube," *Tunnels and Tunneling International*, December, pp. 18-20.
- Madden, K., Madoy, L., Oatmen, R., Larson, A., and Perrone, V., 1994, "Dry Weather Transfer Rainy Weather Storage," Ozdemir, L., and Brierley, G. (eds.), *Soft-Ground Tunneling in Seattle, Washington: Proceedings of North American Tunneling 94*, Denver, June 6-9.
- Makdisi, F.I. and Seed, H.B., 1978, "Simplified Procedure for Estimating Dam and Embankment Earthquake-Induced Deformations," *Journal of the Geotechnical Engineering Division*, American Society of Civil Engineers, Volume 104, Number GT7, pp. 849-867, July.
- Makdisi, F.I. and Seed, H.B., 1979, "Simplified Procedure for Evaluating Embankment Response," *Journal of the Geotechnical Engineering Division*, American Society of Civil Engineers, Volume 105, Number GT12, pp. 1427-1434, December.
- Manson, M.W., Keefer, D.K., and McKittrick, M.A., 1990, "Preliminary Map and Descriptions of Landslides and Related Ground Failures in the Santa Cruz Mountains Triggered by the Loma Prieta, California Earthquake of 17 October 1989," *Eos*, Volume 71, Number 43, pp. 1455.
- Marston, A., 1930, *The Theory of External Loads on Closed Conduits in the Light of the Latest Experiments*, Bulletin 96, Iowa State College, Ames, Iowa.
- Marston, A., Schlick, W.J., and Clemmer, H.F., 1917, *The Supporting Strength of Sewer Pipe in Ditches and Methods of Testing Sewer Pipe in Laboratories to Determine Their Ordinary Supporting Strength*, Bulletin 31, Iowa State College, Ames, Iowa.
- Mathsoft, 1998, *Mathcad 8.0*, copyright 1996-1998, Mathsoft, Inc.
- McCauley, M.L., Works, B.W., and Naramore, S.A., 1985, *Rockfall Mitigation*, Report No. FHWA/CA/TL-85/12, Federal Highway Administration, Washington, DC, 147 pp.
- McCusker, T., 1989, "The Development and Care of Precast Concrete Tunnel Linings," Pond, R.A. and Kenny, P.B. (eds.), *Proceedings, Rapid Excavation and Tunneling Conference*.

- McGrath, T.J., Tigue, D.B., and Heger, F.J., 1988, "PIPECAR and BOXCAR Microcomputer Programs for the Design of Reinforced Concrete Pipe and Box Sections," *Culverts and Tiebacks*, Transportation Research Record No. 1191, Transportation Research Board, Washington, DC, pp. 99-105.
- McGrath, T.J., Selig, E.T., and Beach, T.J., 1996, "Structural Behavior of Three-Sided Arch Span Bridge," *Structures, Culverts, and Tunnels*, Transportation Research Record No. 1541, pp. 112-119, National Academy Press, Washington, DC.
- Merritt, J.L., Monsees, J.E., and Hendron, A.J. Jr., 1985, "Seismic Design of Underground Structures," *Proceedings, 1985 Rapid Excavation and Tunneling Conference*, American Institute of Mining, Metallurgical, and Petroleum Engineers, American Society of Civil Engineers, New York, June 16-20.
- Meyerhoff, G.G., 1953, "The Bearing Capacity of Foundations Under Inclined and Eccentric Loads," *Proceedings, Third International Conference on Soil Mechanics and Foundation Engineering*, Volume 1, pp. 440-445.
- Millar, G., Parker, H.W., and Godlewski, P.M., 1991, "Taller Tunnels," *Civil Engineering Magazine*, Volume 61, Number 9, pp. 50-53.
- Miyajima, M. and Kitaura, M., 1991a, "Performance of Pipelines During Soil Liquefaction," *Lifeline Earthquake Engineering, Proceedings of the Third U.S. Conference*, American Society of Civil Engineers, pp. 470-479.
- Miyajima, M., and Kitaura, M., 1991b, "Response of Buried Pipelines Located Through Liquefied and Non-Liquefied Ground," *Sixth Canadian Conference on Earthquake Engineering, Proceedings*, S.A. Sheikh and S.M. Uzumeri, (eds.), University of Toronto Press, Toronto, Canada, pp. 253-260.
- Mononobe, N. and Matsuo, H., 1929, "On the Determination of Earth Pressures During Earthquakes," *Proceedings of the World Engineering Congress*, Volume 9, pp. 176.
- Mooney, H.M. and Bolt, B.A., 1966, "Dispersive Characteristics of the First Three Rayleigh Modes for a Single Surface Layer," *Bulletin of the Seismological Society of America*, Volume 56, pp. 43 - 47.
- Morrison, E.E. and Ebeling, R.M., 1995, "Limit Equilibrium Computation of Dynamic Passive Earth Pressure," *Canadian Geotechnical Journal*, Volume 32, pp. 481-487.
- Musser, S.C., 1989a, *CANDE-89 User Manual*, Report No. FHWA-RD-89-169, Federal Highway Administration, Washington, DC.
- Musser, S.C., 1989b, *Design Calculations, Missile Storage Igloos*, FY89 MCP Project No. KNMD 890913, Hickam Air Force Base, Oahu, Hawaii, Syro Steel Company, Centerville, Utah, (internal publication).

- NCMA (National Concrete Masonry Association), 1996, *Design Manual for Segmental Retaining Walls*, second edition, National Concrete Masonry Association, Herdon, Virginia.
- NAVFAC DM-7, 1982, *The Naval Facilities Design Manual*, Department of the Navy, Naval Facilities Engineering Command, pp. 89-112.
- Navin, S.J. and Hutchinson, H.L., 1992, "Diamond Fork Hydroelectric Power Development," *American Society of Civil Engineers Water Conference Proceedings*, June.
- Neelakantan, G., Budhu, M., and Richards, R., 1992, "Balanced Seismic Design of Anchored Retaining Walls," *Journal of Geotechnical Engineering*, American Society of Civil Engineers, Volume 118, Number 6, pp. 873-888.
- Newmark, N.M., 1965, "Effects of Earthquakes on Dams and Embankments," *Geotechnique*, Volume 15, Number 2, pp. 139-160.
- Newmark, N.M., 1967, "Problems in Wave Propagation in Soil and Rock," *Proceedings, International Symposium on Wave Propagation and Dynamic Properties of Earth Materials*, University of New Mexico Press, Albuquerque, New Mexico, August 23-25.
- Newmark, N.M. and Hall, W.J., 1975, "Pipeline Design to Resist Large Fault Displacement," *Proceedings, U.S. National Conference on Earthquake Engineering*, Ann Arbor, Michigan.
- Norrish, N.I. and Wylie, D.C., 1996, *Rock Slope Stability Analysis: Landslides Investigation and Mitigation*, Special Report 247, Transportation Research Board, pp. 391-438.
- Okabe, S., 1926, "General Theory of Earth Pressure," *Journal of the Japanese Society of Civil Engineers*, Volume 12, Number 1, Tokyo, Japan.
- Olander, H.C., 1950, *Stress Analysis of Concrete Pipe*, Engineering Monograph No. 6, U.S. Department of the Interior, Bureau of Reclamation.
- Olsen Engineering, Inc., 1996, "Nondestructive Testing of Unknown Subsurface Bridge Foundations- Results of NCHRP Project 21-5," *Research Results Digest*, No. 213, National Cooperative Highway Research Program, Transportation Research Board, Washington, DC, 42 pp.
- Ono, K., Shimamura, S., and Kasai, H., 1992, "Seismic Isolation of Underground Structures," *Proceedings of the Fourth U.S.-Japan Workshop on Earthquake Disaster Prevention for Lifeline Systems*, Special Publication 840, National Institute of Standards and Technology.
- O'Rourke, M.J. and Wang, L.R.L., 1978, "Earthquake Response of Buried Pipelines," *Proceedings, Specialty Conference on Earthquake Engineering and Soil Dynamics*, American Society of Civil Engineers, Volume 2, pp. 720-731.
- O'Rourke, M.J., Castro, G., and Centola, N., 1980, "Effects of Seismic Wave Propagation Upon Buried Pipelines," *International Journal of Earthquake Engineering and Structural Dynamics*, Volume 8, pp. 455-467.

- O'Rourke, M.J. and Castro, G., 1981, "Design of Buried Pipelines for Wave Propagation," *Lifeline Earthquake Engineering, The Current State of Knowledge*, American Society of Civil Engineers, New York, pp. 32-47.
- O'Rourke, M.J., Bloom, M., and Dobry, R., 1982, "Apparent Propagation Velocity of Body Waves," *Earthquake Engineering and Structural Dynamics*, Volume 10, pp. 283-294.
- O'Rourke, M.J., Castro, G., and Hossian, I., 1984, "Horizontal Soil Strain Due to Seismic Waves," *Journal of Geotechnical Engineering*, Volume 110, Number 9, pp. 1173-1187.
- O'Rourke, M.J. and Hmadi, K.E., 1988, "Analysis of Continuous Buried Pipelines for Seismic Wave Effects," *Earthquake Engineering and Structural Dynamics*, Volume 16, pp. 917-929.
- O'Rourke, M.J. and Ayala, G., 1990, "Seismic Damage to Pipeline: Case Study," *Journal of Transportation Engineering*, American Society of Civil Engineers, Volume 116, Number 2, pp. 123-134.
- O'Rourke, T., Grigoriu, M., and Khater, M., 1985, "Seismic Response of Buried Pipeline: A State-of-the-Art Review," *Decade of Progress in Pressure Vessel Technology-1985*, C. Sundararajan, (ed.), American Society of Mechanical Engineers, pp. 281-323.
- O'Rourke, T.D. and Lane, P.L., 1986, "A Case Study of Seismic Hazards and Pipeline System Response for San Francisco," *Proceedings of the Third U.S. National Conference on Earthquake Engineering*, Earthquake Engineering Research Institute, Volume III, pp. 2,167-2,178.
- O'Rourke, T.D. and Jones, C.J.F.P., 1990, "Overview of Earth Retention Systems: 1970-1990," *Design and Performance of Earth Retaining Structures, Proceedings of a Specialty Conference*, Ithaca, New York, Geotechnical Special Publication 25, American Society of Civil Engineers, pp. 22-51.
- O'Rourke, T.D. and Shiba, Y., 1997, "Seismic Performance and Design of Tunnels," *NCEER Highway Project Annual Report*, Report to the Multidisciplinary Center for Earthquake Engineering Research for Federal Highway Administration contract DTFH61-92-C-00106.
- Oughourlian, C.V. and Powell, G.H., 1982, *ANSR-III, General Purpose Computer Program for Nonlinear Structural Analysis*, UCB/EERC 82/21, Earthquake Engineering Research Center, November.
- Owen, G.N. and Scholl, R.E., 1981, *Earthquake Engineering of Large Underground Structures*, Report Number FHWA/RD-80/195, prepared for the Federal Highway Administration and National Science Foundation.
- Papageorgiou, A.S. and Kim, J., 1993, "Propagation and Amplification of Seismic Waves in 2-D Valleys Excited by Obliquely Incident P- and SV-Waves," *Earthquake Engineering and Structural Dynamics*, Volume 22, Number 2, pp. 167-182.
- Paris, J.M., 1921, "Stress Coefficients for Large Horizontal Pipes," *Engineering News Record*, Volume 87, Number 19.

Peck, R.B., Hansen, W.E. and Thornburn, T.H., 1974, *Foundation Engineering*, Second Edition, John Wiley & Sons.

Peck, R.B., Hendron, A.J., and Mohraz, B., 1972, "State of the Art of Soft Ground Tunneling," *Proceedings of the Rapid Excavation and Tunneling Conference*, Chicago, Illinois, Volume 1.

Pei, D. and Papageorgiou, A.P., 1996, "Locally Generated Surface Waves in Santa Clara Valley: Analysis of Observations," *Earthquake Engineering and Structural Dynamics*, Volume 25, pp. 47-63.

Penzien, J., 2000, "Seismically Induced Racking of Tunnel Linings," *Earthquake Engineering and Structural Dynamics*, Volume 29, pp. 683-691.

Penzien, J. and Wu, C., 1998, "Stresses in Linings of Bored Tunnels," *International Journal of Earthquake Engineering and Structural Dynamics*, Volume 27, pp. 283-300.

Pierson, L.A. and Van Vickle, R., 1993, *Rockfall Hazard Rating System, Participant's Manual*, Report No. FHWA SA-93-057, Federal Highway Administration, Washington, DC.

PTI (Post-Tensioning Institute), 1996, *Recommendations for Prestressed Rock and Soil Anchors*, Third Edition, Post-Tensioning Institute, Phoenix, AZ.

Power, M.S., Rosidi, D., Kaneshiro, J., Gilstrap, S.D., and Chiou, S.J., 1998, *Summary and Evaluation of Procedures for the Seismic Design of Tunnels*, Draft Report, Multidisciplinary Center for Earthquake Engineering Research, September.

Prakash, S., Wu, Y., and Rafnsson, E.A., 1995a, "On Seismic Design Displacements of Rigid Retaining Walls," *Proceedings, Third International Conference on Recent Advances in Geotechnical Earthquake Engineering and Soil Dynamics*, St. Louis, Missouri, pp. 1183-1192.

Prakash, S., Wu, Y., and Rafnsson, E.A., 1995b, *Displacement Based Aseismic Design Charts for Rigid Walls*, Shamsheer Prakash Foundation, Rolla, Missouri.

Priestly, N.J., Singh, J.P., Youd, T.L., and Rollins, K.M., 1991, "Bridges," *Costa Rica Earthquake of April 22, 1991 Reconnaissance Report, Earthquake Spectra*, Volume 7, Supplement B, pp. 59-91.

Prysoc, R.H. and Egan, J.P., 1981, *Roadway Damage During the San Fernando, California Earthquake of Feb. 9, 1971*, Report No. FHWA/CA/TL-80/17, California Department of Transportation, 184 pp.

Public Works Research Institute, Ministry of Construction, Japan, 1976, *Earthquake Resistant Design of Tunnels and an Example of its Application*, Technical Memorandum Number 1169, PWRI, 53 pp.

Rabcewicz, L.V., 1964, "New Austrian Tunneling Method," *Water Power*.

- Rafnsson, E.A. and Prakash, S., 1994, "Displacement Based Aseismic Design of Retaining Walls," *Proceedings, XIII International Conference on Soil Mechanics and Foundation Engineering*, New Dehli, Volume 3, pp. 1029-1032.
- Rathje, E.R., Abrahamson, N.A., and Bray, J.D., 1998, "Simplified Frequency Content Estimates of Earthquake Ground Motions," *Journal of Geotechnical and Environmental Engineering*, American Society of Civil Engineers, Vol. 124, No. 2, pp. 150-159.
- Reiter, L., 1990, *Earthquake Hazard Analysis - Issues and Insights*, Columbia University Press, New York, 254 pp.
- Research Engineers, 1995, *STARDYNE User's Manual*.
- Richards, R. and Elms, D.G., 1979, "Seismic Behavior of Gravity Retaining Walls," *Journal of the Geotechnical Engineering Division*, American Society of Civil Engineers, Volume 105, Number 4.
- Richards, R., Elms, D.G., and Budhu, M., 1990, "Dynamic Fluidization of Soils," *Journal of Geotechnical Engineering*, American Society of Civil Engineers, Volume 116, Number 5, pp. 740-759.
- Richards, R. and Shi, X., 1991, "Seismic Bearing Capacity of Shallow Foundations," *Proceedings of the Pacific Conference on Earthquake Engineering*, Auckland, New Zealand.
- Richards, R., Elms, D.G., and Budhu, M., 1993, "Seismic Bearing Capacity and Settlements of Foundations," *Journal of Geotechnical Engineering*, American Society of Civil Engineers, Volume 119, Number 4, pp. 662-674.
- Richards, R. and Shi, X., 1994, "Seismic Lateral Pressures in Soils with Cohesion," *Journal of Geotechnical Engineering*, American Society of Civil Engineers, Volume 120, Number 7, pp. 1230-1251.
- Richards, R., Fishman, K.L., and Divito, R., 1996, "Threshold Accelerations for Rotations or Sliding of Bridge Abutments," *Journal of Geotechnical Engineering*, American Society of Civil Engineers, Volume 122, Number 9, 752-759.
- Ritchie, A.M., 1963, "Evaluation of Rockfall and Its Control," *Highway Research Record 17*, HRB, National Research Council, Washington, DC, pp. 13-28.
- Rosenbleuth, E., 1977, "Soil and Rock Mechanics in Earthquake Engineering," *Proceedings of International Conference on Dynamic Methods in Soil and Rock Mechanics*.
- Rowe, R., 1992, "Tunneling in Seismic Zones," *Tunnels and Tunneling*, December.
- Russell, H.A., 1987, *The Inspection and Rehabilitation of Transit Tunnels*, William Barclay Parsons Fellowship, PBQ&D, Inc.

- Russell, H.A., 1993, "The Control of Groundwater in Tunnel Rehabilitation," Bowerman, L.D. and Munsees, J.E. (eds.), *Proceedings of the Rapid Excavation and Tunneling Conference*, Chapter 32, Boston.
- Russell, H.A., 1999, "Rehabilitation of Tunnel Liners with Shotcrete," Fernandez, G., and Bauer, R.A. (eds.), *Proceedings, Geo-Engineering for Underground Facilities*, Geotechnical Special Publication Number 90, American Society of Civil Engineers, pp. 925-935.
- Sabatini, P.J., 1997, *Earth Retaining Systems, Geotechnical Engineering Circular No. 2*, Report No. FHWA-SA-96-038, Federal Highway Administration, Washington, DC.
- Sabatini, P.J., 2002, *Evaluation of Soil and Rock Properties, Geotechnical Engineering Circular No. 5*, Report No. FHWA-IF-02-034, Federal Highway Administration, Washington, DC.
- Sabatini, P.J., Pass, D.G., and Bachus, R.C., 1998, *Ground Anchors and Anchored Systems, Geotechnical Engineering Circular No. 4*, Report No. FHWA-SA-99-015, Federal Highway Administration, Washington, DC.
- Sadigh, R.K. and Egan, J.A., 1998, "Updated Relationships for Horizontal Peak Ground Velocity and Peak Ground Displacement for Shallow Crustal Earthquakes," *Proceedings of the Sixth U.S. National Conference on Earthquake Engineering*, Seattle, Washington.
- Sakurai, A. and Takahashi, T., 1969, "Dynamic Stresses of Underground Pipelines During Earthquakes," *Proceedings, Fourth World Congress of Earthquake Engineering*, Santiago, Volume II, pp. B4, 81-95.
- San Francisco Bay Area Rapid Transit (SFBART), 1960, *Technical Supplement to the Engineering Report for Trans-Bay Tube*, July.
- Sarma, S.K., 1975, "Seismic Stability of Earth Dams and Embankments," *Geotechnique*, Volume 25, Number 4, pp. 474-761.
- Schmidt, B. and Hashash, Y.M.A., 1998, "Seismic Rehabilitation of Two Immersed Tube Tunnels," *World Tunnel Congress*, Sao Paulo, Brazil, April 25-30.
- Schmidt, B. and Hashash, Y.M.A., 1999, "Preventing Tunnel Flotation due to Liquefaction," *Proceedings of the Second International Conference on Earthquake Geotechnical Engineering*, Lisbon, Portugal, June 21-25, pp. 509-512.
- Schnabel, P.B., Lysmer, J., and Seed, H.B., 1972, *SHAKE: A Computer Program for Earthquake Response Analysis of Horizontally Layered Sites*, Report No. UCB/EERC-72/12, Earthquake Engineering Research Center, University of California, Berkeley, December, 102 pp.
- Schwartz, C.W. and Einstein, H.H., 1980, *Improved Design of Tunnel Supports, Volume 1-Simplified Analysis for Ground-structure Interaction in Tunneling*, Report No. UMTA-MA-06-0100-80-4, U.S. Department of Transportation, Urban Mass Transportation Administration.

- Scott, R.F., 1971, "San Fernando Earthquake, 9 February 1971, Preliminary Soil Engineering Report," *Engineering Features of the San Fernando Earthquake February 9, 1971*, California Institute of Technology, pp. 299-331
- Seed, H.B., 1979, "Considerations in the Earthquake-Resistant Design of Earth and Rockfill Dams," the Rankine Lecture, *Geotechnique*, Volume 29, Number 3, pp. 215-263.
- Seed, H.B., Idriss, I.M., and Keifer, F.W., 1968, *Characteristics of Rock Motions During Earthquakes*, Report Number EERC-68-5, Earthquake Engineering Research Center, University of California, Berkeley, September.
- Seed, H.B. and Whitman, R.V., 1970, "Design of Earth Retaining Structures For Dynamic Loads," *Lateral Stresses in the Ground and Design of Earth Retaining Structures, Specialty Conference*, American Society of Civil Engineers, New York, pp.103-148.
- Seed, H.B. and Idriss, I.M., 1982, *Ground Motions and Soil Liquefaction During Earthquakes*, Monograph Series, Earthquake Engineering Research Institute, 134 pp.
- Seed, R.B. and Harder, L.F., 1990, "SPT-Based Analysis of Cyclic Pore Pressure Generation and Undrained Residual Strength," *Proceedings of the H. Bolton Seed Memorial Symposium*, May 1990, Volume 2, pp. 351-376.
- Segrestan, P. and Bastic, M.J., 1988, "Seismic Design of Reinforced Earth Retaining Walls - The Contribution of Finite Element Analysis," *Theory and Practice of Earth Reinforcement*, Yamanouchi, T., Miura, N., and Ochiai, H. (eds.), Balkema, *Proceedings of the International Geotechnical Symposium on Theory and Practice of Earth Reinforcement*, Fukuoka, Kyushu, Japan, pp. 577-582.
- Shah, H.H., and Chu, S.L., 1974, "Seismic Analysis of Underground Structural Elements," *Journal of the Power Division*, American Society of Civil Engineers, Volume 100, Number PO1, pp. 53-62.
- Sharma, S., 1997, *XSTABL An Integrated Slope Stability Analysis Program for Personal Computers* (V5 Documentation List), Interaction Software Design Inc., Moscow, ID.
- Sharma, S. and Judd, W.R., 1991, "Underground Opening Damage from Earthquakes," *Engineering Geology*, Volume 30.
- Sharp, R.V., Lienkaemper, J.J., Bonilla, M.G., Burke, K.B., Fox, B.F., Herd, D.G., Miller, D.M., Morton, D.M., Ponti, D.J., Rymer, M.J., Tinsley, J.C., Yount, J.C., Kahle, J.E., and Hart, E.W., 1982, *Surface Faulting in the Central Imperial Valley*, U.S. Geological Survey Professional Paper 1254, pp. 119-143.
- Shi, G.H., 1989, *Discontinuous Deformation Analysis - A New Numerical Model for the Static and Dynamics of Block Systems*, Ph.D. thesis, University of California, Berkeley, August.
- Shi, X., 1993, *Plastic Analysis for Seismic Stress Fields*, Ph.D. Dissertation, University at Buffalo, 150 p.

- Siddharthan, R., Gowda, P., and Norris, G., 1991, "Displacement Based Design of Retaining Walls," *Proceedings, Second International Conference on Recent Advances in Geotechnical Earthquake Engineering and Soil Dynamics*, pp. 657-661.
- Siddharthan, R., Ara, S., and Norris, G., 1992, "Simple Rigid Plastic Model For Seismic Tilting of Rigid Walls," *Journal of Structural Engineering*, American Society of Civil Engineers, pp. 469-487.
- Siegel, R.A., 1975, *STABL Users Manual*, Joint Highway Research Report No. JHRP-75-9, School of Civil Engineering, Purdue University, West Lafayette, Indiana, 47907.
- Silva, W. 1997, "Characteristics of Vertical Ground Motion for Applications to Engineering Design," *Proceedings of the FHWA/NCEER Workshop on the National Representation of Seismic Ground Motion for New and Existing Highway Facilities*, Burlingame, California, Technical Report NCEER-97-0010, National Center for Earthquake Engineering Research, University at Buffalo, pp. 205-252.
- Sitar, N. and Clough, G.W., 1983, "Seismic Response of Steep Slopes in Cemented Soils," *Journal of Geotechnical Engineering*, American Society of Civil Engineers, Volume 109, GT2, pp. 210-227.
- Smith, D.D. and Duffy, J.D., 1990, *Field Tests and Evaluation of Rockfall Restraining Nets*, California Department of Transportation, Transportation Materials and Research, Report No. CA/TL 90/05, pp. 138.
- Soast, A., 1989, "Tunnel Rehabilitation, New Methods Slash Time and Costs, Water Jetting and Pumped Shotcrete are Restoring an Aged Aqueduct," *Engineering News Record*, May 25, pp. 86-87.
- St. John, C.M. and Zahrah, T.F., 1987, "Aseismic Design of Underground Structures," *Tunnelling and Underground Space Technology*, Volume 2, Number 2.
- Structural Software Development Co., 1981, *PIPLIN*, Berkeley, California.
- Takada, S., Katagiri, S., Yamashita, A., and Shinmi, T., 1991, "Hybrid Response Analysis of Buried Corrugated Pipeline Under Seismic Wave," *Lifeline Earthquake Engineering, Proceedings of the Third U.S. Conference*, American Society of Civil Engineers, pp. 452-459.
- Tatsuoka, F., Koseki, J., and Tateyama, M., 1995, "Performance of Geogrid Reinforced Retaining Walls During The Great Honshin-Awaji Earthquake, January 17, 1995," *Proceedings of the First International Conference for Geotechnical Earthquake Engineering*, Tokyo, Japan, Volume 1, pp. 55-62.
- Terzaghi, K., Peck, R.B., and Mezeri, G., 1996, *Soil Mechanics in Engineering Practice*, Third Edition, John Wiley & Sons, Inc., New York.

- Tokimatsu, K. and Seed, H.B., 1987, "Evaluation of Settlements in Sands Due to Earthquake Shaking," *Journal of Geotechnical Engineering*, American Society of Civil Engineers, Volume 113, No. 8, pp. 861-878.
- Trifunac, M.D. and Todorovska, M.I., 1997, "Northridge, California, Earthquake of 1994, Density of Pipe Breaks and Surface Strains," *Soil Dynamics and Earthquake Engineering*, Volume 16, pp. 193-207.
- Turner, A.K. and Schuster, R.L., (eds.), 1996, *Landslides Investigation and Mitigation*, Special Report 247, Transportation Research Board, 673 pp.
- Uni-Bell, 1991, *Handbook of PVC Pipe*, Uni-Bell PVC Pipe Association, Third Edition, Dallas, Texas.
- U.S. Army Corps of Engineers, 1970, *Engineering and Design – Stability of Earth and Rockfill Dams*, Engineering Manual EM 1110-2-1902, Department of the Army, Corps of Engineers, Office of the Chief of Engineers, April.
- U.S. Army Corps of Engineers, 1997, *Engineering and Design, Tunnels and Shafts in Rock*, Engineering Manual, EM 1110-2-2901, Department of the Army, Corps of Engineers.
- U.S. Geological Survey (USGS), 1996, *National Seismic Hazard Mapping Project*, Open File Report 97-131, <http://eqhazmaps.usgs.gov/html/genmap.html>.
- U.S. Steel International, 1975, *USS Steel Sheet Piling Design Manual*.
- Varnes, D.J., 1978, "Slope Movement Types and Processes," Schuster, R.L., and Krisek, R.J., (eds.), *Landslides, Analysis and Control*, Special Report 176, Transportation Research Board, National Academy of Sciences, Washington, DC, pp. 11-33.
- Vesic, A.S., 1973, "Analysis of Ultimate Loads on Shallow Foundations," *Journal of the Soil Mechanics and Foundation Division*, American Society of Civil Engineers, Volume 99(SM1), pp. 45-73.
- Vidale, J.E. and Helmberger, D.V., 1988, "Elastic Finite-Difference Modeling of the 1971 San Fernando, California Earthquake," *Bulletin Seismological Society of America*, Volume 78, pp. 122-141.
- Wang, L.R.L., Zhang, H., and Ishibashi, I., 1991, "Seismic Response of Buried Pipeline System in a Soil Liquefaction Environment," *Lifeline Earthquake Engineering, Proceedings of the Third U.S. Conference*, American Society of Civil Engineers, pp. 460-469.
- Wang, J.N., 1993, *Seismic Design of Tunnels- a Simple State-of-the-art Design Approach*, Monograph 7, Parsons Brinckerhoff.
- Wang, Z.L. and Makdisi, F.I., 1999, "Implementing a Bounding Surface Hypoplasticity Model for Sand into the FLAC Program," *Proceedings of the International Symposium on Numerical Modeling in Geomechanics*, Minnesota, September, pp. 483-490.

Wells, D.L. and Coppersmith, K.J., 1994, "New Empirical Relationships Among Magnitude, Rupture Length, Rupture Area, and Surface Displacement," *Bulletin of the Seismological Society of America*, Volume 84, Number 4, August, pp. 974-1002.

Whitman, R.V., 1991, "Seismic Design of Earth Retaining Structures" (state-of-the-art paper), *Proceedings, Second International Conference on Recent Advances in Geotechnical Engineering and Soil Dynamics*, St. Louis, Missouri, Volume II, pp. 1767-1778.

Wieczorek, G.F., Wilson, R.C., and Harp, E.L., 1985, *Map Showing Slope Stability During Earthquakes in San Mateo County, California*, U.S. Geological Survey miscellaneous investigation series, map I-1257-E.

Wilson, E.L., 1998, *SADSAP 4.1, Static and Dynamic Structural Analysis Program*, Structural Analysis Programs, Inc., El Cerrito, California.

Wilson, R.C. and Keefer, D.K., 1985, "Predicting Areal Limits of Earthquake-Induced Landsliding," *Evaluating Earthquake Hazards in the Los Angeles Region--An Earth-Science Perspective*, Professional Paper 1360, U.S. Geological Survey, pp. 316-345.

Wood, J.H., 1973, *Earthquake-induced Soil Pressures on Structures*, Report Number EERL 73-05, California Institute of Technology.

Wright, S.G., 1991, *UTEXAS3, A Computer Program for Slope Stability Calculations*, Shinoak Software, Austin, Texas.

Wyllie, D.C., 1991, "Rock Slope Stabilization and Protection Measures," *Proceedings, National Symposium on Highway and Railway Slope Stability Association of Engineering Geologists*, Chicago, pp. 41-63.

Wyllie, D.C. and Norrish, N.I., 1996, *Stabilization of Rock Slopes: Landslide Investigations and Mitigation*, Special Report 247, Transportation Research Board, pp. 474-504.

Yashinsky, M., 1998, *The Loma Prieta, California Earthquake of October 17, 1989 - Highway Systems, Performance of the Built Environment*, T.L. Holzer, coordinator, U.S. Geological Survey Professional Paper 1552-B.

Yegian, M.K., Marciano, E.A., and Gharaman, V.G., 1991, "Earthquake-Induced Permanent Deformations: Probabilistic Approach," *Journal of Geotechnical Engineering Division*, American Society of Civil Engineers, Volume 117, Number 1, pp. 35-50.

Yeh, G.C.K., 1974, "Seismic Analysis of Slender Buried Beams," *Bulletin of the Seismological Society of America*, Volume 64, Number 5.

Yeh, Y.H., and Wang, C.M., 1991, "Inelastic Behaviors of Pipelines Buried Through Liquefiable Zone," *Lifeline Earthquake Engineering, Proceedings of the Third U.S. Conference*, American Society of Civil Engineers, pp. 480-489.

- Yerkes, R.F., 1992, "Effects of the San Fernando Earthquake as Related to Geology," *San Fernando, California, Earthquake of February 9, 1971*, U.S. Department of Commerce, National Oceanic and Atmospheric Administration, Volume III, pp. 137-154.
- Yerkes, R.F., Bonilla, M.G., Youd, T.L., and Simms, J.D., 1974, "Geologic Environment of the Van Norman Reservoirs Area," *The Van Norman Reservoirs Area, Northern San Fernando Valley, California*, U.S. Geological Survey circular 691-A, pp. A1-A35.
- Yokoyama, H., 1996, "Predominant Period of Sedimentary Surface Wave and Analysis of Earthquake in the Osaka Plain," *Eleventh World Conference on Earthquake Engineering*, Paper No. 87.
- Youd, T.L., 1998, *Screening Guide for Rapid Assessment of Liquefaction Hazard at Highway Bridges Sites*, Technical Report NCEER-98-0005, National Center for Earthquake Engineering Research, University at Buffalo.
- Youd, T.L. and Hoose, S.N., 1978, *Historic Ground Failures in Northern California Triggered by Earthquakes*, U.S. Geological Survey Professional Paper No. 993.
- Youd, T.L., Chung, R.M., and Harp, E.L., 1995, "Liquefaction and Other Geotechnical Effects," *Hokkaido Nansei-Oki Earthquake and Tsunami, Earthquake Spectra*, Volume 11, Supplement A, pp. 49-94.
- Youd, T.L. and Beckman, C.J., 1996, *Highway Culvert Performance During Earthquakes*, Technical Report NCEER-96-0015, National Center for Earthquake Engineering Research, University at Buffalo.
- Yun, H.D. and Kyriakides, S., 1988, "Buckling of Pipelines in Seismic Environments," *Earthquake Engineering and Structural Dynamics*, R.W. Clough, (ed.), Volume 16, Number 6, pp. 2179-2189.
- Zeng, X. and Steedman, R.S., 2000, "Rotating Block Method for Seismic Displacement of Gravity Walls," *Journal of Geotechnical and Geoenvironmental Engineering*, American Society of Civil Engineers, Volume 126, Number 8, pp. 709-717.

This report was prepared by MCEER through a contract from the Federal Highway Administration. Neither MCEER, associates of MCEER, its sponsors, nor any person acting on their behalf makes any warranty, express or implied, with respect to the use of any information, apparatus, method, or process disclosed in this report or that such use may not infringe upon privately owned rights; or assumes any liabilities of whatsoever kind with respect to the use of, or the damage resulting from the use of, any information, apparatus, method, or process disclosed in this report.

The material herein is based upon work supported in whole or in part by the Federal Highway Administration, New York State and other sponsors. Opinions, findings, conclusions or recommendations expressed in this publication do not necessarily reflect the views of these sponsors or the Research Foundation of the State of New York.



EARTHQUAKE ENGINEERING TO EXTREME EVENTS

University at Buffalo, The State University of New York

Red Jacket Quadrangle ▪ Buffalo, New York 14261

Phone: (716) 645-3391 ▪ Fax: (716) 645-3399

E-mail: mceer@buffalo.edu ▪ WWW Site <http://mceer.buffalo.edu>



University at Buffalo *The State University of New York*